Inertial Fusion Energy
Reactor Design Studies
Volume II

DOE/ER-54101
MDC 92E0008
March 1992

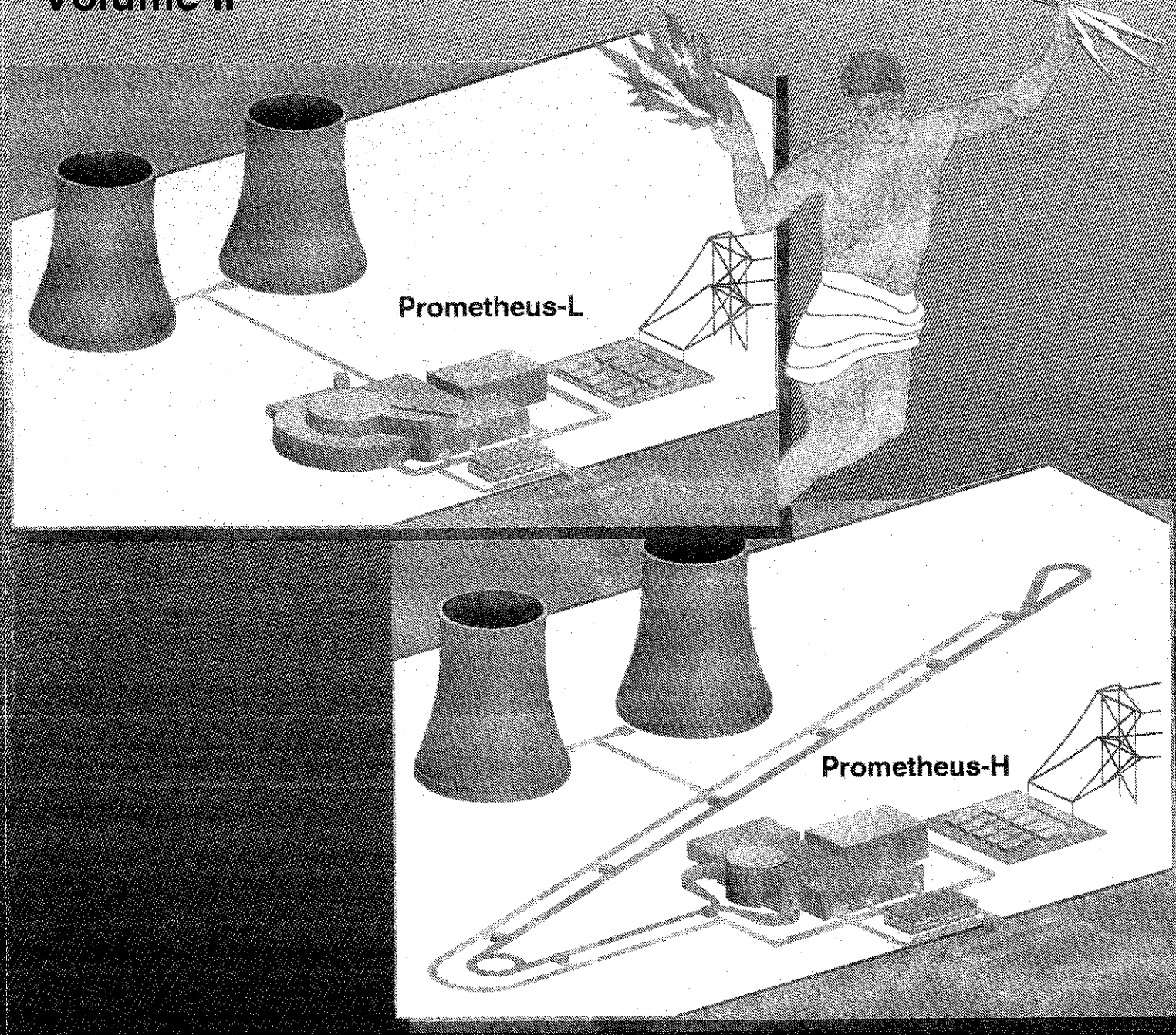

McDonnell Douglas Aerospace Team

Canadian Fusion Fuels Technology Group • Ebasco Services, Inc. • KMS Fusion, Inc.
SPAR Aerospace, Ltd. • TRW Space & Technology Group • University of California at Los Angeles

Final Report

GP33-0272-0001-VC

DOE/ER-54101
MDC 92E0008

INERTIAL FUSION ENERGY REACTOR DESIGN STUDIES

PROMETHEUS-L
PROMETHEUS-H

FINAL REPORT
MARCH 1992

The manuscripts for this document were prepared for publication in March 1992.
The review of the document by DOE delayed publication until July 1993.

Volume II

Copy No. 191

McDonnell Douglas Aerospace
P.O. Box 516
St. Louis, MO 63166-0516

Canadian Fusion Fuels Technology Project
Mississanga, Ontario, Canada

Ebasco Services, Inc.
New York, NY

KMS Fusion, Inc.
Ann Arbor, MI

SPAR Aerospace, Ltd.
Brampton, Ontario, Canada

TRW Space and Electronics Group
Redondo Beach, CA

University of California-Los Angeles
Los Angeles, CA

McDonnell Douglas Aerospace

This work was supported by the US Department of Energy, Office of Fusion Energy, under contract DE-AC02-91ER54101.

CONTRIBUTING AUTHORS

McDONNELL DOUGLAS AEROSPACE

Lester M. Waganer, Daniel E. Driemeyer, V. Dennis Lee

Robert L. Calkins | Henry B. Wald | Forrest R. Williams

CANADIAN FUSION FUELS TECHNOLOGY PROJECT

Ronald S. Matsugu, Otto K. Kveton

K. Kalyanam | Savtantar K. Sood

EBASCO SERVICES, INC.

Stephen L. Ostrow, Stephen F. Marschke

Paul J. Estreich | Marvin J. Parnes

KMS FUSION, INC.

Douglas J. Drake[1]

SPAR AEROSPACE, LTD.

Julian W.F. Millard

John Ballantyne, Chris English, Terry Haines, Clive Holloway, Don Perrot, Andy Turner

TRW SPACE AND ELECTRONICS GROUP

Gary J. Linford | **Steven W. Fornaca** | **Alfred W. Maschke**

UNIVERSITY OF CALIFORNIA, LOS ANGELES

Mohamed A. Abdou, Nasr M. Ghoniem, Mark S. Tillack

James E. Eggleston, Anter El-Azab, Zinovy R. Gorbis, Insoo Jun, Farrokh Issacci, A. Rene Raffray, Shahram Sharafat, Alice Y. Ying, Mahmoud Z. Youssef, Li Zhang

1. Now associated with Interscience, Inc, Germantown, MD

ACKNOWLEDGMENT

The McDonnell Douglas team wishes to thank a great number of people who supported and contributed to this overall effort. Their time and effort are greatly appreciated.

Oversight Committee

Ronald C. Davidson, Chairman	Princeton Plasma Physics Laboratory
Charles C. Baker	Oak Ridge National Laboratory
Roger O. Bangerter	Lawrence Berkeley Laboratory
E. C. Brolin	Princeton Plasma Physics Laboratory
Daniel R. Cohn	Massachusetts Institute of Technology
Donald L. Cook	Sandia National Laboratories
Donald J. Dudziak	North Carolina State University
William Hogan	Lawrence Livermore National Laboratory
David B. Harris	Los Alamos National Laboratory
Robert A. Krakowski	Los Alamos National Laboratory
Thomas E. Shannon	Oak Ridge National Laboratory
Charles P. Verdon	University of Rochester

Target Working Group

Roger O. Bangerter, Chairman	Lawrence Berkeley Laboratory
George Allhouse	Sandia National Laboratories
John Lindl	Lawrence Livermore National Laboratory
William Mead	Los Alamos National Laboratory
Charles P. Verdon	University of Rochester

ARIES Project Staff

Ronald L. Miller	Los Alamos National Laboratory

Lawrence Berkeley Design Staff

Edward Lee	Lawrence Berkeley Laboratory
Andy Faltens	Lawrence Berkeley Laboratory

We would also like to acknowledge the contributions of other people who made this report possible.

David B. Harris, LANL, who facilitated the review process at his facility
Phillip Lang, LANL, Technical Review
Linda M. Merritt, MDA, Principal Text and Graphics Coordinator and Senior Editor
David E. Morgan and J. Warren Stultz, MDA, Technical Editors
Joanne Matheson , SPAR Aerospace, Ltd, Secretarial Support
Bruce Sayer, SPAR Aerospace, Ltd, Graphics Support
Thomas Chao, Alan Chen, Winn Hong, Billy Jimenez, and Faiz Sherman: UCLA Technical Support
Julie Austin, UCLA Secretarial Support
Matt Durkan, UCLA Administrative Support

TABLE OF CONTENTS

TABLE OF CONTENTS

LIST OF PAGES – VOL. II

LIST OF FIGURES – VOL. II

LIST OF FIGURES – VOL. II (CONT.)

LIST OF FIGURES – VOL. II (CONT.)

LIST OF FIGURES – VOL. II (CONT.)

LIST OF FIGURES – VOL. II (CONT.)

LIST OF TABLES – VOL. II

LIST OF TABLES – VOL. II (CONT.)

ABBREVIATIONS AND ACRONYMS

ADS	Air Detritiation System
ALARA	As Low As Reasonably Achievable
ANL	Argonne National Laboratory
ARIES	Advanced Reactor Innovations and Evaluation Study
ASE	Amplified Spontaneous Emission
ASWS	Auxiliary Service Water System
ATA	Advanced Test Reactor
AVLIS	Atomic Vapor Laser Isotope Separation
BCSS	Blanket Comparison and Selection Study
BHP	Biological Hazard Potential
BOP	Balance of Plant
BQ	Beam Quality
BRP	Blanket/Reflector/Plena
BW	Bandwidth
CANDU	Canadian Deuterium Uranium (Fission Reactor)
CAS	Compressed Air System
CASCADE	LLNL IFE reactor concept using rotating ceramic-granuale blanket
CCWS	Closed Cooling Water System
CCW	Component Cooling Water
CD	Cryogenic Distallation
CDS	Central Difference Scheme
CEA	Commissariat A L'Energie Atomique
CEBAF	Continuous Electron Beam Accelerator Facility
CECE	Combined Electroysis and Catalytic Exchange
CERN	Centre for European Research, Nuclear
CET	Chemical Equilibrium Thermodynamic Code
CFFTP	Canadian Fusion Fuels Technology Project
CH	Hydro-Carbon based material
COE	Cost Of Electricity
CRAM	(beam) Crossed Raman Accumulator
CTMS	Cooling Tower Makeup System
CS	Constant Spot
CSS	Condensate Storage System
CVD	Chemical Vapor Deposition
CVI	Chemical Vapor Infilteration
CWS	Circulating Water System
DAC	Derived Air Concentrations
DBTT	Ductile-to-Brittle Transition Temperature
DCG	Derived Concentration Guide
DD	Direct Drive (target)
DEMO	Demonstration Power Plant
DESY	Deutsches Elektron-Synchrotron
DOD	Department of Defense
DOE	Department of Energy
DPA	Displacements Per Atom
DPP	Demonstration Power Plant
DRTF	Darlington Tritium Removal Facility
DSTI	Dual-Sided Target Irradiation
DT	Deuterium-Tritium
DTX	Dose-To-Flux
E/O	Electro-Optical
EADS	Exhaust Atmosphere Detritiation System
EBEEL	Electron Beam Excited Excimer Laser
EBEL	Electron Beam Excimer Laser
EBSEDL	Electron Beam Sustained Electric Discharge Laser
EDEL	Electric Discharge Excimer Laser

ABBREVIATIONS AND ACRONYMS (CONT.)

EDS	Electrical Distribution System
EEDS	Exchaust Effluent Detritiation System
EGDS	Exhaust Gas Detritiation System
ELD	Excimer Driver Laser
ELMO	Excimer Laser Master Oscillator
ELP	Excimer Laser Preamplifier
ELPA	Excimer Laser Power Amplifier
EMRLD	Excimer Mid-range Raman-shifted Laser Device
ENEA	European Nuclear Energy Agency
EP	Exhaust Purfication
EPA	Environmental Protection Agency
EPR	Experimental Power Reactor
EPRI	Electric Power Research Institute
ER	Energy Research
ESECOM	Environmental, Safety, and Economic Aspects of MFE COmmittee
ESCWS	Essential Services Cooling Water System
ETF	Engineering Test Facility
ETHEL	European Tritium Handling and Experimental Laboratory
ETR	Engineering Test Reactor
FCU	Fuel Cleanup Unit
F	Fluence
FEL	Free Electron Laser
FET	Field Effect Transistor
FFTF	Fast Flux Test Facility
FINESSE	Fusion Integrated Nuclear Experiments Strategy Study Effort
FMEA	Failure Modes and Effects Analysis
FODO	Focus-Drift-DeFocus-Drift
FPCCS	Fuel Processing Closed Coolant System
FPS	Freeze Protection System
FPS	Fuel Processing System
FPY	Full Power Year
FRC	Fiber Reinforced Composite
FRRA	Forward Rotational Raman Amplifier
FSMS	Fuel Storage and Management System
FSS	Fuel Storage System
FW/B	First Wall/Blanket
FW	First Wall
FWS	First Wall System
GB	Grain Boundary
GBCS	Glove Box Cleanup System
GBFEL	Ground-Based Free Electron Laser
GC	Gas Chromatographic
GDP	Glow Discharge Polymerization
GIA	Grazing Incidence Angle
GIMM	Grazing Incidence Metal Mirror
HI	Heavy Ion
HIBALL	Heavy Ion Beams and Lithium Lead
HID	Heavy Ion Driver or Driven
HIF	Heavy Ion Fusion
HIFSA	Heavy Ion Fusion Systems Assessment
HIP	Hot Isostatic Pressing
HITEX	High Temperature Isotopic EXchange
HR	High Reflectivity
HVAC	Heating, Ventilation, Air Conditioning
HYLIFE	High-Yield Lithium-Injection Fusion Energy
IADS	Inert Atmospheric Detritiation System

ABBREVIATIONS AND ACRONYMS (CONT.)

IB	Inverse Bremsstrahlung
ICCOMO	Inertial COfinement systems performance and COst MOdel
ICF	Inertial Confinement Fusion
ICFSS	Inertial Confinement Fusion System Study
ICRP	International Commission on Radiological Protection
ID	Indirect Drive (target)
IDLD	Indirect Drive, Laser Driven (targets)
IDLH	Immediately Dangerous to Life or Health
IDPR	IFE Experimental Power Reactor
IEEE	Institute of Electrical and Electronic Engineers
IEPR	IFE Experimental Power Reactor
IFE	Inertial Fusion Energy
IFERDS	Inertial Fusion Energy Reactor Design Study
ILSE	Induction Linac System Experiment
IS	Inherent Safety
ISI	Induced Spatial Incoherence
ISR	Ion Storage Ring
ISS	Isotope Separation System
IT	Impurity Treatment
ITER	International Thermonuclear Experimental Reactor
IVVS	In-Vessel Vehicle System
JAERI	Japan Atomic Energy Research Institute
JET	Joint European Torus
KfK	Kernforschungszentrum Karlsruhe
LA	Large Aperture
LAM	Large Aperture Module
LANL	Los Alamos National Laboratory
LBL	Lawrence Berkeley Laboratory
LD	Laser Driver or Driven
LIA	Linear Induction Accelerator
LIACEP	Linear Induction Accelerator Cost Evaluation Program
LIBRA	Light Ion Beam Fusion Reactor Conceputal Design Study
LINAC	LINear ACcelerator
LLE	Laboratory for Laser Energetics
LLNL	Lawrence Livermore National Laboratory
LLW	Low Level Radioactive Waste
LMF	Laboratory Microfusion Facility
LOCA	Loss of Coolant Accident
LOE	Level Of Effort
LOFA	Loss of Flow Accident
LRO	Local Raman Oscillator
LSA	Level of Safety Assurance
LTA	Long Term Activation
LTE	Local Thermodylnamic Equilibrium
LV	Low Voltage
M	Blanket or Nuclear Power Multiplication
MARS	Mirror Advanced Reactor Study
MB	Multiple Beam
MBL	Multiple Beam Linac
MCF	Magnetic Confinement Fusion
MD	Molecular Dynamics
MDA	McDonnell Douglas Aerospace
MDESC	McDonnell Douglas Electronic Systems Company
MDMSC	McDonnell Douglas Missile Systems Company
MFE	Magnetic Fusion Energy
MHD	Magneto-Hydromanmic

ABBREVIATIONS AND ACRONYMS (CONT.)

MINIMARS	Mini-Mirror Advanced Reactor Study
MOPA	Master Oscillator Power Amplifier
MPC_a	Maximum Premissible Concentration in Air
MSM	Master-Slave Manipulator
MTA	Maintainability Task Analysis
MTBF	Mean Time Between Failure
MTTR	Mean Time To Repair
MUF	Mass Utilization Factor
MV	Medium Voltage
NASA	National Aerospace and Space Administration
NECDB	Nuclear Energy Cost Data Base
NET	Next European Torus
NIOSH	National Institute for Occupational Safety and Health
NLO	Non Linear Optical
NMFECC	National Magnetic Fusion Energy Computer Center
NPB	Neutral Particle Beam
NPBIE	Neutral Particle Beam Integrated Experiment
NPR	New Production Reactor
NPRD	Non-electrical Parts Reliability Data
NRC	Nuclear Regulatory Commission
NRF	Neutron Reflection Factor
NRL	Naval Research Laboratory
OEL	Optimized Excimer Laser
OFE	Office of Fusion Energy
ORNL	Oak Ridge National Laboratory
PC	Pulse Compression
PF	Pulse Forming
PFL	Pulse Forming Line
PFN	Pulse Forming Network
PHA	Preliminary Hazards Analysis
PKA	Primary Knock-on Atom
PPPL	Princeton Plasma Physics Laboratory
PRA	Preliminary Risk Analysis
PRF	Pulse Repetition Frequency
PSA	Pressure Swing Adsorption
PWR	Pressurized Water Reactor
PVA	PolyVinyl Acetate
R&D	Research and Development
RA	Resonance Absorption
RA	Resonant Absorption
RAC	Raman Accumulator Cell
RADS	Recirculating Air Detritiation System
RAM	Reliability, Availability, Maintainability
RCRA	Resource, Conservation, and Recovery Act
RCS	Replacement Collision Sequences
RECON	A UCLA Heat and Mass Transfer Computer Model
RF	Radio Frequency
RHR	Reactor Heat Removal
RMCS	Remote Manipulator and Control System
RMS	Remote Monitoring System
RMSD	Remote Manipulator Systems Division (SPAR)
RPE	Reactor Plant Equipment
RPM	Revolutions Per Minute
RR	Repetition Rate
RT	Rayleigh-Taylor (instability)
RT	Room Temperature

ABBREVIATIONS AND ACRONYMS (CONT.)

SB	Single Beam
SBFEL	Space-Based Free Electron Laser
SBL	Single Beam Linac
SBS	Stimulated Brillouin Scattering
SCR	Silicon Controlled Rectifier
SDI	Strategic Defense Intitative
SDIO	Strategic Defense Intitative Organization
SENRI	A Japanese Fusion Reactor Design Study
SEP	Socie'te' Europeenne de Propulsion
SIRIUS	A Symmetric Direct Drive Laser Fusion Reactor Study (Univ of Wisc)
SLAC	Stanford Linear Accelerator
SNL	Sandia National Laboratories
SOLASE	Experimental Inertial Reactor Study (at Univ of Wisc)
SOW	Statement Of Work
SP	Single Pulse
SPAR	Spar Aerospace, Ltd
SPTF	Single Pulse Test Facility
SRRS	Stimulated Rotational Raman Scattering
SRS	Stimulated Raman Scattering
SSC	Superconducting Super-Collider
SSTI	Single-Sided Target Irradiation
STEM	Storage Tubular Extendible Member
STP	Standard Temperature and Pressure
TARM	Telescoping Articulating Remote Maniupulator
TBCCWS	Turbine Building Closed Cooling Water System
TBR	Tritium Breeding Ratio
TCPSA	Thermally Coupled Pressure Swing Adsorption
TCPSA	Thermally Coupled Pressure Swing Adsroption
TDRF	Threshold Dose Release Fractions
TEXTOR	Tritium Experiment for Technology Oriented Research
TFTR	Tokamak Fusion Test Reactor
TPD	Two Plasmon Decay
TPR	Tritium Production Rate
TRIUMF	Tri-University Meson Facility
TRM	Total Remote Maintenance
TSA	Thermal Swing Adsorption
TSDS	Tritium Storage and Delivery System
TSTA	Tritium System Test Assembly
TVD	Total Variation Diminishing
TWA	Time Weighted Averages
TWI	Target Debris-Wall Interaction
TWG	Target Working Group
UCLA	University of California at Los Angeles
UHS	Ultimate Heat Sink
US	United States
UV	Ultraviolet
VLS	Vapor-Liquid-Solid
VPCE	Vapour Phase Catalytic Exchange
VS	Ventilation System
WD	Water Distillation
WD	Water Detritation System
WJSA	W.J. Schafer Associates
XDL	Times Diffraction Limit
ZS	Zoomed Spot

This page intentionally left blank.

TABLE OF CONTENTS – CHAPTER 3

CHAPTER 3
OBJECTIVES, REQUIREMENTS, AND ASSUMPTIONS

3.1 Introduction

The primary objective of the Prometheus study is to develop two conceptual designs of a commercial fusion electrical power plant based on inertial confinement, one with KrF Laser Driver (Prometheus-L) and the other with Heavy Ion Beam Driver (Prometheus-H). In addition, the study emphasized the following goals.

- State-of-the-art advancement of Inertial Fusion Energy (IFE) power plant design
- Assessment of inertial power production including technical feasibility, economics, safety, and environmental aspects
- Identification and characterization of key technical issues including R&D requirements to resolve each issue
- Comparison of the two IFE reactor design concepts
- Development of information necessary to compare the IFE designs to other concepts based on Magnetic Fusion Energy (MFE).

In order to meet the above objectives and goals, it was necessary to develop a set of requirements and guidelines based on (1) recommendations by an Oversight Committee[1] commissioned by DOE, and (2) study management effort. The Oversight Committee, chaired by Ronald Davidson (PPPL), had two working groups, one chaired by Robert Krakowski (LANL) responsible for guidelines as to the study approach and content, and the other chaired by Roger Bangerter (LBL/LLNL) responsible for developing unclassified guidelines[2] for the target information. These guidelines were developed for the Prometheus team and a parallel study team led by W. J. Schafer Associates. The study management refined and augmented the Oversight Committee guidelines based on the project specific needs.

This chapter discusses the important requirements and guidelines adopted in the course of the study. The current data base for IFE is not sufficient to fully develop a complete conceptual reactor design and accurately predict its performance; therefore, assumptions were made where knowledge gaps exist. These assumptions were carefully made after consultation with experts and are summarized in this chapter.

3.2 General Guidelines

- The IFE reactor plant is to serve as a commercial central station electric power plant. The only product is electricity.

- The reactor is operated on the deuterium-tritium fuel cycle and must satisfy tritium self-sufficiency conditions assuming a mature fusion power economy.

- The design is for tenth-of-a-kind commercial power plant. Thus, the machine performance will be highly predictable and it will have resulted from an extensive R&D program and utility operating experience from earlier plants. This also implies that the development costs have been amortized over prior plants.

- The net electric power output of the plant is 1000 MW. The power level of the plant affects the economics and is important to the utility's ability to finance. The smaller size (e.g., 500 MWe and below) is easier to finance, construct, and incorporate into existing grids but the cost of electricity will be higher. The economy of scale is important for both magnetic and inertial fusion reactors, albeit for different reasons. For example, tokamaks have a minimum size dictated by plasma burn and ignition considerations. In IFE reactors, a larger size is typically more economical because drivers represent a significant fraction of the Cost of Electricity (COE) and the strong dependence of gain on driver energy. The study adopted 1000 MW net electric power as a nominal size for comparison purposes with previous and ongoing MFE and IFE reactor design studies.[3-9] Assessments of the advantages of the larger and smaller sizes will be made.

- The design will have a single generating unit at the site. The target factory will be included in the power plant description.

- The data base used in the design will need to be extrapolated in many areas of physics, technology, and economics. For the purpose of this extrapolation, the plant is assumed to start operation in the year 2040-2050 time frame; thus, the data base should be that available in the period 2030-2040. It is difficult to extrapolate to such a distant future and such extrapolations will necessarily involve judgment that varies among experts. The designers are asked to: (a) strive for a balance between credibility and attractiveness; (b) be consistent with assumptions made for MFE where similar conditions prevail (for example, the development of a particular structural material such as SiC has to assume the same probability of success in MFE and IFE subsystems experiencing the same environment. In contrast, if different conditions can lead to different probabilities of success for MFE and IFE, such conditions will have to be delineated); and (c) assumptions on extrapolation and probable outcome of R&D should be clearly documented. The study should identify the key feasibility issues and assess, for each major reactor system, the development program that is needed to advance the physics and technology from its present status to the status that is required for the performance of that system as specified in the design. This assessment should attempt to quantify the magnitude of the extrapolations involved relative to prior advances. An evaluation of the role of the IFE Defense Program and the ongoing MFE Program in resolving these issues is needed.

- The plant lifetime is 40 years for engineering design and 30 years for economic analysis.

- The construction time is assumed to be six years.

- The power plant availability is very difficult to predict because of the lack of a data base for both IFE and MFE designs. At present, the logical approach is to define "goal" availability consistent with current experience from other types of existing power plants and to make an effort to quantify the requirements on component lifetimes and maintenance as well as the R&D to achieve such a goal. The following goals are suggested. Assume an overall plant availability goal of 75% as a "base case." This is consistent with availability factors attained on the average in the nuclear industry. A commonly used goal for PWR designs is 80%. Current practice in many power plants calls for an annual shutdown for about 30 days to perform maintenance and inspection. This 30-day period can be used for scheduled maintenance simultaneously on both the reactor and balance of plant. Furthermore, present data indicate that 20 days downtime per year is caused by failures in balance of plant. Given a 75% overall plant availability implies a total downtime of 91 days per year. The 91 days can be allocated as 30 days for annual scheduled maintenance on both the reactor and balance of plant, 20 days for unscheduled maintenance on balance of plant, and 41 days for unscheduled maintenance on the reactor.

  The following is a summary of recommendations on "base case" availability.

Downtime Allocations for an Overall Plant Availability Goal of 75%			
Reactor		Balance of Plant	
Scheduled	Unscheduled	Scheduled	Unscheduled
30	41	30	20

- Differences in the achievable availability between Laser- and Heavy Ion-Driven reactors are expected. Also, one would anticipate differences between IFE and MFE reactors. These differences will be identified and their impact on the achievable availability and/or the required R&D program will be quantified. This impact will be assessed at least comparatively relative to the "base case."

- The study will perform and document tradeoff studies for key design choices, for example, direct versus indirect drive targets. The study will also analyze and document the impact of key design assumptions and extrapolations in physics, technology, and economics; for example, target gain and target cost.

- Studies to evaluate the sensitivity of power plant figures of merit (e.g. COE, safety features, attractiveness, cost of R&D) to variations in key design assumptions are encouraged.

- The limitations on the resources for the study dictate a focused approach that will emphasize key IFE reactor components such as target, driver, cavity, and fuel cycle. The effort on the balance-of-plant and other areas that are similar in many respects to MFE should be limited. The study will also devote some special effort to those technical areas that affect the comparative evaluations where previous effort was limited; for example, fuel cycle modeling analysis, evacuation of the reactor chamber, tritium and debris recovery, material recycling, and final optics design.

- Generating data sufficient to compare IFE designs with different drivers and to compare IFE to MFE is an important part of the study. Designers of each subsystem must provide the information specified in the Evaluation Methodology.

3.3 Target and Driver Guidelines

The requirements and the design of all systems, except perhaps the BOP, are strongly influenced by target physics and design. Most target designs and performance data are classified. The charter to do classified target physics and design resides at Los Alamos National Laboratory (LANL), Lawrence Livermore National Laboratory (LLNL), Sandia National Laboratories (SNL), and KMS Fusion. This study is to accomplish its objectives based on unclassified information. The Target Working Group[2] (TWG) has provided the study team with unclassified information and requirements on capsule designs, target gain, and driver performance and coupling to the target. The target designs encompass both direct and indirect drive targets for a range of physics assumptions from conservative to optimistic, consistent with extrapolations to the 2030-2040 time frame.

3.3.1 Target Factory - Targets are currently hand-crafted for a few shots per day. For economical power production, the cost of targets must drop many orders of magnitude and the production rate must be increased to about 10^5-10^6 targets per day. Therefore, mass production techniques must be introduced. These extrapolations in cost and production rates are sufficiently large that, despite some excellent previous studies, large uncertainties remain. It is important to reduce the uncertainties since target production costs appear to contribute significantly to total COE. Therefore, the studies must continue to address this issue, with prototype development of actual target fabrication facilities.

The most recent and complete DOE-supported study of target costs was performed for the Heavy-Ion Fusion Systems Assessment.[6,9] Since the completion of this study, there has been some evolution in target design and substantial progress in hand-crafted target fabrication techniques. Furthermore, some of the newer target fabrication techniques appear suitable for mass production; therefore, continuing studies are needed. The studies must include conceptual techniques for fabricating the targets and must be performed by a group that includes individuals with industrial experience and demonstrated expertise in the mass production of small, high precision components. These individuals must be familiar with advanced manufacturing R&D. Also, target inventory and shelf life and tritium inventory, handling, and control must be addressed. Target factory development needs must be detailed.

The target factory must be on site and financially possible. The maximum allowable cost per target for an IFE plant to be economically competitive can be derived from simple arguments. The presently projected COE from an IFE plant may exceed that from conventional and nuclear power plants because of the presence of large expensive reactor components such as the driver. Therefore, the cost of the targets should be no more than about 10% of the busbar COE for an IFE plant. At present, a reasonable goal for the busbar COE is 5¢/kWh. For a power plant with a net electric power output of 1000 MW, the cost of energy per day is $1.2 million. With the 10% assumption, the maximum allowable cost for the targets is $0.12 million per day. For a pulse repetition rate of about 6 per second, the number of targets required is about 0.52 million targets per day; therefore, the total cost per target should not exceed about 23 cents per target. This is the suggested maximum cost per target including materials, fabrication, and delivery.

3.3.2 Direct-Drive KrF Laser Target and Driver - Direct-drive KrF target designs are relatively mature as they have undergone a number of iterations with respect to issues associated with hydrodynamic stability, effect of long-wavelength drive nonuniformities, and laser energy coupling. However, these direct-drive (DD) targets have not been tested at anything resembling IFE reactor-level laser energies. Current DD target experiments are being conducted at laser energies three orders of magnitude below the ~4 MJ Prometheus-L design. The gain curves for directly driven laser targets are given by the TWG in Figures 3.3-1 and 3.3-2. The direct-drive target described in this report is similar to the target used in determining the gain curves.

The gain curves for the direct-drive target were based on an unclassified code (University of Rochester). The curves in Figure 3.3-1 assume that the laser focal spot radius is constant in time and equal to the target radius. Also assumed is a spatial intensity profile described by $\sin^2 x/x^2$. Because detailed target designs are not

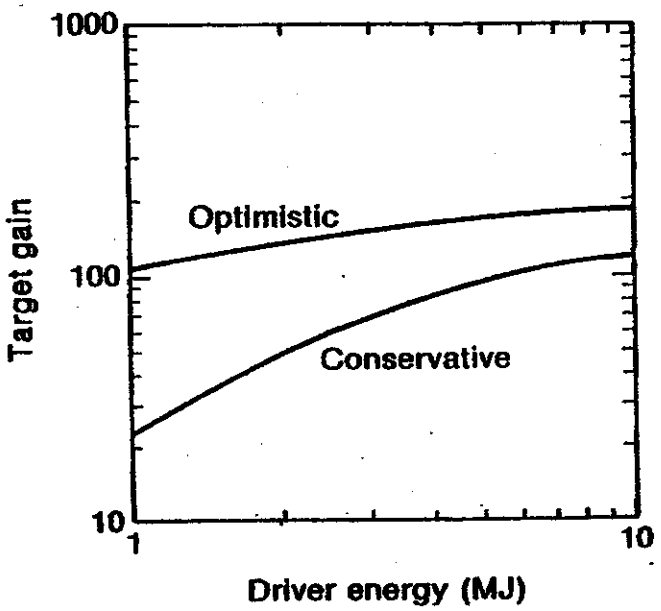

Figure 3.3-1. Gain as a Function of Energy for Directly-Driven Laser Targets[2]

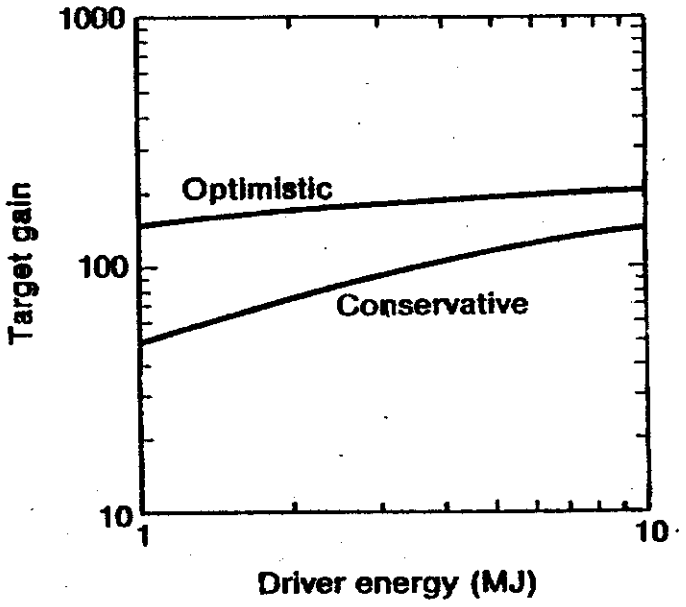

Figure 3.3-2. Gain as a Function of Energy for Directly Driven Laser Targets. These Curves Assume Zooming.[2]

available to this study, we have assumed the well-known hydrodynamic scaling laws to obtain the focal spot radius, (i.e., assume the radius scales as $E_L^{1/3}$ (where E_L is laser energy)). Using a radius of 2.8 mm at 4 MJ has allowed us to compute the coefficient of the gain curves. Similarly, we assumed the peak power scales as $E_L^{2/3}$. We then used a peak power of 500 TW at 4 MJ to get the value for gain curve coefficient. The curves in Figure 3.3-2 assume that the focal spot radius is "zoomed" so that it remains equal to the critical surface throughout the implosion. Detailed guidelines are provided below for the cases in Figure 3.3-1; i.e., for a laser focal spot radius that is constant in time. In Figures 3.3-1 and 3.3-2 the gain curves are shown as a band to represent the current "level of risk" understanding associated with hydrodynamic stability issues. The upper curve represents the optimistic case while the lower curve represents the conservative case. For the purpose of this study, the base line gain should be taken to be the arithmetic mean of the optimistic and conservative curves.

Illumination uniformity requirements were provided by the TWG for the designs represented in Figure 3.3-1. The requirements are summarized as follows:

(a) A minimum of 60 beams is required and the initial focal spot radius should equal the radius of the capsule.

(b) Power balance must be better than about 5% rms for 1% rms illumination uniformity.

(c) Random beam mispointing must be less than 0.1 of the capsule radius to obtain better than about 1.2% rms illumination uniformity.

(d) Capsule mispositioning with respect to the center of the chamber must be less than 0.1 of the capsule radius in order to maintain the nonuniformity below 1% rms.

(e) The required level of individual beam uniformity is difficult to specify accurately at present. Some form of beam smoothing technique is required (asymptotic level of illumination nonuniformity will have to be less than about 1% rms), and smoothing (or averaging) times will have to be as short as possible (less than about 10-20 picoseconds).

Details of the illumination uniformity requirements are provided below.

Illumination Uniformity Requirements for Direct-Drive KrF - The near-field laser beam irradiation pattern on the capsule can be represented as the product of two factors: (1) a single-beam factor that depends on the focusing geometry, the f-number of the lens, the capsule conditions, and the individual beam profiles; and (2) an interbeam interaction factor that is determined by the number, orientation, synchronization, polarization, and bandwidth of the individual beams about the capsule and the energy or power imbalance between the beams. (The balance-of-time, integrated, individual beam energies do not preclude the occurrences of instantaneous differences in intensity between beams at different times in the pulse.)

Number of Beams and Focal Spot Radius - Figure 3.3-3 illustrates the predicted rms irradiation nonuniformity on the capsule for 24-, 32-, 60-, and 96-beam irradiation configurations. The individual beam radial-beam profiles in all cases are assumed to be $\sin^2 x/x^2$ characteristic of the intensity envelope produced by distributed phase plates. This intensity distribution function is, however, characteristic of far field diffraction from a rectangular aperture and is inconsistent with the near-field laser illumination scenario. All of the beam configurations provide adequate uniformity at a focal ratio (beam radius at the 5% intensity point divided by the capsule radius) of ~1 (tangential focus). However, as the capsule implodes, this ratio increases due to the inward motion of the critical surface. By the time the laser pulse has finally turned off,

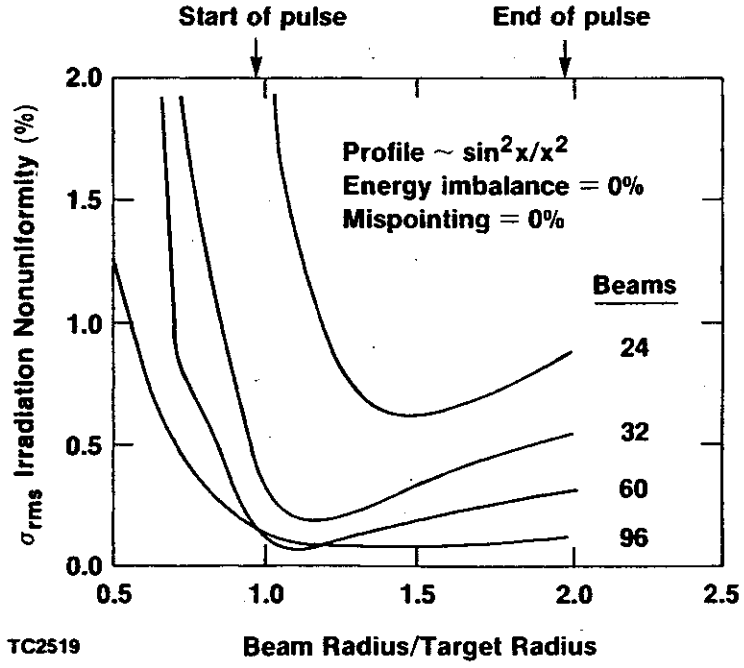

Figure 3.3-3. Irradiation Non uniformity (σ rms) as a Function of Focus Ratio for 24-, 32-, 60-, and 96-Beam Geometries, assuming a Smooth $\sin^2 x/x^2$ Radial Beam Profiles.[1]

the focal ratio typically doubles. From Figure 3.3-3, clearly a minimum of 32 beams is required to obtain a high level of uniformity over the duration of the laser pulse. However, when issues associated with other contributions to illumination nonuniformity are included, it is found that a 32-beam system requires much more control over power balance and beam mispointing than a system with more beams. Therefore, in terms of stating a requirement on the number of beams and their focal spot radii, a minimum of 60 beams is required and the initial focal spot radius should equal the radius of the capsule. As to the beam placement, assuming that the 60 beams are symmetrically disposed about the capsule is a good first approximation.

Power Balance and Beam Alignment - The effects of beam (power) imbalance and beam alignment on capsule performance result in temporally varying illumination nonuniformities with spectral magnitudes that vary with time. Analysis has shown that these illumination nonuniformities produce mainly low-order modes ($l < 6$). Two-dimensional simulations of designs representing the upper gain curve have shown that the $l \leq 6$ modes must have amplitudes less that 1-2% (rms). Using this requirement, an estimate of the power imbalance and beam alignment (mispointing) can be obtained. Figure 3.3-4 shows that a 60-beam system requires power balance

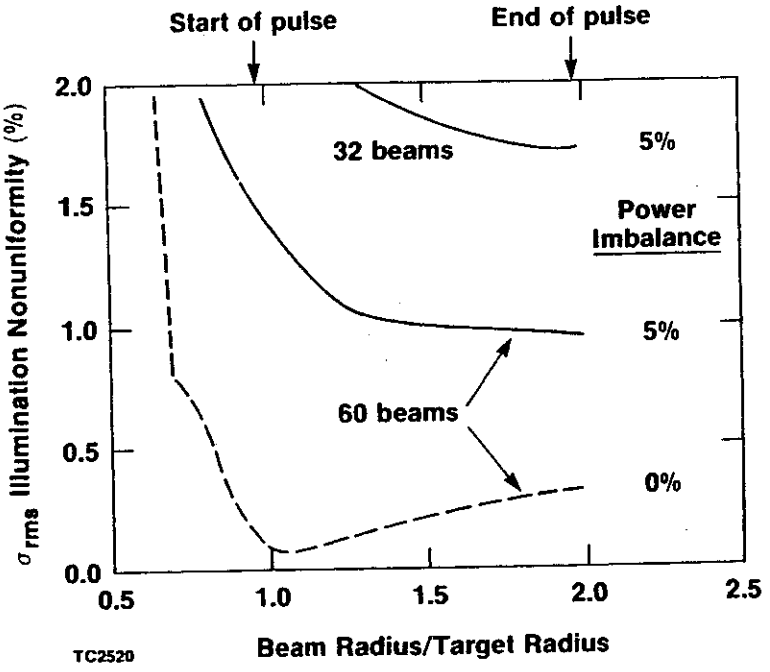

Figure 3.3-4. Irradiation Non uniformity (σ rms) as a Function of Focus Ratio for 32 and 60 Beams, assuming a 5% Power Imbalance and Smooth $\sin^2 x/x^2$ Radial Beam Profiles. The dashed line is the reference σ rms for 5% rms power imbalance for the 60-beam system.[1]

which must be better than ~5 rms for 1% rms illumination nonuniformity for $1 \leq l \leq 6$. The amount of beam mispointing that can be tolerated is shown in Figure 3.3-5. The rms nonuniformity is plotted as a function of the maximum beam mispointing, measured in terms of the target radius. The mispointing is chosen to be random in magnitude (up to the maximum indicated) and random in direction; the error bar indicates the spread in values that is obtained for different sets of pointing errors at a given maximum. For a 60-beam system, a random mispointing of 0.1 of the capsule radius will result in ~1.2% rms illumination nonuniformity. The calculations in Figure 3.3-5 assume perfect power balance. The combined results of power imbalance and beam mispointing add in quadrature.

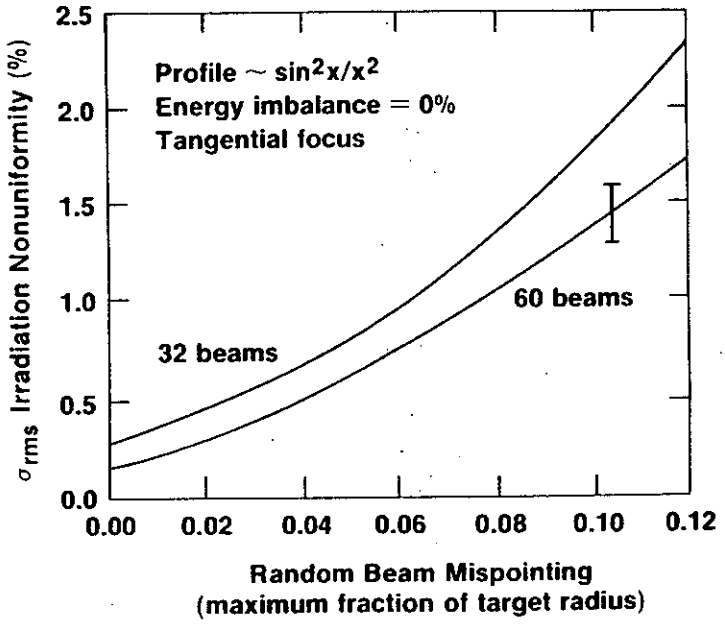

TC2521

Figure 3.3-5. Effect of Beam Pointing Error on Irradiation Non uniformity for 32- and 60-Beam System. A smooth $\sin^2 x/x^2$ radial beam profile is assumed.[1]

Capsule Positioning - Uniformity calculations indicate that the capsule mispositioning with respect to the center of the chamber must be less than 0.1 of the capsule radius in order to maintain the nonuniformity below 1% rms. These calculations did not take into account the time dependent effects on the capsule drive of the energy that misses the capsule due to its miscentering. This would depend on the particular capsule design and the pulse shape under consideration.

Individual Beam Uniformity - The required level of individual beam uniformity is still an area of active research. It is difficult to give a precise answer as to the uniformity requirements because capsule performance is affected by both the magnitude of the nonuniformity as well as the modal content of the resulting beam overlap pattern. Some form of beam smoothing technique will be required, and smoothing (or averaging) times will have to be as short as possible (tens of picoseconds). Therefore, since this study is limited to a KrF laser system, some form of induced spatial incoherence (ISI) beam smoothing may have to be employed. As an estimate of the level of illumination uniformity required, initial calculations indicate that the asymptotic level of illumination nonuniformity will have to be <1% rms and that the averaging times must be less than 10-20 ps.

3.3.3 Indirect-Drive KrF Laser Target and Driver - Target gain, using indirectly driven capsules for inertial fusion energy production, will be a function of a large number of variables, including laser geometry, focusability, pointing accuracy, wavelength, and possibly beam smoothness and bandwidth, as well as target performance determined by such effects as hydrodynamic instabilities and plasma physics effects in hohlraums. Most of these effects are coupled and a system optimization must be carried out to determine the best set of operating conditions. Since most of the target physics is classified, many of the choices that go into any particular set of gain curves must remain classified. Figure 3.3-6 shows two gain curves that we believe span the range of target gains likely to be achievable using standard capsule and hohlraum designs. The lower curve is based on detailed target design studies carried out for the Department of Energy Defense Programs LMF (Laboratory Microfusion Facility). This gain curve is consistent with an extrapolation to the megajoule scale of all current data. This curve represents the present best estimate of the gain that would be achieved in a first-of-a-kind experimental high gain facility. The higher gain of the upper curve results from an increased coupling efficiency that we believe can be achieved after optimization of both the laser-plasma interaction effects and the target geometry. Advanced target designs could have gains of about a factor of two higher than the upper curve. These designs have increased physics uncertainties and have been less thoroughly analyzed than our baseline designs; however, for these studies the enhanced performance curve should be used as the base case. The LMF baseline curve is the conservative case. The enhanced performance curve should be multiplied by 2 to give the more optimistic case called for in the Guidelines; however, the optimistic case should not be used for laser energies less than 2.5 MJ. Figure 3.3-7 shows the peak power requirements for the two gain curves in Figure 3.3-6. The power curve for enhanced hohlraum performance may be used for the optimistic case. About 70% of the total energy is delivered during the peak power part of the pulse. The rest is delivered in a precursor pulse that is 4-5 times the duration of the peak power pulse.

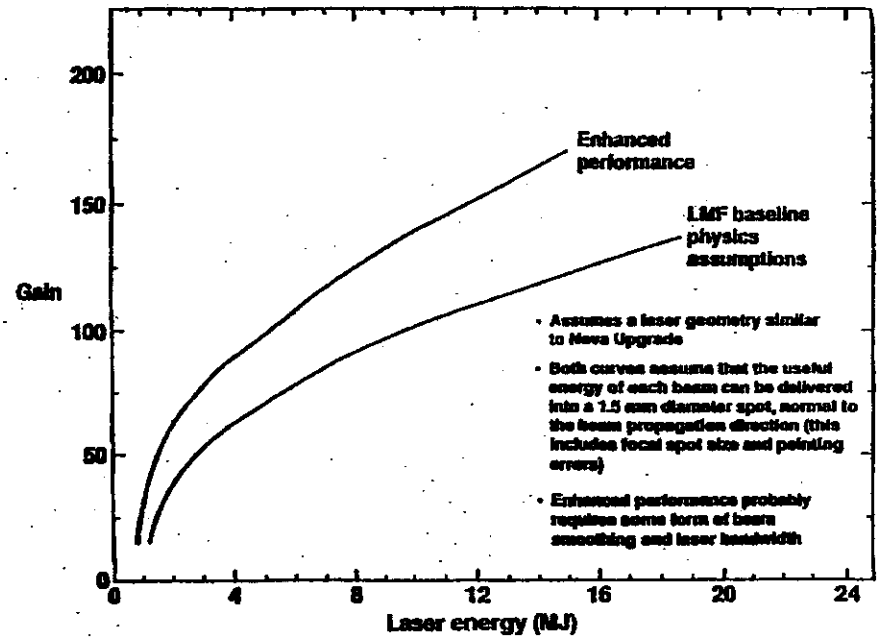

Figure 3.3-6. Gain as a Function of Laser Energy for Indirectly-Driven Targets[2]

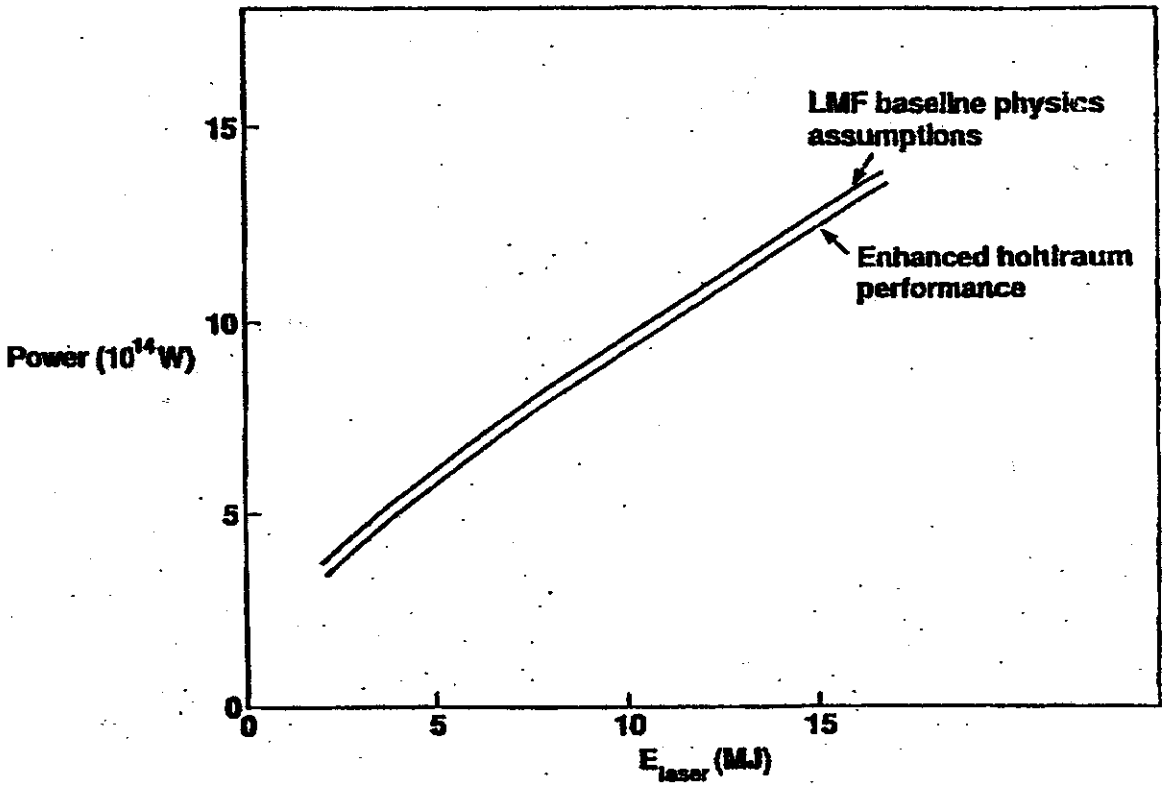

Figure 3.3-7. Power as a Function of Laser Energy for Indirectly-Driven Targets[2]

In order for the laser energy to be efficiently utilized, it is necessary that the laser beam be capable of achieving a spot size that is nearly diffraction limited. It is also important that the pointing errors be limited to a few microradians. A convenient way of stating these requirements is to specify a focal spot within which the laser energy can be delivered. Both gain curves in Figure 3.3-6 assume that all of the useful energy of each beam can be delivered into a 1.5-mm diameter spot. This spot size includes both the size of the focal spot and any pointing errors. All energy outside this spot will not be useful in driving an implosion. However, this divergent energy could adversely affect an implosion if it exceeds even 0.1% of the total energy. Plasma closure phenomena can significantly affect the time-dependent delivery of laser energy to the secondary targets within the hohlraum. In addition, both curves assume a laser geometry similar to that being planned for the Nova Upgrade. The Nova Upgrade laser plan calls for 288 independently pointed beams. The beams are distributed in three or four rings of beams on each side of the target at angles between approximately 30 and 60 degrees from the target axis. The large number of beams allows great flexibility for achieving irradiation uniformity at the capsule while complicating the beams' alignment problems. It also relaxes the instantaneous power and energy balance requirements and allows an rms variation of 10% or more. It may ultimately be possible to reduce the number of beams to a total ranging between 20 and 50. With a smaller number of beams, the power balance must be better than about 5% and the gain may be lower. For these studies we recommend a minimum of 50 beams.

3.3.4 Indirect-Drive Heavy Ion Beam Target and Driver

Target Performance - Figure 3.3-8 gives target gain as a function of driver energy, ion range, and focal spot size for targets driven by two diametrically opposed beams or beam clusters. The peak power requirements for these targets are given in Figure 3.3-9.

The curves in Figures 3.3-8 and 3.3-9 should be considered the "base case." Concepts exist that should give gains about a factor of two higher. Thus the gain can be multiplied by a factor of two (only for cases with driver energies above the ~200 MJ "knee" in the base case curves) to give a more speculative case. The power curves remain unchanged for this case. For a lower limit, the gain should be multiplied by 0.7; the power curves again remain unchanged.

Ion range as a function of ion mass and kinetic energy is given in Figure 3.3-10.

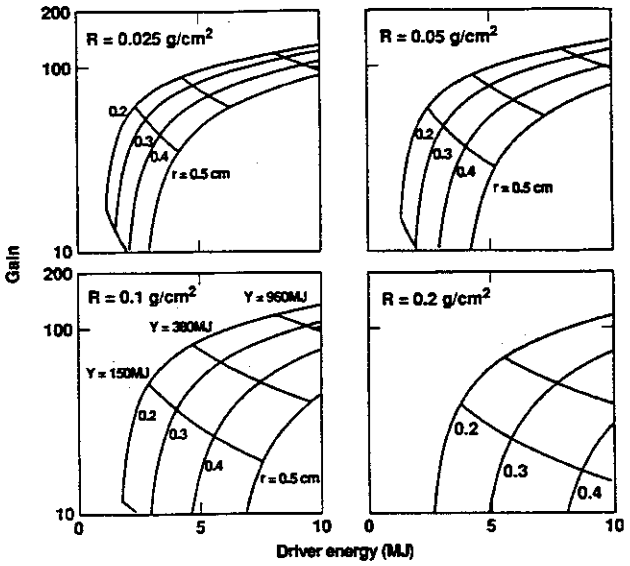

Figure 3.3-8. Target Gain for Indirect-Drive Heavy Ions as a Function of Driver Energy,Ion Range, and Focal Spot Size for Targets Driven by Two Diametrically Opposed Beams[1]

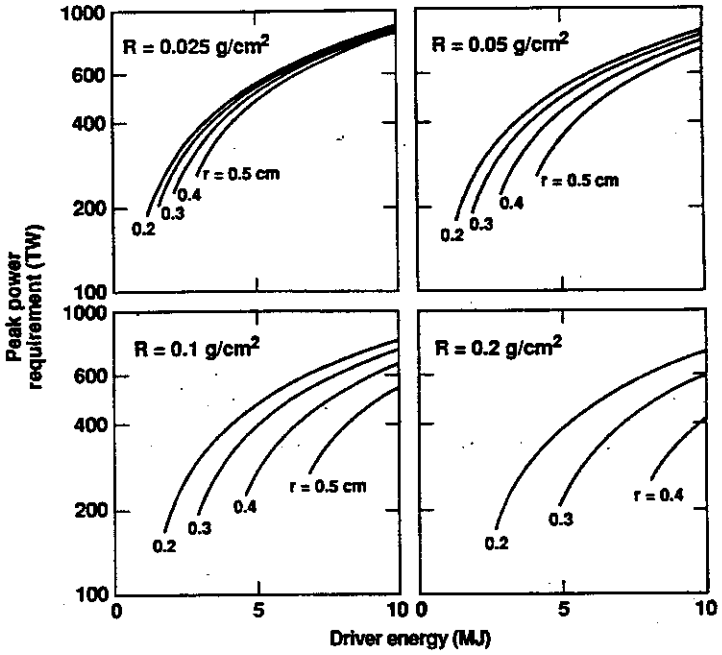

Figure 3.3-9. Peak Power Requirements for Indirect-Drive Heavy Ions as a Function of Driver Energy, Ion Range, and Focal Spot Size for Targets Driven by Two Diametrically Opposed Beams[1]

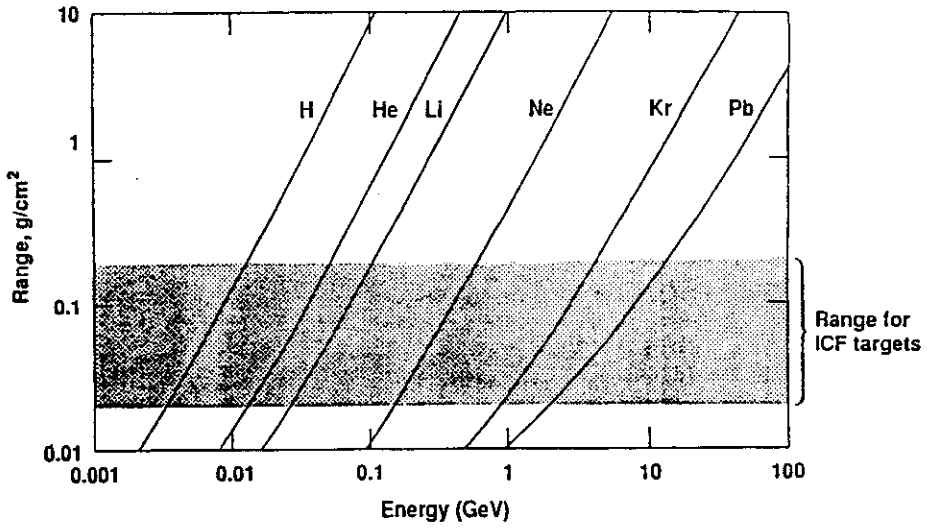

Figure 3.3-10. Ion Range as a Function of Ion Mass and Kinetic Energy[1]

Pulse-Shape Precision, Power Balance, and Beam Alignment - As noted in the previous section, there is considerable flexibility in pulse shape; however, once a pulse shape is chosen, the power at any time during the pulse must be within 3% of its nominal value. This requirement must be met for both beam clusters.

The center of each beam or beam cluster must be aligned within 10% of the focal spot radius. If beam clusters are used and if the beam errors are statistically independent, each beam can clearly have looser tolerances than the tolerance on the entire cluster.

Misalignment and imperfections in the beams and lenses may lead to some fuzziness in the beam radius. If the conditions on power balance and centroid alignment are satisfied, the effect of beam fuzziness can be estimated by using only that fraction of the beam energy that falls in the focal spot radius when using Figures 3.3-8 and 3.3-9. Thus, within limits, there is a trade-off between target gain and beam alignment and radius.

3.4 Reactor Systems

The two drivers to be considered are the KrF excimer laser and the Heavy Ion (HI) beam. A design will be developed for each driver. Most of the key requirements on the driver were specified earlier in discussing the requirements on target design information.

The study should evaluate the technical issues and perform trade-off studies to select among the options and design variables and to determine the performance for each driver design. Key considerations include physics and engineering feasibility, cost, efficiency, reliability, lifetime, safety, and environmental impact. Some of the selection decisions that have to be made for the designs include: (1) direct versus indirect drive, (2) pulse shape and number of beams for the KrF laser, (3) double- or single-sided HI

illumination, and (4) configuration and radiation protection schemes for the driver systems (e.g., optics for laser).

In addition to the target and driver system discussed earlier, other reactor systems included are the reactor chamber evacuation system, first wall and its protection system, blanket, radiation shield, tritium system, and primary heat transport system. The evacuation system provides for vacuum pumping of the reactor chamber between pulses down to the pressure required for efficient transmittal of the driver beams to the target. The function of the wall protection system is to absorb the x-rays, charged particles, and target debris generated from the fusion reactions, target disintegration, and interactions with the background gases in the reactor chamber. Depending on the specific design, the amount of nuclear heating generated by neutrons and gamma rays in the wall protection system can be a significant fraction of the energy of the fusion neutrons. The function of the blanket is to breed tritium at the rate required by tritium self-sufficiency condition and to convert the kinetic energy of neutrons and associated gamma rays into sensible heat. The function of the tritium system is to process tritium from the wall protection system, blanket, reactor chamber exhaust and from other reactor components and to supply tritium to the target factory and to a storage system. The function of the primary heat transport system is to transport the recoverable heat from the blanket, wall protection, driver system, and from other reactor components to the secondary energy conversion system.

These reactor systems have important technical feasibility issues and they greatly influence the potential attractiveness of fusion reactors. The study should develop viable engineering solutions that enhance the potential attractiveness of IFE reactor power plant designs with respect to cost of energy, safety, and environmental impact. Selection of the design for various components and the overall reactor configuration should emphasize simplicity, reliability, and maintainability. Tradeoff studies and the rationale for selection of materials and engineering design features should be documented. Key technical issues and the R&D programs required to resolve these issues must be identified.

These reactor systems in the IFE reactors will have similarities to, as well as differences from, corresponding systems in MFE reactor designs. Applicable experience and data base from MFE designs and R&D programs should be fully utilized. Extrapolations required for materials and technology R&D to meet the feasibility and attractiveness goals should be consistent with those assumed for MFE.

3.5 Economic Guidelines

Many of the previous requirements and criteria have profound effects on the economics of the power plant. These would include such items as the net power output, the tenth-of-a-kind assumption, and technology assumptions. The Oversight Committee also recommended some specific economic groundrules in concert with

the NECDB methodology[10] and the latest ARIES costing methodology.[11,12,13] The economic requirements and guidelines shown in Table 3.5-1 have been worked out with the Economics Working Group, headed by Robert Krakowski of LANL and Ron Miller for ARIES.

Table 3.5-1 Prometheus Economic Guidelines

Plant Operating Lifetime, yrs		30			
Plant Construction Lead Time, yrs		6			
Contingency Factor, Project and Process		See below, may add risk factor			
Spare Parts Multiplier		1.0 (no spares)			
Constant Year Dollars		1991			
Nominal Year Dollars		1997			
Inflation Rate		.05			
Escalation Rate		.05			
		Average	Tax-Adjusted		
Effective Cost of Money, Nominal Dollars		.1135	.0957		
Effective Cost of Money, Constant Dollars		.0605	.0435		
Fixed Charge Rate, Nominal Dollars		.1638			
Fixed Charge Rate, Constant Dollars		.0966			
Indirect Cost Factors	LSA	1	2	3	4
91 Constr Serv & Equipment	(x TDC)	.113	.120	.128	.151
92 Home Office Engr & Services	(x TDC)	.052	.052	.052	.052
93 Field Office Engr & Services	(x TDC)	.052	.060	.064	.087
94 Owners Cost	(x TDC+91+92+93)	.150	.150	.150	.150
95 Process Contingency	(x TDC+91+92+93+94)	.000	.000	.000	.000
96 Project Contingency	(x TDC+91+92+93+94)	.1465	.173	.184	.195
		Constant $	Nominal $		
97 IDC Factor		.1652	.3178		
98 EDC Factor		-0	.2436		
Operations and Maintenance Cost [$91]		$78.9x(L^*)\ (P_E/1200)^{0.5}$			
LSA Factor, L*		0.7[1]; 0.85[2]; 0.952[3]; 1.0[4]			
Decommissioning Allowance, mill/kWeh		0-1 (LSA-dependent)			
Deuterium Fuel Cost, mill/kWeh		-0.05			
Learning Curve		85-90% on fusion systems, 75-100% on non-fusion systems			
Quantity Assumption		10th of kind commercial plant + Prototype and Demo if applicable			
Other Factors Influencing the Economics					
Plant Availability/Capacity		Value derived from design approach Will use typical MCF values (.75) as a starting value			
Cost Adjustment Factor up to 1991$		Use Gross National Product Implicit Price Level Deflators [1982 Basis]			

References for 3

1. R. C. Davidson, et. al, "Inertial Confinement Fusion Reactor Studies Recommended Guidelines," September 1990.

2. R. Bangerter, "Revised Target Information for ICF Reactor Studies," memo from R. Bangerter, February 1991.

3. W. J. Hogan, G. L. Kulcinski, Fusion Technology 8, 17 (1985).

4. The HIBALL studies are good examples. "HIBALL: A Conceptual Heavy Ion Beam Driven Fusion Reactor Study," UWFDM-450, University of Wisconsin Fusion Technology Institute (1981); see also KfK-3202, Kernforschungszentrum Karlsruhe (1981) and "HIBALL II: An Improved Heavy Ion Beam Driven Fusion Reactor Study," UWFDM-625, University of Wisconsin Fusion Technology Institute (1984); see also KfK-3480, Kernforschungszentrum Karlsruhe (1984) and FPA-84-4, Fusion Power Associates (1984).

5. The HYLIFE study is a good example. J. A. Blink, W. J. Hogan, J. Hovingh, W. R. Meier, and J. H. Pitts, Lawrence Livermore National Laboratory Report UCRL-53559, (1985).

6. The Heavy-Ion Fusion Systems Assessment (HIFSA) is a good example. Fusion Technology, 13, No. 2 (1988).

7. F. Najmabadi, "The ARIES-I Tokamak Reactor," 9th Topical Meeting on Technology of Fusion Energy, Oakbrook, Illinois, 7-11 October 1990)

8. R. O. Bangerter, J.W.-K. Mark, and G. Magelssen, "Simple Target Models for Ion Beam Fusion Systems Studies," LLNL Report UCID-20578 (1985).

9. J. H. Pendergrass, D. B. Harris, and D. J. Dudziak, Fusion Technology 13, 375 (1988).

10. "Nuclear Energy Cost Data Base: A Reference Data Base for Nuclear and Coal-Fired Powerplant Power Generation Cost Analysis," US Department of Energy Report DOE/NE-0095, September 1988.

11. J. P. Holdren et. al., "Report of the Senior Committee on Environmental, Safety and Economic Aspects of Magnetic Fusion Energy," LLNL Report URL-53766, 25 September 1989.

12. J. G. Delene, "Updated Comparisons of Economics of Fusion Reactors with Advanced Fission Reactors," 9th Topical Meeting on Technology of Fusion Energy, Oakbrook, Illinois, 7-11 October 1990.

13. R. L. Miller, "Options and Optimizations for Tokamak Reactors: ARIES," 9th Topical Meeting on Technology of Fusion Energy, Oakbrook, Illinois, 7-11 October 1990.

TABLE OF CONTENTS – CHAPTER 4

CHAPTER 4
RATIONALE FOR DESIGN OPTION SELECTION

This chapter will document the rationale for the selection of the main design options for the two IFE reactor design studies. As stated in the study objectives, the study team was empowered to seek innovative approaches that would offer increased safety, performance, and economic attractiveness. Many of these factors were quantified and trade studies were employed to make fact-based decisions. Other decisions were predicated upon the more qualitative factors that were stressed as important to the success of fusion as a future energy source.

Another factor that determined why certain key design options were selected depends upon the technology basis assumed. Naturally, state-of-the-art hardware, software, materials, and designs would be employed for systems to be built in the near time frame, but these design studies assumed not today's technology, not tomorrow's technology, but technology some 20 years or more in the future. The project was trying to be visionary as to the future of the applicable technologies. To assure the credibility of the technology extrapolation, results of promising, evolving technologies were founded upon today's experimental evidence, computer modeling, and expert opinion.

The results of the trade studies indicated a specific choice that was easy to select. Other times, the results were not so clear. This is especially true given the clarity of the looking glass into the future. When a choice was particularly difficult, the team opted to choose the more innovative option. Not only was this the charter to follow, but this choice would afford the opportunity for the technical community to examine this option in more detail and consider the merits of future development and examination.

4.1 Selection of Reactor System Technology Options

An inertial fusion power plant involves several major systems including reactor plant, driver, target plant, and balance of plant. The rationale for choosing design options for these major systems involved complicated trade-offs between many issues including economics, safety, engineering feasibility, technical risk, etc. In many instances, design choices were made without considering the impact on the overall system performance. However it was useful (and sometimes essential) to consider an overall figure of merit when selecting design options. The Inertial Confinement systems performance and COst MOdel (ICCOMO) was updated to assist the design process in such instances. This code has evolved over many years. The models were originally developed as part of the STARFIRE reactor design study[1] and were adapted to IFE as part of the HIFSA project.[2] The code contains parametric scaling and cost models for all major power plant subsystems and design options and, as such, it evolved along with the design. It includes KrF laser and heavy ion LINAC drivers, reactor cavity systems, main heat transport systems, target energetics, target manufacturing plant, fuel stream and waste processing, and all balance-of-plant systems.

A key aspect of the systems modeling involves the assessment of projected performance and cost of subsystems that, in many cases, employ technologies at vastly different stages of development. In developing the code, the cost projections were normalized to an equivalent state of engineering maturity across subsystems. This was difficult where comparable hardware does not exist today. Costs were normalized to assumptions made for recent MFE reactor and technology studies[3,4] to provide a common basis for comparison. Elsewhere, costs were based on the best judgment of experts. All cost models were normalized to first production unit costs and updated to conform with the economic guidelines discussed in Section 3. A detailed description of the final cost models is presented in Appendix C.

The study guidelines recommended that costs be developed for a tenth-of-a-kind power plant. However, technology development will not be dictated by projected tenth-of-a-kind costs but rather by those for the first production unit. The trade studies presented in this section thus include no learning curve adjustments. They consider only first production unit costs. Most results are therefore presented in the form of relative comparisons in order to avoid confusion in relating them to the tenth-of-a-kind costs discussed elsewhere in this report.

4.1.1 Laser System Option Selection - The Prometheus-L design point is an outgrowth of a number of different trade studies. These studies are summarized in Table 4.1.1-1. Many design options were evaluated within individual subsystems;

Table 4.1.1-1. Summary of Design Options Considered for KrF Laser System

Parameter	Baseline Value	Options/Range Considered
Target:		
Type	Direct Drive	Indirect Drive
Gain Curves*	Constant Spot	Optimistic, Conservative
Gain Curves	Constant Spot	Zoomed Spot
Number Beams*	60	30-90
Illumination	Tangential Focus	Nested Focus
Incident Energy (MJ)*	4	2-8
Reactor Cavity:		
Wall Protection	Wetted Wall (Lead)	Dry Wall with Fill Gas
Breeder	Li_2O	FLiBe; LiPb Eutectic
Thermal Cycle (He Coolant)	Advanced Rankine	Direct Brayton
Coolant Pressure (MPa)	1.5	1-5
Driver System:		
Laser Amplifier	Electric Discharge w/Raman Accumulator	Large Area E-Beam Pumped
Pulse Compression	Stimulated Brillouin Cell	Angular Multiplex, Hybrid
Amplifier Energy (kJ)*	5.6	3-10
Amplifier Run Time (ns)	250	200-500
Optical Fluence (J/cm^2)*	10	3-10
Final Mirror:		
Type	Grazing Incidence Metal on Ceramic Structure	Grazing Incidence Metal on Metallic Structure
Protection	Distance; Residual Gas; Deflection Magnets	Shutters; Cover Gas; Gas Prism

* The results of this trade study are presented in Section 6.2

however, some selections could not be quantified within a subsystem. The systems code was used to resolve these choices. The discussion presented in this section concerns itself only with the rationale for choosing between technology options, e.g., indirect versus direct drive targets, single versus multiple beam LINAC, etc. The trade studies directed toward selection of an operating range in parameter space for the baseline technology options are discussed in Section 6.2 as noted in the table.

Gain curves for the present study were provided by a DOE-appointed Target Working Group (TWG). The TWG endeavored to level the technical optimism between the various laser illumination concepts (direct drive constant spot - CS, direct drive zoomed spot - ZS, and indirect drive - ID) and the indirect drive heavy-ion targets. For the laser driver, they provided their results in the form of upper and lower bounds on the expected gain as a function of incident driver energy for each option. The TWG recommended an arithmetic mean of the upper bound (optimistic) and lower bound (conservative) as a baseline gain curve for system studies. Figure 4.1.1-1 compares the reference gain curves for direct and indirect drive targets using a KrF laser-driver. These gain curves formed the basis for target design options. The position of the ignition cliff ~2 MJ determines the minimum driver size, and the slope of the curves determines the attractiveness of going to higher driver energy to improve ηG.

Driver performance characteristics are also an important factor in the trade studies. The Prometheus-L driver design is based on the use of non-linear optics (NLO) to improve beam quality and system reliability. Detailed analyses and rationale supporting the design are presented in Section 4.2. A brief overview of the design is presented here to illustrate how it is represented in the systems code.

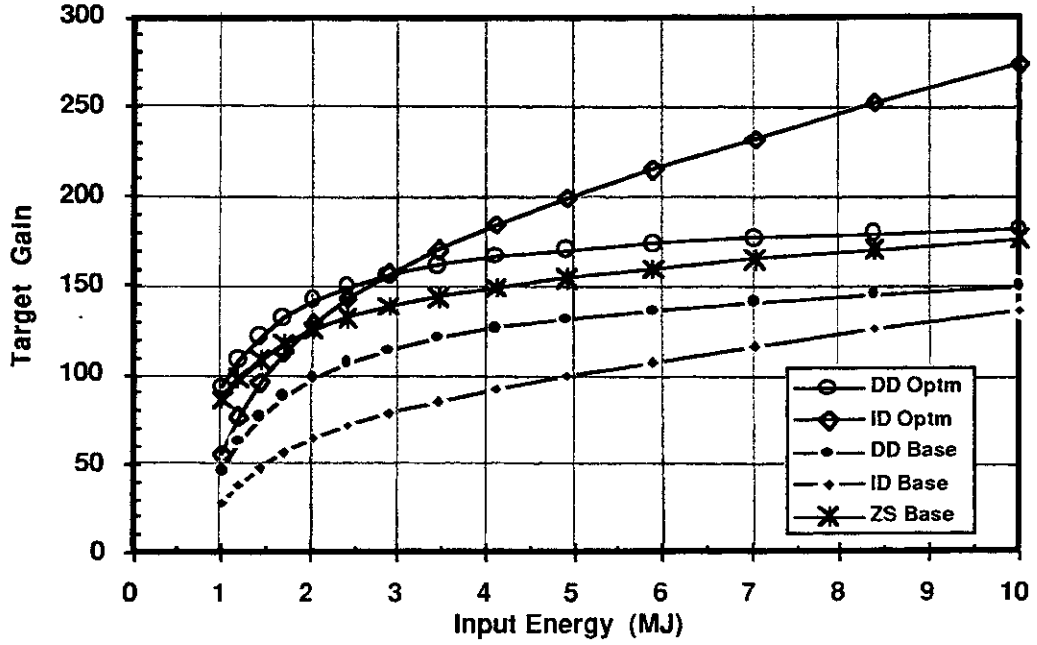

Figure 4.1.1-1. Comparison of Baseline and Optimistic Gain Curves for Direct and Indirect Drive Targets. Direct Drive Curves Assume Constant Focal Spot

The general driver architecture for one of the 60 beamlines is illustrated schematically in Figure 4.1.1-2. It consists of crossed Raman accumulators optically pumped by sixteen 5.9 kJ discharge lasers arrayed four to a side. A Stokes seed is generated for the Raman extraction by splitting off ~1% of the energy from each discharge laser and passing it through a spatially filtered Raman oscillator. The beams are then combined to form a spatially smooth seed that is spectrally and temporally matched to the pumps for maximum extraction efficiency. In addition, the crossed beam geometry serves to smooth out intensity fluctuations across the Raman output aperture. The low quality beams from the discharge lasers are thereby combined to form 60 high brightness beams with very uniform spatial intensity. This permits the downstream optics to operate at higher optical fluence levels (~10 J/cm^2) because local intensity peaking effects are minimal. Simulation studies of such cells by TRW indicate that more than 90% of the discharge laser energy can be Raman converted to the output Stokes beam as discussed in Section 4.2.

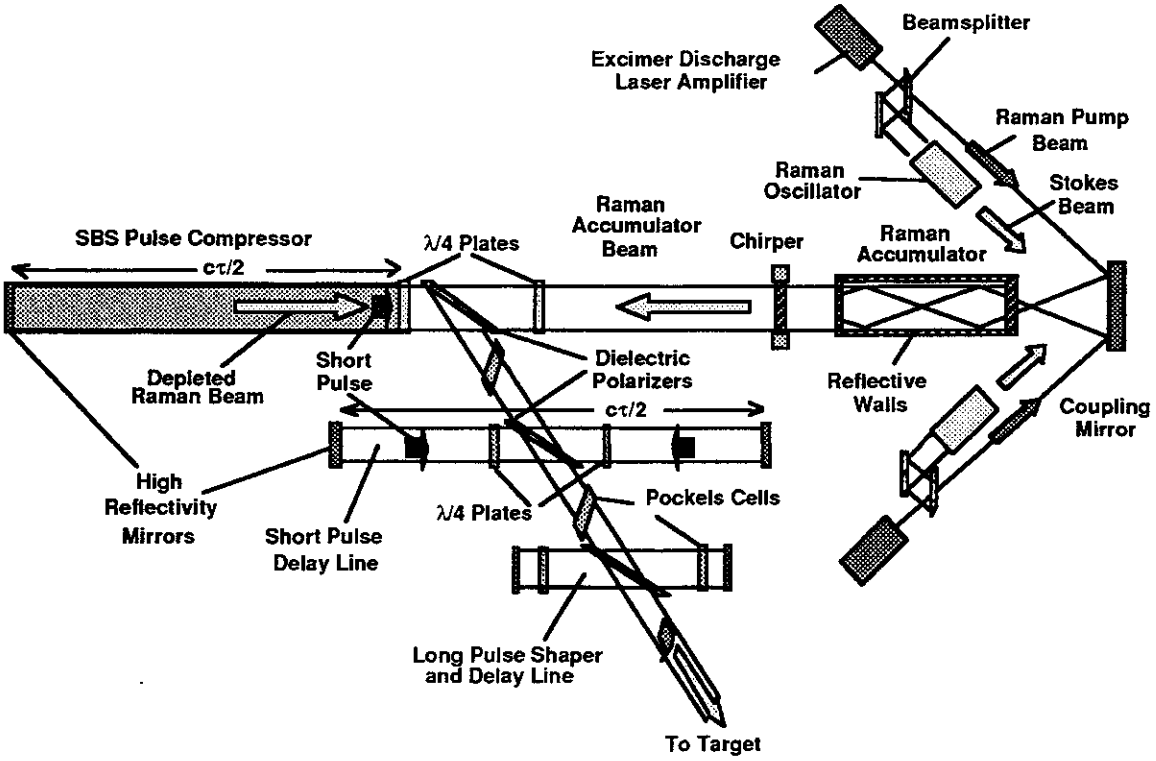

Figure 4.1.1-2. Laser System Architecture for Prometheus-L Driver Design

The output from each Raman accumulator then passes through a precisely timed, electro-optical "chirper" which frequency shifts the first ~10 ns of the beam. The beam continues on into a Stimulated Brillouin Scattering (SBS) cell of length cτ/2. The frequency shift of the "chirped" leading edge is designed to match the SBS shift in the SF_6 gain medium that fills the SBS cell. This enables the leading edge to extract energy from the remainder of the beam as it reflects off the end mirrors and travels back through the optically-pumped medium producing a short duration, high intensity

main pulse appropriate for target implosion. Although the quantum efficiency of this SBS extraction is very high (>99%), the energy tends to be concentrated in a sub-nanosecond pulse at the front of the chirped portion unless care is taken to ramp the amount of power that is chirped. This reduces the efficiency of the SBS extraction to ~65%, as discussed in Section 4.2. However, the unconverted energy is not lost, it still resides in the trailing portion of the pulse.

An optical delay line is provided to interchange the leading edge of the pulse with a portion of the trailing edge. This allows the undepleted SBS pump beam energy to be used as the target prepulse. This is accomplished using a large-aperture Pockels cell to vary the polarization of the leading and trailing portions of the pulse. A dielectric polarizer thus reflects the high intensity leading edge into the delay line but passes the undepleted pulse so that it now becomes a prepulse. The length of the delay line, $c\tau/2$, is chosen to match the prepulse duration requirements, τ = 80 ns. The portion of the undepleted pump extending beyond the 80 ns delay is lost, but this contains < 10% of the total energy. An efficiency of 90% is achieved for the combined SBS/delay line system. It should be noted that the resulting prepulse may have the wrong shape for preparing a proper target atmosphere for the main pulse. Additional pulse shaping may be required. One possible approach utilizes three, large aperture fast Pockels cells in an electro-optical switchyard as indicated in Figure 4.1.1-2. This possibility is discussed further in Section 4.2. Such Pockels cells require significant engineering advances over currently available technology due to the short (~10 ns) repetitive switching times.

The systems code represents the Prometheus-L driver in terms of simple scaling relations for component efficiencies and costs. These relationships are summarized in Table 4.1.1-2, and they lead to a projected overall efficiency of ~6.5% for the laser driver system. To help offset this low efficiency, the excimer discharge laser gas waste heat is recovered and used for feedwater heating. This leads to an effective efficiency of ~8.5% for the laser system.

A significant number of high-quality, large size optics are required for the Prometheus-L system. These optics require good surface figure control, low absorption, anti-reflective and high-reflectivity dielectric coatings at ~250 nm. The optics are sized based on the relations indicated in Table 4.1.1-2. Costs for these components are determined using the algorithms summarized in Table 4.1.1-3. These costs are based on estimates which LLNL developed for the LMF facility.[5] Table 4.1.1-4 summarizes the size and quantity of high power optical components for the 4 MJ Prometheus-L design point to illustrate typical optics requirements for the NLO laser architecture. Optics larger than 1 m linear dimension are segmented to reduce their cost. This should have little effect on performance because a minimum coherent aperture of ~0.5 m is maintained.

Table 4.1.1-2. Laser System Scaling Summary

Item	Effcy/Pwr Rqmt	Sizing Relationship	Cost Relationship (M$)
Front End Systems	Not specifically		
MO and Encoders	accounted for		2.0
Discharge Front End			0.2 N_{DL} E_{DL} / G_{DL}
Discharge Pre-Amps			0.02 C_{DL}
Discharge Lasers	95%*	l = 2 m	
Cavities	15%	w, h based on 3 J/cm^2	0.02 N_{DL} (E_{DL} / 4)$^{0.75}$
E-Beams			0.02 N_{DL} (E_{DL} / 4)$^{0.75}$
Guide Magnets		3 per group, N_{BL} groups	0.209 N_{BL}
Raman Accumulator	96%**	l = 5 m	
Cells	90%	w, h Based on 5 GW/cm	0.01 N_{BL}
Stokes Front End		limit on (intensity *x* length)	0.1 N_{BL}
Stimulated Brillouin	96%**	l = $c\tau$/2	
Cells	90%	10 J/cm^2	0.03 N_{BL}
Chirper System			0.01 N_{BL}
Downstream Optics	95%	10 J/cm^2	
Pulsed Power System	64.3%***	2 m Ceramic PF Lines	
Pulsed Power	Scaled based on		0.005 N_{DL} (E_{DL} / η_{DL})
Discharge Pre-Amps	utilization factor		0.02 C_{DL}
Gas Flow System	1.5 MW	One loop with	
Discharge Gas Flow	Scaled based on	intermediate heat	5.31 N_{BL} (P_G / 18 N_{BL})$^{0.75}$
Discharge Pre-Amps	rep rate, clearing	exchanger for each	0.02 C_{DL}
Gas Purification	stack of 4 cavities	beamline	15.0
Alignmt/Control System			2.84 + 0.194 N_{BL}
Diagnostic System			8.52 (N_{DL} / 960)$^{0.75}$
Pockels Cell Control		4 per beamline	0.02 N_{BL} 4
Power Conditioning			0.084 P_D exp(-0.0005 P_D)
Driver Building		Annulus around reactor	\$88 / m^3
Optics Components			See Tables 4.1.1-3 & 4

* Discharge intrinsic efficiency of 15% and gas pumping effectiveness of 95% are assumed.
** Input and output window transmission efficiency of 98% is assumed.
*** Product of: 94% high voltage, 92% energy storage, 90% pulse forming and $\tau / (\tau + 0.64\ \tau_{rise})$.

Table 4.1.1-3. Optics Cost Basis for Prometheus-L Trade Studies

Component	Type	Blank Cost (\$/cm^3)	Finishing Cost (\$/cm^2)	Coating Cost (\$/cm^2)	Thickness (cm)
Flat Mirror	1	0.13	0.50	0.60	d/16
Spherical Mirror	2	0.13	0.50	0.60	d/16
Window	3	0.60	1.00	0.04	d/16
Lens	4	0.60	1.00	0.04	d/8
Beam Splitter	5	0.60	1.00	0.62	d/8
Thick Window	6	0.60	1.00	0.04	d/10
Thick Lens	7	0.60	1.00	0.04	d/10
Grazing Incidence Mirror	8	540	0.25	0	10, 20% dense
Low Quality Mirror	9	0.13	0.25	0.30	d/16

Blank Size: $w = w_o + 4$ $h = h_o + 4$
Finishing/Coating Area: $A = w\,x\,h$ $d = (w^2 + h^2)^{1/2}$
Mount/Stand Cost: 30% of Blank Cost

Table 4.1.1-4. Prometheus-L Design Point Optical Component and Cost Summary

Component	Quantity	Type	Size (w x h, cm)	Cost (M$)
Discharge Amplifier Windows	920 x 2	3	44 x 44	16.07
Discharge Output Turning Mirrors	960	2	90 x 90	18.54
Raman Accumulator Stokes Mirrors	60	2	18 x 18	0.04
Raman Accumulator Input Windows	36 x 60	3	45 x 45	18.92
Pump Beam Secondary Mirrors	40 x 60	9	90 x 49	14.06
Raman Output Windows	4 x 60	6	90 x 90	19.18
Stimulated Brillouin Polarizer Plates	8 x 60	3	41 x 45	3.79
Brillouin 1/4 Wave Plates	4 x 60	3	45 x 45	2.10
Brillouin Chirper Crystals	4 x 60	3	45 x 45	3.00
Brillouin Cell Mirrors	4 x 60	1	45 x 45	0.96
Delay Line Pockels Cells	4 x 60	3	90 x 90	12.82
Delay Line Polarizer Plates	2 x 8 x 60	3	41 x 45	7.57
Delay Line 1/4 Wave Plates	2 x 4 x 60	3	45 x 45	4.21
Delay Line Turning Mirrors	4 x 60	1	90 x 90	4.64
Relay Turning Mirrors	2 x 60	1	97 x 69	0.93
Vacuum Interface Windows	60	3	97 x 69	2.52
Turning/Pinhole Focusing Mirrors	60	1	97 x 69	0.93
Pinhole Collimating Mirrors	60	2	97 x 69	0.93
Target Focusing Mirrors	60	2	97 x 69	0.93
Grazing Incidence Mirrors	60	8	395 x 69	3.60

Baseline Direct Drive Versus Indirect Drive - The resulting comparison between direct and indirect drive targets for the baseline gain curves is illustrated in Figure 4.1.1-3. This figure highlights the strong preference for direct drive predicted by the baseline gain curves supplied by the TWG. The minimum cost of electricity is ~10% higher for indirect drive and the requisite driver energy increases from 4 to 6 MJ. The driver is thus more complex (2160 discharge lasers as compared to 960 for the direct drive case) and costly (~$250M). This is a direct result of the ηG penalty for the baseline indirect-drive gain curve. For the projected Prometheus-L driver efficiency of 6.5%, the 4 MJ direct drive system has an ηG of 8.2 compared to only 7.0 for the 6 MJ indirect drive case. Illumination symmetry requirements complicate the reactor cavity design for direct drive; however, the analyses discussed in the remainder of this section led to the conclusion that for 60 beams, the cost implications of direct drive illumination are not significant. This was further reinforced by TWG guidance that indirect drive illumination, while not symmetric, would also require roughly 60 beams arrayed on two 60° half-angle cones. Direct drive targets were thus selected for the Prometheus-L system design.

Optimistic Direct Drive Versus Indirect Drive - Figure 4.1.1-4 shows how the direct to indirect drive comparison changes for the optimistic gain curves indicated in Figure 4.1.1-1. As expected, the direct drive advantage is significantly reduced for this case, but it is still favored over indirect drive. The driver costs are virtually

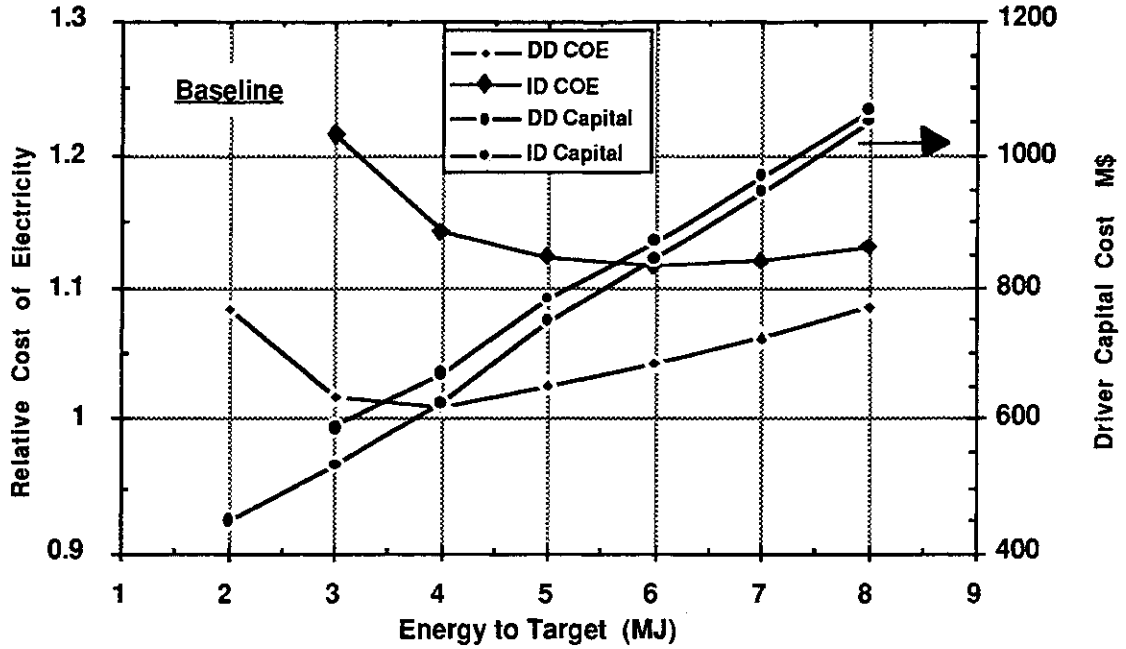

Figure 4.1.1-3. System Performance Comparison for Direct (Solid) and Indirect (Dashed) Drive Targets with Baseline Gain Curves

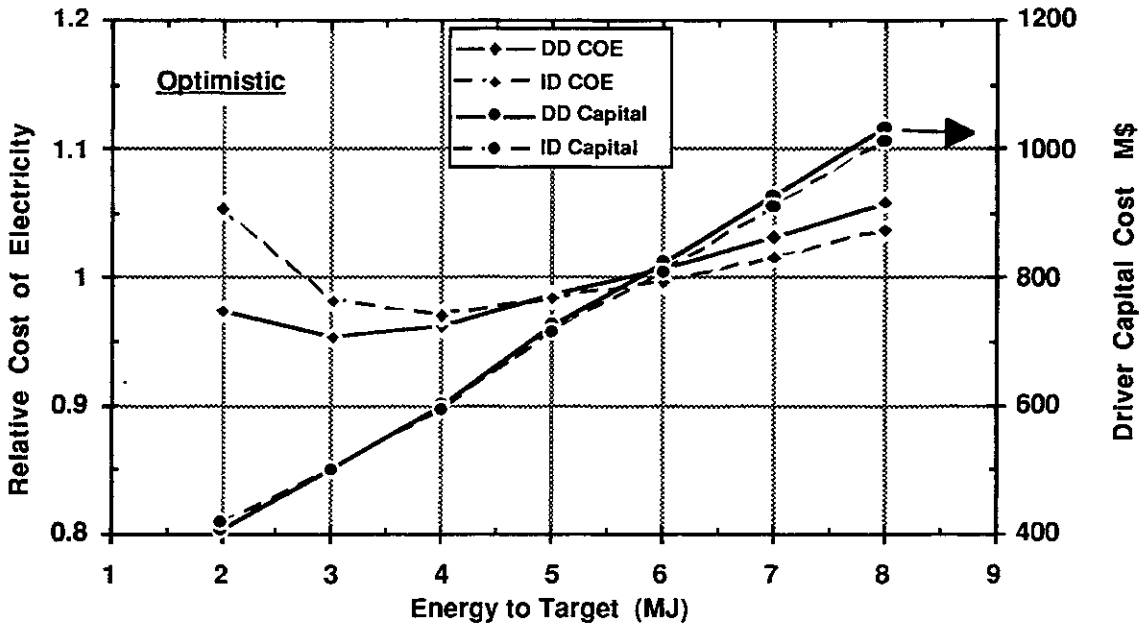

Figure 4.1.1-4. System Performance Comparison for Direct (Solid) and Indirect (Dashed) Drive Targets with Optimistic Gain Curves

identical, but the higher direct-drive gain at low energies leads to a cost advantage for this system. In fact, the minimum indirect drive system cost occurs at 4 MJ even though gain increases significantly beyond that energy. This highlights an important point relative to target design, namely that higher gain is not always beneficial once sufficient ηG has been achieved. The benefit of increasing drive energy depends on the tradeoff between gain curve slope and incremental driver cost. Figure 4.1.1-1 shows that the projected Prometheus-L incremental cost of ~$100/Joule does not favor higher driver energies even if gain scaling is comparable to optimistic expectations.

Constant Spot Versus Zoomed Spot - The final laser design option trade study involves incorporating the capability to zoom the beam focal spot to follow the implosion of the critical energy absorption surface at the target. This leads to higher gain, as indicated in Figure 4.1.1-1, because less energy is wasted in heating the atmosphere around the target, however it complicates the driver design. In order to assess the attractiveness of this possibility, a trade study was conducted with the most optimistic assumption being no added driver cost for zooming. The result of this study is shown in Figure 4.1.1-5. It shows that a zoomed focal spot potentially leads to ~3% lower COE. For the Prometheus NLO laser architecture, the only viable way to zoom the focus involves modifying the rf-driven frequency chirpers for the SBS cells to enable them to introduce a time-varying wavefront curvature. This requires an annular rf field variation around the chirper that significantly complicates its design. The benefit of focal spot zooming was not sufficient to warrant this added complexity. It

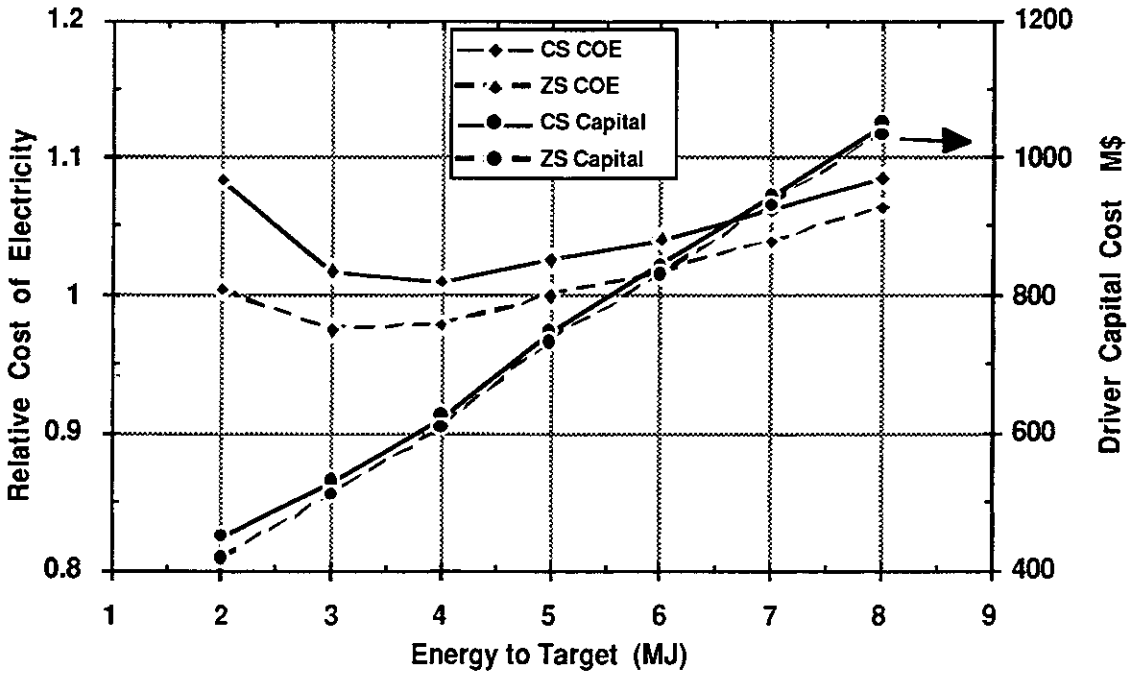

Figure 4.1.1-5. System Performance Comparison for Constant (Solid) and Zoomed (Dashed) Spot Gain Curves

should be noted, however, that the NLO laser architecture provides sufficient beam quality to allow nesting trapezoidally apodized beam focal spots on the target as opposed to the baseline tangential focus option. This possibility, which is discussed in more detail in Section 4.6, may provide the benefit of focal spot zooming without the complications of adding time-varying wavefront curvature.

4.1.2 Heavy Ion System Design Option Selection - The Prometheus-H design point is also based on a number of different trade studies. These studies are summarized in Table 4.1.2-1.

Table 4.1.2-1. Summary of Design Options Considered for Heavy Ion System

Parameter	Baseline Value	Options/Range Considered
Target:		
Type	Indirect Drive	[No Direct Drive Data]
Ion Range (g/cm^2)	0.045 (4 GeV Lead)	0.025-0.2
Spot Size, Radius (mm)*	3	2-5
Illumination	Two Sided	One Sided
Incident Energy (MJ)*	7	4-9
Transport Efficiency (%)*	90	70-100
Reactor Cavity:	Wetted Wall (Lead)	Same as Laser System
Driver System:		
LINAC Type	Single Beam with Storage Rings	Multiple Beam
LINAC Scaling*	$\alpha = 0.2$; $K = -0.15$	$\alpha = (0.2 - 0.5)$; $K = (-0.2 - 0.0)$
Ion Type*	+2 Lead	+1 to +3 Lead
Ion Energy (GeV)*	4	4-8
Focusing Quads	Superconducting	Normal
Cavity Transport	Self-formed Channel	Ballistic; Pre-formed Channel

* The results of this trade study are presented in Section 6.2

The heavy-ion driver has more scaling flexibility because it produces the requisite total energy by combining several ion beamlets at a discrete kinetic energy. The choice of ion charge state and kinetic energy lead to significant differences both in the accelerator configuration and in the target performance that must both be considered in determining the optimum design point. These issues are discussed in Section 6.2.2 along with the results of sensitivity studies which were run to document the leverage of key design parameters indicated in the table on the overall system performance. The discussion presented here focuses on the rationale for choosing a single beam LINAC with intermediate storage rings versus a multiple beam LINAC. The rationale for selecting a self-formed channel for cavity transport and the resulting target focal spot size and channel energy transport efficiency is presented in Section 4.3. Finally, the rationale leading to the choice of a wall protection scheme identical to that for the laser system is presented in Section 4.4, and a discussion of target issues for the heavy ion system is presented in Section 4.6.

Multiple Beam Versus Single Beam - One of the main induction LINAC design challenges involves the space charge limit on transportable current in a periodic focusing lattice. This limit requires multiple transport channels (typically >10 beamlets)

for heavy ion fusion drivers. Past studies[2] have envisioned a multiple beamlet transport lattice consisting of a closely packed quadrupole bundle surrounded by massive induction cores for inertial fusion drivers. The Prometheus-H design considers an alternative approach consisting of a single beam transport lattice coupled with intermediate storage rings to accumulate the required number of beamlets. The approaches are illustrated schematically in Figure 4.1.2-1. This figure highlights the key potential advantages of the single beam system, namely that the accelerator hardware that surrounds the beam(s) (i.e., induction cores, insulator rings, structure and the focusing magnets themselves) are smaller, less complex, and consequently less costly for the single beam system. This simplification, however, is accomplished at the expense of system efficiency which is lower for the single beam approach. The induction cores must be cycled many times (once for each beamlet) to produce each main pulse as compared to one cycle for each main pulse in the multiple beam case. The systems code was used to quantify this tradeoff.

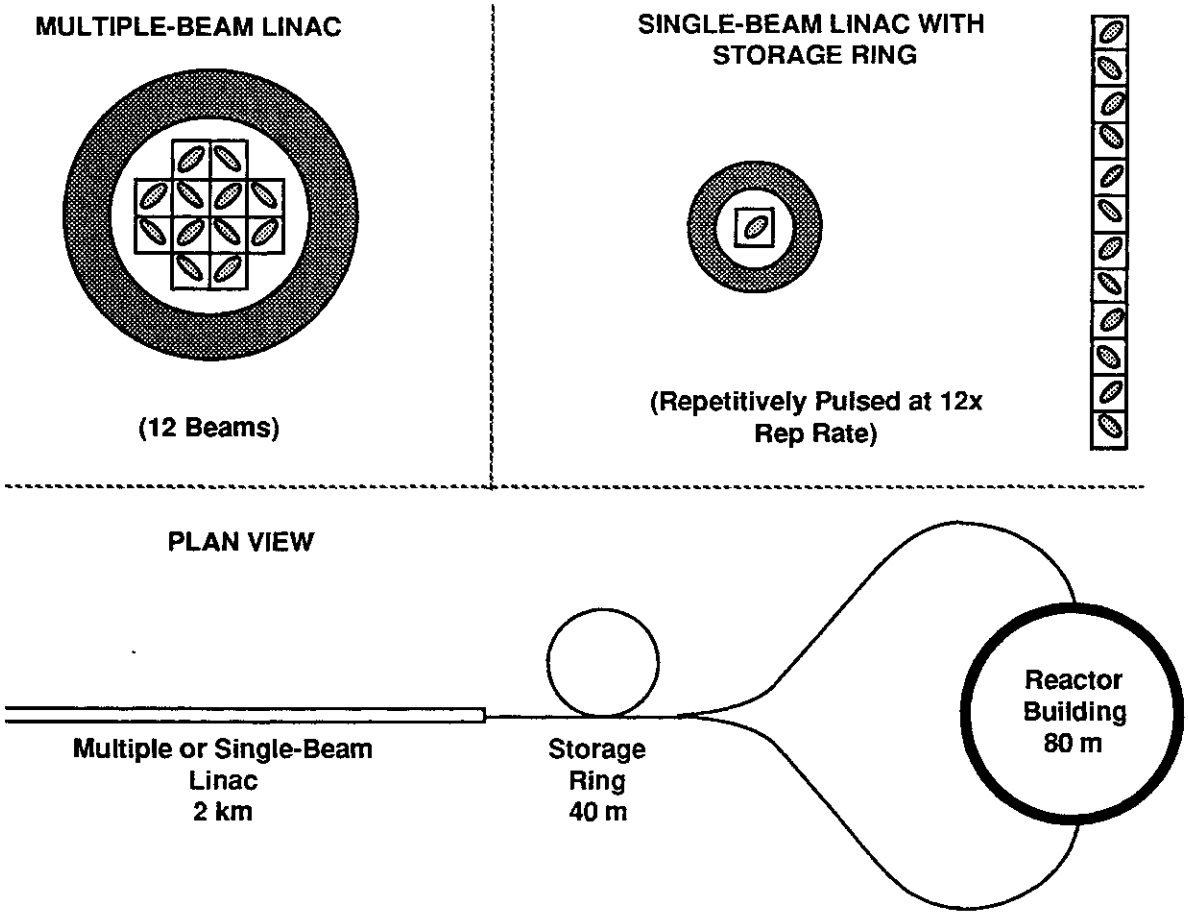

Figure 4.1.2-1. Comparison of Multiple and Single Beam LINAC Configuration

The systems code modeling is based on the general relations summarized in Table 4.1.2-2. The LINAC is sized assuming a maximum accelerating gradient of 1 MV/m. Focusing magnet quantities are determined using continuous limit focal lattice scaling laws developed by Maschke[6]. These scaling relations are summarized in Section 6.2. Injector costs (ion source plus acceleration up to 3 MV) are assumed to be $10M per injector for a single beam system. Multiple beam systems are assumed to require four such injectors. Insulator and accelerator structure costs are calculated based on the final column voltage, V_F, and inner core radius, R_{Ci}, from estimates LBL developed for a 0.83 m radius multiple-beam LINAC.

Table 4.1.2-2. Heavy-Ion System Scaling Summary

Item	Effcy/Pwr Rqmt	Qty/Sizing Relationship	Cost Relationship (K$)
Injector	3 MeV	1 SB; 4 MB	10,000 per injector
Linear Accelerator		Length based on 1 MV/m	
Insulator		Radius scaled with R_{Ci}	10 V_F (R_{Ci} / 0.83)
Structure		from 0.83 m reference	8.76 V_F (R_{Ci} / 0.83)
Induction Core	V_{Core} (J/m^3) N_{Bmlet}	Scaled with G, τ, ΔB, R_{Ci}	32 V_{Core}; $5 / kg
Focusing Magnets		Based on lattice scaling	(55 + 10 N_W + 5 L_M) N_M f_{LC}
Cryogenic System	1000 W_{Cold}	W_{Cold} = N_M (3 W/mag)	4 W_{Cold}
Vacuum System		Scaled with length	5.08 L_{Acc}
Storage Rings		1 per beamlet*	
Magnets		Based on lattice/bending	(55 + 10 N_W + 5 L_M) N_M f_{LC}
Cryogenic System	1000 W_{Cold}	W_{Cold} = N_M (3 W/mag)	4 W_{Cold}
Vacuum System		Scaled with length	5.08 L_{SR}
Final Transport		Main beamlets + prepulse**	
Buncher	2 MB LINACs	Based on bunching rqmts	Same as main LINAC
Drift Section		2 sides, 180 m long	
Magnets		Based on lattice scaling	(55 + 10 N_W + 5 L_M) N_M f_{LC}
Cryogenic System	1000 W_{Cold}	W_{Cold} = N_M (3 W/mag)	4 W_{Cold}
Vacuum System		Scaled with length	5.08 L_{FT}
Pulsed Power	60%***	Core loss + Beam energy	10 / kJ****
Instrument & Control			0.05 C_{Tot}
Auxiliary Systems			0.02 C_{Tot}
Beamline Tunnel		W_{Tun} = 5.0 R_{Co}	$120 / ft^2
PFN Building		0.5 W_{Tun}	$50 / ft^2

* Each main pulse beamlet has its own storage ring, prepulse beamlets are grouped in two rings
** Main pulse beamlets are bundled into one buncher, two prepulse beams in the other
*** Product of 70.6% for high voltage and energy storage and 85% for pulse shaping
**** Pulsed power costs are increased by a factor of 10 for the single beam system

Induction cores are sized based on R_{Ci} and the product of acceleration gradient, G, and pulse length, τ, at each point along the LINAC. The core radius is chosen so that it clears the outer radius of the quadrupole bundle as depicted in Figure 4.1.2-1. Core losses in J/m^3 are determined using the loss curve shown in Figure 4.1.2-2. The figure

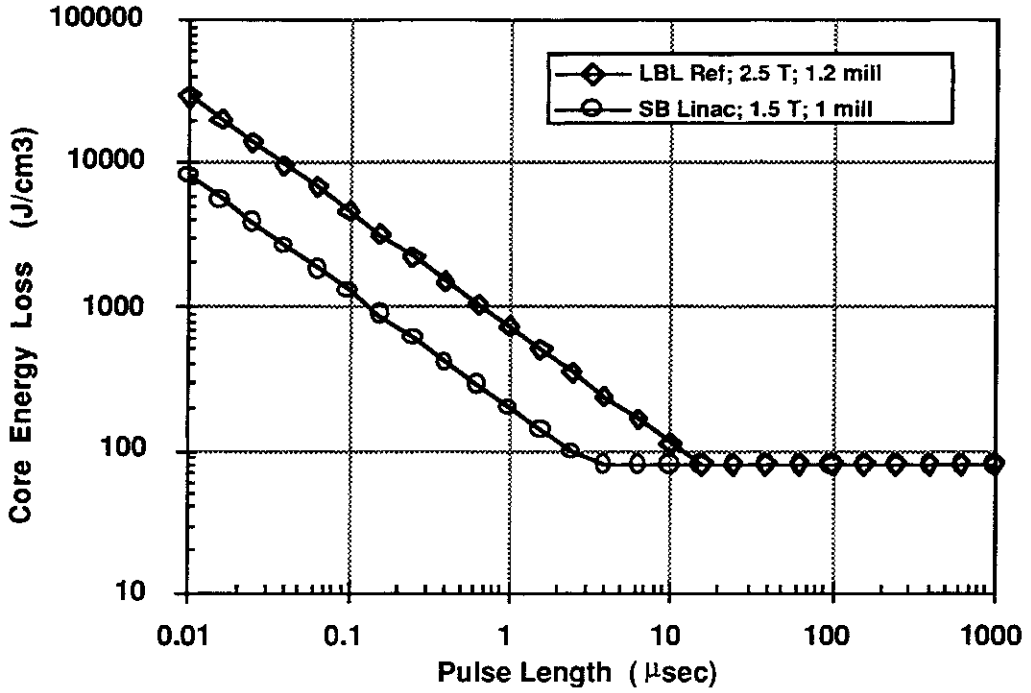

Figure 4.1.2-2. Assumed Metglas Loss Scaling with Pulse Length for LINAC System Studies

depicts the measured losses for a flux swing $\Delta B = 2.5$ T and a winding thickness $t = 1.2$ mills. These are scaled to the lower curve using the relation

$$\text{Core Losses} = \text{Core Losses}_o \left(\frac{\Delta B}{\Delta B_o}\right)^{1.8} \left(\frac{t}{t_o}\right)^2$$

for the flux swing of 1.5 T and winding thickness of 1 mill assumed here. For the single beam system, core losses are multiplied by the number of beamlets, N_{Bmlet}, to account for recycling. Core costs are estimated using \$5 per kilogram of Metglas. An 80% packing fraction is assumed in calculating the core volume. Pulsed power requirements are determined based on the sum of the core losses and the energy gained by the beam. Costs for pulsed power are estimated at \$10 per joule for the multiple beam system and \$100 per joule for the single beam case. These costs are based on information provided by LBL for the multiple beam system[7] and LLNL for the rapidly cycled (10's of kHz) single beam system. The factor of 10 increase recommended for the single beam case is based on recent LLNL work on recirculating LINAC systems.[8]

Magnet costs are based on data for similar quadrupoles for the Superconducting Super-Collider. This indicates that each cryostat will cost \$55,000 with an additional \$10,000 for each quadrupole winding plus \$5000 per meter of length. These costs are adjusted using an 85% learning curve factor, f_{LC}, to determine the magnet costs for the "first production" driver considered here. Cryogenic system costs are based on the

total number of magnets per section, including quadrupoles and dipoles, N_M, with a heat leak of 3 watts per magnet. A cost of $4000 per cold watt, W_{Cold}, is assumed with a power consumption of 1 kW per cold watt. Vacuum system costs are estimated at $5100 per meter of length for each section and tunnel costs at $120 per square foot. The tunnel width is taken to be five times the maximum core outer radius R_{Co}. Finally, I&C and auxiliary systems are assumed to be 5% and 2% respectively of the total cost.

The resulting comparison between projected system performance for the multiple and single beam LINAC drivers is illustrated in Figure 4.1.2-3. This comparison uses lattice scaling suggested by Ed Lee[9], since it was thought to be most favorable for multiple beam systems. The final single beam design uses an alternative lattice scaling discussed in Section 6.2 and therefore has lower capital cost than those presented here. Nevertheless, this figure still highlights the significant advantage projected for the single-beam approach in spite of its lower efficiency (15% as compared to 37%). Driver capital costs for the single beam system are roughly half those for the multiple beam system and this leads to a 12% reduction in COE. The single beam system was therefore selected for the baseline driver in the Prometheus-H design study.

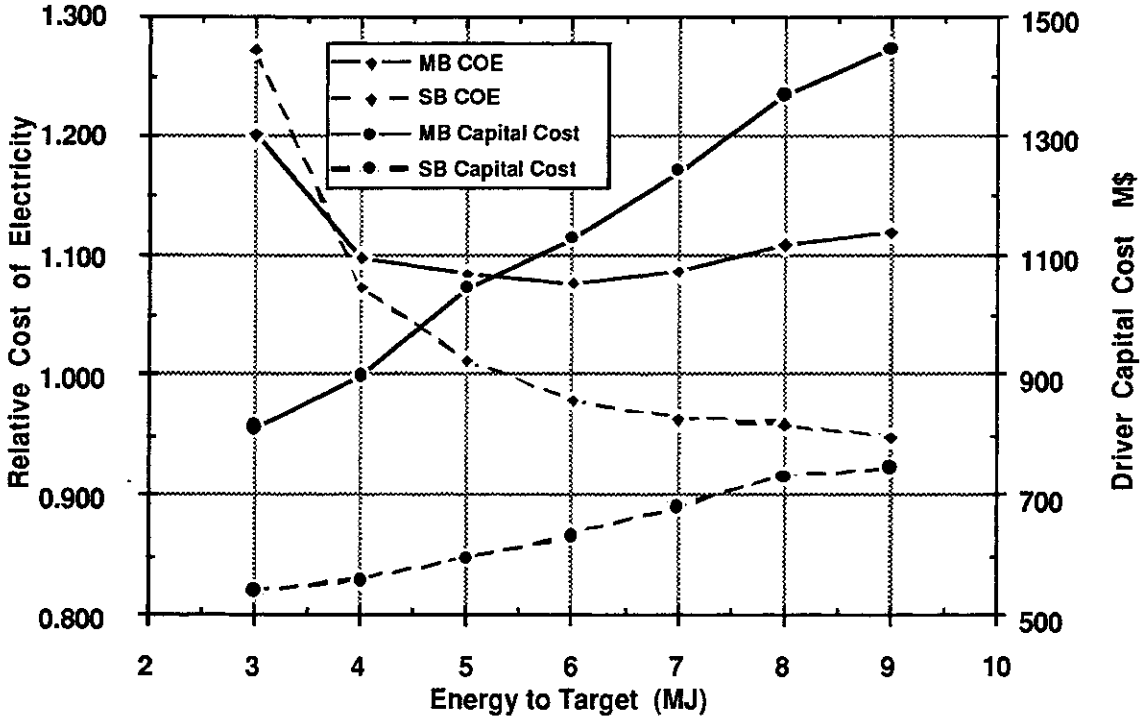

Figure 4.1.2-3. Comparison of Projected COE and Driver Capital Cost for Multiple and Single Beam LINACs. Systems are all 4 GeV, +2 Lead with 3 mm Radius Focal Spot.

It should be noted, however, that the multiple-beam system remains a viable driver option. Its COE is comparable to that for the KrF laser system, and the alternative transport lattice scaling discussed in Section 6.2 leads to significantly lower MB capital costs than those presented here. In addition, it avoids technical issues associated with beam stability and particle loss in the storage rings. These are critical R&D concerns for the single beam approach and they are highlighted in Section 5.

In spite of these concerns the Prometheus-H design point represents a tantalizing development goal. The single beam configuration dramatically lowers the driver cost and technology development challenge while still providing sufficient ηG for an attractive overall system. Furthermore, the 4 GeV ion energy is more attractive to target designers due to its reduced range. Significant issues need to be resolved concerning the storage rings but the starting point is much more appealing than any previously envisioned for induction LINAC drivers.

References for 4.1

1. C. C. Baker, M. A. Abdou, et al., "STARFIRE - A Commercial Tokamak Fusion Power Plant Study," ANL/FPP-80-1, September 1980.

2. D. S. Zuckerman, et al., "Induction LINAC Driven Heavy Ion Fusion System Model," Fusion Technology, Vol. 13, #2, 1986.

3. R. L. Miller, "Options and Optimizations for Tokamak Reactors: ARIES, " 9th Topical Meeting on Technology of Fusion Energy (Oakbrook, Illinois, 7-11 October 1990)

4. Ronald L. Miller, Robert A. Krakowski, David A. Ehst, ARIES System Study Results (Draft), 15 February 1991.

5. D.B. Harris, et al., KrF Laser Driven Laboratory Microfusion Facility Conceptual Design Report," LANL Report LA-UR-91-2915, December 17, 1991.

6. Mr. Alfred Maschke, TRW, Personal Communication, 1991.

7. Unpublished cost analyses performed for LBL HI LMF conceptual design, c.f. Ref 9.

8. J.J. Barnard, et. al., "Study of Recirculating Induction Accelerators as Drivers for Heavy Ion Fusion," LLNL Report UCRL-LR-108095, September 21, 1991

9. Edward P. Lee, et.al., "Heavy Ion Driven LMF Design Concept," LBL Report LBL-31-248, August 1991.

4.2 KrF Laser Driver Options

As described in Section 2.4, the KrF laser was selected as one of the most promising inertial fusion energy (IFE) laser drivers for three principal reasons:

(1) The KrF laser operates at a favorable ultraviolet (UV) wavelength (λ_{KrF} = 248 nm) for inverse Bremsstrahlung coupling to the DT target.
(2) The KrF laser is relatively efficient (ξ = 0.12) for generating UV pulses.
(3) KrF laser amplifiers can be scaled to produce significant UV pulses. (Experimental prototypes have produced as much as 20 kJ.)

There are also some significant drawbacks to the KrF lasers that have been constructed to date. These include:

(1) The KrF laser is a non-storage active medium which, when pumped electrically, means that the duration of the laser pulse is approximately equal to the length of the electrical excitation pulse.
(2) The presently developed type of electrical pulsed power for the KrF is electron-beam excitation which has an optimum pumping pulse duration >600 ns.
(3) E-beam excited excimer lasers have not been demonstrated as being sufficiently reliable to reach the ICF reactor goal of ~10^9 firings between amplifier failures.

Similar comments may be made about the ArF excimer laser (λ = 193 nm) with the additional comments that ArF may be slightly more efficient than KrF owing to a lack of dimer or Kr_2F absorption losses in ArF lasers; but the shorter wavelength coupled with less experimental data on ArF performance in large amplifiers would require additional research to be performed on ArF excimer lasers before recommendations could be made to replace KrF. These two excimer laser media are sufficiently similar that systems originally optimized for KrF may be adapted to use ArF as an alternative gain medium, assuming, of course, that the optical systems were modified to deal with the shorter wavelength (as well as the concomitant hazards of mirror damage, linear absorption, multi-photon absorption, color-center formation, etc.).

It is a given[1] for laser-driven implosion of IFE targets that the laser driver must have a pulse duration, τ_{pulse} ~ 6 ns, an output energy, E_{pulse} 4 to 6 MJ, at a wavelength, λ_{laser} ~ 250 nm, in order to achieve the target irradiation conditions appropriate for efficient implosion of the DT fuel. As is evident from the preceding discussion, the present largest KrF laser prototypes produce pulses of excessive[2] pulse length (~100x) and inadequate[3,4,5] energy (~10%) for a 25-beam (200 kJ/beam) ICF laser driver.[6,7,8] Thus, a future KrF laser driver[9,10] suitable for IFE reactor operation will need to produce efficient shorter UV laser pulses at higher energies.

Another problem common to all large aperture, high energy lasers is the large aperture optics problem. Optical elements (particularly UV optical elements) become very expensive for elements larger than ~50 cm. On the basis of the volumetric cost of the optics alone, scaled optics of aperture, d, have costs proportional to d^3. Typically, the manufacture of larger optics exhibit a lower yield than smaller optics so that, in fact, the costs for large optics scale, with exponents ranging from 3.5 to 7 depending upon yield, grinding and polishing hazards, coating problems, etc. If a large optic of aperture D is synthesized by n^2 subapertures of diameter d (where n = D/d), then the costs of the synthesized optic would be proportional to D^2. Since UV optical damage thresholds tend to limit the maximum laser fluence, Φ_{laser}, tolerable to values ~5 J/cm^2, in order to generate laser pulses of 5 MJ, effective apertures having collective areas of ~10^6 cm^2 for the laser will be required. The costs associated with procuring this large optical surface area can be minimized if the required apertures (and corresponding optical component areas) are synthesized from smaller, cost and performance-optimized optical elements.

After reviewing the KrF laser amplifier literature2-10 and performing our own optimization analyses, we have found that potentially more reliable and efficient excimer laser amplifiers having apertures of ~30x30 cm may be feasible9,10. Accordingly, the fundament of our IFE design for the KrF laser driver is that the most efficient, reliable, cost-effective excimer laser amplifier produces a laser beam of reduced energy (E_{laser} ~ 4 kJ) using an electric discharge excimer laser (EDEL) excitation scheme9,10 which, even with an optimized electrical excitation pulse shape, has a duration too long (EDEL ~ 250 ns) to be useful as a laser driver in IFE target implosions. As a consequence, in order to exploit the high efficiency and cost effectiveness of optimized EDEL amplifiers,9,10 it was necessary to develop: (1) a laser beam combination system to synthesize higher energy laser beams than can be achieved efficiently in a single laser amplifier, and (2) a pulse compression system to shorten the optimum EDEL pulse to the required duration.

There are two general types of optical beam combinations and pulse compressions which have been studied[10-13] during the past decade: linear (use of linear optics, such as lenses and mirrors, to effect parallel beam combination; use of a mirror-based geometry referred to as "angular multiplexing" for temporal pulse compression) and non-linear (Raman beam combination, non-linear optical pulse compression) laser beam configurations.

Linear laser beam manipulation techniques[7,8,9] utilize, by definition, linear optical elements (such as lenses, mirrors, beam-splitters, etc.) to accomplish the objectives of beam combination and pulse compression using long pulse excimer laser light as input. Although typically large numbers of optics and generous amounts of real estate are required, this approach may have advantages since it is fundamentally simple and the spectral bandwidths of potentially wide-bandwidth excimer laser beams are

generally unaffected by linear beam manipulation processes. A major disadvantage of linear beam manipulation techniques is that their optical complexities are approximately proportional to the number of beams to be accumulated or the pulse compression factor.

Non-linear laser beam manipulation[10-18] employs advances in innovative non-linear optical (NLO) processes to accomplish the objectives of beam combination and pulse compression using stimulated quantum mechanics techniques. These NLO processes promise to achieve not only the general objectives of laser beam combination and pulse compression with much simpler optical configurations, but also to smooth excimer laser spatial intensity distributions and improve the accumulated laser beam quality. Given the significant advances demonstrated in the laboratory during the last decade, all of these advantages may be achieved while reducing both cost and risk. Lastly, NLO processes are able to accommodate significant changes in the number of laser beams to be accumulated, or in the pulse compression factor, without substantial changes in configuration or design. Both linear and NLO laser beam manipulation techniques will be described in additional detail in the discussions below.

4.2.1 Linear Optical Manipulation Techniques - In order to allow the KrF laser amplifiers to meet the fundamental fusion target irradiation requirements, two major goals must be achieved: (1) beam combination, and (2) pulse compression. Beam combination is necessary in order to permit the addition of a large number of optimized laser beams to achieve the required laser energy per beam line. This permits the optimization of the output energies of individual excimer laser modules (discussed below in Section 4.2.2) while meeting the requirements for achieving a specific laser energy delivered per individual laser beamline. Thus, for example, if the Prometheus design would require a 6 MJ laser driver delivering the 6 MJ of energy in 60 beam lines, each laser beam line requires laser pulses of approximately 81 kJ each. If, however, the optimization of the excimer laser amplifiers produces a design which is capable of producing only 5kJ/amplifier, then it will be necessary to combine at least 20 such excimer laser beams in order to reach the required energy level of 81 kJ for each beamline.

In an analogous manner, pulse compression can be achieved using linear optics by synthesizing a long pulse of duration, $N\tau$, from a series of N shorter pulses, each of duration τ, and propagating at unique angles, θ_k, to the system axis.[2-8]. In this connection, linear pulse compression techniques (i. e., angular multiplexing) are increasingly difficult to utilize as N increases. Thus, since the optimum pumping pulse duration of the EDEL[9,10] is approximately half that of the EBEL,[2] the angular multiplexing system for the EDEL would have less than half the number of beam lines as the corresponding system for the EBEL. Each of these linear beam combination techniques is briefly described below.

Use of linear optical elements, including lenses, mirrors, beamsplitters, optical delay lines, and adaptive optics, permit the spatial and temporal manipulation of high power laser beams. By linear optical elements, it is understood that these optical elements function substantially in the same manner for laser beams of low intensity as well as laser beams at high intensity.

4.2.1.1 Linear Beam Combination - Linear beam combination is a process which involves directing the output beams of individual laser amplifiers using appropriate mirrors and beamsplitters to accomplish the following objectives:

(1) Accumulate the requisite energy in a series of nxn parallel-propagating beams which, when summed, form an array whose beam diameter is sufficiently large to avoid optical damage to the mirrors and windows in the optical train.

(2) Be timed such that the net path delays among all of the beamlets are significantly less than 1 ns. (This techique may involve phase-matching the individual beamlines using linear adaptive optics techniques.)

(3) Be directed within an alignment angle of the order of the diffraction-limited divergence of the array elements themselves.

The advantage of this type of linear beam combination is that it does not adversely affect the spectral bandwidth of the excimer laser light. The major disadvantage is that the optical system suitable for combining the laser beams tends to be relatively large and unwieldy; difficulties also arise with regard to beam fill factors and near field (Fresnel) diffraction effects from the "egg-crate" multiple mirror mounts unless image relaying is employed.

4.2.1.2 Angular Multiplexing - Linear pulse compression has some of the same characteristics as linear beam accumulation, except that each beamline is injected through the laser amplifiers at a different angle of incidence. This leads to a significantly more complicated optical design, as discussed below.

Previous IFE KrF driver designs[3-8] have featured an optical technique known as angular multiplexing to accomplish the important task of reducing the optimum pulse length for excimer laser amplifiers, $\tau_{excimer}$ ~ 250 ns, by approximately a factor of 45 to meet the target illumination requirement of τ_{pulse} ~ 6 ns. Although this technique is attractive for relatively small compression ratios (<20), complexities arise when compression ratios of >40 are needed. As discussed in Section 6.5.1.2, optimized electric discharge excimer laser (EDEL) amplifiers[9,10] produce pulse durations of ~250 ns, whereas optimized e-beam excited excimer laser (EBEL) amplifiers[2] generate pulses of ~600 ns. In the latter case, angular multiplexing would need to generate a pulse compression ratio of ~100 in order to meet the requisite compressed

pulse duration. A schematic of the angular multiplexing pulse compression concept is shown in Figure 4.2.1-1.

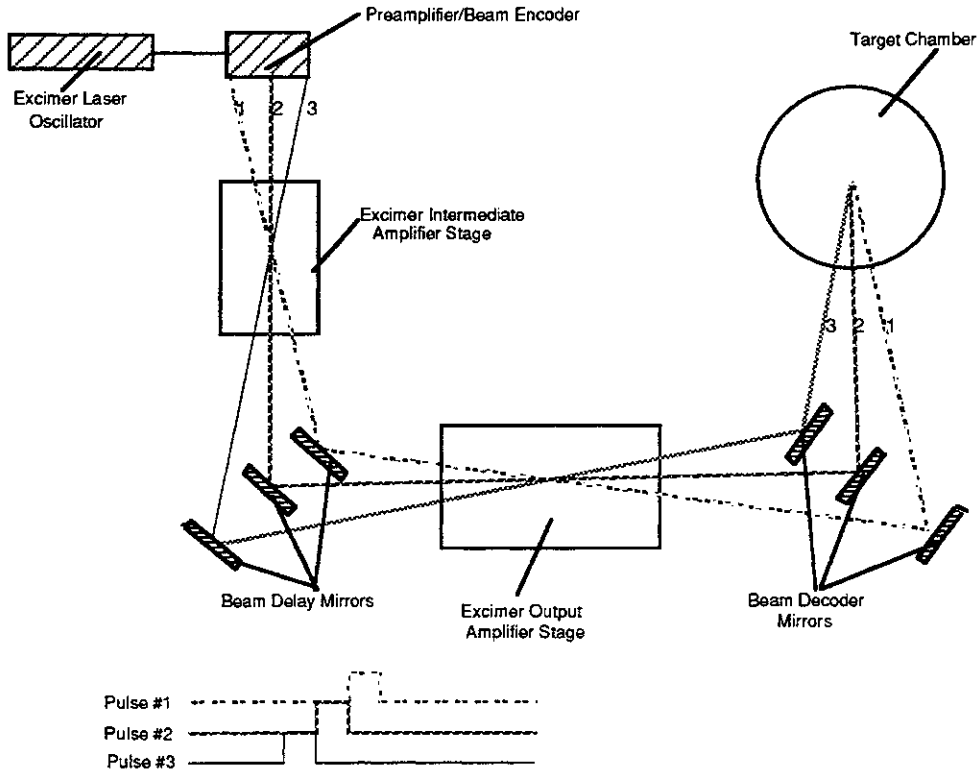

Figure 4.2.1-1 Angular Multiplexing is Accomplished by Synthesizing a Long Laser Pulse from a Series of Suitably Delayed Shorter Laser Pulses Each Propagating at a Specific Angle With Respect to the Optical Axis of the System

Figure 4.2.1-1 illustrates the angular multiplexing concept when a pulse compression of three is desired. As previously discussed, the number of angular-encoded sub-beams required in an angular multiplexer is equal to the pulse compression ratio. Thus, when a pulse compression factor of 100 is required, 100 separate, angular-encoded beam lines (each propagating at a unique angle relative to the system axis) are needed for the angular multiplexing system. Even with careful design, angular multiplexing for large compression factors may result in an unwieldy optical configuration; for small interbeam angles, cross-talk problems between adjacent channels can occur; and unextracted excimer laser volumes can result since beam vignetting occurs. This design does, however, permit broad-bandwidth excimer laser pulses to be compressed while retaining the large bandwidths, a property useful for minimizing adjacent beam interference effects on the target and reducing stimulated scattering processes in plasma atmospheres ablated from targets.

4.2.2 Non-Linear Optical Beam Manipulation Processes - Both of our Prometheus studies and numerous publications[10-17] have shown that two different types of non-linear optical (NLO) systems can be used to accomplish the tasks of

beam combination and pulse compression with both relatively high efficiency (>50%) and flexiblity. Whereas for the linear beam manipulation techniques, there is a proportional penalty for the degree to which (i. e., n beams) beam accumulation is necessary or the fractional pulse compression ratio (i. e., 1/n), for the NLO approaches, it is generally an easier task to accommodate increases (or decreases) in the number of beams to be accumulated or pulse-compressed. Thus if n beams are to be accumulated, the linear optical approach requires n parallel optical systems; whereas the NLO accumulator simply combines n excimer pump beams into a single output beam. Similarly, if the desired pulse compression ratio is n, then the angular multiplexing pulse compressor requires n separate beam lines, each at a separate angle, whereas the NLO compressor performs the pulse compression in a single beam line folded back upon itself.

Each of these systems is briefly described below.

4.2.2.1 NLO Laser Beam Combination - This section will summarize the Prometheus architecture of the non-linear optical beam combination system based on forward rotational Raman scattering.[10,15] As previously discussed, beam combination gives the laser designer the important option to optimize the performance of the excimer laser amplifiers independently of the overall IFE reactor system requirements to deliver a specific amount of laser energy in each beamline to the target. Thus, were it not for the concept of coherent beam combination, it would be necessary to deliver some 81 kJ in each beamline to the target. For coherent beam combination, this might mean, for example, that the 81 kJ of energy would have to be delivered from a single excimer laser amplifier; a feat which has not yet been demonstrated.[5,9] Moreover, the single point failure of any one of these 60 large excimer laser amplifiers would cause the misfiring of the fusion target on that (and presumably successive) shots, thereby forcing the shutdown of the IFE reactor.

During the study, the design architecture for the Raman accumulator system has evolved from earlier considerations of extremely large e-beam pumped excimer lasers (producing 50 to 100 kJ each) to the present conservative (~4 kJ) pump excimer laser amplifier–forward rotational Raman accumulator system. These Raman accumulators work well with either the 600 ns pulse durations of the EBELs or the ~ 250 ns pumping pulse durations of the EDELs. The fundamental purpose of the forward rotational Raman accumulator is coherent beam combination in which a number (e. g., 4x4 = 16) of excimer laser beams of modest energy (~6 kJ) and aperture (~30 cm) are combined into a high energy beam (~81 kJ) and relatively large aperture (~120 cm). In order to achieve a high quantum efficiency, ξ, it is convenient to select specific rotational Raman transitions in hydrogen (or deuterium). The Raman convertor quantum efficiency, ξ, is defined by the expression:

$$\xi = \frac{h\nu_{laser} - \Delta E_{rot}}{h\nu_{laser}} \qquad (4.2.2\text{-}1)$$

where h is Planck's constant, ν_{laser} is the frequency of the excimer laser, and ΔE_{rot} is the energy of the rotational Raman phonon. In order to achieve the highest Raman gain, the polarization state of both the excimer pump beam and the Stokes seed beam must be circular and of opposite helicities. As an example, for two such rotational transitions in room temperature hydrogen, values of $\Delta E \sim 587\ cm^{-1}$ (for S[1]–S[3]) and $354\ cm^{-1}$ (for S[0]–S[2]) have been measured. The relationship of the Stokes seed wavelength, λ_S, to the laser wavelength, λ_{laser}, is given by the simple expression:

$$\lambda_S = \frac{\lambda_{laser}}{\xi} \qquad (4.2.2\text{-}2)$$

where ξ is defined in Eq. 4.2.2-1. Since for $\lambda_{laser} \sim 248$ nm there is only a very slight wavelength difference between λ_{laser} and λ_S, it is difficult to separate the pump and Stokes seed beams spectrally. However, by injecting the Stokes seed beam at an angle θ to the excimer pump beam(s), it is possible to inject the Stokes seed beam efficiently into the Raman accumulator cell. Moreover, intensity averaging occurs under these circumstances, which can lead to an improvement[10,14,15] in Stokes beam quality compared to that of the excimer laser pump. An example of how this beam combination task might be accomplished is shown in Figure 4.2.2-1.

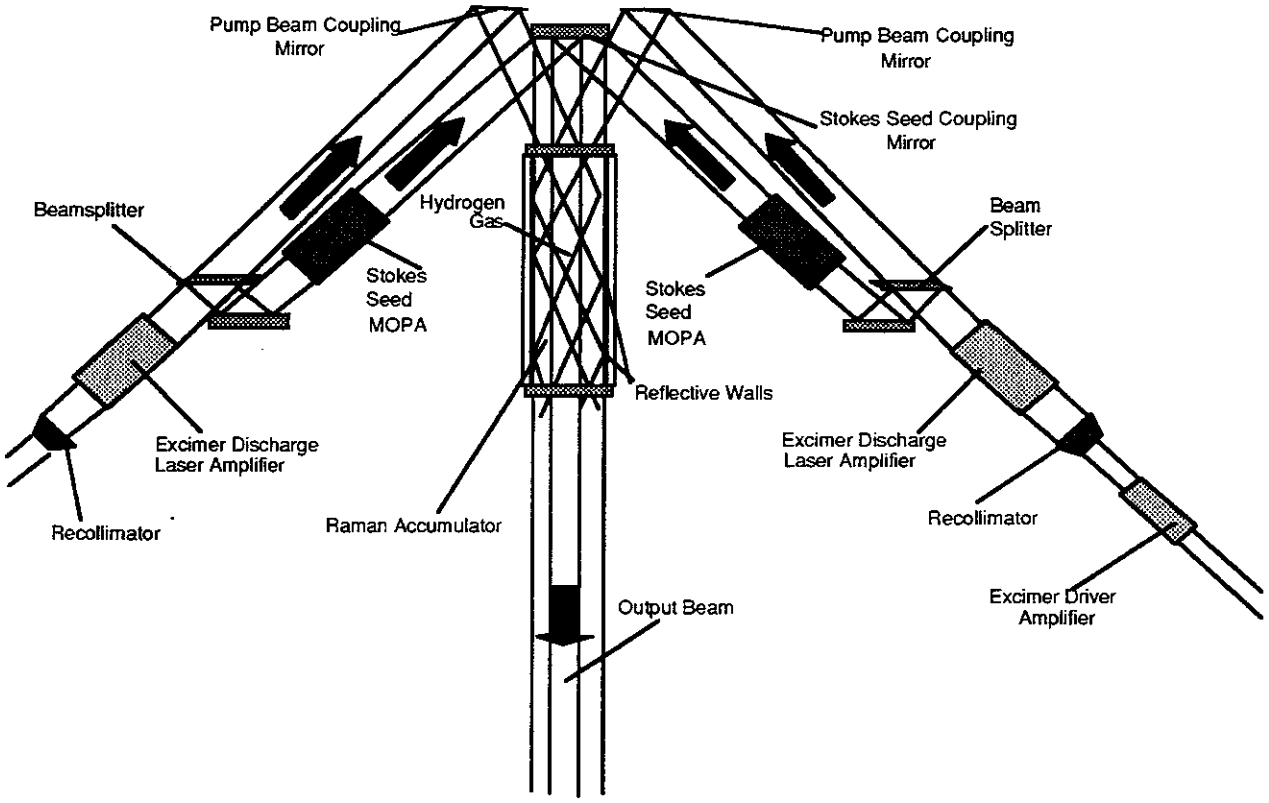

Figure 4.2.2-1 The Forward Rotational Raman Accumulator Permits 16 Separate KrF Laser Beamlets to be Combined in a Single Coherent Beam

The crossed Raman (or CRAM) configuration illustrated schematically in Figure 4.2.2-1 provides an example of a Raman seed beam derived from the original excimer pump, thereby guaranteeing that the highest Raman gain will be achieved. To achieve high gain with the bandwidth of the excimer pump greater than the Raman linewidth, this configuration requires that the optical path length of the seed generator be matched to the main excimer pump path length.[14] In this case, the optical gain, G_R, of the Raman amplifier is given by the expression:

$$G_R = \exp\left[g_R(\rho,\theta)\, I_{laser} L_{interaction}\right] \qquad (4.2.2\text{-}3)$$

where $g_R(\rho,\theta)$ is the rotational Raman gain coefficient (dependent upon the gas density, ρ, and the angle between the pump and Stokes beams, θ). An important parameter in stimulated Raman scattering is the bandwidth, $\Delta\nu_R$, of the Raman transition. An expression[15] for the Raman bandwidth, $\Delta\nu_R$, is:

$$\Delta\nu_R = \frac{K_1 \left|K_p - K_s\right|^2}{\rho} + K_2\rho \qquad (4.2.2\text{-}4)$$

where K_1 and K_2 are two constants which depend upon the Raman medium, ρ is the medium density in amagat, K_p is the pump wave vector, and K_s is the Stokes wave vector. In turn, the rotational Raman gain coefficient, g_R, is dependent[10,15] upon Raman bandwidth, $\Delta\nu_R$, the gas density, ρ, and the angle, θ, according to the expression:

$$g_R = \frac{2\lambda_s^2 \Delta N}{h\upsilon_p \pi \Delta\nu_r(\theta,\rho)} \frac{d\sigma}{d\Omega} \qquad (4.2.2\text{-}5)$$

where λ_s is the Stokes wavelength, ΔN is the density of scatterers, $h\nu_p$ is the quantum pump energy, $\Delta\nu_r(\theta,\rho)$ is the Raman linewidth, and $d\sigma/d\Omega$ is the differential cross-section for rotational Raman scattering. A plot of the dependence of g_R on ρ and θ is illustrated in Figure 4.2.2-2 for $\lambda_{laser} \sim 248$ nm, $\theta = 0°$, 5°, and 10°.

As indicated in Figure 4.2.2-2, for $\theta \sim 10°$, a significant reduction in $g_R(\theta)$ is observed for densities of $H_2 < 1.5$ amagat. As a consequence, we have considered using angles smaller than $\theta = 10°$ (i. e., $\theta = 5°$) if gas pressures above 1 atm are to be avoided. High H_2 pressures lead to the requirement for thick Raman cell windows and produce higher relative optical gains for competing vibrational Raman transitions (for $\rho > 2$ amagat).

As an illustration of the effect the Raman gain coefficient has on the predicted conversion efficiency of the accumulator, plots of the conversion efficiency vs. Raman cell length for the S(1) rotational hydrogen Raman with $\lambda_{laser} = 248$ nm, $E_{laser} = 4$ kJ, $D_{beam} = 30$ cm, $\tau_{pulse} = 600$ ns, ρ ranging from 1.0 to 2.0 amagat, and θ ranging from 5 to 10° are illustrated in Figure 4.2.2-3.

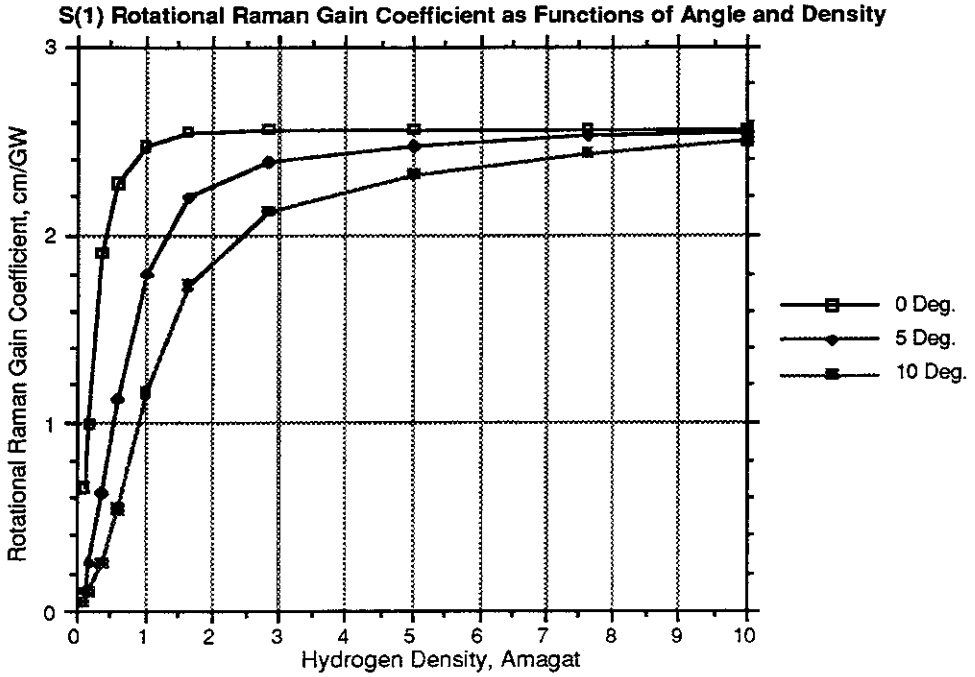

Figure 4.2.2-2 S(1) Rotational Raman Gain Coefficient as a Function of ρ for Different Values of CRAM Angle, θ

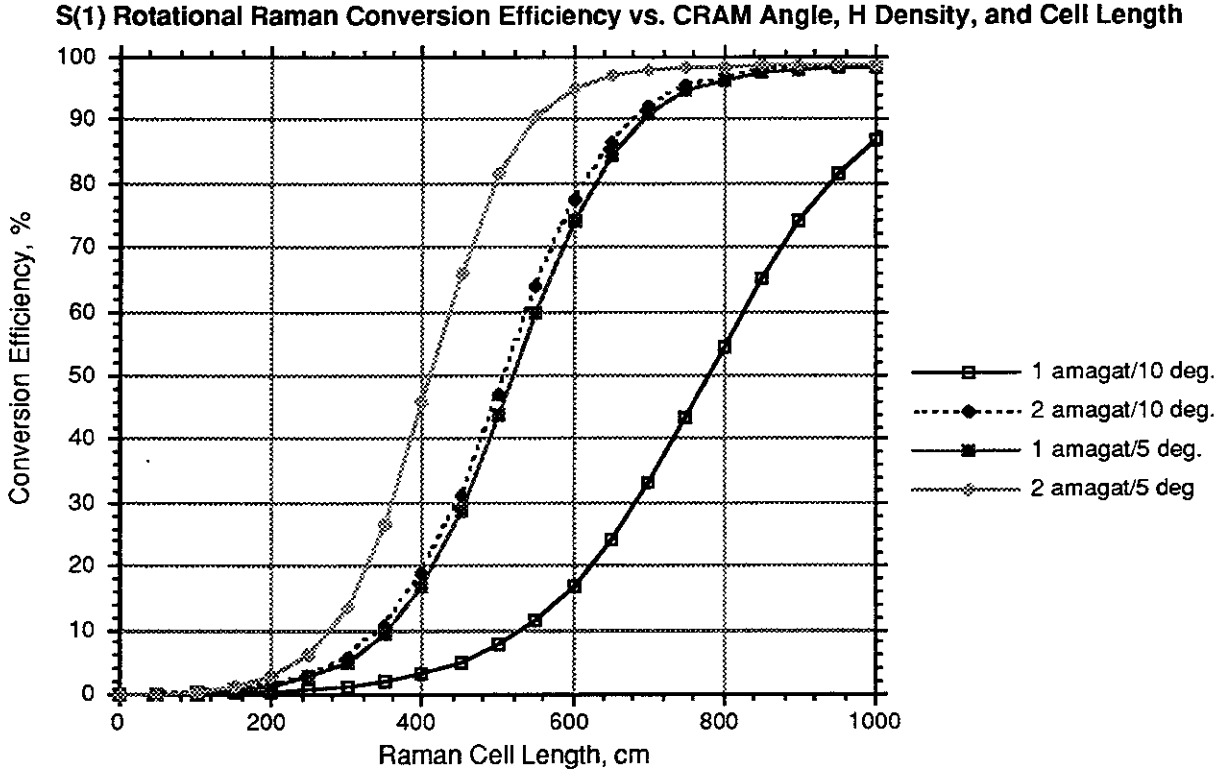

Figure 4.2.2-3. Accumulator Conversion Efficiencies as a Function of Cell Length with ΔE = 4 kJ, D_{amp} = 30 cm, τ_{pulse} = 600 ns, and λ_{laser} = 248 nm

As indicated, for $\theta = 10°$ and $\rho = 1$ amagat, 90% conversion is not achieved for $L < 1000$ cm, whereas for $\theta = 5°$ and $\rho = 2$ amagat, 90% is achieved at $L = 530$ cm. The axial ($\theta = 0$) small signal Raman gain given by Eq. 4.2.2-5 ranges from 10 nepers for $L = 500$ cm (acceptable) to 20 nepers for $L = 1000$ cm (marginal). It would be preferable if high conversion efficiencies ($\xi_R > 90\%$) can be achieved for interaction lengths, $L < 6$ m. In the present case, the fluence on the cell windows is only 4.4 J/cm^2. Higher fluences (either smaller beam diameters or higher energies) would permit efficient beam conversion in shorter distances. If higher energies can be achieved in the electric discharge excimer lasers (i. e., $\Delta E = 4.8$ kJ), then efficient conversion in the Raman accumulator cells can be achieved in a shorter distance. These results are shown in Figure 4.2.2-4.

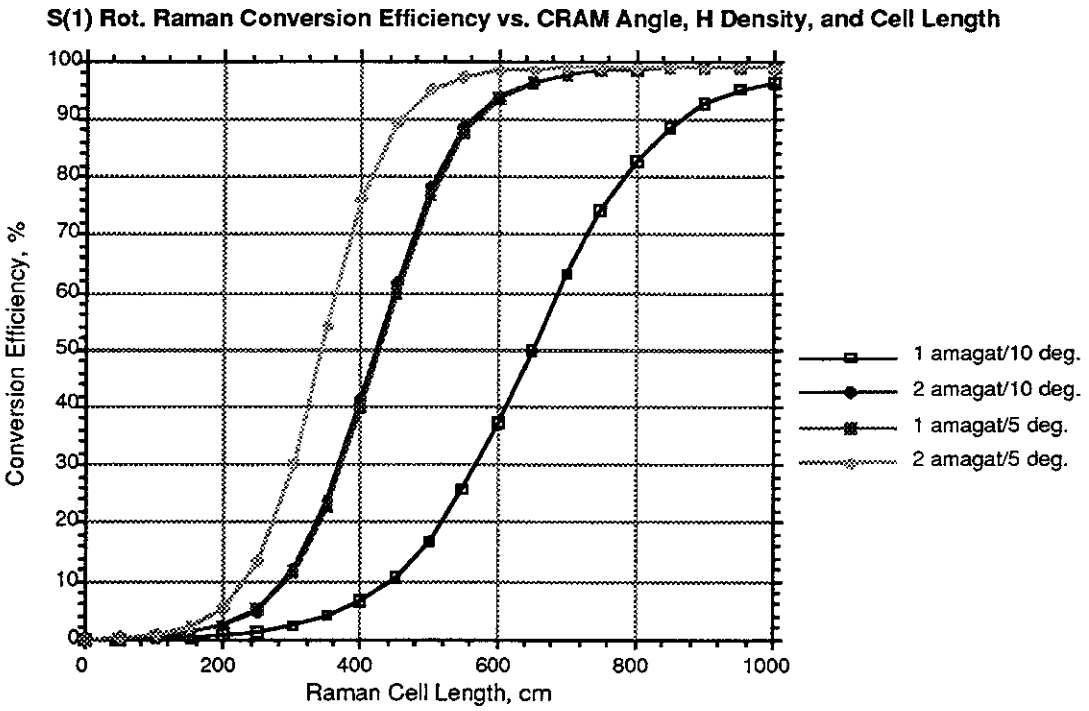

Figure 4.2.2-4 The Accumulator Conversion Efficiency Depend on the Raman Cell Length with $\Delta E = 4.8$ kJ, $D_{amp} = 30$ cm, $\tau_{pulse} = 600$ ns, and $\lambda_{laser} = 248$ nm

In this case, with a modest increase to a flux loading of 5.3 J/cm^2, a reduction in Raman cell length could be achieved. This increase in fluence could be achieved either by increasing the excimer output energy, ΔE, from 4 to 4.8 kJ, or by decreasing the amplifier aperture slightly, from 30 cm to 27.5 cm. As indicated, for $\theta = 10°$ and $\rho = 1$ amagat, 90% conversion is attained only for $L = 860$ cm, whereas for $\theta = 5°$ and $\rho = 2$ amagat, 90% is achieved at $L = 440$ cm. The axial Raman gain ($\theta = 0$) in this case for $L = 500$ would be approximately 12 nepers. These considerations apply primarily to Raman conversion of a single e-beam excimer laser (EBEL) amplifier, since EBEL laser amplifier pulse lengths are relatively long (~600ns). For electric-discharge excimer laser (EDEL) amplifiers, a shorter (~250 ns) pulse duration appears to be more optimum. These shorter duration, proportionally higher output power

pulses produce higher Raman gains. Shown in Figure 4.2.2-5 are Raman accumulator cell (RAC) conversion efficiency curves for 4x4x6 kJ EDEL pump amplifiers (~81 kJ) delivered to the RAC in a pulse duration of 250 ns. This represents the Prometheus-L laser driver design point.

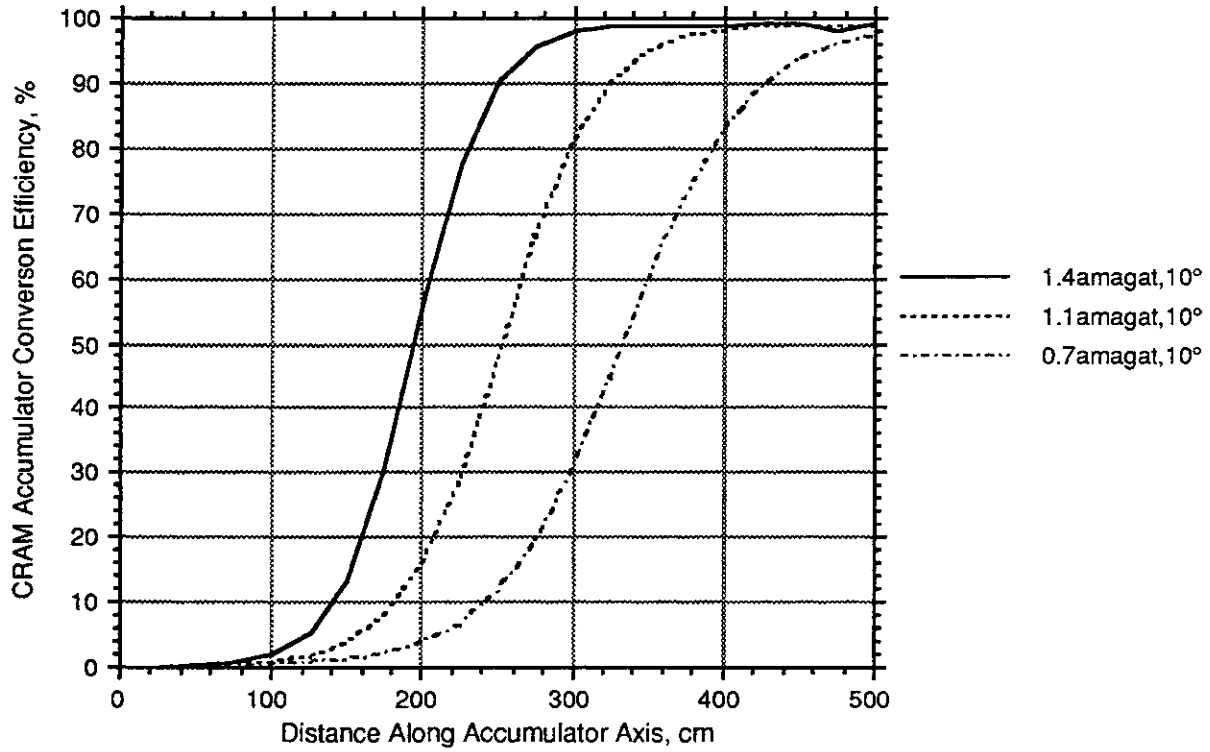

Figure 4.2.2-5. With an Input of 81 kJ in a 250 ns Pulse for λ = 248 nm in Deuterium at Sensitivities of 0.7, 1.1, and 1.4 amagat with the CRAM Angle = 10°, the Conversion Efficiency Depends Upon the RAC Length.

It is important not to exceed Raman conversion efficiencies greater than ~90% since the danger arises that some conversion to higher order Stokes lines could occur. Under controlled conditions (i.e., deliberately injecting a second Stokes seed), this could permit an increase in the effective bandwidth of the RAC laser beam since it would contain two discrete wavelengths (corresponding to the first and second Stokes order in D_2). The separation of wavelengths would depend upon whether the Raman lines selected were rotational or vibrational. If, for example, the S(2)–S(0) rotational transition in hydrogen were optimized ($\Delta E \sim 354\ cm^{-1}$), then the wavelengths of the first and second Stokes would be 250.2 and 252.4 nm (separated by 2.2 nm), assuming that the 248 nm KrF laser were used as a pump. If the S(3)–S(1) rotational transition in hydrogen were optimized ($\Delta E \sim 587\ cm^{-1}$), then the first and second Stokes would lie at 251.6 and 255.2 nm (separated by 3.6 nm). These Raman lines would represent 0.87 and 1.45% bandwidths, respectively.

In addition to the simulations of RAC performance for KrF laser pumps, a number of Raman conversion calculations were carried out assuming that ArF (λ = 193 nm) were the pump wavelength. It should be noted that, if further excimer laser research revealed that ArF were a superior excimer gain medium to KrF but that problems associated with two-photon absorption and/or color center formation in transmissive optics made operation at λ_{laser} = 193 nm unattractive, using the Q(1) vibrational transition in H_2 (corresponding to a phonon energy of 4155.2 cm^{-1}) or the Q(2) vibrational transition in D_2 (for an energy shift of 2987.2 cm^{-1}) would permit the Stokes output wavelength from the accumulators to be either λ_{Stokes} = 210 nm (for H_2) or λ_{Stokes} = 205 nm (for D_2); these longer wavelengths may prove to be an acceptable compromise between 248 and 193 nm.

4.2.2.2 Backward Raman Pulse Compression - As discussed above, as a consequence of the complexity of angular multiplexing as applied to the present problem, other pulse compression techniques were examined. Two different methods which use non-linear optical techniques were considered:

(1) Backward stimulated Raman scattering (SRS) pulse compression.[11,12]
(2) Backward stimulated Brillouin scattering (SBS) pulse compression.[10,15,17]

These non-linear pulse compressors both utilize stimulated scattering processes which are capable of using the long pulse excimer laser pump beams for efficient conversion to higher radiance Stokes beams with differing wavelengths, directionality, phase aberrations, and temporal durations. Because these non-linear optical techniques are enormously flexible, such a dual-architecture system permits a wide variety of pulse shapes, wavelengths, etc., to be achieved without requiring any significant changes in the overall system configurations.

A schematic of a backward Raman pulse compressor[11,12] is illustrated in Figure 4.2.2-6.

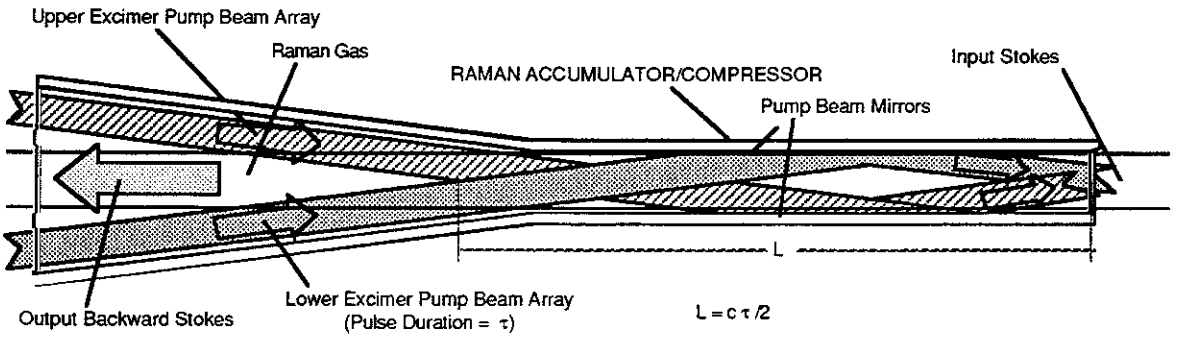

Figure 4.2.2-6 The Backward Raman Pulse Compressor Overlaps the Long Excimer Laser Pulse with a Shorter, Backward-Propagating Stokes Seed to Achieve Pulse Compression.

As indicated in Figure 4.2.2-6, a Raman cell having a length, $L_R = c\tau_{laser}/2$, has a Stokes seed of wavelength, λ_S (defined in Eq. 4.2.2-2). Although such a device can accomplish both the functions of beam accumulation and pulse compression, experiments and analyses have shown that backward Raman pulse compression typically can achieve efficient operation only for pulse compression factors of 5 or less.[11,12] Thus, in order to achieve an overall pulse compression of 100, it would be necessary to have three successive backward Raman pulse compressors. Hitherto, this has been an unattractive solution because of the reduced overall conversion efficiency.

4.2.2.3 SBS Pulse Compression - A third pulse compression technique utilizing stimulated Brillouin scattering (SBS) has been considered for performing the function of laser pulse compression. The SBS process[10,16,17] exhibits optical gain in a functional form similar to that given for SRS Eq. 4.2.2-3 as shown in Eq. 4.2.2-6:

$$G_{SBS}(\rho, \Delta\nu, t) = \exp\left(g_{sbs}[\rho, \Delta\nu]\, I_{laser}(\Delta\nu, t)\, L_{cell}\right) \qquad (4.2.2\text{-}6)$$

where the SBS gain coefficient, $g_{SBS}(\rho,\Delta\nu_{pump})$, is primarily a function of the gas density and the bandwidth of the pump laser, $\Delta\nu_{pump}$. The physics of SBS differs from that of SRS in that the scattering of incident excimer laser photons from sound waves in the SBS medium occurs, as compared with the scattering of light from molecular energy states, as the basis of the SRS process. The difference in frequency between the excimer laser, ν_{laser}, and the Stokes seed, ν_{SBS}, is simply the Doppler shift, $\Delta\nu_D$, suffered by the pump photons when scattered from the moving density waves in the Brillouin gain medium. Thus, $\Delta\nu_D = 2\nu_{laser}v/c$ where v is the sound speed in the SBS medium and c is the speed of light. As a result, the quantum efficiency for the SBS process defined in Eq. 4.2.2-6 can be very high, $\xi \sim 100\%$.

The Brillouin gain coefficient, g_B, is defined by the relation:[16]

$$g_b = \frac{k_s^2 \gamma_e^2}{nc\nu_s \rho \Gamma_B} \qquad (4.2.2\text{-}7)$$

where k_s is the wave vector of the Stokes beam, γ_e is the electrostrictive coefficient (of the SF_6 SBS gain medium), n is the refractive index, c is the speed of light, v_s is the speed of sound in the gas, ρ is the density, and Γ_B is the spontaneous Brillouin linewidth.

Building upon the work of Mak,[17] et al. in the Soviet Union, we have analyzed the case in which the leading edge of the long, 600 ns excimer laser pulse is electronically chirped in frequency by an amount equal to the SBS seed frequency, $\Delta\nu_{SBS}$, and then ramped in modulation depth to encourage the generation of pulses >1 ns duration. We then have a very flexible method of generating a variety of output compressed

pulse shapes in a single non-linear, self-seeding, pulse compressor. A schematic of the SBS pulse compression concept is shown in Figure 4.2.2-7.

It is assumed that the SBS pulse compressor has, as an input beam, a long pulse (τ_{pulse} ~ 600 ns) output beam from a Raman accumulator. This long pulse beam is shown as the first waveform in Figure 4.2.2-7. The first step in the SBS pulse compression process[17] is to "chirp" the first few nanoseconds of the leading edge of the long, τ_{laser} ~ 600 ns laser pulse originating in the Raman accumulators (described above). In Step II, this long laser pulse with the "chirped leading edge" is then directed into a gas-filled SBS cell of approximate length $L = c\tau_{laser}/2$ equipped with a 100% reflecting mirror at the far end of the cell. The purpose of this mirror is to reflect the short duration, "chirped" SBS "seed" beam back down the cell where the high, stimulated Brillouin gain can effect an efficient conversion of long pulse energy into a short pulse Stokes beam. Thus, upon reaching the 100% mirror and being retroreflected, the chirped leading edge of the excimer pulse serves as the SBS Stokes "seed" beam to extract the majority of the power in the original long pulse excimer beam in a time, $\tau_{pulse} << \tau_{laser}$. Since the characteristics of this "chirped" SBS seed are electronically determined, this method permits a wide variety of pulses to be generated. An operational diagram of how such pulse compressors could be configured is shown in Figure 4.2.2-8.

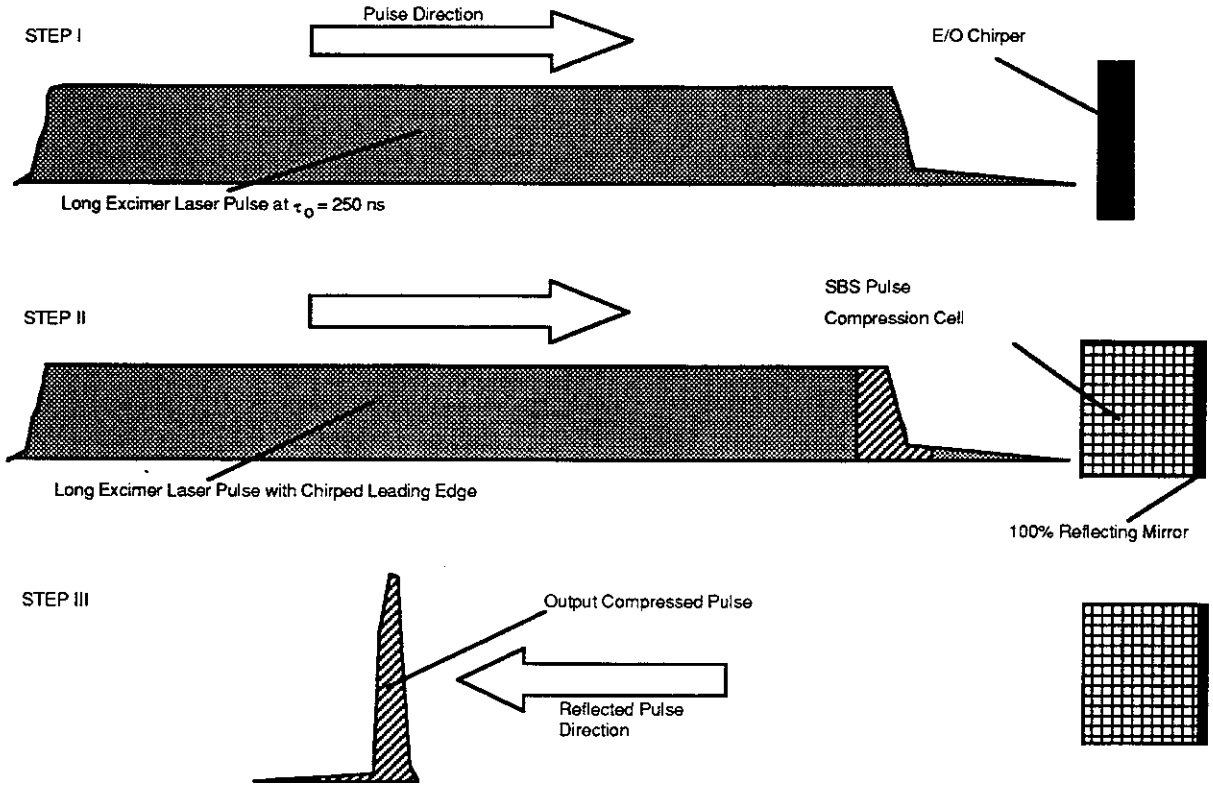

Figure 4.2.2-7 The Three Steps Associated with Pulse Compression in the SBS Pulse Compressor.

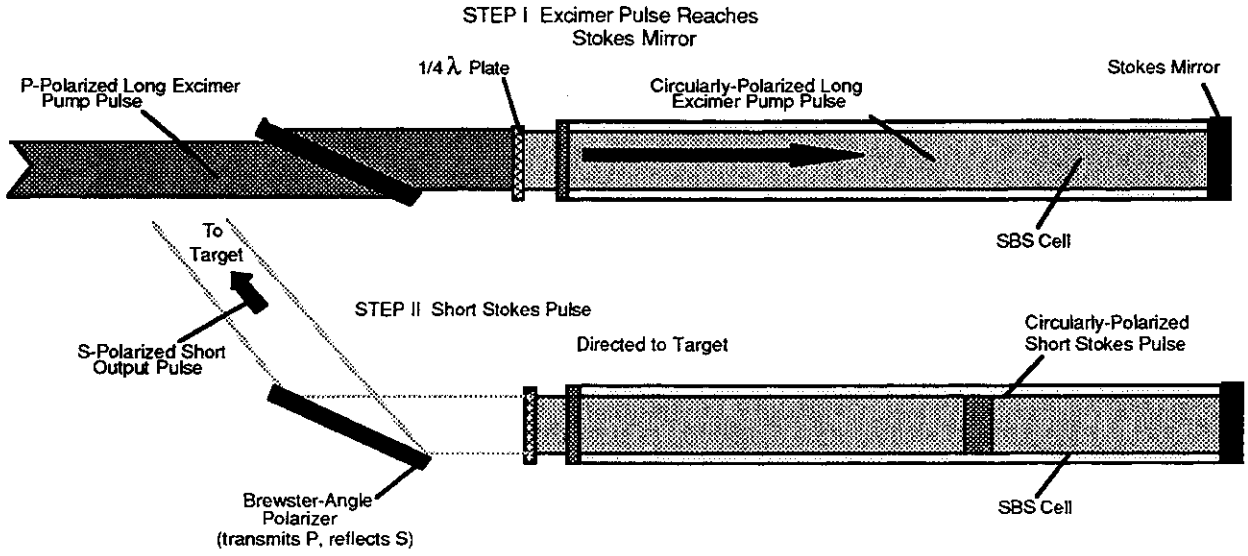

Figure 4.2.2-8 Use of SBS Pulse Compressor Cell Coupled With Polarized Input and Output Laser Beams Facilitates Integration into Reactor

As indicated in Figure 4.2.2-8, the use of linearly-polarized light, together with a large aperture, dielectric-polarizer, and a quarter-wave plate, permits the long pulse input and short pulse output beams to be readily separated with high efficiency. It is not convenient to separate the compressed pulse from the input long pulse spectrally because the SBS frequency shift is nearly negligible in comparison with the laser frequency. Similarly, it is generally not convenient to have a significant angle, θ, between the temporally long incident pump pulse and the short Stokes compressed pulse because poor spatial overlap would then occur with a concomitant reduction in conversion efficiency. A schematic of the placement of the SBS pulse compressor relative to the Raman accumulators is illustrated in the diagram shown in Figure 4.2.2-9.

One of the useful properties of these non-linear devices (i. e., the Raman accumulators and the SBS pulse compressors) is that essentially none of the excimer laser light is lost in the devices. Any laser light that is not converted can be collected and put to additonal uses, recirculated, etc. In this case (shown in Figure 4.2.2-9), any long pulse excimer laser power not converted in the Raman accumulator cells would be available for generating complex pulse shapes for target illumination.

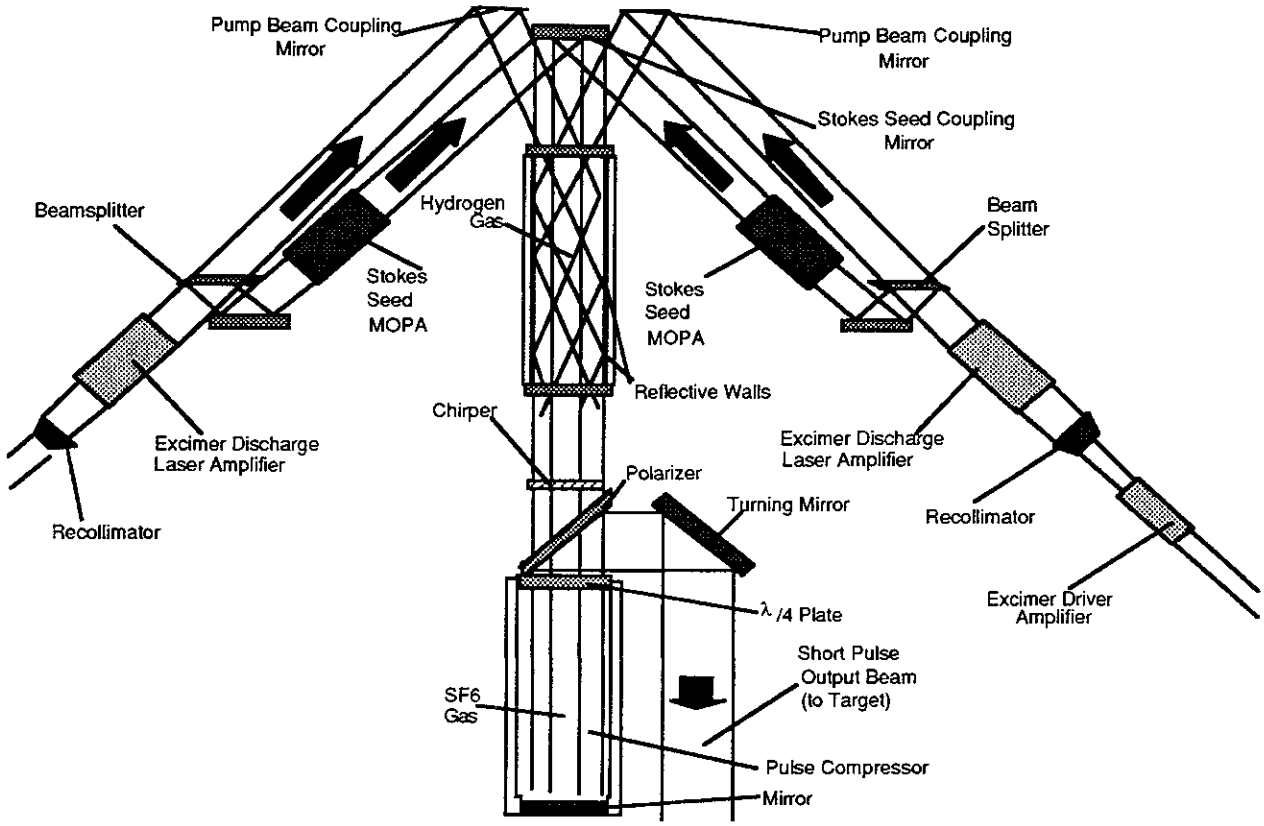

Figure 4.2.2-9 The SBS Pulse Compressor is Readily Integrated into the Reactor Driver System Following the Raman Accumulators

In order to explore the capabilities of the SBS pulse compressor for delivering a variety of output Stokes pulse shapes to meet target compression requirements, a series of calculations were carried out using a series of different temporal "chirped" SBS seed pulse shapes. Examples of the input Stokes pulse shapes used in these simulations are shown in Figure 4.2.2-10.

In Figure 4.2.2-10, the ratios indicated are the final powers in the SBS Stokes Seeds to the initial powers. Thus, a ratio of 10^4:1 indicates that the power of the Stokes seed increases by a factor of 10,000 during the course of the nominal 10 ns Stokes seed pulse duration. The variation of spontaneous SBS linewidth with SF_6 density is important to calculate.

Using experimental data[18] substituted into Eq. 4.2.2-7, the spontaneous SBS linewidth, Γ_B, is calculated as a function of the SF_6 density with the results plotted in Figure 4.2.2-11.

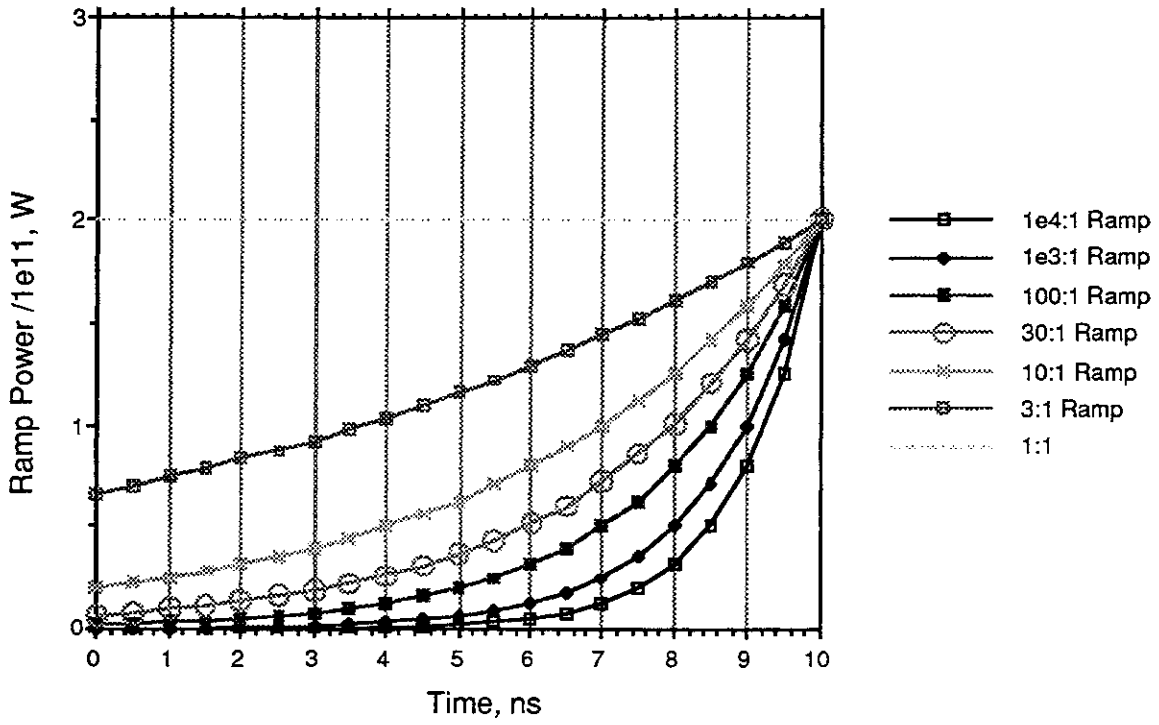

Figure 4.2.2-10 By Selecting Various Temporal Ramp Pulse Shapes for "Chirped" SBS Stokes Seeds a Variety of Compressed Pulse Shapes Can Be Generated

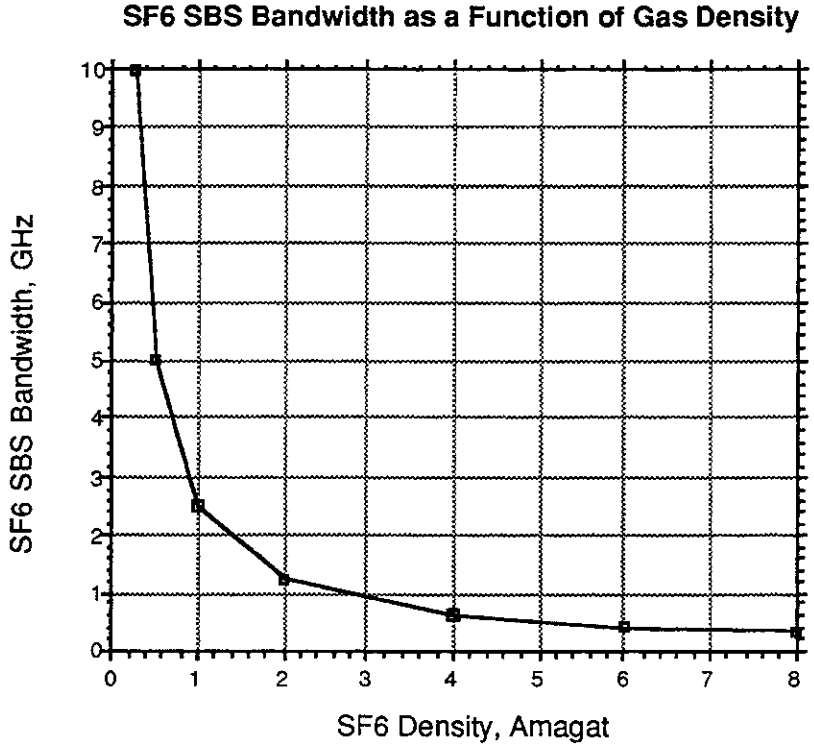

Figure 4.2.2-11 The Dependence of Spontaneous SBS Linewidth with SF_6 Density Defines Limitations on the Compressed Pulse Bandwidth

Our design point is taken near ρ = 1 amagat for SF_6 in order to trade off sufficient Brillouin gain together with adequate bandwidth (assuming an excimer/Raman pump beam bandwidth of approximately 10 GHz). From Eq. 4.2.2-7, it is evident that higher densities of SF_6 lead to increased SBS gain but over a narrower bandwidth.

Simulations of the SBS pulse compression process were carried out using the assumptions summarized in Table 4.2.2-1:

Table 4.2.2-1
Parameters Appropriate for SBS Pulse Compressor Calculations

Parameter	
Pulse Duration of Long Excimer Laser Pulse:	τ_{laser} =250 ns
Energy in Long Raman Accumulator Pulse:	E = 120 kJ
Type of SBS Gain Medium:	SF_6
Pressure of SBS Gain Medium:	2 amagat
Bandwidth of Excimer Laser Pulse:	5 GHz
SBS Stokes Seed Frequency Shift:	98 GHz
Quantum Efficiency:	99.9%
Length of SBS Cell = $c\tau_{laser}/2$	38 m
Pulse Length of Compressed Pulse:	see below
Conversion Efficiency:	see below

The effective pulse lengths and conversion efficiencies of the simulated output pulses from the SBS cell depended upon the shape of the Stokes seed used. Results of these calculations illustrating examples of the different output pulse shapes generated by the example SBS pulse compressor cell are shown in Figure 4.2.2-12.

The efficiencies of the pulse compressors as functions of ramp ratios are illustrated in Figure 4.2.2-13 for 1 amagat SF_6 and 1 meter aperture SBS cells.

Additional increases in conversion efficiency can be achieved by optimization of gas density, cell aperture, and SBS medium used. Since the calculated SBS pulse compression efficiencies depend upon the shape of the output Stokes pulse, it is necessary to specify the temporal shape of the output Stokes pulse in order to define a specific SBS conversion efficiency. Examples of ouptut Stokes pulse shapes are triangular, rectangular, etc. Use of a "picket fence" series of short output pulses synthesizing the main compression pulse can permit a significant increase in the SBS conversion efficiency up to the limit of the quantum efficiency of >99%. Without a more precise definition of the required pulse shape, the design point selection must remain imprecisely defined.

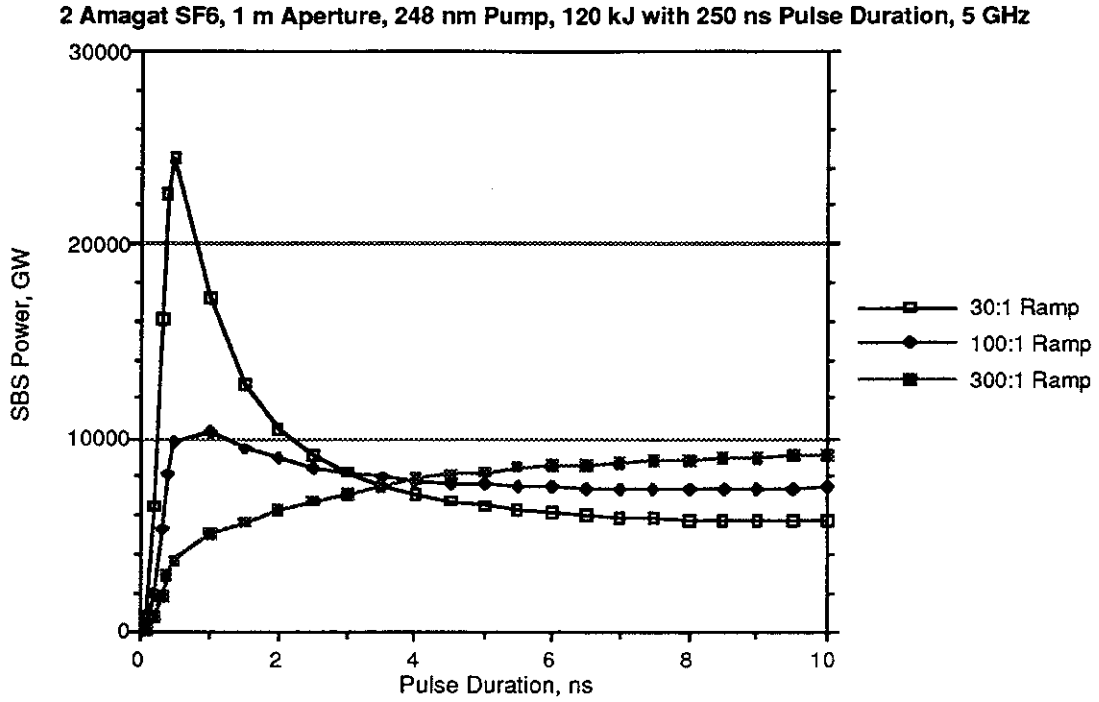

Figure 4.2.2-12 A Variety of Output SBS Pulse Shapes in SF_6 as Functions of SBS Stokes Seed Ramp Ratios is Available for D/T Target Compression

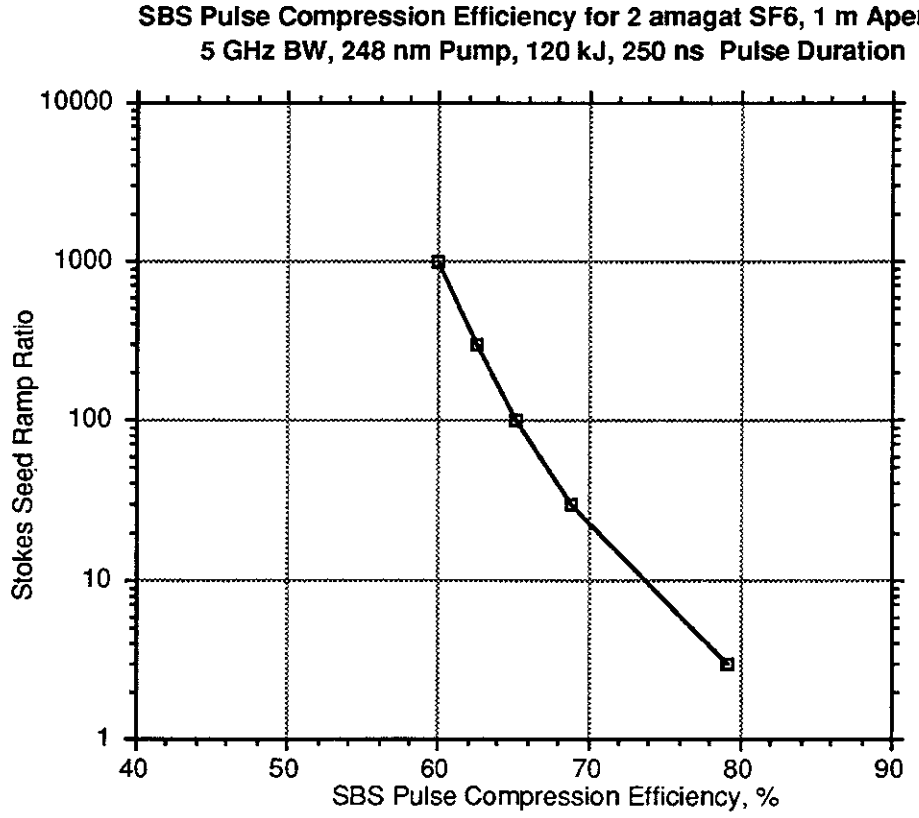

Figure 4.2.2-13 The SBS Conversion Efficiency Depends on SBS Seed Ramp Ratios

4.2.2.4 Summary of Laser Beam Conditioning Strategies - The approach for designing the KrF laser driver for a circa 2030 inertial fusion energy (IFE) power plant was to optimize the performance, efficiency, reliability, safety, and cost effectiveness of the excimer laser amplifiers independently of the DT target pellet irradiation requirements. Since optimized excimer lasers (OELs) are likely to produce ultraviolet laser pulses that are too low in energy (E ~ 3-5 kJ) to meet the IFE pellet requirement of E_{pulse} ~ 5 MJ, and with pulses that are much too long (λ_{laser} ~ 250 ns) for estimated ideal target compression scenarios using 6 ns pulses, a fundamental aspect of our design strategy is to design coherent laser beam accumulators to collect a sufficient number (~2000) of OEL beams in order to achieve the requisite 5 MJ energy level while using integated pulse compressors to generate the needed 6 ns pulse durations. Although there are conventional techniques for incoherent beam combination and angular multiplexing for pulse compression, two non-linear optical techniques for achieving coherent beam combination and pulse compression were selected because of their inherent simplicity, flexibility, and outstanding performance capability.

The non-linear optical architectures selected for achieving coherent beam combination and pulse compression are the forward rotational stimulated Raman scattering in hydrogen (for beam combination)[10,15] and the backward-seeded stimulated Brillouin scattering[17] in SF_6 (for pulse compression). Computer simulations were used to estimate the performance of each of these systems. The forward Raman conversion should have an efficiency of 90% and the SBS pulse compression from 70% to 95%, depending upon whether the main laser pulse format is a single 6 ns pulse or a 6 ns pulse synthesized from a series of "picket fence" composed of shorter pulses. Longer, flat-topped monolithic SBS Stokes output pulses are achieved in this design at the expense of conversion efficiency. Higher order Stokes conversion in the Raman accumulators is controlled by limiting both the H_2 path length in the cells and minimizing the angle, θ, between the pump and Stokes beams to control ASE seeding higher order Stokes beams.

By selecting both H_2 and SF_6 pressures near 1 atmosphere, no dangers associated with high pressure optical cells occur. The electric discharge excimer lasers are operated at relatively low voltages producing minimal x-ray hazards. The Raman accumulators are pumped with atmospheric pressure electric discharge excimer lasers producing only a few kilojoules each and the failure modes of the electric discharge excimer lasers are non-catastrophic. This architecture also permits further development of potentially efficient ArF (λ_{laser} = 193 nm) excimer laser amplifier modules. Use of vibrational H_2 or D_2 transitions in the Raman accumulators could be used to shift the wavelength out to λ = 210 nm. This laser driver architecture emphasizes safety, reliabilty, and efficient operation in wavelengths that couple well with the targets.

References for 4.2

1. "Inertial Confinement Fusion Reactor Design Studies Recommended Guidelines," prepared for the Department of Energy Office of Fusion Energy, Dr. Ronald C. Davidson (Chairman), Massachusetts Institute of Technology, Cambridge, MA, September 1990.

2. "Electron-Beam Sources for Pumping Large Aperture KrF Lasers," Louis A. Rosocha and Kenneth B. Riepe, Fusion Technology 11, pp. 576-611 (1987).

3. "Performance of the Aurora KrF ICF Laser System," J. E. Jones, et al., Proceedings of the International Conference on Lasers '89, pp. 88-95, 3-8 December 1989.

4. "Aurora Multi-kilojoule KrF Laser System Prototype for Inertial Confinement Fusion," Louis A. Rosocha, *et al.*, Fusion Technology 11, pp. 497-531 (1987).

5. "KrF for Fusion: An Overview of Laser Issues," Reed Jensen, Fusion Technology 11, pp. 497-531 (1987).

6. "Design of a 100 kJ KrF Power Amplifier Module," J. Allan Sullivan, Fusion Technology 11, pp. 684-704 (1987).

7. "The Aurora Laser Optical System," John A. Hanlon and John McLeod, Fusion Technology 11, pp. 636-653 (1987).

8. "Aurora Multi-kJ KrF Laser System Prototype for Inertial Confinement Fusion," Louis A. Rosocha, et al., Fusion Technology 11, pp. 497-531 (1987).

9. "Future Developments and Applications of KrF Laser-Fusion Systems", David B. Harris, et al., Fusion Technology 11, pp. 705-731 (1987).

10. "New Techniques for KrF Laser Fusion Systems," M. J. Kushner, J. J. Ewing, J. M. Egglestron, D. B. Lowenthal, R. G. Berger, Interim Report for the Los Alamos National Laboratory, Spectra Technololgy, Inc., Seattle, WA (1985).

11. "Raman Pulse Compression of Excimer Lasers for Application to Laser Fusion, " J. R. Murray, et al., IEEE J. Quant. Elect., QE-15, pp342-368 (1979).

12. "Optical Pulse Compressor Systems for Laser Fusion, " J. J. Ewing, et al., IEEE J. Quant. Elect., QE-15, pp368-379, (1979).

13. "Beam Combination through stimulated Brillouin scattering,", Richard H. Moyer, et al., JOSA, 5 pp. 2473--2489 (1988).

14. "Raman Beam Combining Program," Final Report for Contract #F29601-85-C-0053, prepared for the Air Force Weapons Laboratory, Kirtland Air Force Base, New Mexico, Shirley J. Pfeifer, K. Allardyce, R. Johnson, G. Linford, H. Injeyan, and J. Betts, TRW Applied Technology Division, Redondo Beach, CA, and H. Komine, G. Lombardi, W. Long, and E. Stappaerts, Northrop Research & Technology Center, Palos Verdes Peninsula, CA, September 1986.

15. "Raman Oscillator Studies," Final Report for Contract F29601-84-C-0051, prepared for AFCMD, Kirtland Air Force Base, New Mexico, Jerry Oldenettel and Michael Terpka, Western Research Corporation, San Diego, CA, March 1987.

16. Laser Handbook, edited by F. T. Arecchi, North-Holland Book Co., W. Kaiser, M. Maier, "Stimulated Rayleigh, Brillouin, and Raman Spectroscopy," pp. 1116-1120.

17. "Optical Methods for Laser Beam Control," Arthur A. Mak and Leonid N. Soms, Proceedings of SPIE, Vol. 1415, Modeling and Simulation of Laser Systems II, pp. 110-119, (1991).

18. "Direct Measurement of the Acoustic Decay Times of Hypersonic Waves Generated by SBS," M. J. Damzen, M. Hutchinson, & W. Schroeder, IEEE J. of Quant. Electronics QE-23, pp. 328-334 (1987).

4.3 Rationale for Heavy Ion Driver Options

The configuration of the Prometheus-H Heavy Ion Driver was significantly influenced by the projected cost of electricity of the plant. Two key design choices for the simplification of the driver were the substitution of a single beam LINAC plus storage rings for the multiple beam LINAC and the channel transport of the entire beam through a single small aperture in the first wall/blanket rather than through many large apertures.

4.3.1 Single Beam LINAC Plus Storage Rings Vs. Multiple Beam LINAC - The total energy requirements for the target are such that many beamlets must be accelerated and combined. The major cost drivers in the accelerator are the quadrupole focusing magnets that contain the beamlets, the induction cores that maintain the acceleration gradient for the duration of the pulse, and the pulsed power systems that provide the total energy gain for all of the beamlets.

In the case of a multiple beam LINAC, there are N beamlets per reactor shot to be accelerated in parallel. The cross-sectional area is proportional to N, as in Figure 4.3.1-1.

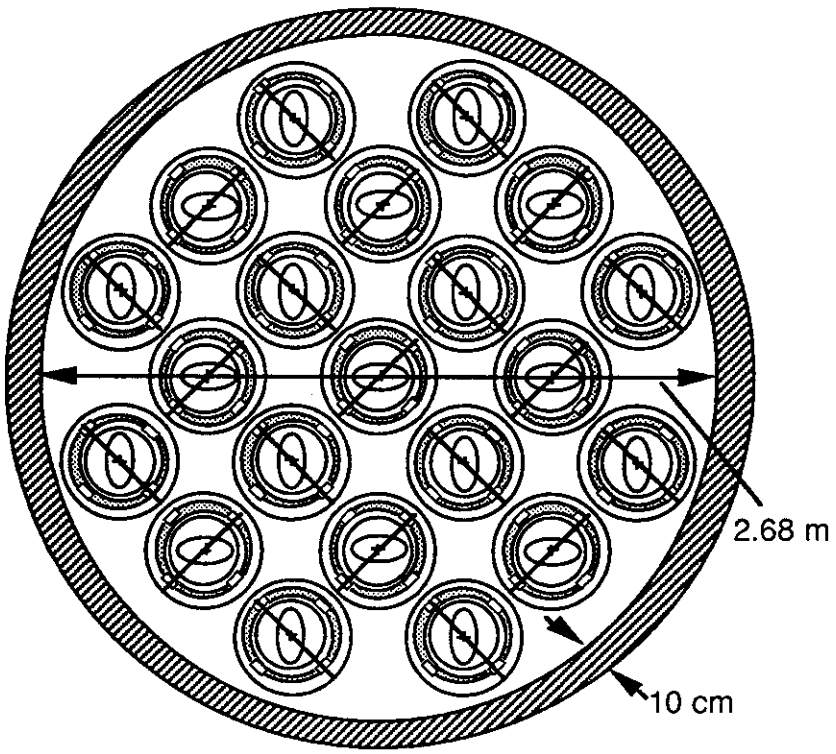

Figure 4.3.1-1 Multiple Beam LINAC Cross-Section

In the multiple beam LINAC, there are N magnets per unit length in order to confine each beamlet. The induction core that surrounds the magnets has a thickness, t, to provide the required volt-seconds (voltage/meter x pulse length = ΔB x area/meter = t), so the volume of the core is $2 \pi N^{1/2}$ t. The total energy supplied by the pulsed power is the beam energy plus the losses in the cores (which are proportional to the core volume) times a factor to account for the efficiency of the pulsed power. Since beam energy is fixed by the target requirement, the variables are the core losses and the pulsed power efficiency.

In the case of a single beam LINAC, the same N beamlets per reactor shot can be accelerated serially. The cross-section for this configuration appears in Figure 4.3.1-2.

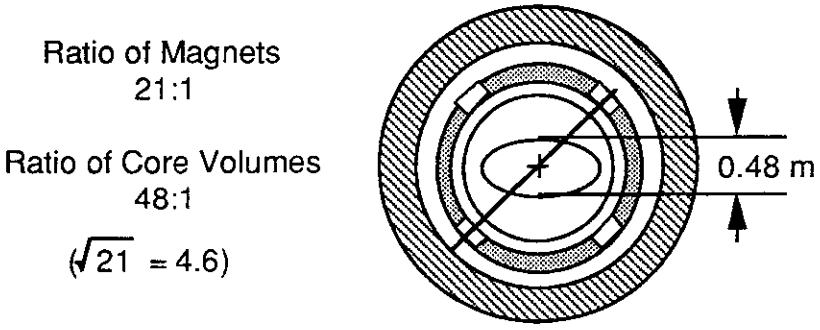

Figure 4.3.1-2 Single Beam LINAC Cross-Section

There is only one magnet per unit length, a factor of N improvement. Although the core has the same thickness, t, to provide the same number of volt-seconds, the inner radius and the core volume are reduced a factor of $N^{1/2}$. Although the core volume is reduced, the core is fired N times rather than once, leading to a net increase in the core losses per reactor shot. Total beam power is the same; therefore, there is no intrinsic reason why the efficiency of the pulsed power should change. However, the cost per joule of the pulsed power will go up due to the high repetition rate capability.

Based on the cost model, this single beam LINAC is the more cost-effective system. The technology of the single beam LINAC is more developed. The complication is that there is a time delay of the order of milliseconds between the first and last of the serially-generated beamlets. A number, N, of separate storage rings must be used to function as delay lines for the beamlets so they may arrive at the target simultaneously. The technical feasibility of storing high current ion beams for millisecond time scales must be demonstrated, since there is a possibility of instabilities. This is identified as a Critical Issue for the Heavy Ion Driver. Given that storage is feasible, the cost impact of the rings is relatively minor. Since there are no acceleration modules in the storage rings, the only cost driver is the superconducting magnets, which now include dipole bending magnets as well as quadrupole focusing magnets. Thus, the total number of magnets in all of the storage rings is roughly equal to the number in the final 10% of

the multiple beam LINAC. Even with the storage rings added to the LINAC, the much lower cost associated with the single beam system yields a more attractive driver for the 1000-MWe power reactor.

4.3.2 Pinched Channel Transport Vs. Ballistic Focusing - The indirect drive target is illuminated from two sides with proper access for the beams through the shielding, blanket, and first wall elements. Following the target implosion, neutrons and gas flow out of the access ports, back toward the final focus magnetic optics and the rest of the linear accelerator with concomitant damage and contamination of those elements.

The superconducting final focus magnets are susceptible to damage from the neutrons with little room for shielding. More robust, iron-dominated, room temperature quadrupoles are available; however, they are large, inefficient, and expensive. At 2 MW electrical per normal conducting quadrupole lens (the value used for HIBALL-II[1]) the reactor power balance is skewed since this is roughly the time-averaged kinetic power per beamlet in Prometheus-H.

The gas load is also a problem since, within the reactor chamber, the partial pressure of the noncondensibles (primarily hydrogen) is about 100 mtorr just before a shot, and it peaks at hundreds of torr soon after. This gas leaves the chamber primarily through pumps but also through the target chamber apertures, where it heads back toward the accelerator. The accelerator must be kept in the 10^{-7} to 10^{-10} torr regime for beam propagation. There is strong motivation to keep the number and size of apertures small. There are two scenarios possible in the relatively low energy ($E < 10$ GeV) and high charge ($Q > 1$) regime.

The first case, ballistic focusing, is illustrated in Figure 4.3.2-1. Each of N beamlets can come through a 20 to 40 cm diameter hole in the reactor wall, individually focussed on the target by its final focus magnets. The beams propagate approximately 5 m through whatever gas is within the target chamber, which includes both burn products and additives. The beamlet must be at least partially neutralized to overcome space charge repulsion, and although there is presumably plenty of plasma within the beam duct to provide electrons, this plasma will also collisionally strip the beam ions to higher charge states. The beam is entirely within the target chamber before the first ion strikes the target. The precursor beamlets (containing one-fourth to one-third of the beam power) continue to strike the target for 30 to 40 ns before the rest of the beamlets arrive, generating x-rays that photo-ionize the beam, further increasing the beam charge state and interfering with the space-charge neutralization process that permits focusing to small spot sizes. After ignition, the neutrons and gas head back up the ducts to the magnets and the rest of the accelerator.

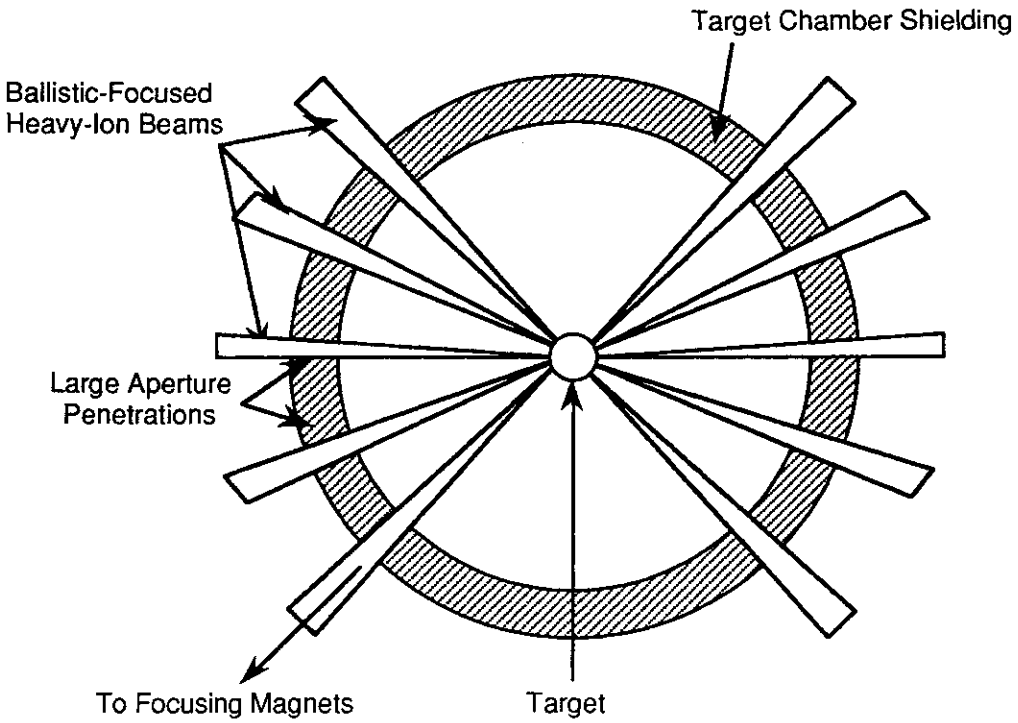

Figure 4.3.2-1 Ballistic Focusing of HI beams

The second case, pinched channel transport, is illustrated in Figure 4.3.2-2. The beamlets again focus down from 20 to 40-cm diameters, but are now directed to a common spot outside the blanket rather than the target pellet. The region they traverse has a controlled amount of gas or plasma, permitting fine tuning to control the degree of neutralization and collisional stripping. The beam ions converge on a thin layer of gas at the outside of the blanket, completely stripping ($Q > 50+$ within a few millimeters) and increasing the beam electrical current by a very large factor. The envelope begins to collapse under the influence of the pinch current, overcoming the tendency of the outer beamlets to separate. The coalesced beam propagates to the target through a 2-cm diameter hole in the blanket. Because the ions are already completely stripped, the x-rays caused by the precursor have no effect. After ignition, the small flow of backstreaming gas through the 2-cm aperture is blocked by the same gas layer that stripped the beam ions. There is room to add additional shielding for the magnets to protect them from neutrons that pass through the ducts in the main shielding.

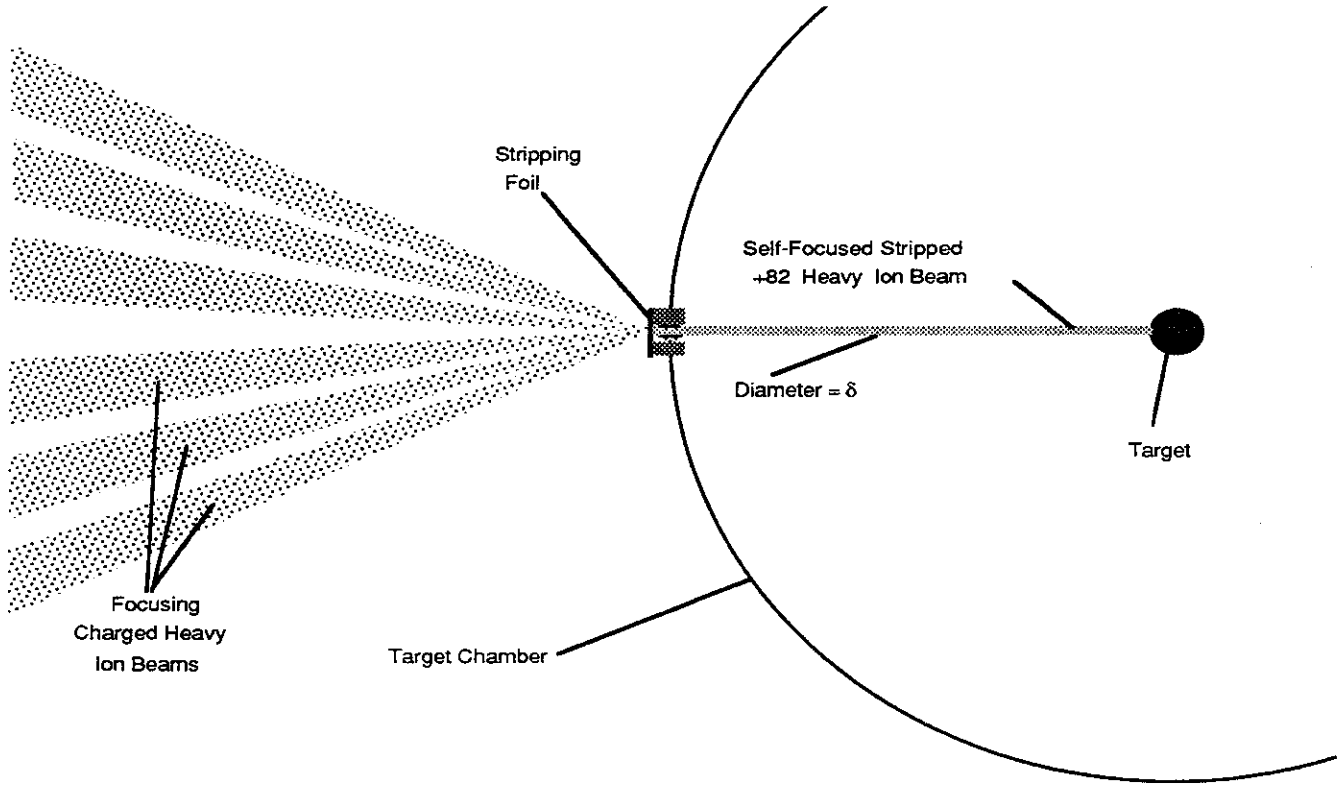

Figure 4.3.2-2. Pinched Channel Transport in Target Chamber

Both methods rely on the detailed response of the plasma and are, therefore, speculative. Neither has been demonstrated with anything approaching a relevant heavy ion beam. Some computer simulations have indicated the beam pinch will not form, but contrary results are obtained when different input conditions are assumed. Although the pinched channel transport is probably riskier, the engineering advantages it affords make it worthwhile to carry along as a baseline until a relevant experiment can be performed.

References for 4.3

1. B. Badger, et al., "HIBALL II - An Improved Conceptual Heavy Ion Beam Driven Fusion Reactor Study," UWFDM-450/KfK 3840 , Fusion Engineering Program, University of Wisconsin (July 1985).

4.4 Cavity Design Options

The cavity environment is very severe for an IFE reactor. Not only is the time-averaged neutron fluence similar to that of an MFE reactor, the pulsed nature of IFE adds blast effects, instantaneous high heat loads, and high levels of X ray and gamma radiation. A large number of IFE cavity design studies have been performed during the past ten years. The selection of a cavity concept for Prometheus was preceded by a thorough review of existing designs. The trade studies for the wall protection and the blanket are described in the following sections.

4.4.1 Wall Protection Concept - The protection of the wall is one the most critical engineering challenges in the reactor plant. The adverse environment is very harsh because of the pulsed nature of the inertial fusion reaction. A majority of the energy release occurs almost instantaneously in the form of prompt X rays, neutrons, and photons. The debris ions provide the remainder of the energy deposition a short time later. After the initial energy release, the cavity chamber is "relatively quiescent" which allows the environment and chamber wall/structure to equilibrate, thermally and mechanically. This process
is repeated many times a second and hundreds of millions of times per year which imposes a daunting fatigue challenge to design and manufacture a reliable and long-lived first wall system.

4.4.1.1 Wall Protection Design Options – The major cavity options and variants considered in the study are noted in Table 4.4.1–1. The major classes of protection include gas, thin liquid films, thick liquid jets, and solid granules. In addition, a number of more "exotic" ideas have also been proposed, including a frost first wall (for the LMF), a pool-type reactor (Pulse*Star[11]), and magnetic protection.

Table 4.4.1–1. Main Wall Protection Design Options Considered

1. Granular Solid Protection
   - Centrifugally Rotated (CASCADE)[1]
   - Gravity-Driven
2. Thick Liquid Jet
   - Gravity-Driven (HYLIFE I)[2]
   - Magnetically-Guided (SENRI)[3]
   - Advanced Flow Types (HYLIFE-II)[4,5]
3. Liquid Film
   - HIBALL/INPORT,[6] LIBRA[7,8]
   - Porous Composite Wall
4. Gas or Magnetic Protection
   - SOLASE[9]
   - SIRIUS[10]

Granular Solid Protection – An example of a granular solid protection scheme is the one proposed for the CASCADE[1] concept. It consists of a three-layered flowing blanket of pyrolytic carbon, BeO, and solid breeder ceramic (such as $LiAlO_2$) granules. Here, the flowing granules provide both protection and blanket functions. The reactor rotates about its horizontal axis and the moving granule blanket is held against the reactor wall by centrifugal force. The granules are fed by gravity and the rate of flow is controlled by the rotation speed. This concept has attractive safety, efficiency, and low-activation features. Issues are linked to the discontinuity of the heating rate at the BeO/solid breeder interface and to possible aggregation of the granules.

Liquid Protection – Liquid protection schemes use liquid metals or Flibe in the form of either a liquid metal spray, a thick liquid metal wall, or a hybrid concept using a porous solid wall with liquid metal film. Advantages of a spray include the potential uniformity of protection afforded by the mist and the shorter renewal time, while a key issue relates to the stability of the spray formation.

A thick liquid wall was investigated in the HYLIFE-I [2] design study. The concept consists of a liquid lithium waterfall surrounding the micro-explosion area. The lithium fall protects the first wall from the photon and ion fluxes and attenuates the neutron flux so that wall damage is considerably reduced. In this case, the flowing liquid metal provides functions of protection but also of tritium breeding and energy removal. This concept offers advantages in tritium breeding and energy multiplication. However, because of the time necessary to replenish the waterfall, it is mostly suitable for low repetition rate systems. Issues include the effect of the impact on the first wall of liquid lithium slugs propelled by the pressure of lithium vapor created during the micro-explosion. A possible way to alleviate this problem is to use an array of individual jets which could reduce this lithium gas pressure driving force. HYLIFE-II [4,5] continued the concept of a thick liquid jet, but replaced Li with Flibe as the protectant.

An interesting variation for this concept is the use of a magnetic field to guide and stabilize the liquid lithium flow and control flow velocity, as in the SENRI design.[3] The benefit of flow control must be evaluated against the added design complexity resulting from the introduction of magnetic fields.

Another variation of the liquid protection concept is the hybrid (solid/liquid) design, where the falling liquid metal is enclosed in porous solids to prevent disassembly of the liquid following each micro-explosion. For example, in the INPORT modules used in the LIBRA[7,8] and HIBALL[6] design studies, the LiPb columns are made to flow inside porous SiC sleeves. A source of uncertainty is the design and lifetime of these sleeves.

Gas Protection – Gas protection schemes, such as the one used for the SOLASE design,[9] involve filling the reactor cavity with a buffer gas to attenuate the charged particles and soft x-rays before they reach the first wall. Neon is an attractive buffer

gas because of its relatively high stopping power for ions and x-rays and its inertness. Issues include energy re-radiation from the gas to the first wall and its time scale and the effect of impurities and gas breakdown on target performance. The blanket heat removal and tritium breeding function are then carried out separately from the wall protection function. For example, in SOLASE[1], a flow of Li_2O solid breeder particles behind the first wall is used for these functions.

4.4.1.2 Evaluation Criteria - The choice of a cavity wall protection design concept reflects concern over a large number of competing factors. The protection scheme chosen for Prometheus uses a thin liquid Pb film supplied through a porous structure of SiC composite material. The more important concerns which were considered in choosing a thin film protection scheme include:

(1) Configurational Compatibility (Beam Line Accommodation) – Granular and thick film schemes appear nearly impossible to engineer when there are a large number of beam lines. Thick falling films must be guided around all penetrations, without sacrificing protection at any point. We assume that any spot which is not fully covered is likely to be destroyed, such that the protection scheme should be reliable and "passively stable". The beam lines themselves should be protected beyond the first wall, as a significant amount of energy may be deposited there as well. The porous structure could easily be extended into the beam lines.

(2) Engineering Simplicity – One of the unattractive features of a thick falling film is the coupling of functions, including wall protection, breeding, energy conversion, and shielding. While removing components may appear to simplify the design, there are serious disadvantages. The design window is reduced whenever multiple constraints are imposed on a single system. Much of the existing blanket technology from MFE can be applied if a separate blanket is used.

In addition, the technical feasibility of flowing large quantities of liquid at high velocity over large path lengths (and in some cases complex flow schemes) is questionable, especially considering the requirements for beam propagation. There are geometric advantages of a thin film fed from behind the first wall. The flow rate of the film can be very small in comparison.

(3) Safety and Environmental Attractiveness (Minimum Liquid Inventory) – Contamination of the protective film will be very difficult if the inventory is large and, consequently, the required purity level is low. In addition, the reduction in inventory and thickness allows us to choose from a larger number of liquids for the protective medium.

(4) Cavity Clearing – Compared with thick liquid jets, thin films should have better repetition rates. The amount of liquid which can be ejected is limited, and the presence of the porous backing should help contain the film.

(5) Lifetime – The choice of SiC for the structural material has good radiation resistance and safety and environmental advantages. The protective film material can be selected based in part on minimizing radioactivity. In addition, the relatively thick independent first wall system coolant protects the blanket, thus increasing the blanket lifetime.

(6) Versatility – This configuration should be applicable for both HI and laser, for both direct- and indirect-drive schemes.

Gas-protected "dry-wall" concepts, such as SOLASE and SIRIUS, have many desirable features as well, offering good accommodation of beam penetrations, flexibility, and probably the best cavity clearing capability. However, these designs suffer from several problems of their own. Problems arise from the high required gas pressure, including laser-induced gas breakdown and target penetration. Other problems include long energy re-radiation time of the gas and damping of the mechanical impulse from the blast. From past studies, the cavity diameter is likely to be much larger than liquid-protected designs, implying several times as much material and consequently higher cost.

4.4.1.3 Wall Protection Design Choices – The protection scheme chosen for Prometheus uses a thin liquid Pb film supplied through a porous structure of SiC composite material. The SiC structure must be flexible enough to withstand cyclic loading from the blast, but strong enough to support itself and the internal pressure of the film. A supply region behind the porous structure serves to slowly feed the liquid and to remove the heat from the first wall (40% of the total fusion power). Blast energy is removed from the cavity initially by evaporation. During the recondensation phase of each pulse, heat is conducted through the relatively thin film and into the first wall coolant.

The film material is Pb, which offers many advantages:

(1) Appropriate Temperature Ranges – Pb has excellent saturation temperatures in the pressure range of interest (1 mtorr ~ 100 torr). It is high enough for good conduction heat transfer from the film surface to the coolant, but not too high for limits on material properties and compatibility. It is also high enough to provide a high coolant temperature, resulting in good thermal conversion efficiency.
(2) High Thermal Conductivity
(3) Good Neutron Multiplier - Pb is an adequate neutron multiplier which allows elimination of Be in blanket.

(4) Safety Advantages - Since the film contains no Li, the chemical reaction hazard and mobility of Li and LiPb is not a problem.
(5) Chemical Compatibility with SiC
(6) Good Fit with Pb in Hohlraum Targets - Since Pb has been selected as the main high-Z component in the indirect-drive hohlraum targets, impurity control in the liquid is easier.

The main disadvantages of Pb are its weight, low tritium solubility leading to higher permeation, radioactivity (which can be reduced with impurity control), health hazard of Pb vapor, and lower energy multiplication as compared with a Be multiplier.

Having rejected Li and LiPb protectants for safety reasons, Flibe (Li_2BeF_4) was considered as an alternative. Flibe has been extensively studied in the HYLIFE-II[5] reactor studies. While it offers some potential advantages, several concerns led us to select Pb. These areas of concern for Flibe include:

- Poor thermal conductivity (0.8 vs. 34 W/m-K for Pb)
- Dissociation
- Coolant chemistry
- Short-term activation of fluorine
- Chemical reactivity of fluorine
- Mobility of Be and F in vapor form (transport into vacuum system)

The overall configuration of Prometheus is a low aspect ratio cylinder with hemispherical end caps. This configuration was selected for several reasons:

(1) Maintenance of a cylinder is easier than a sphere. Maintenance paths are all straight vertical. The configuration allows independent removal of first wall panels and blanket modules.
(2) A cylinder provides better control of film flow. Problems protecting the upper hemisphere can be reduced with higher aspect ratio, in which the distance from the blast to the upper end cap can be maximized.
(3) A cylindrical configuration is more consistent with conventional plant layouts.

The main disadvantage of this concept is nonuniform power distribution and higher peak loads. The higher peak-to-average loading leads to larger size and higher cost for a given total reactor power. To minimize these disadvantages, the aspect ratio is kept relatively low—of the order of 1-2; however, this also limits the advantage of upper end cap protection.

Another main feature of the Prometheus design is the separate blanket region. This blanket is protected from the blast and is designed to optimize breeding, energy conversion, reliability, and maintainability. A more detailed explanation of the blanket is found in the following section.

The concept described above can be applied to both laser and heavy ion reactor designs. This feature is important in reducing the R&D required for cavity development.

4.4.2 Blanket Concept – The design of the Prometheus blanket was strongly influenced by the desire to maximize safety and reliability. Safety considerations led to the choice of a helium coolant, low-activation solid breeder, and SiC for the structure and neutron reflector. Higher reliability is sought by a combination of vertical maintenance with easily-detachable blanket modules, low coolant pressure with double containment, and relatively conventional configuration adapted from magnetic fusion reactors.

The overall configuration consists of several rings, each containing a number of modules. The modules are configured into the rings outside of the reactor. If any module requires replacement, the entire ring can be removed easily, and then repairs are made to individual modules externally. The module is composed of layers of coolant and breeder. The pressurized He coolant is contained in U-bend woven SiC tube shells. The Li_2O breeder is placed in packed-bed form between the tube shells and is purged by He flowing along the axis of the module.

The Li_2O breeder has many attractive features, including low activation, good temperature window, low tritium inventory, and good existing data base. Of the candidate solid breeder materials, it has the best TBR and, in conjunction with the first wall Pb coolant, provides the potential for adequate tritium breeding without the need for Be as a multiplier.

He coolant also has many advantages. It is chemically inert and can operate at high temperature. This allows high thermal cycle efficiency, but also eliminates the need for a thermal resistance region between the breeder and coolant (all solid breeder materials must operate at high temperature to release their tritium).

In previous blanket design studies, the disadvantages of using He at high pressure have been assessed. These include high pressure stresses, possibly leading to failures, and the fear of leakage problems. In order to reduce these concerns, we took advantage of the unique possibility for low-pressure operation in our design. Inertial fusion inherently produces less neutron power than magnetic fusion. In the Prometheus design, the thick first wall system substantially moderates the neutrons and further reduces the neutron power to the blanket. Only 60% of the thermal power is in the blanket system. Because of the low power density in the Prometheus blanket, the coolant pressure was reduced from the more traditional 5 MPa to only 1.5 MPa. The pressure is so low that the breeder module walls and purge system were designed to withstand coolant tube rupture, resulting in a much higher reliability than higher-pressure designs.

The major penalty paid for this pressure reduction is higher pumping power, resulting in lower thermal cycle efficiency. In this design, the tradeoff was judged favorably for the low pressure design.

Finally, the Pb FW coolant is the sole multiplier. Eliminating Be from the blanket makes the blanket design simpler and also avoids the well-known problems of resource limitations and high cost. Overall, the Prometheus blanket is a very simple and conventional blanket design, yet offers excellent safety, environmental, reliability, and lifetime characteristics.

References for 4.4

1. J. H. Pitts, "Development of the CASCADE Inertial-Confinement Fusion Reactor," Fusion Technology, Vol. 8, No. 1, Part 2B, p. 1198, July 1985.
2. J. A. Blink, et al., "The High-Yield Lithium-Injection Fusion-Energy (HYLIFE) Reactor," UCRL-53559, LLNL, Livermore, December 1985.
3. C. Yamanaka, et al., "Concept and Design of ICF Reactor -SENRI-I," Institute of Laser Engineering Report ILE-8127 P (1981).
4. R. W. Moir, "A Review of Inertial Confinement Fusion (ICF), ICF Reactors, and the HYLIFE-II Concept Using Liquid FLiBe," UCID-21748, 25 September 1989.
5. R. W. Moir, "HYLIFE-II Inertial Confinement Fusion Reactor Design," Fusion Tech. 19 617–624 (May 1991).
6. B. Badger, et al., "HIBALL - A Conceptual Heavy Ion Beam Driven Fusion Reactor Study," UWFDM-450, Fusion Engineering Program, University of Wisconsin (1981).
7. G. A. Moses, et al., "Overview of LIBRA Light Ion Beam Fusion Conceptual Design", Fusion Technology, Vol. 15, No. 2, Part 2A 756, (1989).
8. M. E. Sawan, et al., "Chamber Design for the LIBRA Light Ion Beam Fusion Reactor," Fusion Technology, Vol. 15, No. 2, Part 2A 766, (1989).
9. R. W. Conn, et al., "SOLASE - A Conceptual Laser Fusion Reactor Design," UWFDM-220, University of Wisconsin, December 1977.
10. S. I. Abdel-Khalik, et al., "SIRIUS-M: A Symmetric Illumination, Inertially Confined Direct Drive Materials Test Facility," 2nd Int. Conf. on Fusion Reactor Mater., April 1986.
11. J. A. Blink and W. J. Logan, "The Pulse*Star Inertial Confinement Fusion Reactor", Fusion Technology, Vol. 8, July 1985.

4.5 Selection Criteria for SiC/SiC Composites

4.5.1 Introduction – An important feature of fusion reactions is that the resulting radioactive products are short-lived. However, the interaction of neutrons with structural materials in fusion power systems can lead to long-lived radioactive decay chains. Proper selection of structural materials can lead to significant reductions in the level and duration of environmentally hazardous radioactive products. Several neutronic and conceptual fusion-reactor studies have concluded that the post-shutdown radioactive inventories of FW/B structures made of pure SiC are dramatically lower than any metallic alloy considered for fusion so far.[1-4] The same assessments have shown conclusively that decay heat generated in the reactor, in case of a loss of coolant accident, can be safely and passively removed without the danger of radioactivity release to the environment. It is also realized that long-term radioactive inventories will be mainly controlled by the level of impurities in the structure. Therefore, processing technologies which offer the potential for significant reductions in the level of impurities should be attractive for the development of SiC structures.

Another important feature of SiC structural materials is their high temperature capabilities. Operational temperatures approaching 1000°C are potentially attainable, which can lead to improved thermal cycle efficiency. For these important reasons, the development of SiC structural components is perceived to be of paramount significance to the successful commercialization of fusion energy. This section analyzes and reviews the body of knowledge which is relevant to the application of SiC as a structural material in the inertial confinement reactor concept Prometheus. The relevant features and data base of SiC/SiC composites are presented. On the basis of the available data base and reasonable extrapolations, selection criteria are developed.

4.5.2 Processing of SiC/SiC FRC's - Several methods have been developed for production of SiC fibers for use as reinforcements in high-temperature composites. Continuous yarns of 500 fibers are now in commercial production by Nippon Carbon Company[1] under the trade name Nicalon. The process starts by dechlorinating dichlorodimethylsilane with molten metallic sodium to produce the solid polymer. Further processing steps are polymerization, and densification of amorphous Si and C at high temperatures (1200°C-1500°C). The final microstructure is crystalline β-SiC of density in the range 3.16 g/cm^3, and of crystallite size of 20-50 μm. The final product is continuous multifilament tows comprised of 500 filaments.

SiC monofilaments can also be prepared by the chemical vapor deposition (CVD) process, as described in References 2 and 3. SiC is deposited from vapor mixtures of alkyl silanes and H_2 onto a substrate formed by a resistance-heated W wire or C filament. The substrate has a diameter of 10-25 μm and forms the fiber core. The final

filament is commonly 100-150 μm in diameter. Although deposition at high temperatures (above 1300°C) is fast, the resulting structure is coarse crystalline and is weaker than the amorphous structure obtained at lower temperatures. If any free silicon appears in the microstructure, further weakening will result.

Whiskers of SiC can be prepared either from rice hulls[4] or by a vapor-liquid-solid (VLS) process.[5] Rice hull whiskers contain around 10% SiO_2 and between 0%-10% Si_3N_4. Around 10% of SiC is in the β crystalline phase, and the remainder is composed of α-SiC particulates. Whiskers produced from rice hulls are short, with lengths around 50 μm. Longer and smoother whiskers are prepared at Los Alamos[5] by the VLS process. Such whiskers possess superb mechanical properties, with an average strength of 8.4 GPa and an average elastic modulus of 580 GPa.

Multifilament fibers can be assembled into two- and three-dimensional structures by interlacing, intertwining, or interlooping. Combining the high strength of fibers with proper matrix-fiber interface frictional properties, fiber architectures will expand the design options for tough and reliable fusion structural materials. Fiber architectures can be classified into four categories: discrete, continuous, two-dimensional, and fully integrated (three-dimensional). Selection of one of these architectures for F/B or high heat flux applications will depend on a number of factors. These are: (1) the capability for in-plane multi-axial reinforcements, (2) through-thickness reinforcements, (3) the capability for final shape manufacturing, and (4) leak-tightness of the final components during high-temperature operation. Selection of a particular form of architecture for fusion may be premature at present, because matrix processing techniques are still evolving. While 3-D architectures provide an orthotropically tougher composite, the CVI technology employed at present is limited to low fiber volume fractions, and the procedure is quite lengthy. On the other hand, 2-D laminates can be produced at much greater speeds and can achieve higher fiber volume fractions. The final component mechanical properties will be anisotropic. This feature will certainly lead to reduced capabilities of components to carry shear loads. In summary, processing technologies for the manufacture of SiC/SiC FRM's are available at present. However, further development is needed for production of components on a commercial scale.

4.5.3 Data Base - SiC is known to have high intrinsic strength and stiffness (E = 450 GPa at RT), high-temperature stability (decomposition temperature = 2830°C), and excellent oxidation resistance. Its relatively high conductivity ($k = 0.25$ W cm^{-1} $°C^{-1}$ at 200°C) and low coefficient of thermal expansion ($\alpha = 3.8 \times 10^{-6}$ $°C^{-1}$ at 200°C) results in favorable thermal shock resistance when compared to other ceramic materials. The thermal conductivity of CVD SiC, k(W cm^{-1} $°C^{-1}$), and the specific heat, C_p (J Kg^{-1} $°C^{-1}$), are given by empirical equations of the form:

$$\text{Property} = \sum_{i=1}^{4} M_i T^j$$

where T is temperature in °C. Values of the polynomial fit coefficients are shown in Table 4.5.3-1. Graphical representation of these properties as functions of temperature is shown in Figure 4.5.3-1.

Table 4.5.3-1. Coefficients of Polynomial Fits to Selected Properties of SiC

$$\text{Property} = \sum_{i=1}^{4} M_i T^j$$

Property Coefficient	Thermal Conductivity $W\,m^{-1}\,K^{-1}$	Specific Heat $J\,Kg^{-1}\,K^{-1}$	Fracture Stress, σ_f MPa	Young's Modulus GPa	Swelling δV/V <1000°C	Swelling δV/V >1000°C
M_0	62.84	435.53	−993.9	605.632	1.43	−71.19
M_1	−0.04	3.08	7.42	−1.407	0.0059	0.15
M_2	6.25×10^{-6}	−0.0047	−0.013	0.003	-1.56×10^{-9}	1.09×10^{-4}
M_3	0	3.31×10^{-6}	9.54×10^{-6}	-2.087×10^{-6}	8.58×10^{-9}	2.56×10^{-8}
M_4	0	-8.41×10^{-10}	-2.42×10^{-9}	0	0	0

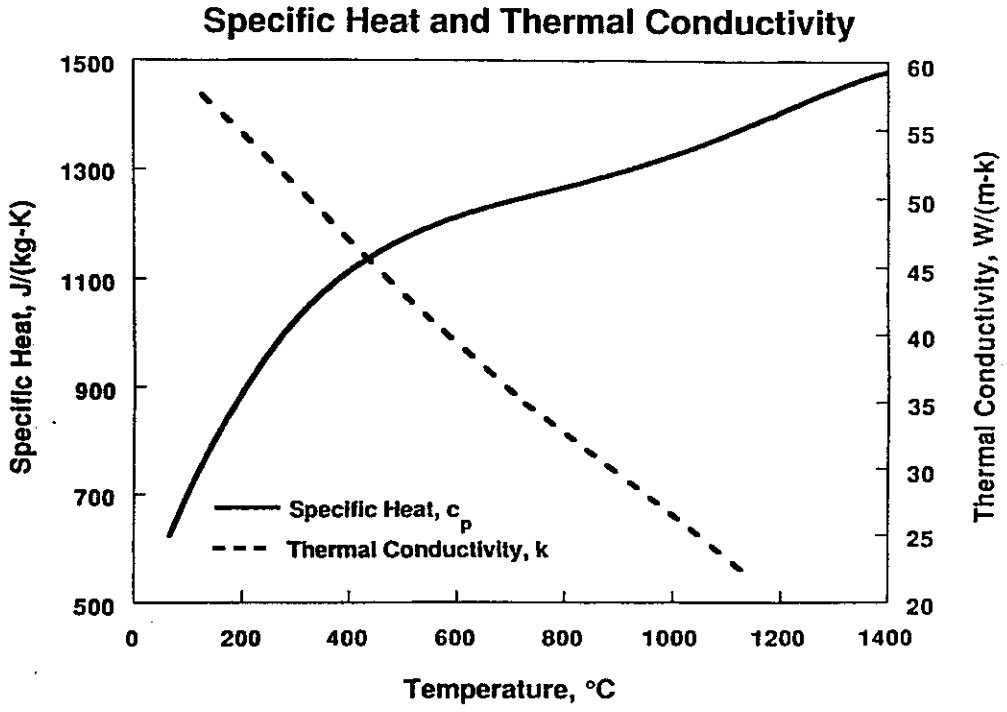

Figure 4.5.3-1. Dependence of the Specific Heat and Thermal Conductivity of SiC on Temperature

Assessment of the data base and development of a proper fusion-specific SiC composite is an iterative process. For this reason, we discuss here the available mechanical and radiation effects data base so that ways for further improvements can be found.

4.5.3.1 Mechanical Properties – The tensile strength of Nicalon fibers is statistical because of the existence of defects (e.g. voids and cracks) during the manufacturing process. It is also strongly influenced by heat treatment, test atmosphere, and test temperature. Commercial Nicalon fibers in various atmospheres show degradation in strength at or above 1000°C.[6] Strength deterioration is attributed to: (1) chemical reaction between SiO_2 and free C, leading to surface damage; (2) crystallization of the amorphous structure; and (3) oxidation in gaseous atmospheres. The tensile strength of CVD-prepared SiC fibers on C cores is retained only up to 800°C. The 100 h rupture strength of CVD fibers was shown to degrade greatly above 1100°C.[7] While the average tensile strength of unirradiated monofilaments is 2.8 GPa at temperatures below 900°C, preform wires have an average flexural strength of only 1.3 GPa. The uniform elongation at fracture is 1.5-2.0%.

For CVD fibers, it was observed that fiber creep is anelastic (i.e. recoverable) and is a result of grain boundary sliding,[8] controlled mainly by a small amount of free silicon in the grain boundary. Fiber creep activation energy of 480 kJ $mole^{-1}$ was concluded to be similar to sintered SiC material, and the resulting creep rate is about an order of magnitude greater than the Nicalon fibers.[8] The lower creep resistance of the more commercial Nicalon fibers was attributed to the lower grain boundary (GB) viscosity of free Si, which results from the polymerization process. Diffusional creep by GB sliding has an activation energy estimated at 611 kJ $mole^{-1}$ and a pre-exponential of 3.1×10^{-7} m^2 s^{-1}.[Ref.9]

These observations indicate that high-temperature creep properties of the composite may be life-limiting in fusion. In particular, the crack bridging mechanism, which is the main feature for enhancement of the composite's toughness, will have to be critically examined since the bridging fibers may creep at a faster rate than the matrix itself.

The high-temperature deformation characteristics of hot-pressed SiC have been experimentally investigated and may be taken as indicative of the matrix in a composite.[8,9] The activation energies for power law as well as lattice diffusion creep were found to be about 912 kJ $mole^{-1}$.[Ref.9] Transition from power law creep at high stresses to diffusional creep at low stresses was also observed.[10] However, the diffusional matrix creep rates were found to be very small. A power law index of 5 was found to be similar to that of pure Si. The mechanical properties of unirradiated reaction sintered SiC (i.e., Young's modulus, E (GPa), and bend strength, σ_f (MPa)) as

functions of temperature, T (°C), are also given by polynomial fits, with coefficients defined in Table 4.5.3-1. Graphical representation is shown in Figure 4.5.3-2.

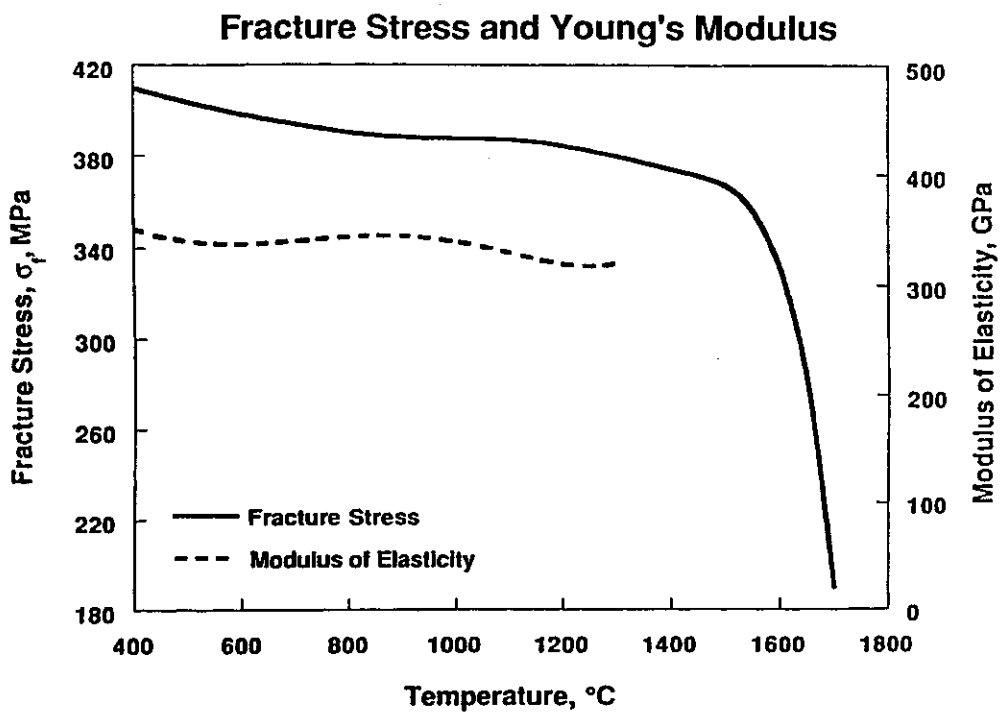

Figure 4.5.3-2. Temperature Dependence of the Fracture Stress and Young's Modulus of SiC

The critical stress intensity factor of the SiC matrix is expected to be low, as compared to metallic alloys. However, the bridging of cracks with the strong fibers will possibly allow for higher values of an apparent K_{IC}, especially when one is concerned about catastrophic through cracks. Room temperature values of K_{IC} for an unbridged hot pressed SiC range from 2.6 to 5.7 $MN.M^{-3/2}$ and is independent of temperature up to 1000°C. Sintered SiC shows temperature-independent K_{IC} of about 3 $MN.M^{-3/2}$ up to 1500°C.

An allowable design stress for SiC FRC's will depend on a wide range of manufacturing and operational factors. For example, recent fracture test results at PNL at 800°C on SiC FRM's from several vendors showed them to have strengths in the range 300-600 MPa in the unirradiated condition. Neutron irradiation at the same temperature, and up to approximately 10 dpa, showed that the fracture strength declined by about a factor of 2–2.5.[11] It is possible then, with modest technology extrapolation, that low pressure FW/B components would be designed to operate reliably in a fusion environment.

4.5.3.2 Coolant Compatibility – SiC has excellent resistance to oxidation up to 1000°C, because of the formation of a protective stable SiO_2 layer. Rapid oxidation may occur, however, depending on the physical state of the oxide layer between 100°C and 1300°C. The porous oxide layer offers no resistance to the diffusion of oxygen to react with the SiC forming volatile Si and C oxides. The stability of the SiO_2 layer is dependent on the O_2 partial pressure, being unstable at pressures lower than 10^{-10} to 10^{-8} atmospheres.[12] In a primary helium loop, the partial pressure of O_2 is expected to exceed these values. However, the reaction of the interfacial layer between the fibers and the matrix with oxygen will ultimately determine the upper usable temperature of the composite, as far as compatibility is concerned. At present, this layer is either C, BC_4, or BN. While carbon oxidation will severely limit the upper temperature, the production of He and H from nuclear reactions in B compounds is expected to degrade the strength of SiC FRC's. An important factor which needs yet to be studied is the possible reduction of the passive SiO_2 layer by tritium or hydrogen.

Compatibility studies of SiC in molten Li indicated that intergranular penetration degrades its fracture strength.[13] Reaction with the glassy phase at the GB is thought to be the cause of this rapid penetration. In a molten lithium environment, the uniform corrosion rate was reported to be extensive.[13] However, the reported data was obtained at O_2 activities thought to be much higher than anticipated in a typical Li loop of a fusion reactor.[11]

4.5.3.3 Radiation Effects – The strong directional bonding and the mass difference between Si and C atoms render the crystalline form of β-SiC exceptional radiation resistance characteristics. Recent Molecular Dynamics (MD) studies[14] show that Replacement Collision Sequences (RCS's) are improbable, and that the displacement of C atoms is much easier than Si. MD computer simulations[14] show that while the average threshold displacement energy (E_d) is 15 eV for C, it is about 90 eV for Si. This result would directly lead to the conclusion that the stoichiometry of the displacement cascade will differ substantially from that of the matrix. It is also observed that energetic Si PKA's displace multiple C atoms which end up on <111> planes. Thus, C-rich interstitial dislocation loops will tend to form on <111> planes. Experimental observations at temperatures below 1000°C tend to corroborate this conclusion.[15] Vacancies and He atoms exhibit considerable mobility above 1000°C. These fundamental considerations may explain some of the observed features of SiC dimensional changes as a function of temperature and fluence.[15-18]

The ease by which C atoms can be displaced, as compared to Si, would indicate that C-rich interstitial loops may tend to be prevalent as a result of irradiation. Energetic Si atoms traveling the <111> gap induce simultaneous displacements of multiple C atoms on {111} planes. Price[15] observed Frank-type loops on {111} planes which may be C-rich. Below 1000°C, point defects tend to form loops on {111} planes and swelling is therefore expected to saturate. For example, Harrison and Correli[19] observed large loops (10-200 nm) in RB-SiC after neutron irradiation to a fluence of

1.8×10^{23} cm^{-2}. At temperatures above 1000°C, cavities form and swelling does not saturate. The presence of helium results in further increases in the swelling rate by the known gas-driven swelling mechanism, as observed in the swelling of nuclear fuels. Swelling data with helium generation are scarce and need future considerations. Swelling of β-SiC in the temperature range 625-1500°C and at a neutron fluence (E > 0.18 MeV) of 1.2×10^{22} [Ref.15] is represented by two separate polynomials, with two different sets of coefficients below and above 1000°C, respectively. The coefficients and the general swelling behavior as a function of temperature is shown in Figure 4.5.3-3. Additional helium will drive swelling to higher values, particularly at temperatures above 1200°C.[20]

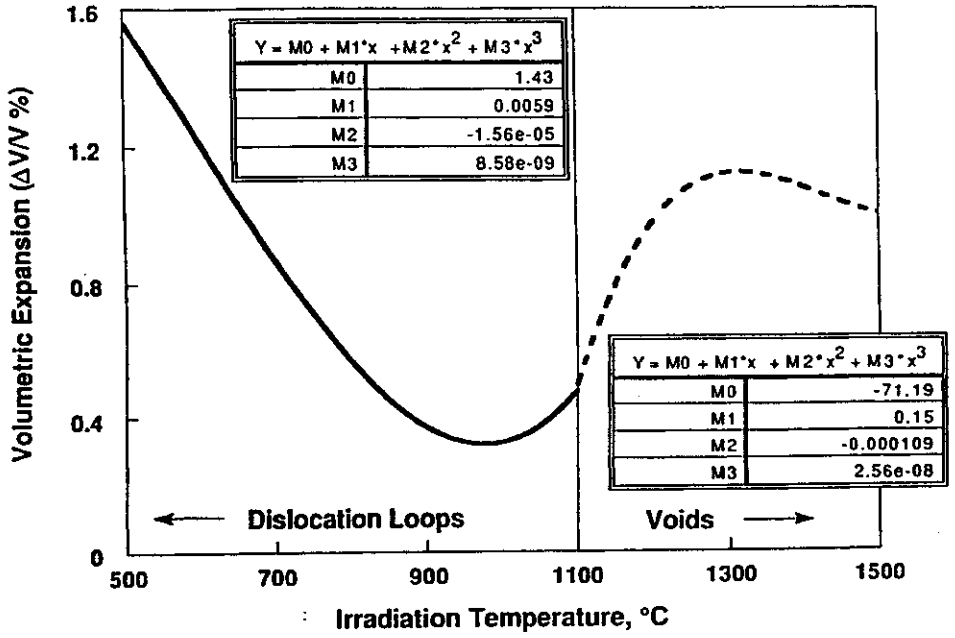

Figure 4.5.3-3. Volumetric Swelling of SiC as a Function of Temperature at a Neutron Fluence of 1.2×10^{22} n cm^{-2} (E>0.18 MeV)

A significant irradiation damage problem which results in the deterioration of the mechanical properties of SiC is the crystalline-to-amorphous phase transition phenomenon. For example, the strength of Nicalon fibers is degraded by irradiation-induced re-crystallization. Crystallites growing out of the fibers into the matrix form nucleation sites for cracks leading to delamination of the interface. The limited accumulated evidence from radiation effects data indicate that the upper temperature limit for use of SiC in structural design is in the range of 900-1000°C.

4.5.4 Design With SiC/SiC Composites – Design rules for SiC/SiC composites in the high-temperature and radiation environment of fusion reactors are obviously not established, mainly because the test data base is not complete. This data base for mechanical properties must also be made on full-size components. It is interesting to note that the fracture behavior of the composite is totally different from monolithic

behavior, and exhibits considerable apparent ductility, as shown in Figure 4.5.4-1. However, this increased toughness is caused by the dissipation of the elastic energy in slow micro-cracking processes. Failure stresses will have to be determined for particular applications (e.g. load bearing but not leak-tight components, leak-tight components, components which resist thermal stresses, etc.). A promising failure approach would be to use an interactive theory, such as the Tsa-Wu criterion. In such an approach, the failure stress tensor is measured. This would give failure stress

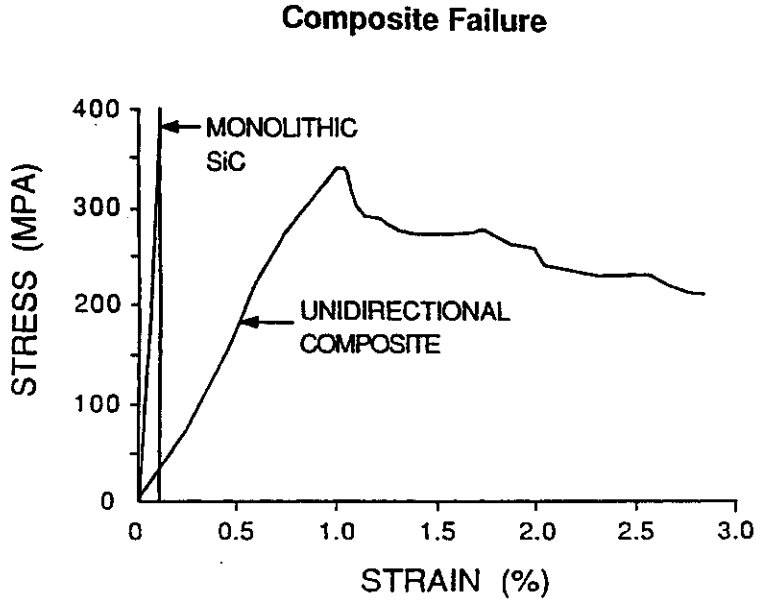

Figure 4.5.4-1. Stress-Strain Behavior of Monolithic and Unidirectional Composite SiC at Room Temperature

components in tension, compression, and shear, for both in-plane and out-of-plane components. Structural analysis would be fairly complete and would result in the definition of safety factors in each direction. This approach would take into account the probabilistic variability of properties, as determined by experimental measurements. There will be no need to use Weibull statistical analysis because safety factors and the experimental failure tensor would guarantee safe operation, as desired, from a particular component.

4.5.5 Selection Rationale – SiC/SiC FRC's are excellent, low-activation, safe structural materials for the high-temperature and radiation environment in commercial fusion reactors. Their superior mechanical and physical properties would allow for operational temperatures approaching 900–1000°C, thus achieving high thermal cycle efficiencies. The strong covalent bond between Si and C results in promising resistance to the damaging effects of neutron irradiation. Increased toughness because of the reinforcement with strong fibers will make deterministic design

approaches possible. However, considerable research and development will be needed before the material will be able to meet its promise.

References for Section 4.5

1. S. Yajima, K. Okamura, J. Hayashi and M. Omori, J. Amer. Ceram. Soc., 59 (1976) 324.
2. E. Fitzer, D. Kehr, and M. Shahibkar, in: Silicon Carbide-1973, Marshal, Faust and Ryan, Eds. (Univ. of South Carolina Press, USA, 1974) p33.
3. H. E. DeBolt, V. J. Krukonis, and F. E. Wawne, in: ibid., p.168.
4. I. B. Cutler, "Production of SiC from Rice Hulls," U.S. Patent # 3,754,076, 1976.
5. G. Hurtley and J. Petrovic, in: Proc. Adv. Composites Conf., M. W. Liedtke and W. H. Todd, Eds., ASM, 1985, p.401.
6. S. Yajima, H. Kayaro, K. Okamura, M. Omori, J. Hayashi, T. Matsuzwa, and K. Akutsu, Am. Chem. Soc. Bull., 55 (1976) 1065.
7. I. Ahmad, D. N. Hill, and W. Hefferman, in: Proc. Inter. Conf. Comp. Mater., AIME, 1976, vol 1, p. 85.
8. J. Decarlo, J. Mater. Sci., 21 (1986) 217.
9. P.M. Sargent and M. F. Ashby, Scripta Met., 17 (1983) 951.
10. A. Djemel, J. Cadoz and J. Philibert , in: Creep and Fracture of Engineering materials and Structures, B. Wilshire and D. R. J. Owen, Eds., Pineridge, Swansea, U.K., 1981, p. 381.
11. R. H. Jones, in: Fusion Reactor Materials Semiannual Progress Report, March 1991, DOE/ER-0313/10, p. 215.
12. E. A Gulbransen and S. A. Jansson, Oxid. Met., 4 (1972) 181.
13. D. R. Curran and M. F. Amateau, Amer. Cer. Soc. Bull., 65 (1986) 1419.
14. A. Elazab and N. M. Ghoniem, ICFRM-5.
15. R. J. Price, J. Nucl. Mater., 46(1973)268.
16. R. Blackstone and E. H. Voice, J. Nucl. Mater. 39(1971)319.
17. A. M. Carey, F. J. Pineau, C. W. Lee, and J. C. Corelli, J. Nucl. Mater., 103&104(1981)789.
18. K. Hojou and K. Izui, J. Nucl. Mater., 160(1988)334.
19. S. D. Harrison and J. C. Corelli, J. Nucl. Mater., 122&123(1984)833.
20. T. Suzuki and T. Iseki, J. Nucl. Mater., 170(1990)113.

4.6 Target Selection

Given that laser and heavy ions can be built to deliver MJ of pulses onto small foci, a key element in an inertial fusion energy (IFE) reactor is the design of the DT target. The IFE driver designs are dictated, in large part, by the target configuration as well as the requirements set forth by the target designers for achieving a uniform DT target implosion. Depending upon the stringency of DT target irradiation requirements in terms of uniformity of illumination (in the case of the laser driver) or in the beam diameters on target (in the case of the heavy ion driver), the requirements placed on the drivers may be sufficiently demanding that the resulting driver costs would be unaffordable. Thus it is of vital importance that the target irradiation requirements for both Prometheus-L and Prometheus-H be well understood. The following section describes the types of DT targets and target irradiation requirements currently being considered for both laser-driven and heavy ion-driven IFE reactors.

4.6.1 Laser Driver Target - The Target Working Group (TWG) has provided the study team with prescriptions for target illumination for both direct and indirect laser-driven targets.[1] At the present time, owing to the higher target gain, we selected the direct-drive IFE laser target was selected as the baseline. Therefore efforts were concentrated on the direct-drive laser target illumination problem. A schematic of this target is shown in Figure 4.6.1-1.

The direct-drive laser target consists of a polystyrene shell surrounding a layer of DT ice and a central region of DT vapor. As an example, for a driver energy of 1.6 MJ, the radius of such a target would be 0.2 cm.

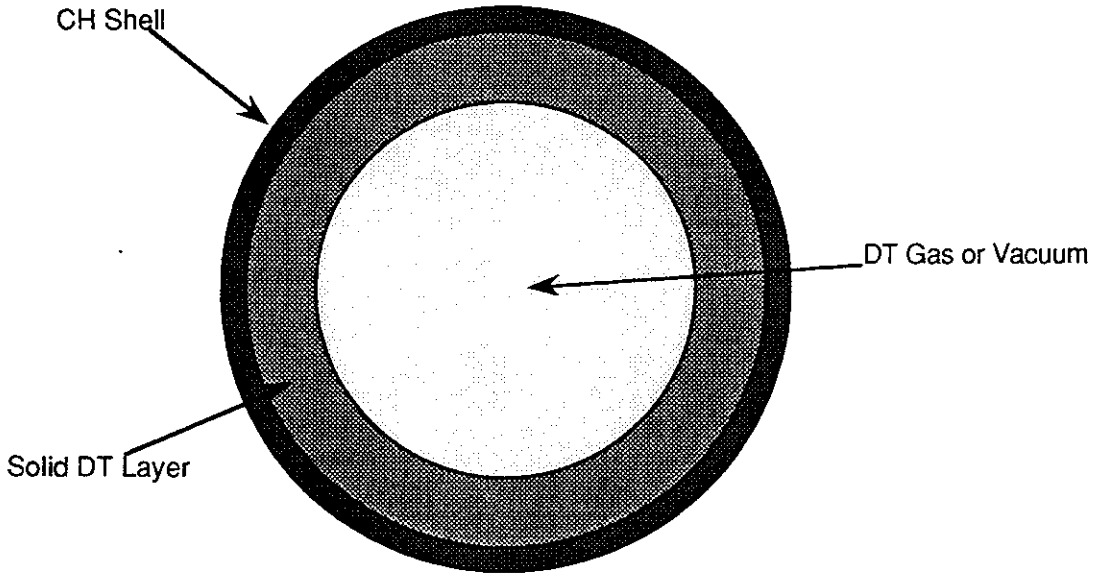

Figure 4.6.1-1 Schematic of Laser Direct-Drive IFE Target Structure.

In addition to the direct drive targets, the team also examined the indirect-drive laser IFE targets. It was assumed the fuel containing pellet or capsule of indirect-drive laser targets would be similar to the DD design. No further information on the geometry of laser indirect drive targets was supplied. As most of the information on these targets is classified, it is difficult to fill in the details needed to arrive at developing credible indirect-drive target illumination schemes. In considering the laser IFE indirect-drive (ID) target further, it was necessary to make a number of assumptions regarding ID laser targets based on the scant details available in the open literature. Additional details regarding these laser ID IFE target considerations can be found in Section 6.5.

A laser driver energy of 4 MJ was selected for reasons outlined in Sections 4.2 and 6.2. Mass scaling data was used to estimate that a target similar to that illustrated in Figure 4.6.1-1 scaled to a driver energy of 4 MJ would contain ~6.5 mg of DT and 16.5 mg of CH. This was used as the base target for the Prometheus-L design study. The possibility of adding thin layers of various materials to the basic DD target structure to act as permeation barriers, shine shields, etc., was also considered. However, with the possible exception of target alignment requirements, such additions were found to be unnecessary for the point design chosen. Therefore, the basic design shown in Figure 4.6.1-1 was used without modification.

Following the completion of the Prometheus-L laser driver design, a number of questions have emerged regarding the direct-drive target illumination requirements set forth by the TWG. Thus, when the requirements set forth by the TWG for direct-drive target illumination are compared with some of the known considerations applying to the laser beam illumination physics and the physics of light/plasma interaction, some serious questions arise regarding some of the TWG direct-drive target illumination requirements.[2] Facts and known requirements associated with the TWG guidelines, the laser driver, and target coupling physics are briefly summarized below.

4.6.1.1 Optimized Target Interactions - By considering the impacts of the TWG direct-drive target illumination requirements with the newly defined capabilities of the Prometheus-L laser driver and the known physics requirements of laser light/plasma interactions, it should be possible to optimize the laser/target coupling interaction significantly. This laser/target interaction optimization may result in a significant reduction in the laser energy required to reach a given DT target gain. The TWG has already specified that implementation of a "zoom" optical system which follows the imploding surface of critical density could guarantee an increase in target coupling efficiency of a factor of at least two.

Each of these three areas of discussion is briefly described below:

4.6.1.2 TWG's Direct-Drive Target Illumination Requirements - The TWG direct-drive target irradiation scenario includes the following elements:

(1) There will be at least 60 laser beams incident on the target.
(2) The target will be illuminated uniformly such that the intensity variation anywhere on the spherical surface will not vary more than ±1%.
(3) λ_{laser} ~ 250 nm, increasing the importance of Bremsstrahlung absorption over resonant absorption.
(4) The pulse duration of the main pulse will be approximately 6 ns with an approximately 60 ns lower intensity precursor "foot"; all beams must produce similar pulse shapes such that the uniformity requirement (2) is met.
(5) The laser beam size on the target will be equal to the target diameter.
(6) The spherical direct drive DT target will be approximately 0.6 cm in diameter.
(7) During the course of the laser pulse, the critical surface of the target will shrink to a diameter ~0.3 cm.
(8) The spatial intensity distribution of each laser beam incident on the target shall approximate $I(\theta) \sim (\sin \theta/\theta)^2$.

The penalty associated with failing to meet target illumination requirements is poor or no target yield.

4.6.1.3 Laser Driver Requirements/Characteristics - In addition to the preceding eight requirements set forth by the TWG, there are a number of requirements and/or characteristics of the laser driver and its associated optics which need to be taken into consideration.

(1) Excimer laser amplifiers produce optical beams having square cross-sections.
(2) Square laser beams map efficiently onto spherical surfaces only if the dimensions of the squares are significantly smaller than the sphere radius.
(3) The degree of trapezoidal apodization and the requirements for an efficient laser amplifier fill factor can be traded off to yield an optimum value.
(4) Optical elements cost least when sized according to an optimum aperture; optical vendors can be geared up to produce square (or rectangular) optics.
(5) Large aperture optics can be synthesized from an array of square (or rectangular) subelements using optimized aperture sizes.
(6) Trapezoidal (or pyramidal) laser beam apodization can reduce angular pointing requirements for the array mirrors.
(7) For a final focusing mirror focal length, f_m, of 40 m and an effective aperture, D_m, of 1 m, the f/number of the focusing optics is relatively large (~40).
(8) Automatic "zooming" of the optical system on the collapsing surface of critical density occurs when the foci of each of the 60 mirrors are located at the center

of the target. (This arrangement is impractical in the present case[2] since it would require a prohibitive number of beamlines.)

(9) For constant beam quality and laser wavelength, the far field focal spot size depends only on the f/number of the final focusing mirror; in the present case, the focal diameter for each laser beam is estimated to lie between 10 and 15 microns (assuming an f/40 system and λ = 248 nm).

(10) Research has been performed on high power optical techniques for generating negative non-linear refractive indices, thereby making possible (in principle) automatic "zooming" optical systems for high power lasers.

(11) The surface of the 0.6 cm diameter target sphere lies in the near field of each of the 60 laser beams, thereby permitting beams of predetermined shape and apodization to be placed on the target's critical surface (typically, laser beams do not follow spatial intensity profiles ~ $(\sin \theta/\theta)^2$ [this is a far-field diffraction intensity profile]).

(12) Although a variety of laser beam cross-sectional shapes and apodizations are possible, square beams with trapezoidal apodizations appear to be an optimum choice for efficiently placing a homogeneous intensity distribution on the spherical target surface.

(13) Even with careful computer control of the laser amplifier power conditioning, it will take strenuous efforts to achieve the ±1% target illumination homogeneity requirements set forth by the TWG.

The penalties for not heeding the physics of laser drivers are low efficiency, high driver cost, impaired performance, and difficult alignment problems.

4.6.1.4 Laser/Plasma Interaction Physics Requirements - The following observations regarding laser/plasma interactions can be made:

(1) The primary mechanism for coupling UV laser light into an imploding plasma having densities at or greater than the critical density is inverse Bremsstrahlung.

(2) Resonance absorption can also play a role, especially for large angles of incidence. In the case of linearly polarized laser light, resonance absorption is concentrated in two lobes aligned along the polarization vector.[3]

(3) Laser light interacts weakly with plasma below the critical density with the primarily effects being SBS, SRS, and refraction of the incident laser light.

(4) Laser light cannot propagate through plasmas having densities greater than critical density.

(5) Planar target interaction experiments have shown that the inverse Bremsstrahlung absorption depends upon the fifth power[3] of the cosine of the angle of incidence, q (where the angle of incidence is the angle between the

Poynting vector and the normal to the critical surface) for linear plasma density profiles and on the $(\cos\theta)^3$ for exponential plasma density profiles.

(6) Rayleigh-Taylor (RT) instabilities are driven primarily by laser beam intensity inhomogeneities occurring at the beginning of an implosion.

(7) Higher-order RT instabilities are more serious than low-order instabilities.

(8) Laser intensities above 10^{15} W/cm^2 tend to produce undesirable nonlinear optical effects in the plasma atmosphere (including stimulated Raman scattering, stimulated Brillouin scattering, harmonic generation at $\omega^{3/2}$, etc.).

(9) Resonance absorption (RA) depends upon the polarization vectors of each of the laser beams, which means that RA can spoil the homogeneity of target illumination even if the intensity is homogeneous. The TWG did not address the polarization issue.

The penalties associated with ignoring these plasma physics issues are inefficient light/plasma coupling, low target yield, and impaired system performance.

4.6.1.5 Global IFE Implications of Conflicting Requirements - The implications of this brief review of characteristics and requirements for the TWG direct-drive target prescription, the current laser driver design, and the physics of laser/plasma interactions are that significant improvements in IFE performance may be attained if careful tradeoffs are made to find optimum solutions which simultaneously satisfy all the requirements. This, then, is the purpose in examining these issues at this time so that unnecessary or inappropriate requirements which may actually impair IFE performance can be identified and, if possible, altered to permit a more optimum design to be generated.

4.6.1.6 Possible Conflicts Among the TWG Requirements: IB vs. RA - The two principal laser/plasma absorption mechanisms are inverse Bremsstrahlung (IB) and resonant absorption (RA). The TWG requirements that the direct-drive target be homogeneously (±1%) illuminated with ~60 randomly polarized laser beams equal to the diameter of the target may produce significant laser beam/plasma coupling inefficiencies and absorption non-uniformity. The most efficient excimer laser beam cross-section is rectangular, a shape which couples inefficiently onto a sphere unless the laser spot size is significantly smaller than the radius of the sphere. Furthermore, for full sphere illumination, most of the laser beam power will be incident on the critical surface of the target at incidence angles, θ_o, greater than 45° (when inverse Bremsstrahlung absorption[3] is proportional to $[\cos\theta_o]^5$) and additional laser/plasma coupling inhomogeneities due to resonant absorption may result. These problems are explored in detail below.

4.6.1.7 Calculation of Laser/Plasma Tangential Coupling Efficiencies for IB and RA - In general, calculations of laser/plasma coupling efficiency are extremely involved even when performed using magneto-hydrodynamics computer codes (i.e., LASNEX) on large machines. However, some simple considerations which can be performed on microcomputers are in order here. The first case considered is that of the specified target illumination scenario in which the incident laser beams are of dimensions equal to the diameter of the DT target. This scenario corresponds to the target illumination guideline furnished by the TWG. Both IB and RA calculations will be made. Resonant absorption (RA) depends approximately on $(\cos \theta_0)^2$, whereas for inverse Bremsstrahlung the absorption is proportional to $(\cos \theta_0)^5$ for linear plasma density gradients and proportional to $(\cos \theta_0)^3$ for exponential density gradients. The RA absorption also depends upon the polarization state of the absorbed laser light, and, in general, the RA absorption is a complex, two-lobed spatial function. Each of these two major light/plasma absorption mechanisms will be discussed below.

First, a specification is required for the laser pulse temporal format delivered in 60 beams to the direct-drive target in order to generate the target implosion scenario. An approximate sketch of each of the 60 laser beam pulses as specified by the TWG is shown below in Figure 4.6.1-2.

As indicated in Figure 4.6.1-2, the prepulse "ramp" precedes the main laser pulse in order to ablate a dilute plasma from the direct-drive DT target and form a critically-dense surface in preparation for arrival of the main pulse(s). At the end of the prepulse "ramp," the target is nominally still 0.6 cm in diameter, although the extent of the dilute plasma atmosphere ablated from the target is contained within a sphere of radius, R_a, given by the expression:

$$R_a = R_o + v_{plasma}\, \tau_{ramp} \qquad (4.6.1\text{-}1)$$

where $R_o \sim 0.3$ cm is the initial radius of the DT target, and where $v_{plasma} \sim 4 \times 10^7$ cm/sec according to measurements made by Auerbach[4], et al. For $\tau_{ramp} \sim 60$ ns, $R_a \sim 2.7$ cm. The primary linear effect of this spherical atmosphere of dilute plasma would be to refract the incident laser light slightly in such a manner that the converging beam would focus more quickly, but at a point well beyond the target. The tangential target illumination geometry which occurs at the beginning of the main laser pulse is shown in Figure 4.6.1-3.

It is presumed that the dilute plasma atmosphere surrounding the target only produces a slight focusing of the incident rays. As discussed below, however, the nonlinear effects (stimulated Brillouin scattering, stimulated Raman scattering) can produce a significant number of hot electrons which can lead to target preheat.

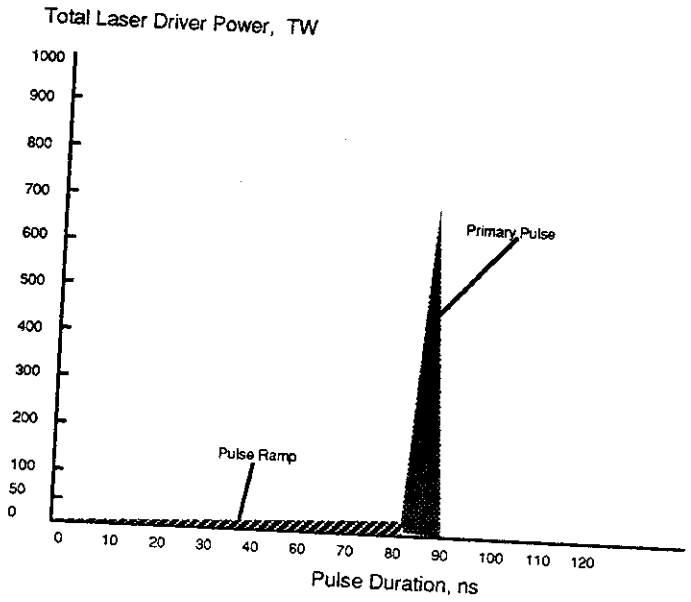

Figure 4.6.1-2 The Laser Pulse Features a 80 ns Prepulse Containing 30% of the Energy

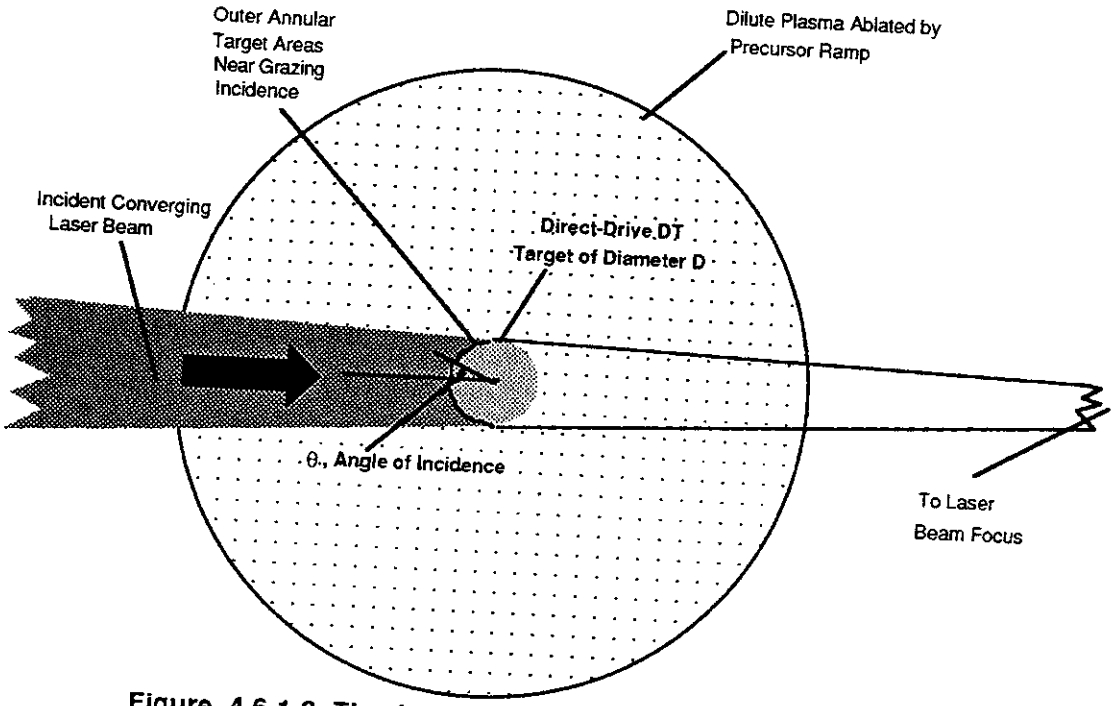

Figure 4.6.1-3 The Laser Prepulse Ablates a Dilute Plasma Atmosphere 3.2 cm Deep from the Target

Inverse Bremsstrahlung Absorption - It is apparent from Figure 4.6.1-3 that most of the incident laser power will be incident on the target critical surface at angles greater than 45°. Numerous well-characterized, laser-induced plasma experiments have been conducted on planar targets for which the angle of incidence, θ_o, was well known. An expression[3] for the fractional absorption, f_{ib}, as a function of θ_o due to inverse Bremsstrahlung for a plasma is:

$$f_{ib} = \left(\frac{16\nu}{15\omega}\right) \kappa\Delta R \cos^5\theta_o \qquad (4.6.1\text{-}2)$$

where the ratio ν/ω is evaluated at the critical density. Since the focal ratio of the laser driver is ~f/40 to first order, the incident laser beams can be regarded as plane waves. Simple laser/plasma absorption calculations have been carried out using Eq. 4.6.1-2 for λ = 248 nm, assuming a "top-hat" beam intensity profile apodization and that the $f_{ib}(\theta_o = 0) \sim 1$ on the surface of critical density. The results are shown below in Figure 4.6.1-4 for a time immediately prior to the target implosion.

Although these calculations were carried out using a larger laser amplifier fill factor than the $(\sin\theta)^2/\theta^2$ apodization assumed by the TWG, efficient extraction from excimer laser amplifiers (and the Raman accumulators) would involve the use of high efficiency apodizations and not be limited by far field diffraction profiles such as $(\sin x)^2/x^2$. Using the top-hat apodization and assuming that the laser beam spot sizes are equal to 0.6 cm, then the laser energy is absorbed by the target as a function of the target diameter and angle of incidence. This relationship is shown in Figure 4.6.1-5.

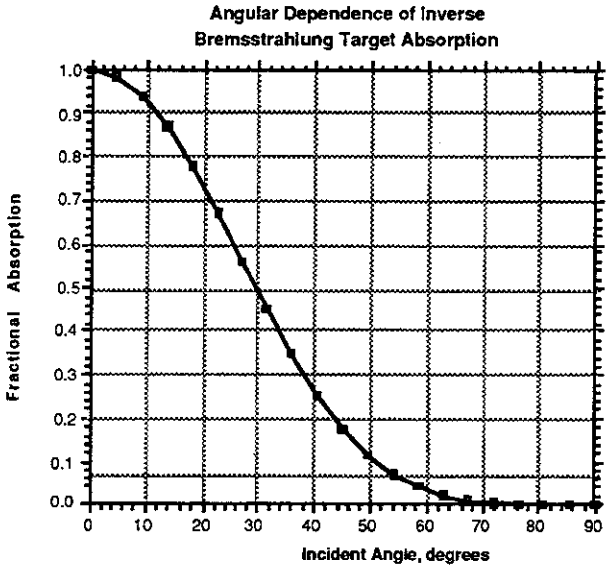

Figure 4.6.1-4. The Laser/Plasma Inverse Bremsstrahlung Absorption Fraction Depends on the Incident Angle, θ_o

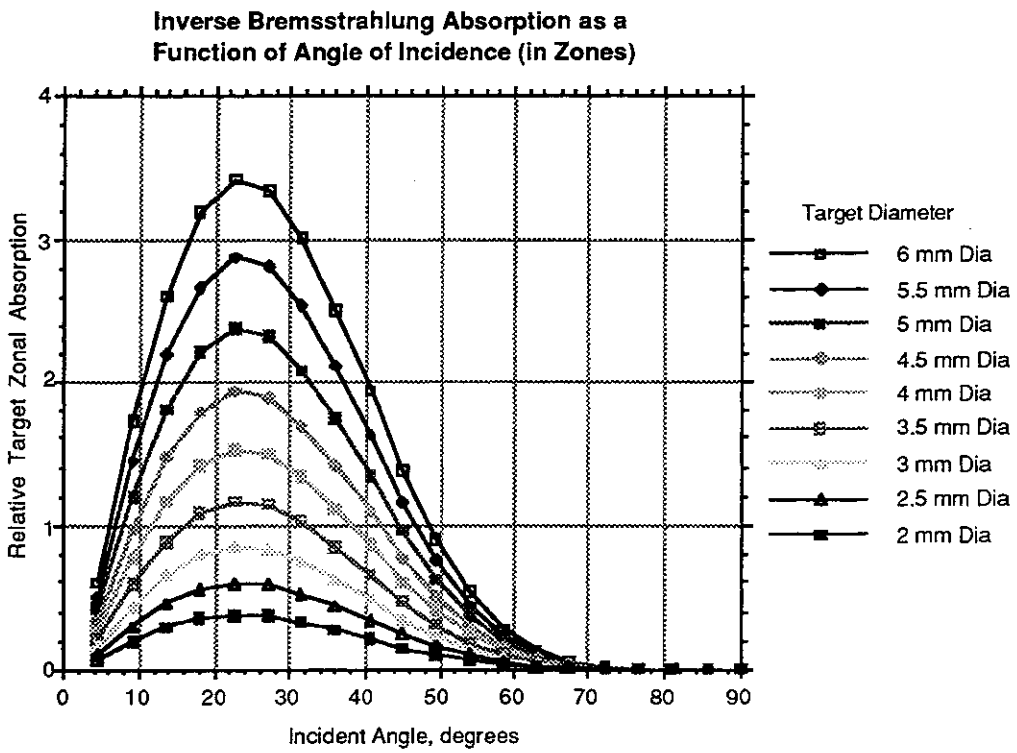

Figure 4.6.1-5. The Inverse Bremsstrahlung Energy Absorbed by Direct-Drive Targets Depend on the Incident Angle and Target Diameter (6 mm diameter spot size, 100 kJ beam, 6 ns pulse duration, top-hat apodization)

The initial amounts of absorbed laser energy are small in Figure 4.6.1-5 since the areas of the annular apertures are reduced for small values of θ_o. The geometry used for conducting these calculations is shown below in Figure 4.6.1-6.

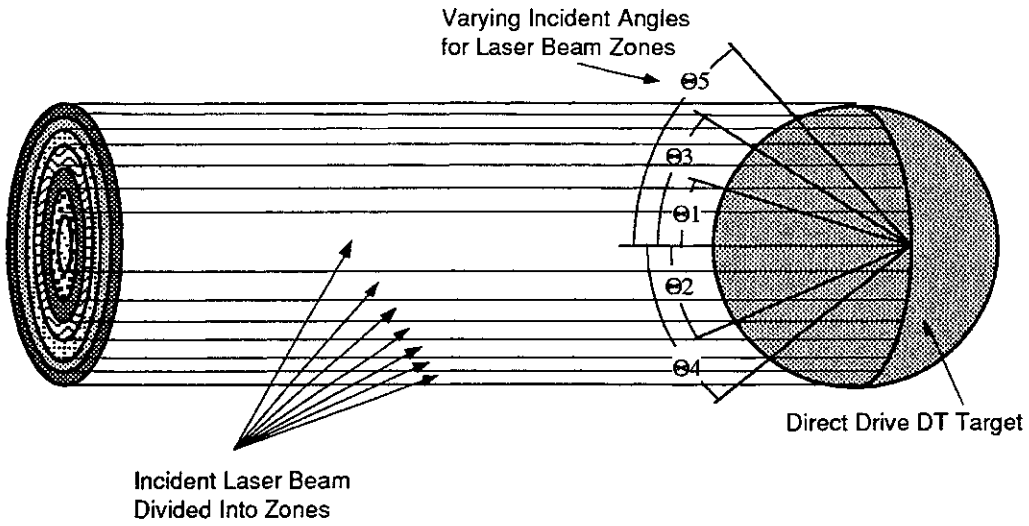

Figure 4.6.1-6 The Incident Laser Beam Can Be Decomposed Into Annular Zones to Calculate Absorption Efficiencies

The variation of the absorbed laser energy/beam for inverse *Bremsstrahlung* as a function of target diameter was calculated assuming that the diameter of the critical surface remains constant during the entire high power pulse duration (which was assumed to be a temporal top hat distribution as well) and the results are shown below in Figure 4.6.1-7.

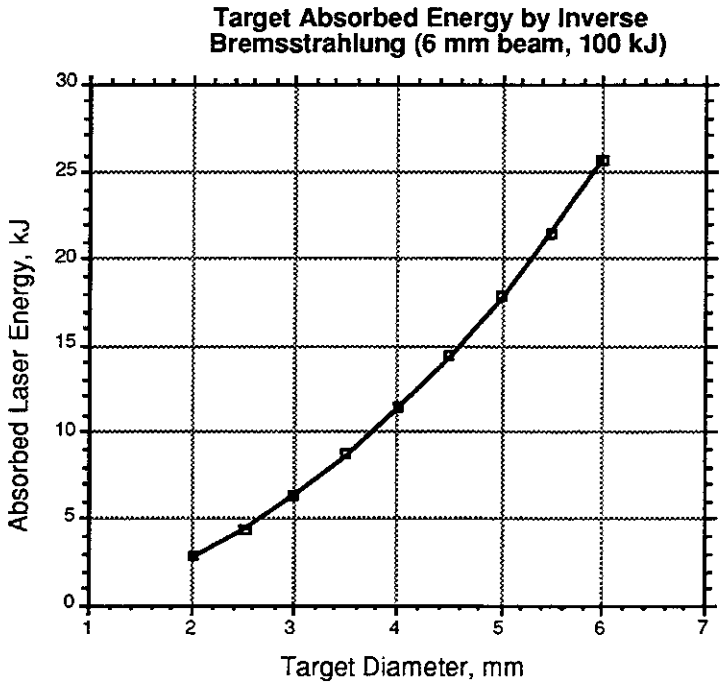

Figure 4.6.1-7 The Absorbed Laser Energy/Beam Depends on the Direct Drive Target Diameter for Inverse Bremsstrahlung (assuming 100 kJ/Beam and 6 mm diameter laser spot sizes) for Static Target Diameters

As indicated, when the critical density target diameter decreases to a value of R_T ~ 3 mm, the laser power couples only approximately 7% into the target. Although it was assumed that the radius of the target remained constant during the laser pulse in calculating the results for Figure 4.6.1-7, it is straightforward to estimate the energy absorbed by the target as it implodes. Thus if the rate of target implosion, dR_T/dt, is constant (here $dR_T/dt \sim 2.5 \times 10^7$ cm/sec) during the main portion of the laser pulse, then the total energy absorbed by the target is calculated from the expression:

$$E_{tot} = \frac{1}{N} \sum_{k=0}^{N} E_{abs}(R_k) \qquad (4.6.1\text{-}3)$$

where N is the number of iterations taken between $R_1 = 3$ mm and $R_N = 1.5$ mm. Taking the further approximation that the laser power is constant during the implosion of the target, then the energy absorbed by the target is calculated from Eq. 4.6.1-3 to be 15.2 kJ/beam line, or approximately 15% of the available laser energy. Much of the

laser light simply misses the critical surface of the target under these circumstances. This geometry is illustrated below in Figure 4.6.1-8.

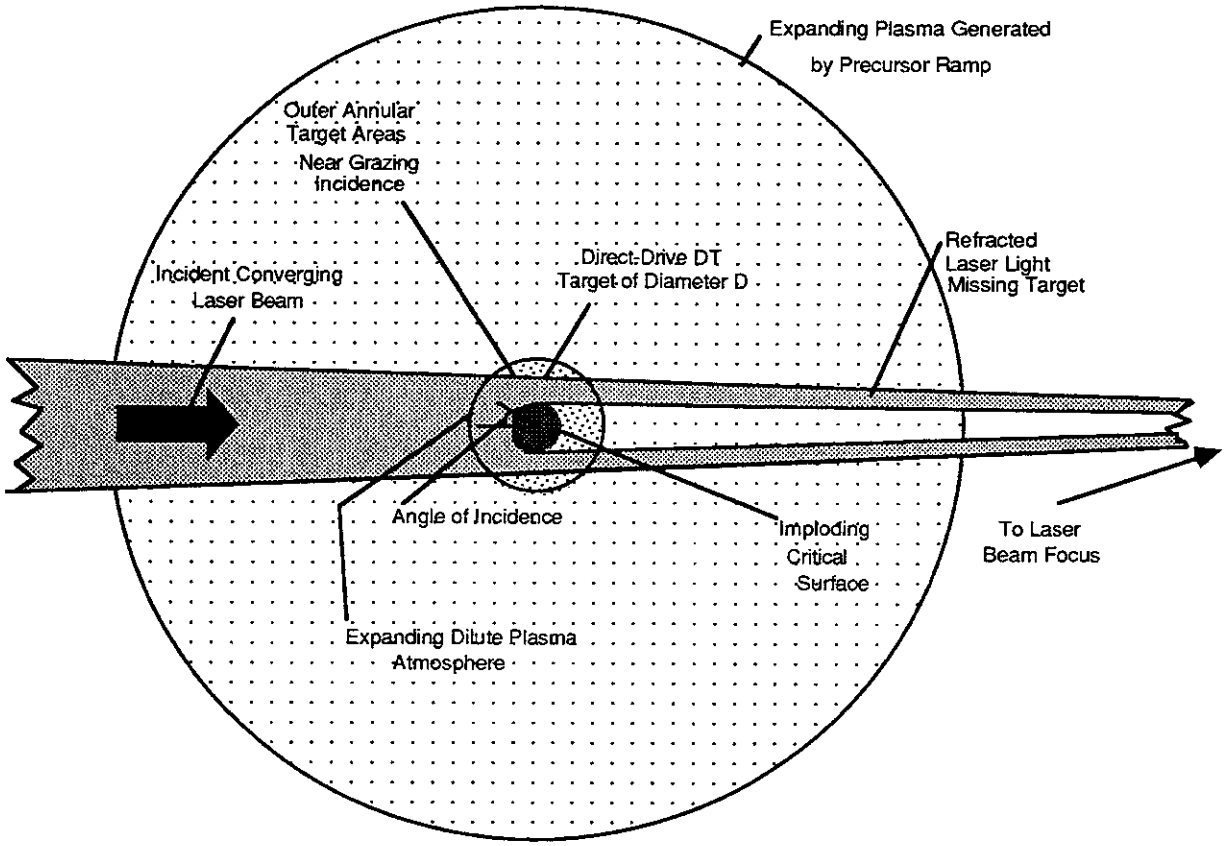

Figure 4.6.1-8. The Direct Drive Target Diameter Implodes to Half the Laser Beam Diameter by the End of the Main Laser Pulse

Resonance Absorption Calculations - The energy absorbed by resonant-driven fields in the plasma is described by the expression:[3]

$$E_{abs} = \int \frac{\upsilon(<E_r^* E_r>)}{8\pi} r^2 \, dr \, \sin\theta \, d\theta \, d\phi \qquad (4.6.1\text{-}4)$$

where E_r is the radial electric field of the laser beam. Near the critical density, the expression for E_r is given by:

$$E_r = \frac{\ell(\ell+1)}{(i\varepsilon k^2 r^2)} a_1 \left(\ell - \alpha_\ell^2\right)^{\frac{1}{4}} P_\ell^1(\cos\theta) \cos\phi \exp(i\delta) \frac{\Phi^2(\tau_1)}{2\pi\gamma\alpha_\ell^2} \qquad (4.6.1\text{-}5)$$

where a_l is given by the expression:

$$\alpha_\ell = \frac{\sqrt{\ell\,(\ell+1)}}{k\,R_c} \qquad (4.6.1\text{-}6)$$

(where R_c is the radius of the plasma critical density) and where $\Phi^2(\tau_l)$ is the absorption function for the lth mode. The fraction absorption of the lth mode, f_{RA}, is given by:

$$f_{RA} = \frac{\Phi^2(\tau_l)}{2\pi} \sqrt{1 - \alpha_l^2} \qquad (4.6.1\text{-}7)$$

so that the total power absorbed from the laser beam as a consequence of resonance absorption is given by:

$$P_{RA} = \sum_l \frac{P_l}{2\pi} \Phi^2(\tau_l) \sqrt{1 - \alpha_l^2} \qquad (4.6.1\text{-}8)$$

where P_l is the laser power in the lth mode.

The net result of performing the integral in Eq. 4.6.1-4 is to show that resonance absorption generally depends upon $(\cos \theta_o)^2$. Perhaps a more serious result of these analyses[3] is that the spatial absorption distribution function is not uniform over the target sphere. The calculated RA distribution for a vertically polarized laser beam is shown in Figure 4.6.1-9.

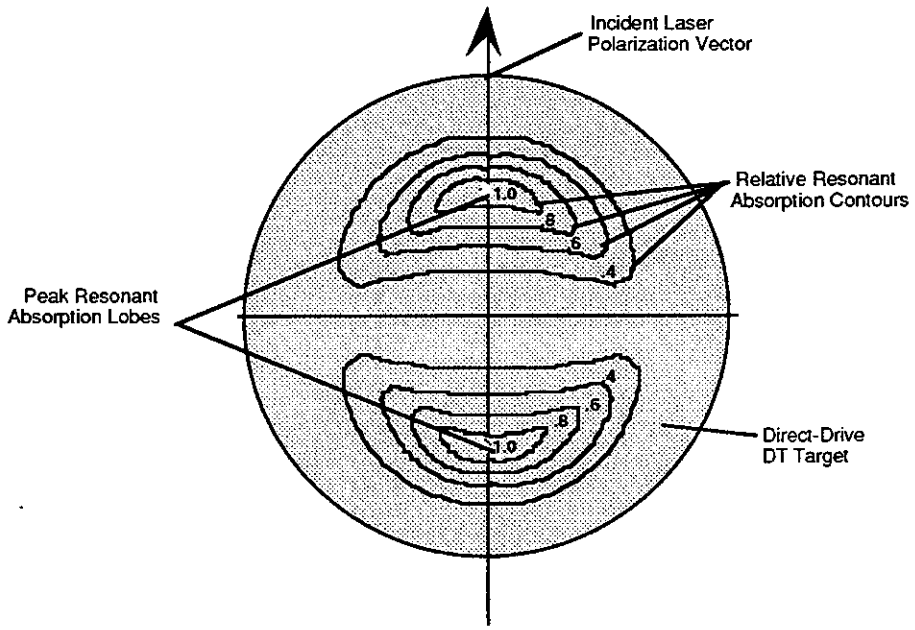

Figure 4.6.1-9. The Calculated Spatial Dependence of the Laser Power Absorbed by Resonance Absorption Is Not Homogeneous

As shown, resonance absorption is predicted to produce two symmetrical "hot spots" of absorption at mid-latitudes on the sphere when illuminated with linearly polarized light. This may constitute an absorption uniformity problem because this process occurs even when the sphere is uniformly illuminated. However, by using λ = 248 nm

laser radiation, the effects of resonance absorption are not expected to be reduced relative to inverse Bremsstrahlung.

Simple laser/plasma absorption calculations have been carried out using Eq. 4.6.1-7 and Eq. 4.6.1-8 for $\lambda = 248$ nm, assuming a "top-hat" beam intensity profile apodization and assuming that $f_{ra}(\theta_o = 0) \sim 1$ (and $f_{ra} = \xi\,[\cos\theta]^2$) on the surface of critical density. The results are shown below in Figure 4.6.1-10 for the case prior to the implosion.

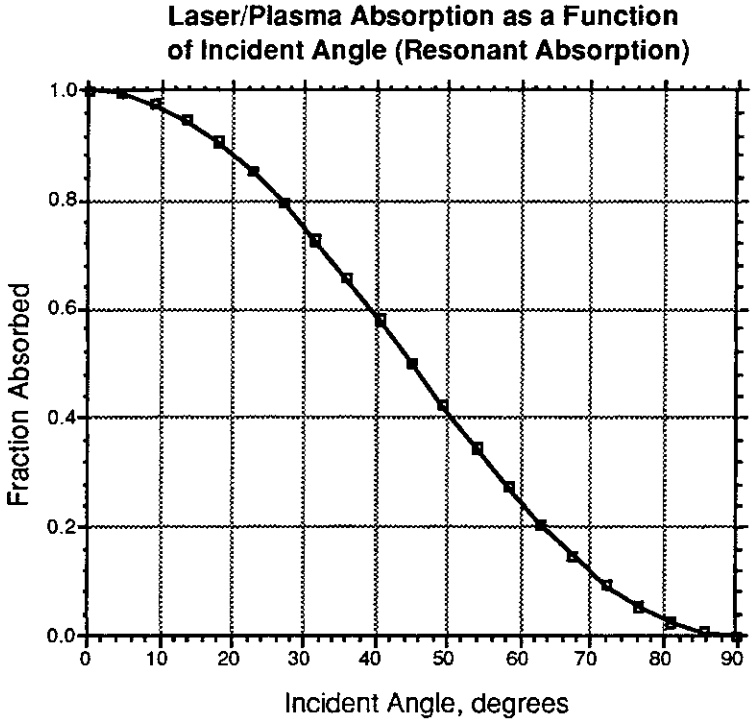

Figure 4.6.1-10. The Fraction of Laser Power Absorbed Via Laser/Plasma Resonance Absorption Is a Function of the Incident Angle, θ_o

As before, although these calculations were carried out using a "top-hat" intensity profile (i.e., a larger laser amplifier fill factor than the $(\sin x)^2/x^2$ apodization assumed by the TWG), efficient extraction from excimer laser amplifiers (and the Raman accumulators) would involve the use of such high efficiency apodizations. Using the top-hat apodization and assuming that the laser beam spot sizes are equal to 0.6 cm, then the laser energy absorbed by the target as a function of target diameter and angle of incidence is shown in Figure 4.6.1-11.

As calculated above for the inverse Bremsstrahlung case, the initial amounts of absorbed laser energy are small in Figure 4.6.1-11 since the areas of the annular apertures are reduced for small values of θ_o, in accordance with the calculation procedure illustrated in Figure 4.6.1-6.

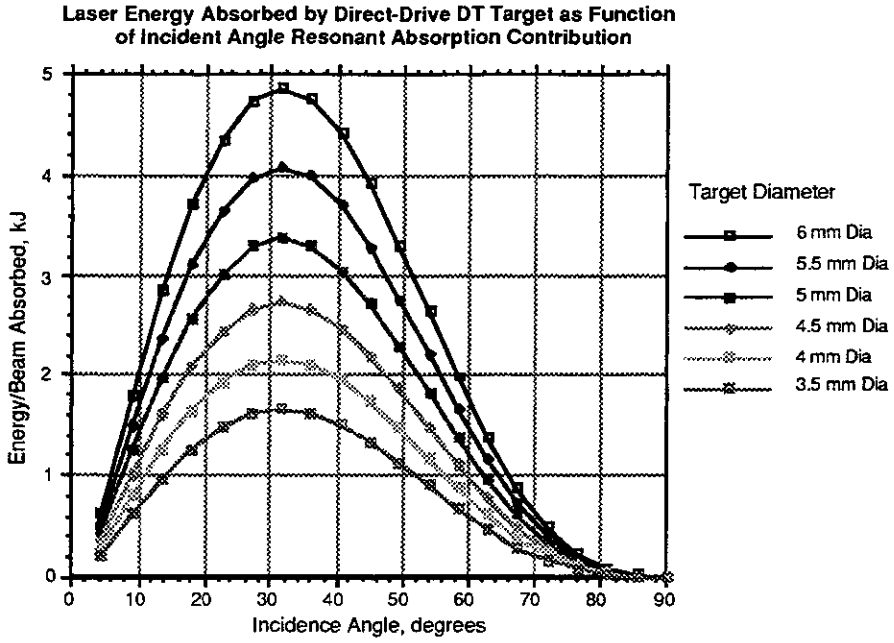

Figure 4.6.1-11. The Resonance Absorbed Energy for Direct-Drive Targets is a Function of Both Incident Angle and Target Diameter (6 mm diameter Spot Size, 100 kJ Beam, 6 ns Pulse Duration, Top-Hat Apodization)

Following in a manner similar to that for the IB case above, the variation of the absorbed laser energy/beam for inverse Bremsstrahlung as a function of target diameter was calculated assuming that the critical surface remains constant at a constant diameter during the delivery of the high power laser pulse (which was assumed to be a temporal top hat distribution as well) and the results are shown in Figure 4.6.1-12.

As indicated in Figure 4.6.1-12, when the critical density target diameter is reduced to $R_T \sim 3$ mm (with the laser beam diameter equal to 6 mm), the laser power couples only approximately 11% into the target. The target radius was held constant during the arrival of the laser pulse in calculating the results for Figure 4.6.1-7. It is straightforward to estimate the energy absorbed by the target as it implodes using Eq. 4.6.1-1 above; it is calculated that 27.7 kJ/beam would be absorbed by the target (assuming resonant absorption accounted for 100% of the laser/plasma target interaction) or approximately 28%, based on the approximations that $f_{RA}(\theta_o = 0) = 1$, and $f_{RA}(\theta_o) = \xi(\cos \theta_o)^2$.

In actual fact, resonance absorption is not the primarily laser/plasma absorption mechanism and, consequently, the fraction of laser light, ξ_{RA}, absorbed by the resonance absorption mechanism must be added to the fraction of laser light absorbed by inverse Bremsstrahlung, ξ_{RA}, to produce a total absorption, ξ_{tot}, given by

$$\xi_{tot} = \xi_{IB} + \xi_{RA} \qquad (4.6.1\text{-}9)$$

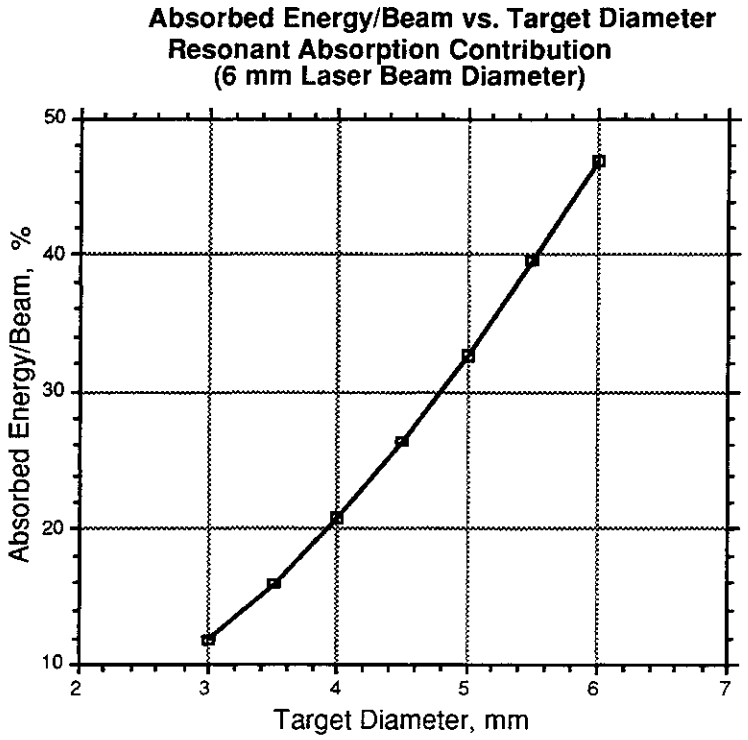

Figure 4.6.1-12. Estimated Absorbed Laser Energy/Beam vs. Direct Drive Target Diameter for Resonance Absorption (100 kJ/Beam, 6 mm Diameter Laser Beam) Assuming Constant Target Diameter

Comparison of the Target Absorption Results of IB and RA - As indicated above, simple incident angle-dependent calculations regarding resonant absorption have produced the results that only approximately 28% of incident laser light would be absorbed by a 6-mm diameter sphere that uniformly implodes to a diameter of 3 mm during the laser pulse. The previous result calculated for inverse Bremsstrahlung under the same circumstances produced a value of ξ_{IB} ~ 15%. If it is assumed that IB accounts for approximately two-thirds of the target absorption and RA the remaining one third, then the overall absorption efficiency of a tangentially-illuminated 6 mm DT direct-drive target would be approximately 20%. Thus, for a laser energy of 5 MJ delivered to the target, these rough estimates suggest that only 1 MJ would be coupled into the target!

4.6.1.8 Calculation of Laser/Plasma Nested Trapezoidal Beam Coupling Efficiency - In a similar manner, the coupling efficiency for a laser beam with a trapezoidal apodization focused down to an intermediate spot size, δ_{laser}, given approximately by the expression:

$$\delta = R_T \sqrt{\frac{4\pi}{N}} \qquad (4.6.1\text{-}10)$$

where, as before, R_T is the radius of the direct-drive DT target and N is the number of laser beams (N ~ 60). In the case in which R_T ~ 0.6 cm, then δ_{laser} = 0.137 cm and θ_{max} ~ 26.2°.

A schematic of meshing trapezoidal intensity distributions is illustrated in Figure 4.6.1-13.

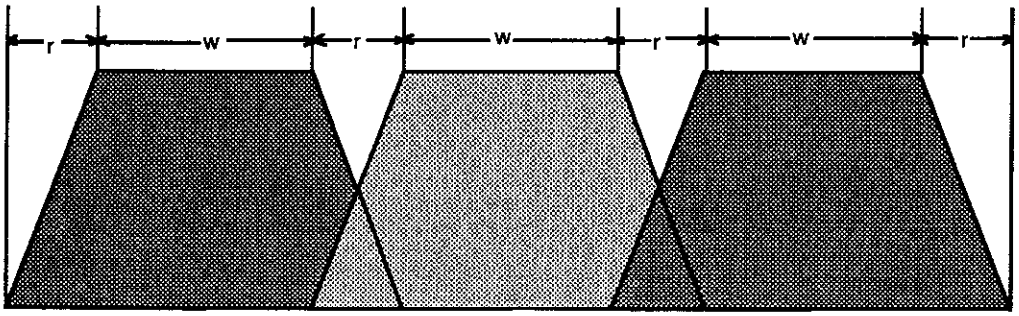

Figure 4.6.1-13. Meshing Trapezoidal Intensity Distributions Permits Smooth Near-Field Illumination of Direct Drive Targets

By varying the fill factor of these trapezoidal beams, the relative interbeam alignment accuracy of the optical system can be traded off against laser amplifier efficiency (i.e., steep trapezoidal shoulders [large w/r ratios] mean high amplifier efficiency). Figure 4.6.1-13 illustrates a case of a high w/r ratio. An example of nested trapezoidal beams with a low w/r ratio is shown below in Figure 4.6.1-14. Since these beams are in the near field (with a Fresnel number > 100), relatively detailed apodization profiles are possible, although the impact of the apodization on the amplifier apodization must be calculated.

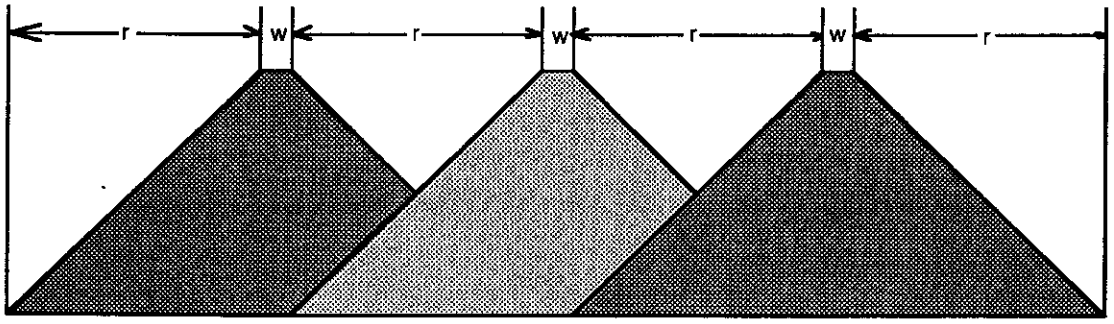

Figure 4.6.1-14. Meshing Trapezoidal Intensity Distributions with Low w/r Ratios Relaxes Near-Field Laser Beam Alignment Tolerances

In practice, it may be important to include the capabilities of on-board computer control systems to permit interferometric alignment accuracy of the final focusing mirrors onto a surrogate target to be attained. Precise erection of a surrogate target at the center of the target chamber would be a key feature of permitting laser beams to be aligned to

submicroradian accuracy. Such precise angular alignment must be carried out for both q and f corresponding to the two beveled directions of the trapezoidal apodization. An isometric view of the trapezoidal apodization is shown below in Figure 4.6.1-15.

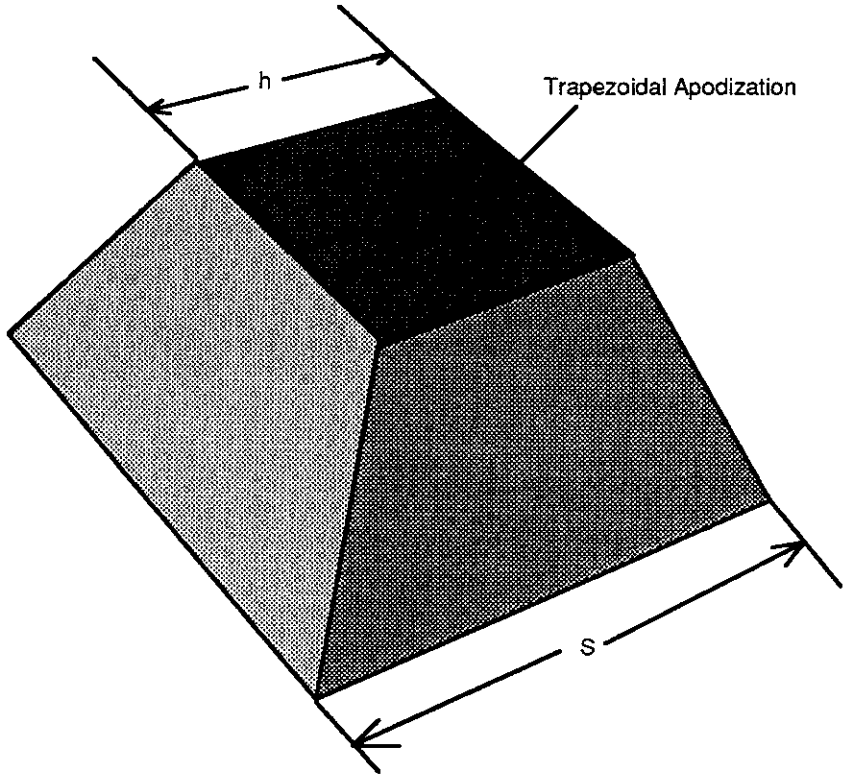

Figure 4.6.1-15. An Isometric View of Trapezoidal Beam Illustrates the Interlocking of Multiple Near-Field Laser Beams Aligned on Direct Drive Fusion Targets

The use of nested trapezoidal beams can be applied to direct-drive targets illuminated with a variety of beam architectures. Considered briefly here are beam configurations starting with cubic symmetry (for which N = 6) and going out as far as N = 240. The nested trapezoidal parameters for these cases are summarized in Table 4.6.1-1.

Table 4.6.1-1
Parameters for Direct-Drive Nested Trapezoidal Beam Arrangements

No.	No. of Beams	Spot Size on Target (mm)	Coupling Efficiency (%)
1	6	4.34	47.4
2	12	3.07	69.2
3	20	2.38	80.4
4	28	2.01	85.6
5	32	1.88	87.3
6	60	1.37	93.1
7	80	1.19	94.8
8	120	0.97	96.5
9	240	0.69	98.2

The laser/target coupling efficiencies tabulated in Table 4.6.1-1 were calculated using Eq. 4.6.1-2 above with the incident laser beam decomposed into annular zones as shown in Figure 4.6.1-6 above, assuming that the diameter of the critical surface was remaining constant.

The near field focusing geometry of the trapezoidal nesting of laser beams is illustrated for a single incident laser beam in Figure 4.6.1-16.

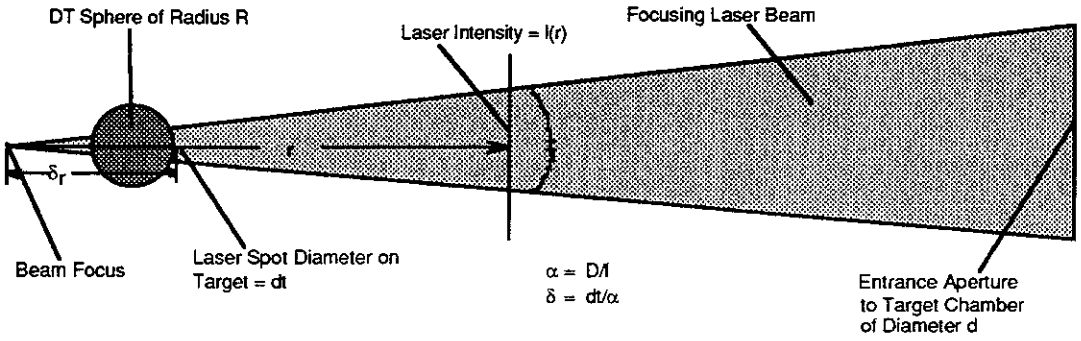

Figure 4.6.1-16. Near-Field Focusing Geometry for Trapezoidal Nesting

Since the DD target is located in the near field, the positional accuracy, $d = \Delta x$, of each beam incident on the target sphere is related to the required DD target illumination uniformity, Ψ, and the trapezoidal spacing parameter, r, via the simple relation:

$$d = \Delta x = \Psi r \qquad (4.6.1\text{-}11)$$

Thus, if the TWG requirement for the required DD illumination uniformity (Ψ) is equal to 0.01, then $\Delta x = r/100$. The angular pointing requirement, $\Delta\theta$, of the GIMM would therefore be given by the expression:

$$\Delta\theta = d/(R1) = \Psi r/R1 \qquad (4.6.1\text{-}12)$$

where R1 is the distance from the GIMM to the target. The values for the summit width of the trapezoid, w (see Figure 4.6.1-13 and 4.6.1-14 for a definition of w), are calculated as a function of the number of laser beam lines, N, and the results presented above in Table 4.6.1-1. For a fixed target diameter (d = 0.6 cm), there are other limitations on r since, in addition to optical alignment accuracy, $\Delta\theta$, r affects the laser beam fill factor, ξff. An expression for ξff is given by:

$$\xi_{ff} = \frac{w^2}{w^2 + 2r(w + r)} \qquad (4.6.1\text{-}13)$$

where w and r are defined previously. In order for laser amplifier power extraction to be efficient and to minimize optical damage, it is important that ξff ~ 1, which would force r = 0. This would be undesirable for the requirement noted above for the

alignment accuracy, $\Delta\theta$. As shown below in Figure 4.6.1-17, a ray from an alignment laser would be deflected in angle, $\Delta\alpha = 2d/R$, assuming that a shine shield is available on the DD target to assist in target alignment.

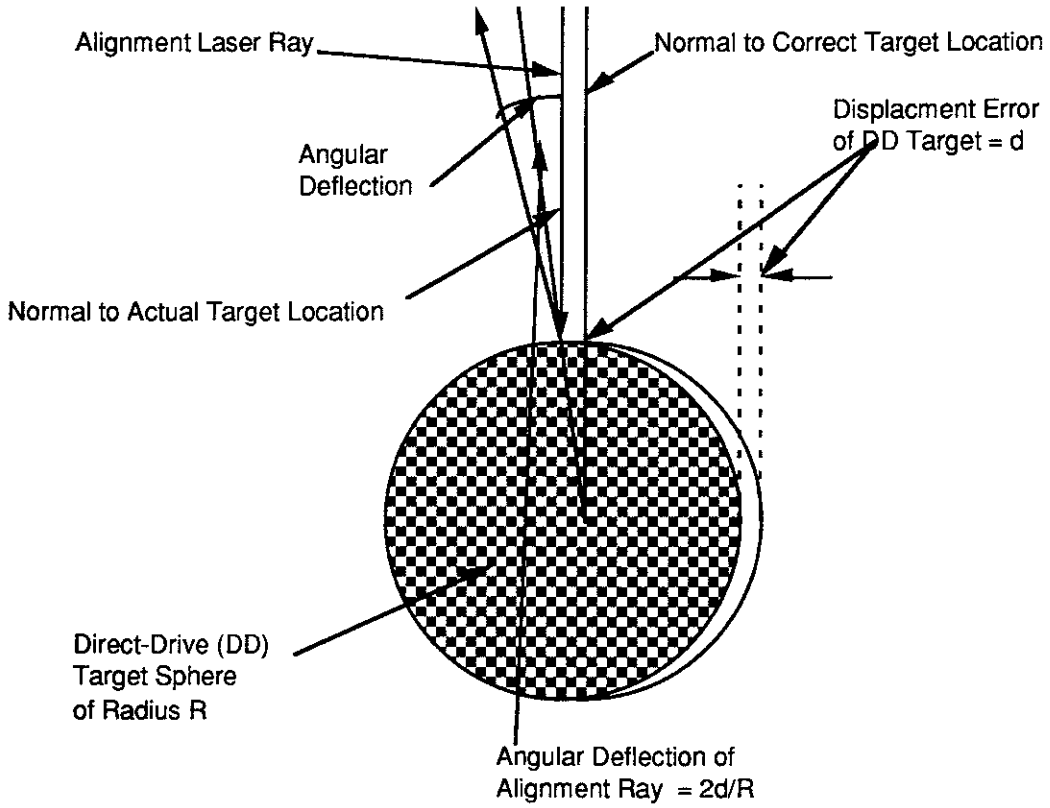

Figure 4.6.1-17 DD Target Misalignment Geometry for Alignment Laser Reflecting Off of Shine Shield: Angular Deflection = $\Delta\alpha$.

The dependence of the laser beam fill factor, ξff, on r is illustrated in Figure 4.6.1-18 for the cases of N = 60, 80, and 120 beams.

If values of the Prometheus-L laser beam fill factors, ξff > 0.8, are desired, then for 60 beams, w = 0.137 cm, r = 0.017 cm, and the alignment accuracy, $\Delta\theta$, equals $\Psi r/R1 \sim 9\times10^{-8}$ radians or ~0.1 μR. The corresponding sensing angle, $\Delta\alpha$, from the DD target shine shield is ~2r/R ~ 100 μR. Although these are challenging requirements for the Prometheus-L laser/target beam alignment system, the resulting cost reductions possible may be worth the additional technical investment.

The laser/target coupling efficiency, ξ, is plotted as a function of the number of laser beams in Figure 4.6.1-19. To be conservative, these calculations included only the $f_{IB} = \xi(\cos\theta_o)^5$ inverse Bremsstrahlung contributions and did not include any resonant absorption components.

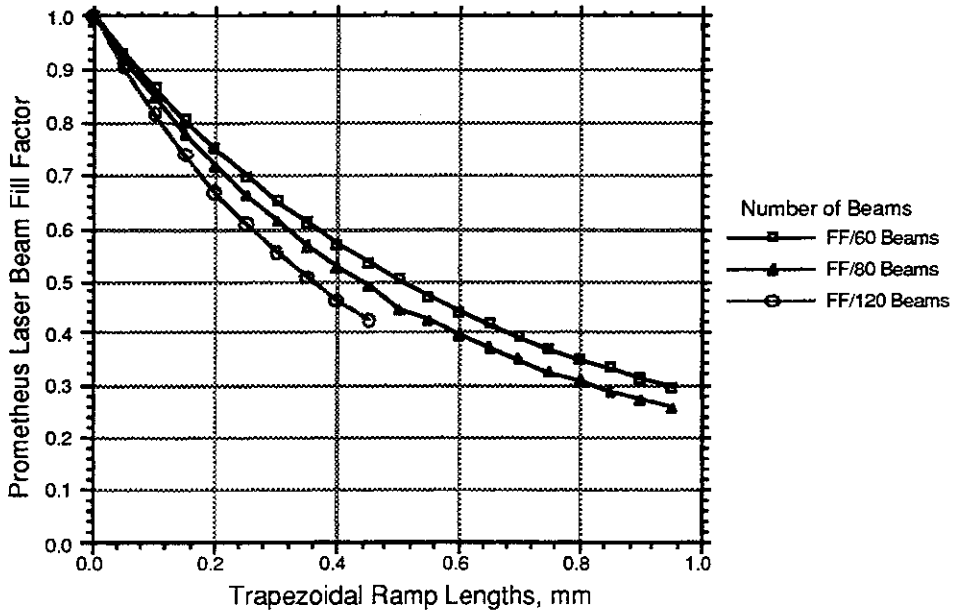

Figure 4.6.1-18 Laser Beam Fill Factors as a Function of Trapezoidal Ramp Lengths, r.

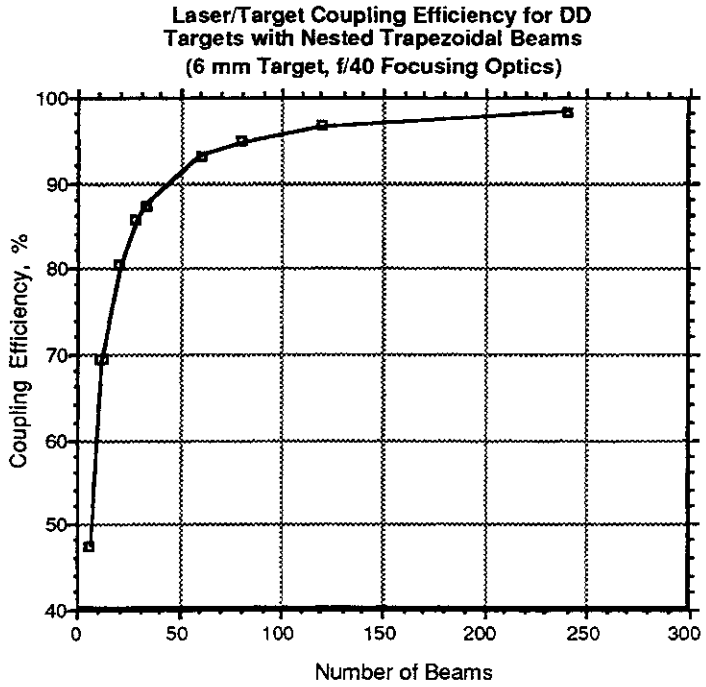

Figure 4.6.1-19. The Laser/Target Coupling Efficiency, ξ_T, Depends on the Number of Laser Beams Illuminating the Direct Drive Target (Constant 6 mm DD DT Target Diameter and IB Interaction)

As shown for large numbers of laser beams, the laser/plasma coupling efficiency exceeds 90% for a static target. When these calculations are repeated for N = 60 for critical surfaces ranging from 6 mm to 3 mm diameters while keeping the beam diameter at the target constant (~1.37 mm), the coupling efficiency, ξ_T, drops from 93% to 75%, as illustrated in Figure 4.6.1-20.

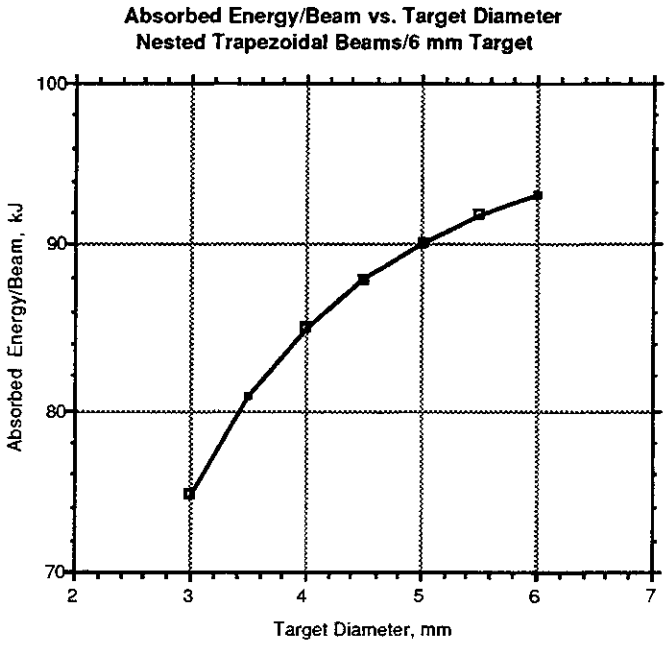

Figure 4.6.1-20. The Laser/Target Coupling Efficiency, ξ_T, Depends on the Critical Surface Target Diameter (60 Beams, f/40 Optics, 1.37 mm Spot Size, Trapezoidal Beam Nesting)

When the variation of laser target coupling efficiency with imploding target diameter is calculated, the integrated energy absorbed by the imploding target was calculated to be 86.2% of the incident laser energy for the 60 beam case, 6 mm DT target, f/40 optics, and trapezoidal beam nesting. This is to be compared with the 20% integrated coupling efficiency calculated for the tangential target illumination case above.

4.6.1.9 Summary of Laser/Target Interaction Physics - During the course of designing the IFE KrF laser driver, some questions have arisen with regard to the final focusing requirements in order to achieve efficient target coupling. The TWG guideline has adopted a conservative approach by illuminating the target with at least 60 beams having diameters at the target approximately equal to the diameter of the target. Elementary calculations of the laser/plasma coupling assuming that the primary coupling process is inverse Bremsstrahlung suggest that this conservative approach may result in less than 15% of the laser beam energy actually being coupled into the target (with an estimated additional 5% absorption coming from resonant absorption for a total of 20%). Similar IB calculations carried out for trapezoidal beam nesting to

minimize the angle of incidence with the critical surface while maintaining illumination homogeneity suggest that approximately 85% of the laser beam energy can be coupled into the target. These calculations also suggest that the importance of "zooming" the laser beams to follow the imploding critical surface is not as important for trapezoidal beam nesting as for tangential target illumination. Thus, there is evidence that we should be able to take advantage of the "zoomed optics" benefit in calculating the amount of laser energy necessary to drive a given target. A potential key problem with the trapezoidal beam nesting is intensity inhomogeneities arising from beam overlapping on the imploding target. This is illustrated in Figure 4.6.1-21.

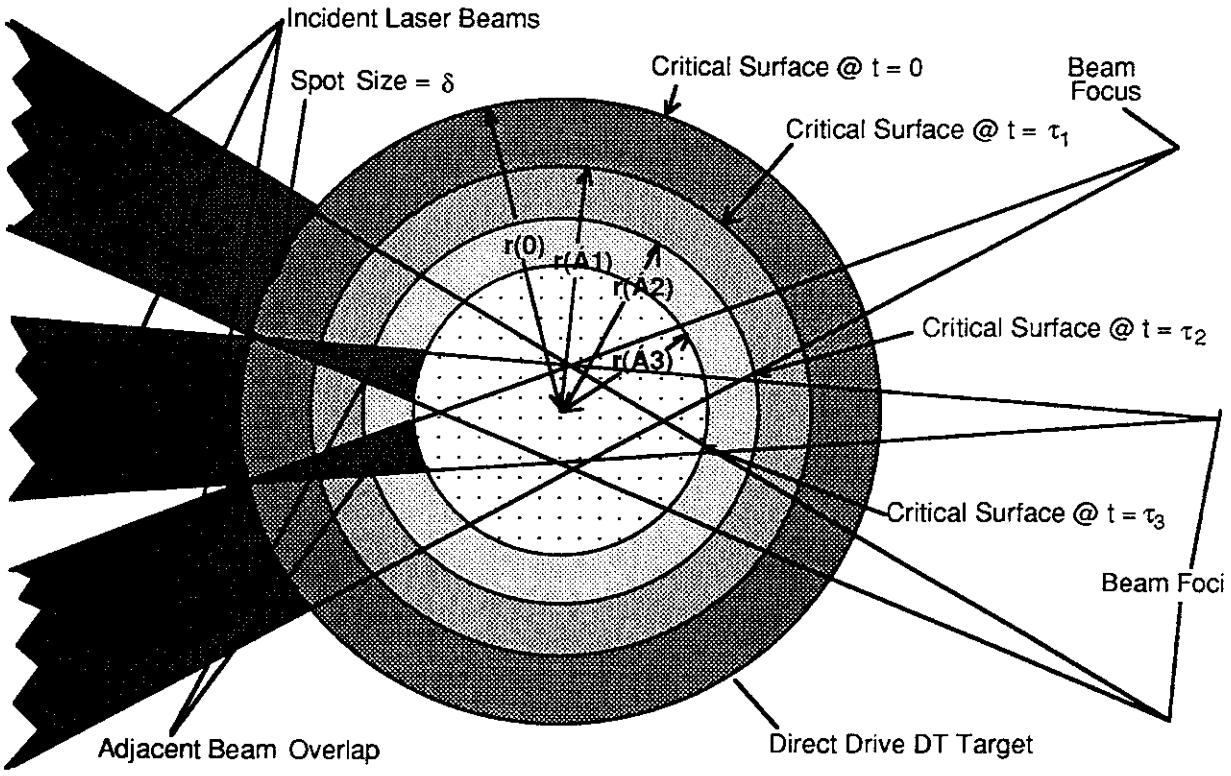

Figure 4.6.1-21. The Imploding Direct Drive Target Critical Surfaces Requires Zooming of the Near-Field Laser Beams to Maintain Homogeneous Illumination

Since this overlapping would occur late in the target implosion, it is thought likely that no Rayleigh-Taylor instabilities would be driven by this overlap.

Lastly, these considerations raise a concern that even if we were to achieve the remarkable level of illumination homogeneity (±1%) defined in the TWG Guidelines, the two-lobe absorption distribution of resonant absorption (Figure 4.6.1-9) may make this stringent illumination homogeneity specification meaningless.

4.6.2 Heavy Ion Driver Targets - In direct analogy with the two types of laser-driven (LD) IFE targets, there are two general types of Heavy Ion Driver (HID) targets: (1) direct drive targets, and (2) indirect drive targets.

Although these HID targets bear some general similarities with their laser-driven target counterparts, there are some significant structural differences in the HI targets as well as major differences in the energy coupling mechanisms to the targets. For example, the HI driver delivers a 6 ns pulse containing approximately 6 MJ of energy in the form of non-relativistic, high-Z ions having an energy per ion of approximately 4 GeV. This 6 MJ of energy is assumed to be stopped in a relatively thin layer of converter material. The LD, on the other hand, delivers a 6 ns laser pulse containing approximately 4 MJ of energy in the form of ultraviolet photons having wavelengths of approximately 250 nm.

4.6.2.1 Heavy Ion Direct Drive Target Description - At first glance, the design of the Heavy Ion Driver (HID) direct-drive target is similar to the LD direct-drive target illustrated in Figure 4.6.1-1. A diagram of the HID direct-drive target is presented below in Figure 4.6.2-1.

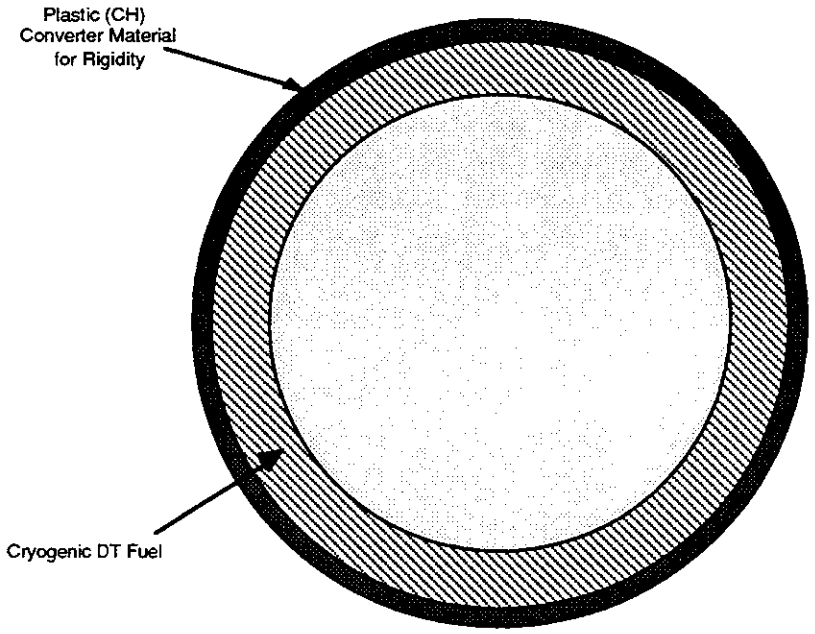

Figure 4.6.2-1 The Direct Drive HID Target Has Spherical Symmetry and Requires Uniform Power Loading of its Converter Shell

As indicated, the HID direct-drive target is a spherical, multi-shelled structure containing successive layers of converter material, structural CH (as needed for robust target construction), and cryogenic DT located at the center of the target. An alternative design is shown in Figure 4.6.2-2.

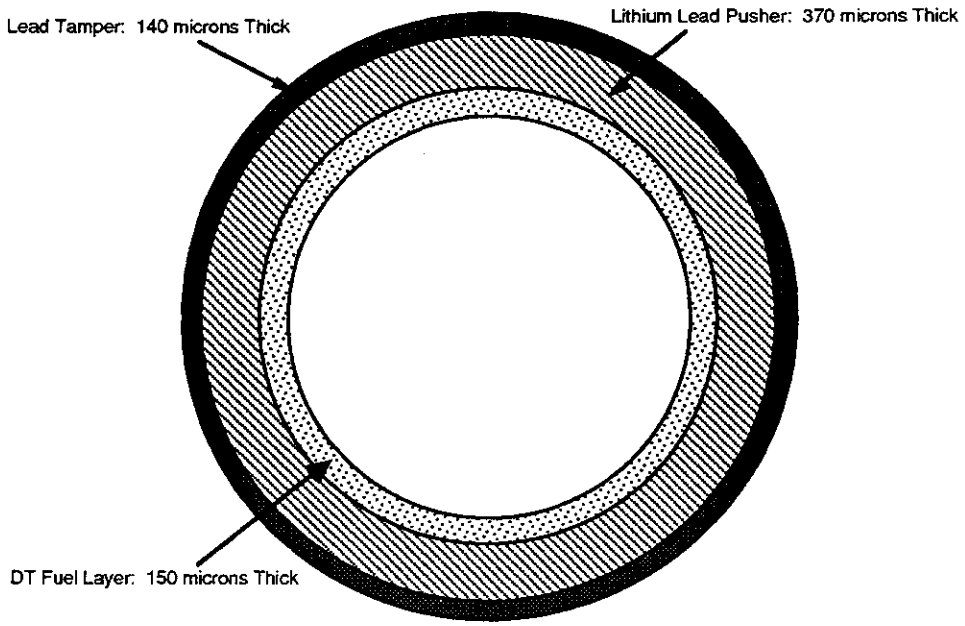

Figure 4.6.2-2. Alternative Direct Drive HID Target with Pb Tamper and Li-Pb Pusher (HIBALL-I)[5]

Heavy Ion Driver (HID) direct-drive targets yield fusion energy based upon the following scenario. At a time t = 0, the spherical HID direct-drive target is enveloped by approximately 100 HID beams symmetrically focused on the converter shell of the HID direct-drive target and synchronized to achieve the required degree of power loading uniformity. These focused HID beams consist of non-relativistic ions having individual energies of approximately 4 GeV. Implosion of the HID direct-drive target is accomplished by the generation of a homogeneous, spherical implosion wave capable of isentropically and uniformly compressing the DT fuel to a level of approximately 20 times liquid density. The direct-drive HID target uniformity of power loading requirements are similar to those of the LD direct-drive target: Power loading from the direct drive HID beams[5] must be ±1% uniform in order to permit isentropic compression without Rayleigh-Taylor instabilities. This high uniformity of power loading requirement represents the single most serious HID direct-drive target engineering problem since it involves the simultaneous achievement of equal beam currents together with synchronization of the beams arriving in 4π sterradians. Compared with the indirect drive HID targets described below, the 1% direct drive HID target irradiation requirements are extremely difficult to achieve, thereby making this target design unattractive for HID. Furthermore, having ~100 beam penetrations of the target chamber for the ~100 HID beamlines would cause serious radiation problems for the focusing quadrupole magnets and the downstream components.

4.6.2.2 Heavy Ion Driver Indirect Drive Targets - Although the HID indirect-drive targets are geometrically similar to their LD counterparts (i.e., energy deposition is achieved with two-sided geometries with the HID energy being converted into x-rays within a radiation hohlraum enclosure), there are, in fact, some substantial differences between the LD and HID indirect drive targets.

The design of the HID indirect-drive target is fundamentally different than the LD indirect-drive target design described in Section 4.6.1. According to the HID/target interaction data[1] supplied by the Target Working Group (TWG), the gain of the indirect HID target is more well known and defined than the direct-drive HID target. As a consequence of these data provided by the TWG, the indirect-drive HID target was selected for the baseline. As a further specification of the HID indirect-drive target, two-sided illumination was selected for the Prometheus-H HID baseline design.

Compared with the corresponding LD indirect-drive target, there are substantial differences between the LD and HID indirect-drive targets. Depending upon the plasma atmosphere generated in the LD indirect-drive target, significant numbers of hot electrons can be produced by the laser/plasma interaction; whereas in the case of the HID indirect-drive targets, relatively few hot electrons are produced in the interactions between the decelerating heavy ions and the converter plugs placed at each end of the HID hohlraum. In addition, for the laser-driven hohlraum, the duration of the high intensity portion of the laser pulse is limited by closure of the entrances to the capsule, whereas no comparable effect occurs for the HID hohlraum. This may permit HID indirect-drive targets to outperform LD indirect-drive targets at the same driver energy levels.[6,7]

Selection of parameters for the ID heavy ion target was complicated by the fact that most of the details of such targets are classified. It was known that the targets consist of a fuel capsule surrounded by a radiation case with a high-Z material. The TWG directed the fuel capsule parameters. No details were supplied for the radiation case .

According to TWG guidelines, ". . .*single-sided illumination is still sufficiently speculative that the contractors should continue to carry a two-sided option, . . .*".[8] Based upon this TWG recommendation and information in the open literature[9,10], it was decided to assume two-sided illumination for the Prometheus-H baseline target design.

No guidance was provided on how the DT capsule was to be suspended in the Hohlraum radiation case. A scheme was developed to support the DT fuel capsule with sufficient structural rigidity to tolerate accelerations of 100 g's. Dimensions of the case were chosen for ease of fabrication and ability to withstand the necessary levels of acceleration. The supplied heavy ion ID gain curves indicated energy converter region diameters depending on the ion range and driver energy chosen. The

converter region was determined for the driver design point chosen, allowing some beam misalignment with the target.

References for 4.6

1. Ronald C. Davidson (MIT), et al., "Inertial Confinement Fusion Reactor Design Studies Recommended Guidelines," prepared for DOE Office of Fusion Energy, September 1990.

2. R. L. McCrory, Director, University of Rochester Laboratory for Laser Energetics Annual Report, 23, p. 126, 1984-85.

3. J. J. Thomson, C. E. Max, J. Erkkila, and J. E. Tull, "Laser Light Absorption in Spherical Plasmas," Physical Review Letters 37, pp. 1052-1056 (1976).

4. J. Auerbach, N. C. Holms, J. T. Hunt, and G. J. Linford, "Closure Phenomena in Pinholes Irradiated by Nd:Laser Pulses," Applied Optics 18, 510 (1979).

5. Kessler and von Moellendorff, **Fusion Technology**, 11, 378 (1987).

6. Richard C. Arnold and Rolf W. Mueller, "Parameter Study for Adapting a Heavy-Ion Collider to Drive IFE Ignition Experiments," Theoretische Quantenelektronik, Technische Hochschule, Darmstadt and GSI, Darmstadt, p. 36.

7. R. O. Bangerter, J. W. Mark, and G. Magelssen, "Simple Target Models for Ion Beam Fusion Systems Studies," LLNL Report UCID-20578 (1985).

8. R. Bangerter, et al., "Revised Target Information for IFE Reactor Studies," memo from Roger Bangerter, Chairman TWG, February 1991.

9. R. Bock, "Status and Perspectives of Heavy Ion Inertial Fusion," Gesellschaft fuer Schwerionenforschung mbH, Darmstadt, Germany, GSI-91-13.

10. J. Meyer-ter-Vehn and K. Unterseer, **Laser and Particle Beams**, 3 (3), pp. 283-311.

4.7 Design Rationale for the GIMM

The last and closest optical component in the laser system before the laser light enters the reactor cavity will be subjected to intense transient thermal loading, as well as charged particle and neutron irradiation. For these reasons, it is has been shown in previous laser fusion studies that the engineering design of a long life and reliable last mirror is a major challenge. In this section, the rationale behind the materials selection and design philosophy will be outlined.

Materials Selection - The optical properties of the mirrors surface have been decoupled from the mechanical properties of the supporting structure. In this regard, a great degree of flexibility has been achieved in the design. The surface of the GIMM was chosen to be metallic, because dielectric materials show great sensitivity to the effects of ionizing radiation. The absorption coefficient of MgF_2, and the optical transmission of ZnS degrade by an order of magnitude, after a fluence limit of 10^{16} n/cm^2 accumulates. Even if most of the color centers are annealed out periodically, remaining residual defects would lead to very short lifetime.

The leading high reflectivity candidate metals are aluminum, magnesium, silver, gold, and copper. To select between these metals, the following criteria was considered:

(1) High reflectivity in the wavelength of interest (i.e. 250-500 nm).
(2) Effects of radiation on absorptivity.
(3) Surface temperature rise during the laser pulse.
(4) Thermal fatigue resistance.
(5) Radiation effects on surface deformation.

Although silver has excellent reflectivity, neutron-induced micro-craters are expected to distort the mirror's surface. Near-surface collision cascades in silver will be very dense, because of the high electronic stopping power of silver. On the other hand, copper was excluded on the basis of its high neutron-induced swelling, particularly when it is pure. the higher fatigue strength of aluminum results in a smaller mirror size, when it is compared to magnesium. In addition, the neutron-induced swelling rate of commercial grade aluminum is lower than that of magnesium. For the above reasons, aluminum has been chosen as the material for the surface of the mirror.

The structural support of the mirror is composed of two parts: a low swelling composite SiC high-rigidity component, and a concrete shell for control of thermal deformations. The SiC structure is designed to have small helium cooling channels, running along the length of the mirror. Two other layers are attached immediately underneath. Each one of these two layers is stiffened by I-beams. The SiC composite construction is chosen for the following reasons:

(1) Very low neutron-induced deformations by thermal and irradiation creep mechanisms in the temperature range of 500-700 K.
(2) For porosity of approximately 10-15%, no neutron swelling is to be expected, thus mechanical deformations of the mirror's surface are minimized.
(3) SiC is a low activation material. The choice of SiC will allow passive safety, and shallow land burial of the mirror at the end of life.

In addition to the SiC structure, a concrete shell is designed to provide complete restraint to out-of-plane deformations. This is achieved by sliding bolting mechanisms for the attachment of the bottom of the SiC structure to the concrete shell.

Since the coefficient of thermal expansion of aluminum is higher than that of SiC, a shear graphitic layer is deposited first on the surface of the SiC composite, and the aluminum is added on top of the graphitic shear layer. With this arrangement, in-plane mismatch thermal expansions of the aluminum can be isolated from the SiC composite structure.

More details and design specifics on the GIMM can be found in Section 6.5.1.8, Summary of Laser Driver Subsystems, Grazing Incidence Metal Mirror.

TABLE OF CONTENTS – CHAPTER 5

TABLE OF CONTENTS – CHAPTER 5 (CONT.)

CHAPTER 5
KEY TECHNICAL ISSUES AND R&D REQUIREMENTS

This chapter presents the key technical issues and R&D requirements found during the conduct of the two IFE reactor design studies. The presentation of these issues and requirements will hopefully benefit the technical community and the decision makers to help them better formulate the program and technical plans toward the goal of commercial fusion energy.

5.1 Introduction

Purpose - Although significant progress has been made in inertial fusion energy research during the past decades, the field is still in its early stage of research and development and the present data base is severely limited. Therefore, many uncertainties exist in the actual performance and operation of present fusion reactor conceptual designs. The expected consequences of these uncertainties vary in magnitude: on one extreme, the uncertainties are so large that the feasibility of the reactor design is at stake, and, on the other extreme, the uncertainties may simply require moderate redesign, reduced performance, or increased cost.

This chapter contains a comprehensive list of key physics and engineering issues for the IFE conceptual reactor designs developed in this study. The chapter also includes an attempt to determine the additional research and development (R&D) needed to develop critical systems and reduce development risks for each of the two reactor design concepts.

The list of key technical issues, shown in Section 5.2, explicitly defines the uncertainties associated with the physics and engineering operation of IFE reactors and addresses the potential consequences resulting from each issue. It is believed that this list will be useful to engineering and physics researchers, reactor designers, experimentalists, and program planners in identifying the areas of greatest concern and their impact on the development and potential attractiveness of inertial fusion reactors.

The key issues identified in this work are large in number and they cover specific technical issues ranging in complexity and importance. Each of these issues impacts aspects of feasibility, safety, and/or economic potential of fusion reactors. Resolving these issues requires new knowledge through experiments, models, and theory. The issues identified here represent great details that are necessary to accurately prescribe the R&D necessary to resolve the issues. However, such details have made the list relatively long with each issue having a focus on a narrow technical area.

To provide a brief summary of the most important issues, a smaller number of issues, called critical issues, were identified in Section 5.3. A critical issue is broader in scope than a key issue; each critical issue may encompass several key issues.

In general, the issues identified here are for the two reactor design concepts developed in the Prometheus[1] study. However, many of the issues tend to be generic to IFE and are fairly independent of the specific selections made here. To maximize the usefulness of the list of issues, the degree of dependence of the issue on design specificity is explicitly identified. Many technical issues for IFE correspond to similar technical issues in MFE. The degree of similarity is also indicated to facilitate identifying areas of R&D that are of common interest to MFE and IFE.

There is an intentional bias towards testing issues–those likely to require testing (experiments) before a commercial reactor could confidently be built. However, it is not limited to testing alone, the entries in the list are described as "Issues/Technical Areas" to allow broader categories. The issues serve to identify the R&D needs which are listed later in the Section 5.5. Also, the quantification of the test requirements depends heavily on the issues.

The precise definition of an issue is difficult. One reason for this is the interrelated nature of the technical disciplines and the phenomena involved. For example, in the solid breeder blanket, thermal stresses may be a primary cause of structural failures. The thermal stresses are a function of temperature distributions, which depend on the allowable operating temperature window, which in turn is highly dependent on tritium transport and inventory, which in turn is a strong function of radiation effects on the solid breeding material. Structural failures are also affected by material property changes due to irradiation.

It is arbitrary to some extent how to break out pieces of the overall behavior of a reactor component and call them separate issues. Consider, for example, the blanket as a reactor component. The only real issue for the blanket is the demonstration of adequately meeting its functional requirements of tritium breeding and energy conversion at economical and safe conditions. To help alleviate this problem and still retain technical specificity in the issues, an attempt is made to illuminate the logical pathway to the ultimate consequences or failure modes. For the blanket, these relate to the basic functions of structural integrity, tritium breeding, heat transport, materials compatibility, etc.

Organization - The key issue list is arranged according to the major reactor components shown in the Table 5.1-1. A concise table (several pages) of the key issues appears in Section 5.2, together with table entries for potential impact, design specificity, level of concern, relevant operating environment conditions, and degree of relevance to MFE. Section 5.3 focuses on the critical issues. In Section 5.4, each issue identified in Section 5.2 is explained in detail, giving the rationale behind the table entries. For some of the issues, more detailed analysis of the issue is given. The numbering of the issues write-ups in Section 5.4 exactly corresponds to the numbering of the table in Section 5.2. The R&D requirements to resolve these issues are addressed in Section 5.5.

Table 5.1-1 Organization of Components and Technical Areas for which Technical Issues are Identified

A. Target
B. Driver
   - Laser
   - Heavy Ion
C. Vacuum System and Evacuation
D. Tritium Processing System
E. Cavity Design
   - Wall Protection
   - Blanket
   - Shield
F. Materials
G. Heat Transport and Secondary Energy Conversion
H. Maintenance and Configuration
I. Balance of Plant
J. Safety and Environment
K. Subsystem Interactions

Entries and Abbreviations - The entries for Table 5.2-1 and the rest of this chapter are explained below. The "Reactor Concept" entry simply indicates whether the issue is relevant to the Laser-Driven or the Heavy Ion-Driven reactor design, or both. The "Potential Impact" entry for each issue helps to determine the level of concern, or importance, of the issue. Seven possible impact categories have been defined in the FINESSE[2] study and are used here as defined in Table 5.1-2. The abbreviations used in Table 5.2-1 for "Potential Impact" are also defined in this table. These are divided into two classes of issues: feasibility issues and attractiveness issues. In general, a feasibility issue is more serious because it could rule out a component concept on scientific grounds without considering the cost, complexity, or safety implications relative to alternate energy sources. The most serious issues are those which can close the device operating window, or design window, thereby eliminating the design. The attractiveness issues may still be very serious, rendering a reactor design impractical on the basis of economics or safety.

Table 5.1-2 Definition of Potential Impact Abbreviations

Feasibility Issues:	DW	May Close the Design Window
	US	May Result in Unacceptable Safety Risk
	UL	May Result in Unacceptable Reliability, Availability, or Lifetime
Attractiveness Issues:	RP	Reduced System Performance
	RL	Reduced Component Lifetime
	IC	Increased System Cost
	RS	Less Desirable Safety or Environmental Implications

The Design Specificity entry indicates if the issue is generic to all the plant systems, components, or materials specific to an individual item. To reduce the table size, abbreviations are used to denote the specificity of components, specific design concepts, etc. These abbreviations are given in Table 5.1-3. Any feasibility issue that is generic to a class of component designs is considered to possess a critical level of concern. Other issues are regarded as high, medium or low levels of concern depending on a qualitative judgment on their overall severity.

Table 5.1-3 Definition of Design Specificity Abbreviations

System Abbreviation

B	Blanket
CBOP	Conventional Balance of Plant
DHI	Driver-Heavy Ion
DL	Driver-Laser
FW	First Wall
S	Shield
T	Tritium System
TF	Target Factory
V	Vacuum System
WP	Wall Protection

Other Abbreviations

CS	Ceramic Structure
DS	Draw Salt
LB	Liquid Breeder
LM	Liquid Metal
LS	Laser System
SB	Solid Breeder
SiC	Silicon Carbide
TC	Ternary Ceramic

The relevant environmental conditions in Table 5.2-1 indicate those particular parameters of the operating environment for the component that influence the issue severity. Those environmental conditions are particularly useful in defining the R & D required to resolve the issues and in identifying major facilities needs. Operating environment parameters such as temperature, stress, and surface heat flux are abbreviated as noted in Table 5.1-4. The influence of neutrons in the operating environment on a particular issue is important to clarify because of the large effect on the type of facilities required for the R&D. The effect of neutrons on the particular issue is indicated by three categories: bulk heating, material damage, and specific reactions. These are abbreviated in the Issue Tables as H, D, and R, respectively, with the abbreviations also given in Table 5.1-4.

Table 5.1-4 Key to Operating Environments

Neutron Effects

H	Bulk Heating
D	Materials Damage (Displacements, helium production, etc.)
R	Specific Reactions (Tritium breeding, helium production, hydrogen production, activation, sputtering, radiolytic decomposition, etc.)

General

F	Fluence	TWI	Target debris-Wall interactions
ϕ	Flux	G	Geometry
S	Spectrum	Q	Power Density
T	Temperature	t	Time
σ	Stress State	q	Surface Heat Flux
C	Chemical Environment	P	Pressure
I	Impurities	P_t	Tritium Pressure
H	Tritium	v	Velocity
A	Dimensions (Area)	N	Cyclic Operation
B	Magnetic Field Strength	s	Surface Condition
b	Transient Magnetic Field	γ	Gamma Radiation
L	Laser	HI	Heavy Ion
TG	Tritium Generation	IB	Beam Current
D	Debris	ρ	Pulse Shape
OF	Optical Energy Fluence	EI	Ion Energy
ρ_g	Background Gas Density	E	Beam Energy
n	Neutron Environment	V	Vacuum Environment

References for 5.1

1. Prometheus Study, This Report.

2. M. A. Abdou, et. al., FINESSE: A Study of the Issues, Experiments and Facilities for Fusion Nuclear Technology Research and Development, Interim Report, Volume 11, UCLA-EGG-84-30, p. 821, October 1984.

This page intentionally left blank.

5.2 Identification of Key Issues

This section contains the IFE Key Issues Summary, Table 5.2-1. For each issue, this table indentifies the applicable reactor concept, potential impact as to feasibility or attractiveness, specificity to the system design, level of concern, assessment of the neutron and general environment, and relevance to MFE. Each issue is discussed in detail in section 5.4.

Table 5.2-1 IFE Key Issues Summary

Issue/Technical Area	Reactor Concept	Potential Impact	Design Specificity	Level of Concern	Operating Environment		Relevance to MFE
					Neutron	General	
A) Target							
A.a Target physics							
A.a.1 Direct Drive Target Coupling	L/HI	DW,UL, RP	Generic	Critical		H, L, TWI, G, N	None
A.a.2 Indirect Drive Target Coupling	L	DW, RP, IC, RS	Generic	Critical		L,TWI,G,Q, N,I,S,F,T, q,s,t	None
A.a.3 Survivability of Targets in Chamber Environment	L/HI	DW, RP	Generic	High		S, T, A, G, Q, t, q, P, v	Low
A.b Beam/Target Interaction							
A.b.1 Demonstration of Injection and Tracking of Targets Coupled with Beam Steering	L/HI	UL	Generic	Critical		A, TWI, P	Low
A.c Fabrication							
A.c.1 Manufactur-ability of High Quality, Low Cost DD and ID Targets	L/HI	UL, RP, IC, RS	Generic	High		H, TWI, N	Medium
B. Driver							
B.a Laser							
B.a.1 D/T Target Illumination	L	DW, UL, RP, IC	DL	High		L, t, G	None
B.a.2 Large Laser Bandwidth	L	RP, IC	DL	High		L, t, G	None
B.a.3 Final Optics Pointing System	L	DW, UL, RP, IC	DL, S	High	H, D, R	L, t, G	None

Table 5.2-1 IFE Key Issues Summary (Continued)

Issue/Technical Area	Reactor Concept	Potential Impact	Design Specificity	Level of Concern	Operating Environment		Relevance to MFE
					Neutron	General	
B.a.4 Grazing Incidence Mirror Damage	L	DW, UL, RP, IC	DL, S, V Mirror	High	H, D, R	L, F, TWI, Q, q, γ	None
B.a.5 SBS Pulse Compressor	L	IC	DL	High		L, t, G	None
B.b Heavy Ion							
B.b.1 Timing of Heavy Ion Beam	HI	RP, IC	DHI	High		P,Q,I,B,G, N,T,E,EI,p, HI	Low
B.b.2 Channel Formation	HI	RP, IC	DHI	High		P,Q,I,B,G, N,T,E,EI,p, HI	Low
B.b.3 Channel Transport	HI	RP, IC, RS, RL	DHI	High		P,Q,I,B,G, N,T,E,EI,p, HI	Low
B.b.4 Stripping of HI Beam	HI	RP, IC	DHI	High		P,Q,I,B,G, N,T,E,EI,p, HI	Low
B.b.5 Alignment of Indirect HI Target		RP, IC	DHI	High	H, D, R	P,Q,I,B,G, N,T,E,EI,p, HI	Low
C. Vacuum System and Evacuation							
C.1 Vacuum Seal Compound Survival in Nuclear Environment	L/HI		Generic	Low			High
C.2 Cryogenic Pump - Hydrogen Capacity	L/HI		Generic	High			High
C.3 Chemical Stability of the Reactor Exhaust	L/HI		Generic	Medium		C	None

Table 5.2-1 IFE Key Issues Summary (Continued)

Issue/Technical Area	Reactor Concept	Potential Impact	Design Specificity	Level of Concern	Operating Environment		Relevance to MFE
					Neutron	General	
D. Tritium Processing System							
D.1 Tritium Inventory Mean Residence; Time of Tritium in the Subsystems; Tritium Losses from the Subsystems	L/HI	RS	B,T, TF	Medium			High
D.2 Tritium Permeation from the First Wall Coolant - Liquid Pb	L/HI						
E. Cavity							
E.a Wall Protection							
E.a.1 Cavity Vapor Hydrodynamics	L/HI	DW, UL	Generic	Critical		S,A,G,TWI, Q, t, q, P	None
E.a.2 Cavity Structure Mechanics Response to Blast	L/HI	UL, RP, IC	All	High		F,T,σ,A, TWI,G,Q, q,P,N,s	Low
E.a.3 Vapor Condensation Rate	L/HI	DW, RP, IC	WP	Critical		T,A,TWI,G, t, q, P	None
E.a.4 Radiation Heat Transport in Partially-Ionized Gas	L/HI	RP, RL	Generic	High		T,A,TWI,G, Q, t, q	Low
E.a.5 Film Flow Control: Injection, Uniform Thickness and Drainage	L/HI	DW	Generic Thin Film	Critical		A, G, v	Low
E.a.6 Film Flow Stability and Response to Impulsive Loading	L/HI	DW	Thin Film	High		A, G, v	Low

Table 5.2-1 IFE Key Issues Summary (Continued)

Issue/Technical Area	Reactor Concept	Potential Impact	Design Specificity	Level of Concern	Operating Environment		Relevance to MFE
					Neutron	General	
E.a.7 Pb/Sic Wetability	L/HI	RP, RL, IC	Specific	Medium		C, I, s	Low
E.a.8 Pb Compatibility with Steel	L/HI	RP, RL, RS	Specific	Medium		T, C, v	Medium
E.b Blanket							
E.b.1 Tritium Self-Sufficiency	L/HI	DW	Generic	Critical	H, D, R	F,ϕ,S,T,C, I,TG,A,G, Q,t,P_t,N,γ	High
E.b.2 Tritium Inventory, Recovery, and Containment	L/HI	DW, US, IC	SB	Critical	R, H	F,ϕS, T,C, I,A,G,Q	High
E.b.3 Breeder/Structure Mechanical Interactions	L/HI	RL, RP	SiC, SB	High	H, R	F,T,C,I,A,t, N,σ,P	High
E.b.4 Off-normal and Accident Conditions	L/HI	IC, RS	SiC	High	H	T,s,G,Q,t, P_t,V,P,N, TG	High
E.b.5 Structural Response and Failure Modes	L/HI	RS, UL	SiC	High	H, D, R	F,T,σ,C,I, A,G,Q,t,N, P	Medium
E.b.6 Corrosion and Mass Transfer	L/HI	DW	SB	High	H, R	F, T, C, I, t P_t, N	High
E.b.7 Tritium Permeation	L/HI	US, UL	Generic	High	R, D	F, N, T, P_t, I	High
E.b.8 Fabrication	L/HI	IC, UL	SB, SiC	High		A, G	Medium
E.b.9 Heat Generation and Power Production	L/HI	RP, RS	Generic	High	R, H	ϕ,S,G,Q,t, γ	High
E.c Shield							
E.c.1 Effective of Bulk Shield							
E.c.1.1 Biological Dose during Operation and Maintenance	L/HI	RS, UL	Generic	High	R, D	ϕ, F, S, G	High
E.c.1.2 Radiation Streaming	L/HI	RS, US	Generic	High	R, D	ϕ, F, S, G	High

Table 5.2-1 IFE Key Issues Summary (Continued)

Issue/Technical Area	Reactor Concept	Potential Impact	Design Specificity	Level of Concern	Operating Environment		Relevance to MFE
					Neutron	General	
E.c.1.3 Analytical Techniques and Data Base	L/HI	RS, UL	Generic	High	R, D	ϕ, S, G, F	High
E.c.2 Shield Compatibility with Cavity and Vacuum Boundary, Inclucing Assembly/ Disassembly	L/HI	RS, UL	Generic	High	R, D	ϕ, F, S, G	High
E.c.3 Activation of Reactor Building Components Outside the Cavity	L/HI	RS, UL	Generic	Low	R, D	ϕ, F,S, G	High
E.c.4 Shielding of Final Mirrors	L	UL, RP, RL, IC	Mirror	High	D, R, H	ϕ, F, S, G	None
E.c.5 Shielding of Quadrupole Magnets	HI	UL, RP, RL, IC	Magnets	High	D, R, H	ϕ, F, S, G	Medium
F. Materials							
F.a Viability of SiC Structure	L/HI	RP,RL,UL	FW, B	High	D, R	γ, T, σ	High
F.b Thermo-Mechanical and Materials	L	DW, RP	DL	High	D, R, H	γ, T, σ	Low
G. Heat Transport and Secondary Energy Conversion		No Key Issue Identified					
H. Maintenance and Configuration							
H.1 Computer Reliability	L/HI	UL	Generic	Low		t	High
H.2 Total Remote Maintenance	L/HI	DW, UL	Generic	Low		F,S,T,C,H, B	High

Table 5.2-1 IFE Key Issues Summary (Continued)

Issue/Technical Area		Reactor Concept	Potential Impact	Design Specificity	Level of Concern	Operating Environment		Relevance to MFE
						Neutron	General	
H.3	Material Joining	L/HI	DW, IC	Generic	High		F,S,T,C,H, B	High
H.4	Lead Flushing	L/HI	IC	Generic	Medium		F, T, H	Low
H.5	Seal life	L/HI	DW, IC	Generic	High		F,S,T,C,H, B	High
H.6	Embrittlement Temperature	L/HI	DW, IC	Generic	Medium		T	High
I.	Balance of Plant		No Key Issue Identified					
J.	Safety and Environment							
J.1	Overall plant tritium inventory	L/HI	IC, RS	T	Medium		H	Medium
J.2	Permeation of Tritium	L/HI	RP	T	Medium		H	Medium
J.3	Normal Operation Tritium Release	L/HI	IC	T	Medium		H	Medium
J.4	Neutronic Cross Sections/Data Library for Activation Analysis	L/HI	US	Generic	High	R	F,ϕ,S,Q,γ	High
J.5	Removing Decay Heat from Lead Coolant Under Accident Conditions	L/HI	US, IC, RS	FW	Medium	R	F,ϕ,s,Q,γ	Medium
J.6	Hydrogen Burn Due to Rupture of Diffusion Vessel	L/HI	RP, IC	TF	Medium		H, P_t	None
J.7	Detection of Local Dry Spots Prior to Failure	L/HI	US, IC	FW	High		F,ϕ,S,T,Q, σ	High

Table 5.2-1 IFE Key Issues Summary (Continued)

Issue/Technical Area		Reactor Concept	Potential Impact	Design Specificity	Level of Concern	Operating Environment		Relevance to MFE
						Neutron	General	
J.8	Detailed Accident Analysis	L/HI	IC, RS	All	High	-	All	Medium
J.9	Removal of Contaminants from the Liquid Lead	L/HI	RP, RS	WP	Medium	-	I	None
J.10	Impact of Large Quantities of Lead on Waste Disposal	L/HI	IC, RS	WP	Low	-	I	None
K.	Subsystem Interactions							
K.1	Laser System/ Cavity Interface and Final Mirror Protection	L	UL	DL	Critical		F,OF,S,C, T,n,γ,V,s, q	Low
K.2	SiC/Metal Piping Transition Interface	L/HI	IC	CS/ CBOP	Critical		C,T,H,A,P, Q,I,v	High
K.3	Heavy-Ion System/Cavity Interface and Beam Propagation, Focusing and Optics	HI	DW	DH, WP	High	-	ρ_g,Q,IB,G, N,T,E,EI,p	Low

This page intentionally left blank.

5.3 Prometheus Reactor Design Study Critical Issues

This section presents the critical issues identified for the laser and heavy ion driver, reactor cavity and balance-of-plant systems considered for the Prometheus IFE power plant design study. Each critical issue is broad in scope and covers several of the most important key issues for a number of components and technical disciplines. The final list of critical issues is presented in Table 5.3-1. References are collected at the end of each issue discussion

Table 5.3-1. List of Critical Issues Identified by the Prometheus Design Study

1. Demonstration of Moderate Gain at Low Driver Energy
2. Feasibility of Direct Drive Targets
3. Feasibility of Indirect Drive Targets for Heavy Ions
4. Feasibility of Indirect Drive Targets for Lasers
5. Cost Reduction Strategies for Heavy Ion Drivers
6. Demonstration of Higher Overall Laser Driver Efficiency
7. Tritium Self Sufficiency in IFE Reactors
8. Cavity Clearing at IFE Pulse Repetition Rates
9. Performance, Reliability, and Lifetime of Final Laser Optics
10. Viability of Liquid Metal Film for First Wall Protection
11. Fabricability, Reliability and Lifetime of SiC Composite Structures
12. Validation of Radiation Shielding Requirements, Design Tools, and Nuclear Data
13. Reliability and Lifetime of Laser and Heavy Ion Drivers
14. Demonstration of Large-Scale Non-Linear Optical Laser Driver Architecture
15. Demonstration of Cost Effective KrF Amplifiers
16. Demonstration of Low Cost, High Volume Target Production Techniques

5.3.1 Critical Issue No. 1: Demonstration of Moderate Gain at Low Driver Energy - The U.S. National Energy Strategy[1] envisions three major facilities for IFE/ICF applications development: a Laboratory Microfusion Facility (LMF) for high gain target performance characterization and advanced military applications development; an Engineering Test Facility (ETF) to provide high pulse rate capability supporting fusion energy technology development and testing; and a Demonstration Power Plant (DPP) to validate long term economic, reliability, availability and maintainability issues for IFE. The total development cost associated with this plan will be formidable because each facility will likely cost more than $1B. It therefore is worthwhile to consider development paths that might enable a single facility to address both LMF and ETF research and development needs. Hogan discusses the prospects for such a facility in a recent paper[2]. Target experiments could be carried out in a separate, single-shot cavity. Engineering development would be conducted in another cavity with the target design and driver pulse rate selected to produce relatively low yield and fusion power. This approach would dramatically lower the cost of IFE development potentially leading to a more near-term DPP.

Reactor design studies have typically focused on high-gain, multi-megajoule incident energy target concepts that are appropriate for economic power production. However, engineering development, is usually cost limited. It therefore is worthwhile to consider if target designs that provide moderate gain (20-50) at low drive energy (1-2 MJ) are justified. Such targets would lower the facility cost associated with IFE engineering testing and fusion power demonstration. Target design studies for the Nova Upgrade have identified conditions under which the ignition "cliff" is shifted to much lower drive energy with the penalty of lower gain. This is illustrated in Figure 5.3.1-1 which compares the projected gain for two different sets of implosion velocities and associated hohlraum temperatures to that projected for the LMF conditions. (The shaded region at the low energy end of the curves represents the uncertainty in the location of the ignition "cliff" due to uncertainty in the capsule surface finish.)

As indicated, the alternative target designs coupled with a driver comparable to the Nova upgrade (1-2 MJ) would be above the ignition cliff and repeatably produce the output distribution (neutron/debris/x-ray split) and energy spectra of higher gain targets. Reactor component development testing could thereby be conducted at low drive energy with a cavity radius scaled appropriately to duplicate the relevant reactor parameters. In principle, this should provide the capability to achieve most of the ETF goals at relatively low power levels with full thermonuclear effects in a moderate cost facility.

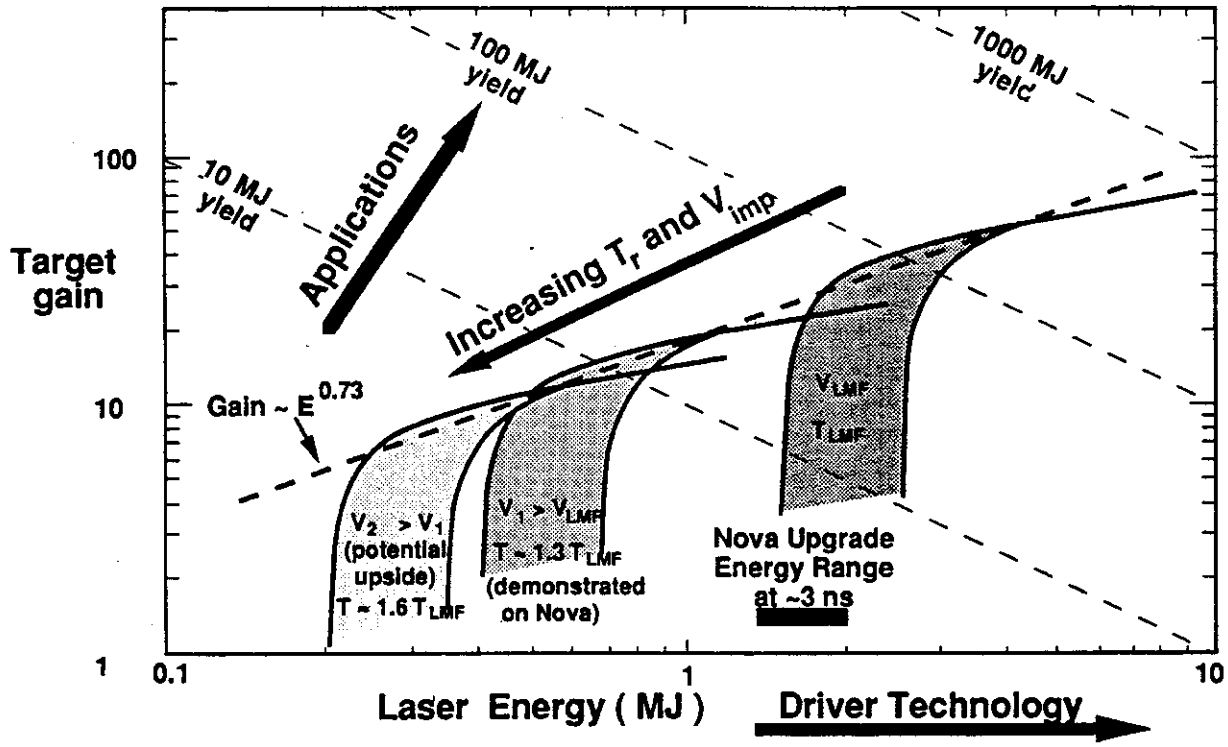

Figure 5.3.1-1. Gain Curve Scaling With Hohlraum Temperature Relative to Gain for the LMF Conditions. Nova Upgrade Will Characterize the 1-2 MJ Region of Gain Space and Reveal How Well the Location and Height of the Ignition Cliff Can Be Controlled. (Figure Courtesy LLNL).

Issue Resolution Strategy - To help identify the region of gain space that is attractive for reducing IFE development costs, the Prometheus driver, reactor and balance-of-plant design/cost scaling relations were used to project curves of target gain versus driver energy for a fixed capital cost facility. A 100 MWe demonstration power plant was chosen for illustration purposes. The costs are for a first-of-a-kind plant and include only direct construction costs. A summary of the cost elements included in the study and their scaling with yield (Y in MJ), pulse repetition rate (RR in pps), thermal power (P_{th} in MW), recirculating and gross powers (P_r and P_g in MWe) and driver energy (E_d in MJ) is presented in Table 5.3.1-1.

The resulting driver cost variation with output energy is shown in Figure 5.3.1-2 over the energy range of interest. This figure shows that projected laser costs are typically less than those for a multiple-beam LINAC but more than those for the 2 GeV single-beam system. The multiple-beam LINAC efficiency, however, is much higher than that for the other two driver options which offsets its higher cost.

Table 5.3.1-1. Summary of Demonstration Power Plant Direct Cost Scaling Used in Required Gain Curve Study

Cost Element	Cost Scaling Relationship (M$)
KrF Laser Driver (NLO)	$113 + 163\ E_d$
Single-Beam LINAC (4 GeV)	$288 + 76\ E_d$
Multiple-Beam LINAC (4 GeV)	$292 + 117\ E_d$
Single-Beam LINAC (2 GeV)	$218 + 35\ E_d$
Multiple-Beam LINAC (2 GeV)	$244 + 116\ E_d$
Land and Structures	$60 + 150(P_f/500)^{0.3}$
Reactor Plant	$50 + 480(P_{th}/3000)^{0.5} + 320(Y/500)^{0.5}$
Turbine Plant	$13 + 176(P_a/1000)^{0.8} + 20(P_{th}/2860) + 59((P_{th}-P_a)/1860)^{0.8}$
Electric Plant	$71.5 + 67(P_a/1000)$
Miscellaneous Plant	$57(P_n/1000)^{0.3}$
Target Factory	$50 + 100(RR/5.6)^{0.7}$

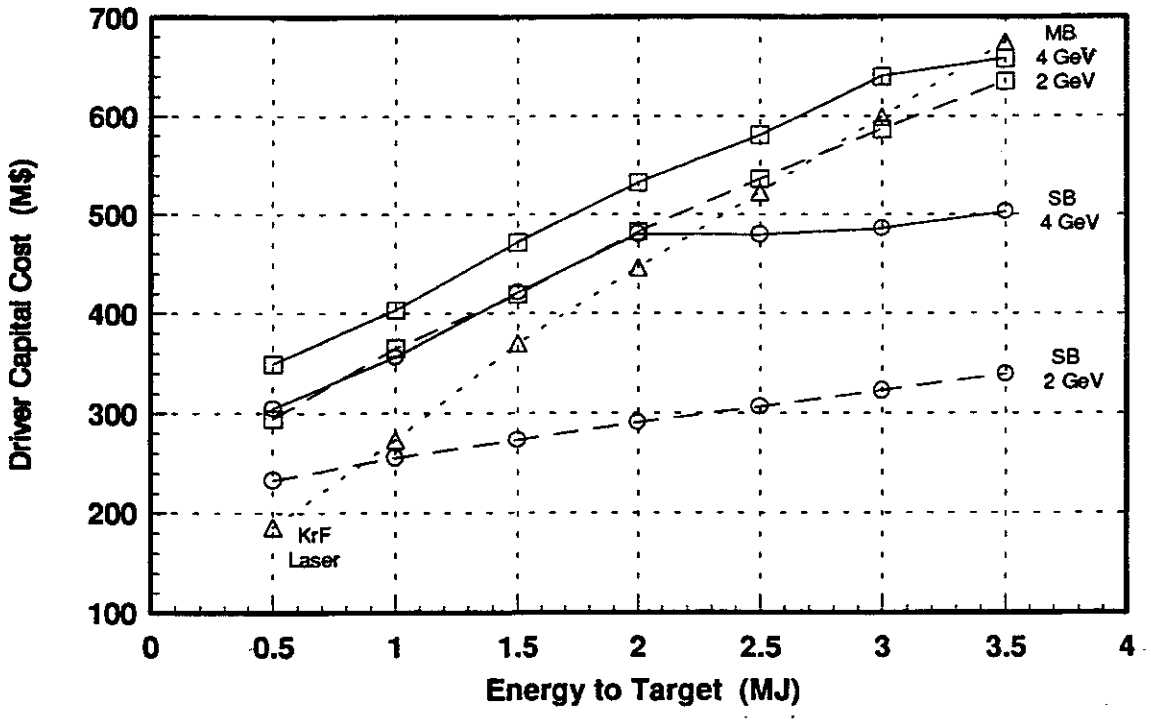

Figure 5.3.1-2. Projected Cost Scaling for Small-Size KrF Laser and Heavy-Ion LINAC Drivers

Efficiency plays a key role in minimizing the reactor and balance of plant costs for small plants where the net power is comparable to that required by the driver. This is because the recirculating power is equal to $P_{th} / (M \eta_d G)$ where M is the blanket energy multiplication (1.1-1.4). If the recirculating power exceeds the gross power ($\eta_{th} P_{th}$), no net power is generated. Conversely, if $M \eta_d G$ exceeds $1/\eta_{th}$ by more than a factor of two, the reactor and blance-of-plant costs are determined primarily by the net power requirement. As a result, in a cost-limited scenario, the gain (hence yield and associated plant cost) required to produce net power scales directly with driver efficiency. Figure 5.3.1-3 shows the projected efficiencies for the drivers considered in this study. The 10% Prometheus-L system efficiency may ultimately be increased to 15%, but both values are well below the 30% efficiency possible with a MB LINAC. This makes the MB LINAC an attractive option in spite of its higher capital cost.

It also is worthwhile to note that as driver energy increases, eventually there is no gain which will support both the recirculating and net output power requirements in a fixed-cost facility. The driver portion of the cost becomes too large. The required gain curves thus asymptote to infinity at some driver energy which is a function of the specified capital cost.

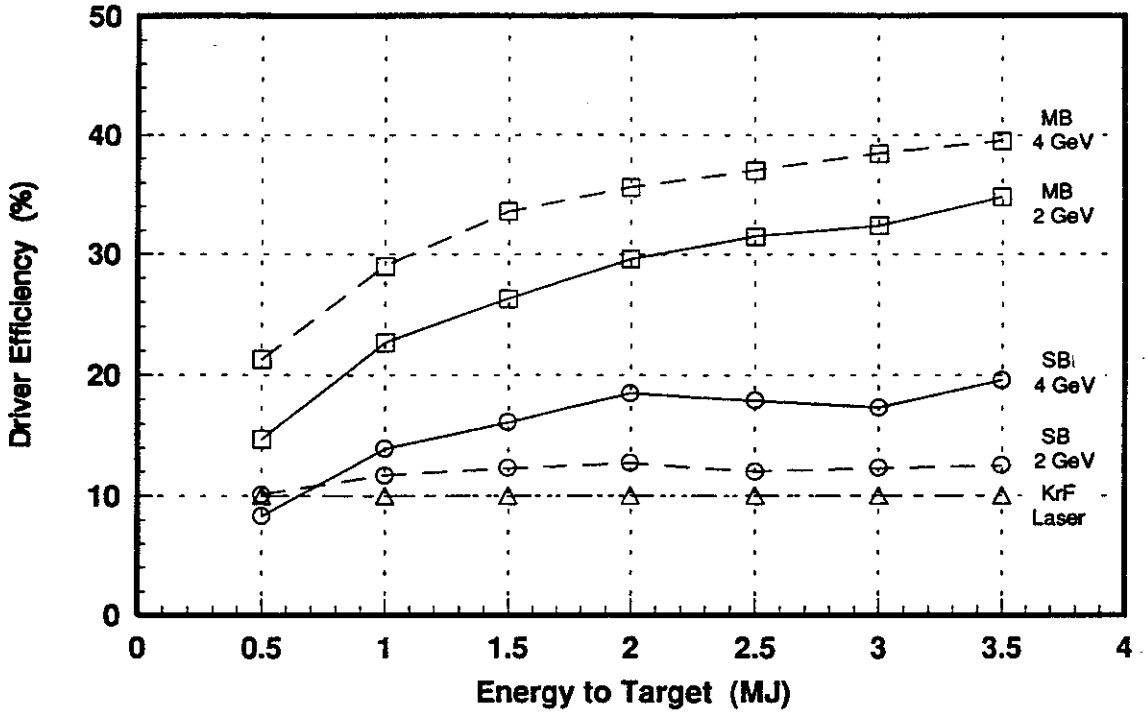

Figure 5.3.1-3. Projected Efficiency Scaling For Small-Sized KrF Laser And Heavy-Ion LINAC Drivers

These simple power balance and cost relations were used to define curves of required gain versus driver output energy for different fixed direct capital costs. Figure 5.3.1-4 shows the result for a 100 MWe power plant based on the Prometheus-L driver design at 10 and 15% efficiency. It should be noted that the target design windows for cost-limited development are the important consideration here not the projected capital costs. Absolute costs may change, but the parametric scaling should result in similar design windows. To assess whether the design windows are feasible, Figure 5.3.1-4 compares the gain requirement curves to possible optimistic and pessimistic physics limitations on target gain for indirect-drive targets suggested by Hogan[3].

The figure shows that target gains of 30-50 at a drive energy of 1-2 MJ provide a possible DPP design window for either 10 or 15% laser efficiency. Improved efficiency enlarges the design window (or conversely reduces the cost). But the gain required for a 10% efficient laser is less than conservative limits on possible target gain, with only $300M in additional funding beyond that needed to provide any design window. Therefore, there is significant motivation to develop target designs appropriate for this region of gain space. This is reinforced by the fact that such designs could likely be validated on Nova Upgrade.

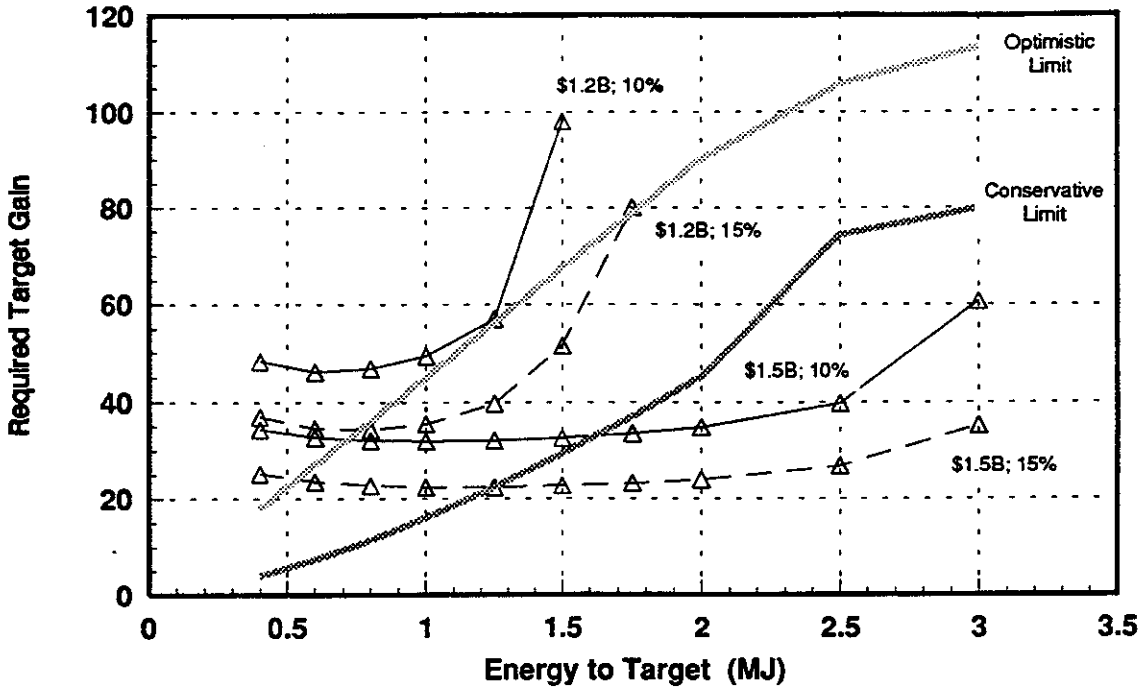

Figure 5.3.1-4. Projected 100 MWe Demonstration Power Plant Gain Space Windows for the Prometheus-L Driver Configuration. Values Indicated Only Include Direct Costs.

The simple power balance and cost relations were also used to evaluate the gain space appropriate for heavy-ion drivers. Figure 5.3.1-5 shows these results for a

comparable 100 MWe power plant with a single-beam (SB) LINAC driver based on the Prometheus-H design configuration. To assess the feasibility of such designs, Figure 5.3.1-5 again includes possible optimistic and conservative limits on gain suggested by Hogan[3]. This figure shows that SB power plants only require gains of 20-30 at a drive energy of 1-2 MJ due to the higher driver efficiency. This is greater than the conservative limit on gain scaling would suggest, but it is well below the optimistic gain scaling limit. A driver with 2.5 MJ output is required to surpass possible conservative limits on gain.

It is also worthwhile to note that the 2 GeV option may provide an extremely attractive development path. As indicated in Figure 5.3.1-2, this driver costs ~60% of the 4 GeV system because it is half as long. At driver energies above 3 MJ, the number of beams becomes excessively large (greater than 40) for a 2 GeV system. However, if viable target designs are possible in the 1-2 MJ energy range, this option provides a very low-cost driver (<$300M) with a number of beams comparable to that proposed for the Prometheus-H plwer plant. Further characterization of heavy-ion target designs in this region of gain space thus is clearly justified.

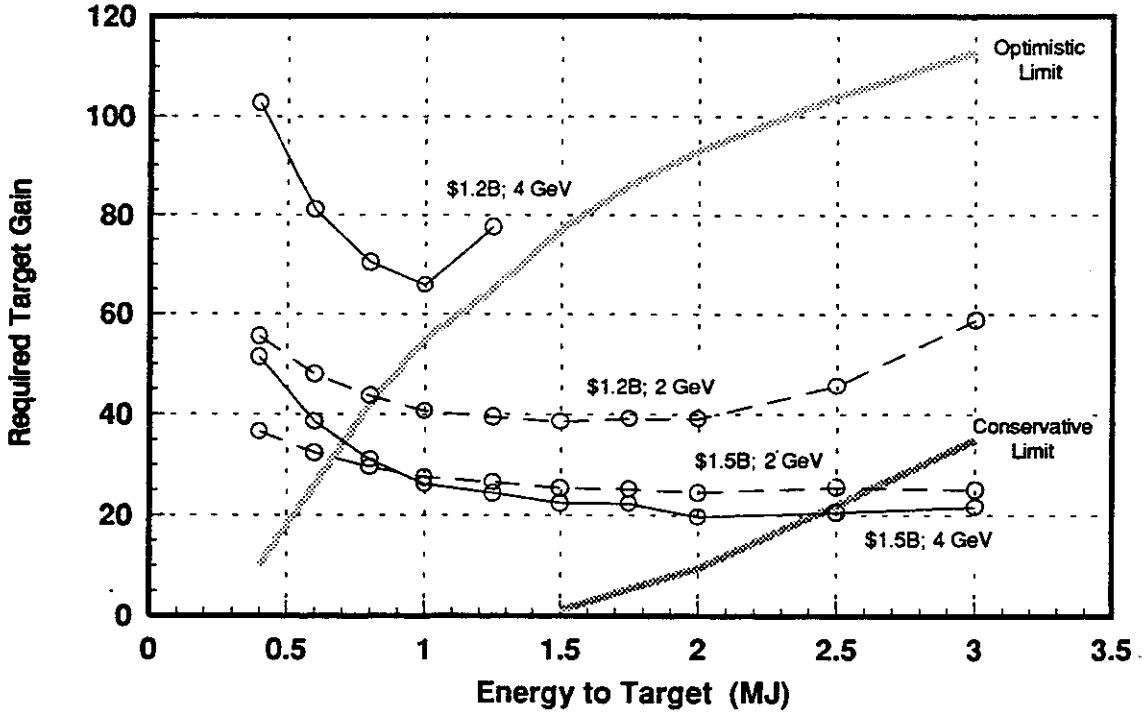

Figure 5.3.1-5. Projected 100 MWe Demonstration Power Plant Gain Space Windows for the Single Beam Prometheus-H Driver Configuration. Values Indicated Only Include Direct Costs.

Figure 5.3.1-6 shows these same gain space design windows for a 100 MWe power plant with a multiple-beam (MB) LINAC driver. This option eliminates the core recycling and storage rings required for the single beam design, which leads to

efficiencies between 20 and 40% as indicated in Figure 5.3.1-3. This makes the MB LINAC an attractive option for a DPP in spite of its higher capital cost, as indicated in Figure 5.3.1-2, since recirculating power is significantly lower. This is highlighted in Figure 5.3.1-6, which shows that the required gain curves for an MB LINAC are actually lower than those for the SB LINAC once funding is large enough to get over the hump of its higher capital cost. Gains of 10-20 at driver energies between 1 and 2 MJ are all that is required to build a small DPP using an MB LINAC driver.

The figure also shows that the 2 GeV design may once again offer an attractive development pathway. The cost advantage of a 2 GeV system is reduced for the MBL driver, as indicated in Figure 5.3.1-2, but its efficiency is comparable to that at 4 GeV. Furthermore, target performance will likely be improved at this energy because of the shorter ion range. A 2 GeV MB LINAC may therefore prove to be the best option for a heavy ion DPP. The SBL capital cost is significantly lower, but this is offset by reduced BOP costs for the higher MB efficiency for a small DPP where there is little excess ηG.

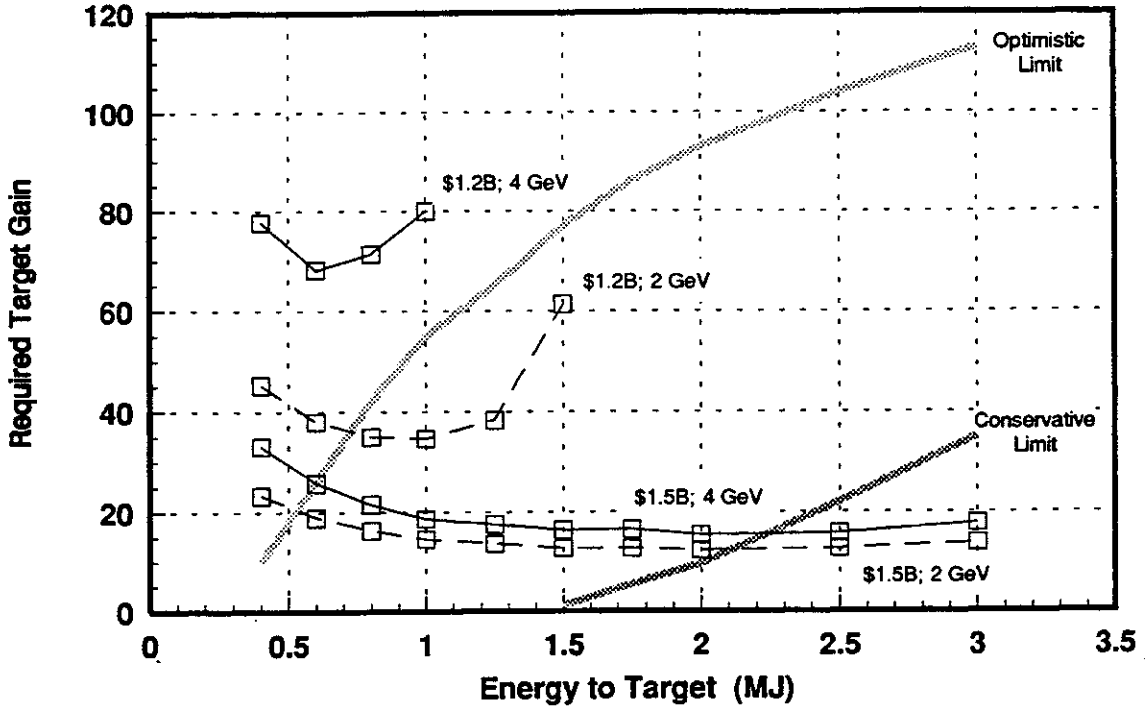

Figure 5.3.1-6. Projected 100 MWe Demonstration Power Plant Gain Space Windows for a Multiple Beam LINAC Driver. Values Indicated Only Include Direct Costs.

It, therefore, is critical that the Nova upgrade or a similar plant be implemented in a timely manner. Target experiments could then be conducted to characterize the location of the ignition cliff and the height of the gain curves for advanced target designs. This will establish a database for designing the ETF/LMF facility. An early ~2000 demonstration of low drive energy (1-2 MJ) target designs with repeatable

gains comparable to those projected by this study would also provide strong justification for a lower-cost IFE development pathway utilizing such moderate-gain targets. This could provide the impetus to accelerate the engineering development and commercialization of IFE technology.

References for 5.3.1

1. National Energy Strategy, First Edition 1991/1992, U.S. Department of Energy, Washington, DC, February 1991.
2. W. J. Hogan, "Small Inertial Fusion Energy (IFE) Demonstration Reactors," to be published, Proceedings 14th IEEE/NPSS Symposium on Fusion Engineering, San Diego, CA, October 1991.
3. W. J. Hogan, private communication, 1992.

5.3.2 Critical Issue No. 2: Feasibility of Direct Drive Targets

Description of Problem - There are strong incentives to consider direct-drive (DD) laser targets because of higher gains. However, the feasibility and performance characteristics of DD targets are presently uncertain. These discussions are likely also applicable to heavy ion, direct drive targets, but the database is non-existent. The fundamental laser driver architecture of the Prometheus IFE Reactor Design is strongly influenced by the direct-drive (DD) target illumination requirements given by the Target Working Group (TWG). Unfortunately, the specified TWG requirements may contain some serious inconsistencies with published plasma physics requirements for efficient laser/target coupling. The laser driver spatial intensity profile in the target plane provided by the TWG is not consistent with the Fresnel number of the beam at the location of the target. In addition, there are concerns that the long, 80 ns precursor pulse may produce significant deleterious effects, such as generation of non-linear scattering processes which may lead to target preheat, thereby preventing an efficient DT implosion from occurring. Designs for DD targets appear to have been anchored on experiments conducted on miniature DD targets illuminated with only a few kJ of laser energy. Large reactor sized, multi-MJ DD targets apparently require entirely different illumination scenarios. For reactor operation, the DD targets must also be accurately injected into the target chamber with a tracking/alignment system capable of meeting the illumination uniformity requirements set forth below.

Review of Target Illumination Requirements Supplied by TWG - The TWG has provided the project with laser direct drive target illumination requirements which include the following elements:

(1) ≥ 60 beam illumination with $\pm$ 1% illumination homogeneity of a 6-mm diameter target
(2) 80 ns precursor pulse containing 30% of energy, followed by 6-ns main pulse (long prepulse generates underdense plasma atmosphere 3.2-cm deep prior to arrival of main pulse, thereby risking generations of SBS, SRS, hot electrons, and resonant absorption mechanisms)
(3) UV wavelength (<300 nm) with approximately 5 MJ of energy
(4) Tangential illumination (beam diameter at target = target diameter); no mention of focal zoom; beams are circular in cross-section, (very wasteful of laser light, excimer laser beams are square, may encourage resonant absorption in underdense plasmas)
(5) The spatial intensity distribution of the incident laser beams in the target plane is described by $I_{target}(x) = (\sin^2 x) / x^2$ (inappropriate apodization for homogeneous illumination and efficient excimer laser extraction)

There were no TWG specified requirements on beam polarization, bandwidth, or beam quality, all of which are important parameters in laser/target interactions. During the 6-ns main pulse duration, the direct drive (DD) target implodes from an initial 6 mm diameter down to 3 mm, which corresponds to an implosion speed of 2.5×10^7 cm/sec. Approximately 30% of the DT fuel is fused during the resulting implosion.

Physics of Target Implosion - Using the TWG criteria, the DD target is assumed to be a 6-mm CH spherical shell containing a layer of frozen DT. The initial laser photons incident on the CH shell blow off an underdense plasma from the CH shell to permit the main pulse to interact primarily with the plasma atmosphere. The intention is to drive a symmetrical implosion of the D/T fuel to at least 20 times liquid density. A diagram of a single beam (one of many) tangentially illuminating a spherical direct-drive target at the start of the laser pulse is shown below in Figure 5.3.2-1.

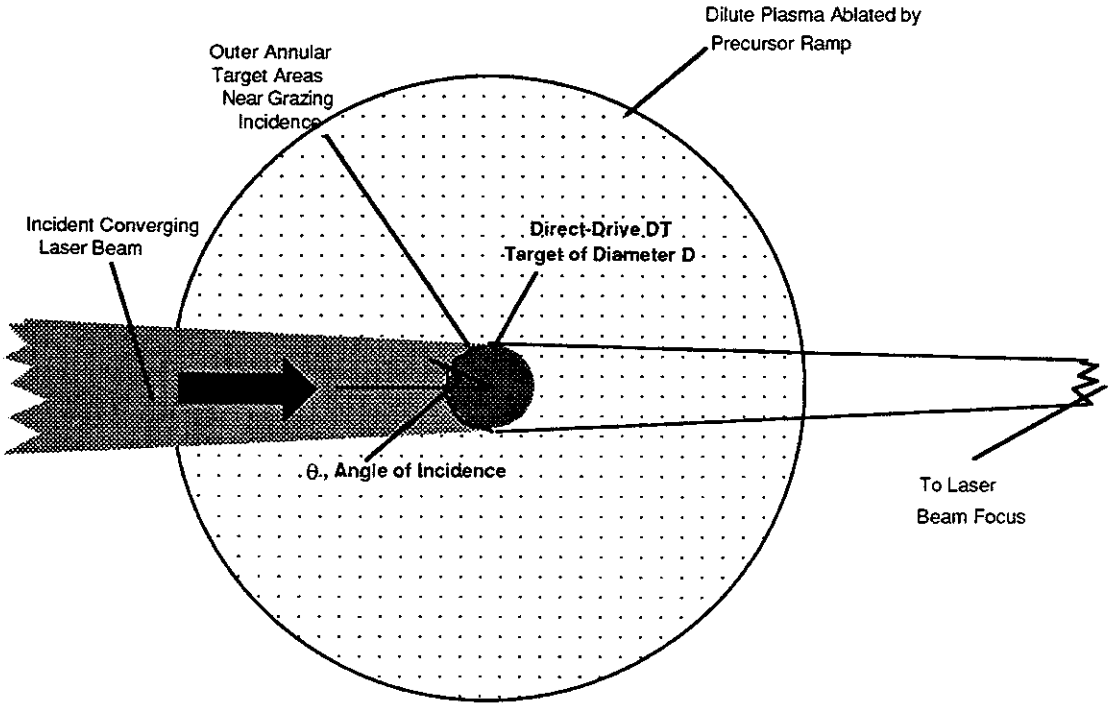

Figure 5.3.2-1. Diagram of Tangential Direct-Drive Target Illumination Geometry at Start of Main Pulse

A precursor pulse this long produces an underdense atmosphere 3.2 cm deep by the arrival of the main pulse, thereby providing a long gain length for non-linear processes which can cause target pre-heat. During the resulting implosion occurring at a speed of approximately 2.5×10^7 cm/sec., the target compresses to ~50% of its original diameter. Unless the laser beam focal spot sizes are also reduced by 50%, a

significant amount of laser light would consequently miss the target. A diagram illustrating this problem is shown in Figure 5.3.2-2.

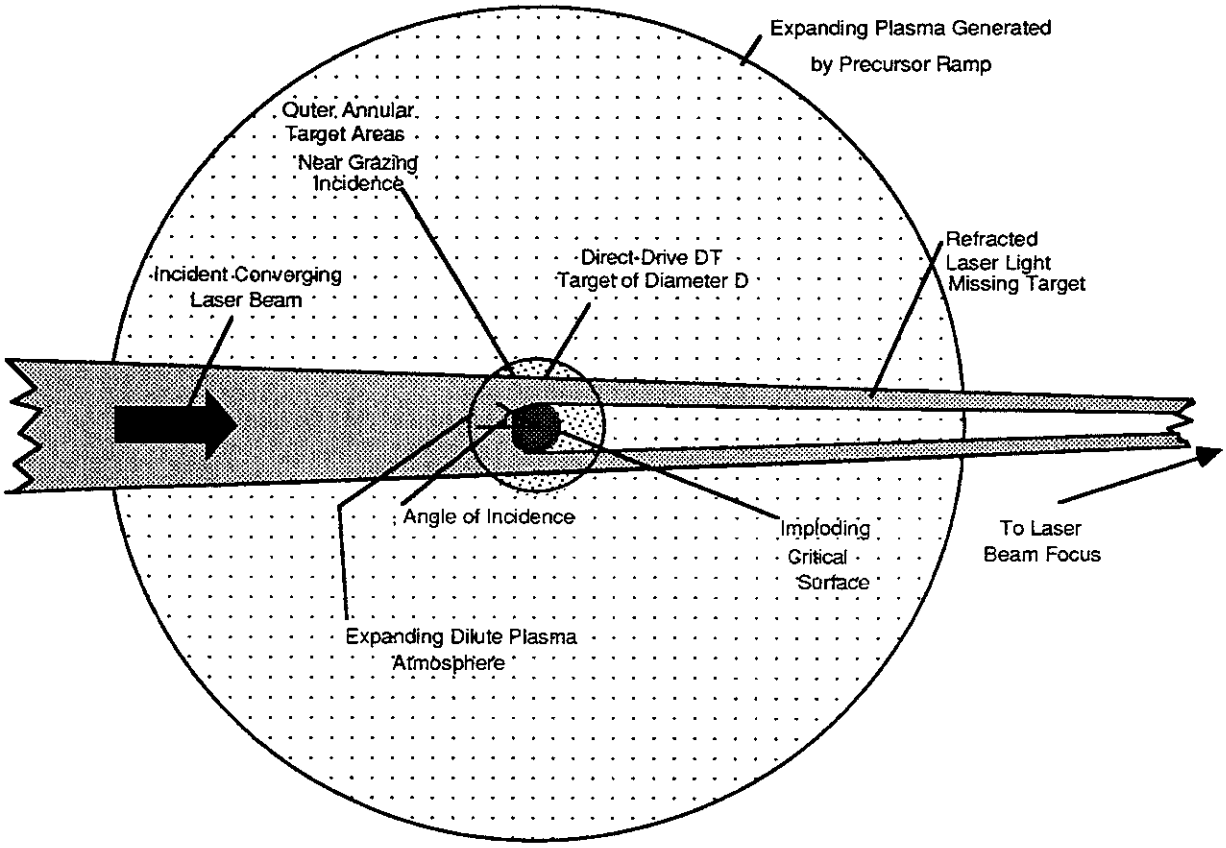

Figure 5.3.2-2. Diagram of Tangential Laser Illumination Geometry at end of 6 ns Laser Pulse

Recapitulation of Published Plasma Physics Target Coupling Requirements -
Uniformity of target illumination for multiple beam geometries is essential for preventing the growth of Rayleigh-Taylor instabilities. However, it is also important that the angle of incidence, θ, between the incoming laser beams and the target be minimized in order to absorb the incident beam efficiently into the critically-dense plasma atmosphere blown off from the target. According to Kruer,[1] the fractional absorption, f_A, for a linear plasma density profile is given by the expression:

$$f_A = 1 - \exp\left(\frac{32\, v_{ei}\, L}{15c}\cos^5\theta\right) \qquad (5.3.2\text{-}1)$$

which, as indicated, depends upon $\cos^5 \theta$. Here, v_{ei} is the plasma collision frequency evaluated at the critical density, n_{crit}. In addition, since an obliquely incident optical wave reflects from the plasma at a lower density than the critical density, less collisional plasma is traversed by these waves, further decreasing the coupling fraction. Calculations were carried out using this absorption function using the geometry shown below in Figure 5.3.2-3.

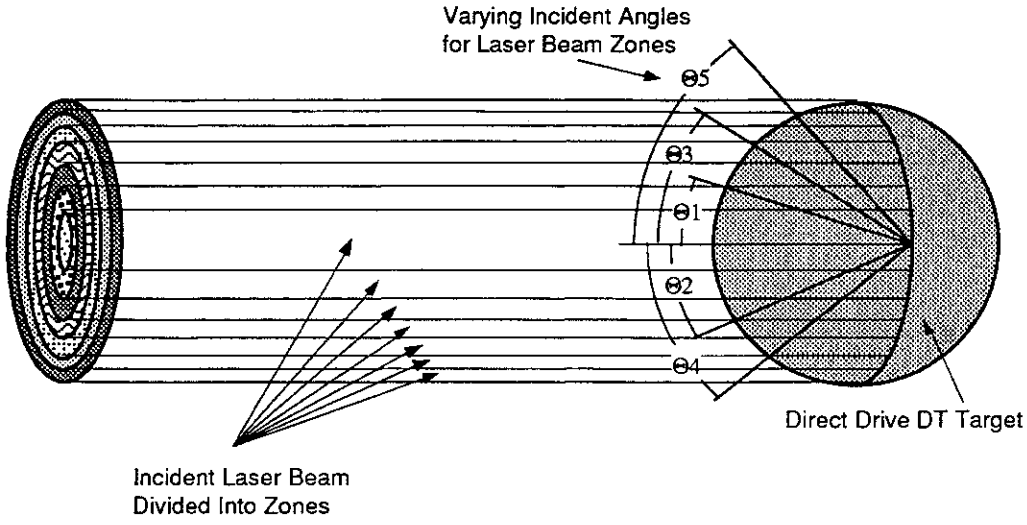

Figure 5.3.2-3. Geometry for Computing Angular-Dependent Light/Plasma Coupling Efficiencies

Using this geometry and Eq. 5.3.2-1, the target coupling efficiency was calculated assuming that $f_A = 1$ for $\theta = 0$ with a top hat apodization; the results are plotted below in Figure 5.3.2-4.

For a linear density profile averaged over the implosion time, these simulations estimate that only 15% of the laser light incident on the target will be absorbed. Since the actual beam shapes from the excimer lasers are square, a further reduction in target absorption efficiency of $\pi/4$ occurs. For an exponential electron density profile in the plasma ($n_c = n_{crit} \exp(-z/L)$, the fractional absorption, f_A, is given by the expression:

$$f_A = 1 - \exp\left(\frac{8\, v_{ei}\, L}{3c} \cos^3\theta\right) \qquad (5.3.2\text{-}2)$$

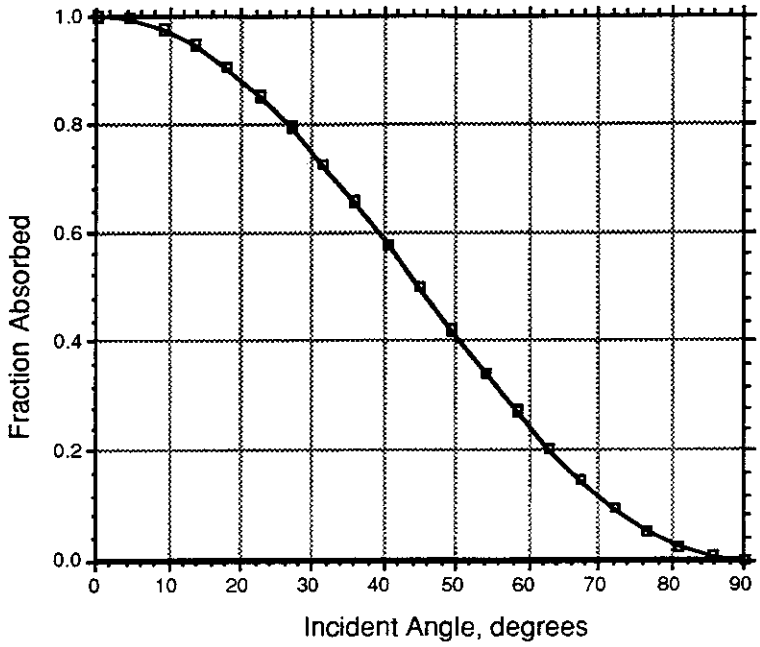

Figure 5.3.2-4. Fraction of Incident Laser Light Absorbed For Linear Plasma Density Profile

which, as indicated, depends upon $\cos^3 \theta$. Calculations were also carried out using this absorption function with a top hat apodization. In this case, 28% of the energy incident on the target would be absorbed.

Resonance Absorption Calculations - The energy absorbed by resonantly driven fields in the plasma is described by the expression:[2]

$$E_{abs} = \int \left(\frac{v\,(\langle E_r^* E_r \rangle)}{8\pi}\right) r^2\, dr \sin\theta\, d\theta\, d\phi \qquad (5.3.2\text{-}3)$$

where E_r is the radial electric field of the laser beam. Near the critical density, the expression for E_r is given by:

$$E_r = \frac{\ell\,(\ell+1)}{(i\varepsilon k^2 r^2)} a_\ell (1-\alpha_\ell^2)^{\frac{1}{4}} P_\ell^1(\cos\theta) \cos\phi \exp(i\delta) \frac{\Phi^2(\tau_\ell)}{2\pi\gamma\alpha_\ell^2} \qquad (5.3.2\text{-}4)$$

where α_l is given by the expression:

$$\alpha_\ell = \frac{\sqrt{\ell\,(\ell+1)}}{k\,R_c} \qquad (5.3.2\text{-}5)$$

(where R_c is the radius of the plasma critical density) and where $\Phi^2(\tau_l)$ is the absorption function for the lth mode. The fraction absorption of the lth mode, f_{RA}, is given by:

$$f_{RA} = \frac{\Phi^2(\tau_\ell)}{2\pi}\sqrt{1-\alpha_\ell^2} \qquad (5.3.2\text{-}6)$$

so that the total power absorbed from the laser beam as a consequence of resonance absorption is given by:

$$P_{RA} = \sum_\ell \frac{P_\ell}{2\pi}\,\Phi^2(\tau_\ell)\sqrt{1-\alpha_\ell^2} \qquad (5.3.2\text{-}7)$$

where P_l is the laser power in the lth mode. The net result of performing the integral in Eq. 5.3.2-3 is to show that resonance absorption generally depends upon $(\cos\theta_0)$;[2] the implication is that tangential target illumination proposed by the TWG would favor resonant absorption over inverse Bremsstrahlung for large angles of incidence. Perhaps a more serious result of these analyses[2] is that the spatial absorption distribution function is not uniform over the target sphere. The calculated RA distribution for a vertically polarized laser beam is shown in Figure 5.3.2-5.

As shown, resonance absorption is predicted to produce two symmetrical "hot spots" of absorption at mid-latitudes on the sphere when illuminated with linearly polarized light. This may constitute an absorption uniformity problem because this process occurs even when the sphere is uniformly illuminated. However, by using $\lambda = 248$ nm laser radiation, the effects of resonance absorption are not expected to be reduced relative to inverse Bremsstrahlung.

DD Target Injection, Tracking, and Alignment Problems - The 6-mm DD target is assumed to be injected into the target chamber with speeds of the order of 200 m/sec. Owing to the vagaries of mechanical and/or electromagnetic injection methods, tracking of the target and alignment of the 60 beamlines to the anticipated location of the target is mandatory. If tangential illumination is used, beams need to be aligned with an accuracy of ±500 μ (corresponding to an angle $\Delta\alpha = 25$ μrad as seen by the FEM) relative to the target. If pyramidal apodization is used, much more accurate

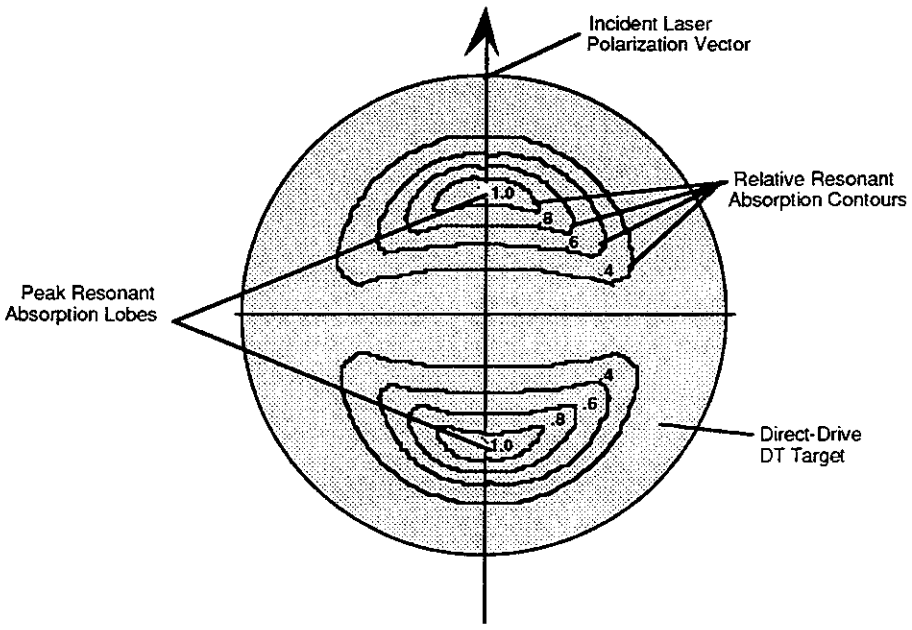

Figure 5.3.2-5. Resonant Absorption Contours on Spherical DD Target

target alignment is required (estimated to be ±5 μ [corresponding to an angle $\Delta\alpha = 0.25$ μrad as seen by the GIMM]). In order to achieve the requisite alignment accuracy in this case, a reflective "shine shield" on the direct drive target is strongly recommended. Although DD target injection, tracking, and alignment present technological challenges, it is believed that these problems can be solved using careful engineering, parallel dedicated computer processing, and advance metrology techniques.

Summary - Present specifications for the DD target illumination requirements such as those provided by the TWG, are based upon work performed at only a few kJ of laser energy. Elementary plasma physics and optics calculations suggest that the current TWG DD target illumination specifications are seriously flawed. It is essential that DD target results obtained at hundreds of kilojoules to megajoules be carried out as soon as possible to permit realistic DD target driver requirements to be generated. Such experiments could be performed using the Nova Upgrade laser proposed to be built at the Lawrence Livermore National Laboratory.[3,4] Using advances in laser technology together with SDIO tracking technology, we anticipate that high gain DD targets could be developed which require only a few MJ of laser energy to achieve optimum performance. These large reductions in the requirements for laser energy can lead to significant reductions in COE as well as an increase in reliability. More importantly, the development steps will have facilities of much smaller size and moderate costs.

References for 5.3.2

1. The Physics of Laser Plasma Interactions, William L. Kruer, Chapter 5, "Collisional Absorption of Electromagnetic Waves in Plasma," pp. 45-56.

2. "Laser Light Absorption in Spherical Plasmas," J. J. Thomson, C. E. Max, J. Erkkila, and J. E. Tull, Physical Review Letters 37, pp. 1052-1056 (1976).

3. "Nova Upgrade Facility for Ignition and Gain," LLNL ICF Program, UCRL-LR-106874, LLNL, Livermore, CA 94550, March 1991.

4. "Nova Upgrade–A Proposed ICF Facility to Demonstrate Ignition and Gain by the Year 2000," LLNL ICF Program, UCRL-LR-106736, LLNL, Livermore, CA 94550, March 1991.

5.3.3 Critical Issue No. 3: Feasibility of Indirect Drive Targets for Heavy Ions

Description of Problem - The feasibility of the indirect drive (ID) targets for the heavy (HI) ion driver is, in part, linked to: (1) the properties of the method used to transport and focus the HI beam to the target, (2) the accuracy and reproducibility of the repetitive HI target launch system which injects the ID targets to the center of the target chamber, and (3) the ability of the high-Z hohlraum cavity to efficiently convert and smooth the radiation incident on the DT capsule. This study is involved with finding innovative solutions only to the first and second tasks.

There are several methods of transport of the heavy ion beams across the cavity and focusing onto one or more locations on the target, either direct drive or indirect drive. Sections 4.3.2 and 6.5.2.6 discuss these options in some detail. Two methods are worthy of note, ballistic transport and channel transport. A concurrent IFE Reactor Design Study[1] was accomplished by a team lead by W.J. Schafer Associates. This team selected the ballistic approach while the MDA-led tema chose the channel transport. In the interest of brevity, the discussion of this issue will be limited to the channel transport option although may aspects of the issue are common and generic.

In the approach being investigated for the Prometheus-H IFE Reactor Design, a number of HI beams is focused onto a stripping foil or cell placed in front of a pre-ionized channel. The HI beam(s) are then completely stripped, yielding mega-ampere currents which overcome space charge repulsion to self-focus the beam(s), thereby trapping the ions in a small diameter (a few mm) channel whose direction is accurately determined by the pre-ionizing beam. This self-focused, small diameter beam is subsequently directed to the convertor regions of the moving hohlraum target capsule. The target has been injected to arrive at the center of the reactor target chamber synchronously with the arrival of the HI beam(s).

Two types of indirect drive, heavy ion fusion targets were considered:

(1) Single energy convertor ID hohlraum targets designed for single-sided target irradiation (SSTI), and
(2) Dual energy convertor ID hohlraum targets designed for dual-sided irradiation (DSTI).

The feasibility of efficiently imploding both of these ID targets depends upon the solution of a series of technical problems, including:

(1) Providing return paths for the 13.3 $x10^6$ A current for the SSTI beam and for 6.7 $x10^6$ A for each beam for the DSTI case.
(2) Successful injection and self-pinching of the HI beams passing through the stripping foil(s) into a self-focused, small diameter beam directed at the SSTI or DSTI ID target.
(3) Accurate pointing of the pre-ionized channel(s) at the energy convertor(s) of the ID target.
(4) Precision launching of the HI ID targets to arrive repeatedly at the center of the target chamber and synchronized with the arrival of heavy ion beams.

Review of Target Irradiation Requirements Supplied by TWG - The Target Working Group (TWG) supplied the team with several unclassified documents[2,3] which were used to design a suitable HI driver design. The following general HI driver requirements were determined from the TWG recommendations:

(1) Tightly focused HI beams containing approximately 5 MJ of energy are to be delivered in a main beam pulse duration of 6 ns,
(2) The incident HI beam diameters need to be ≤6 mm at the $1/e^2$ points,
(3) The HI beams must intercept the convertor regions with an accuracy of ±0.5 mm.

Physics of Single-Sided HI ID Target Irradiation - Key to both the HI ID target irradiation of both single-sided and double-sided targets for the Prometheus IFE reactor is the collapse of all the separate HI beams into a single, pre-ionized channel of small dimensions. In the Prometheus IFE reactor design concept, this feat is accomplished by focusing the separate, bunched beams with large quadrupole magnets down to a common focus coinciding with a thin stripping foil. A schematic of this configuration is shown below in Figure 5.3.3-1. Background gas is present to permit autoneutralization of the focusing beams. Immediately prior to the arrival of the bunched beams, a non-bunched, precursor HI beam is precisely directed through the foil to the predicted location of the HI target. The target moves approximately 10 μm while the beams cross the cavity. Care must be taken to avoid damaging the HI ID target with the non-bunched beam. A dilute gas (Pb vapor) at a pressure of ~100 millitorr is present in the target chamber. The non-bunched precursor HI beam forms an ionized channel in the dilute lead vapor from the foil to the HI target.

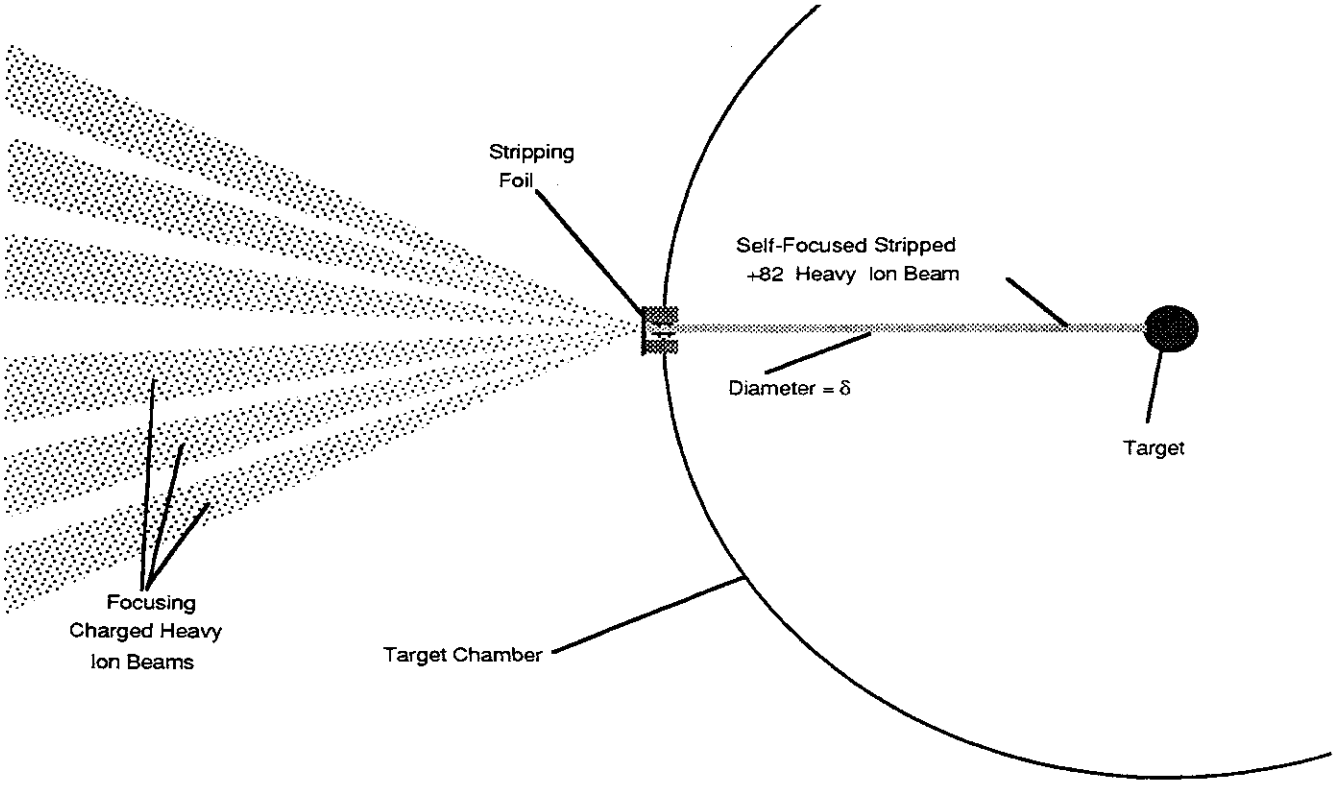

Figure 5.3.3-1. Schematic of Prometheus Approach for Heavy Ion Single Sided ID Target Irradiation

Following the arrival of the bunched HI beams, each +2 ion is stripped to an ~ +80 charge state, thereby increasing the current to a level of approximately 6 MA. This beam current is more than an order of magnitude larger than is necessary to self-pinch the combined beams, thereby leading to a trapped, self-focused HI beam precisely directed to the energy convertor of the single-sided HI target. The diameter, δ, of the self-pinched beam oscillates transverse to the beam direction with an amplitude determined by the original beam emittance and a period of approximately 20 cm.

Physics of Double-Sided HI ID Target Irradiation - The technical problems associated with double-sided HI ID target irradiation are similar to those described above for the single-sided HI ID target case. An additional constraint is that the two HI pulses must not only arrive near simultaneously at each of the target energy convertors, but they must also be accurately aligned spatially. A schematic of the double-sided HI ID target irradiation geometry is shown below in Figure 5.3.3-2.

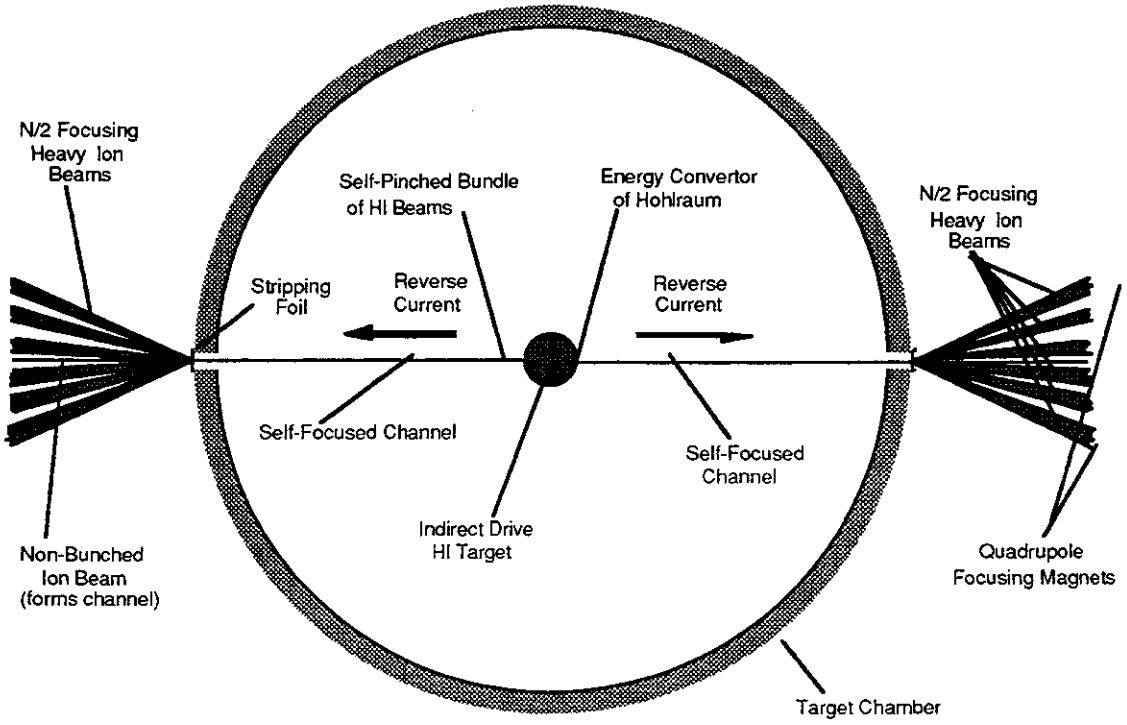

Figure 5.3.3-2. Schematic of Double-Sided Heavy Ion ID Target Irradiation Geometry

As noted above, key to the Prometheus HI ID double-sided target irradiation concept is the collapse of the two sets of separate HI beams into each of the two pre-ionized channels of ≤6 mm diameter. In this case, the non-bunched precursor HI beams create the ionized channels in the low pressure (100 millitorr or less) lead vapor prior to the arrival of the HI ID target.

In a manner similar to that described above for single-sided irradiation, following the arrival of the N/2 bunched HI beams, each +2 ion is stripped to a ~ +80 charge state, thereby increasing the current to a level of approximately 6 MA. This is sufficient to self-pinch the combined beams, thereby leading to a pair of colliding, self-focused HI beams precisely directed to the energy convertor of the double-sided HI target. Previous work performed with heavy-ion beams has shown that high degrees of precision can be achieved with regard to both timing of pulse arrival as well as intercepting a small aperture, providing the divergence associated with non-compensated space charge have been overcome.

ID HI Target Transport Problems - The problems asociated with transport of the indirect drive heavy ion beam target relates to two general categories:

(1) Protection of the cryogenic target from thermal radiation, primarily emanating from the cooling interior of the reactor chamber

(2) Accurate delivery of the indirect drive, heavy ion beam target to a location where the beams can successfully illuminate the target.

Indirect drive targets by their very nature are relatively fragile and difficult to accelerate rapidly. In general, accelerations greater than 100 m/sec^2 are to be avoided. Target velocities should be in the range of 200 m/s to minimize the transit time across to the center of the chamber. Since the cryogenic DT capsule is relatively well protected from the thermal radiation present in the target chamber, the HI ID target is predicted to be less prone to heating. Because of the 100 mtorr residual lead vapor pressure, the effect of viscous drag and turbulence on the motion of the target in the chamber must be determined.

As mentioned earlier, the target injector and the beams must work in conjunction with each other to provide the required illumination on every target. To date, the experimental targets have been stationary and the beams and/or target adjusted to achieve the desired illumination requirements. In demonstration power or commercial reactors, this degree of accuracy must be achieved every time, several times a second. This can be accomplished either with a highly precise target injector and the target can be tracked and the beams adjusted to the known or predicted location of the target.

The factors which effect the final position of the target include the velocity vector at release and the environment during the transit to the final position. The magnitude of the vector, if measurable, is not a serious problem as the timing of the beams can be adjusted to compensate. Alignment of the injector can easily be corrected. The alignment of the single-sided injector would be easiest because it would enter from the opposite side of the chamber and would be aligned coaxial with the beam. The alignment of the injector with dual-sided illumination is more difficult because coaxial injection is not permitted due to the on-axis precursor beams. The Prometheus recommendation was to locate the injector off axis by 10° to clear the beamline cone. This severely complicates the alignment because the lateral component of target motion relative to the nominal beam axis. Timing of the beam becomes more critical and/or beam adjustments are required.

One of the more serious difficulties is ensuring that during the release of the target from the injector no lateral forces are induced which would influence the target velocity

vector. The precision of the injector can be analytically modeled and then tested experimentally to verify the required precision. The environmental influences within the chamber are more difficult, especially predicting how the environment will behave a few tenths of a second after the prior fusion reaction. Modeling and experimental evidence will be required to develop the necessary database.

Upon leaving the injector, the velocity and position of targets must be determined. The targets could be tracked (with difficulty) through the shield, blanket, and into the actual cavity. Depending upon the known characteristics and behavior of the cavity environment, the required degree of tracking is determined – the better the environment is known, the less tracking is required and vice versa. Sensors can be protected to some degree, but high levels of radiation hardening will be required inside the shield area.

Summary - In the Prometheus IFE reactor concept, the feasibility of indirect drive heavy ion targets is largely based upon the successful and efficient collapsing of a large number of low ionization state particles into one or two single, highly ionized, self-pinched ion beams that are accurately guided to the energy convertor(s) of a heavy ion indirect drive hohlraum. Since the TWG specifications for HI ID targets were vague, the Prometheus IFE reactor concept has necessarily incorporated a great deal of flexibility in the final focus and transport portions of the heavy ion driver design.

It is important to demonstrate the validity of the Prometheus heavy ion final focus and self-pinched propagation physics experimentally. Since these experiments must be performed at full scale, it will be necessary to construct a substantial heavy ion driver machine in order to demonstrate the concept. It is strongly recommend that this be accomplished within the next decade.

References for 5.3.3

1. W. R. Meier, et al., "OSIRIS and SOMBRERO Inertial Fusion Power Plant Designs," W.J. Schafer Associates Report, WJSA-923-01 (March 1992)

2. "Inertial Confinement Fusion Reactor Design Studies; Recommended Guidelines," Ronald C. Davidson, et al., prepared for the Department of Energy Office of Fusion Energy, September 1990.

3. "Revised Target Information for IFE Reactor Studies," received form Roger Bangerter, Lawrence Berkeley Laboratory, Bldg. 47, room 112, 28 February 1991.

5.3.4 Critical Issue No. 4: Feasibility of Indirect Drive Targets for Lasers

Description of Problem - As in the case of the indirect drive heavy ion fusion target, the indirect drive (ID) laser fusion target being considered by the Prometheus IFE Reactor Design is a symmetric, two-sided hohlraum design. The feasibility of efficiently imploding this ID laser target has difficulties arising from three major sources:

(1) Plasma closure of the two entrance apertures to the hohlraum,
(2) Accurate target tracking and pointing of the multiple laser beams to coincide with the two entrance apertures of the moving ID target, and
(3) Accurate and reproducible indirect drive target propagation from the pellet injector to the center of the target chamber.

Significant misalignment of the laser beams could damage the radiation casing of the target capsule and cause a target misfire.

Review of Target Irradiation Requirements Supplied by TWG - As in the case of the heavy ion indirect drive targets, the Target Working Group (TWG) has supplied the team with unclassified documents. In the original inertial confinement fusion driver guideline document[1] supplied us, all references to indirect drive laser targets had been removed. A second document,[2] obtained much later, has some information concerning indirect drive laser targets. After careful examining of the information in these documents[1,2] from the TWG, the following laser driver requirements were surmised:

(1) Using the Nova Upgrade laser plan of 288 independently pointed beams arranged in three or four rings of beams on each side of the target with the beams distributed in angles ranging from 30° to 60° from the target axis, the indirect laser target illumination requirement is achieved. It should be possible to reduce the total number of beams to approximately 50. This would require an energy balance between beams of 5%. (Achieving a 5% balance of power among the laser beams is significantly easier than the 1% illumination uniformity required for direct drive laser targets)

(2) Nearly diffraction-limited laser beams are required with essentially all of the ~2.5 MJ in each of the two beams being contained inside a 1.5-mm diameter spot. Pulse durations range from around 8 ns at a 5 MJ energy level to 10 ns at 10 MJ. of 6 ns. (This is readily achieved since the focal spot size from a 1-m aperture mirror located 20 meters from the target chamber can achieve a 15-μm spot size.)

(3) A laser wavelength is needed for which efficient inverse Bremsstrahlung can be achieved [UV Wavelength (<300 nm)].

(4) A precursor laser pulse containing 30% of the energy and having a duration of 40 to 50 ns is required.

In general, these requirements are easier to meet than those specified for the laser direct-drive target. There are, however, some additional problems associated with ID laser targets which may seriously affect performance.

ID Laser Target Transport Problems - As noted, indirect drive laser targets are relatively fragile and difficult to accelerate rapidly. In general, accelerations greater than 100 m/sec^2 are to be avoided. Since the cryogenic DT capsule is relatively well protected from the thermal radiation present in the target chamber, the laser ID target can survive for longer periods in the target chamber (i.e., the propagation speed of the laser ID target need not be as great as that required for the laser direct drive target owing to this protective feature). See Section 5.3.3 for a list discussion of similar problems.

Summary - The feasibility of indirect drive laser targets is largely based on overcoming a number of potential technical problems: (1) directing 50 nearly diffraction limited laser beams accurately to the entrance apertures of the target and (2) reliably transporting the indirect drive target to the center of the target chamber with great precision. A great deal of flexibility in the final laser beam focus and transport portions of the laser architecture was incorporated to accommodate the range of specified requirements. As in the case of the direct drive target, technical development of high speed tracking and laser pointing systems are required in order to assure that all laser beams would be properly positioned on the entrance apertures of the ID target.

References 5.3.4

1. "Inertial Confinement Fusion Reactor Design Studies; Recommended Guidelines," Ronald C. Davidson, et al., prepared for the Department of Energy Office of Fusion Energy, September 1990.

2. "Revised Target Information for ICF Reactor Studies," Received from Roger Bangerter, Lawrence Berkeley Laboratory, Bldg. 47, room 112, 28 February 1991.

5.3.5 Critical Issue No. 5: Cost Reduction Strategies for the Heavy Ion Driver

Description of Problem - The attraction of the Heavy Ion (HI) approach to IFE has always been related to the fundamental technical feasibility of building a system with the required properties to drive a pellet to ignition. The basic accelerator technology is well developed, the beam physics is tractable, and existing accelerator systems have exhibited 25-year lifetimes with 95% availabilities. A system to provide the required average power could have been built ten years ago. The problem is cost. A 10-GeV linear accelerator built with today's technology would cost billions of dollars.

There are two key issues associated with HI driver cost reduction:

(1) Space charge limited transport of a bunched beam, and
(2) High current storage rings for heavy ion beams.

Space Charge-Limited Transport of a Bunched Beam - Experiments and computer simulations have shown that transporting beams for several kilometers at their space charge limit should be possible, with little emittance growth. However, this HI beam transport has only been demonstrated with low energy, low power, unbunched beams.

If the HI beams have to be transported at currents lower than the space charge limit, then the accelerator will have to have a longer pulse (in the case of an induction LINAC) or more quadrupole transport channels within the same accelerator, thereby increasing the cost of the accelerator.

High Current Storage Rings for Heavy Ion Beams - One of the characteristic properties of linear accelerators is their ability to run at rather high average powers and relatively high repetition rates. Since the clearing time in the IFE reactor chamber precludes very high repetition rates for the DT pellet ignition, the LINAC is forced to operate at uneconomically slow repetition rates. This problem can be eliminated if the beams for the LINAC can be stored for a short period of time. By operating the induction LINAC in the burst mode, the induction cores are used over and over, and of course, each core is therefore smaller in diameter.

The issue here is one of demonstrating that a HI beam of the required intensity can be stored in a storage ring for the requisite time, typically on the order of 1 to 2 milliseconds. The issues are similar to those associated with bunched beam transport, but have the additional complications associated with closed orbit synchrotrons, such as betatron and synchrotron resonances, etc., which can give rise to emittance growth or beam loss. Furthermore, beam induced vacuum instability is another problem which must be overcome. All of these issues can only be resolved with an experimental storage ring with parameters reasonably close to what is required.

5.3.6 Critical Issue No. 6: Demonstration of High Overall Laser Driver Efficiency

Description of Problem - The excimer laser driver system has a number of components which can individually be optimized to yield high efficiencies. The achievement of high efficiency is viewed as a crucial requirement for the laser driver. In addition to the achievement of high efficiency is the corresponding goal of highly reliable components. The laser driver consists of the following four major elements:

(1) Excimer laser amplifiers
(2) Raman accumulators
(3) SBS pulse compressors
(4) Computer controlled and self-aligning optical train which directs the laser beams through the various optical components and down into the target chamber.

The latter three elements require some additional development and testing before they can be judged adequate to be incorporated into a mature laser driver design. The major problem to be addressed here is the first element, the excimer laser amplifiers.

The fundament of an efficient, reliable laser driver is the successful design, construction, and testing of excimer laser amplifier modules.

During the past five years, relatively little work has been carried out in the USA with regard to improving the efficiency and the reliability of moderate sized excimer laser amplifiers. Some analytical studies[1] have been carried out on both electron-beam excited excimer lasers (EBEELs) and electron-beam sustained electric discharge lasers (EBSEDLs) which offered (on paper) gross wall plug efficiencies as high as 17%. These efficiencies, however, are more likely to be reduced significantly if incorporated into a large laser system architecture. The main concern is that no experimental work in excimer amplifier development is either currently in progress or planned by the Department of Energy (DOE).

Work in the Soviet Union with sliding discharge cathodes in CO_2 discharge lasers has produced some promising results which may offer alternatives to the EBSEDLs. The electric discharge lasers offer an inherently higher efficiency than the EBEELs since excitation of the excimer species occurs along the neutral channel, thereby avoiding the excitation of a large number of higher-lying states (which may contribute relatively little to the overall amplifier extraction efficiency). Moreover, by avoiding transmitting large beam currents through foils, hibachis, etc., the overall pumping efficiency may be significantly higher.

Required Future Work on Excimer Laser Amplifier Modules - There are several problems with the electric discharge excimer lasers which require further experimental work. These include:

(1) Characterization of the optimum pulse duration and gas mixture to achieve efficient operation with a matched, efficient, pulsed power system.
(2) Sensing and prevention of the formation of arcs in the discharges.
(3) Extension of the operating lifetimes of the amplifiers to reach levels of 10^9 to 10^{10} amplifier firings between failures.
(4) Control of color center formation and chemical attack of amplifier windows during the 10^9 to 10^{10} shot operational periods.

If these problems were analyzed theoretically and solutions found experimentally during a series of technological development programs granted by DOE to industry, the workhorse of the Prometheus excimer laser driver could be developed to the point that it could be incorporated into a credible IFE reactor system by the year 2030.

Summary - The major obstacle to the development of a reliable, highly efficient excimer laser driver for IFE reactors is the lack of work previously performed or currently planned on moderate-sized (2-4 kJ output) excimer laser amplifier modules. It is strongly recommended that DOE support an aggressive excimer laser amplifier program with the goal of producing a 2 to 4 kJ amplifier with a wall plug efficiency of 12% and a mean time between failures of between 10^9 and 10^{10} shots.

Amplifier modules this size can fail in operation without producing a deleterious effect on the overall operation of the IFE reactor. Additional work would be needed on the Raman accumulators, SBS pulse compressors, and beam conditioning systems as well in order to achieve the objective of an efficient, reliable, operational IFE laser driver by the year 2030.

Reference for 5.3.6

1. "New Techniques for KrF Laser Fusion Systems," Interim Report for Los Alamos National Laboratory, pp. 2-70 through 2-72, Los Alamos, New Mexico, written by Spectra Technology, Inc., Seattle, Washington.

5.3.7 Critical Issue No. 7: Tritium Self-Sufficiency in IFE Reactors

Introduction - Fuel self-sufficiency is a critical requirement for a renewable energy source. The first generation of fusion power reactors will operate on the DT cycle. Since tritium is not available in nature, tritium must be bred internally in fusion reactors using neutrons generated in the DT reactions. Therefore, careful analysis of the fuel cycle is necessary to evaluate the conditions that must be met in a fusion reactor design. These conditions must then be used as absolute criteria in selection among design concepts and in defining the range of acceptable performance parameters. Self-sufficiency requirements must be included in a prudent plan for fusion research and development.

Several characteristics of tritium and fusion reactors that make fuel cycle analysis complex are (1) tritium is a gas in the natural state, (2) tritium undergoes radioactive decay with a relatively short, 12-yr half life, (3) tritium must be fed nearly continuously into the reaction chamber, (4) the fractional burnup, i.e. the fraction of the tritium atoms fed into the reaction region that undergo fusion reaction before they are removed out of the reaction region, is relatively low, (5) removal and processing of the fuel exhaust from the reaction region involve many physical, chemical and thermal processes and, generally, require a significant amount of time, (6) tritium bred in the blanket surrounding the reaction region must be extracted and processed through several processes that take time and, (7) the amount of tritium that can be produced in the blanket per fusion reaction is sensitive to the choices of particular technologies of key reactor components (e.g. neutral beams vs. rf in MFE or laser vs. heavy ion beams in IFE) and to many of the specific design features and performance parameters for a given technology (e.g. penetrations associated with direct or indirect KrF laser driver).

In previous work,[1] fuel cycle analysis was performed and fuel self-sufficiency conditions were derived for magnetic fusion reactors. There are substantial differences in the fuel cycle and in the reactor characteristics, and hence in fuel self-sufficiency conditions and requirements between MFE and IFE reactors. The purposes of this work are (1) to develop a mathematical model for the fuel cycle in IFE reactors, and (2) to derive fuel self-sufficiency conditions and requirements. Future work should compare the requirements and potential for attaining self-sufficiency in future IFE and MFE reactors.

Self-sufficiency Condition - The tritium breeding ratio (TBR), Λ is defined[1] as:

$$\Lambda = \frac{\dot{N}^{+}}{\dot{N}^{-}} \qquad (5.3.7\text{-}1)$$

where $\dot{N}^+$ is the rate of tritium production in the system (primarily, the blanket) and $\dot{N}^-$ is the rate of burning tritium in the fusion reaction chamber (i.e., the fuel target in IFE or the plasma in MFE). Defining two specific breeding ratios, the required TBR, Λ_r, and the achievable TBR, Λ_a; the condition to attain tritium self-sufficiency in fusion reactors can then be written as:

$$\Lambda_a \geq \Lambda_r \qquad (5.3.7\text{-}2)$$

Since fusion is in a relatively early stage of R & D, accurate and clear definition of Λ_r and Λ_a must be general enough to account for uncertainties in reactor system description and in predicting its performance.

The required TBR (Λ_r) in a self-sustained fusion power economy must exceed unity by a margin, G, necessary to (a) compensate for losses and radioactive decay of tritium during the period between production and use, (b) supply a holdup inventory in various reactor components, and (c) provide inventory for startup of other fusion reactors.

The required Λ_r, as shown later, is a function of many reactor parameters as well as the doubling time, t_d, and the radioactive decay constant for tritium. Examples of these parameters are the fractional tritium burnup in the target, and the mean residence time and tritium inventory in various reactor components such as the target factory, blanket, and tritium processing systems. Many of these parameters vary from one design to another; and, for a given design, the prediction of some of these parameters is subject to uncertainties. We write:

$$\Lambda_r = 1 + G_o + \Delta_G \qquad (5.3.7\text{-}3)$$

where G_o is the breeding margin for a reference conceptual design based on a given estimate of its performance parameters, and where Δ_G is the uncertainty in estimating the required breeding ratio $(1 + G_o)$.

The achievable TBR, Λ_a, is also a function of the reactor design with particularly strong dependence on the first wall/blanket design concept. At present, accurate prediction of Λ_a suffers from two types of uncertainties:

(1) Uncertainties in system definition: Fusion reactor design concepts are evolving. The choices for many of the design features, materials, and technology options have not been made. The achievable TBR is strongly dependent on many of these choices.

(2) Inaccuracies in prediction: For a well-specified reactor system, the prediction of the achievable breeding ratio is subject to uncertainties. These are due to approximations or errors in the various elements of the calculations, e.g., in basic nuclear data, data representation, calculational methods, and geometric representation. We write the achievable TBR, Λ_a, as:

$$\Lambda_a = \Lambda_c - \Delta_a \qquad (5.3.7\text{-}4)$$

where Λ_c = TBR calculated for a specified blanket in a specified reactor system

Δ_a = uncertainty in calculating the achievable TBR

$$\Delta_a = \sqrt{\Delta_s^2 + \Delta_p^2} \qquad (5.3.7\text{-}5)$$

where

Δ_s = uncertainty associated with system definition; i.e., the changes in Λ_c due to probable changes in the system definition

Δ_p = uncertainty in predicting the breeding ratio (Λ_c) for the specified system due to nuclear data uncertainties, numerical approximations, geometrical modeling, etc.

In comparing the potential to achieve tritium self-sufficiency among various reactor concepts or among various blanket options for a given reactor design, it is useful to define a "figure of merit." One such figure of merit is

$$\varepsilon = \Lambda_a - \Lambda_c = (\Lambda_c - \Delta_a) - (1 + G_o + \Delta_G) \qquad (5.3.7\text{-}6)$$

Required TBR - The analytic model developed in Reference 1 was modified to describe the various elements of the tritium cycle in an IFE reactor. The model is shown schematically in Figure 5.3.7-1. A set of differential equations was written down to relate the tritium inventories in the various components of Figure 5.3.7-1 to their operating parameters. The equations were solved analytically to derive explicit expressions for the functional dependence of the tritium inventories. An exact expression for the required TBR as a function of the doubling time and the tritium cycle operating parameters was derived. A computer program was written, using these equations, to calculate the dependence of the required TBR on the key physics and technology parameters of an IFE reactor. Table 5.3.7-1 denotes the abbreviations used in Figure 5.3.7-1.

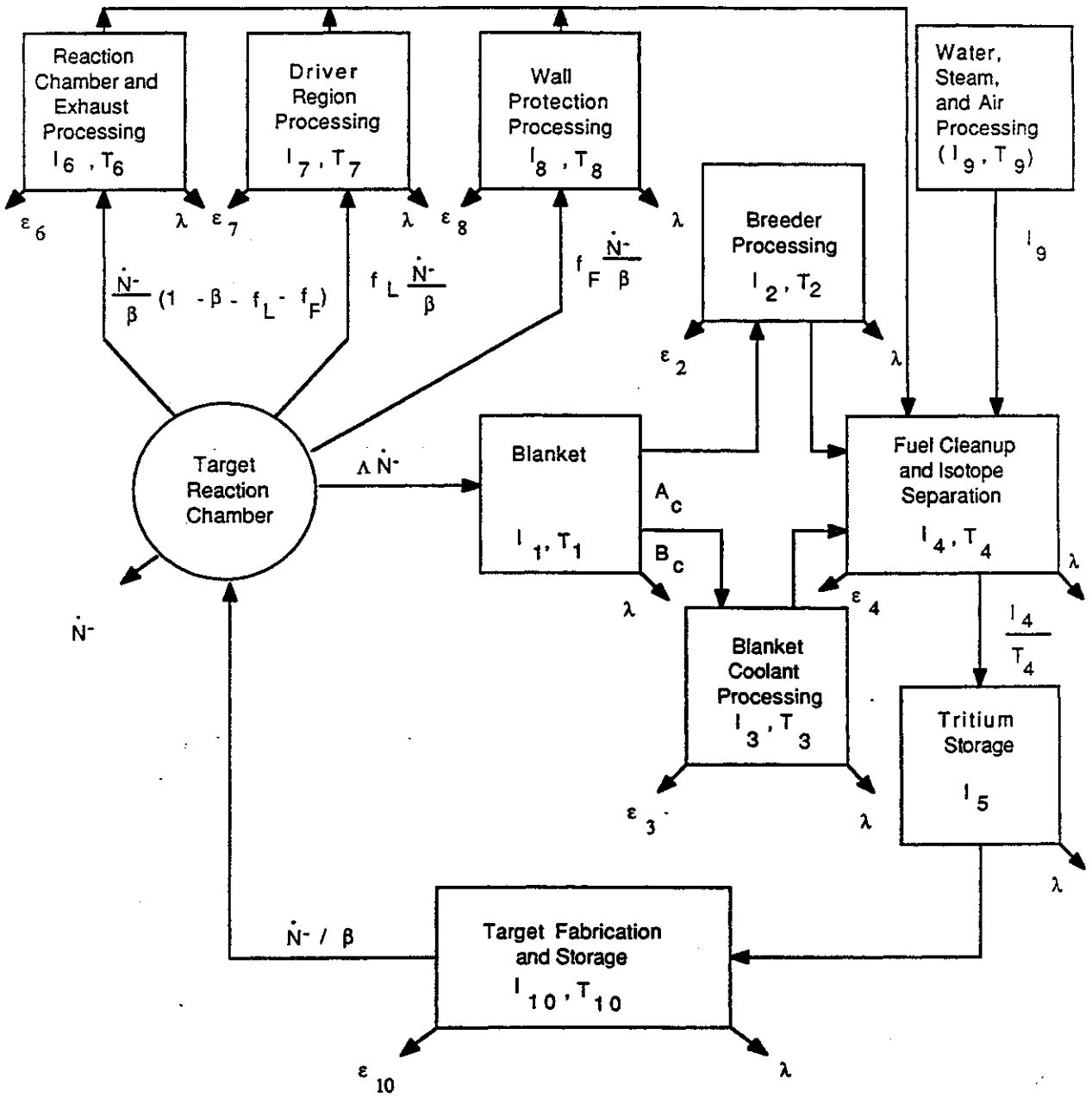

Figure 5.3.7-1. Schematic Model of the Fuel Cycle for IFE Reactor Operated on the DT Cycle

Table 5.3.7-1 Abbreviations Used in Figure 5.3.7-1

Λ = TBF
$\dot{N}^-$ = tritium burn rate in the target
I_i = tritium inventory in compartment i
T_i = mean residence time of tritium in compartment i
ε_i = nonradioactive loss fraction of tritium in compartment i
λ = tritium decay constant
β = tritium fractional burnup in the target
f_i = tritium fractional leakage to compartment i
I_g = constant flow rate of tritium recovered from waste, steam, and air processing units

$$A_c = \frac{I_1}{T_1}(1 - f_c)$$

$$B_c = \frac{I_1}{T_1} f_c$$

A set of reference parameters was selected to represent the present best estimate. This reference parameter set is shown in Table 5.3.7-2. The calculated value of the required TBR with this reference parameter set is 1.05. A sensitivity study was then performed to determine the sensitivity of Λ_r to variations in various parameters. It was found that the required TBR is most sensitive to:

- β tritium fractional burnup in the target
- T_{10} the tritium mean residence time in the target factory
- t_r the number of days of tritium reserve on site
- t_d the doubling time

Figure 5.3.7-2 shows the variation of the required TBR with these most important parameters. It can be seen from this figure that the required TBR can increase to ~1.25. Figure 5.3.7-3 shows the variation of Λ_r with simultaneous change in the values of β and T_{10}. The required TBR increases dramatically, e.g. to ~1.5 if β drops to 5% and T_{10} becomes 20 days. Such high TBR can not be achieved in a fusion reactor.

Table 5.3.7-2. Reference Parameter Set for Tritium Self-Sufficiency Calculation

Tritium consumption (burn in plasma), $\dot{N}$ (kg/day)	0.3
Doubling time, t_d(yr)	5
Tritium fractional burnup in plasma, β(%)	30
Time reserved for independent tritium supply, t_r(day)	2
Non radioactive losses (chemical tie-up in radioactive waste, etc.) in	
Breeder processing, ε_2(%)	0.02
Blanket coolant processing, ε_3(%)	0.001
Fuel clean up and isotope separation units, ε_4(%)	0.0
Reactor chamber and exhaust processing, ε_6(%)	0.05
Driver region processing, ε_7(%)	0.1
Wall protection processing, ε_8(%)	0.1
Target fabrication processing, ε_{10}(%)	0.1
Tritium mean residence time in	
Blanket, T_1(day)	1
Breeder processing, T_2(day)	0.1
Blanket coolant processing, T_3(day)	100
Fuel cleanup and isotope separation units, T_4(day)	1
Reaction chamber and exhaust processing, T_6(day)	1
Driver region processing, T_7(day)	100
Wall protection coolant processing, T_8(day)	100
Target fabrication and target storage, T_{10}(day)	10
Tritium fractional leakage from	
Breeder to blanket coolant processing, f_C(%)	0.001
Plasma to limiter processing, f_L(%)	0.01
Plasma to wall protection processing, f_F(%)	0.01
Constant tritium flow returned from the waste, steam and air processing, 19(g/day)	0.01

The achievable TBR is generally in the range of 1.1 to 1.3 with about 20% uncertainty due to system definition and prediction capability. Two important conclusions arise from this analysis:

(1) R&D effort for IFE must aim at achieving certain range of parameters that have direct impact on tritium self-sufficiency. For example, the R & D goals should be to achieve $\beta > 20\%$ and $T_{10} < 10$ days.
(2) Tritium self-sufficiency is a critical issue in IFE, as it is in MFE. Demonstration of tritium self-sufficiency must be a goal for early integrated test facilities.

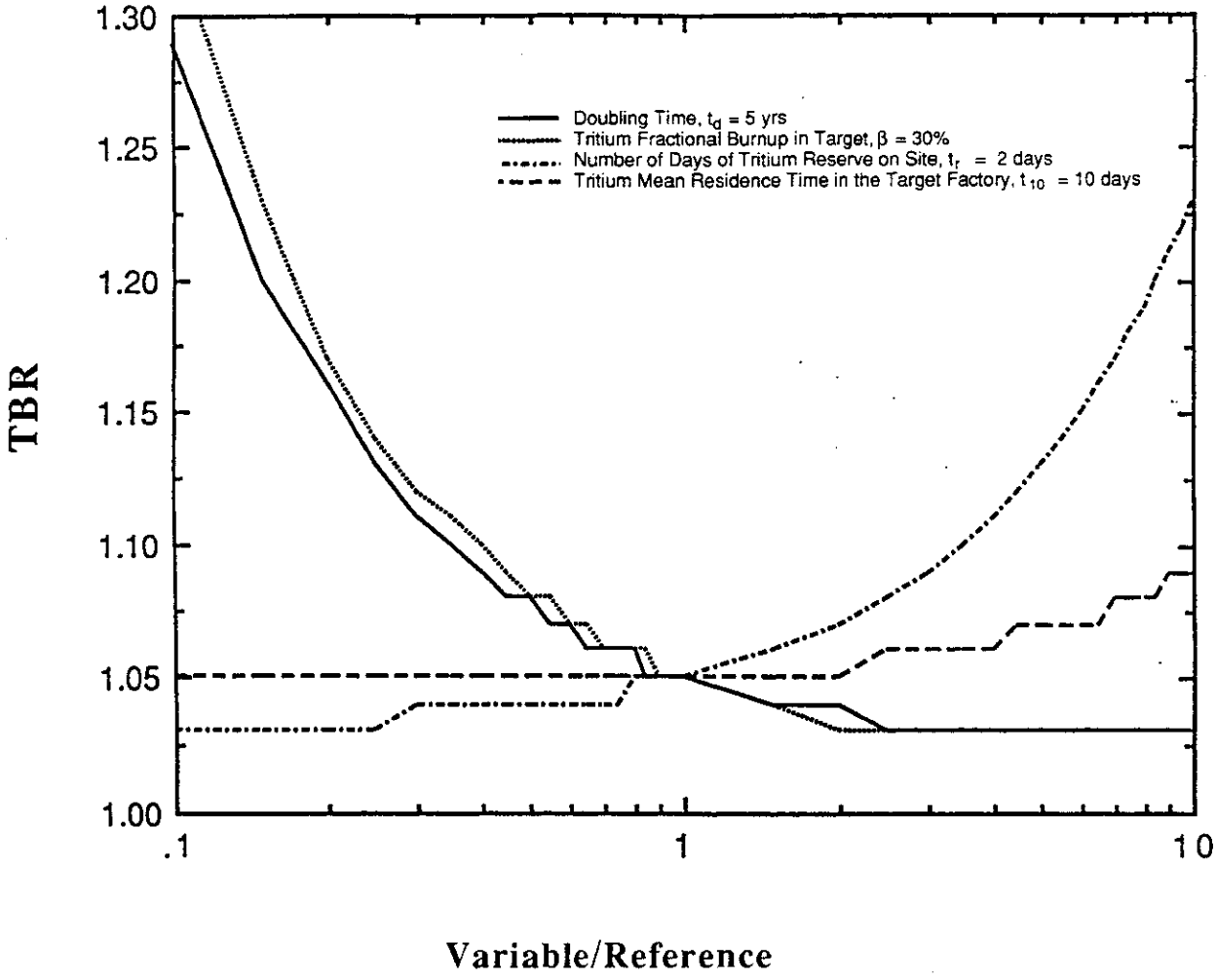

Figure 5.3.7-2. Variation of Required TBR with Reactor Parameters

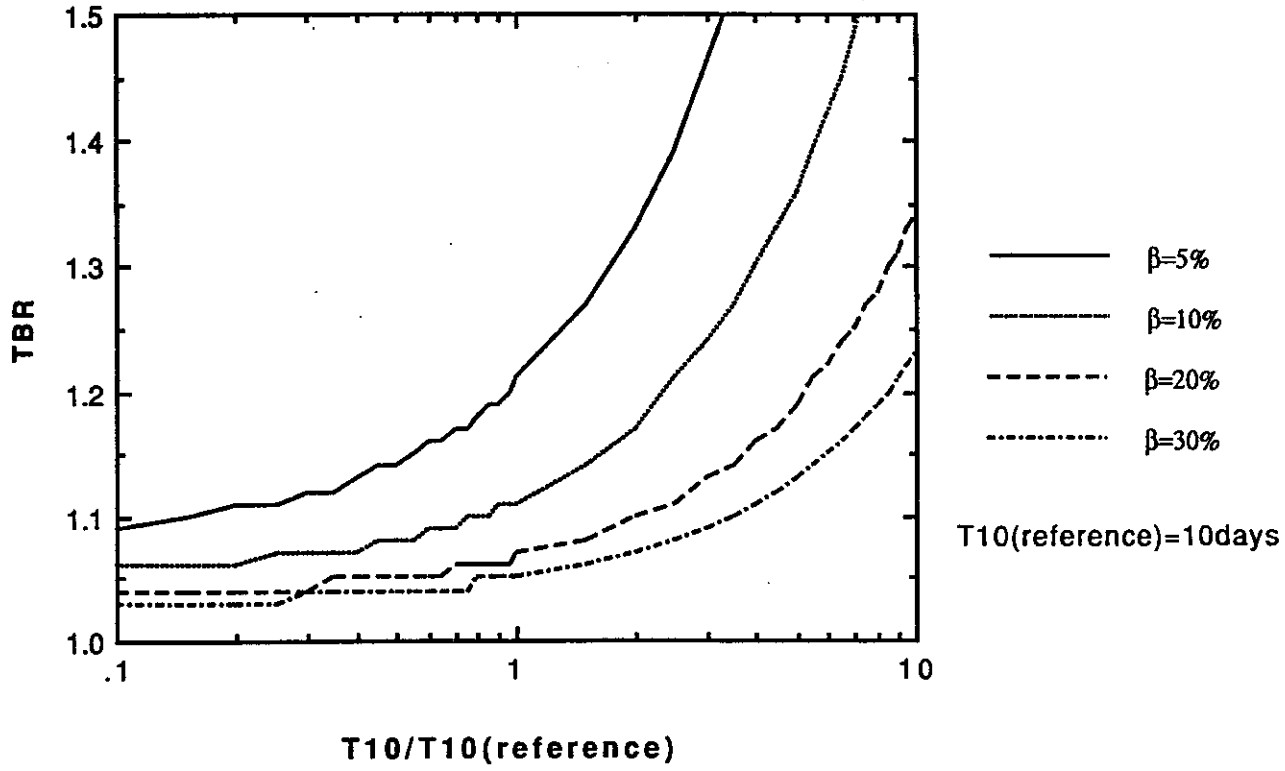

Figure 5.3.7-3. Variation of Required TBR as a Function of T_{10} (Residence Time in Target Factory) for Various Values of the Tritium Fractional Burnup (β).

References for 5.3.7

1. M. A. Abdou, et al, "Deuterium-Tritium Fuel Self-Sufficiency in Fusion Reactors," Fusion Technology, vol. 9, pages 250-284 (March, 1986).

5.3.8 Critical Issue No. 8: Cavity Clearing at IFE Pulse Repetition Rates

Description of the Problem - Following each pellet explosion, the cavity fills with target debris and material evaporated or otherwise ejected from the cavity surfaces. This material must be removed from the cavity before the next target is injected. In the Prometheus designs, the cavity is cleared by recondensing the condensable gases onto the surface of the first wall, and by pumping non-condensable gases out through large ducts.

Operation of a power reactor requires continuous operation at several (i.e., ~5-10) pulses per second. For a fixed reactor thermal power, lower repetition rates require higher yields, which in turn produce unacceptably high driver energy requirements and excessive loads on the surrounding components. In order to ensure that a feasible design window exists, the cavity pressure must be reduced to the level required for target and driver energy propagation.

Evacuation requirements are based on propagation limits for both targets and driver energy. Base pressure requirements are important for two reasons: (1) the time to evacuate the chamber depends on the pressure, and (2) the level of protection to the first wall (and final optics) afforded by the cavity background gas depends strongly on the pressure. If a sufficiently high background pressure could be allowed, the survivability of the solid surfaces might be substantially enhanced.

Analysis - Driver propagation requirements depend on the type of driver. For the Prometheus-L design, the Pb pressure limit for laser propagation was estimated as ~1 mtorr@0°C. Above this value, gas breakdown is expected to occur, in which case the laser beams would be degraded. Target gain would start to decline.

Due to the innovative, heavy-ion channel transport mechanism used in Prometheus-H, a much higher base pressure is considered acceptable. In this case, the 100 mtorr limit is determined also by target transport. Target propagation limits depend on the target design. Indirect drive targets are generally more robust than direct drive, and can propagate at higher base pressure with less degradation. In order to resolve this aspect of the issue, accurate estimates of maximum allowable base pressure need to be determined for each target and driver design to be pursued.

Under idealized conditions, achievable cavity clearing times can be estimated by analyzing mass and energy transport within the cavity. Figure 5.3.8-1 shows the results of such a calculation. Cavity vapor temperature and pressure histories are plotted for a Pb wetted-wall cavity design. In this case, approximately 3 kg of Pb are evaporated by direct energy deposition from the x-rays which reach the first wall. The

initial average cavity vapor pressure and temperature are estimated as 49 kPa and 3 eV, respectively. A much larger amount of Pb is subsequently evaporated due to rapid radiation cooling of the cavity vapor. Before the recondensation phase begins, about 80 kg of Pb (10 μm) is evaporated.

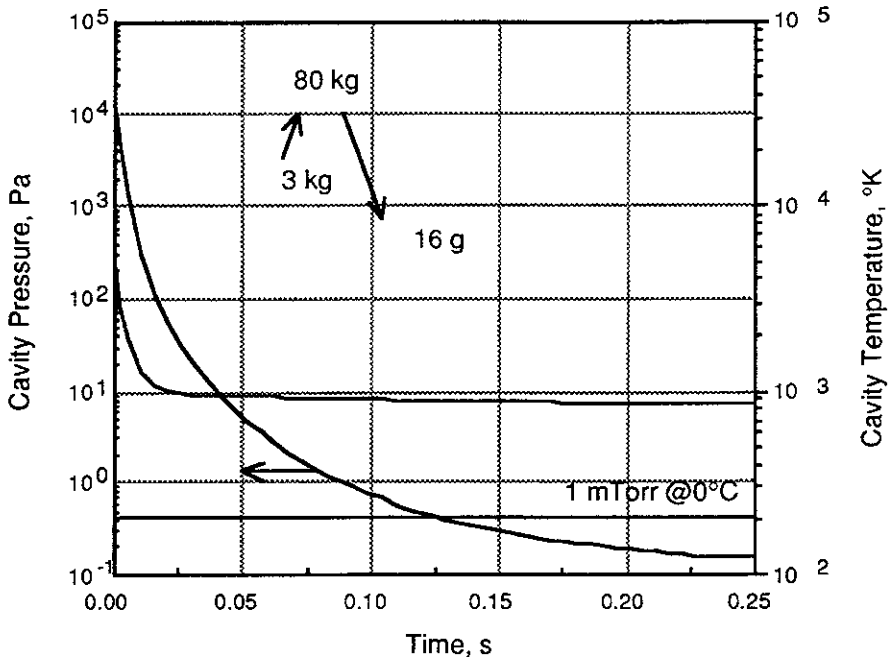

Figure 5.3.8-1. Cavity Vapor Pressure and Temperature Histories Following the Blast.

Based on this analysis, the cavity pressure drops below 1 mtorr before the next shot. However, the actual physics of energy and mass transport and vapor recondensation is very complex under the extreme conditions following a target explosion. The cavity gas is partially ionized, and subject to highly time-dependent processes such as hydrodynamic shock waves. Non-ideal effects such as liquid droplet formation and effects of penetrations provide additional uncertainties.

While many uncertainties exist, there are also various design solutions which can be adopted to improve the cavity clearing rate. For example, condensing surfaces (or cold jets) could be added. Some design proposals use large slugs of cold liquid to evacuate the chamber. More research is needed to better understand clearing requirements, the recondensation process, and to develop design solutions to this critical issue.

5.3.9 Critical Issue No. 9: Performance, Reliability, and Lifetime of Final Laser Optics

Description - In this study, successful conceptual mirror designs were introduced. These designs involved both the dielectric turning and focussing mirror and the final optical component, the Grazing Incidence Metal Mirror (GIMM). Analysis of the proposed design indicated that, with proper selection of materials and mechanical configuration, the GIMM lifetime can be very long–on the order of the plant lifetime. Clever shielding designs and materials selection for the dielectric elements can likewise lead to great improvements in the overall laser reactor concept. In all previous studies of laser fusion so far, it has always been concluded that the final mirror will have to be at distances in excess of 30-40 m away from the cavity center and that the lifetime and reliability will be small. Preliminary analyses of the Prometheus design approach indicated the mirror could be a life-of-plant component and yet be located 20 meters from the cavity center. An in-depth study of the performance, reliability, and lifetime of the final optical components is necessary. Advances in this area will, undoubtedly, lead to significant improvements of the entire concept and will likely benefit other technological areas which rely on the reliable performance of large laser mirror systems.

Analysis -

Turning Mirror - As far as the turning mirror is concerned, two categories of research will be pursued:

(1) Shielding design of a neutron dump, and pinhole for minimization of the damage caused by ionizing radiation (i.e. neutronic and photonic).
(2) Materials selection and data base analysis for the optimum choice of dielectrics with the minimum amount of damage. In this area, rate theory would be used to compute the accumulation rates of color centers and their impact on the optical properties of the dielectric. To our knowledge, this approach has not been attempted so far. A model with these capabilities can actually lead to the development of annealing strategies for the elimination or reduction of the effects of radiation on the optical properties of the dielectric materials.

Grazing Incidence Metal Mirror - The design of a reliable, long-life GIMM is critical to the success of the laser fusion concept. A detailed thermo-mechanical design involves the following features:

(1) De-coupling between the optical and structural functions of the mirror. A high strength aluminum alloy is deposited on top of a composite SiC stiffened

support structure. A very thin graphitic shear layer would be desirable, such that the larger thermal expansion of the aluminum surface does not lead to buckling patterns on the mirror's surface which would degrade the optical quality of the laser beam.

(2) A low activation, zero swelling composite structural support of the aluminum surface. Thermal deformations of the surface are corrected for by uniform end moments . These correcting moments can be induced by clamping the structural support to a rigid concrete shell, which would also give only one two degrees of freedom for thermal expansion. Design of mechanical sliding/bolting systems must be demonstrated in order that the deflections caused by the small temperature gradient across the mirror's surface can be completely eliminated.

(3) Detailed structural analysis of the aluminum optical layer, the supporting composite structure, and the graphitic shear layer.

(4) Determination and analysis of the possible modes of damage to the mirror. This would involve fatigue and creep damage assessments. It is to be borne in mind that fatigue analysis of the composite structural substrate does not follow the established rules for metal systems. On the other hand, fatigue of the surface aluminum layer (a few mm thick) can also be minimized, or perhaps eliminated, if more effort is directed toward stress redistribution in between the optical aluminum layer and the structural substrate.

(5) Investigation of the possibility of piezoelectric, or other error detection and correction mechanisms, for final mechanical control of the optical quality of the mirror's surface.

5.3.10 Critical Issue No. 10: Viability of Liquid Metal Film for First Wall Protection

Description of the Problem - In the Prometheus designs, a thin liquid metal film wets the first wall in order to prevent the solid structures from rapidly degrading due to the extremely high instantaneous heat and particle loads. To prevent liquid from entering the cavity, the thickness of the film is maintained as small as possible. For this scheme to be successful, all structures exposed to the blast must be covered. Analysis of dry spots suggests that operation for periods of time greater than 10-15 minutes will cause irreparable damage to the first wall.

While a great deal of research has been carried out on film flows, the materials, configuration, and environmental conditions for inertial fusion are unique, and little effort has been expended in the IFE community to determine how films will behave under these conditions in a real engineering system. The major uncertainties include:

- Film feeding and thickness control
- Blast effects
- Flow around geometric perturbations (such as beam penetrations)
- Protection of inverted surfaces

The film thickness must be relatively uniform in Prometheus because the surface power conducts through the film. The local film thickness determines the local surface temperature, which strongly influences the condensation rate. Even for very thin films, the flow becomes turbulent and instabilities are likely to develop. Therefore, better understanding of the nature of instabilities and possible remedies are critical. Good wetting between the solid surface and liquid film is very important.

Explosive effects resulting from the blast may lead to further problems. Several effects are present:

(1) A large impulse is imparted to the film following rapid evaporation at the surface
(2) Additional shock waves strike the wall as the cavity vapor responds to the blast. These shocks cause motion of the solid structures which could eject liquid into the chamber
(3) Rapid "isochoric" bulk heating of the liquid creates high pressures, which can cause fragmentation of the liquid film.

The problem of wall protection with films is particularly difficult near inverted surfaces (such as the upper hemisphere or tops of beamlines) or at penetrations and

nonuniformities in the cavity interior. Dripping is likely to occur from inverted surfaces, so that the concept of slow porous flow may need to be supplemented with alternate methods, such as inertial jets or magnetic guiding.

Figures 5.3.10-1 and 5.3.10-2 show the jet velocity required, and the film thickness and minimum flow rate required for film attachment on the upper hemisphere. The velocity and thickness can be high, leading to large flow rates. The option of using MHD guiding has been shown to be capable of resolving this problem, but adds design complexity to the device.

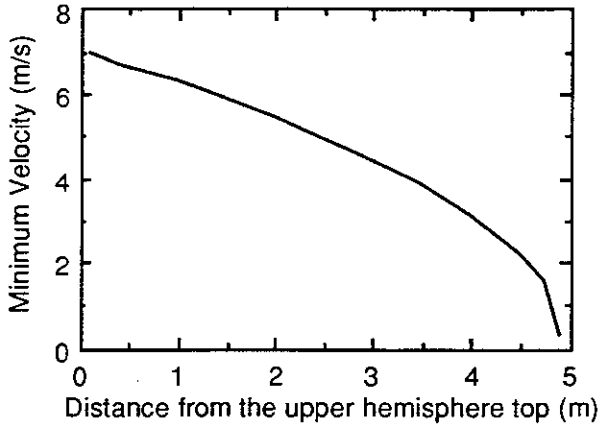

Figure 5.3.10-1. Minimum Velocity Required for Film Attachment on the Upper Hemisphere

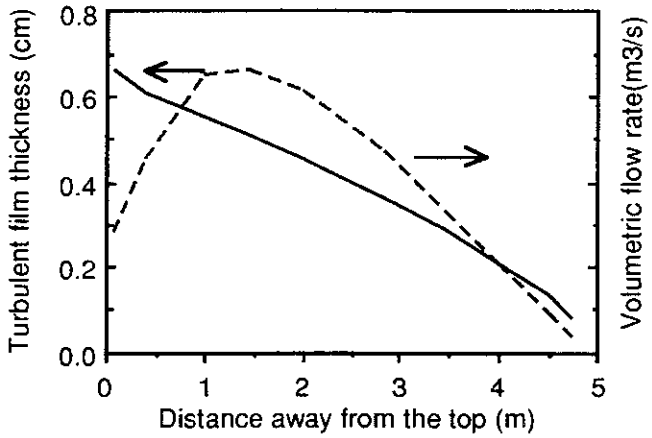

Figure 5.3.10-2. Turbulent Film Thickness and Minimum Flow Rate Required for Film Attachment on the Upper Hemisphere

5.3.11 Critical Issue No. 11: Fabricability, Reliability, and Lifetime of SiC Composite Structures

Description of the Problem - The viability of using SiC structures in the first wall and blanket is a key consideration of the laser and heavy ion designs. If these concepts are to be believable, efforts should be made to assess the factors involved in determination of acceptable lifetimes, and to determine the appropriate manufacturing methods and their economics. Anticipated lifetimes for FW/B components are not well known. Limited resources allocated to this area precluded a realistic assessment of the anticipated lifetimes. Without this knowledge, system reliability, maintenance and economics would be seriously challenged. In order to perform this task, several investigations need be considered. It is too simplistic, and perhaps misleading, to use the accumulated fluence, or displacements per atom, to make projections of lifetimes. The determination of such lifetimes would need knowledge of the various effects of radiation. The most prominent of those are neutron induced swelling, embrittlement, fiber shrinkage, and/or detachment from the matrix, creep crack propagation at high temperatures, and crack bridging mechanisms during irradiation.

On the other hand, the technology to process and manufacture SiC composites is at its infancy. An evaluation of manufacturing methods, potential, and costs is needed. Manufacturing methods are classified into fiber production techniques and matrix processing technologies. A variety of possibilities exist, with potential consequences on both economics and design.

Analysis

(1) Radiation Effects on the properties of SiC Composites: The relevant effect of irradiation to be investigated are: displacement damage production in various neutron spectra; swelling rate dependence on temperature, fluence and porosity; irradiation induced creep; irradiation embrittlement by amorphization; high temperature crack nucleation and propagation under static and dynamic conditions.

(2) Lifetime assessment of the FW: A realistic determination of FW lifetime would require analysis of a number of material and structural properties of the first wall. The data base accumulated under item (1) above would have to phenomenalogically modeled in the form of appropriate design equations. These equations will include crack growth under cyclic loading at high temperature, radiation creep rate, thermal creep rate, and swelling rate. These mechanical property equations will then be used in a structural analysis code

for determination of stress and strain fields under time-dependent loading conditions. The lifetime of the FW/B structure will be dictated by:

(a) fatigue crack growth.
(b) maximum allowable inelastic deformations.
(c) maximum stress/strain criteria under the complex multiaxial loading situation in the structure.

(3) Manufacturing and reliability: Existing manufacturing techniques involve CVD, CVI, and HIP technologies for the matrix. A wide range of fibers and architecture are also possible. The structural performance, lifetime and reliability are all dependent on the manufacturing method of the composite. In addition, cost is an important factor, which will be also determined by the manufacturing technique.

5.3.12 Critical Issue No. 12: Validation of Radiation Shielding Requirements, Design Tools, and Nuclear Data

Description of the Problem - Radiation shielding must protect both personnel and sensitive reactor components. Components with the most stringent protection requirements include the final optics in a laser-driven fusion reactor. Other components with important radiation protection requirements include magnets in the heavy ion driver, instrumentation and control. Two important requirements must be imposed on the radiation shield in order to enhance attractive environmental and safety features of IFE reactors. First, the bulk shield (immediately surrounding the blanket) must be designed so that the long-term activation in reactor components outside the cavity and inside the reactor building is minimum. Such components include the heat transport system, heat exchanger and/or steam generators, and a variety of auxiliary system and constitute a large material inventory that would tremendously increase the waste disposal problem if allowed to be highly radioactive. Second, the IFE shield should be designed to permit some personnel access to the reactor building outside the bulk shield within days after shutdown. Although full remote maintenance should be planned for, having personnel access capability after shutdown is deemed necessary in a number of foreseen cases and unforeseen events.

These critical requirements on the shield combined with the fact that the shield is one of the largest (in volume and weight) and more expensive components in an IFE reactor necessitate careful shield design. Sophisticated capabilities for predicting the radiation field and associated radiation response in materials are required. Although advanced capabilities exist, uncertainties in accuracy remain due to modeling complexities, nuclear data uncertainties, limitations of calculational methods in void regions and deep radiation penetration problems, and time dependent behavior of materials and components. For example, it is likely that components will deform during operation, which may head to unpredictable streaming paths. Improvements in methods, data and experimental verification of prediction capabilities are needed.

Establishing accurate radiation protection requirements is necessary, particularly for components whose shielding is either physically difficult (e.g. final optics in laser driver) or results in substantial economic penalty. Thus, quantitative and reliable knowledge of the effect of radiation on materials and components is required.

5.3.13 Critical Issue No. 13: Reliability and Lifetime of Laser and Heavy Ion Drivers

Description of Problem - The reliabilities and lifetimes of excimer laser and heavy ion beam driver systems profoundly affect the operating characteristics of an inertial fusion energy (IFE) reactor. Although both the excimer laser and the heavy ion beam drivers are powered with somewhat similar pulsed power systems, the critical issues associated with these two drivers are sufficiently distinct that they should be considered separately. There are presently no known technical problems which could keep either of these driver types from performing reliably as IFE drivers.

Reliability and Lifetimes of Excimer Laser Drivers - Two general types of excimer laser amplifiers have been considered for IFE:

(1) Direct electron-beam pumping through a foil, and
(2) Electric-discharge pumping.

The first category can be constructed in larger sizes (and hence output energies) than the latter. Theoretical simulations suggest that the electric-discharge laser may be more reliable than the e-beam pumped laser. There are, in addition, a number of similarities which these two types of excimer lasers share. First of all, a key parameter for each of the lasers is the small signal optical gain, G_o given by the expression:

$$G_o = \exp(\sigma N L) \qquad (5.3.13\text{-}1)$$

where σ is the stimulated emission cross-section for the excimer laser transition, N is the inversion density of the excimer laser amplifier, and L is the length of the active excimer gain medium. Typically, G_o must be less than some fixed number (such as 20-30) in order to avoid unwanted parasitic oscillations in the amplifier volume. A somewhat higher limit is set by the superfluorescent limit which defines a relationship between the amplifier solid angle, Ω_a, and the small signal gain, G_o. A simplified expression[1] for the superfluorescent limit on amplifier gain is given by the inequality:

$$4\frac{\sqrt{\ln G_o^2}}{\sqrt{(G_o - 1)^3}} < \Omega_a \qquad (5.3.13\text{-}2)$$

where the amplifier solid angle is given approximately by d_a^2/L^2 for a rectangular amplifier (where d_a is the amplifier aperture). Since σ is nominally a fixed parameter, in order to keep G_o below the parasitic limit, L and/or N must be adjusted. The

difficulty here is that the excimer inversion density, N, is related to the inversion energy, E_S, in the medium given by the expression:

$$E_S = NhvLd_a^2 \qquad (5.3.13\text{-}3)$$

where, as before, d_a is the amplifier aperture, h is Planck's constant, and v is the laser frequency. An important parameter for laser amplifiers is the inversion energy per unit volume, $\rho_S = E_S/V = Nhv$. In optimizing amplifiers, frequently ρ_S is maximized in order to obtain the highest output energy/cm^3 form the excimer amplifier gain volume. A typical limit for ρ_S is 20 J/liter, or more typically 10 J/liter.[1] Thus, in order to keep G_o below either the parasitic limit or the superfluorescent limit, it is easiest to adjust L, the gain length. In carrying out these optimizations at constant σ and N, the results tend to reduce the size of the excimer laser amplifier to dimensions of the order of 50x50x200 cm with a volume of approximately 500 liters. Amplifiers this size tend to produce less than 5 kJ of output energy, an amount of energy which is only 0.1% of the total driver energy of 5 MJ; this is an important factor in performing the overall driver failure mode analyses. Designers of e-beam pumped lasers, however, have produced designs for much larger amplifiers, theoretically producing output energies of hundreds of kilojoules.

Each of these two types of excimer lasers is briefly described below:

E-Beam Pumped Excimer Lasers - Direct electron-beam pumping permits large volumetric excitation of the excimer gain media (typically a mixture of noble gasses plus a halogen). All of the pumping energy delivered to the gas is delivered by the e-beam. This excitation scheme has been attractive for the construction of large excimer lasers since it is readily scalable to large apertures (~100 cm), energies, and volumes (thousands of liters).

The e-beam is generated under hard vacuum conditions (10^{-7} torr or better), whereas the excimer gain medium is approximately 1 amagat (or 760 torr). A thin foil is used to separate the high vacuum e-beam from the corrosive halogen atmosphere inside the laser amplifier. Since the excitation area is given by the product d_aL, a relatively large foil area in a typical e-beam pumped excimer laser amplifier (such as the LAM[2] with a ~100x200 = 2x10^4 cm^2 area) is exposed to the vacuum interface. In order for the thin (several micron) foil mechanically to support the force exerted by 760 torr, a mechanical bridge-type structure (often referred to as a Hibachi) which may block a portion of the incident e-beam is installed to stiffen the foil structure. In operation, the high power e-beam is accelerated through potentials in excess of 10^6 V, and upon traversing the foil, some fraction (30-50%) of the electron beam energy is lost. The action of this large amount of energy is deposited into the small volumes of the foil and

Hibachi, thereby greatly stressing these elements, particularly the foil in cases in which the beam current density is not uniform. The problem increases significantly in repetitive operation since it necessitates water-cooled Hibachis. The repetitive operation of an e-beam pumped excimer laser has hitherto been unreliable because of periodic foil ruptures. In order to overcome this problem, e-beam pumped excimer laser have received a considerable amount of technological development.

Even with the greater energy capabilities of EBELs, a substantial number, n, of EBELs is required to generate the ~5 MJ of energy required for the Prometheus laser driver. (The required laser energy on target is 4 MJ but, owing to optical inefficiencies associated with beam combination, propagation, and pulse compression, the output energy from the EBELs needs to be at least 25% greater than the desired net energy.) Assuming that each of the n optimized e-beam pumped excimer amplifiers produces an output energy = 5 MJ/n (which is presumably more than 1% of the total driver output energy), the mean number of amplifier firings between failures must be at least n x 10^8 if the IFE reactor operation is not to be interrupted between maintenance periods.

Electric-Discharge Excimer Lasers - Much less experimental work has been carried out on electric discharge excimer lasers. In this case, excitation of the excimer gain medium occurs on the neutral channel with relatively low-lying species being produced. This can enhance the efficiency of the amplifier. Unlike the e-beam pumped excimer laser, the full pumping power does not flow through a foil/Hibachi structure, and predictions are that this design would be more reliable following an intensive development effort.

Owing to the nature of the electric discharge, the available pulse duration is shorter than that for the e-beam (200 ns compared with ~ 500 ns). Electric discharge lasers for which d_a > 30 cm appear to have serious discharge stability and efficiency problems. As a consequence, using the scaling relations outlines above, the electric discharge lasers tend to optimize at energies of a few kilojoules. For energies this small, the overall reliability of the IFE reactor would not be impaired if several electric discharge amplifiers failed. Assuming such amplifiers could readily be replaced by robotics, the impact of discharge amplifier failure on reactor operation is regarded as minimal. As a consequence, if failed electric discharge excimer lasers can be replaced more rapidly than they fail, then the mean time between failure characteristics the IFE reactor will be independent of the excimer amplifiers.

Reliability and Lifetimes of Heavy Ion Drivers - The fundament of an efficient, reliable Prometheus heavy ion driver is the successful design, construction, and testing of a full scale accelerator suitable for operation in a burst mode (~50 kHz) to fill storage rings with 18 beamlets at a rate of ~3.5 pulses/sec. Accelerators can be made to be very

reliable if great care is taken with regard to the control of the magnets, particularly in the (recommended) case of superconducting dipoles, quadrupoles, and triplets. A large amount of data is available on the failure modes of linear accelerators (LINACs), and there are no serious technical problems which would render this design unreliable. The key element for long, reliable operation of the LINAC is a very fast, highly automated control system which can sense beam mispointing before superconducting magnets are either heated sufficiently to make them go "normal" or damaged by the beam. Under competent computer control, the heavy ion driver would only require attention during regular IFE reactor maintenance intervals (possibly every two years). A key element in this HI driver reliability assessment is the development of an adequate computer control system employing the latest developments in artificial intelligence, parallel processing, and expert systems (see Section 6.5.3.3).

Accurate simulations of the dynamics of the LINAC, the filling of the storage rings, the bunching, the rapid expansion to the triplet focusing magnets, the focusing down into the pre-formed channels, the complete stripping of the heavy ions, and the dynamics of self-focused heavy ion beams propagating down the channels to the target are too difficult to attempt presently, and the results, even if favorable, would require experimental verification to be trusted. Thus, the major emphasis on demonstrating the feasibility of heavy ion drivers should be experimental.

It is essential that a carefully planned heavy ion driver developmental program be designed to test each of the key elements of the proposed Prometheus-H IFE heavy ion driver in order to create a design data base sufficient to permit suitable modifications allowing the driver to reach its full reliability potential. In particular, experimental results on beamlet accumulation (without emittance growth) for ms time scales in storage rings, self-focused beam stabilities, locking the focused beams into a pre-formed channel, etc., are crucial for developing this promising driver concept.

References for 5.3.13

1. G. J. Linford, E. R. Peressin, W. R. Sooy, and M. L. Spaeth, "Very Long Lasers," Applied Optics 13, pp 379--390, (1974).

2. L. A. Rososha, et al., "Aurora Multi-kJ KrF Laser System Prototype for ICF," Fusion Technology 11, pp. 497-531, (1987).

5.3.14 Critical Issue No. 14: Demonstration of Large-Scale Non-Linear Optical Laser Driver Architecture

Description of Problem - The fundament of the Non-Linear Optical Subsystems proposed for the Prometheus-L driver is based upon the very strong experimental and theoretical bases of non-linear optics. Since both proposed subsystems are simply large optical cells filled with H_2 and SF_6 respectively, there are very few components present which can fail. The primary question is how well the system will function properly on the first pulse. If the electro-optical subsystems can be tailored to achieve first time operation, the overall architecture should prove to be as reliable as other state-of-the art, high speed, high voltage electronics. A balance must be struck between the extremely high gains (and concomitant high conversion efficiencies) of which these systems are capable. Thus, the reliabilities and lifetimes of the two types of non-linear optical subsystems proposed for the Prometheus-L IFE reactor design hinge primarily on the support optical equipment that is associated with the non-linear optical (NLO) devices. The two NLO devices are:

(1) The Raman accumulators
(2) The SBS pulse compressors

Numerous key non-linear optical (NLO) subscale experiments and analyses have been performed in the last twenty years which demonstrate the capabilities of these two types of NLO devices. In order to properly implement them, however, each needs to be supplied a Stokes seed beam, and therein lies most of the questions regarding the success of the architecture reliabilities and lifetimes.

Generation of Stokes Seeds for Raman Accumulators - To achieve highest efficiency while averaging excimer laser intensities across the accumulator aperture, the proposed Prometheus Raman accumulator system uses crossed stimulated rotational Raman scattering. This architecture sets limits on the bandwidth, $\Delta\nu_{lasers}$ of the excimer pumps, on the crossed Raman angle, θ, and on the dimensions of the gain length (to avoid generating higher order Stokes beams). The physics is relatively well understood. A detailed design could be made now using present understanding. Tests at full scale could be made if approximately 30 two-kilojoules KrF excimer laser amplifiers were available as pump sources.

The required Stokes seeds can be derived from taking a small portion of the available excimer pump light, injecting the pump light into a Raman oscillator filled with the same gas used in the Raman amplifier. This process generates an automatic frequency shift, $\Delta\nu_R$, equal to the required Raman shift. Injecting this Stokes seed beam into the Raman amplifier at an angle θ to the pump beams permits a high quality

(in the case of the Prometheus-L design, 80 kJ) output beam to be generated following path matching of the seeds to the original pump beams.

If stimulated rotational Raman scattering proved to be too difficult to control under the required test conditions (higher order Stokes, etc.), stimulated vibrational Raman scattering could suffice, at a slight reduction in overall operating efficiency. The Raman accumulators should be able to achieve high degrees of reliability.

Generation of Stokes Seeds for SBS Pulse Compressors - The Stokes seeds for the SBS pulse compressors are generated electronically by "chirping" (acoustical-frequency shifting) the leading edges of the 80 kJ output beams from the Raman accumulators. Some technological development needs to take place to permit full aperture "chirpers" to be installed, but subscale tests with small crystals have produced promising results. Work at the Lawrence Livermore National Laboratory has already produced Pockels cells having conducting electrodes with apertures of approximately 30 cm. Experimental verifications need to be made of theoretical predictions of compressed pulse shapes and conversion efficiencies given the specific requirements on pulse shape established by the Target Working Group.

In the same vein, fast, large aperture (~100 cm) Pockels cells to be used for pulse-shaping the depleted pump beams from the SBS pulse compressors for synthesizing the required precursor pulses need to be demonstrated.

Although the development of large aperture Pockels cells may prove difficult, there do not appear to be any serious technological problems associated with synthesizing large aperture electro-optical (E/O) switches from smaller components. This synthesis may have significant advantages, for example, in the suppression of transverse SBS losses in the Pockels cells.

The SBS pulse compressors and attendant E/O switchyards currently represent the highest risk elements in the Prometheus-L driver design. Failure of any of the Pockels cells or "chirper" modulators would mean the loss of an entire 80 kJ beamline, with consequent failure of direct drive targets. In some cases, continued operation with indirect drive targets could be considered even if one of the 80 kJ beamlines went down.

5.3.15 Critical Issue No. 15: Demonstration of Cost Effective KrF Amplifiers

Description of Problem - One of the key elements associated with developing a cost effective KrF laser driver for the Prometheus reactor design study is the design of the output KrF laser amplifier module. These KrF amplifier modules represent the fundamental building-blocks of the KrF driver, generate the output energy pulses for the KrF laser driver, and the nature of their design represents a major fundament of the laser driver reliability. These KrF amplifiers need not only meet requirements of output energy, pulse duration, beam quality, beam diameter, wavelength, bandwidth, etc., but also stringent requirements on reliability, consistency of operation, etc. In order to prevent catastrophic failure of the IFE reactor, the Prometheus has designed a laser driver which can permit the occasional failure of a KrF amplifier without requiring the concomitant shutdown of the reactor. As this freedom from KrF amplifier failure is predicated upon the choice of IFE reactor operation with direct drive targets, a limit is placed upon the laser energy delivered by each KrF amplifier such that the 1% direct drive target illumination uniformity requirement is met. Given 60 beams arranged symmetrically around the spherical direct drive target, together with a nominal laser driver energy of 5 MJ, the loss of 5 kJ (or approximately 6%) from each of the 60 beams from time to time should still permit target illumination uniformity to be maintained, at least for tangential target illumination schemes. KrF amplifier output energies of 5 kJ represent a significant derating of current designs and successful development of reliable amplifier prototypes should be achievable during the next decade if sufficient funding is made available.

Previous Department of Energy (DOE) and Department of Defense (DoD) excimer laser research and development programs have identified two general excimer laser amplifier design configurations:

(1) Direct electron beam excitation of relatively large ($V > 1000$ liters) excimer laser amplifier volumes, and
(2) Electric discharge excimer laser amplifiers with the excitation of the KrF excimer achieved along the neutral channel for geometries involving moderate ($V < 200$ liters) volumes.

The first excimer laser amplifier design configuration, electron beam excited excimer lasers (EBEL), has received extensive development from both the DOE and the DoD with KrF amplifier modules as large as 2000 liters being constructed. The second configuration, electric discharge excimer lasers (EDEL), has been much less thoroughly investigated; some preliminary theoretical work was funded by DOE[1] several years ago, but little experimental verification of the predicted high EDEL

efficiency was made. Each of these two KrF amplifier design configurations has its supporters and detractors. The EBEL has received priority development over the EDEL because the EBEL scales to larger volumes (and hence larger output energies) much more readily than does the EDEL. For single-shot DOE applications and for some DoD applications, this scalability advantage of the EBEL has been important. For an IFE reactor application in which reliability for c. 10^9 over long periods of time at repetition rates of 3-10 Hz is crucial, the potentially higher reliability of the EDEL makes this configuration of greater interest than formerly.

During the course of the reactor design study (including reviews with Government scientists), the question has been raised whether or not KrF amplifiers can be designed to fulfill all the technical requirements (summarized below), while still achieving a cost effective level of performance to permit the overall cost of electricity (COE) for the IFE reactor to be competitive. Our design should significantly reduce the risk of developing a cost-effective KrF final amplifier design for three reasons:

(1) The amplifier output energy has been reduced from the 250 kJ level suggested for EBELs down to levels of the order of 5 kJ,
(2) Since the dimensions of the laser amplifier are of the order of 30x30x200 cm, parasitic oscillations and superfluorescent losses are more easily controlled,
(3) Optics costs and risks are significantly reduces as the effective aperture of the amplifier is reduced to 30 cm.

The new non-linear optical beam combination design approach which has made it technically feasible to relax the energy, volume, and aperture requirements for the KrF laser amplifiers is the implementation of forward stimulated rotational Raman scattering amplifiers for beam combination, larger aperture synthesis, and improved beam quality. Nonetheless, there remain a series of developmental problems associated with both types of amplifiers.

In evaluating the relative risks associated with the two excimer laser designs, the requirement performance parameters of each is summarized below in Table 5.3.15-1 and Table 5.3.15-2.

Note that the large volume EBEL amplifier module must have a saturating laser pulse passing through the active volume in order to prevent serious superfluorescence and parasitic oscillation losses associated with the high (13.8 neper) small signal gain of the amplifier.

Table 5.3.15-1 Design Requirements for EBEL

Requirement Description	Design Value
Output Energy	240 kJ
Amplifier Aperture	3x3 m
Pulse Duration	500 ns
Amplifier Volume	54 m^3
Amplifier Gain Length	6 m
Amplifier Gain Coefficient	.023/cm
Energy Storage Density	7 J/liter
Energy Extraction Efficiency	0.7
Final Anode Voltage	3.3 MV
Overall Efficiency	10%
Bandwidth	1% or 10^{13} Hz
Laser Wavelength	248 nm
Active Medium	KrF
Total Gas Pressure	760 torr
Pulse Compressor	Angular Multiplexing
Laser Beam Quality	1.4 XDL
Peak to Peak Laser Beam Homogeneity	20%
Number of Shots Between Failures	10^{10}
Repetition Rate	5 Hz

Table 5.3.15-2 Design Requirements for EDEL

Requirement Description	Design Value
Output Energy	4 kJ
Amplifier Aperture	30x30 m
Pulse Duration	200 ns
Amplifier Volume	0.18 m^3
Amplifier Gain Length	2 m
Amplifier Gain Coefficient	0.05/cm
Energy Storage Density	22 J/liter
Energy Extraction Efficiency	0.7
Final Anode Voltage	50 MV
Overall Efficiency	12%
Bandwidth	10^{10}Hz
Laser Wavelength	248 nm
Active Medium	KrF
Total Gas Pressure	760 torr
Pulse Compressor	Chirped SBS
Laser Beam Quality	1.1 XDL
Peak to Peak Laser Beam Homogeneity	5%
Number of Shots Between Failures	10^9
Repetition Rate	5 Hz

Comparison between Table 5.3.15-1 and Table 5.3.15-2 will indicate that the requirements for the EBEL are generally much more difficult to attain than those listed for the EDEL, with regard to the required optics, the pulsed power, and the performance of the amplifiers themselves. The key developmental problems

associated with each of these two types of excimer laser amplifiers are summarized below in Tables 5.3.15-3 and 5.3.15-4.

Table 5.3.15-3 EBEL Developmental Problems

#	Description of Problem Area	Possible Solution
1	Foil Rupture	Homogenize E-Beam Current Density
2	Parasitic Oscillations	Lower Amplifier Reflectivities
3	Amplified Superfluorescence	Reduce Amplifier Solid Angle
4	High Cost of Large Windows	Segmented Optics
5	Radiation Damage from E-Beams	Lower Anode Voltage
6	Reduced Beam Quality	Phase Conjugation
7	Optics Damage	Reduce Radiation Fluence
8	Catastrophic Failure Mode	Redesign Foil Support Structure

These EBEL developmental problems are relatively well understood in view of the extensive theoretical and experimental studies of these amplifiers carried out by both the DOE and the DoD. For successful implementation into an IFE reactor, the most important development for the EBEL is the need for a dramatic increase in the mean number of amplifier firings between failures. As summarized below in Table 5.3.15-4, there are also significant problems associated with the EDEL approach, but since the amount of research and development for these amplifiers is relatively small, larger uncertainties in this excimer laser design exist:

Table 5.3.15-4 EDEL Developmental Problems

#	Description of Problem Area	Possible Solution
1	Stabilization of Discharge	Discharge Uniformity; Control F_2 Burn
2	Uniformity of Discharge Excitation	Elimination of Cathode Fall Region
3	Reduced Excimer Beam Quality	Beam Combination in Raman Cell
4	Achieve 10^9 Shot Lifetime	Engineer Pulsed Power/Electrodes
5	Optics Damage	Reduce Radiation Fluence
6	Verify Excitation Efficiency	Conduct Full Scale Experiments

Compared with the EBEL, the developmental problems for the EDEL appear to be more tractable although relatively little work to date has been completed for these devices.

Summary - Considerable developmental work has been carried out during the last decade on EBEL amplifiers. Although much progress has been made in achieving the ambitious design goals for EBEL amplifiers, these devices are currently not believed to be capable of meeting a 10^9 shots-between-failure requirement. Moreover, the primary advantage of the EBEL design over the EDEL is the ability of the e-beam excitation to scale to larger amplifier volumes. This is not desirable for a reactor design since it causes the excimer laser amplifier to become the cause of a single point failure.

It must be emphasized that significant KrF amplifier development work must be carried out in the next decade if the demanding requirements for the KrF driver amplifiers are to be met. Thus, the essence of this Critical Issue is that substantial development effort will be required in order to provide the KrF amplifiers which will be the workhorses of the future IFE reactor. Details will be defined in the associated Research and Development section.

References for 5.3.15

1. Mark Kuschner, et al., "New Techniques for KrF Laser Fusion Systems," Interim Report for Los Alamos National Laboratory, Spectra Technologies, Inc., Seattle, WA (1986).

5.3.16 Critical Issue No. 16: Demonstration of Low Cost, High Volume Target Production Techniques

Description - Target production for IFE reactors will require technologies which are presently either nonexistent or insufficiently developed for such an application. It is, therefore, very difficult to accurately estimate the production costs of such targets. These difficulties are further aggravated by the potential need for sabots to deliver the targets to the reaction chamber and, in the case of indirect drive, for an outer case which must meet stringent engineering requirements. Target cost is clearly a critical issue in light of the fact that IFE reactors will consume huge numbers of targets (on the order of 10^8 per year), and will be uneconomical and, therefore, impractical if these targets are too expensive.

This page intentionally left blank.

conditions. Failure to meet symmetry requirements would reduce system performance by forcing the reactor to operate on a less favorable gain curve.

Design Specificity - (Generic)

Overall Level of Concern - (Critical) Unpredicted target coupling deficiencies are not expected to lead to a gradual drop off in target gain. Instead, because of the physics of implosion, hot spot generation and propagating burn presently envisioned for all reactor types, failure would be sudden and catastrophic.

Operating Environment - (H, L, TWI, G, N) Tritium inventory will be affected by the efficiency of target burn. Laser type and wavelength will influence coupling efficiency more than choice of heavy ion driver design parameters. Poor target coupling can lead to incomplete vaporization and the generation of solid target debris. Beam geometry will affect coupling efficiency. The severity of the technical problem is increased by the need for cyclic operation.

Degree of Relevance to MFE - None

Analysis - A code has been written to analyze the problem of target coupling efficiency. Results obtained to date will be reported at an upcoming IEEE conference.

Issue A.a.2 Indirect Drive Laser Target Coupling

Description - The indirect-drive IFE laser target design consists of a cryogenic DT fuel capsule located inside a radiation-enclosing cavity (or hohlraum) designed to accomplish the following three goals:

(1) Convert the incident laser energy efficiently into soft X-rays,
(2) Using the particular shape of the hohlraum enclosure, these soft X-rays are focused into a uniform irradiation of the cryogenic DT fuel capsule,
(3) Uniform irradiation (and consequent absorption) of the soft X-rays by the DT fuel capsule leads to ablation and the resulting rocket reaction produces a uniform DT target compression permitting the interior of the DT Target to reach values of ρr (product of density [ρ] and compressed target diameter [r]) with 3/2kT ~ 25 KeV adequate to achieve rapid fusion of the fuel via the reaction:

$$ {}_1D^2 + {}_1T^3 = {}_2He^4 + {}_0n^1 \ (14 \text{ MeV}) $$

A number of problems have been identified with achieving these three indirect-drive laser driven (IDLD) IFE target goals.

5.4 Key Issues Description

This section provides more detail on the key issues previously identified in Section 5.2, Table 5.2-1. The same designation noted in Table 5.2-1 will be used in this section. Each issue will be described in depth, followed with more detail regarding each of the table entries. The same abbreviations and notations explained in Section 5.1 and used in Table 5.2-1 are used in this section. Some of the issues have substantiating analyses.

Issue A. Target

A.a Target Physics

Issue A.a.1 Direct Drive Target Coupling

Description - Absorption of driver radiation by direct drive laser targets is a complex process involving inverse bremsstrahlung, resonance absorption and various light scattering instabilities such as stimulated Brillouin scattering (SBS), stimulated Raman scattering (SRS), laser light filamentation and two plasmon decay (TPD). These processes occur both at the critical surface and in the volume space about the target. All of these processes can play a potentially critical role in affecting the uniformity of direct drive illumination and target coupling efficiency.

It is now believed that illumination nonuniformities in IFE reactors must be kept below 1% to avoid the excitation of hydrodynamic instabilities. This is a difficult technical requirement in view of the fact that on the order of half a million targets per day must all be accurately illuminated by approximately 60 laser beams. These targets will not be mounted on stalks and accurately positioned before each shot as has been done in previous laser fusion experiments. Rather, they will be injected into the reaction chamber with the aid of pneumatic, electromagnetic, centrifugal, or other accelerating devices. Inaccuracies will inevitably occur in this complex process in the form of slight variations in injection velocity, beam pointing errors, etc. It is necessary to consider all these factors in judging the technical feasibility of a reactor design.

Reactor Concept - Laser and Heavy Ion

Potential Impact - (DW, UL, RP) The design window may be closed if a beam arrangement cannot meet illumination symmetry requirements under realistic conditions. Unavoidable beam pointing and target injection errors may result in unacceptable reliability even if a beam arrangement would work under ideal

Attainment of Goal #1 - Goal #1, the efficient conversion of incident laser energy into soft X-rays is hampered by the physical structure of current ID LD targets. Access of the incoming laser beams to the hohlraum wall is attained by transmitting the high power laser beams through two small apertures (in the case of 2-sided laser illumination scenarios) in the radiation-opaque ID LD target casing. Great care must be taken to avoid allowing high intensity portions of the incident laser beams to irradiate the opaque ID LD target casing.

Previous research has demonstrated that the interaction of the high power laser light with the edges of the entrance apertures to the hohlraum produces sufficient densities of plasma above the critical density to reduce the transmission of laser light significantly into the ID LD target capsule. This plasma closure process is time dependent.

Attainment of Goal #2 - Uniform irradiation of the DT target with the soft X-rays generated by the target represents a difficult technical problem requiring the simultaneous achievement of homogeneous X-ray conversion together with isotropic illumination by the quasi-ellipsoidal optical figure of the radiation enclosure itself. Physical optical analyses of such homogeneous irradiation have indicated that a high degree of DT target irradiation uniformity is very difficult to achieve in certain design configurations.

Attainment of Goal #3 - DT target implosion, avoiding any significant Rayleigh-Taylor instabilities, is a complex magnetohydrodynamic process requiring stringent initial conditions on the irradiation uniformity, spectral distribution of the incident X-rays, avoidance of target preheating by hot electrons or hard X-rays, etc. The achievement of this goal is crucial to the success of both indirect-drive and direct-drive laser IFE targets.

Reactor Concept - Laser

Potential Impact - (DW, RP, IC, RS) The design window may be closed if the majority of the laser light cannot propagate into the hohlraum for efficient soft X-ray conversion. This would necessitate increased laser irradiation energies, shortening of the laser pulse duration, etc. If the optical figure of the hohlraum radiation enclosure is unable to provide uniform irradiation of the DT fuel capsule, high yield will not be obtained from the target implosion. This would force the IFE reactor to operate at a lower efficiency.

Design Specificity - (Generic)

Overall Level of Concern - (Critical) Low conversion efficiency of incident laser light by the target may result in the laser light interacting strongly with the plasma cloud

generated around the IFE target. These laser/plasma interactions may result in the generation of hot electrons and hard X-rays which may cause catastrophic target preheat, leading to enormous fluctuations in IFE reactor output power.

Operating Environment - (L, TWI, G, Q, N, I, S, F, T, q, s, t) Operating power for the laser driver will be strongly affected by the target coupling efficiency and target yields. The tritium inventory will be affected by the target yields. Poor target coupling for indirect drive targets can lead to additional debris problems. Enlargement of the hohlraum may lead to increase in contaminants if materials other than Pb are used.

Degree of Relevance to MFE - None

Analysis - Several codes are available to analyze the problems of indirect-drive laser IFE target physics. These analyses must be anchored to realistic laser IFE experiments before the issues can be resolved.

Issue A.a.3 Survivability of Targets in Chamber Environment

Description - The chamber environment is hostile to the cryogenic integrity of the target and could even potentially cause significant ablation of the target surface. The precise physical conditions which will exist in an IFE reactor chamber is still a very open question. The evaporation/recondensation issue requires realistic experimental investigation for its resolution, and the radiation background will likely be non-LTE for much if not all of the cycle. However, parameter studies can be undertaken to find when chamber conditions become a serious threat to target survival.

Reactor Concept - Laser and Heavy Ion

Potential Impact - (DW, RP) If the present projections of chamber temperature, pressure, and radiation background prove overly optimistic, the cryogenic survival of the target in the chamber may be threatened.which would have a deleterious effect on system performance.

Design Specificity - (Generic)

Overall Level of Concern - (High) Target designs should protect the cryogenic fuel. It appears that significant departures from presently projected chamber conditions would be necessary for significant deterioration of target performance to occur.

Operating Environment - (S, T, A, G, Q, t, q, P, v) All factor which affect conditions in the chamber have an impact on target integrity. Background radiation and pressure are key factors.

Degree of Relevance to MFE - (Low) There is some similarity between this issue and the issue of ablation from the cryogenic pellets which may be used to refuel MFE reactors.

Analysis - Analysis of the question is presently being conducted by the team with the aid of a 3D hydrodynamics computer code. A parameter search is planned which will show at what levels various chamber conditions begin to pose a threat to the target. At the same time, the study will determine the ability of background gases in the chamber to affect the trajectory of the target. This work is not yet finished.

Issue A.b Beam/Target Interaction

Issue A.b.1 Demonstration of Injection and Tracking of Targets Coupled with Beam Steering

Description - According to the Target Working Group, illumination nonuniformity must be kept below 1% rms. This means that injection and tracking must be sufficiently accurate to keep target mispositioning at less than 0.1 of the capsule radius during illumination. Assuming the target is exactly where is should be, beam mispointing errors must also be kept below about 0.075 of the target radius to assure adequate illumination uniformity. To meet these stringent requirements, some sort of a real time tracking system along with electronic beam steering is necessary.

Reactor Concept - Laser and Heavy Ion

Potential Impact - (UL) Symmetric implosions are critical to the success of inertial fusion. Excessive departures from adequate illumination symmetry will not lead to a gradual fall-off in target gain. rather, gain will show a steep drop to near zero levels if generation of hydrodynamic instabilities disrupts the implosion process.

Design Specificity - (Generic)

Overall Level of Concern - (Critical) Unless adequate illumination symmetry can be guaranteed, IFE is technically out of the question.

Operating Environment - (A, TWI, P) Cavity dimensions will have an affect on the impact of small deviations in injection velocity. Target failure due to beam mispointing and injection velocity errors will lead to the generation of solid target debris. Fluctuations in background pressure could potentially affect target velocity.

Degree of Relevance to MFE - (Low) Injection systems must also be used in MFE solid cryogenic pellet refueling schemes. However, although accurate pellet trajectories are important, they are not as critical as in IFE.

Analysis - A code has been written to study the effects of various combinations of injection velocity errors and beam mispointing on IFE reactor performance. Results obtained with the code will be provided as they become available.

A.c Fabrication

Issue A.c.1 Manufacturability of High Quality, Low Cost DD and ID Targets

Description - Previous target production for ICF has been in very small batches, often with each target custom made. Inspection for flaws in surface finish, concentricity and thickness could be made almost at leisure. Fusion energy generation will require the production of hundreds of thousands of targets of uniformly high quality ever day. These targets must be produced with a low turn around time to avoid high tritium inventories. Efficient fill techniques must be demonstrated for reactor size targets. The ability to create uniform fuel layers using the beta heating process or some other procedure must be demonstrated. The feasibility of using artificial intelligence and mechanization for accurate mass inspection must be proved. For an indirect drive target, a case must be mated to the capsule, probably under cryogenic conditions, which assures symmetric burn while at the same time providing a sufficiently robust overall configuration to survive acceleration and transit through the target chamber.

Reactor Concept - Laser and Heavy Ion

Potential Impact - (UL, RP, IC, RS) To avoid high tritium inventories it is advisable to produce targets on a "just in time" basis. Therefore, if any of the major steps in the production process proves unreliable, reactor shutdown would result. Failure of inspection and quality assurance procedures to assure uniformly high quality targets would result in lower gain and poor system performance. Targets must be manufactured cheaply or the large consumption of targets will lead to excessive costs. Target manufacture will require the presence of large tritium inventories in the

factories. Rapid fill rates and efficient beta heating must be demonstrated to assure that these inventories do not become excessive.

Design Specificity - (Generic)

Overall Level of Concern - (High) Resolution of this issue will mainly affect the issue of cost. Inability to produce targets efficiently will not preclude the generation of fusion power. It will simply make it economically unattractive.

Operating Environment - (H, TWI, N) Reactor tritium inventories will be strongly affected by the efficiency of the target fill and beta heating processes. Poor target quality will lead to incomplete burn and the resultant generation of target debris. The continuous operation of the reactor assumes no interruption of the target supply.

Degree of Relevance to MFE - Similar problems will be faced in MFE if solid fuel pellets must be produced and injected into the reactor on a cyclic basis. This presently seems a likely MFE refueling method.

Analysis - A technical note is available from KMS on required factory tritium inventories. Theoretical and experimental work on the beta heating process presently indicates that the process will generate uniform fuel layers efficiently and quickly under ideal conditions. It remains to be shown that such conditions can be provided for millions of targets at once in a factory environment. Diffusion filling of a reactor size CH (plastic) target has not been demonstrated to date. However, diffusion rates for CH are well known and this step in the production process is not expected to present any technical problems. However, diffusion filling will require large tritium inventories.

Issue B. Driver

B.a. Laser Driver

Issue B.a.1. DT Target Illumination Issues

Description - Current Target Working Group (TWG) Guidelines[1] call for tangential illumination of the direct-drive spherical DT target with at least 60 beams producing an overall ~1% intensity uniformity, no polarization specification, a pulse duration of 6 ns, an incident laser energy (at λ = 248 nm) of 5 MJ, together with a pre-pulse ramp of 60-80 ns with ~1% of the laser energy. The TWG stated the laser/target coupling efficiencies are implicitly included in the provided target gain curves. Elementary calculations for inverse Bremsstrahlung (IB) assuming an laser light/target coupling

dependence of $(\cos \theta_o)^5$ derived from planar target experiments[2] indicate that DD coupling may be relatively inefficient. Furthermore, the prepulse is expected to generate a 6-cm diameter underdense plasma atmosphere around the DT target which in the presence of summed laser intensities as high as 10^{15} W/cm^2 could give rise to significant stimulated Brillouin scattering (SBS) and stimulated Raman scattering (SRS) together with attendant production of suprathermal electrons unless very high laser bandwidths were available. Lastly, the influence of resonant absorption (RA) has been assumed to be negligible assuming that the laser driver operated in the 250 nm wavelength range. Since RA deposits energy in the plasma in a two-lobed pattern[2], the concern arose that if this mechanism were enhanced by the tangential illumination criterion of the TWG, it would not be possible to meet the ~1% target illumination uniformity requirement.

The worst case scenarios for the direct-drive illumination issues break down into two possibilities: (1) the DD illumination can be accomplished with inefficient coupling of laser light into the target, and (2) it may be necessary to go to an indirect drive target design.

There are additional key issues associated with indirect-drive laser-driven targets; i. e., plasma closure of the hohlraum entrance apertures preventing laser pulses from efficiently coupling to the target.

References

1. Ronald C. Davidson (MIT), et al., "Inertial Confinement Fusion Reactor Design Studies Recommended Guidelines," prepared for DOE Office of Fusion Energy, September 1990.
2. J. J. Thomson, C. E. Max, J. Erikkila, and J. E. Tull, "Absorption of Focused Light by Spherical Plasmas," Physical Review Letters, 37, pp. 1052-1056, (1976).

Issue B.a.2 Large Laser Bandwidth Issues

Description - By virtue of their quantum mechanical properties, excimer lasers are theoretically capable of generating efficient, high power, partially-coherent laser beams having relatively large bandwidths of up to 0.1%. Thus, for $\lambda = 250$ nm, the laser frequency would be $\nu = c/\lambda = 1.1 \times 10^{15}$ Hz, so that the maximum bandwidth would be $\Delta\nu \sim 10^{12}$ Hz or 1000 GHz. Hitherto excimer lasers operated with very wide bandwidths have exhibited temporally unstable oscillation characteristics in part

because of the complex mixture of laser modes which broad-band resonators would permit to exist within the laser. A second problem arises if non-linear optical (NLO) processes (such as stimulated Raman scattering [SRS] and stimulated Brillouin scattering [SBS]) are required for beam combination and pulse compression. Both SRS and SBS become inefficient for laser bandwidths significantly greater than 10 GHz unless careful attention is paid to the NLO device design. Lastly, propagating intense, broad-bandwidth laser pulses through a significant number of dioptric elements can produce both temporal and angular dispersion, thereby endangering the target illumination uniformity budgets.

From a target illumination standpoint, laser beams having broad-bandwidths may solve some problems. Coherent beams incident at relatively small angles produce interference fringes on the surface of the target which "wash out" in a period of time, τ_c, of the order of $1/\Delta\nu$, which for $\Delta\nu$ = 10 GHz, τ_c ~ 100 ps. Secondly, intensity thresholds for SBS and SRS in the underdense plasma atmosphere around the target increase as the bandwidth of the illuminating laser is increased for $\Delta\nu_{laser} > \Delta\nu_{SBS}$ or $\Delta\nu_{laser} > \Delta\nu_{SRS}$.

Thus broad bandwidth illumination could reduce DT target preheat from suprathermal electrons.

Other key laser amplifier issues have to do with demonstrating a well-engineered laser amplifier design: This category of key issues includes:

(1) Developing a fail-safe design (i. e., if an excimer laser amplifier fails, no reactor shutdown will be required)
(2) Meeting a wall-plug efficiency of c. 12%
(3) Achieving a mean number of firings between failures of 10^9
(4) Producing a very high quality output beam quality. (This factor can be mitigated if a Raman accumulator is used to improve beam quality.)

Issue B.a.3 Final Optics Pointing System

Description - The final optics pointing system must meet a precise requirement for achieving target illumination uniformities using 60 laser beams defined in Section 3.1, above. This pointing requirement will be made for fusion targets moving at a high speed (possibly ~1 km/sec) through a residual atmosphere in a cylindrical target chamber. It is assumed that the nominal focal length of the focusing mirrors will be ~40 m, so that if the focusing mirrors were used also for pointing the laser, interbeam pointing accuracies of the order of $\Delta\theta$ ~ 1×10^{-6} rad would be required, depending also

upon the near-field apodizations of the 60 tangential illuminated laser beams. An additional uncertainty would be the degree to which all 60 beams would have to be deflected to compensate for a ballistic DT target that was off course by a distance, Δx. Small spatial misalignments, Δx, are not as serious for meeting the target illumination requirements (Issue B.a.1, above) since such a misplaced target would experience only second-order illumination uniformities since the interbeam alignment stringencies set the first order target illumination requirements.

Hitherto, IFE target alignment systems have had to deal with fixed targets so that the final optics pointing system would be significantly more complicated than previous systems. Methods and techniques exist to align the 60 beams relative to a precision surrogate target. Where needed, this methodology needs to be incorporated into the design of the mirror pointing and centering system.

Issue B.a.4 Grazing Incidence Mirror Damage

Description - A key issue for the excimer laser driver is the control of optical damage on mirrors and windows in the system. Excimer laser amplifiers put their amplifier windows at particular risk since these windows are simultaneously exposed to ionizing radiation, UV laser light, and the corrosive effects of F_2 gas. A key element in controlling optical damage is to design the laser elements to produce spatially smooth beams with little or no intensity ripples. Use of a Raman accumulator with excimer laser pump beams has hitherto proven to be the most effective method for controlling intensity spikes from excimer lasers.

The grazing incidence mirror for the Prometheus-L reactor is currently situated at distances of the order of 20 m from a source of X-rays, neutrons, charged particles, etc. having a total power of the order of 2.8 GW of which approximately 1/4% will be incident on the grazing incidence mirrors, assuming a pulse repetition rate of 5 Hz, a target gain of 124, and a laser energy of 4 MJ/pulse. In addition, assuming that the each of the 60 beam lines will have an energy/pulse of approximately 70 kJ delivered at an angle of incidence of 80°, these mirrors will be exposed to 6 ns pulses of ultraviolet laser radiation at an average fluence of $\Phi_{laser} \cos(80°) \sim 2$ J/cm^2. At the present time, a composite mirror structure of aluminum and silicon-carbide is proposed for the grazing incidence mirror, and with the leading edge of the mirror located at a distance of 20 m from the center of the chamber, swellings on the optical surfaces of the order of $\lambda/4$ are expected to occur during the first year of operation. Calculations by UCLA indicate that swelling in the aluminum layer will be sufficiently minor that piezoelectric-activated transducers for mirror figure control may not be necessary.

One of the serious hazards faced by grazing incidence mirrors is potential damage due to particles that may be deposited on the surface of the mirrors. These particles are illuminated not with fluences of 2 J/cm^2, but with much more dangerous fluences of 10 J/cm^2 since the cos (80°) does not apply in this case. Although many particles are expelled from mirrors under these circumstances, particles that stick to the mirror surface in the presence of laser fluences this high can produce catastrophic damage to optical surfaces.[1]

Reference

1. G. J. Linford, "Simulations of Intracavity Laser Heating of Particles," Proceedings of SPIE, 1415, pp. 196-210, (1991).

Issue B.a.5 SBS Pulse Compressor

Description - Although many experiments and theoretical analyses concerning the behavior of stimulated Brillouin scattering have been carried out, the use of large scale (E_{laser} > 1 kJ) SBS cells for performing 100:1 pulse compression with high efficiency has not yet been carried out in the United States. Calculations[1,2] have suggested that ~100:1 SBS pulse compression can be achieved, but it has been shown theoretically that it may be difficult to achieve 6 ns pulse durations with high conversion efficiencies. Mak,[3] et al., reported that in work performed in the Soviet Union, 100:1 compressions of long pulse KrF lasers had been achieved with 99% efficiencies at energy levels of the order of 1 kJ.

Additional experimental work needs to be performed to demonstrate that the Soviet approach using a "chirped" input Stokes, possibly in a ramped format, can achieve the requisite pulse shape with a high conversion efficiency. There does not seem to be a serious concern that the SBS pulse compressor can achieve the requisite pulse compression ratio and pulse shape—the primary problem appears to be that the conversion efficiency may lie between 50 and 70%. Use of large aperture Pockels cells and appropriate delay lines can permit the depleted SBS pump (representing the remaining 30% of the energy in the SBS cell) to be used as the 80 ns precursor for the main laser beam.

References

1. "New Techniques for KrF Laser Fusion Systems; Stimulated Brillouin Architectures," Spectra Technology interim report for Los Alamos National Laboratory, pp. 1-3 through 1-6, (1989?).

2. "Ramp Stokes Seeds for SBS Pulse Compressors," TRW IOC from Gary Linford to ICFRDS Team, K323-L-91-142, 18 July 1991.

3. Arthur A. Mak and Leonid N. Soms, "Optical Methods for Laser Beam Control," Proceedings of SPIE, 1415, pp. 110-120, (1991).

B.b Heavy Ion

Issue B.b.1 Timing of Heavy Ion Beams

Description - In order to meet the TWG's requirements for the heavy ion indirect drive target, it will be necessary to achieve better than a ~0.5-ns time difference among all 16 HI beams through the LINACs, channel formation, channel transport, stripping, and focusing into the hohlraum. This degree of precision is currently not within the state of the art and will need development to attain.

Issue B.b.2 Channel Formation

Description - A complete description of the individual beam properties including current, charge state, density, energy charge density profile, rise time, degree of symmetry, and beam radius will be required to characterize channel formation in the background gas. In addition, the physics of interaction with the beam in terms of the background gas properties must be made. These background gas properties are: composition (Pb, D_2, DT, He, plastics, etc.), density, ionization potentials, degree of ionization, etc. It is presumed that the heavy ions will have Z ~ 82, initial charge state +2, current tens of MA, and energies of approximately 5 GeV.

Issue B.b.3 Channel Transport

Description - There are key issues associated with the transport of space-charge limited heavy ion beams through the reactor cavity to the target. The problems associated with HI channel transport include collapse of channel due to pinching, motion of plasma within the solenoidal magnetic field, recirculating neutralization currents, attraction of elections, repulsion of ions, etc. In addition, it will be necessary to know the betatron period vs. the ionic charge state. Development of instabilities such as "kink" and "sausage" need to be understood, both experimentally and theoretically.

There are several critical issues which will require validation through experimentation and modeling before self-formed transport channels can be considered truly viable. Foremost among these is a laboratory demonstration of a self-pinched heavy ion beam transport channel. The transport characteristics of the channel must then be

assessed including: (1) fraction of the beam ions initially captured in the channel, (2) fraction of the beam energy lost due to background collisions and back EMF, (3) fraction of the beam energy lost near the target where opposing side channel currents begin to cancel the confining azimuthal field, (4) fraction of the prepulse energy eroded during channel formation, (5) capability of the channel to re-image the focal spot at the channel entrance onto the target, (6) limitations on beam focal spot size at the channel entrance, (7) demonstration of sufficient control over the channel to accurately position the focal spot on the target, and (8) characterization of background gas conditions/limitations for stable channel formation.

Reactor Concept - Prometheus-H

Potential Impact - RP, IC, RS, RL

Design Specificity - DHI (Driver, Heavy Ion)

Overall Level of Concern - High
The capability to form a stable, self-pinched transport channel to re-image a heavy ion beam focal spot on a target would have significant positive economic and technical impact on design of a heavy ion-driven inertial fusion power plant.

Operating Environment

P	-	Background Gas Density	T	-	Temperature
Q	-	Power Density	E	-	Beam Energy
IB	-	Beam Current	EI	-	Ion Energy
G	-	Geometry	p	-	Pulse Shape
N	-	Cyclic Operation	HI	-	Heavy Ion

Relevance to MFE - Low
This development issue is not directly relevant to MFE.

Issue B.b.4 Stripping of HI Beam

Description - The stripping of the HI beam in a thin foil needs to be understood in terms of the momentum vector of the completely stripped beam. In addition, if an ionizing laser is used to generate a channel, the interaction of the stripped HI beam with the weakly ionized channel through the gas needs to be thoroughly investigated. The precision with which the HI beam follows the laser beam needs to be established accurately since it strongly impacts the accuracy with which the HI beams can be delivered to the indirect drive target. In addition, a reliable method is required for the introduction of the laser beam through the foil area and into the impact region for the injected indirect-drive target. In addition, the phenomenon of self-focused beam capture inside the pre-formed channel needs to be investigated experimentally.

Issue B.b.5 Alignment of Indirect HI Target

Description - Although the alignment stringencies of the HI beams to the indirect drive target are less severe than those placed on the excimer laser driver irradiating a direct-drive target, it is necessary to combine the 16 HI beams into a bundle of sufficiently small size (~1 mm) to permit the efficient irradiation of the target without damaging the capsule. This problem is therefore intimately related to the channel transport issues raised above in sections 3.3 and 3.4.

Issue C Vacuum System and Evacuation

Issue C.1 Vacuum Seal Compound Survival in Nuclear Environments

Description - Elastomers such as Viton, Buna and teflon are frequently used for seals in vacuum designs. These as well as other candidate elastomeric compounds may be quite susceptible to degradation and alteration of properties in a nuclear environment.

Reactor Concept - Laser and Heavy Ion

Potential Impact - Alternative, more expensive and labor intensive designs utilizing metal seals will be required if nuclear hardening of elastomeric seal materials is not accomplished.

Design Specificity - This issue is generic to all reactor concepts.

Overall Level of Concern - Low. This problem will have to be solved and may add to remote maintenance costs. the problem has been encountered before and existing seal designs are available.

Operating Environment -

Degree of Relevance to MFE - High. Magnetically confined fusion devices have encountered this problem and have sponsored studies to determine applicable alternative seal designs.

Analysis - None.

Issue C.2 Cryogenic Pump Hydrogen Capacity

Description - The largest design factor affecting the vacuum system is cryopump hydrogen capacity. Current pumps have relatively limited capacity which drives designers to choose between large numbers of pumps or frequent pump regeneration. Increases in hydrogen capacity may be accomplished through pump design trade-offs, sacrificing the ability to pump large amounts of heavier gas species.

Reactor Concept - Laser and Heavy Ion

Potential Impact - Vacuum system design may be changed due to increases in hydrogen capacity. Reductions in the number and/or size of cryogenic pumps has impact on remote maintenance systems, shielding requirements, reactor exhaust reprocessing system as well as the vacuum system.

Design Specificity - This issue is generic to all inertial confinement reactor concepts.

Overall Level of Concern - High. This issue could significantly reduce the size of the reactor vacuum system. As shown in the potential impact statement, the issue has a ripple effect through several reactor subsystems. Significant cost reductions are possible.

Operating Environment

Degree of Relevance to MFE - High. MFE reactors have significant gas loads and the vacuum system spatial restrictions are significant.

Analysis - See Section 6.6 of report.

Issue C.3 Chemical Stability of the Reactor Exhaust

Description - The carbon and hydrogen isotopes contained in the reactor exhaust could combine to form various hydrocarbon molecules. This chemical recombination could produce flammable and/or toxic compounds. Vacuum and reactor exhaust systems operation and design could be affected.

Reactor Concept - Laser and Heavy Ion

Potential Impact - Vacuum system design may be changed due to reduced atomic hydrogen gas loads as well as the potential health and safety hazards. The exhaust system design may also need alteration to allow separation of the hydrocarbons for potential cracking/reprocessing operations.

Design Specificity - This issue is generic to all inertial confinement reactor concepts that introduce carbon into the reactor.

Overall Level of Concern: - Medium. This issue could significantly reduce the size of the reactor vacuum system. It also has the potential to increase safety problems and to add to the fuel reprocessing complexity. This issue will have to be addressed prior to design of the first reactor.

Operating Environment - High temperature carbon and hydrogen exhaust gases.

Degree of Relevance to MFE - None. Carbon and other chemically reactive compounds are probably present in only insignificant amounts in an MFE reactor.

Analysis - None.

Issue D Tritium Processing System

Issue D.1 Tritium Inventory

Description - The Tritium Fuel Cycle System is required to manage and process all tritium containing streams in the IFE plant. These include supply of tritium to target fabrication, processing of reactor chamber exhaust to remove protium and impurities, and treating tritiated impurities to recover tritium. In addition, tritium is to be recovered from the breeder blanket to ensure self-sufficiency. Also, various systems such as coolant, beam lines, reactor building atmosphere and waste water need to be decontaminated to remove tritium.

The key issue in the Tritium Fuel Cycle System is the tritium inventory and mean residence time of tritium in the subsystems and tritium losses from the subsystems, due to the radiological hazard posed by tritium. Tritium is a weak beta emitter with a half life of 12.3 years. It is a particular biological hazard because hydrogen is an important chemical component of the life cycle and the hydrogen isotopes are extremely mobile.

Reactor Concept - Laser and Heavy Ion. The design of the Tritium Fuel Cycle System is relatively independent of the driver design and is similar whether the Heavy Ion or Laser driver is selected.

Potential Impact - (RS) Containment and control of tritium present some special problems because tritium can permeate through materials and form volatile species. Tritium cleanup and safety systems are provided to protect the plant staff, the public and the environment from exposure to too much tritium, by effectively limiting the escape of tritium. They must also quickly recover all the tritium deposited in reactor systems to limit inventories and prevent decay losses.

Design Specificity - (B, T, TF) There are three subsystems of the Tritium Fuel Cycle System in an IFE plant with potentially large tritium inventories, i.e. the blanket, the exhaust processing system and the target factory.

Level of Concern - (Medium) Several strategies are suggested for controlling tritium to very low concentrations and for limiting the escape of tritium to the environment. By proper selection of material combinations, highly reliable processing systems and their operating conditions and multiple barriers, the tritium inventories and leakage can be minimized. Tritium escaping to the plant containment can be removed by gas cleanup systems.

Operating Environment -

Relevance to MFE - The tritium issue is virtually identical for IFE as for MFE with the exception of a large tritium inventory associated with the target fabrication for IFE.

Analysis - A critical issue is a serious problem which only R&D can resolve. A problem which can be resolved through conservatism in design and where R&D has only economic justification, could be termed a technical issue.

For DT fuel cycle self-sufficiency the blanket performance is a critical issue. The tritium breeding required defines a number of concerns of which only a few quality as issues. For example, the tritium inventory in the blanket is one of the parameters of the blanket issue. Tritium recycling from the chamber is, for steady state conditions, not an issue. The chamber tritium inventory (at steady state) may be an issue which could be packaged with another parameter; i.e., the tritium content of the first wall protection material, into a broader issue. Tritium inventories in the fuel processing systems are not an issue. for the given design the amount of tritium in the system is known and is acceptable. If however, the reference design changes to some different concept, this

may become an issue. The time required for target fabrication and target storage could be packaged into a broader target fabrication issue.

Based on the above comments and on the present design, there is no critical issue in the Fuel Cycle Design.

Issue D.2 Tritium Permeation from the First Wall Coolant - Liquid Pb

Description - Approximately 40% of the heat produced in the reactor will be removed by liquid lead and transferred into the ultimate heat transfer medium steam which will convert this into energy in a steam turbine. The permeation rate from the Pb side of the heat exchanger is of serious concern. Any permeation rate in excess of the release limit is unacceptable for direct heat exchange in a steam generator for directly driving the turbine. The following theoretical mitigating options exist:

(1) Double wall [1.1] or composite heat transfer tubes [1.2]. Option [1.1] could have an interspace between tubes which would be purged and evacuated. Alternatively, option [1.2], would feature a composite heat transfer tube wall which would have tailored permeation barriers consisting of dissimilar metals and/or oxide barriers.

(2) Use of an intermediate coolant loop. Such loop would transfer heat between Pb and steam, and provide opportunity for recovering permeated tritium.

Option 1.1 is, from the fuel cycle design point of view, very simple. In this case a purge gas would sweep the interspace under vacuum. The gas would be processed in one of the main fuel processing loops such as PSA (if He is used) or fuel purification loop if hydrogen is used. However, from the heat transfer point of view this option may be very difficult to implement as the heat transfer from liquid lead to steam may be severely restricted.

Option 1.2 would have no impact on the fuel cycle since the permeation would be restricted to values below noticeable levels. There would be no additional processes required.

Option 2 would, due to the high temperatures, involve a medium other than water. Such medium would most likely have to be liquid metals (or steam) since even known organic coolants could be used only to some 420°C.

In order to see if the concern is relevant the permeation rate was attempted to be calculated:

Solubility of T in Liquid Lead - Upper Permeation Limit - Ghoniem[1] suggests solubility values of 0.11-0.25 [cc T/100 mg Pb] at 500 and 600°C respectively. Such high figures appear to be in agreement with Opie and Grant[2] which were never experimentally duplicated;[4] and Hofman and Maatsch[3] could not measure figures above 0.01 which apparently was the detection limit of their instruments. Even this lower figure, when extrapolated for the high Pb flow of 20,311 kg/s [1] (or 7.3×10^{11} [g/h]), will yield tritium transport figures in excess of the 29.29 mol/h fueled into the chamber. However, a more useful source of solubility dependency on pressure is shown in Reference 4 and Figure 5.4-1. From this the solubility is 1.2×10^{-2} [appm H in Pb/torr$^{1/2}$]. The simplifying news is that the solubility appears not to be temperature dependent. Consequently cooling of Pb will not release any T in the heat exchanger. This leads to an assumption that the partial pressure of T on the Pb side of the heat exchanger is equal to the pressure at which the equilibrium solubility was established in the chamber. The chamber pressure[6] appears to follow a decay exponential from 10^4 Pa to 0.2 Pa during each of the 0.25 sec interval between explosions. An approximate integration of that pressure indicates that the average pressure is in the 130 Pa region. If the mole fraction of T_2, mt $_T$ is 0.208, the partial pressure of T_2 is:

$$p_T = mfT \times 130 = 0.208 \times 130 = 27 \text{ [Pa] or } 0.205 \text{ [torr]}.$$

The amount of tritium dissolved in Pb transferred to the heat exchanger is:

$$T_2 = \frac{p_T^{1/2} \times K_6}{10^6} \times \frac{A_T}{A_{pb}} \times Q\left(\frac{gT}{h}\right)$$

where:

p_T	=	partial pressure of Tritium in the chamber [torr];
K_3	=	Solubility = 1.2×10^{-2} [appm H in Pb/torr$^{1/2}$];
A_T	=	atom number for tritium = 3;
A_{pb}	=	atom number for lead = 207.2;
Q	=	Flow of lead to the heat exchanger 20311 kg/s or 7.3×10^{10} [g/h]

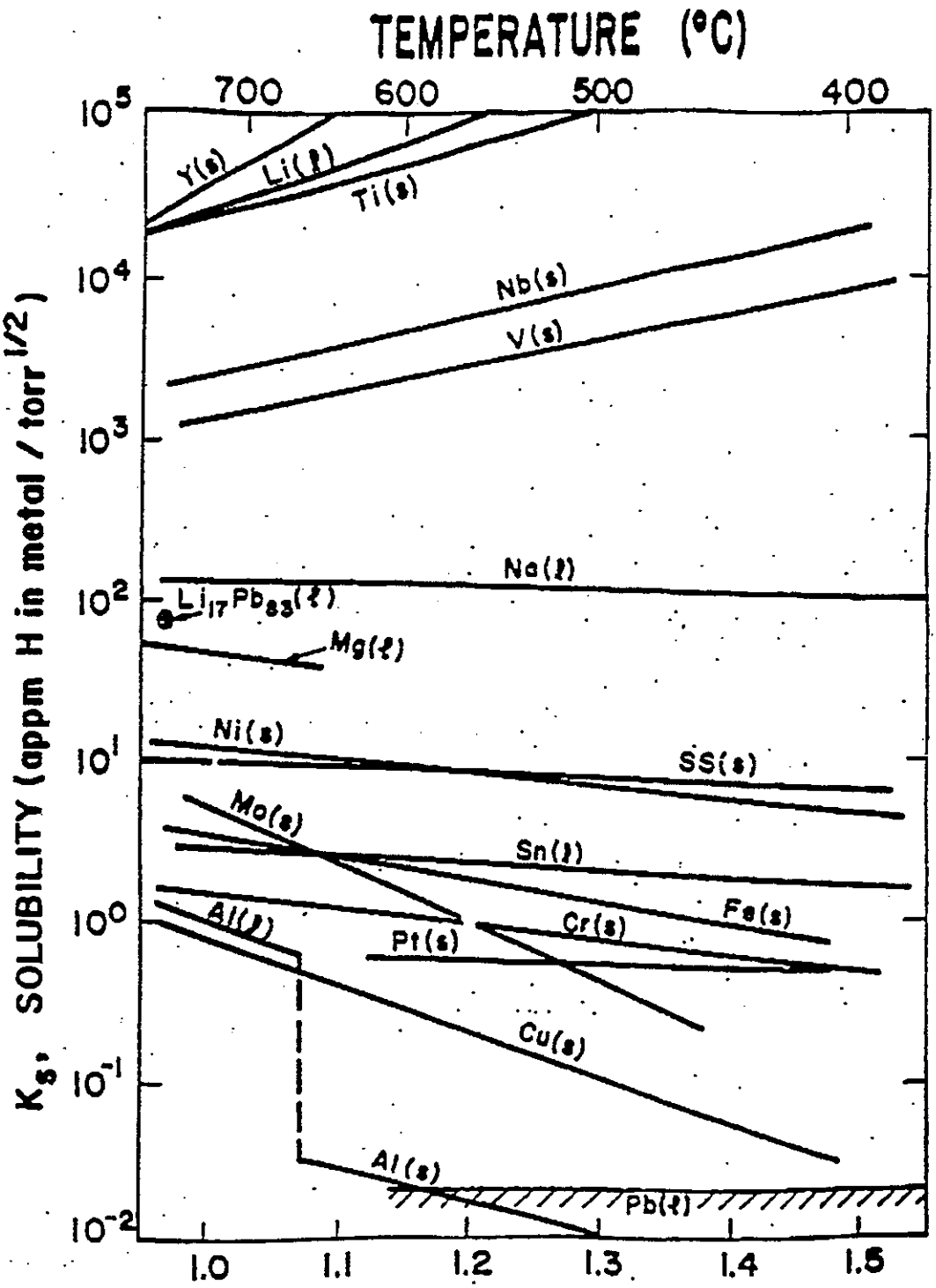

Figure 5.4-1. The Solubility of Hydrogen in Selected Metals and Alloys[4]

McDonnell Douglas Aerospace

The resulting tritium flow in solution is:

$$T_3 = \frac{(0.205)^{1/2} \times 1.2 \times 10^{-2}}{10^6} \times \frac{3}{207.2} \times 7.3 \times 10^{10} = 5.7\left(\frac{g}{h}\right)$$

This represents the upper limit for the permeation, since no more tritium can be carried out of the chamber.

Tritium Permeation - From Reference 5, the following correlation applies for a group of steel based materials:

$$\text{perm} = 0.5 \times \exp\left(\frac{-15000}{RT}\right) = 1.41 \times 10^{-5}; \text{cm}^3 \text{ (STP)} \times \frac{\text{mm}}{\text{cm}^2 \times \text{min} \times \text{torr}^{1/2}}$$

if: perm = Permeability (see above);

and for Gas constant R = 1.98, wall temperature T = 723 K, and:

A = Heat transfer area 1.5×10^6 [cm^2]
t_p = Wall thickness of the heat transfer tubes = 2 [mm];
p_T = Partial pressure of Tritium = 0.205 [torr];

The T permeation rate is:

$$T_{perm} = \frac{60 \times \text{perm} \times A \times (p_T)^{1/2} \times M_T}{2 \times 1000 \times 22.4} =$$

$$\frac{60 \times 1.2 \times 1.41 \times 10^{-5} \times (0.205)^{1/2} \times 6}{2 \times 1000 \times 22.4} = X \times (0.205)^{1/2} = 16.8 \times 0.25 = 7.56 \left(\frac{g}{h}\right)$$

It is apparent that the permeation flux through clean tubes in the Pb heat exchanger is exceeding the amount of tritium dissolved in Pb. From the mass balance, the amount of tritium "dropped out" of the solution must be in balance with the amount permeated. From the material balance, the permeation rate must be equal to the amount of tritium left in the heat exchanger. This balance will be reached at a lower partial pressure where the dissolved tritium is equal to the permeation flow. For such balance, the following applies:

T permeated = T supplied with Pb - T returned in Pb

or:

$$\frac{7.56 \times (px)^{1/2}}{(0.205)^{1/2}} = 5.7 - \frac{5.7 \times (px)^{1/2}}{(0.205)^{1/2}}$$

Consequently:

$$(px)^{1/2} = 0.194; \text{ and } p_x = 0.037 \text{ torr};$$

The new permeation rate is:

$$T_{3x} = 5.7 \times \frac{(px)^{1/2}}{(p_{chamber})^{1/2}} = 5.7 \times \frac{(0.037)^{1/2}}{(0.205)^{1/2}} = 2.45\left(\frac{g}{h}\right)$$

And the tritium flow returning to the chamber will be:

$$T_{sr} = 5.7 - 2.45 = 3.25\left(\frac{g}{h}\right)$$

Permeation with Oxide Barriers - Bell[5] offers permeation impedance factors ranging from 100 to 1000 for stainless steel conditioned by water oxidation at 600°C. For Incaloy 800 the corresponding figures are ranging from 167 to 319. This still leaves permeation flux in the range of 7 to 70 [mg/h] or in terms of Ci/h 70 to 700 Ci/h. Even the lower of the two figures could still cause a tritium extraction problem. With composite walls and or space the permeation flux could be reduced by 4 orders of magnitude which could bring the permeation into the range of 7 Ci/h or 167 Ci/day which is still hardly acceptable. It appears that the permeation control may have resorted to much more drastic steps such as oxidizing the permeated tritium in the tube interspace (or in the intermediate loop or on the Pb side of the heat exchanger) which should lower the permeation rate.

Tritium Inventory for the Fuel Cycle Components - As the design progresses, the earlier preliminary estimate of tritium inventories for the fuel cycle has been updated from the earlier figures extrapolated from ITER. These are shown in Table 5.4-1.

Table 5.4-1: Tritium Inventories for Fuel Cycle Systems

Service or System	Process	T Inventory [g]
Isotope Separation (ISS)	Cryo-distillation	56
Impurities from Fuel	Permeation	5
Tritium from Impurity reject	HITEX	0.5
Tritium from Solid Breeder	Pressure Swing Adsorption	2.8
Tritium from Water	Distillation + VPCE	0.3
Tritium from Atmospheres	Recombiner/Dryer	25
Solids removal from Pb	TBD	0
Fuel Management and Storage	Zr/Co or U beds	600-800
Breeding Blanket	Solid, He purged, He cooled	50-500
Coolant	Helium	0
Solid Waste De-tritiation	TBD	TBD
Total		740-1400

References

1. N. M. Ghoniem, UCLA, "Laser Reactor Chamber Design," IFE Reactor Design Studies Project Meeting, 6 August 1991.

2. W. R. Opie and N. J. Grant, "Solubility of Hydrogen in Molten Lead," Trans. AIME 191, 244-245 (1951).

3. W. Hofman and J. Maatsch," Loslichkeit von Wasserstoff in Aluminum," Blei-und Zinkachmelzen , Z. Metallkunde 47, 89-95 (1956).

4. E. M. Larsen, M. S. Ortman, K. E. Plute, University of Wisconsin, "Comments on the Hydrogen Solubility Data for Liquid Lead, Lithium, and Lithium-Lead Alloys and Review of a Tritium-Solubility Model for Lithium-Lead Alloys," UWFDM-415 (1981).

5. J. T. Bell, J. D. Redman, Chemistry Division, Oak Ridge National Laboratory, "Tritium Permeation Through Steam Generator Materials," American Chemical Society, 8412-0513- 2/79/0779-331, 1979.

6. N. M. Ghoniem et al., UCLA, Partial pre-print of UCLA draft contribution to the IFE Report, Rev. 14, September 1991.

Issue E. Cavity

E.a Wall Protection

Issue E.a.1 Cavity Vapor Hydrodynamics

Description - Vapor hydrodynamics following the blast affects both the pressure loads seen at the wall and also the condensation rate for cavity clearing, both of which are serious issues. Hydrodynamic phenomena in the cavity are very complex, involving temporally and spatially dependent energy deposition, shock propagation and vapor mass transfer. The hydrodynamics is also intimately coupled to cavity heat transfer, which is itself very complex.

Reactor Concept - Laser and Heavy Ion

Potential Impact - (DW, UL) Vapor hydrodynamics strongly affects recondensation and cavity clearing; if the cavity clearing rate is too slow, the reactor concept is not

feasible. Unacceptably high pressures at the first wall would cause early failures or result in conservative designs that increase cost and lower performance.

Design Specificity - (Generic) Dry wall protection schemes use cover gases, whereas liquid protection schemes fill the cavity with evaporated liquid. In either case, this is an important issue.

Overall Level of Concern - (Critical)

Operating Environment - (S, A, G, TWI, Q, t, q, P) Many factors affect cavity hydrodynamics. Initial conditions are set by the blast yields and spectra. Vapor and surface conditions are important, including temperature, pressure, power density and heat flux. Dimensions, geometry, and wall interactions also affect the phenomena.

Degree of Relevance to MFE - (None) This work is only slightly related to plasma disruptions.

Issue E.a.2 Cavity Structure Mechanical Response to Blast

Description - The main sources of loading on the first wall are due to: (1) impulse from rapid evaporation, (2) shock waves in the cavity gas, and (3) weight of the Pb. If the resulting stresses and strains are too large, then the fatigue life of the first wall may be unacceptably short, or the cavity will have to be designed more conservatively. Many failure modes will depend on the mechanical responses in the first wall structures. Mechanical response is very design dependent, and is difficult to predict currently due to the unique material design, component configuration and attachment scheme, as well as the complex loading conditions. Innovative design approaches can be envisaged to reduce the peak stresses; these require analysis and testing to determine the extent to which they are successful.

Reactor Concept - Laser and Heavy Ion

Potential Impact - (UL, RP, IC) If the resulting stresses and strains are too large, then the fatigue life of the first wall may be unacceptably short, or the cavity will have to be designed more conservatively.

Design Specificity - (All IFE reactors must address this issue.)

Overall Level of Concern - (High)

Operating Environment - (F, T, σ, A, TWI, G, Q, q, P, N, s) Mechanical responses depend very strongly on the local conditions in the first wall, including temperature, stress state, etc., and are strongly influenced by geometric factors. In addition, simulation of proper loading conditions is important, such that the requirements on the environmental conditions are very difficult.

Degree of Relevance to MFE - (Low) This problem resembles the response to disruptions, and to some extent the mechanical response of large components (such as the blanket) under cyclic operating conditions.

Issue E.a.3 Vapor Condensation Rate

Description - For liquid-protected first walls, evaporated material must be removed from the cavity quickly to allow rapid firing of the targets and beams. In most designs, this requires condensing the vapor on the wall or on separate condensing surfaces. Noncondensables must be pumped separately. The condensation rate is limited by processes in the cavity and by heat transfer to the cooling medium. The condensing surface must be adequately cooled to a temperature lower than the saturation temperature at the desired cavity base pressure. The basic heat and mass transfer processes under ideal conditions are relatively well known, but insufficiently studied at present. Lack of experimental data makes the modeling predictions very uncertain. More seriously, non-ideal effects, such as nucleate recondensation, aerosol transport, droplet generation and transport, 3D effects contribute very large uncertainties.

Reactor Concept - Laser and Heavy Ion

Potential Impact - (DW, RP, IC) Inadequate cavity clearing lowers the allowable repetition rate, raising the yields and/or lowering the power produced. If the yields become too high, the driver energy and wall loads may become prohibitively high. Alternatively, one could reduce the net power produced, although this would almost certainly destroy the economics.

Design Specificity - (Most wall protection schemes)

This issue is relevant, with the possible exception of a few schemes such as HYLIFE-II, in which the cavity is cleared by liquid slugs.

Overall Level of Concern - (Critical)

Operating Environment - (T, A, TWI, G, t, q, P) The main parameters which dominate recondensation are the temperature and pressure in the cavity and at the first wall.

Degree of Relevance to MFE - (None) Some possible relationship to plasma disruptions.

Issue E.a.4 Radiation Heat Transport in Partially-Ionized Gas

Description - The x-ray and debris energy is absorbed in the cavity background gas or in the vapor shield which arises from film evaporation. This leads to vapor temperatures up to several eV. In this partially-ionized regime, emission and transport of thermal radiation is very difficult to model. Thermal radiation is particularly important for the analysis of dry spots (or dry walls), but also contributes to the determination of the cavity clearing time.

Reactor Concept - Laser and Heavy Ion

Potential Impact - (RP, RL) Thermal radiation affects vapor recondensation and cavity clearing time, although its importance in this regard is uncertain (the time constant may be fast enough such that thermal conduction and mass transport dominate). It is more important when dry spots occur; when no liquid is present, evaporation of the dry wall due to thermal radiation is more important.

Design Specificity - (Generic)

Overall Level of Concern - (High)

Operating Environment - (T, A, TWI, G, Q, t, q) Target yields and spectra determine the initial conditions. The background gas pressure and temperature and wall temperature are the most important parameters.

Degree of Relevance to MFE - (Low) Thermal radiation in partially-ionized gases shares some similarities with the plasma edge region of an MFE reactor, although the materials are different.

Issue E.a.5 Film Flow Control: Injection, Uniform Thickness, and Drainage

Description - Any solid surface exposed to the blast will rapidly deteriorate; complete wall coverage is mandatory. Further, if the thickness of the film varies too much, then

the wall temperature will vary, limiting recondensation. Excessive variation of film thickness will lead to overly conservative design, driven by the hot spots. Many problems have been identified with control of the film thickness. One of the most difficult problems is protection of inverted (upper) surfaces. Any finite-thickness film is subject to Rayleigh-Taylor instability and will drip down into the cavity. Proposals to aid in upper end-cap protection include inertial jet injection and magnetic guiding. Drainage is another serious concern, as large pools at the bottom of the cavity would become hot and limit recondensation.

Reactor Concept - Laser and Heavy Ion

Potential Impact - (DW) Inability to adequately protect the solid surfaces makes this design concept impractical.

Design Specificity - (Generic to thin film wall protection.)

Overall Level of Concern - (Critical)

Operating Environment - (A, G, v) Most aspects of this issue are independent of the radiation and blast environments.

Degree of Relevance to MFE - (Low) Some similarity to free-surface films as innovative divertor protection.

Issue E.a.6 Film Flow Stability and Response to Impulsive Loading

Description - The ability to maintain a constant film supply through a porous wall under impulsive loading is highly uncertain. Resolution of this issue requires a good understanding of the time-dependent surface pressure and the interaction of the fluid and structure. Rapid heating from the blast, sometimes called isochoric heating, can cause liquid to eject into the cavity. In this event, beams and targets would not propagate into the chamber.

Reactor Concept - Laser and Heavy Ion

Potential Impact - (DW) If liquid is ejected into the cavity, then beams and targets would not propagate and the film concept would be impractical.

Design Specificity - (Thin film protection schemes.)

Overall Level of Concern - (High)

Operating Environment - (A, G, v) Requires simulating both the film conditions as well as the blast conditions which establish the time-dependent loads.

Degree of Relevance to MFE - (Low) Some similarity to free-surface films as innovative divertor protection.

Issue E.a.7 Pb/SiC Wettability

Description - Good wetting between Pb and SiC is necessary to provide reliable supply and coverage of Pb to the first wall. Preliminary experiments indicate that the two materials do not wet, even in a very pure atmosphere. Wetting is particularly important at inverted surfaces, where capillary action is needed to help support the film. Chemical additives to the SiC matrix (e.g. metals) may be necessary to encourage wetting.

Reactor Concept - Laser and Heavy Ion

Potential Impact - (RP, RL, IC) If good wetting can not be obtained, then the film supply system would become very complex and more subject to failures.

Design Specificity - (Specific to this design, using Pb and SiC in a thin-film configuration.)

Overall Level of Concern - (Medium) Wetting is important, but it is predicted that solutions to this problem can be obtained without a huge R&D investment.

Operating Environment - (C, I, s) This is primarily a materials issue, with little effect from the operating environment.

Degree of Relevance to MFE - (Low) Possible relationship to LiPb breeders in SiC blankets, although this combination is not one of the principal MFE design concepts.

Issue E.a.8 Pb Compatibility with Steel

Description - The maximum bulk outlet temperature of the Pb first wall coolant is limited by compatibility with steel in the pipes and heat exchanger. Dissolution of steel is controlled primarily by temperature. Previous studies have set limits of the order of 10 mm/yr erosion to prevent heat exchanger plugging. This translates to a coolant bulk outlet temperature limit of approximately 500–550°C. These estimates are based

on extrapolation from data obtained for sodium-steel interactions, and may not be valid for Pb-steel. Since the bulk coolant temperature is important in determining the thermal cycle efficiency, accurate measurements are important. Impurity control methods, such as cold trapping may allow an increase in the allowable temperature, and should be explored as well.

Reactor Concept - Laser and Heavy Ion

Potential Impact - (RP, RL, RS) - Lower temperatures result in lower thermal cycle efficiencies. If the corrosion rate is too high, heat exchanger plugging may result. Transport of steel constituents into the reactor cavity would result in additional radioactivity.

Design Specificity - (Specific to Pb-steel systems.)

Overall Level of Concern - (Medium)

Operating Environment - (T, C, v) The concern is outside the radiation environment. The major parameters are temperature, impurity content (especially oxygen), and coolant velocity.

Degree of Relevance to MFE - (Medium) Material compatibility is a generic issue. Pb corrosion is related to LiPb corrosion, which is an important issue for MFE.

E.b Blanket Issues

Key technical issues for blankets can be listed in the following categories (major sources of uncertainties for each issue category are also shown).

1. Tritium self-sufficiency
   - Uncertainties in achievable breeding ratio (inventory)
   - Uncertainties in required breeding ratio (production rate, burn up)
2. Tritium inventory and recovery
   - Tritium transport mechanisms
   - Solid breeder micro-structure
   - Chemical trapping
   - Surface processes
   - Irradiation effects
   - Temperature limits
3. Breeder/structure mechanical interactions
   - Swelling

- Interface heat transfer

4. Off-normal and accident conditions
   - LOFA, LOCA
   - Tritium behavior during transients
   - Module pressurization
5. Structural response and failure modes
   - Uncertainties
6. Corrosion and mass transfer
   - LiOT formation and vaporization
   - Breeder/clad corrosion under irradiation and temperature
   - Coolant impurities
7. Tritium permeation
   - Surface kinetics
8. Fabrication & Assembly
9. Heat generation and power production
   - Nuclear heating rates and energy multiplication

Each issue is described in more detail below.

E.b.1 Tritium Self-Sufficiency

Description - Tritium self-sufficiency is a necessary goal for fusion, which is satisfied when the achievable tritium breeding ratio equals or exceeds the required tritium breeding ratio. Blanket-related uncertainties in the achievable tritium breeding ratio include uncertainties in tritium production rates due to limitations in neutronics predictive capability and data base and to material and configuration choices. Uncertainties in the required tritium breeding ratio relate mostly to the blanket inventory.

Reactor Concept - L/H

Potential Impact - (DW) Tritium self-sufficiency is a critical issue that may close the design window since it is a required goal for a fusion reactor.

Design Specificity - Generic

Overall Level of Concern - Critical

Operating Environment -

Neutron: H, D, R

Parameters: F, ϕ, S, T, C, I, TG, A, G, Q, t, P_t, N, γ

Degree of Relevance to MFE - High

E.b.2 Tritium Inventory and Recovery

Description - Tritium inventory and recovery in the solid breeder blanket is important for two reasons. First, the feasibility of the blanket depends on whether or not it can breed enough tritium to satisfy the tritium self-sufficiency requirement. The required tritium breeding ratio increases with increasing breeder inventory. Secondly, this tritium inventory may be a large safety risk, depending on its magnitude and mobility. Uncertainties in the tritium transport mechanisms are large and are associated with both lack of fundamental property data and with the effect of integrated operation in a fusion environment. Achieving acceptable levels of tritium inventory and recovery would also impose temperature limits on the breeder and blanket and affect design configuration and operating flexibility.

Reactor Concept - L/H

Potential Impact - (DW, US, IC) The impact of tritium recovery and inventory on tritium self-sufficiency makes it a critical issue as it may be responsible for closing the design window. In addition, a large tritium inventory is a major safety concern because of hazard during accidents, as well as an economic penalty because of the larger initial tritium supply required before the device becomes self-sufficient.

Design Specificity - Solid breeder blankets

Overall Level of Concern - Critical

Operating Environment -

Neutron: H, R
Parameters: F, ϕ, S, T, C, I, A, G, Q

Degree of Relevance to MFE - High

E.b.3 Breeder/Structure Mechanical Interactions

Description - The mechanical interactions between the solid breeder material and the structural material can lead to either degradation of the performance or seriously limit the useful lifetime or safe operation of the blanket module. These interactions are driven by differences in thermal expansion, creep and swelling behaviors.

Reactor Concept - L/H

Potential Impact - (RP, RL) Material property changes such as melting points, and compatibility between structure and breeder under irradiation and temperature and in the presence of impurities may limit the lifetime or performance of the blanket.

Design Specificity - Solid Breeders/SiC

Overall Level of Concern - High

Operating Environment -

Neutron: H, R
Parameters: F, T, C, I, A, t, N, σ, P

Degree of Relevance to MFE - High

E.b.4 Off-Normal and Accident Conditions

Description - The reactor would have to be designed to withstand several types of accident transients with no (or minimum) loss of investment. These transients include loss of flow and loss of coolant accidents and tube sheet failure inside the blanket module. Adequate ability to predict system response to such transients, including tritium behavior and module pressurization effects, is needed.

Reactor Concept - L/H

Potential Impact - (IC, RS) Inaccurate predictions could lead to either over-design with associated costs, or under-design with potential for serious fault conditions.

Design Specificity - generic, SiC

Overall Level of Concern - High

Operating Environment -

Neutron: H
Parameters: T, s, G, Q, t, P_t, v, P, N, TG

Degree of Relevance to MFE - High

E.b.5 Structural Response and Failure Modes

Description - Knowledge of failure modes and rates in blanket components is necessary because of their critical impact on the economic potential and safety. Virtually no data exist on failure modes and rates of components in a fusion environment. Possible failure modes that need to be examined experimentally are crack growth under cycling and irradiation, and cracking at welds and discontinuities. However, the most important information from experiments is expected to be the identification of unforeseen failure modes.

Reactor Concept - L/H

Potential Impact - (RS, UL) Understanding of structural response and identification of failure modes are critical to the economic potential and safety of a fusion reactor.

Design Specificity - Generic, SiC

Overall Level of Concern - High

Operating Environment -

Neutron: H, D, R
Parameters: F, T, σ, C, I, A, G, Q, t, N, P

Degree of Relevance to MFE - Medium

E.b.6 Corrosion and Mass Transfer

Description - With helium as coolant, the key concern are the impurities and their effect on the structural material. Of concern also is the material interaction at the breeder/clad interface including the effect of burnup, and the formation of LiOT enhanced by moisture impurity and formation which could lead to LiOT vaporization and Li mass transfer, as well as enhanced corrosion.

Reactor Concept - L/H

Potential Impact - DW (particularly for Li_2O) LiOT formation and vaporization is of particular concern for LiOT. Mass transfer of LiOT to cooler regions could result in plugging purge flow paths and loss of breeder material.

Design Specificity - Solid breeder (Li_2O), SiC

Overall Level of Concern - High

Operating Environment -

Neutron: H, R
Parameters: F, T, C, I, t, P_t, N

Degree of Relevance to MFE - High

E.b.7 Tritium Permeation

Description - Tritium permeation from the breeding material into the coolant may be a problem at interfaces where large areas of relatively thin walls separate breeder and coolant. In the absence of cracks, tritium will diffuse through structural components at a rate determined by surface kinetics, tritium vapor pressure and permeability. Corrosion/chemistry at both interfaces of structural components may either inhibit or enhance tritium permeation. Alternately, cracking of engineered or natural barriers will strongly affect permeation.

Reactor Concept - L/H

Potential Impact - (US, UL) Tritium permeation into the coolant is a substantial safety penalty since it may be difficult to prevent further tritium transfer outside of the primary coolant. A major tritium permeation problem would require replacing the faulty blanket module(s).

Design Specificity - Generic

Overall Level of Concern - High

Operating Environment -

Neutron: D, R
Parameters: F, T, I, P_t, N

Degree of Relevance to MFE - High

E.b.8 Fabrication

Description - Manufacture and assembly of the SiC tube sheets and modules are uncertain and need to be demonstrated. In addition, the fabrication of the solid breeder is uncertain. The basic material must be produced and assembled into the desired form with the desired microstructure and packing fraction. Precautions with Li_2O are necessary because it is hygroscopic and LiOH is corrosive.

Reactor Concept - L/H

Potential Impact - (IC, UL) Blanket cost and reliability are dependent on ease of fabrication and assembly.

Design Specificity - Solid Breeder, SiC

Overall Level of Concern - High

Operating Environment -

Neutron:
Parameters: A, G

Degree of Relevance to MFE - Medium, depending on MFE blanket design similarity

E.b.9 Heat Generation and Power Production

Description - Uncertainties in the prediction of nuclear heating rates due to inaccuracies in neutronics data and/or transport code affect temperature levels and gradients, which govern most blanket phenomena. Uncertainties in predicting the energy multiplication factor for the blanket affect the power production. In addition, uncertainties associated with decay heat production would affect accommodation of afterheat under normal and accident conditions.

Reactor Concept - L/H

Potential Impact - (RP, RS) Poor prediction of heat generation during operation has implications on the design limit and the performance of the blanket.

Design Specificity - Generic, solid breeder

Overall Level of Concern - High

Operating Environment -

Neutron: R, H
Parameters: ϕ, S, G, Q, t, γ

Degree of Relevance to MFE - High

E.c Shielding

Issue E.c.1 Effective of Bulk Shield

Issue E.c.1.1 Biological Dose During Operation and After Shutdown for Maintenance

Description - During reactor operation, the occupational exposure limits outside the reactor site (outside reactor building) must be maintained. The bulk shield thickness/material outside the FW/Blanket system and the reactor building thickness/material must be designed to ensure meeting these exposure limits during reactor operation. After shutdown, the activation level attained in the bulk shield due to prolonged irradiation during reactor operation determines the waiting period before accessing reactor building. This also applies to the shielding materials of the laser beam lines and the beamlets (including the prepulsed beams) in HI reactors. Extra shield may be required at localized zones to ensure maintaining the exposure limits

(e.g. around the laser windows at the inlet of laser beams to reactor building and at the far ends of the HI beams). Primary uncertainties in actual dose levels arise from tolerances in bulk shield assemblies, distortion resulting from thermal and radiation effects, and neutron streaming through gaps and penetrations.

Reactor Concept - Laser and Heavy Ion.

Potential Impact - (RS, UL) If shielding is insufficient, this will require additional shield and/or components rearrangement. This could lead to delayed plant operation and/or reduced period of operation, imposing economical and availability penalties.

Design Specificity - (Generic)

Overall Level of Concern - (High)

Operating Environment - (R, D; ϕ ,F, S, G) Fusion neutrons are required to interact with bulk shield/reactor building as the source of radiation. Dose levels are governed by the material selection (for both during operation and after shutdown cases), neutron and gamma fluxes and spectra, and the actual geometry and arrangement of the bulk shield. Heat deposition and removal in bulk shield (due to neutrons/gammas interactions during operation and due to decay heat after shutdown) is an important design issue which has safety/reliability implications.

Relevance to MFE - (High)

Issue E.c.1.2 Radiation Streaming

Description - Neutrons stream through: (a) the relatively large opening of the laser and HI beams, and (b) the gaps/slits between shield assemblies (of the bulk shield, shielding of the beamlines, shielding of vacuum ducts, etc.). Neutrons/gammas reaching the ends of the beamlines will increase local exposure dose and radiation damage to components in the vicinity. Neutrons/gammas streaming through gaps/slits impeded in the bulk shield design also increase local flux levels which will require safety factors to be impeded in the design of shielding segments.

Reactor Concept - Laser and Heavy Ion

Potential Impact - (RS, UL) Accurate estimates of neutrons streaming through the relatively large openings of the laser and HI beamlines penetrating the bulk shield is

essential for protecting laser windows and sensitive components and for the designing of the extra local shield around these components.

Design Specificity - (Generic for both laser and HI)

Overall Level of Concern - (High)

Operating Environment - (R, D; ϕ, F, S, G) In general, level of neutrons/gammas at the end of openings/gaps/slits depends on the energy, spectrum, and the fluence of the primary neutrons streaming through these opening. The size and shape of the openings/gaps/slits (e.g. Diameter/Length of large openings, straight vs. irregular or stepped shape for gaps/slits) is a determining factor to the flux level at the ends of these penetrations.

Relevance to MFE - (High) Large laser and HI beamline openings are similar to the openings of the neutral beam injectors/ vacuum ducts in MFE.

Issue E.c.1.3 Analytical Techniques and Data Base

Description - Neutron and gamma transport codes and nuclear data base are used to predict the nuclear performance of the bulk shield and dose level behind it during operation and after shutdown. The adequacy of these codes/data in predicting this performance as well as neutrons/gammas streaming through penetrations impeded in the bulk shield is an important design issue not only pertaining to bulk shield design but to the design of all other nuclear components. Uncertainties in estimating the operating environment of sensitive components are best relieved by additional conservatism in bulk and penetrations shield thicknesses.

Reactor Concept - Laser and Heavy Ion

Potential Impact - (RS, UL) The additional conservatism in designing the bulk and penetrations shield (or safety factors) to cover the current uncertainties in nuclear data (transport and response data) and the approximations used in the transport calculations has an adverse impact on the overall cost of the reactor. Integral experiments are needed to test and validate the design safety margins and/or to improve the data base used in design.

Design Specificity - (Generic)

Overall Level of Concern - (High)

Operating Environment - (R, D; ϕ, F, S, G) Integral experiments dedicated to test and validate the neutron/gamma transport codes/data used in shielding design will require either a 14.1 MeV point source or a simulated line source. The latter is more suitable for streaming experiments.

Relevance to MFE - (High)

Issue E.c.2 Shield Compatibility with Cavity and Vacuum Boundary, Including Assembly/Disassembly

Description - Shields are generally heavy, weighting more than a 50 tons apiece. They must be fitted together with such accuracy that the slit width between them is small enough to maintain the level of radiation streaming through these slits/gaps below a certain specified level. The design of support mechanism for the blanket and shield must consider various factors such as competition for space, differences in the amount and direction of thermal expansions, clearance against earthquakes, etc. In the process of assembling/disassembling the shield, activation level of shield materials may require remote handling.

Reactor Concept - Laser and Heavy Ion

Potential Impact - (RS, UL) Mechanical interactions between the various segments of the shield and/or other components may lead to mechanical failures. Additionally, the type of maintenance (vertical vs. horizontal) is a determining factor to reactor reliability/availability. From a safety stand viewpoint, if the precision of the assembly/disassembly is not enough, neutrons/gamma streaming could occur leading to unacceptable radiation dose levels.

Design Specificity - (Generic)

Overall Level of Concern - (High) Because of the complexity and serious consequences of mechanical failures with regard to shield compatibility with cavity and vacuum boundary, the level of concern is high in this case. Furthermore, although radiation streaming through slits/gaps between the shield segments seems to be inevitable, reduction in the streamed neutrons/gammas could be achieved by considering stepped slits/gaps or by adding additional shielding when feasible.

Operating Environment - (R, D, ϕ, F, S, G)Although irradiation creep has some effect on mechanical failures, neutrons and transported gammas have the dominant role in generating bulk heating in the shield segments and thus causing thermal expansions. Neutrons are also the source of concern with regard to streaming and activation issues.

Relevance to MFE - (High)

Issue E.c.3 Activation of Reactor Building Components Outside the Cavity

Description - The combined thickness of the blanket and bulk shield is an important contributing factor in determining the fusion power and economics of a reactor. The bulk shield thickness should be chosen such that activation of components located in the reactor building and outside the cavity is kept minimal (e.g. activation of heat exchangers, vacuum pumps, etc., if the design calls for installing them in the reactor building). The situation in laser and HI reactors are more relaxed compared to MFE since no inboard shield is required to protect the superconducting magnets in these reactors. However, the protection of the final mirrors and the quadrupole magnets (see issues # D.3.4 and D.3.5) are key design issues for IFE.

Reactor Concept - Laser and Heavy Ion

Potential Impact - (RS, UL)

Design Specificity - (Generic)

Overall Level of Concern - (Low)

Operating Environment - (R, D ; ϕ, F, S, G) Neutrons/gammas are required to interact with components located outside the cavity. Level of activation of these components depends on their location, size, and materials.

Relevance to MFE - (High)

Issue E.c.4 Shielding of Final Mirrors

Description - Neutrons and gammas stream through the laser beam ducts from the center of the cavity all the way to the Grazing Incidence Metal Mirrors (GIMM), the turning mirrors, and the laser windows. Streamed neutrons can also end up in the

laser building and hence cause damage to the sensitive optical components. Because the beam duct from the GIMM to the cavity is conical in shape, most of the radiation damage to the GIMM (quantified in terms of dpa/FPY) is caused by the uncollided neutrons streaming directly from the cavity center to the GIMM. In addition to these neutrons and the collided ones in the shielding materials located in the vicinity of the GIMM , neutron-induced gammas deposit substantial part of their energies in the GIMM . This impact the life-time of the GIMM. To minimize neutrons' damage effect in the GIMM, a neutron trap zone is normally located behind the GIMM to absorb transmitted neutrons and lessen neutron reflection to the GIMM. Damage to the turning mirrors are primarily caused by collided neutrons in the liner/shield materials around the beam duct. Excessive dose absorbed in the laser windows leads to their damage.

Reactor Concept - Laser

Potential Impact - (UL,RP,RL,IC) GIMM transmission characteristics adversely affected by radiation damage caused by neutron streaming leading to short life-time. Thermal stresses cause deformation and reduced performance. Frequent replacement of the GIMM impacts system cost and the overall reactor availability. This applies as well to the turning mirrors and the laser windows whose life-time are generally longer than the GIMM's.

Design Specificity - (Mirrors)

Overall Level of Concern - (High)

Operating Environment - (R, D, H; ϕ, F, S, G) High-energy neutrons (~12 MeV) for GIMM, relatively moderated neutrons (several MeV) for the turning mirrors and laser windows are the main cause for reduced performance due to radiation damage. Geometry of the mirrors impacts life-time (e.g. flat vs. paraboloid or ellipsoid mirrors, grazing incident angle, mirror thickness, etc.)

Relevance to MFE - (None)

Issue E.c.5 Shielding of Quadrupole Magnets

Description - Focusing magnets in a HI beam driven reactor are damaged by neutrons streaming through the beam ducts unless adequate shielding is provided to protect these superconducting magnets. The damage is quantified in terms of the dpa/FPY to the Cu stabilizer, the peak radiation dose to the insulator, the fast neutron (> 0.1 MeV)

fluence and peak power density in the magnet. Radiation damage is more serious in the quadrupole magnets closer to the cavity where shielding is needed most.

Reactor Concept - Heavy Ion

Potential Impact - (UL,RP,RL,IC) Radiation damage to the epoxy (or to the more radiation-resistant polyimide) insulator is not reversible. Frequent repair has the most impact on the driver cost. Shielding should protect excessive radiation dose to the insulator such that the insulator could last the life-time of the reactor. Peak radiation damage to the Cu stabilizer (reversible) should be kept below a specific design limit to allow for few (if not at all) annealing processes during the plant life-time and, hence, increasing the plant availability. Total heat deposited in the magnet should also be kept below a specific integrated value to avoid magnet warm-up.

Design Specificity - (Magnets)

Overall Level of Concern - (High)

Operating Environment - (R,D,H ; ϕ, F, S, G) Neutrons streaming through the HI beam ports at the FW and colliding in the beamline shielding materials are the main cause of magnet damage. Neutrons and gamma heating in the insulator, when excessive, is a life-limiting factor.

Relevance to MFE - (Medium) Although there is a degree of relevance exists to MFE but the geometrical arrangement of the magnet relative to the primary neutron source in HI IFE reactor is different from MFE. In the latter, neutrons streaming through the beamlines are incident with a glancing angle to the magnet shield, relaxing the shielding requirements in this case.

Issue F. Material

Issue F.a Viability of SiC Structures

Description - The viability of using SiC structures in the first wall and blanket is key consideration of the laser and heavy ion designs. If these concepts are to be believable, efforts should be made to assess the factors involved in determination of acceptable lifetimes, and to determine the appropriate manufacturing methods and their economics. Anticipated lifetimes for FW/B components are not well known. Limited resources allocated to this area precluded a realistic assessment of the anticipated lifetimes. Without this knowledge, system reliability, maintenance and

economics would be seriously challenged. In order to perform this task, several investigations need be considered. It is too simplistic, and perhaps misleading, to use the accumulated fluence, or displacements per atom, to make projections of lifetimes. The determination of such lifetimes would need knowledge of the various effects of radiation. The most prominent of those are neutron induced swelling, embrittlement, fiber shrinkage, and/or detachment from the matrix, creep and fatigue crack propagation at high temperatures, and crack bridging mechanisms during irradiation.

On the other hand, the technology to process and manufacture SiC composites is at its infancy. An evaluation of manufacturing methods, potential, and costs is needed. Manufacturing methods are classified into fiber production techniques and matrix processing technologies. A variety of possibilities exist, with potential consequences on the economics and design.

Reactor Concept - Laser and Heavy Ion. The work is applicable to both Laser and Heavy Ion designs.

Potential Impact - (RP, RL, UL) Short lifetime of the SiC structure would result in an unacceptable reliability and/or availability. Additionally, reduced performance and reduced component lifetimes are expected.

Design Specificity - (FW, B) SiC structures are used in both the First Wall and Blanket components.

Overall Level of Concern - (High) Without reasonable and reliable lifetime of structural components, the entire design is compromised.

Operating Environment - (D, R; γ, T, σ) Neutron and gamma radiation, high temperatures, and moderate stress levels.

Degree of Relevance to MFE - (High) The development of low activation SiC composites is one of the important technology goals of magnetic confinement fusion.

Analysis -

(1) Radiation Effects: Assessment of the effects of radiation on SiC has not been thoroughly made. Experimental data and theoretical analyses will be available in the near future through the MFE materials program. Assessment will include mechanical properties, swelling, and high temperature creep.

(2) Fatigue Life: Fatigue analysis of the FW/B structure can be very involved. It requires accurate determination of the mechanical loading imposed by ablasion and repetitive reflections of pressure shock waves. A study of fatigue crack initiation and propagation in the structure is necessary. Reasonable assessments on this basis will require, at least, 2-D finite element analysis of the FW/B front and side walls. Considerations of the effects of radiation on fatigue crack growth will have to be on the basis of theory/extrapolation.

(3) Manufacturing of the FW/B: Existing manufacturing techniques involve CVD, and CVI processing technologies for the production of the composite's matrix. The fibers can be produced by the Yajima method (Nicalon), the Rice hulls method (US), the Los Alamos method (Whiskers). Combinations of fiber and matrix processing produces the composite. Assessment of the cost, reliability, and the capability for large component fabrication is desirable.

Issue F.b Thermomechanical and Materials Design of Laser Optics

Description - The mirror designs which we introduced in this study have been successful, at least conceptually. Nevertheless, greater improvements can be achieved, and more certainty and recognition may be realized, once we perform the proper thermostructural analysis. This will include materials selection data base, possible various configurations which would minimize surface deformations, laser energy density limits, and thermal fatigue limits. More work is needed on the dielectric tuning mirror, since it is quite sensitive to radiation effects.

Reactor Concept - Laser. The work is applicable only to the KrF Laser design.

Potential Impact - (DW, RP) The lifetime and design of the optics system in the neutron environment systems has long been identified as key to the performance of the system. The window may actually be closed if the lifetimes of the turning and grazing incidental mirrors are too short for economic feasibility. Additionally, the reliability of the entire system hinges on the reliability of the optics system.

Design Specificity - (DL) This issue is specific to the Driver Laser (DL).

Overall Level of Concern - (High) Without reasonable and reliable performance of the optics system, the laser concept is at risk.

Operating Environment - (D, R, H; γ, T, σ) Neutron and gamma radiation, high temperatures, and moderate stress levels.

Degree of Relevance to MFE - (Low) Optical components are used in MFE designs for RF heating and for diagnostics. However, the environment is not as severe, and the problem is not perceived to be a concern to the MFE community.

Analysis - Research is expected to be along two major fronts; Materials selection and thermomechanical design. This research will be concerned with the detailed design of the two final mirrors; the turning and the grazing incidence. The turning mirror will likely be selected of a dielectric material, which will be very sensitive to the effects of both neutron and gamma radiation. The neutron fluence limit is generally on the order of 10^{16} n/cm^2. The effort will involve shielding design to reduce neutron and gamma fluence, material selection for better solutions to the problem and analysis for accurate determination of the radiation limits. Further innovative thermomechanical designs of the GIMM may reduce its size and bring it closer to the cavity.

Issue H Maintenance and Configuration

Issue H.1 Computer Reliability

Description - Current guidelines on the relative safety of plant operation equate manual operation, mechanical interlocks, double electrical interlocks and triple computer interlocks. These guidelines date from the early days of the fission industry and need to be updated to reflect technological advances since that time. In other industries single computer systems are proving more "safe" than both mechanical and electrical interlocks when used in complex manufacturing plants. New guidelines are needed to put requirements for different levels of safety criticality and task complexity with approval procedures that equalize approval requirements for computers with other technology. IAEA study on this issue started in mid-1991 with seminar in Vienna in July.

Reactor concept - This issue applies equally to Laser and Heavy Ion options.

Potential Impact - (UL) This issue will result in unacceptable reliability and availability through the use of older less suitable technological solutions in areas where regulation hinders the adoption of computer based solutions.

Design Specificity - (Generic) This issue is generic and has impact to various degrees in all current power production options with increasing impact with plant size.

Overall Level of Concern - (Low) The level of concern ascribed to this issue is low based on the current level of action from the International Atomic Energy Authority among others.

Operating Environment - (t) Operating environment for this technology is assumed to be STP with the only key parameter time although current work on radiation hardness of electronics could bring in far more onerous conditions on a limited proportion of computer equipment.

Degree of Relevance to MFE - Due to its generic nature this issue is equally applicable to MFE.

Analysis - The current treatment of computer systems in the nuclear industry is thought to be overly restrictive given the current proliferation in many industries of computers with increasing power and reliability. While the need for verification of computers is not questioned, the current procedures are restrictive. In software QA, the seven-level process model for software development, starting with specification requirements and ending with traceable software code, is thought by many to be unusable and costly without guaranteeing software reliability. The International Atomic Energy Agency recognizes computer systems can play a significant role in improving nuclear plant safety and economics but this needs to be supplemented with an update of the current implementation standards.

Issue H.2 Total Remote Maintenance

Description - The design of plant to only have services for robotics and not humans is not something done in 1992 unless radiation levels or regulation force the issue. Given the overall trends in automation, it is probable that this tenth-of-a-kind plant should be designed for exclusive use of automation in key areas.

Reactor Concept - (Laser and Heavy Ion) This issue could bring in significant cost savings and design advantages if total remote maintenance (TRM) is used.

Potential Impact - (DW, UL) This issue could bring in significant cost savings and design advantages if TRM is used.

Design Specificity - (Generic) This issue is generic and applicable to all design options with toxic and/or radioactive elements or compounds and high radiation environments.

Overall Level of Concern - (Low) The level of concern on this issue is low, based on the assumption that TRM will be accepted in future decades.

Operating Environment - (F, S, T, C, H, B)

Degree of Relevance to MFE - (High) Due to its generic nature this issue is equally applicable to MFE.

Analysis - Designing the reactor building to accommodate robots and not humans is a contentious point though by 2030 the 'risk' in planning to keep humans out of all hazardous areas should be accepted. Even with no HVAC or human walkways, human access for emergency purposes can be accomplished with suited workers on mobile platforms.

Issue H.3 Material Joining

Description - The joining of and to silicon carbide is a largely untried process particularly at elevated temperatures.

Reactor Concept - This issue applies equally to Laser and Heavy Ion options.

Potential Impact - (DW, IC) This issue has the potential to close the design window though with R&D it is probable it can be solved.

Design Specificity - (Generic) This issue is general to all design solutions using ceramic composites which, by 2030 will probably mean a majority.

Overall Level of Concern - (High) High due to the lack of knowledge in this area.

Operating Environment - (F, S, T, C, H, B)

Degree of Relevance to MFE - (High) Due to its generic nature this issue is equally applicable to MFE.

Analysis - Joining of silicon carbide structural parts is not well understood. This will also be affected by the presence of lead coolant. Composite joints are often handled using metal implants though in this case further problems due to differential expansion would occur. Joining of composites to metals is an area needing research, especially with differential expansion issues at flanges, etc., particularly the joint between the silicon cooling pipes to stainless steel in the helium cooling lines.

Issue H.4 Lead Flushing

Description - When the reactor vessel is allowed to cool the lead coolant will solidify in the first wall requiring some sort of draining or flushing process to remove lead and allow the first wall tiles to be taken out individually. Any lead that remains will cause severe sealing problems on reassembly in the key primary cooling tubes.

Reactor concept - This issue applies equally to Laser and Heavy Ion options.

Potential Impact - (IC) This problem could have a significant cost impact as well as potentially decreasing the availability of the reactor.

Design Specificity - (Generic) This issue is specific to designs using a liquid metal coolant.

Overall Level of Concern - (Medium) Concern on this issue is high primarily due to the lack of information on the use of lead coolants particularly in silicon carbide structures.

Operating Environment - (F, T, H)

Degree of Relevance to MFE - (Low)

Analysis - Due to the high melting point (325°C) of lead, the presence of lead in pipes etc., will be a problem during maintenance. Flushing the lead out also brings more problems from the flushing medium.

Issue H.5 Seal Life

Description - The life of seals on the vacuum duct between the vacuum pumps and the reactor vessel is anticipated to be a problem, particularly as each vacuum pump needs an isolation valve at its junction with the duct. The issue is also applicable to a lesser degree to helium cooling pipes.

Reactor Concept - This issue applies mainly to laser options though as the issue applies to helium cooling pipes as well it does impact heavy ion.

Potential Impact - (DW, IC) This issue could severely close the design window as well as reducing availability and increase costs.

Design Specificity - (Generic) This issue is not specific to designs in general though liquid first walls and use of cryopumps increase the problem.

Overall Level of Concern - (High) Level of concern is high as the temperature range and types of materials which seals encounter are at the limit of current technology.

Operating Environment - (F, S, T, C, H, B) Key environmental parameters in this issue are temperature range and the materials (like helium) which come into contact with the seals.

Degree of Relevance to MFE - (High) Due to its generic nature this issue is equally applicable to MFE.

Analysis - Seals in vacuum pumps on the vessel only have a two-hour life in ITER MFE conditions, this will also be a problem on IFE on all flanges and valves near the reactor vessel. In the heavy ion option the problem is less severe as roots vacuum pumps are far less rigorous in environment than cryo or turbomolecular vacuum pumps. The life of seals in helium pipe is an accepted problem which none the less needs a solution if problems with this reactor are to be minimized.

Issue H.6 Embrittlement Temperature

Description - Material embrittlement problems are decreased if the temperature of much of the reactor pipework is kept above 150°C at all times, including during maintenance. This will be a maintenance challenge to operate at this elevated temperature.

Reactor Concept - This issue applies equally to laser and heavy ion options.

Potential Impact - (DW, IC) This issue will both close the design window for the reactor maintenance equipment and cause an increase in cost.

Design Specificity - (Generic) This issue is generic as it applies to a feature that will be found in most designs.

Overall Level of Concern - (Medium) This issue is of medium concern mainly due to the potential cost impact.

Operating Environment - T (Tritium)

Degree of Relevance to MFE - Due to its generic nature this issue is equally applicable to MFE.

Issue J Safety and Environmental

Issue J.1 Overall Plant Tritium Inventory

Description - The overall plant tritium inventory will directly impact the potential for large radioactivity releases, with their associated off-site exposures. Also, large amounts of tritium within the plant will require more complex engineered barriers to minimize occupational exposures. In addition to the amount, the form (i.e., whether HT or HTO) and location within the plant of the tritium will directly impact the design.

Reactor Concept - Laser and Heavy Ion

Potential Impact - (IC, RS)

This issue is an Attractiveness Issue, since there are engineered feature which can be implemented to mitigate the impacts of tritium, once its amount form, and location has been identified.

Design Specificity - T (Tritium)

Overall Level of Concern - Medium. Since there are engineered features to mitigate the impacts associated with this issue, an overall level of concern of medium has been specified.

Operating Environment - H (Tritium)

Degree of Relevance to MFE - Medium. The methods developed to mitigate the impacts of tritium for this plant are directly applicable to MFE, however, the amount, form and location will differ.

Issue J.2 Permeation of Tritium

Description - Tritium will be carried by the liquid lead first wall coolant and will readily permeate through the walls of the heat exchanger. Unless engineered design features are provided, the permeated tritium will be released to the environment, resulting in unacceptable off-site exposures.

Reactor Concept - Laser and Heavy Ion

Potential Impact - (RP) This issue is an Attractiveness Issue, since there are engineered feature which can be implemented to mitigate the permeation of tritium, (e.g., secondary loop, permeation barrier, duplex heat exchanger, etc.).

Design Specificity - T (Tritium)

Overall Level of Concern - (Medium) Since there are engineered features to mitigate the impacts associated with this issue, an overall level of concern of medium has been specified.

Operating Environment - H (Tritium)

Degree of Relevance to MFE - Medium. The methods developed to mitigate the impacts of tritium for this plant are directly applicable to MFE, however, the amount form and location will differ.

Issue J.3 Normal Operation Tritium Release

Description - This issue is closely linked to the previous issue, however, this issue extends the scope to controlling tritium releases from all portions of the plant.

Reactor Concept - L/HI

Potential Impact - IC. This issue is an Attractiveness Issue, since there are engineered feature which can be implemented to mitigate the release of tritium, (e.g., desiccant systems).

Design Specificity - T (Tritium)

Overall Level of Concern - (Medium) Since there are engineered features to mitigate the impacts associated with this issue, an overall level of concern of medium has been specified.

Operating Environment - H (Tritium)

Degree of Relevance to MFE - Medium. The methods developed to mitigate the release of tritium for this plant are directly applicable to MFE.

Issue J.4 Neutronic Cross Sections/Data Library for Activation Analysis

Description - As emphasis on safety and environmental impact of fusion reactor has greatly increased, an accurate predictive capability of radioactivity and its related parameters such as decay heat has become necessary. The basic elements of such predictive capability are a computer code based on an accurate mathematical model and a library of basic nuclear data including decay data and transmutation cross sections. Recent studies[1] point out that inadequate reaction cross section and decay data exist in the codes and data libraries widely used in fusion community. Example calculations show that the inadequacy in the RACC libraries underestimates the photon yield by a factor of as large as 1000 in the ITER first wall tungsten zone during operation and at times after shutdown. The study concludes that the accuracies of neutronic cross sections and data library are essential for activation analysis.

Reactor Concept - Laser and Heavy Ion. The work is applicable to both Laser and Heavy Ion designs.

Potential Impact - (US) Inadequate prediction of radioactivity and decay heat for a fusion reactor design may result in unacceptable safety risk.

Design Specificity - (Generic) All components exposed to radiation environment are affected.

Overall Level of Concern - High

Operating Environment - (R; ϕ, F, S, Q, γ)

Degree of Relevance to MFE - High

Reference

1. I. Jun, "Comparison Study Between Computed and Measured Radioactivity Decay Rates from Neutron Irradiation of Zirconium and Tungsten in a Simulated Fusion Environment," UCLA-FNT-55, November 1991

Issue J.5 Removing Decay Heat From Lead Coolant Under Accident Conditions

Description - Following the accident conditions, such as a loss of coolant due to a lead cooling tube rupture, the radioactive lead coolant spills and might pose a threat to the safety and environment. One of the design criteria requires that under this condition, the radioactive lead will be collected into a "containment" through gravity driven lead drain paths. If such a collection is fully successful, the lead can be cooled either actively or passively. However, some amount of lead might stay inside the reactor and knowing the location of lead is needed to mitigate the safety concern. Analysis indicates that if a failure of removing lead coolant decay heat occurs, the lead coolant (for the case of after two full power year operation) can reach about 1000°C at 8 hours following the accident. This temperature might damage the local structure and results in the migration of lead radionuclide into other plant components. Design reactor chamber with residual heat removal system (such as containment fan cooling) and/or with the development of lead detecting devices increase the plant cost.

Reactor Concept - Laser and Heavy Ion. The work is applicable to both laser and heavy ion designs.

Potential Impact - (US, IC, RS) Inadequate cooling in lead decay heat may result in unacceptable safety risk. Design inclusion of residual heat removal system increases the plant capital cost.

Design Specificity - FW

Overall Level of Concern - Medium.

Operating Environment - (R; ϕ, s, Q, γ)) The levels of decay heat following the reactor shutdown due to short lived radionuclides depend on the amount of neutron flux prior to the accident occurs, which is sensitive to the reactor power. The magnitude of long term decay heat is determined by the total neutron fluence regardless of the temporal variation of flux.

Degree of relevance to MFE - Medium. This issue is only preferentially relevant to MFE if lead is considered as the multiplier in the blanket design. Developing active means for lead decay heat removal under a cooling tube rupture (LOCA) is important for MFE blanket design.

Issue J.6 Hydrogen Burn Due to Rupture of Diffusion Vessel

Description - The diffusion vessel in the Target Factory could rupture resulting in either an explosion or burning of the tritium and deuterium contained within the vessel. Such an explosion could result in the environmental release of, and associated off-site exposures to, HTO unless proper engineered barriers are provided.

Reactor Concept - Laser and Heavy Ion

Potential Impact - (RP, IC) This issue is an Attractiveness Issue, since there are engineered feature which can be implemented to mitigate the impacts of a hydrogen burn, (e.g., dividing the inventory into smaller vessels, increasing the robustness of the building walls, etc.).

Design Specificity - TF (Target Factory)

Overall Level of Concern - (Medium) Since there are engineered features to mitigate the impacts associated with this issue, an overall level of concern of medium has been specified.

Operating Environment - (H, P_t)

Degree of Relevance to MFE - None

Issue J.7 Detection of Local Dry Spots Prior to Failure

Description - The dry spots on the first wall may be created due to the following mechanisms: (1) poor wetting of lead on the SiC material; (2) hydrodynamic instability of film subjected to pressure impulses; and (3) integrity of fibrous SiC material which is immersed in lead metal and subjected to a severe radiation environment. Once a dry spot is formed on the surface, the heat deposited on the SiC may result in a wall sublimation if at which the heat can not be adequately conducted away. Analysis shows that the sublimation rate of SiC is about 0.67 Kg/m^2 per shot, which corresponds to a layer of thickness of 1.1 mm per shot. If the film can not be reestablished and the dry spot remains, the time to failure (or a hole formation on the SiC wall) for a wall thickness of 0.5 cm is about 17 minutes. A failure of first wall reduces the plant availability, in addition it raises a safety concern if a hole is created and lead floods the chamber. This result indicates that the ability of local dry spot detection and remedy of removing dry spot is needed to reduce this issue.

Reactor Concept - Laser and Heavy Ion. The issue is applicable to both laser and heavy ion designs.

Potential Impact - US, IC

Design Specificity - Cavity FW

Overall Level of Concern - High. The abilities to detect and remedy the first wall dry spot are essential for the first wall structural integrity and reactor safety.

Operating Environment - (F, ϕ, S, T, Q, σ)

Degree of relevance to MFE - (High) Analytical method (or numerical modeling) for the SiC sublimation is relevant to the modeling used in the plasma disruption phenomenology studies, when the FW or high heat flux components undergo melting and subsequent vaporization. Technology for detection of dry spot is needed for the liquid film divertor concepts.

Analysis - The rate of SiC sublimation due to radiation re-emitted to the surface by the cavity gas depends on the gas conditions (pressure, temperature, charge state) as a function of time. The vapor entering the cavity from the X-ray deposition following the explosion is expected to be at a temperature of several eV. With gas at a temperature of several eV, the gas becomes ionized and excited. The gas temperature is estimated by knowing the equation of state properties, which are calculated by assuming the interparticle potentials are small.[1] The internal energy for an ion is computed relative to the ground state energy of the neutral atom and is given as:

$$e(Z) = \frac{3}{2}(1 + \langle Z \rangle) KT + Q(Z)$$

where Q is the energy required to remove the Z electrons from the neutral atom and is written as:

$$Q(Z) = S\, I_i \; ; \qquad \text{for} \quad i=1,\text{---}, Z$$

I_i= ionization potential for the ith charge state.

The degree of gas ionization and excitation (ignored in the present analysis) depends on the gas temperature and number of density and is obtained from LIBRA.[2] The cooling rate of the ionized gas is calculated based on the analytical method developed by Zel'dovich et al.[1] This is given as:

$$q''' = \frac{4sT^4}{l_1}$$

where s is the Stefan-Boltzmann constant and l_1 is the radiation mean free path and is given as:

$$l_1 = \frac{1.1 \times 10^{23} T^{3.5}}{n^2 <Z> (<Z> + 1)^2 \frac{I}{KT}}$$

where n is the number of density and T is gas temperature.

The aforementioned model is only valid for optically thin gas. If the photon mean free path approaches the characteristic length of the cavity, the gas is assumed to act as a black body. Under the circumstance that the radiative energy flux into the SiC exceeds the rate at which the conduction carry away, some amount of SiC is sublimated. The heat of sublimation is estimated by averaging the potential energy of both Si and C in the SiC lattice based on Pearson et al.[3] This is found to be equal to 1.91x107 J/kg. The amount of SiC sublimated is about 0.67 Kg per shot per m^2. This corresponds to a layer thickness of 1.1 mm.

Present calculation assumes thermal-hydrodynamic equilibrium, further analysis shall include the effect of nonthermal-hydrodynamic equilibrium, gas excitation, self-shielding, etc. Better modeling of radiative heat flux shall be incorporated to the cases where the optically thin gas theory breaks down.

References

1. Y. B. Zel'dovich et al., "Physics of Shock Waves and High Temperature Hydrodynamic Phenomena", Volume I, Academic Press, New York, 1966

2. "LIBRA, A Light Ion Beam Fusion Conceptual Reactor Design," UWFDM-800, July, 1989

3. E. Pearson et al., "Computer Modeling of Si And SiC Surfaces and Surface Processes Relevant to Crystal Growth From the Vapor", J. of Crystal Growth 70 (1984) 33-40.

Issue J.8 Detailed Accident Analysis

Description - A number of accident scenarios/initiating events have been identified for Prometheus (see Table 5.4-2). However, due to limitations on the scope of this study it is not feasible to perform a detailed analysis of each of these accidents to determine what detailed design features are necessary to prevent/mitigate each of the identified accidents. Nonetheless, the viability of design which has been proposed is not expected to be negated by the detailed analysis of these, or other, accidents.

Reactor Concept - Laser and Heavy Ion

Potential Impact - (IC, RS)

Design Specificity - (All) Accident initiating events have been postulated that involve many (all) of the plant's systems.

Overall Level of Concern - (High) The potential exists for some of the yet unanalyzed accidents to require extensive and complex engineered features to mitigate their effects, however, it is not believed that any of the identified accident scenarios will negate the viability of the basic plant design.

Operating Environment - (All) Accident initiating events have been postulated that involve many (all) of the plant's parameters.

Degree of Relevance to MFE - (Medium) A number of the identified accident scenarios have direct applicability to MFE, (e.g., accidents in the blanket or the tritium systems).

Table 5.4-2 Potential IFE Reactor Accidents by Subsystem

Accident	Concern
A. Laser System	Reliability
1. Partial Input Beam Blockage	
2. Single Raman Accumulator Failure	
3. Single SBS Pulse Compressor Failure	
4. Loss of Inerting Gas	
a. Inadvertent Personnel Entry	Personnel Health
b. Loss of Containment	
5. Laser Misalignment	
a. Single Beam Misses Target	
b. Multiple Beams Miss Target	
6. Fluorine Release	Toxic Chemical Release
B. Reactor System	Reliability
1. Loss of Vacuum	
a. Vacuum Pump Failure	
b. Laser Building "Window" Failure	
c. Break in Instrument Line	
2. First Wall Unlocking	
3. Target Manufacturing Errors	
a. Contains Excess Tritium	
b. Contains Shortage of Tritium	
4. Loss of Wet Wall	
C. Blanket Coolant System	Reliability
1. Heat Exchanger Tube Rupture	
2. Pump Failure	
3. Increase in Coolant Flow Rate	
D. Driver Coolant System	
1. Heat Exchanger Tube Rupture	
2. Pump Failure	
3. Increase in Coolant Flow Rate	
E. First Wall Protection System	Toxic Material (Pb) Release
1. Plugged SiC Tube	
2. Pump Failure	
3. Increase in Coolant Flow Rate	
F. Secondary Coolant System	Reliability
1. Steam Line Break (Break Size Equal to Area of Safety Valve Throat)	
2. Decrease in Heat Removal (e.g. Pump Failure)	
3. Increase in Heat Removal (e.g. Decrease in Feedwater Temperature	
G. Target Delivery System	Reliability
1. Failure to Deliver Target	
2. Target Misalignment	Toxic Material (Pb) Release
a. Target Arrives Too Soon/Late	
b. Target Off-Center	
H. Target Factory	Tritium Release
1. Loss of Cryogenics	
2. Storage Tank Failure	
I. Containment Cooling (HVAC) System	Tritium Release
1. Loss of Cooling	
2. Loss of Containment Integrity	
J. Radwaste System	Tritium Release
1. Gas Collection Tank Failure	Methane Release
2. Liquid Waste Tank Failure	
K. Turbine-Generator System	Reliability
1. Loss of Load	
2. Loss of Condenser Vacuum	
L. Maintenance Systems	Personnel Exposures
1. Blanket Section Change-Out Accidents	
a. Stuck	
b. Dropped	
c. Broken	

Issue J.9 Removal of Contaminants from the Liquid Lead

Description - The Prometheus design includes the use of liquid lead for first wall protection. This lead, and any impurities within it, will become activated and contaminated with target debris, and will have to be processed to remove these contaminants. Since this is a new and innovative use of lead, these cleanup processes have not been developed.

Reactor Concept - Laser and Heavy Ion

Potential Impact - (RP, RS)

Design Specificity - WP (Wall Protection)

Overall Level of Concern - (Medium) The development of processes to remove contamination from lead is expected to be evolutionary, rather than innovative.

Operating Environment - I (Impurities)

Degree of Relevance to MFE - None

Issue J.10 Impact of Large Quantities of Lead on Waste Disposal

Description - The Prometheus design includes the use of liquid lead for first wall protection. This lead will become activated, and will have to periodically replaced, generating large quantities of radioactive lead for disposal. Because lead is a hazardous material, this waste must be disposed of as mixed waste (i.e.; both radioactive and hazardous) falling under NRC's 10CFR Part 61 and EPA's RCRA regulations. Finally, since the amount of radioactive lead which is currently generated is so small, it is not specifically identified in NRC regulations. However, if large quantities are to be generated, the NRC may modify their regulation to specifically address lead.

Reactor Concept - Laser and Heavy Ion

Potential Impact - (IC, RS)

Design Specificity - WP (Wall Protection)

Overall Level of Concern - Low. The NRC and EPA are currently developing procedures for addressing the disposal of mixed waste. It can be assumed that by the time Prometheus is operational (i.e., 2030), these procedures and regulations will be in place. Regardless, there will be a high unit cost associated with the disposal of all radioactive, hazardous and mixed wastes from Prometheus or any other source.

Operating Environment - I

Degree of Relevance to MFE - None

Analysis - An analysis of the disposal of fusion reactor materials, including radioactive lead (Pb-205) was presented in "Recycling and Shallow Land Burial as Goals for Fusion Materials Development," Carlo Ponti, Fusion Technology, January 1988. This analysis presents a proposed concentration limit of $1x10^6$ (Bq/cm^3) for Pb-205.

K. Subsystem Interactions

Issue K.1 Laser System/Cavity Interface and Final Mirror Protection

Description - The Interface between the laser system and the reactor cavity represents a key development issue for the laser driver. The beam port walls and final optics must be protected from heating, blast and radiation damage effects. Furthermore, the protection mechanism(s) must not interfere with the laser beam propagation. The problem is complicated by the fact that the optics require a clean-room environment and special radiation-sensitive coatings to control their energy absorption while maintaining a direct line-of-sight to the target.

We investigated a multi-layer defense for the laser system/cavity interface that is illustrated schematically in Figure 5.4-2. The protection mechanisms include:

(1) The use of a flowing, liquid lead film to protect the port wall structure from surface vaporization. The port wall design employs a porous SiC first wall structure that slowly allows the liquid lead to seep through providing film replenishment around ports between shots.
(2) The residual lead vapor from the cavity walls which helps attenuate debris and x-rays before they even reach the wall boundary.
(3) A magnetic field in each beamline to deflect ions and electrostatically charged particles.

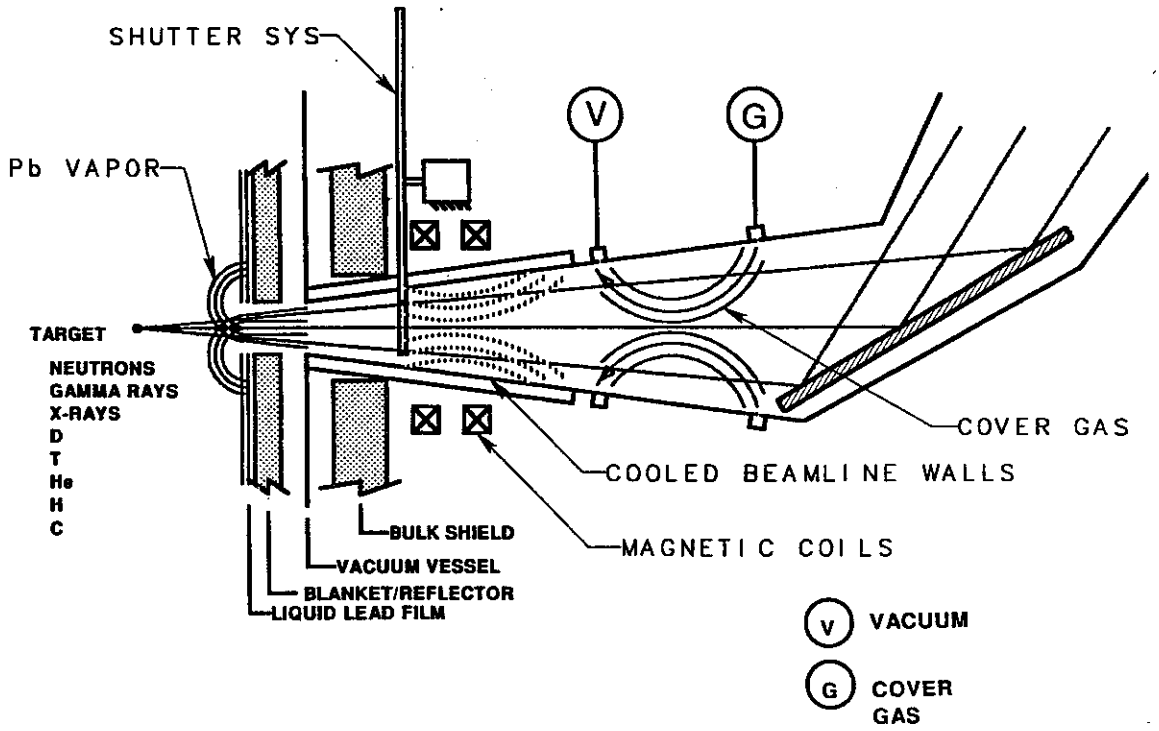

Figure 5.4-2. Protection Options for Final Optics Protection

(4) A flowing neon cover gas in each beamline, injected at one location and vacuum pumped at another to stop the remaining x-rays and sweep out vaporized gas. Alternatively, the beamline walls downstream of the GIMM can be heated to vaporize a portion of the protective liquid lead film providing a lead vapor protection gas. Any lead vapor recondensing on the GIMM surface will be vaporized by the laser prepulse beams.

(5) Cooling the beamline walls below the mirror surface temperature to assure that condensable gases stick to the walls instead of the optics.

(6) A low speed shutter system to intercept lead droplets that are blown off the walls and may make their way down the lower beamlines.

(7) Placement of the final optic element at a significant distance (25 m) form the target blast center to minimize shock waves and allow for $1/r^2$ attenuation of the heat flux and radiation.

(8) Use of a Grazing Incidence Metal Mirror (GIMM) as the final optic in each beamline to remove the dielectric-coated focusing mirrors from line-of-sight radiation. We feel that all of the above mechanisms are required to assure viable system performance. Lifetime is still an issue for the GIMM but swelling analysis indicates that it can be life-of-plant using the design approach we have developed. This topic is discussed as part of the GIMM critical issues.

Our baseline design employs all the protection methods above except the use of the neon cover gas and cooled beamline walls. The neon cover gas resulted in extremely difficult vacuum pumping requirements. Therefore, we chose to heat the beamline walls providing a Pb vapor cover gas and depending on the laser beams to remove recondensed vapor on the GIMM surfaces.

Reactor Concept - Prometheus-L

Potential Impact - (UL) The final optics are large area, expensive items subjected to a very harsh environment. If they are not properly protected, their lifetime will not be sufficient for economic power production.

Design Specificity - (DL) This issue is specific to the laser driver, but generic to the design of any laser-driven inertial fusion energy power plant.

Overall Level of Concern - (Critical) The design of the laser system/cavity interface is critical to the successful development of laser-driven inertial fusion energy power plants. The final optics are expensive and must repeatedly and reliably deliver their portion (~100 kJ) of the total energy to the target with microradian pointing accuracy for successful operation. These optics must furthermore have a multi-year lifetime for the plant to be economically competitive.

Operating Environment - (OF, F, S, C, T, n, γ, V, S, q)

Relevance to MFE - Low. This development issue is not directly relevant to MFE but there may be some aspects of the problem which have MFE relevance. For instance, some MFE plasma diagnostics may needs to operate in environments comparable to those expected for the final mirrors.

Analysis - Extensive literature reviews and analyses were conducted to substantiate the proposed laser system/cavity interface design. This activity is summarized in Table 5.4-3. This table indicates the sources of mirror degradation and the primary and secondary protection mechanisms for each source of degradation.

Table 5.4-3 Final Mirror Protection Summary

Source/Debris or Radiation	Debris or Radiation State	Range of Speed (m/s)	Protection Method*
Target			
X-rays	Radiation	$3x10^8$	SD; PBv; CG
Gamma Rays	Radiation	$3x10^8$	SD; PBv; CG
Neutrons	Particle	$3x10^8$	SD
Hydrogen	Ionized; Vaporized	(TBD)	PBv; M; CG; CBW; VP; S?
Deuterium	Ionized; Vaporized	(TBD)	PBv; M; CG; CBW; VP; S?
Tritium	Ionized; Vaporized	(TBD)	PBv; M; CG; CBW; VP; S?
Helium	Ionized; Vaporized	(TBD)	PBv; M; CG; CBW; VP; S?
Carbon	Ionized	(TBD)	PBv; M; CG; CBW
First Wall Film			
Lead	Ionized; Vaporized Liquid Droplets	(TBD) 9.8+	M; CG; CBW; S?

* Protection Methods

SD	Mirror Surface Design	CBW	Cooled Beamline Walls
PBv	Lead Vapor	VP	Vacuum Pumping
M	Magnetic Field Lines	S	Shutter System
CG	Cover Gas		

Issue K.2 SiC/Metal Piping Transition Interface

Description - The proposed Prometheus first wall and blanket are fabricated using low activation SiC/SiC composite materials to minimize the generation of high-level radioactive waste in these regions thus achieving an inherently safe design. However, the main heat transfer piping and steam generators can employ conventional high-temperature piping/structural materials since they are located outside the bulk shield where neutron activation is minimal. Furthermore, there is significant cost incentive to transition to conventional materials as soon as possible outside the bulk shield to achieve an economically attractive design. The transition interface between low activation SiC structure and conventional metal piping is therefore a key development issue for our Prometheus cavity design.

The transition from SiC to conventional piping involves large diameter piping that must be leak tight to 1.5 MPa (15 atm) helium and 23 MPa (20 atm) lead coolants and resistant to corrosion by impurities in the coolant streams. These joints must furthermore be capable of being broken and rejoined using remote handling equipment. Pipe diameters ranging from 1.0 m for the lead lines to 2.8 m for the helium lines are presently being considered. Therefore, both the material change and the pipe sizes make this a key development issue.

Reactor Concept - Prometheus-L and -H

Potential Impact - (IC) The primary heat transport/steam generator system(s) in a large nuclear power plant is complex and expensive. The bulk of this system is located in a low radiation environment and can therefore be fabricated from conventional materials to keep the cost for these items under control while still maintaining a low radioactive material inventory.

Design Specificity - (CS/CBOP) This issue is generic to any advanced nuclear reactor design employing ceramic reactor structures to achieve high levels of inherent safety but using conventional steam-cycle balance-of-plant systems to control costs. In the Prometheus design the transition interface involves the use of helium and lead coolants for primary heat transport.

Overall Level of Concern - Critical. The design of the piping transition interface is critical to the successful development of advanced, low-activation, ceramic structure nuclear power plants.

Operating Environment - (C, T, H, A, P, Q, I, v)

Relevance to MFE - High. This development issue is directly relevant to MFE designs that employ advanced ceramic structures.

Issue K.3 Heavy-Ion System/Cavity Interface and Beam Propagation, Focusing, and Optics Protection

Description - The interface between the heavy-ion system and the reactor cavity/target represents a key research and development area for the heavy ion-driver, heavy ion systems studies have typically proposed some form of ballistic focusing with varying degrees of and mechanisms for space-charge neutralization. Ballistic focusing requires large conical envelopes on two-sides of the target where multiple (typically 8 or more per side), large area (typically 1-m diameter) openings must be provided through the shield, breeding blanket and first wall. Since the beams converge at the target, this approach leads to significant line-of-sight radiation streaming down the center of the final focusing magnets which typically precludes the use of superconducting magnets for this purpose. This also complicates the wall protection system design since the interior walls of these beamlines must be protected from heating, blast and radiation damage effects. Furthermore the protection mechanism must not interfere with the propagation and focusing of the beams which must form a tightly-focused (<1-cm diameter) spot at the target. This typically requires background gas pressures of order 1 mtorr with Li vapor.

Our design instead proposes to use a self-formed transport channel to re-image the beam focal spot from outside the blanket onto the target. This has significant implications relative to the above issues for ballistic focusing. It moves the conical arrays of focusing magnets out of line-of-sight into the cavity minimizing the opening size in both the blanket and the first wall to something of order 10 cm diameter. This minimizes shielding concerns for these magnets, permitting superconducting coils to be employed. It also greatly simplifies the wall protection system design for the heavy ion-driver since the transport channels can be formed in a significantly higher (100 mtorr lead vapor) background gas environment than is possible using ballistic focusing. This enables us to consider using the same lead wetted-wall design for the laser and heavy-ion drivers.

Channel formation using light ion beams with pre-formed plasma channels is well documented and has even been considered for near-term applications such as the light-ion LMF, but self-formed channels are a different matter. Analyses indicate that stable, self-formed channels cannot be generated using light ions. These analyses are not valid for heavy-ions due to their higher energies (GeV as compared to MeV for light ions) and significantly greater mass (200 amu versus 7 amu). We have evaluated the first-order physics of heavy-ion channel formation and find no fundamental limitations. However, the dynamics of the problem are extremely complex and beyond the scope of our study. We have therefore targeted this as a key R&D area.

There are several critical issues which will require validation through experimentation and modeling before self-formed transport channels can be considered truly viable. Foremost among these is a laboratory demonstration of a self-pinched heavy-ion beam transport channel. The transport characteristics of the channel must then be assessed including: (1) fraction of the beam ions initially captured in the channel, (2) fraction of the beam energy lost due to background collisions and back EMF, (3) fraction of the beam energy lost near the target where opposing side channel currents begin to cancel the confining aximuthal field, (4) fraction of the prepulse energy eroded during channel formation, (5) capability of the channel to re-image the focal spot at the channel entrance onto the target, (6) limitations on beam focal spot size at the channel entrance, (7) demonstration of sufficient control over the channel to accurately position the focal spot on the target, and (8) characterization of background gas conditions/limitations for stable channel formation.

Reactor Concept - Prometheus-H

Potential Impact - (DW) The use of liquid lead for wall protection is probably not compatible with ballistic transport using our present design. An alternative, lower-Z

wall protection material would be needed, or a different cavity design using a condensing vapor spray or a wall geometry with more exposed surface area.

Design Specificity - (DH, WP) This issue is specific to the heavy-ion driver coupled with a liquid lead wall protection scheme.

Overall Level of Concern - (High) The capability to form a stable, self-pinched transport channel to re-image a heavy-ion beam focal spot on a target would have significant positive economic and technical impact on design of a heavy ion-driven inertial fusion power plant.

Operating Environment - (ρ_g, Q, IB, G, N, T, E, EI, p)

Relevance to MFE - Low. This development issue is not directly relevant to MFE.

Analysis - Our study budgets/priorities did not permit any detailed analysis of heavy ion beam transport channel formation, stability and beam loss dynamics. We have assessed these issues and determined that there is no fundamental reason why self-formed transport channels will not work with heavy-ion beams. The potential technological and economic benefits of this mode of propagating the beams to the target warrants further investigation into their feasibility.

5.5 Research and Development Assessment

An important part of a conceptual reactor design study such as Prometheus is the identification of important research and development needs to resolve the key issues. An R&D assessment has been carried out for Prometheus to serve three purposes: (1) provide programmatic-decision makers with a list of important R&D tasks that need to be carried out, (2) provide part of the input for a comparison study between the Heavy-Ion and Laser-driven reactors, and (3) identify areas of R&D that are common to inertial and magnetic fusion energy.

This assessment has not attempted to develop a comprehensive R&D plan for IFE. Developing such a plan requires detailed analysis of experimental facilities and careful consideration of the time sequence and cost of such facilities in order to minimize the overall R&D cost and time and maximize benefits. Rather, this effort has focused on identifying the R&D required to resolve the critical and key issues described earlier in this chapter.

A specific development goal was selected as the ultimate objective of the R&D items described here. This goal is to develop the physics and engineering data base sufficient to construct an IFE Experimental Power Reactor (IEPR). It is difficult at this stage of IFE research to specify the detailed characteristics of an IEPR. However, IEPR is envisioned as a facility in which the basic physics and engineering performance as well as system integration tests are carried out. IEPR scope and mission similar in many respects to ITER in the magnetic fusion energy program as they both provide the data base necessary to construct a Demonstration Power Plant (DEMO). IEPR will have prototypical components and will probably produce several hundred megawatts of fusion power and operate with about one pulse per second and overall availability of 20-30%.

The R&D assessment here focused primarily on critical components unique to IFE: target, driver, and cavity. Some modest R&D has also been identified for the tritium systems and safety. Because a number of key issues can be resolved through experiments on the same facilities, the R&D presented below has been organized so that each R&D item relates to one key issue or a group of issues. In this latter case, the issues involved are clearly indicated using the numbering system used earlier in the Key Issue Summary Table. A summary of R&D costs for the laser reactor option and heavy ion option is included in Section 7.3.6 in the comparison chapter.

5.5.1 Research and Development Requirements for Targets and Drivers

The majority of the most urgent Research and Development (R&D) requirements for IFE Targets and the two types of drivers are inextricably linked together. Some of the most difficult issues having exclusively to do with the drivers involve the demonstration of the generation and delivery of high energy pulses; these same high energy pulses from the driver are requirements for solving significant issues associated with target design and development.

Target/Driver R&D - IFE target irradiation requirements basically define the driver designs. If faulty target design gives rise to unnecessary or inappropriate driver requirements, expensive and unnecessary driver development may occur without advancing the state of the art. Furthermore, experimental evidence and theoretical simulations have shown that the IFE target implosion physics is strongly dependent upon the scale of the target, so that data derived from small (kJ scale) driver/target interaction experiments cannot be easily extrapolated to aid in the design or predict accurately the performance of reactor-sized targets (requiring irradiation energies of the order of MJ).

Thus, in order to design an optimum reactor-sized DT target, a strong, long-term IFE R&D program involving experiments and analyses associated both with drivers and targets must be established. This would permit the development of a series of DT target designs of increasing scale, beginning at our present stage of understanding, and proceeding in an orderly manner to IFE target ignition and beyond, with the desired optimum reactor targets having yields of the order of hundreds of MJ.

This orderly series of target/driver interaction experiments is crucial to the success of an IFE reactor development program because there are a variety of competing processes to efficient thermonuclear "burns" of the DT fuel which have unique scale lengths. These competing processes can lead to anisotropies in target compression, preheating of the cryogenic DT fuel, generation of plasma instabilities, etc. As target dimensions increase, many of the strengths of these competing processes can grow exponentially. Frequently, variations of one or more parameters in target or driver design can check the growth or otherwise control an undesirable competing process, thereby permitting continued progress toward achieving ignition, thermonuclear break-even, and eventual demonstration of optimized target/driver designs for cost-effective IFE reactor operation.

In the case of the HI driver, a crucial series of driver/target experiments conducted with indirect-drive HI DT targets would be to demonstrate that heavy ion beams converted at each end of an HI indirect-drive target efficiently produce soft X-rays in an energy range suitable for achieving the Rayleigh-Taylor irradiation requirements for a uniform implosion of the DT target within the hohlraum. This could prove to be one of the chief

advantages for the HI IFE driver over a comparable UV excimer laser driver. Verification of the accuracy of this prediction is a crucial step in allowing future IFE reactor designers to make appropriate choices as our database for both targets and drivers is enlarged by implementation of a well thought out IFE R&D plan.

Although some laser/target irradiation experiments could be conducted using subscale beams associated with parallel driver development efforts, a key demonstration for the success of the Prometheus-L laser driver interacting with direct-drive targets is the uniform ~1% target illumination with 60 beams, totaling 4 MJ. Another important series of key, full-scale R&D experiments involving both direct-drive targets and laser drivers would be the demonstration that the long laser prepulse doesn't significantly contribute to target preheat by generating hot electrons and hard X-rays via stimulated Brillouin and Raman scattering in the plasma atmosphere blown off from the target by the long duration prepulse.

Target R&D - Once the riddles of IFE target design are being solved by implementation of an aggressive plan exploiting extensive driver/target R&D experiments and analyses, there are a series of purely target-related requirements which need to be explored in parallel with the other programs. Development of cost-effective, target fabrication methods leading to economical mass production for IFE reactors needs to be carried out. R&D for innovative methods of accurately placing IFE targets at the centers of target chambers at around a 5-Hz rate is of crucial importance. There may be significant target/driver alignment advantages associated with having IFE DT targets injected into reactor target chambers with zero net velocity following injection and, hence, target injection R&D might deal with developing techniques which may permit this goal to be achieved.

Some modifications to target designs may be required in order to enhance the alignment of the DT targets relative to the driver beams. An example might be the addition of a "shine shield" on a direct-drive laser DT target so that aligning laser beams may be used to sense the position of a DT target with a high degree of accuracy.

Driver R&D - Although a series of parallel subscale R&D experiments, analyses, and technological innovations must be carried out for the IFE HI driver, the vast majority of meaningful HI driver R&D developments must be conducted at or near full scale; i. e., at energy levels of the order of MJ with pulse durations of the order of 10 ns. In particular, our understanding of the physics of heavy ion (HI) drivers will not significantly benefit from HI experiments conducted with pulsed energies of the order of only a few tens of kilojoules because these sub-scale experiments do not overlap the HI driver parameter space occupied by candidate HI IFE reactor drivers.

The Prometheus-H heavy ion (HI) driver design calls for the delivery of 7.8 MJ in 18 beamlines, of which 12 are bunched into ~7 ns pulses and the remaining 6 beamlets are bunched into ~30 ns pulses. This corresponds to approximately 420 kJ/beamline. Transport experiments with a single, space-charge limited HI beam may be useful, but a key HI driver demonstration goal will be the successive achievements at full scale energy (~4 MJ) of ballistic focusing, stripping, channel formation, and stable, self-pinched transport to the target. However, as noted above, the same HI facility that can demonstrate these fundamental capabilities for the driver can also be used to test HI target design parameters.

In an analogous manner, off-line HI development programs can be established to develop low emittance, doubly-ionized heavy ion (Pb^{+2}) beam sources, cost-effective superconducting dipoles, expert control systems, channel formation techniques, HI beam alignment systems, etc. R&D programs associated with achieving significant reductions in Metglas losses could be carried out in parallel with other R&D efforts designed to optimize the single beam LINAC operated in a burst mode. Construction of a series of full-scale HI storage rings suitable for demonstrating that a single beam LINAC operated in the burst mode can deliver an adequate number of comparable low emittance beamlets suitable for ballistic focusing into a pre-formed channel.

Although a series of parallel subscale R&D experiments can be conducted for the laser driver, again the vast majority of meaningful R&D developments must be conducted at or near full scale; i. e., at energy levels of the order of MJ with pulse durations of the order of 10 ns. Similarly, there are a number of IFE laser driver issues which require operation of a least one beam line at full scale energy. In the case of the Prometheus-L KrF laser design, this would be an ultraviolet (UV) laser beam of energy ~80 kJ generated from a combination of using a large number (16 to 25) moderate energy (4 to 6 kJ) electric-discharge excimer lasers to pump a large aperture (1.2 m) Raman accumulator cell which, in turn, pumps a backward stimulated Brillouin scattering (SBS) pulse compression cell yielding a pulse duration of approximately 6 ns with a wavelength of ~250 nm.

As described below, the Prometheus-L KrF laser driver requires extensive development of workhorse excimer laser amplifiers, reliably producing output energies ranging from 4 to 6 kJ with moderately good beam quality. An ambitious goal for these laser amplifiers is to have them reach a level of ~10^9 shots between failures.

Again, however, it should be emphasized that the natural consequences of solving these driver component development problems in parallel following an orderly plan is the step-by-step construction of a driver facility suitable for performing full scale target irradiation experiments.

5.5.2 Target R&D

Many of the issues and associated R&D for the target are closely related to those of the driver. In this subsection, the R&D most closely related to the target is discussed. In the next subsection, the required R&D for the driver is presented together with the cost estimate for both the driver and target R&D.

5.5.2.1 Direct Drive Target Coupling (Key Issue A.a.1)

Description - Areas requiring R&D for this issue include:

- Proof of ability to model plasma physics correctly - Experiments with high gain targets to establish agreement with computer models.
- Studies of development of hydrodynamic instabilities and target break up/mixing for reactor size targets - Experiments to show that growth of Rayleigh-Taylor and other instabilities agrees with reactor-size targets and that symmetric implosions can be achieved.
- Illumination symmetry and laser light absorption for reactor size targets - Experiments to demonstrate sufficiently smooth beam profiles with correct apodization and laser light absorption in a agreement with computer models.
- Accurate pulse shaping - Experiments to show that pulses can be shaped with sufficient accuracy to implode targets on a low adiabat and, at the same time, generate converging shocks sufficient to ignite a small, central hot spot (spark plug).

Facility - Direct drive experimental facility: Such a facility would be especially useful should the ignition and gain facility be capable of illuminating indirect drive targets only, but should probably be built in any case. It should be capable of delivering 100 to 500 kJ on target from 60+ beams. It would be used to demonstrate ignition of direct drive targets.

Cost and Time - These will depend on when and how the facility described above is built. Most economical path will probably be a direct drive experimental facility constructed as an upgrade of the OMEGA laser system at the University of Rochester. Cost estimates are given in the next section on the Driver.

5.5.2.2 Survivability of Targets in Chamber Environment (Key Issue A.a.3)

Description - Areas requiring R&D for this issue include:

- Hydrodynamics of target/cavity interaction. Once this environment is known, theoretical studies using modern hydrodynamics and heat transfer algorithms should be able to settle the question of target survivability. Experimental work would be useful to check code results, but should be limited in scope and capable of being carried out in existing facilities.

Facility - It will probably be unnecessary to build a separate facility to address this R&D issue.

Cost and Time - Once the cavity environment has been specified, it will not be expensive to address this issue in either cost or time. A theoretical study coupled with limited experimental research could be conducted at a national laboratory or university. It should be possible to complete the R&D within two or three years.

5.5.2.3 Demonstration of Injection and Tracking of Targets Coupled with Beam Steering (Key Issue A.b.1)

Description - Areas requiring R&D for this issue include:

- Target injection and tracking/beam steering - Experiments to show that targets can be injected reliably and tracked with sufficient precision.
- Illumination symmetry and laser light absorption for reactor size targets - Experiments to demonstrate sufficiently smooth beam profiles with correct apodization and laser light absorption in agreement with computer models.

Facility - The technology required here has not been demonstrated in IFE or any other field. A separate facility should probably be built.

- Target injection/beam steering simulator. This facility will be used to prove that accurate illumination can be achieved in a reactor scenario. Full size steering components will be used, but actual beams need only be sufficiently intense to provide accurate diagnostics. The facility will include a full scale injection system capable of repetition rates of around 10 hertz.

Cost and Time - This facility might be built at Sandia or Los Alamos at a cost of $100-300 million. Annual operating cost would be around $20 million. The facility would take about three years to build. The R&D program would last about five years.

5.5.2.4 Manufacturability of High Quality, Low Cost DD and ID Targets (Key Issue A.c.1)

Description - R&D in this area will establish the ability to mass produce targets at low cost using already demonstrated technologies. Considerable advances have been made in the fabrication of individual targets using microencapsulation, microfabrication, droplet generators, etc. Research in this area will establish whether any of these demonstrated techniques are viable for mass production, and identify alternative methods. To date, no major research effort has been devoted to mass production of IFE targets. The R&D effort in this area would include experimental and theoretical work. Funding should be on a level sufficient to attract significant attention

to the problem. It is likely that numerous existing chemical and industrial processes could be profitably applied to mass produce targets. It is a question of making the best talent aware that the problem exists.

Facility - It will probably be unnecessary to fund major new facilities for this R&D. Once the best processes have been identified, existing facilities at major industrial companies or universities will probably be capable of proving the potential for mass production.

Cost and Time - Although new facilities are probably not needed in this area, significant amounts of time and money will be required to attract the necessary research in the area. Expenditures of $200 million over 10 years would not be unreasonable.

5.5.2.5 Overall R&D - Significant technical R&D will be required in areas of target physics, production, and operation which is not necessarily covered in any of the key issues. Therefore, the following is included as a catch-all for what the key issues for the target area have missed.

Description - Overall R&D covers some of the areas already identified above as well as areas not specifically identified among the target key issues, and the scope of the required R&D is accordingly large. We have tried to cover below all areas which we feel require a significant R&D effort within the target physics and engineering-related areas.

- Target implosion on a low adiabat - Experiments to demonstrate efficient compression without excessive preheat before ignition.
- Test of target designs - Experiments to prove that high gain can be achieved with proposed target designs.
- Proof of ability to model plasma physics correctly - Experiments with high gain targets to establish agreement with computer models.
- Central spark ignition and propagating burn - Experiments to prove that bootstrap heating by fast alpha particles can generate an outward-propagating burn wave leading to efficient thermonuclear burn.
- Studies of development of hydrodynamic instabilities and target break up/mixing for reactor size targets - Experiments to show that growth of Rayleigh Taylor and other instabilities agrees with predictions for reactor-size targets, and that symmetric implosions can be achieved.
- Significant gain for low mass targets - Experiments to prove that economically attractive gain can be achieved with 1-10 MJ drivers.
- Hohlraum physics - Experiments to show agreement with predictions of computer models.

- Non-LTE radiative transfer. Demonstrate agreement of code-predicted radiative transfer with experiments for reactor-size indirect drive targets.
- Target injection and tracking/beam steering - Experiments to show that targets can be injected reliably and tracked with sufficient precision.
- Illumination symmetry and laser light absorption for reactor size targets - Experiments to demonstrate sufficiently smooth beam profiles with correct apodization and laser light absorption in agreement with computer models.
- Accurate pulse shaping - Experiments to show that pulses can be shaped with sufficient accuracy to implode targets on a low adiabat and, at the same time, generate shocks sufficient to ignite a small, central hop spot (spark plug).

Facility - It will probably be necessary to build several facilities to conduct the experimental programs outlined above. These might include:

- Ignition and gain facility: This facility should be capable of delivering at least one megajoule of beam energy. It should have at least 32 beams and an independent backlighting system.
- Target injection/beam steering simulator: This facility will be used to prove that accurate illumination can be achieved in a reactor scenario. Full size optics will be used, but beams need only be sufficiently intense to provide accurate diagnostics. The facility will include a full scale injection system capable of repetition rates of around 10 Hertz.
- Direct drive experimental facility: Such a facility would be especially useful should the ignition and gain facility be capable of illuminating indirect drive targets only, but should probably be built in any case. It should be capable of delivering 100 to 500 kJ on target from 60+ beams. It would be used to demonstrate ignition of direct drive targets.
- Demonstration reactor: This facility will demonstrate IFE production at the 10 to 100 MWe level.

5.5.3 Driver R&D

5.5.3.1 Summary of R&D Tasks for Target and Driver Key Issues - There are a wide variety of research and development (R&D) efforts which need to be carried out to assist with the development of viable target and driver designs.
R&D work relevant to specific key issues associated with the Prometheus laser driver described here include:

A.a.1 Direct Drive Target Coupling,
A.a.2 Indirect Drive Target Coupling,
A.a.3 Survivability of Targets in Target Chamber Environment,
A.b.1 Demonstrating of Injection and Tracking of Targets Coupled with Beam Steering,

A.c.1 Manufacturability of High Quality, Low Cost Direct-Drive and Indirect-Drive Targets,
B.a.1 DT Target Illumination Issues,
B.a.2 Large Laser Development and Bandwidth Issues,
B.a.3 Final Optics Pointing System,
B.a.4 Grazing Incidence Mirror Damage,
B.a.5 SBS Pulse Compressor,

Recommended R&D work associated with the Prometheus-H heavy ion driver include the following relevant key issues:

B.b.1 Timing of Heavy Ion Beams,
B.b.2 Heavy Ion Channel Formation,
B.b.3 Heavy Ion Channel Transport,
B.b.4 Stripping of Heavy Ion Beam,
B.b.5 Alignment of Indirect Heavy Ion Target

Summary of R&D Cost Estimates

Table 5.5-1. Summary of Laser Driver R&D Task and Duration Estimates

No.	Task Description	Estimated Cost	Key Issue	R&D Duration
1	Demo DD Target Beam Nesting	10 M$	B.a.1	3 years
2	Satisfy Bandwidth Requirements	10 M$	B.a.2	3 years
3	Laser Beam/Target Alignment System	12 M$	A.b.1,B.a.3	4 years
4	Demo DD MJ DT Target Ignition*	400 M$	A.a.1,B.a.1	10 years
5	Final optics pointing demo	5 M$	A.b.1,B.a.3	3 years
6	Optics Damage Resistance Demo	5 M$	B.a.4	3 years
7	Develop Robust GIMM	5 M$	B.a.4	4 years
8	Develop excimer laser modules	20 M$	B.a.2	3 years
9	Test to demonstrate 10^9 lifetime	40 M$	B.a.2	5 years
10	Demonstrate single 6 kJ beam line	80 M$	B.a.2	4 years
11	Demonstrate 6x16=96 KJ beam line	120 M$	B.a.2	2 years
12	Develop/Demo Laser Control System	40 M$	B.a.2	5 years
13	Develop 50 J Raman seed generators	2 M$	B.a.2	1 year
14	Demonstrate 6 kJ Raman converter	1 M$	B.a.2	1 year
15	Demo 100 kJ Raman converter	20 M$	B.a.2	2 years
16	Develop programmable SBS chirper	2 M$	B.a.5	1 year
17	Subscale SBS PC demonstration	2 M$	B.a.5	1 year
18	Develop Large Aperture SBS chirper	10 M$	B.a.5	3 years
19	Demo 6 kJ SBS Pulse Compressor	5 M$	B.a.5	2 years
20	Demonstrate 100 kJ Pulse Compressor	20M$	B.a.5	5 years
	Total Laser Driver R&D Costs	829M$		

*Includes cost of Nova Upgrade.
DD = direct drive, GIMM = grazing incidence metal mirror, SBS = stimulated Brillouin Scattering, PC = pulse compression, DT = deuterium/tritium

Table 5.5-2 Summary of Heavy Ion Driver R&D Task and Duration Estimates

No.	Task Description	Estimated Cost	Key Issue	R&D Duration
1	Demo Single Accel. in Burst Mode	15 M$	B.b.1	3 years
2	Develop Brighter Pb^{+2} Source	10 M$	B.b.1	3 years
3	Develop high brightness HI injector	20 M$	B.b.1	2 years
4	Demo low emittance through injector	10 M$	B.b.1	2 years
5	SP HI Pulse Synch. & Timing Demo	10 M$	B.b.1	3 years
6	SP Triplet Focusing Demo	10 M$	B.b.2	2 years
7	SP HI Channel Formation Demo	100 M$	B.b.2	7 years
8	SP Injection of HI Beam in Channel	10 M$	B.b.3	3 years
9	SP Demo of Channel Transport @ MA	50 M$	B.b.3	5 years
10	SP HI Beam Stripping	20 M$	B.b.4	2 years
11	SP HI Neutralization	5 M$	B.b.4	1 year
12	Develop high PRF burst-mode pwr.sup.	30 M$	B.b.3	2 years
13	Demo superconducting quadrupoles	20 M$	B.b.3	3 years
14	Demo storage ring performance	50 M$	B.b.3	3 years
15	Demo bunchers	25 M$	B.b.3	3 years
16	Develop HID Computer Control System	20 M$	B.b.5	5 years
17	Alignment of HI Beam to ID Target	400 M$	B.b.5	10 years
	Total Heavy Ion R&D Costs	805M$		

SP = single pulse, HI = heavy ion, MA = mega-ampere currents,
PRF = pulse repetition frequency, HID = heavy ion driver, ID = indirect drive

Table 5.5-3 Summary of Target R&D Task and Duration Estimates

No.	Task Description	Estimated Cost	Key Issue	R&D Duration
1	Demo Target Survivability in TC	5 M$	A.a.3	2 years
2	Demo Target Injection/Tracking	10 M$	A.b.1,B.a.3	3 years
3	Target Manufacturability Demo	10 M$	A.c.1	2 years
4	Direct Drive Target Experiments (with >1 MJ Laser Driver)	200 M$	A.a.1,A.a.3 A.b.1,A.c.1 B.a.1,B.a.2 B.a.3	5 years
5	Indirect Drive Target Experiments (with >1 MJ Heavy Ion Driver)	200 M$	A.a.3,A.b.1 A.c.1,B.b.5 B.b.1,B.b.2 B.b.3,B.b.4	5 years
6	Pellet Injection Research Facility	200 M$	A.a.3,A.b.1 A.c.1	5 years
7	Alternative DD Target Irradiation Facility (Upgrade Ω-Laser at UofR to 100 kJ)	100 M$	A.a.1,A.a.3 A.b.1,A.c.1 B.a.1,B.a.2 B.a.3	5 years
	Total Target R&D Costs	725M$		

DT = deuterium/tritium fuel, TC = target chamber, DD = direct drive.

5.5.3.2 R&D for Feasibility of Laser Driven Direct Drive Target System

(Relevant Key Issues: A.a.1, A.a.3, A.b.1, A.c.1, B.a.1, B.a.2, B.a.3, B.a.4, B.a.5.)

Description of Problem - Designs for direct drive (DD) laser driven IFE DT targets have been anchored on experiments conducted on miniature DD targets illuminated with only a few kJ of laser energy. Large reactor sized, multi-MJ DD targets may require different illumination conditions making use of recent technological innovations in laser beam propagation and apodization. For reactor operation, the DD targets must also be accurately injected into the target chamber in coordination with a tracking/alignment system capable of meeting the illumination uniformity requirements.

Description of Required R&D Efforts - R&D work relevant to specific key issues associated with the Prometheus laser driver described here include:

- A.a.1 Direct Drive Target Coupling,
- A.a.3 Survivability of Targets in Target Chamber Environment,
- A.b.1 Demonstrating of Injection and Tracking of Targets Coupled with Beam Steering,
- A.c.1 Manufacturability of High Quality, Low Cost Direct-Drive and Indirect Drive Targets,
- B.a.1 DT Target Illumination Issues,
- B.a.2 Large Laser Development and Bandwidth Issues,
- B.a.3 Final Optics Pointing System,
- B.a.4 Grazing Incidence Mirror Damage,
- B.a.5 SBS Pulse Compressor,

Two general types of R&D experiments are required to solve the problems identified in the corresponding Critical Issue #2:[1]

(1) Full-scale DD target irradiation experiments
(2) Realistic DD target injection, tracking, and alignment experiments

Each is briefly described below. (A combination of these two general types of R&D experiments is not recommended at this time as the costs would be prohibitive.)

Direct-Drive Target Irradiation Experiments at > 1 MJ - IFE target irradiation experiments on reactor-sized DD targets can be carried out using a single shot laser irradiation facilities such as that proposed for the Nova Upgrade. Laser driver energies of at least 1 MJ need to be delivered in approximately 60 beamlines with a ~1% illumination uniformity. Both tangential focusing and potentially more efficient, nested and apodized square beamlet DD target illumination configurations need to be investigated. Different laser driver prepulse shapes need to be investigated to ensure that undesirable stimulated Raman and Brillouin scattering processes in the underdense plasma atmosphere do not contribute to target preheating.

Direct-Drive Target Injection Experiments - A separate series of experiments needs to be conducted on DD target injection, tracking, and beam alignment to assure that the static DD target irradiation specifications can be met. This may necessitate the use of a "shine shield" on the DD IFE target.

Facility Requirements - Single-shot DD target irradiation experiments can yield useful data on target design, laser/target coupling, and the relative successes of tangential focusing vs. nested apodized beamlets on the DD targets. For full scale direct-drive laser target irradiation experiments, a new laser facility at least as large as the proposed Nova Upgrade laser irradiation facility will be required. A separate new facility will also be required to perform the target tracking and alignment experiments.

Cost and Schedule - The Nova Upgrade facility has been estimated to cost between $300 M and $400M.[2] If funded promptly, this IFE facility should be on-line by 1998,[3] at which time DD experiments such as those described above could be carried out. The DD target experiments themselves, were they to be conducted in the Nova Upgrade facility, are could be completed in 18 months and are estimated to cost approximately $25M (assuming two series of 100 DD targets shot @ $50k/shot plus $3M for experimental staff, $10M for simulations/data reduction, and $2M for diagnostics).

A relatively simple laboratory facility could be used to test DD target tracking and alignment techniques. With a $500k laboratory conversion (of an existing laboratory) combined with $1.5M for staff salaries and alignment diagnostics, attractive DD target alignment schemes could be tested. A separate source of DD targets (from a target fabrication laboratory) could furnish targets at an estimated cost of $20K (for $2x10^4$ DD targets).

Summary of R&D Cost Estimates

Table 5.5-4 Feasibility of Laser-Driven Direct-Drive Target System R&D Task and Duration Estimates

No.	Task Description	Estimated Cost	Key Issue	R&D Duration
1	Demo DD Target Survivability in TC	$5 M	A.a.3	2 years
2	Demo Target Injection/Tracking	$10 M	A.b.1,B.a.3	3 years
3	Target Manufacturability	$10 M	A.c.1	2 years
4	Demo DD Target Beam Nesting	$10 M	B.a.1	3 years
5	Satisfy Bandwidth Requirements	$10 M	B.a.2	3 years
6	Laser Beam/Target Alignment System	1$2 M	A.b.1,B.a.3	4 years
7	Demo DD MJ DT Target Ignition*	$400 M	A.a.1,B.a.1	10 years
8	Final optics pointing demo	5 M$	A.b.1,B.a.3	3 years
	Total Laser Driver R&D Costs	$459M		

*Includes cost of Nova Upgrade.

References for 5.5.3

1. Gary J. Linford, TRW S&TG/ATD, "ICFRDS Critical Issue #2: Feasibility of Laser Driven Direct Drive Targets," December 1991.

2. "Nova Upgrade Facility for Ignition and Gain," UCRL-LR-106874, Lawrence Livermore National Laboratory, Livermore, CA 94551 (March 1991).

3. "Nova Upgrade: A Proposed ICF Facility to Demonstrate Ignition and Gain by the Year 2000," UCRL-LR-106736, Lawrence Livermore National Laboratory, Livermore, CA 94551 (March 1991).

5.5.3.3 R&D for Feasibility of Heavy Ion Driven Indirect-Drive Target System

(Relevant Key Issues: B.b.1, B.b.2, B.b.3, B.b.4, B.b.5)

Description of Problem - The primary problems associated with the feasibility of heavy ion indirect-drive (HI ID) targets have to do with space-charge-limited heavy ion beam transport and accurate focusing onto the moving HI ID target. There is currently substantial disagreement among HI driver experts with regard to the conditions required for reliable self-focused HI channel formation, even assuming an ionizing precursor (either another charged particle beam or an ultraviolet [UV] laser beam). Furthermore, although calculations show that for two HI beam bundles (each having 3 MJ of 4 GeV lead ions), following passage through the stripping cells, the resulting MA beam current is above the threshold for self-pinching by about two orders of magnitude, the HI ID target experiments would need to be conducted at or near full scale to demonstrate the feasibility of the concept.

Another HI ID target problem is associated with fabricating the HI ID target to be economical, mechanically robust to withstand launch accelerations, and capable of meeting the precise target design requirements for efficient implosion.

Recommended R&D work associated with the Prometheus-H heavy ion driver include the following relevant key issues:

B.b.1 Timing of Heavy Ion Beams,
B.b.2 Heavy Ion Channel Formation,
B.b.3 Heavy Ion Channel Transport,
B.b.4 Stripping of Heavy Ion Beam,
B.b.5 Alignment of Indirect Heavy Ion Target

Description of Required R&D Efforts - Seven types of HI ID R&D experiments are required to solve the problems identified in the corresponding Critical Issue #3:[1]

(1) Demonstration that ~12 to 18 lead HI beams can be accelerated to an energy of 4 GeV, injected and ejected efficiently from the storage rings in timed, synchronized, and bunched prior to injection into the triplet focusing magnets.

(2) Demonstration that the 4 GeV (in a +2 charge state) can be focused down to a spot having a radius of 3 mm.
(3) Demonstration that the focused HI beam will enter a preformed channel (formed by either a precursor ion beam or UV laser beam).
(4) Demonstration that the self-pinched beam will self-focus and follow the preformed channel with an angular accuracy of ~10 microradians.
(5) Efficiently convert the ~6 MJ of HI beam energy to soft X-rays in the target.
(6) Demonstration that all return currents can be conducted without significant HI beam deflection or misalignment.
(7) Demonstration that launched HI ID targets can (a) be directed accurately into the HI ID target firing zone, and (b) meet target robustness requirements.

There is some indication that HI ID target irradiation performance may be improved by single-sided HI ID target irradiation geometries but with the condition that the delivered HI beam energy (and hence the number of HI beams) may need to be reduced.

Acceleration and Transport of HI Beams - It will be necessary to demonstrate the efficacies of the entire single beam accelerator operated in a burst mode, together with the synchronized injection and ejection of beams from the storage rings. Demonstration of required HI beam bunching while minimizing beam losses prior to injection into the triplet focusing magnets.

Focusing of Bundled HI Beams to 3 mm Radius Spot - Injection of approximately a dozen synchronized, bunched, 4 GeV, doubly charged HI beams into the triplet focusing magnets, focusing the HI beams down through a neutralizing cell to achieve a 3 mm radius spot on an electron-stripping gas jet. The current in each of the two beamlines (assuming two-sided HI ID target irradiation) should easily exceed 1 MA after stripping. The focusing geometry must allow a precursor beam (either an ion beam or a UV laser beam) to pre-form the beam channel.

Injection of Focused HI Beams into Pre-formed Channel - By placing the common focus of the overlapping HI beams at the head of a pre-formed ionized channel, it is necessary to demonstrate the efficient capture (~90%) of the combined HI beams into a self-pinched channel. Beam currents of the order of 10 MA are expected.

Propagation of Self-Pinched HI Beams Parallel to Precursor Beam - The dynamic stability of the self-focused HI beams propagating over distances of the order of 5 m must be demonstrated. Propagation of the HI beams within the channel and parallel to the direction established by the precursor beams ~100 mrad must be demonstrated. Limits on interbeam energy imbalances and the effects of there interbeam energy imbalances on the propagation characteristics of the self-focused HI beam channel need to be determined.

Demonstration of Efficient Conversion of 3 MJ 4 GeV HI Beams to Soft X-rays - Full-scale HI ID target experiments must be conducted to demonstrate the required X-ray conversion efficiencies.

Demonstration of Self-Pinched HI Beam Insensitivity to Deflection - With the HI driver running in the burst mode, measurements of HI beam deflections as functions of return current symmetries need to be conducted to assess the effects of external currents reducing the effective pointing accuracies of the HI beams.

HI ID Target Tracking and Performance Verification - A separate series of experiments needs to be conducted on ID target injection, tracking, and beam alignment to assure that the static ID target irradiation specifications can be met. This may necessitate the use of "shine shields" on the two ends of the cylindrical ID IFE target in analogy with measurements required for similar laser-driven targets.

Facility Requirements - A few subscale HI ID experiments can be conducted at existing accelerator facilities. However, the majority of HI ID R&D experiments could only be conducted at a new accelerator site designed to support these HI experiments. This large accelerator facility can be used for conducting the extensive experimental measurements outlined above. Considerable modifications may be required during the course of the HI ID target experiments to modify the ramp gradient, fixed gradient, storage rings, buncher accelerator, and final focusing triplet configurations in accordance with varying HI ID target irradiation requirements. It is highly probable that as HI ID target experiments are conducted, design details of the HI ID targets will evolve, thereby necessitating continued modifications to the HI driver facility. The required accelerator facility would be substantially smaller than that of the proposed Superconducting Super Collider. A smaller facility could be used to perform the target tracking, alignment, and evaluation experiments. Some reconfiguration of these facilities would be required to generate the required target illumination symmetries.

Cost and Schedule - The estimated costs for supporting the ambitious plans defined above are highly dependent upon the availability of existing accelerator facilities. If it were necessary to construct such a facility from the ground up, enormous costs may be involved, possibly as much at $700 M. Depending upon the evolution of optimum HI ID target illumination requirements, some time and money would be needed to reconfigure the accelerator and focusing magnets to meet specific configuration requirements. The HI ID target experiments themselves, could be completed in 18 months and are estimated to cost approximately $20M (assuming two series of 100 ID targets shot @ $40k/shot plus $3M for experimental staff, $7M for simulations/data reduction, and $2M for diagnostics). These HI ID experiments could be performed in conjunction with the R&D experiments associated with cost reduction of a suitable IFE HI driver[2]. Additional experiments and costs are described below in Summary of R&D Cost Estimate.

For HI ID target injection experiments, a laboratory could be equipped for $500k with a budget of $1.5M to perform HI ID target injection experiments. Realistic ID targets

would be supplied by another target fabrication laboratory (to be determined) at an estimated cost of $200k. Additional experiments and costs are described below in Summary of R&D Cost Estimates.

Summary of R&D Cost Estimates

Table 5.5-5 Feasibility of Heavy Ion Driven Indirect Drive Target System R&D Task and Duration Estimates

No.	Task Description	Estimated Cost	Key Issue	R&D Duration
1	Demo DT Target Survivability in TC	$5 M	A.a.3	2 years
2	Demo Target Injection/Tracking	$10 M	A.b.1,B.a.3	3 years
3	Target Manufacturability	$10 M	A.c.1	2 years
4	Demo Single Accel. in Burst Mode	$15 M	B.b.1	3 years
5	Develop Bright Pb^{+2} Source	$10 M	B.b.1	3 years
6	Develop high brightness HI injector	$20 M	B.b.1	2 years
7	Demo low emittance through injector	$10 M	B.b.1	2 years
8	SP HI Pulse Synch. & Timing Demo	$10 M	B.b.1	3 years
9	SP Triplet Focusing Demo	$10 M	B.b.2	2 years
10	SP HI Channel Formation Demo	$100 M	B.b.2	7 years
11	SP Injection of HI Beam in Channel	$10 M	B.b.3	3 years
12	SP Demo of Channel Transport @ MA	$50 M	B.b.3	5 years
13	SP HI Beam Stripping	$20 M	B.b.4	2 years
14	SP HI Neutralization	$5 M	B.b.4	1 year
15	Develop high PRF burst-mode pwr.sup.	$30 M	B.b.3	2 years
16	Demo superconducting quadrupoles	$20 M	B.b.3	3 years
17	Demo storage ring performance	$50 M	B.b.3	3 years
18	Demo bunchers	$25 M	B.b.3	3 years
19	Develop HID Computer Control System	$0 M	B.b.5	5 years
20	Alignment of HI Beam to ID Target	$400 M	B.b.5	10 years
	Total Heavy Ion R&D Costs	$830 M		

References for 5.5.3.3

1. Gary J. Linford, "ICFRDS Critical Issue #3: Feasibility of Indirect Drive Targets for Heavy Ion," TRW S&TG/ATD, December 1991.

2. Alfred Maschke, Gary Linford, and Steven Fornaca, "Research and Development for Critical Issue #5: Cost Reduction for the Heavy Ion Driver," TRW S&TG/ATD, January 1992.

5.5.3.4 R&D for Feasibility of Laser Driven Indirect Drive Target System

(Relevant Key Issues: A.a.2, A.a.3, A.b.1, A.c.1, B.a.2, B.a.3, B.a.4.)

Description of Problem - Although more IFE indirect-drive target experiments have been conducted laser energies between 10 and 30 kJ than have been carried out for direct-drive targets, there remains a gap in laser irradiation energies of more than two orders of magnitude between the current experimental indirect-drive laser DT targets and the proposed IFE reactor-scale targets. Thus the current designs for reactor-scale indirect drive (ID) laser driven IFE DT targets have been anchored on experiments conducted on miniature ID targets illuminated with only a less than 1% of the laser energy required for the IFE reactor laser drivers. Furthermore, reduction or elimination of the transparencies[1] of the hohlraum entrance apertures may be an issue. As was the case also for direct-drive targets, for IFE reactor operation, it must be demonstrated that the ID targets can also be accurately injected into the target chamber with a tracking/alignment system capable of meeting the illumination requirements.

R&D work relevant to specific key issues associated with the Prometheus laser driver described here include:

- A.a.2 Indirect Drive Target Coupling
- A.a.3 Survivability of Targets in Target Chamber Environment
- A.b.1 Demonstrating of Injection and Tracking of Targets Coupled with Beam Steering
- A.c.1 Manufacturability of High Quality, Low Cost Indirect-Drive Targets
- B.a.1 DT Target Illumination Issues
- B.a.2 Large Laser Development and Bandwidth Issues
- B.a.3 Final Optics Pointing System
- B.a.4 Grazing Incidence Mirror Damage

Description of Required R&D Efforts - Two types of R&D experiments are required to solve the problems identified in the corresponding Critical Issue #4:[2]

(1) Gradual scale up to full-scale ID target irradiation experiments.
(2) Brassboard laser driven ID target injection, tracking, and alignment experiments.

Each is briefly described below:

Indirect-Drive Target Irradiation Experiments at >100 kJ to 1 MJ - Initial experiments need to be carried out at lower laser irradiation energies (~100 kJ) and various temporal formats to determine the ranges over which plasma closure of entrance apertures occurs. Then IFE target irradiation experiments on reactor-sized ID targets

can be carried out using single shot laser irradiation facilities such as that proposed for the Nova Upgrade. Laser driver energies ranging up to at least 1 MJ need to be delivered in two symmetric beam bundles with a ~5% illumination uniformity. Different prepulse shapes need to be investigated to ensure that plasma closure of the ID target entrance apertures and undesirable stimulated Raman and Brillouin scattering processes in the underdense plasma atmosphere generated inside the target do not reduce the target coupling efficiency or contribute to DT target preheating.

Indirect-Drive Target Injection Experiments - A separate series of experiments needs to be conducted on ID target injection, tracking, and beam alignment to assure that the static ID target irradiation specifications can be met. This may necessitate the use of "shine shields" on the two ends of the cylindrical ID IFE target. ID target robustness must also be demonstrated; i. e., following a ~200 g accelerated target launch, internal mechanical oscillations must be damped out such that the internal hohlraum components must be in proper position to meet ID implosion requirements.

Facility Requirements - A DT target laser irradiation facility at least as large as the proposed Nova Upgrade laser irradiation facility will be required to permit the needed single pulse laser driven ID target experiments to be performed.

A separate new facility will also be required to perform the target tracking and alignment experiments. Some reconfiguration of the facility would be required to generate the required target illumination symmetries. Since a similar target injection facility would be required for direct-drive target injection experiments, a single laboratory could be designed to serve both experiments if funding were available to perform both experiments. As indicated below, common use of the target injection facility is estimated to save approximately $500K.

Cost and Schedule - The Nova Upgrade facility has been estimated to cost between $300M and $400M.[3] If funded promptly, this IFE facility should be on-line by 1998,[4] at which time ID target experiments such as those described above could be carried out. Depending upon the target illumination symmetries, some time and money would need to be expended to reconfigure the laser to meet specific requirements. The ID target experiments themselves, were they to be conducted in the Nova Upgrade facility, could be completed in 18 months and are estimated to cost approximately $25M (assuming two series of 100 ID targets shot @ $50K/shot plus $3M for experimental staff, $10M for simulations/data reduction, and $2M for diagnostics). Significant cost savings could be realized by combining a test program with that described for direct-drive targets.[5] Additional experiments and costs are described below in Summary of R&D Cost Estimate.

For target injection experiments, a laboratory could be equipped for $500K with a budget of $1.5M to perform target injection experiments. Realistic ID targets would be

supplied by another target fabrication laboratory (to be determined) at an estimated cost of $200K. Additional experiments and costs are described below in Summary of R&D Cost Estimate.

Summary of R&D Cost Estimates

Table 5.5-6 Feasibility of Laser-Driven Indirect-Drive Target System R&D Task and Duration Estimates

No.	Task Description	Estimated Cost	Key Issue	R&D Duration
1	Demo DT Target Survivability in TC	$5 M	A.a.3	2 years
2	Demo Target Injection/Tracking	$10 M	A.b.1,B.a.3	3 years
3	Target Manufacturability	$10 M	A.c.1	2 years
4	Laser Beam/Target Alignment System	$12 M	A.a.2,B.a.3	4 years
5	Demo DD MJ DT Target Ignition*	$400 M	A.a.1,B.a.1	10 years
6	Final optics pointing demo	$5 M	A.b.1,B.a.3	3 years
7	Optics Damage Resistance Demo	$5 M	B.a.4	3 years
8	Develop Robust GIMM	$5 M	B.a.4	4 years
	Total Laser Driver R&D Costs	$452M		

*Includes cost of Nova Upgrade.

References for 5.5.3.4

1. J. M. Auerbach, et al., "Closure Phenomena in Pinholes Irradiated by Nd:Laser Pulses," Applied Optics, 18, 510 (1979).

2. Gary J. Linford, "ICFRDS Critical Issue #4: Feasibility of Laser Driven Indirect Drive Targets," TRW S&TG/ATD, December 1991.

3. "Nova Upgrade Facility for Ignition and Gain," UCRL-LR-106874, Lawrence Livermore National Laboratory, Livermore, CA 94551 (March 1991).

4. "Nova Upgrade: A Proposed ICF Facility to Demonstrate Ignition and Gain by the Year 2000," UCRL-LR-106736, Lawrence Livermore National Laboratory, Livermore, CA 94551 (March 1991).

5. Gary J. Linford, Douglas Drake, and Dan Driemeyer, "R&D for Critical Issue #2 Feasibility of Laser Drive Direct Drive Target Systems," IFERDS Program, MDA, St. Louis, MO (1992).

5.5.3.5 R&D for Cost Reduction for the Heavy Ion Driver

(Relevant Key Issues: A.a.3, A.b.1, A.c.1, B.b.1, B.b.2, B.b.3, B.b.4, B.b.5)

Description of Problem - As described in the associated description provided as Critical Issue #5,[1] the major attraction of the Heavy Ion (HI) approach to inertial fusion energy (IFE) has always been related to the fundamental technical feasibility of building a HI driver system with the required properties to drive a DT pellet to ignition. The basic accelerator technology is well developed, the beam physics is tractable, and existing accelerator systems have exhibited 25 year lifetimes with 95% availabilities. A system to provide the required average power could have been built ten years ago. The major problem is cost. A 10 GeV linear accelerator built with today's technology would cost more than a billion dollars.

There are two key issues associated with HI driver cost reduction:

(1) Space charge-limited transport of a bunched beam to minimize total length of the single beam LINAC (or multiple beam LINAC).
(2) High current storage rings for heavy ion beams (required for single beam LINACs).

In addition, there is an important secondary issue having to do with the losses associated with Metglas (important for high pulse repetition rates in single beam LINACs).

Recommended R&D work associated with the Prometheus-H heavy ion driver include the following relevant key issues:

A.a.3 Survivability of Targets in Target Chamber Environment
A.b.1 Demonstrating of Injection and Tracking of Targets Coupled with Beam Steering
A.c.1 Manufacturability of High Quality, Low Cost Indirect-Drive Targets
B.b.1 Timing of Heavy Ion Beams
B.b.2 Heavy Ion Channel Formation
B.b.3 Heavy Ion Channel Transport
B.b.4 Stripping of Heavy Ion Beam
B.b.5 Alignment of Indirect Heavy Ion Target

Description of Required R&D Efforts - Three types of R&D experiments are required to solve the problems identified in the corresponding Critical Issue #5:[1]

(1) Development of cost effective techniques and demonstrations of space charge-limited transport of a bunched heavy ion beam through an accelerator,
(2) Development of cost effective techniques and design of high current storage rings for heavy ion beams, and
(3) Minimization of Metglas losses to raise the accelerator efficiency.

Each of these required R&D efforts is briefly described below:

R&D Demonstration of Space Charge-Limited Transport of a Bunched Beam - Experiments and computer simulations have shown that transporting beams for several kilometers at their space charge limit should be possible, with little emittance growth. However, this HI beam transport has only been demonstrated with low energy, low power, unbunched beams. It is necessary to demonstrate transport at high σ_0 (undepressed tune), low σ (depressed tune), continually bunching the HI beam to increase current as voltage increases.

If the HI beams have to be transported at currents lower than the space charge limit, then the accelerator will have to have a longer pulse (in the case of a single beam LINAC) or more quadrupole transport channels within the same multiple beam accelerator, thereby increasing the cost of the accelerator.

R&D Demonstrations of High Current Storage Rings for Heavy Ion Beams - One of the characteristic properties of linear accelerators is their ability to run at rather high average powers and relatively high repetition rates. Since the clearing time in the ICF reactor precludes very high repetition rates for the DT pellet ignition, the LINAC is forced to operate at uneconomical repetition rates. This problem can be eliminated if the beams for the LINAC can be stored for a short period of time. By operating the induction LINAC in the burst mode, the induction cores are used over and over, and, of course, each core is therefore smaller in diameter.

The issue here is one of demonstrating that a HI beam of the required intensity can be stored in a storage ring for the requisite time, typically on the order of 1 to 2 milliseconds. The issues are similar to those associated with bunched beam transport, but have the additional complications associated with closed orbit synchrotrons, such as betatron and synchrotron resonances, etc., which can give rise to emittance growth or beam loss. Furthermore, beam induced vacuum instability is another problem which must be overcome. All of these issues can only be resolved with an experimental ring with parameters reasonably close to what is required.

R&D Experiments to Reduce Metglas Losses - The first type of loss in Metglas, that due to BH hysteresis losses may be intrinsic and is probably unavoidable, although further investigations into use of less hysteretic ceramic materials may be very useful. The second type is eddy current loss in the magnet cores which can be minimized by careful core design and attention to detail in proper pulse shaping of the current waveforms. The important physical parameter associated with the eddy current losses is the thickness of the Metglas ribbon and the shape and amplitude of the waveform used. Presently Metglas thicknesses of the order of 35 μ are being employed, although successful experiments have been carried out with Metglas thicknesses as small as 20 μ. By optimizing the voltage waveforms used to drive the beam and to reset the cores, the pulsed power requirements can be minimized.

Facility Requirements - In order to demonstrate the two key HI driver R&D issues, transport of a bunched, space charge-limited HI beam and demonstration of high current HI storage rings will require either the use of an existing suitable induction LINAC or the construction of a new facility capable of meeting the HI driver requirements of transporting megajoules of energy in doubly charged, non-relativistic ~5 GeV lead ions. Assuming typical accelerator gradients of the order of 1 MeV/m, an accelerator having dimensions of several kilometers will be required. In addition, approximately two dozen high current storage rings having diameters of the order of 50 m will be required to investigate technologies associated with achieving the required performance levels while minimizing the cost of the storage rings.

A significant demonstration of the HI beam transport and storage ring configuration could be carried out using a single pulse, a single ring, reduced energy (to possibly 0.5 GeV), pulsed magnets, etc. Such a facility could be installed in the Advanced Test Accelerator Site 300 facility at the Lawrence Livermore National Laboratory (LLNL) at a relatively small cost.

The requirements for the Metglas investigations are even more modest. The required R&D investigations to reduce Metglas losses can be carried out at a variety of accelerator facilities, such as those existing at the Lawrence Berkeley Laboratory (LBL), LLNL, Fermilab, Brookhaven National Laboratory, Argonne National Laboratory, etc.

Support of HI indirect-drive target experiments requires a full-scale HI driver, but a HI driver that runs at a relatively low repetition rate. Thus a major facility advantage would be a significant reduction in installed power requirements since the single beam LINAC would not need to operate at 5 Hz.

Cost and Schedule - The costs associated with carrying out the ambitious HI cost reduction R&D experiments are a strong function of whether or not it would be necessary to construct a new facility to meet the demanding HI driver requirements with regard to beam current, beam energy, particle energy, atomic weight of ions, etc. It is estimated that the total cost to build a conventional induction LINAC with two dozen storage rings to accomplish the R&D experiments would be of the order of $1000M. The experiments themselves would be relatively expensive if promising techniques for reducing cost required frequent rebuilding of the accelerator and storage rings. Such a facility could be constructed in five years once a suitable site had been selected. It would also be a very attractive solution to have this large HI driver facility support the related HI indirect drive target feasibility R&D experiments proposed as R&D Program #3.[2] It is estimated that significant Metglas development could continue at one or more accelerator facilities with a funding level of $1-2M/year. Additional experiments and costs are described below in Summary of R&D Cost Estimate.

Table 5.5-7 Cost Reduction in the Heavy Ion Driver R&D Task and Duration Estimates

No.	Task Description	Estimated Cost	Key Issue	R&D Duration
1	Demo DT Target Survivability in TC	$5 M	A.a.3	2 years
2	Demo Target Injection/Tracking	$10 M	A.b.1,B.a.3	3 years
3	Target Manufacturability	$10 M	B.b.1	3 years
5	Develop Bright Pb^{+2} Source	$10 M	B.b.1	3 years
6	Develop high brightness HI injector	$20 M	B.b.1	2 years
7	Demo low emittance through injector	$10 M	B.b.1	2 years
8	SP HI Pulse Synch. and Timing Demo	$10 M	B.b.1	3 years
9	SP Triplet Focusing Demo	$10 M	B.b.2	2 years
10	SP HI Channel Formation Demo	$100 M	B.b.2	7 years
11	SP Injection of HI Beam in Channel	$10 M	B.b.3	3 years
12	SP Demo of Channel Transport @ MA	$50 M	B.b.3	5 years
13	SP HI Beam Stripping	$20 M	B.b.4	2 years
14	SP HI Neutralization	$5 M	B.b.4	1 year
15	Develop high PRF burst-mode pwr.sup.	$30 M	B.b.3	2 years
16	Demo superconducting quadrupoles	$20 M	B.b.3	3 years
17	Demo storage ring performance	$50 M	B.b.3	3 years
18	Demo bunchers	$25 M	B.b.3	3 years
19	Develop HID Computer Control System	$20 M	B.b.5	5 years
20	Alignment of HI Beam to ID Target	$400 M	B.b.5	10 years
	Total Heavy Ion R&D Costs	$845M		

References for 5.5.3.5

1. Alfred Maschke, "ICFRDS Critical Issue #5: Cost Reduction for the Heavy Ion Driver," TRW S&TG/ATD, December 1991.

2. Gary Linford, Douglas Drake, and Dan Driemeyer, "Research and Development for Critical Issue #3: Feasibility of Indirect Drive for Heavy Ion," IFERDS, MDA, January 1992.

5.5.3.6 R&D for Demonstration of High Overall Laser System Efficiency

(Relevant Key Issues: B.a.1, B.a.2, B.a.3, B.a.5)

Description of Problem - As discussed in Critical Issue #6,[1] the inertial fusion energy (IFE) excimer laser driver system is composed of a number of components which can individually be optimized to yield high efficiencies. The achievement of high operating efficiency is a crucial requirement for the laser driver. Another crucial goal is the development of highly reliable laser driver components. A laser driver that frequently fails will not permit economical IFE reactor operation to be achieved.

The MDA Team Prometheus Reactor Design Study KrF laser driver consists of the following four major elements:

(1) The excimer laser amplifiers
(2) The Raman accumulators
(3) The SBS pulse compressors
(4) The computer controlled and self-aligning linear optical train which directs the laser beams through the various optical components and down into the target chamber.

Significant research and developmental work needs to be performed on the excimer laser amplifier modules. Although there are still R&D issues to be settled, the latter three elements listed above require less additional technological development and experimental verification before they can be judged adequate to be incorporated into a mature laser driver design.

R&D work relevant to specific key issues associated with the Prometheus laser driver described here include:

B.a.1 DT Target Illumination Issues,
B.a.2 Large Laser Development and Bandwidth Issues,
B.a.3 Final Optics Pointing System,
B.a.5 SBS Pulse Compressor,

The Excimer Laser Amplifier Problem - The fundament of an efficient, reliable Prometheus laser driver is the successful design, construction, and testing of excimer laser amplifier modules. The MDA team has found that large excimer laser amplifiers producing >50 kJ of energy may prove to be undesirable for a reactor since the loss of a single excimer laser amplifier would prevent the ~1% direct drive (DD) target illumination uniformity requirement from being achieved. Furthermore, excimer laser amplifiers generating large (>50 kJ) energies also require excitation geometries of unwieldy (~2x2x4 m) dimensions, amplified spontaneous emission (ASE), and parasitic oscillations can reduce laser efficiencies, threaten the safety of the cryogenic target, and complicate the overall optical design of the laser driver. As a consequence, the MDA team has identified a moderate excimer laser amplifier output energy range (from 4 to 6 kJ) as being optimum for constructing an efficient, reliable, and safe IFE laser driver capable of tolerating an occasional amplifier failure without forcing reactor shutdowns. Each of these reduced scale excimer laser amplifiers has modest dimensions (0.3x0.3x2 m). This 4-6 kJ energy level, however, is much lower than the ~100 kJ needed for each of the 60 laser driver beamlines. In order to achieve the requisite beam energies (~100 kJ), the MDA team has selected to combine many excimer beams coherently using Raman accumulators.

During the past five years, relatively little work has been carried out in the USA with regard to improving the efficiency and the reliability of such moderate sized excimer laser amplifiers. Some analytical studies[2] have been carried out on both electron-

beam excited excimer lasers (EBEELs) and electron-beam sustained electric discharge lasers (EBSEDLs) which offered (on paper) gross wallplug efficiencies as high as 17%. These efficiencies, however, are more likely to be reduced significantly if incorporated into a large laser system architecture. The main concern is that no experimental work in excimer amplifier development is either currently in progress or planned by the Department of Energy.

Work in the Soviet Union with sliding discharge cathodes, plasma electrodes, and UV pre-ionization in both excimer and CO_2 discharge lasers has produced some promising results[3,4,5] which may offer alternatives to the EBSEDLs. Although significant experimental work needs to be carried out to demonstrate the potentially higher efficiency of EBSEDLs, the electric discharge lasers may offer an inherently higher efficiency than the EBEELs since excitation of the excimer species occur along the neutral channel, thereby avoiding the excitation of a large number of higher-lying states (which may contribute relatively little to the overall amplifier extraction efficiency) or which end up as excess heat which deleteriously affects excimer amplifier beam quality. Moreover, by avoiding transmitting large electron beam currents through foils, hibachis, etc., the overall excimer laser pumping efficiency may be significantly higher.

Raman Accumulator Problems - A key to achieving high efficiency with Raman accumulators is to start with a design that exhibits a high quantum efficiency, ξ, together with a large Raman gain coefficient, g_R. Stimulated rotational Raman gain in H_2 (or D_2) has been previously investigated and promises to fulfill the requirements for both ξ and g_R. Since the Raman accumulators are also expected to be operated in the crossed Raman configuration (to improve the beam quality of the output Stokes beam), some inefficiencies arise. The Raman accumulators need to be driven with a synchronized Stokes seed having appropriate temporal and spectral components. The primary R&D problem is to demonstrate efficient beam combination with high beam quality while suppressing parasitic oscillations and higher order Stokes components from being generated. Secondary Raman accumulator problems have to do with details associated with efficient generation of synchronized Stokes seeds which are correlated[6] with the excimer pump beams.

Problems Associated with the Stimulated Brillouin Pulse Compressor - The stimulated Brillouin scattering (SBS) process when applied to the problem of temporally compressing long (>250 ns) excimer/Raman accumulator laser pulses tends to produce subnanosecond pulses[2] with high efficiencies (>95%). When a longer pulse (such as the 6 ns main pulse specified by the TWG) is required, the needed compressed pulse length can be generated by a ramped-Stokes seeded SBS cell, but at considerable cost of overall efficiency. Since the sum of the energies of the compressed 6 ns pulse and the long undepleted (>250 ns) pulse is approximately 100% of the original long excimer/Raman accumulator pulse, the overall efficiency of the ramped-Stokes seeded SBS cell can be improved by utilizing the long,

undepleted pump pulse as the long precursor pulse to the target (as specified by the TWG).[7] The following operational details need to be demonstrated in an R&D program:

(1) Demonstration of the performance (efficiency, pulse shape versatility, etc.) of a ramped Stokes seeded SBS cell.
(2) Control over competing processes, parasitic oscillations, multi-order Stokes, etc.
(3) Demonstration of the use of an electro-optical switchyard, pulse delay lines, etc., for utilizing depleted pump as the precursor pulse.
(4) Performance of electro-optical "chirper" SBS Stokes seed generators.

Computer-Control and Alignment Problems - The computer control system must monitor an excimer master oscillator driving ~1000 excimer laser amplifier modules feeding into 60 Raman accumulators, 60 SBS pulse compressors, and 60 beam alignment systems attempting to strike a 6 mm diameter target moving at a speed of 200 m/sec., it is evident that a sophisticated parallel processing computer control system is required.

Description of Required R&D Efforts

Excimer Laser Amplifier R&D - R&D investigations of promising (efficient and reliable) designs of both electron beam excited excimer lasers (EBEELs) and electric-discharge excimer lasers (EDELs) need to be carried out.

EBEEL R&D - In the case of the EBEELs, the primary parameters to be demonstrated are reliability (mean number of shots between failures $>10^9$) and efficiency. Many of the color-center formation problems, chemical attack problems, etc., are similar to those described below for the EBELs.

EBSEDL R&D - Since the EBSEDL has received significantly less R&D in the past than the EBEEL, there are several problems associated with the EBSEDLs which require further experimental work. These include:

(1) Characterization of the optimum pulse duration and gas mixture to achieve efficient neutral channel excimer excitation with a matched, efficient, pulsed power system.
(2) Sensing and prevention of the formation of arcs in the discharges caused by consumption of fluorine, impedance changes, etc.
(3) Extension of the operating lifetimes of the amplifiers to reach levels of 10^9 to 10^{10} amplifier firings between failures.
(4) Control of color center formation and chemical attack of amplifier windows during the 10^9 to 10^{10} shot operational periods.

These problems need to be analyzed theoretically and solutions found experimentally during a series of R&D related technological development programs granted by DOE to industry and the national labs. The direct result of this R&D would permit the excimer laser amplifiers to become the workhorse of the Prometheus excimer laser driver by the year 2030.

R&D for Alternative Laser Drivers - R&D efforts to evaluate other efficient and reliable laser drivers should also be planned. These alternative IFE laser drivers could include:

(1) Semiconductor diode pumped solid-state lasers (λ = 1064 nm).
(2) Chemical oxygen-iodine lasers (λ = 1315 nm).
(3) HF overtone chemical lasers (λ ~ 1350 nm).

These lasers require implementation of high average power harmonic conversion technology to permit efficient operation in the UV portion of the spectrum, but the ultimate reliabilities of these alternative fusion laser drivers may be higher than can be achieved with either EBEELs or EBSEDLs.

Raman Accumulator R&D - The R&D program for the Raman accumulator is relatively simple and straightforward. It builds upon the extensive work already completed. Two types of Raman accumulator systems need to be addressed: single pulse and high repetition rate.

Single Pulse Raman Accumulator R&D - The following single pulse Raman accumulator tasks need to be addressed:

(1) Demonstration of efficient rotational Raman conversion in H_2 (or D_2).
(2) Demonstration of an effective (correlated) rotational Raman Stokes seed generator.
(3) Demonstration of intensity averaging and beam quality enhancement for crossed Raman accumulator geometries.
(4) Coherent, large aperture beam synthesis.
(5) Control of diffraction and egg-crate damage by image relay optics.

Although some of these tasks can be demonstrated at sub-scale energies, the most convincing single pulse Raman accumulator R&D plan would involve a full, 100 kJ beamline.

Repetition Rate Raman Accumulator R&D - These R&D experiments need to deal primarily with the gas circulation problems to remove the phonon heat from the H_2 (or D_2) gas without adversely affecting the accumulator beam quality.

SBS Pulse Compressor R&D - In a manner analogous to the Raman accumulator described above in Section 2.3, the SBS pulse compressor R&D needs to be divided between single pulse proof-of-principle experiments and high average power experiments dealing with control of thermal effects.

Single Shot SBS Pulse Compressor R&D - Both sub-scale and full scale single shot R&D SBS pulse compressor experiments need to be performed. The fundamental working principles of the SBS pulse compressor can be demonstrated in sub-scale experiments. These sub-scale experiments involve full scale physical lengths of the SBS cell ($L_{cell} = c\tau_{pump}/2$) but, to reduce costs, subapertures of perhaps 1/20 full aperture may be employed. These subscale SBS R&D experiments would include the following tasks:

(1) Demonstration of high pulse compression conversion efficiency using a self-seeded, "chirped" input Stokes SBS seed.[8]
(2) Demonstration of versatile SBS pulse compressor output pulse shapes by using a ramped "chirped" Stokes SBS seed, and
(3) Demonstration of the operating principles of an electro-optical "switchyard" involving fast Pockels cells to tailor the undepleted pump pulse into an 80 ns long precursor pulse.

These experiments could be carried out at convenient apertures (~5 cm) using pulse energies of 250 J and 250 ns durations.

In order to conduct the full scale SBS Pulse Compressor R&D experiments, it would be necessary to have large aperture pump beams containing ~100 kJ. The MDA IFERDS SBS Pulse Compressor design features a relatively large aperture, ~1 m. Although this large 1 m aperture can be synthesized from an array of smaller optics supported in an "egg-crate" structure. These full scale experiments would be similar to the sub-scale experiments with the additional feature that transverse SBS parasitics could be investigated as a potential problem.

High Average Power SBS Pulse Compressor R&D Experiments - As described above for the single shot SBS pulse compressor R&D experiments, both subaperture and full aperture high average power R&D experiments can be performed. Since the primary purpose of the high average power experiments is to investigate the influence of phonon-induced thermal effects in the SF_6-filled SBS cell, it is very likely that only subaperture high average power experiments would produce meaningful results for the relative costs.

Computer Control and Alignment R&D Experiments - The computer control and alignment R&D experiments need to cover all aspects of computer control and optical alignment of the MDA Prometheus laser driver system. A variety of techniques has been suggested for performing the difficult moving DT target tracking and alignment tasks using interferometric and holographic techniques. These proposed tracking and alignment techniques require extensive real time, fast response, data processing, possibly requiring a series of dedicated parallel processors, artificial intelligence, expert systems, etc. The R&D program would have to demonstrate adequate performance of these (and other) control designs.

Facility Requirements

Excimer Laser Amplifier R&D Facilities - The facilities required to evaluate the performance of moderate energy (4-6 kJ) excimer laser modules are relatively modest. Assuming these amplifiers were 10% efficient and operated at a pulse repetition rate of 5 Hz, power supplies of ~500 kW would suffice to power the test amplifier.

Since one of the key design issues to be demonstrated for these excimer laser modules, it is essential that a large number of amplifiers be tested in parallel at as high a repetition rate as reasonable. The facilities would have to be designed to accommodate automatic, 24-hour per day operation in order to permit the evaluation of mean number of amplifier firings between firings of 10^9 and 10^{10}.

Raman Accumulator R&D Facilities - The single shot subscale Raman accumulator R&D experiments can be performed with modest laboratory facilities.

The high average power Raman accumulator R&D experiments would require significant input powers from excimer pump amplifiers. If an entire single beam of the laser driver were to be tested, an input energy/pulse of approximately 100 kJ would be required, possibly in the form of either 25 (5x5) 4 kJ excimer laser modules or 16 (4x4) 5.5 kJ excimer laser modules. These experiments could be combined with tests of test excimer laser amplifiers to realize significant cost savings. The full scale Raman accumulators would have apertures of ~1 m and lengths of the order of 10 m.

SBS Pulse Compressor R&D Facilities - The single pulse, subaperture SBS pulse compressor R&D facilities can be performed in a modest laser facility having a long optical path (~50 m) available. For a square 5 cm aperture SBS cell pumped with a Raman accumulator pulse of duration 250 ns and energy of 250 J, a cell length of approximately 38 m would be required.

Full aperture, high average power SBS compressor R&D facilities are similar to those described above for the high average power Raman accumulator experiments with the

additional requirement that sufficient laboratory space be provided for the 38 m long SBS pulse compressor cells.

Computer Control and Alignment R&D Facilities - Relatively modest facilities are required to test the computer control and alignment facilities. Since the most stressing R&D task is the tracking of the moving DT targets, the testing of this capability could be combined with a facility used for testing the DT target launching system.

Cost and Schedule

Costs of Excimer Laser Amplifier R&D - It is estimated that a minimum of $20M and three years would be required to develop candidate excimer laser modules. Additional time and expense would be required to test the amplifiers to demonstrate 10^9 to 10^{10} firings between failures.

In order to demonstrate a single beam line, it would be necessary to construct between 20 and 40 of the excimer laser modules (depending upon their output energies), together with their associated pulsed power. It is estimated that this task would cost approximately $80M once an excimer laser amplifier design had been perfected.

Cost of Raman Accumulator R&D Experiments - Single pulse, subscale Raman accumulator R&D experiments can be performed for $2M. High repetition rate subscale Raman experiments would cost $7M. Combined with the construction of an array of NxN excimer amplifiers described in Section 4.1, above, a full aperture 1x1 m Raman accumulator could be tested for and additional $20M for a total of $100M (NxN excimer amplifiers + Raman accumulator). This would take an estimated five years from beginning to end.

Cost of SBS Pulse Compressor R&D Experiments - The subaperture single SBS pulse compressor experiments could be carried out for $4M over a two-year period. Full aperture, high average power tests of a full scale SBS pulse compressor could be carried out in association with construction of a NxN excimer laser pump array in (excimer laser modules) and a full aperture, high average power Raman accumulator (Raman Accumulator R&D) for an additional $20M for a total cost of $120M ($80M for the excimer lasers, $20M for the Raman experiments, and $20M for the SBS experiments). This is estimated to take eight years from beginning to end.

Cost of Computer Control and Alignment R&D Experiments - It is recommended that these R&D experiments be conducted subscale with the predominant emphasis on testing the target tracking and alignment system. This task is estimated to cost $20M in conjunction with a full scale DT target launching system.

Summary of R&D Cost Estimates

Table 5.5-8 Demonstration of High Overall Laser System Efficiency R&D Task and Duration Estimates

No.	Task Description	Estimated Cost	Key Issue	R&D Duration
1	Demo DD Target Beam Nesting	$10 M	B.a.1	3 years
2	Satisfy Bandwidth Requirements	$10 M	B.a.2	3 years
3	Laser Beam/Target Alignment System	$12 M	A.b.1,B.a.3	4 years
4	Final optics pointing demo	$5 M	A.b.1,B.a.3	3 years
5	Develop excimer laser modules	$20 M	B.a.2	3 years
6	Test to demonstrate 10^9 lifetime	$40 M	B.a.2	5 years
7	Demonstrate single 6 kJ beam line	$80 M	B.a.2	4 years
8	Demonstrate 6x16=96 kJ beam line	$120 M	B.a.2	2 years
9	Develop/Demo Laser Control System	$40 M	B.a.2	5 years
10	Develop 50 J Raman seed generators	$2 M	B.a.2	1 year
11	Demonstrate 6 kJ Raman converter	$1 M	B.a.2	1 year
12	Demo 100 kJ Raman converter	$20 M	B.a.2	2 years
13	Develop programmable SBS chirper	$2 M	B.a.5	1 year
14	Subscale SBS PC demonstration	$2 M	B.a.5	1 year
15	Develop Large Aperture SBS chirper	$10 M	B.a.5	3 years
16	Demo 6 kJ SBS Pulse Compressor	$5 M	B.a.5	2 years
17	Demonstrate 100 kJ PC	$20 M	B.a.5	3 years
18	Dev.Large Aperture Fast Pockels Cells	$20 M	B.a.5	5 years
	Total Laser Driver R&D Costs	$419M		

References for 5.5.3.6

1. Gary J. Linford, "Prometheus Critical Issue #6: Demonstration of High Overall Laser System Efficiency," TRW S&TG/ATD, December 1991.

2. "New Techniques for KrF Laser Fusion Systems," Interim Report for Los Alamos National Laboratory, pp. 2-70 through 2-72, Los Alamos, New Mexico, written by Dr. Mark Kushner, then at Spectra Technology, Inc., Seattle, Washington (1986).

3. V. Yu. Baranov, et al., "Use of a Discharge over a Dielectric Surface for Pre-ionization in Excimer Lasers," Sov. J. Quantum Electron., 11, pp. 42-45 (1981).

4. V. Yu. Baranov, et al., "UV-Pre-ionized Rare Gas Halide Lasers with Plasma Electrodes," Proceedings of the International Conference on Lasers 1981, pp. 968-974 (1981).

5. V. V. Apollonov, et al., "High Power Molecular Lasers Pumped by a Volume Self-Sustained Discharge," J. Opt. Soc. Am. B, 8, pp. 220-229, (1991).

6. Shirley J. Pfeifer, et al., "Final Report of the Raman Beam Combining Program," TRW E&DS, Redondo Beach, CA, and Northrop Research & Technology Center, Palos Verdes Peninsula, CA, Contract # F29601-85-c-0053 (September 1986) submitted to the Air Force Weapons Laboratory, AFSC, Kirtland Air Force Base, NM 87117.

7. Ronald C. Davidson (MIT) et al., "Inertial Confinement Fusion Reactor Design Studies Recommended Guidelines," prepared for the Department of Energy Office of Fusion Energy, Germantown, MD (September 1990).

8. Artur A. Mak and Leonid N. Soms, "Optical Methods for Laser Beam Control," Proceedings of SPIE, 1415, Modeling and Simulation of Laser Systems II, pp. 110-119 (1991).

5.5.3.7 R&D for Reliability and Lifetime of Laser and Heavy Ion Drivers

(Relevant Key Issues: A.a.1, A.b.1, B.a.1, B.a.2, B.a.3, B.a.4, B.a.5, B.b.1, B.b.2, B.b.3, B.b.4, B.b.5)

Description of Problem - Both the Laser Driver (LD) and Heavy Ion Drivers (HID) for an inertial fusion energy (IFE) reactor will be required to operate reliably at approximately a 5 Hz rate over extended periods of time (of the order of years) in order not to impact adversely the IFE reactor cost of electricity (COE). This reliability requirement (corresponding to λ 1.58 x 10^8 shots/year) calls for robust driver designs exhibiting either remarkable durability or capable of being repaired and maintained on-line without requiring IFE reactor shut-down. Each of these two driver designs exhibits different reliability problems, and these reliability problems will be briefly described below. R&D work relevant to specific key issues associated with the laser and target described here include: A.a.1, Direct Drive Target Coupling, A.b.1, Demonstration of Injection and Tracking of Targets Coupled with Beam Steering, B.a.1, DT Target Illumination Issues, B.a.2, Large Laser Bandwidth Issues, B.a.3, Final Optics Pointing System, B.a.4, Grazing Incidence Mirror Damage, and B.a.5, SBS Pulse Compressor. Recommended R&D work relevant to key issues associated with the heavy ion driver include: B.a.1, Timing of Heavy Ion Beams, B.a.2, Heavy Ion Channel Formation, B.a.3, Heavy Ion Channel Transport, B.a.4. Stripping of HI Beam, and B.a.5, Alignment of Indirect HI Target.

KrF Laser Driver Lifetime Issues - The primary lifetime problem to be solved for the KrF excimer laser driver (LD) is associated with the pulsed excimer laser amplifiers. Secondary reliability problems associated with damage protection for optical components, gas circulation systems for Raman accumulators, etc., which require relatively little R&D to improve.

Two types of excimer laser amplifiers have been considered for the Prometheus IFERDS KrF laser driver: e-beam excited excimer laser amplifiers (EBEELs) and e-beam sustained electric discharge excimer lasers (EBSELs). The former has been subjected to substantial research and development but the latter (EBSELs) need substantial further development before the technology could be described as mature.

Our current data on the mean number of EBEEL firings between failures indicates that this type of excimer laser amplifier is currently not capable of meeting a $2x10^8$ firings between failures. The second type of excimer laser, EBSEL, has no significant experimental data regarding reliability, but the EBSEL theoretically appears to be potentially more reliable since the e-beams are not required to operate at high current through foils, hibachis, etc. The MDA Prometheus team selected a excimer laser/Raman accumulator driver which could tolerate occasional (one per month) failures of individual amplifier modules without compromising overall IFE reactor operation.

As a key KrF laser driver reliability issue, the Prometheus team has found that large excimer laser amplifiers producing >50 kJ of energy may prove to be undesirable for a IFE reactor since the loss of a single excimer laser amplifier would prevent the ~1% direct drive (DD) target illumination uniformity requirement from being achieved. Furthermore, excimer laser amplifiers generating large (>50 kJ) energies also require excitation geometries of unwieldy (~2x2x4 m) dimensions, amplified spontaneous emission (ASE), and parasitic oscillations can reduce laser efficiencies, threaten the safety of the cryogenic target, and complicate the overall optical design of the laser driver. As a consequence, the MDA team has identified a moderate excimer laser amplifier output energy range (from 4 to 6 kJ) as being optimum for constructing an efficient, reliable, and safe IFE laser driver capable of tolerating an occasional amplifier failure without forcing reactor shutdowns. Each of these reduced scale excimer laser amplifiers has modest dimensions (0.3x0.3x2 m). This 4-6 kJ energy level, however, is much lower than the ~100 kJ needed for each of the 60 laser driver beamlines. In order to achieve the requisite beam energies (~100 kJ), the MDA team has selected to combine many excimer beams coherently using Raman accumulators. R&D experiments improving the performance of Raman accumulators have been recommended,[1] but since the reliabilities of these devices are well established, no additional R&D is required to increase the reliabilities of the Raman accumulators further.

During the past five years, little or no research has been carried out in the USA with regard to improving the efficiency and the reliability of 4-6 kJ excimer laser amplifiers. Some analytical studies[2] have been carried out on both electron-beam excited excimer lasers (EBEELs) and electron-beam sustained electric discharge lasers (EBSEDLs) which offered (on paper) gross wallplug efficiencies as high as 17%. These efficiencies, however, are more likely to be reduced significantly if incorporated into a large laser system architecture.

Work in the Soviet Union with sliding discharge cathodes, plasma electrodes, and UV pre-ionization in both excimer and CO_2 discharge lasers has produced some promising results[3,4,5] which may offer alternatives to the EBSEDLs. Although significant experimental work needs to be carried out to demonstrate the potentially

higher efficiency of EBSEDLs, the electric discharge lasers may offer an inherently higher reliability and efficiency than the EBEELs since excitation of the excimer species occur via an electric discharge along the neutral channel, thereby avoiding the excitation of a large number of higher-lying states (which may contribute relatively little to the overall amplifier extraction efficiency) or which end up as excess heat which deleteriously affects excimer amplifier beam quality. Moreover, by avoiding transmitting large electron beam currents through foils, hibachis, etc., the overall excitation efficiency of the excimer laser can be increased while, at the same time, eliminating a potential failure mode (i.e., foil rupture). The fundament of an efficient, reliable Prometheus laser driver is the successful design, construction, and testing of excimer laser amplifier modules.

Heavy Ion Driver Lifetime Problems - Although the HID basic accelerator technology is well developed, the beam physics is tractable, and existing accelerator systems have exhibited 25-year lifetimes with 95% availabilities, there are a number of unanswered questions associated with improving known weak links in the HID. Unlike the laser system, failure of almost any single component of the HID is likely to provoke a complete shutdown of the IFE reactor. A major lifetime problem to be solved for the HID has to do with analyzing to what extent redundant or backup systems could be implemented to prevent HID failure and consequent reactor shutdown.

There are a number of HID problems which should be investigated:

(1) High reliability high brightness, doubly charged lead source
(2) Reliability of helium refrigerators, cryostats, and individual magnets for superconducting magnets
(3) Reproducibility of space charge limited transport of a bunched beam
(4) Long term stabilities of high current storage rings for heavy ion beams
(5) Reliability of Metglas to breakdown and long term deterioration

Description of Required LD and HID R&D Efforts - The R&D requirements for each of these HID problems is briefly discussed below.

Excimer Laser Amplifier R&D - R&D investigations of reliable and efficient designs of both electron beam excited excimer lasers (EBEELs) and e-beam sustained electric-discharge excimer lasers (EBSEDLs) need to be carried out. If funding is restricted, emphasis should be given the development of EBSEDLs since they promise to be more reliable and efficient.

EBEEL R&D - In the case of the EBEELs, the primary parameters to be demonstrated are reliability (mean number of shots between failures $>10^9$) and efficiency. Many of the color-center formation problems, chemical attack problems, etc., are similar to those described below for the EBELs.

EBSEDL R&D - Since the EBSEDL has received significantly less R&D in the past than the EBEEL, there are several problems associated with the EBSEDLs which require further experimental work. These include:

(1) Characterization of the optimum pulse duration and gas mixture to achieve reliable, efficient neutral channel excimer excitation with a matched, efficient, pulsed power system.
(2) Sensing and prevention of the formation of arcs in the discharges caused by consumption of fluorine, impedance changes, etc.
(3) Extension of the operating lifetimes of the amplifiers to reach levels of 10^9 to 10^{10} amplifier firings between failures.
(4) Control of color center formation and chemical attack of amplifier windows during the 10^9 to 10^{10} shot operational periods.

These problems need to be analyzed theoretically and solutions found experimentally during a series of R&D related technological development programs granted by DOE to industry and the national labs. The direct result of this R&D would permit the excimer laser amplifiers to become the workhorse of the Prometheus excimer laser driver by the year 2030.

R&D for Alternative Laser Drivers - Extremely reliable pulsed excimer laser amplifiers may prove difficult to construct. Thus R&D efforts to evaluate other efficient and potentially more reliable laser drivers should also be planned. These alternative IFE laser drivers could include:

(1) Semiconductor diode pumped solid-state lasers (λ = 1064 nm).
(2) Chemical oxygen-iodine lasers (λ = 1315 nm).
(3) HF overtone chemical lasers (λ ~ 1350 nm).

None of these alternative laser sources requires the use of high voltage, pulsed power. These near infrared lasers require implementation of high average power harmonic conversion technology to permit efficient operation in the UV portion of the spectrum, but the ultimate reliabilities of these alternative fusion laser drivers may be higher than can be achieved with either EBEELs or EBSEDLs.

R&D Reliability Demonstration Experiments for Heavy Ion Driver - Five types of R&D experiments are required to solve the HID potential reliability problems identified above:

(1) Development of a reliable, high brightness, doubly charged lead ion source.
(2) Demonstration of a highly reliable (possibly redundant) helium refrigeration system, serviceable cryostats, dependable magnets.

(3) Development of reliable, cost effective techniques and demonstrations of space charge-limited transport of a bunched heavy ion beam through an accelerator.
(4) Development of reliable, cost effective techniques and design of high current storage rings for heavy ion beams.
(5) Minimization of Metglas deterioration while minimizing losses to raise the accelerator efficiency.

Each of these required R&D efforts is briefly described below:

Reliable R&D High Brightness Pb^{++} Ion Development - At the present time, no reliable high brightness doubly charged lead ion source is available for providing input to the ramp gradient section of the HID. Redundant systems are recommended here in order to eliminate single point ion-source failures.

R&D Effort for Cryogenic Superconducting Magnets - Although considerable experience has been gained constructing superconducting magnets, it is crucial to perform R&D development experiments on redundant systems wherever possible to provide a fail-safe capability for the superconducting magnets.

These R&D experiments must provide a sufficient data base to permit the mean time between failures to be calculated for the superconducting magnet system.

R&D Demonstration of Reliable Space Charge-Limited Transport of a Bunched Beam - Past experiments and computer simulations have shown that transporting beams for several kilometers at their space charge limit should be possible, with little emittance growth. The key reliability issue has to do with the fluctuations that may occur in beam current from pulse to pulse. In addition the relative beam currents associated with each of the separate beams circulating in the storage rings need to be measured and equalized. In general it is necessary to demonstrate transport at high σ_0 (undepressed tune), low σ (depressed tune), continually bunching the HI beam to increase current as voltage increases.

If the HI beams have to be transported at currents lower than the space charge limit, then the accelerator will have to have a longer pulse (in the case of a single beam LINAC) or more quadrupole transport channels within the same multiple beam accelerator, thereby increasing the cost of the accelerator. The impact of this operational mode on the pulse to pulse equality of beam currents needs to be determined.

Operation of the LINAC at rather high average powers and relatively high repetition rates may affect the pulse to pulse performance of the system. This variation from pulse to pulse needs to be determined and compared with the tolerable limit on

possible beam steering once half the beams are combined in the self-focused channel. Since the clearing time in the ICF reactor precludes very high repetition rates for the D/T pellet ignition, the LINAC is forced to perate at uneconomical repetition rates. By operating the induction LINAC in the burst mode, the induction cores are used over and over, and, of course, each core is therefore smaller in diameter. The reliability of operating the LINAC in the burst mode needs to be demonstrated.

R&D Demonstrations of High Current Storage Rings for Heavy Ion Beams - The key reliability issues here have to do with demonstrating that HI beams can be reproducibly stored in rings for times typically on the order of 1 to 2 milliseconds. The reliability issues are similar to those associated with bunched beam transport, but have the additional complications associated with closed orbit synchrotrons, such as betatron and synchrotron resonances, etc., which can give rise to emittance growth, variations in beam current or outright beam loss. Furthermore, beam induced vacuum instability is another problem which must be overcome in order for long-term stability of the HI driver to be achieved. All of these issues can only be resolved with extensive experiments conducted an experimental ring with parameters reasonably close to what is required.

R&D Experiments to Increase Metglas Reliability While Minimizing Losses - Given the fact that the Metglas is going to be located in an excoriating radiation environment, it is possible that the Metglas will gradually deteriorate until its performance is marginal or until dielectric breakdown in the Metglas begins to occur. It needs to be determined if radiation-resistant Metglas compositions are also efficient, particularly with regard to the two possible types of losses. The first type of loss in Metglas, that due to BH hysteresis losses may be intrinsic and is probably unavoidable, although further investigations into use of less hysteretic ceramic materials may be very useful. The second type is eddy current loss in the magnet cores which can be minimized by careful core design and attention to detail in proper pulse shaping of the current waveforms. The important physical parameter associated with the eddy current losses is the thickness of the Metglas ribbon and the shape and amplitude of the waveform used. Presently Metglas thicknesses of the order of 35 μ are being employed, although successful experiments have been carried out with Metglas thicknesses as small as 20 μ. By optimizing the voltage waveforms used to drive the beam and to reset the cores, the pulsed power requirements can be minimized.

Experiments and computer simulations have shown that transporting beams for several kilometers at their space charge limit should be possible, with little emittance growth. However, this HI beam transport has only been demonstrated with low energy, low power, unbunched beams. If the HI beams have to be transported at currents lower than the space charge limit, then the accelerator will have to have a longer pulse (in the case of an induction LINAC) or more quadrupole transport

channels within the same accelerator, thereby increasing the cost of the accelerator. The effect of beam current vs. HID reliability needs to be evaluated.

R&D Facility Requirements - Unique R&D facilities for both KrF laser and heavy ion driver experiments need to be provided. Since the needs of these two drivers are very different from one another, two separate facilities would be needed for reliability evaluations.

Excimer Laser Amplifier R&D Facilities - The facilities required to evaluate the reliabilities of moderate energy (4-6 kJ) excimer laser modules are relatively modest. Assuming these amplifiers were 10% efficient and operated at a pulse repetition rate of 5 Hz, power supplies of ~500 kW would suffice to power the test amplifier.

Since the KrF laser amplifier reliability is one of the key design issues to be demonstrated for these excimer laser modules, it is essential that a large number of amplifiers be tested in parallel at as high a repetition rate as reasonable. The facilities would have to be designed to accommodate automatic, 24-hour per day operation in order to permit the evaluation of mean number of amplifier firings between firings of $\sim 10^9$.

HID R&D Reliability Facility Requirements - In order to demonstrate the two key HI driver R&D issues, reliable transport of a bunched, space charge-limited HI beam and demonstration of reliable high current HI storage rings will require either the extensive modification of an existing induction LINAC or the construction of a new facility capable of meeting the HI driver requirements of transporting megajoules of energy in doubly charged, non-relativistic ~5 GeV lead ions. Assuming typical accelerator gradients of the order of 1 MeV/m, an accelerator having dimensions of several kilometers will be required. In addition, approximately two dozen high current storage rings having diameters of the order of 50 m will be required to investigate technologies associated with achieving the required performance levels while minimizing the cost of the storage rings.

A significant demonstration of the HI beam transport and storage ring configuration could be carried out using a single pulse, a single ring, reduced energy (to possibly 0.5 GeV), pulsed magnets, etc. Such a facility could be installed in the Advanced Test Accelerator Site 300 facility at the Lawrence Livermore National Laboratory (LLNL) at a small cost.

The requirements for the Metglas investigations are even more modest. The required R&D investigations to reduce Metglas losses can be carried out at a variety of accelerator facilities, such as those existing at the Lawrence Berkeley Laboratory (LBL), LLNL, Fermilab, Brookhaven National Laboratory, Argonne National Laboratory, etc. Support of HI indirect-drive target experiments requires a full-scale HI driver, but a HI driver that runs at a relatively low repetition rate. Thus a major facility advantage would be a significant reduction in installed power requirements since the single beam LINAC would not need to operate at 5 Hz.

Costs and Schedules

Costs of Excimer Laser Amplifier R&D - It is estimated that a minimum of $20M and three years would be required to develop candidate excimer laser modules. Additional time and expense would be required to test the amplifiers to demonstrate 10^9 to 10^{10} firings between failures. In order to demonstrate a single beam line, it would be necessary to construct between 20 and 40 of the excimer laser modules (depending upon their output energies), together with their associated pulsed power. It is estimated that this task would cost approximately 80 M$ once an excimer laser amplifier design had been perfected. Additional experiments and costs are described in Chapter 6.

HI R&D Reliability Experiments Cost and Schedule - The costs associated with carrying out the ambitious HI cost reduction R&D experiments are a strong function of whether or not it would be necessary to construct a new facility to meet the demanding HI driver requirements with regard to beam current, beam energy, particle energy, atomic weight of ions, etc. It is estimated that the total cost to build a conventional induction LINAC with two dozen storage rings to accomplish the R&D experiments would be of the order of $500M. The experiments themselves would be relatively expensive if promising techniques for reducing cost required frequent rebuilding of the accelerator and storage rings. Such a facility could be constructed in five years once a suitable site had been selected. It would also be a very attractive solution to have this large HI driver facility support the related HI indirect drive target feasibility R&D experiments proposed as R&D Program #3.[5] Significant Metglas development could continue at one or more accelerator facilities with a funding level of $1-2M/year. Additional experiments and costs are described below in Summary of R&D Cost Estimates.

Table 5.5-9 Reliability and Lifetime for Laser Driver R&D Task and Duration Estimates

No.	Task Description	Estimated Cost	Key Issue	R&D Duration
1	Demo DD Target Beam Nesting	$10 M	B.a.1	3 years
2	Satisfy Bandwidth Requirements	$10 M	B.a.2	3 years
3	Laser Beam/Target Alignment System	$12 M	A.b.1,B.a.3	4 years
4	Demo DD MJ DT Target Ignition*	$400 M	A.a.1,B.a.1	10 years
5	Final optics pointing demo	$5 M	A.b.1,B.a.3	3 years
6	Optics Damage Resistance Demo	$5 M	B.a.4	3 years
7	Develop Robust GIMM	$5 M	B.a.4	4 years
8	Develop excimer laser modules	$20 M	B.a.2	3 years
9	Test to demonstrate 10^9 lifetime	$40 M	B.a.2	5 years
10	Demonstrate single 6 kJ beam line	$80 M	B.a.2	4 years
11	Demonstrate 6x16=96 kJ beam line	$120 M	B.a.2	2 years
12	Develop/Demo Laser Control System	$40 M	B.a.2	5 years
13	Develop 50 J Raman seed generators	$2 M	B.a.2	1 year
14	Demonstrate 6 kJ Raman converter	$1 M	B.a.2	1 year
15	Demo 100 kJ Raman converter	$20 M	B.a.2	2 years
16	Develop programmable SBS chirper	$2 M	B.a.5	1 year
17	Subscale SBS PC demonstration	$2 M	B.a.5	1 year
18	Develop Large Aperture SBS chirper	$10 M	B.a.5	3 years
19	Demo 6 kJ SBS Pulse Compressor	$5 M	B.a.5	2 years
20	Demonstrate 100 kJ PC	$20 M	B.a.5	3 years
21	Dev.Large Aperture Fast Pockels Cells	$20 M	B.a.5	5 years
	Total Laser Driver R&D Costs	$829M		

*Includes cost of Nova Upgrade.

Table 5.5-10 Reliability and Lifetime for Heavy Ion Driver R&D Task and Duration Estimates

No.	Task Description	Estimated Cost	Key Issue	R&D Duration
1	Demo Single Accel. in Burst Mode	$15 M	B.b.1	3 years
2	Develop Bright Pb^{+2} Source	$10 M	B.b.1	3 years
3	Develop high brightness HI injector	$20 M	B.b.1	2 years
4	Demo low emittance through injector	$10 M	B.b.1	2 years
5	SP HI Pulse Synch. and Timing Demo	$10 M	B.b.1	3 years
6	SP Triplet Focusing Demo	$10 M	B.b.2	2 years
7	SP HI Channel Formation Demo	$100 M	B.b.2	7 years
8	SP Injection of HI Beam in Channel	$10 M	B.b.3	3 years
9	SP Demo of Channel Transport @ MA	$50 M	B.b.3	5 years
10	SP HI Beam Stripping	$20 M	B.b.4	2 years
11	SP HI Neutralization	$5 M	B.b.4	1 year
12	Develop high PRF burst-mode pwr.sup.	$30 M	B.b.3	2 years
13	Demo superconducting quadrupoles	$20 M	B.b.3	3 years
14	Demo storage ring performance	$50 M	B.b.3	3 years
15	Demo bunchers	$25 M	B.b.3	3 years
16	Develop HID Computer Control System	$20 M	B.b.5	5 years
17	Alignment of HI Beam to ID Target	$400 M	B.b.5	10 years
	Total Heavy Ion R&D Costs	$805M		

References for 5.5.3.7

1. Gary J. Linford at TRW/ATD and Dan Driemeyer MDA, "R&D for Critical Issue #6: Demonstration of High Overall Laser System Efficiency," January 1992.

2. "New Techniques for KrF Laser Fusion Systems," Interim Report for Los Alamos National Laboratory, pp. 2-70 through 2-72, Los Alamos, New Mexico, written by Dr. Mark Kushner, then at Spectra Technology, Inc., Seattle, Washington (1986).

3. V. Yu. Baranov, et al., "Use of a Discharge over a Dielectric Surface for Pre-ionization in Excimer Lasers," Sov. J. Quantum Electron., 11, pp. 42-45 (1981).

4. V. Yu. Baranov, et al., "UV-Preionized Rare Gas Halide Lasers with Plasma Electrodes," Proceedings of the International Conference on Lasers 1981, pp. 968-974 (1981).

5. V. V. Apollonov, et al., "High Power Molecular Lasers Pumped by a Volume Self-Sustained Discharge," J. Opt. Soc. Am. B, 8, pp. 220-229, (1991).

6. Alfred Maschke, Gary Linford, and Steven Fornaca, "R&D for Critical Issue #5: Cost Reduction for the Heavy Ion Driver," TRW S&TG/ATD, January 1992.

5.5.3.8 R&D for Demonstration of Non-Linear Optical Laser Driver Architecture

(Relevant Key Issues: B.a.1, B.a.2, B.a.3, B.a.4, B.a.5.)

Description of Problem - As discussed in both Critical Issue #6 and #14,[1,2] the MDA inertial fusion energy (IFE) reactor design study (IFERDS) excimer laser non-linear optical (NLO) architecture is made up of NLO components which can be tailored to permit safe, efficient, and versatile operation of the laser driver.

The MDA Team Inertial Fusion Energy Reactor Design Study NLO architecture consists of two major devices:

(1) The Raman accumulators (used for beam combination in the crossed Raman [or CRAM configuration])
(2) The SBS pulse compressors

Although there are still NLO R&D issues to be settled, the physics of both the Raman accumulators and the SBS pulse compressors is well understood. R&D work relevant to specific key issues associated with the Prometheus laser driver described here include:

B.a.1 DT Target Illumination Issues,
B.a.2 Large Laser Development and Bandwidth Issues,
B.a.3 Final Optics Pointing System,
B.a.4 Grazing Incidence Mirror Damage,
B.a.5 SBS Pulse Compressor,

R&D CRAM Accumulator Problems - A key to achieving high efficiency with Raman accumulators is to start with a design that exhibits a high quantum efficiency, ξ, together with a large Raman gain coefficient, g_R. Stimulated rotational Raman gain in H_2 (or D_2) has been previously investigated and promises to fulfill the requirements for both ξ and g_R. Since the Raman accumulators are also expected to be operated in the CRAM configuration (to improve the beam quality of the output Stokes beam), some inefficiencies arise. The Raman accumulators need to be driven with a synchronized Stokes seed having appropriate temporal and spectral components. The major R&D problems are to demonstrate:

(a) Efficient beam combination
(b) Achievement of high beam quality
(c) Suppression of higher order Stokes orders from being generated
(d) Pump intensity averaging
(e) Suppression of parasitic oscillations

Secondary Raman accumulator problems have to do with details associated with efficient generation of synchronized Stokes seeds which are correlated[3] with the excimer pump beams.

R&D Problems Associated with the Stimulated Brillouin Pulse Compressor - When the stimulated Brillouin scattering (SBS) process is applied to the problem of temporally compressing long (>250 ns) excimer/Raman accumulator laser pulses, the SBS process tends to produce subnanosecond pulses[4] with high efficiencies (> 95%). When a longer pulse (such as the 6 ns main pulse specified by the TWG)[5] is required, the needed compressed pulse length can be generated by a ramped-Stokes seeded SBS cell, but at considerable cost of overall efficiency. Since the sum of the energies of the compressed 6 ns pulse and the long undepleted (>250 ns) pulse is approximately 100% of the original long excimer/Raman accumulator pulse, the overall efficiency of the ramped-Stokes seeded SBS cell can be improved by utilizing the long, undepleted pump pulse as the long precursor pulse to the target (as specified by the TWG).[5] The following operational details need to be demonstrated in an R&D program:

(1) Demonstration of the performance (efficiency, pulse shape versatility, etc.) of a ramped Stokes seeded SBS cell.
(2) Control over competing processes, parasitic oscillations, multi-order Stokes, etc.

(3) Demonstration of the use of an electro-optical switchyard, pulse delay lines, etc., for utilizing depleted pump as the precursor pulse.
(4) Performance of electro-optical "chirper" SBS Stokes seed generators.

Description of Required R&D Efforts

CRAM Accumulator R&D - The R&D program for the CRAM Raman accumulator is relatively simple and straightforward. It builds upon the extensive work already completed. Two types of Raman accumulator systems need to be addressed: single pulse and high repetition rate.

Single Pulse CRAM Accumulator R&D

The following single pulse CRAM R&D accumulator tasks need to be addressed:

(1) Demonstration of efficient (> 80%) rotational CRAM conversion in H_2 (or D_2)
(2) Demonstration of an effective (correlated) rotational CRAM Stokes seed generator
(3) Demonstration of excimer pump beam intensity averaging and beam quality enhancement for CRAM accumulator geometries
(4) Coherent, large aperture beam synthesis
(5) Control of diffraction and egg-crate damage by image relay optics.

Although some of these R&D tasks can be demonstrated at sub-scale energies, the most convincing single pulse Raman accumulator R&D plan would involve a full, 100 kJ beamline.

High Repetition Rate CRAM Accumulator R&D - These CRAM R&D experiments need to deal primarily with the gas circulation problems to remove the phonon heat from the H_2 (or D_2) gas without adversely affecting the accumulator beam quality.

SBS Pulse Compressor R&D - In a manner analogous to the Raman accumulator described above in CRAM Accumulator R&D, the SBS pulse compressor R&D experiments need to be divided between single pulse proof-of-principle experiments and high average power experiments dealing with control of thermal effects.

Single Shot SBS Pulse Compressor R&D - Both sub-scale and full scale single shot R&D SBS pulse compressor experiments need to be performed. The fundamental working principles of the SBS pulse compressor can be demonstrated in sub-scale experiments. These sub-scale experiments involve full scale physical lengths of the SBS cell ($L_{cell} = c\tau_{pump}/2$) but, to reduce costs, subapertures of perhaps 1/20 full aperture may be employed. These subscale SBS R&D experiments would include the following tasks:

(1) Demonstration of high pulse compression conversion efficiency using a self-seeded, "chirped" input Stokes SBS seed.[6]
(2) Demonstration of versatile SBS pulse compressor output pulse shapes by using a ramped "chirped" Stokes SBS seed.
(3) Demonstration of the operating principles of an electro-optical "switchyard" involving fast Pockels cells to tailor the undepleted pump pulse into an 80 ns long precursor pulse.

These experiments could be carried out at convenient apertures (~5 cm) using pulse energies of 250 J and 250 ns durations

In order to conduct the full scale SBS Pulse Compressor R&D experiments, it would be necessary to have large aperture pump beams containing ~100 kJ. The MDA SBS Pulse Compressor design features a relatively large aperture, ~1 m. Although this large 1 m aperture can be synthesized from an array of smaller optics supported in an "egg-crate" structure. These full scale experiments would be similar to the sub-scale experiments with the additional feature that transverse SBS parasitics could be investigated as a potential problem.

High Average Power SBS Pulse Compressor R&D Experiments - As described above for the single shot SBS pulse compressor R&D experiments, both subaperture and full aperture high average power R&D experiments can be performed. Since the primary purpose of the high average power experiments is to investigate the influence of phonon-induced thermal effects in the SF_6-filled SBS cell, it is very likely that only subaperture high average power experiments would produce meaningful results for the relative costs.

Facility Requirements

Raman Accumulator R&D Facilities - The single shot subscale Raman accumulator R&D experiments can be performed with modest laboratory facilities.

The high average power Raman accumulator R&D experiments would require significant input powers from excimer pump amplifiers. If an entire single beam of the laser driver were to be tested, an input energy/pulse of approximately 100 kJ would be required, possibly in the form of either 25 (5x5) 4 kJ excimer laser modules or 16 (4x4) 5.5 kJ excimer laser modules. These experiments could be combined with tests of test excimer laser amplifiers to realize significant cost savings. The full scale Raman accumulators would have apertures of ~1 m and gain lengths of the order of 10 m.

SBS Pulse Compressor R&D Facilities - The single pulse, subaperture SBS pulse compressor R&D facilities can be performed in a modest laser facility having a long optical path (~50 m) available. For a square 5 cm aperture SBS cell pumped with a

Raman accumulator pulse of duration 250 ns and energy of 250 J, a cell length of approximately 38 m would be required.

Full aperture, high average power SBS compressor R&D facilities are similar to those described above for the high average power Raman accumulator experiments with the additional requirement that sufficient laboratory space be provided for the 38-m long SBS pulse compressor cells.

Cost and Schedule

Cost of CRAM Accumulator R&D Experiments - Single pulse, subscale Raman accumulator R&D experiments can be performed for ~$2 M. High repetition rate subscale Raman experiments would cost $7M. Combined with the construction of an array of NxN excimer amplifiers described in Section 4.1, above, a full aperture 1x1 m CRAM accumulator could be tested for and additional $20M for a total of $100M (NxN excimer amplifiers + Raman accumulator). This would take an estimated five years from beginning to end.

Additional experiments and costs are described below in Summary of R&D Cost Estimates.

Cost of SBS Pulse Compressor R&D Experiments - The subaperture single SBS pulse compressor experiments could be carried out for $4M over a two-year period. Full aperture, high average power tests of a full scale SBS pulse compressor could be carried out in association with construction of a NxN excimer laser pump array in (CRAM Accumulator R&D Experiments) and a full aperture, high average power Raman accumulator (SBS Pulse Compressor R&D Experiments) for an additional $20M for a total cost of $120M ($80M for the excimer lasers, $20M for the Raman experiments, and $20M for the SBS experiments). This is estimated to take eight years from beginning to end. Additional experiments and costs are described below in Summary of R&D Cost Estimates.

Cost of Computer Control and Alignment R&D Experiments - It is recommended that these R&D experiments be conducted subscale with the predominant emphasis on testing the target tracking and alignment system. This task is estimated to cost $20M in conjunction with a full scale DT target launching system. Additional experiments and costs are described below in Summary of R&D Cost Estimates.

Table 5.5-11 Demonstration of Non-Linear Optical Laser Driver R&D Task and Duration Estimates

No.	Task Description	Estimated Cost	Key Issue	R&D Duration
1	Satisfy Bandwidth Requirements	$10 M	B.a.2	3 years
2	Laser Beam/Target Alignment System	$12 M	A.b.1,B.a.3	4 years
3	Final optics pointing demo	$5 M	A.b.1,B.a.3	3 years
4	Optics Damage Resistance Demo	$5 M	B.a.4	3 years
5	Develop excimer laser modules	$20 M	B.a.2	3 years
6	Test to demonstrate 10^9 lifetime	$40 M	B.a.2	5 years
7	Demonstrate single 6 kJ beam line	$80 M	B.a.2	4 years
8	Demonstrate 6x16=96 kJ beam line	$120 M	B.a.2	2 years
9	Develop/Demo Laser Control System	$40 M	B.a.2	5 years
10	Develop 50 J Raman seed generators	$2 M	B.a.2	1 year
11	Demonstrate 6 kJ Raman converter	$1 M	B.a.2	1 year
12	Demo 100 kJ Raman converter	$20 M	B.a.2	2 years
13	Develop programmable SBS chirper	$2 M	B.a.5	1 year
14	Subscale SBS PC demonstration	$2 M	B.a.5	1 year
15	Develop Large Aperture SBS chirper	$10 M	B.a.5	3 years
16	Demo 6 kJ SBS Pulse Compressor	$5 M	B.a.5	2 years
17	Demonstrate 100 kJ PC	$20 M	B.a.5	3 years
18	Dev.Large Aperture Fast Pockels Cells	$20 M	B.a.5	5 years
	Total Laser Driver R&D Costs	$414M		

References for 5.5.3.8

1. Gary J. Linford, "ICFRDS Critical Issue #6: Demonstration of High Overall Laser System Efficiency," TRW S&TG/ATD, December 1991.

2. Gary J. Linford, "ICFRDS Critical Issue #14: Demonstration of Non-Linear Optical Laser Driver Architecture," TRW S&TG/ATD and Dan Driemeyer, MDA, December 1991.

3. "Final Report of the Raman Beam Combining Program," Shirley J. Pfeifer, et al., TRW E&DS, Redondo Beach, CA, and Northrop Research & Technology Center, Palos Verdes Peninsula, CA, Contract # F29601-85-c-0053 (September 1986) submitted to the Air Force Weapons Laboratory, AFSC, Kirtland Air Force Base, NM 87117.

4. "New Techniques for KrF Laser Fusion Systems," Interim Report for Los Alamos National Laboratory, pp. 2-70 through 2-72, Los Alamos, New Mexico, written by Dr. Mark Kushner then at Spectra Technology, Inc., Seattle, Washington (1986).

5. "Inertial Confinement Fusion Reactor Design Studies Recommended Guidelines," Ronald C. Davidson (MIT) et al., prepared for the Department of Energy Office of Fusion Energy, Germantown, MD (September 1990).

6. "Optical Methods for Laser Beam Control," Artur A. Mak and Leonid N. Soms, Proceedings of SPIE, 1415, Modeling and Simulation of Laser Systems II, pp. 110-119 (1991).

5.5.4 R&D for the Cavity - This section contains the R&D for the cavity. This includes (1) first wall protection, (2) blanket, and (3) shield.

5.5.4.1 R&D Needs for First Wall Protection - A basic test plan for the first wall protection system has been devised, in which a number of parallel near-term tests are performed on separate or multiple issues, followed by a facility in which integrated cavity responses are simulated. Figure 5.5-1 shows a possible scenario for this test plan.

Near-term R&D tasks are best classified by the types of facilities required. The tasks areas include:

A. Film flow
B. Vapor behavior
C. Component structural responses
D. Material interactions
E. Blast simulation

Facility requirements can be very different for the different tests. Blast simulation is a treated as a separate R&D task even though it is not an issue itself. The ability to perform useful engineering testing prior to construction of an IFE fusion reactor depends greatly on the quality of the blast simulation available.

Following 10-15 years of separate and multiple effects testing, there is a strong need to construct a test facility which combines all of the interrelated factors which impact the feasibility of the cavity concept. Uncertainties in cavity behavior can not be resolved without combining film thermal hydraulics, vapor dynamics and structural responses.

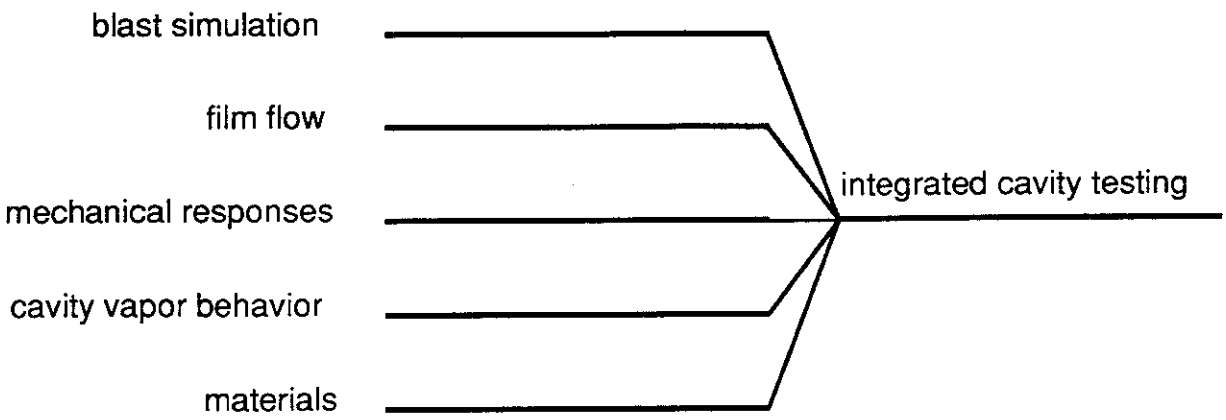

Figure 5.5-1. Testing Logic for the First Wall Protection System

A. Film Flow

Issue #E.a.5. Film flow control: injection, uniform thickness, and drainage
Issue #E.a.6. Film flow stability and response to impulsive loading

Description: Film flow is currently an active research area. Hydrodynamic behavior of films on vertical and curved surfaces is not fully-understood, particularly under the environmental conditions imposed on the Prometheus first wall. In addition, the unique materials and flow paths add uncertainties. In order to resolve issues related to film flow, both experiments and modeling are needed.

These experiments should demonstrate that adequate wall coverage can be attained to prevent first wall structure damage. This includes studies of film stability, development of effective injection and drainage systems, and film thickness control studies. Some specialized tests are needed. For example, the concept of MHD guiding to protect inverted surfaces should be explored. Transient response in the porous wall also requires study.

An active modeling effort will be very useful for this R&D task. There are many possible geometric configurations and component designs. Experimental data alone will validate a single design, but will be difficult to extrapolate to other designs.

Facility Requirements: These issues are grouped together because they can be addressed under a similar set of environmental conditions. Except for the issue of blast effects on film stability, blast simulation is not critical. Many tests can be performed without heating as well. The most important condition to simulate is flow geometry.

Several small-scale facilities can be envisioned. These would be devoted to separate flow issues, such as flow control, injector development, etc. The facilities would consist of a flow loop with process control and loop heaters. Test sections would be installed into the loops and tested. Combining these tests into a single loop facility may reduce costs, although the equipment costs in these tests are minimal. At least one small facility should have the capability to simulate blast pressure effects.

Cost and Time: A possible test plan involves four subtasks, as listed below. Time to perform the tests and cost estimates are also given. Sequential testing leads to a total test time of ~10 years.

Table 5.5-12 First Wall Protection R&D Task and Duration Estimates

R&D Task	Time Required	Facility Cost	Yearly Operating Cost
Film thickness control	3 yrs.	$200k	$100k
Flow on inverted surfaces	3 yrs.	$200k	$100k
Flow around obstructions	3 yrs.	$200k	$100k
Transient flow through porous structures	2 yrs.	$200k	$100k
Stability tests	5 yrs.	$500k	$200k
Injector development	5 yrs.	$2-5M	$1M

B. Cavity Vapor Response to Blast and Clearing Demonstration

Issue #E.a.1. Cavity vapor hydrodynamics
Issue #E.a.3. Vapor condensation rate
Issue #E.a.4. Radiation heat transport in partially-ionized gas

Description: Some models exist to predict the cavity vapor response to the blast (sometimes referred to as the "fireball"). The response includes blast energy deposition, vapor hydrodynamics and mass transport, thermal radiation, and evaporation/recondensation processes. Almost no experimental verification is available, such that confidence in the predictions is very low. Even if the models are accurate for idealized conditions, there are many potential non-ideal effects which could occur, and which are very difficult to accommodate in the models without empirical data. As data becomes available, more effort can be placed on model improvement.

A key to successful testing is to simulate the energy release characteristics from the target explosion. Without this, the responses may bear little resemblance to a real reactor. The experiments should measure the major responses, including time-dependent temperature, pressure, and heat and mass fluxes to the surface. Ideally,

one would measure spatial variations in these parameters. The tests should demonstrate that the time to clear the cavity allows for high repetition rates in a reactor.

Facility Requirements: The major facility for this R&D task consists of a relatively large cavity which represents the wall protection scheme to be tested and simulates the blast energy sources. Surface heating and bulk heating of the cavity vapor are most important, but bulk heating of the surface would be useful to simulate isochoric heating effects.

Since heat transfer to the coolant is a small source of uncertainty, the most important region to simulate is the surface facing the explosions. This surface should use prototypic materials, configurations and environmental conditions. The size of the cavity depends on the blast simulation. In principle, the most important conditions to simulate involve local intensity, and not the total yields. Rapid pulsing may not be required, but would help identify any cumulative effects due to multiple blasts.

Smaller experiments can be devised to address specific aspects of this issue; however, it is unclear how the source term could be reproduced in a small experiment. These might include small, focused tests of shock propagation, vapor condensation, radiation cooling rates and transport in partially ionized Pb, and specialized tests to explore non-ideal effects (multi-dimensional effects, droplet formation & behavior, etc.)

Cost and Time: - The larger integrated facility would be of the order of $10-20M to construct and $1-2M per year to operate.

(1) Separate-effects tests (e.g., shock propagation, vapor condensation, radiation transport and cooling rates, multi-dimensional effects, droplet formation and behavior) are expected to cost ~$100-200k each with annual operating budgets of the order of $100k. Assuming ten such tests, the total is $1.5M+$1M per year.
(2) A single multiple-effects cavity vapor test facility is estimated to cost $1-2M with annual operating cost of $250k.

The total time to complete this task is 10-15 years.

C. Cavity Structure Mechanical Response to Blast

Issue #E.a.2. Cavity structure mechanical response to blast

Description: The response to highly-transient loading in complex, engineered structures (i.e., SiC composites with Pb infiltration) is very uncertain. This issue is important to establish the survivability and lifetime of the solid structures which absorb the blast. Some useful information on failure modes will also be obtained. Assuming

the material properties, such as fatigue lifetime, are well-characterized, the tests do not necessarily have to be performed up to end-of-life. Tests must measure stress and strain in the structures, and run to enough cycles to identify major problem areas. Locations where stresses are highest should be more highly instrumented to ensure the design limits are not exceeded anywhere in the structures.

The structure geometry should be as close to prototypic as possible, including the mechanical support system. Scaling of the tests may be possible, but ultimately a full scale experiment should be performed. First wall panels in Prometheus are modular, such that even the full-scale tests would be only ~2 m × 2 m. The most important environmental condition to simulate is the pressure loading at the front of the wall. Methods to obtain prototypic impulsive loading without fusion explosions should be explored.

Facility Requirements: A range of tests is suggested, from specimen to large-scale tests. The pressure loading can be simulated with a combination of radiant heat deposited in a very short pulse, together with a gas shock. For the more integrated tests, a cavity is required to simulate the multiple shock waves that reflect off of the structures. More sophisticated sources may be needed. Source development is similar to the R&D task described above, except that rapid, continuous pulsing is more important in order to provide adequate cycles.

Cost and Time: A possible test plan involves 4 steps, as listed below. Time to perform the tests and cost estimates are also given. Sequential testing leads to a total test time of 10 years.

R&D Task	Time Required	Facility Cost	Yearly Operating Cost
Sub-scale tests	5 yrs.	$200k	$100k
Scale-model prototypes	5 yrs.	$1M	$500k
Panel tests	5 yrs.	$2M	$1M

D1. Pb/SiC Wettability

Issue #E.a.7. Pb/SiC Wettability

Description: Pb and SiC do not wet naturally. Poor wetting could render the wetted wall concept impractical. Surface modifications to the SiC (such as CVD impregnation with a metal) may provide a wettable surface. Tests should be conducted to determine methods to provide wetting (including fabrication issues), measure the contact angle, and study capillary behavior in porous materials.

Facility Requirements: Most of these tests can be performed without major new facilities.

Cost and Time:

	Test Time	Operating Cost
Fabrication	1-2 years	$250k/yr
Property measurements	2 years	$250k/yr
Capillary flow tests	2 years	$250k/yr

D2. Pb Compatibility with Steel

Issue #E.a.8. Pb Compatibility with Steel

Description: Corrosion of steel by Pb is not well-characterized. In Prometheus, the maximum first wall coolant temperature is determined, in part, by compatibility of Pb with the steel in the heat transport system. These tests should establish supportable temperature limits and explore methods to enhance the compatibility of Pb and steels. This might involve impurity control systems or modifications to the bulk or surface of the steel.

Facility Requirements: Two types of tests are considered: specimen and loop tests. Loop tests can be forced or natural convection. Facility needs are modest in either case. Flow loops are needed with heating and cooling capabilities. Post-test examination has the most demanding facility requirements, but several existing facilities are available.

Cost and Time:

	Equipment	Operating	Test Time
Specimen tests	$100k	$100k/yr	2 years
Loop tests	$500k	$250k/yr	3–5 years

E. Blast Simulation Development

Description: Due to the difficulties of using real pellet explosions as the source term, alternate methods of obtaining a good simulation of fusion explosions must be developed.

F. Partially Integrated Cavity Test Facility (Issues E.a.1–6)

Description: Film flow, cavity hydrodynamics, cavity clearing, and mechanical responses can and should be studied in separate facilities; however, the phenomena present in the cavity are highly interrelated. For example, proper loading conditions on the film and wall structures requires the presence of prototypical hydrodynamics. Cavity clearing depends to a large extent on the film thermal hydraulics. Many large uncertainties will remain until a cavity mock-up test is performed with all of the essential features present.

The ability to simulate the energy deposition from the blast is a critical issue for this facility. If appropriate non-nuclear pulsed energy sources are not feasible, then it may be necessary to perform these engineering tests in a nuclear facility with high-power drivers, targets, etc. The cost of such a facility may be quite high. A separate R&D program will be needed to develop alternative blast simulations. There is a need for both single-shot and repetitively-pulsed tests.

Facility Requirements: There is not sufficient information available to know the degree to which these tests can be scaled. As a minimum, cavities of 1-2 m in diameter will be required. Using prototypical surface power densities, at least 20-40 MW of pulsed power will be needed. A full coolant and film supply system is needed, as well as complete vacuum and impurity control system.

Cost and Time: This facility is a major element in the cavity R&D program. It integrates results from a large number of separate effects tests, and contains all of the necessary subsystems to validate acceptable cavity responses and clearing time.

The cavity or at least parts of it should be replaceable. These test component replacement costs are included in the operating budget. Cost estimates are as follows:

Equipment	Operating	Test Time
$50M	$5M/yr	10 yrs

5.5.4.2 R&D Needs for the Blanket - The blanket R&D needs for IFE solid breeder blankets are very similar to those for MFE solid breeder blankets since the

issues are the same. Reference 1 covers in reasonable details such needs. Here, only a brief description of the important uncertainties and R&D needs is given.

The most important uncertainties in the list of issues for solid breeder blankets relate to tritium breeding, tritium recovery, and breeder thermomechanical behavior. These are particularly large because: (1) there is limited understanding of gas transport in irradiated solids, (2) designs must keep the low thermal conductivity solid breeders within their respective temperature limits under substantial nuclear heating and neutron damage rates, and (3) the resulting designs have a significant amount of non-breeding structure and coolant. The primary safety uncertainties are associated with the behavior of the blanket under off-normal or transient conditions and to the control of tritium under normal conditions.

A coordinated program is needed to address the uncertainties associated with the solid breeder blanket issues. First a material development and characterization program is required. A series of single-effect or partially integrated types of experiments are then required to test either individual or group of issues. Finally, more integrated submodule-size experiments would address several issues. The write-up below gives a brief description of the major tasks required for such a program, following the above classification and listing in each case the solid breeder blanket issues being addressed.

Reference for 5.5.4.2

1. M. A. Abdou, et al., "Technical Issues and requirements of Experiments and Facilities for Fusion Nuclear Technology – FINESSE Phase 1 Report," PPG-909, UCLA-ENG-85-39, University of California, Los Angeles, December 1985.

Material Development and Characterization

(All Issues)

Description: The development of an attractive blanket depends strongly on the development of attractive solid breeder and structural materials. Material development refers to the process of identifying possible classes of materials, understanding the effects of material parameters, such as its microstructure and impurity content, and characterizing the material through measurement of its properties. This task is most effective when done early in the program, and has already been carried out for several years.

The most important needs are:

(1) Measurement of basic properties, such as thermal conductivity of different material forms, swelling and thermal stability, and characterization of the material microstructure. For the solid breeders, other measurements of particular interest include tritium diffusion parameters and tritium surface adsorption/desorption activation energies, while for the SiC composite of interest, tritium permeation needs to be fully characterized.
(2) Fabrication of different material forms, in particular sintered pellet and sphere pac forms for the solid breeders, and tube sheet form for the SiC composite.
(3) Understanding of the importance of the effect of various material parameters on the material properties.

Facility: No major new facility is required.

Cost and Time: The cost is about $12M/yr over about five years.

Neutronics and Tritium Breeding

Issue #E.b.1. Tritium self-sufficiency
Issue #E.b.9. Heat generation and power production

Description: Uncertainties here range from nuclear cross-section uncertainties to the heating profiles in the blanket and achievable tritium breeding ratio. The required tasks include measurement of the neutron spectra and reaction rates (tritium, heating, transmutations) under progressively more relevant blanket geometries to provide for verification of basic nuclear data, data libraries and neutronics analysis techniques. A well-calibrated 14-MeV neutron source is required. Point neutron source measurements have been made, and recently line source experiments have been initiated.

Facility: Existing 14-MeV neutron source facility, such as the one at JAERI, exist and are being used to address these issues. Verification of tritium self-sufficiency would require a fusion facility.

Cost and Time: The program consists of experiments on simple geometry for about three years, followed by experiments on blanket mock-ups for about three years. The capital cost for the test assembly is about $10M for the simple geometry and about $15M for the blanket mock up. The operating cost in both case is about $3M/yr.

Issue #E.b.2. Tritium Inventory and Recovery

Description: Predicting tritium behavior in solid breeder blankets requires understanding tritium transport, retention and chemical form in the breeder material under the influence of the fusion environment. Transport processes include intragranular diffusion, grain boundary diffusion, surface processes, diffusion through

interconnected porosity, and convection by the purge flow. Tritium retention processes include solubility, surface adsorption, and chemical and radiation trapping. The tritium behavior is influenced by many factors, such as temperature, purge gas composition and burnup.

A program of experiments and modeling studies is underway to address this issue. The experiments include:

(1) Laboratory experiments to characterize the microstructure and measure transport and surface properties of lithium ceramics, such as temperature controlled desorption experiments. These experiments are part of the material development and characterization task described above. The effort should be expanded in this area to provide better fundamental data for modeling application, in particular for the surface mechanism activation energies.
(2) Closed capsule experiments in fission reactors followed by controlled anneals in laboratories to address internal grain transport, surface desorption and trapping; some experiments also focus on single crystal specimens in which bulk diffusion tends to be particularly important and from which a better estimate of the diffusive properties of the materials can be obtained.
(3) In-situ tritium recovery experiments which consist of open, actively purged test capsule irradiated in a fission reactor. These tests explore the tritium behavior over a range of parameters, including temperature, temperature gradient, material characteristic, burnup, sweep gas composition and purge flow rate. Advanced in-situ tests would also include the partially integrated effects, such as breeder/clad interaction.

Over the last few years, a vigorous modeling effort has also been carried out in parallel and complementary to the experimental program, resulting in much progress in the understanding of tritium transport mechanisms and in the interpretation of experimental data. The effort needs to be pursued and to concentrate on mechanisms still poorly understood, such as dissolution and chemical and irradiation trapping.

Facility: No major new facility is required, since these experiments are carried out in existing fission reactors.

Cost and Time: Most of the tests are ongoing, except for advanced in-situ tests (which could be part of a more integrated nuclear submodule test). Efforts are still required to better characterize fundamental tritium transport mechanisms, in particular surface fluxes, and irradiation and chemical trapping. In parallel, a vigorous modeling effort should continue to help better understand, interpret and apply the results to blanket situations.

The cost estimates are about $15M for the capital cost of test assemblies, and about $8M/yr as overall operating costs over eight years.

Blanket Thermomechanical Behavior

Issue #E.b.3. Breeder/structure mechanical interactions
Issue #E.b.6. Corrosion and mass transfer

Description: The R&D needs in this category include investigation of breeder-structure thermomechanical behavior, heat transfer and corrosion/mass transfer, in particular the determination of operating temperature limits. Earlier experiments are underway and include laboratory corrosion test of unirradiated material in particular to investigate Li_2O mass transfer at temperature. Small-scale experiments to observe the thermal performance of a breeder/clad/coolant unit cell are also required in conjunction with irradiated capsule test to observe the irradiation effect on the breeder/clad thermomechanical interaction. These irradiated tests can be carried in fission reactors, and the more integrated test could use the same test assembly as that for the advanced in-situ test.

Facility: No major new facility is required, since these experiments are carried out in existing fission reactors or in laboratory facilities.

Cost and Time: Some tests are ongoing. Future efforts should address the thermo-mechanical interaction and corrosion characteristics of solid breeder and SiC.

The cost estimates are about $3M for the capital cost of test assemblies, and about $3M/yr as overall operating costs over 5 years.

Non-Neutron Module Test

Issue #E.b.3. Breeder/structure mechanical interactions
Issue #E.b.4. Off-normal and accident conditions
Issue #E.b.5. Structural response and failure modes
Issue #E.b.6 Corrosion and mass transfer
Issue #E.b.7. Tritium permeation
Issue #E.b.8. Fabrication & Assembly

Description: Nuclear testing is critical for exploring the effects of radiation on issues such as tritium recovery and breeder/structure mechanical behavior over the lifetime of the blanket. However, fission reactor test facilities provide limited test space, and also

impose constraints on the type and severity of transient tests, which limits the test information that can be obtained.

A complementary non-neutron experiment would provide valuable and needed information on prototypical-size integrated modules under near-prototypical conditions (except for irradiation effects) if suitable heat sources can be identified. Such a facility could address all the issues listed above. For example, it could provide for:

(1) Fabrication of a prototypical-size module or even segment if required which would help demonstrate fabrication and assembly techniques for a blanket module.
(2) Thermomechanical test of the blanket module under normal operation, including demonstration of thermal behavior over different power levels and flow conditions, which would help develop design margins.
(3) Thermalhydraulic test of purge flow, as well as test of permeation to the coolant within the blanket by using deuterium or hydrogen added to the purge. Control of the purge flow composition would also allow for observation of any corrosion or material interaction for different gas chemistry (at least over a short time).
(4) Off-normal and severe transient tests (which could be done at the end of the test program with the particular module) including LOCA and LOFA conditions. Structural response and failure mode could also be addressed at the end based on off-normal conditions and/or pressurization.

In addition, a modeling effort is required in order to develop design codes for the thermomechanical behavior of solid breeder blankets. Such a facility would then provide a discriminating test for these design codes.

Facility: A major new facility would be required. It would need to be able to house at least a full-size blanket module (of the order of 1m x 1m x 1m) and to provide for over power and severe transient testing, such as pressurization test. Heat sources to simulate the nuclear heat generation and coolant and purge flow systems would be required. Test module instrumentation would include strain gauges and thermocouples.

Cost and Time: The capital cost is estimated at about $20M for the facility, and about $15M for fabrication of a module, and the operating cost at $3M/yr. Testing in this facility would follow the initial single and multiple-effect types of experiments and would last about four years.

Nuclear Submodule Test

Issue #E.b.2. Tritium inventory and recovery
Issue #E.b.3. Breeder/structure mechanical interactions
Issue #E.b.5. Structural response and failure modes
Issue #E.b.6. Corrosion and mass transfer
Issue #E.b.8. Fabrication & Assembly

Description: Such a submodule test would be carried out in a fission reactor. Size constraint would mean that only part of a module assembly could be tested. However, a test submodule would comprise solid breeder, clad, purge and coolant in a prototypical arrangement under near-prototypical operating conditions, including the key effect of irradiation. This would be the most integrated test under irradiation with prototypical temperatures, flow rates and purge chemistry, and would provide key information, particularly on tritium recovery and breeder/clad interaction including corrosion. Parameters such as the submodule interface with the reactor and the solid breeder enrichment would be chosen in function of the facility to try to reproduce prototypical tritium generation and nuclear heating rate profiles.

The test would also provide for small-scale fabrication of part of a module assembly and PIE tests would provide valuable information on tritium inventories as well as on structural material conditions following operation at near-prototypical conditions, including irradiation.

Results would also help to validate design models, in particular for tritium recovery and inventory.

Facility: No major new facility is required, since this experiment will be carried out in existing fission reactors. The choice of fission reactor will depend on a number of parameters, such as available test space and ability to reproduce nuclear heating and tritium production rates over time.

Cost and Time: This test would start approximately at the same time as the non-neutron module test and will last about seven years per submodule.

The capital cost for a test submodule fabrication is about $15M, and the operating cost is about $3M/yr.

5.5.4.3 R&D Needs for Shielding

Effectiveness of Bulk Shield

Issues: #E.c.1.1 Biological Dose During Operation and After Shutdown for Maintenance.
#E.c.1.2 Radiation Streaming.
#E.c.1.3 Analytical Techniques and Data Base.

Description: Integral experiments should be planned to resolve the above technical issues associated with the effectiveness of the bulk shield. The prediction accuracies of calculated occupational dose, neutron and gamma flux level outside the biological shield, and the safety factors impeded in the design to account for higher flux level around gaps/slits due to neutron streaming through these paths or through larger penetrations (e.g. vacuum ducts) are estimated based on comparing predicted values to experimental measurements.

An intense 14-MeV neutron source with intensities $>10^{13}$ n/s and continuous operation capability should be used. Experiments should be conducted first to characterize the boundary conditions and background levels prior to the shielding performance experiments. The size of the mock-ups should be 100-150 cm wide and 80-150 cm long. The material constituents of the mock-ups could be conventional (316SS, water and concrete) or innovative materials that have superior attenuation capabilities (SiC+Pb+B_4C+water.) Arrangements can be in homogeneous or heterogeneous set-ups. Figures 5.5-2 through 5.5-6 show examples of possible configurations that also include discontinuities and penetrations. Measured parameters are: (a) Neutron spectrum ($E_n > 2$ MeV, 1 keV< E_n< 1 MeV), (b) Gamma spectrum, (c) Dose equivalent behind shield, and (d) Gamma heating during and after irradiation.

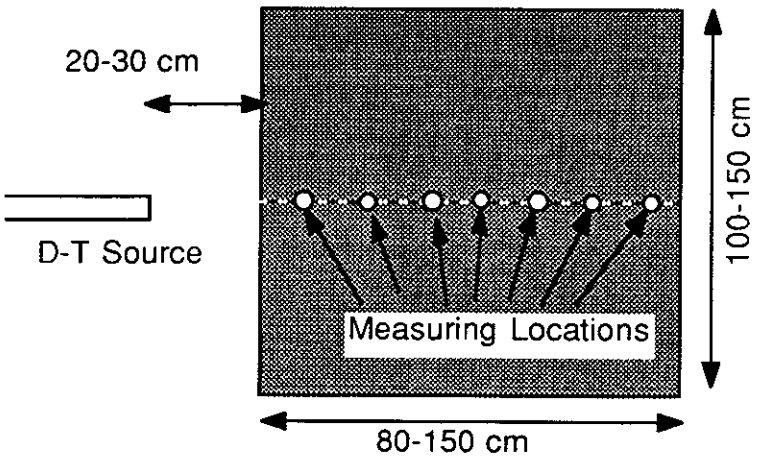

Figure 5.5-2. Example Bulk Shield Test Assembly – Homogeneous Assembly

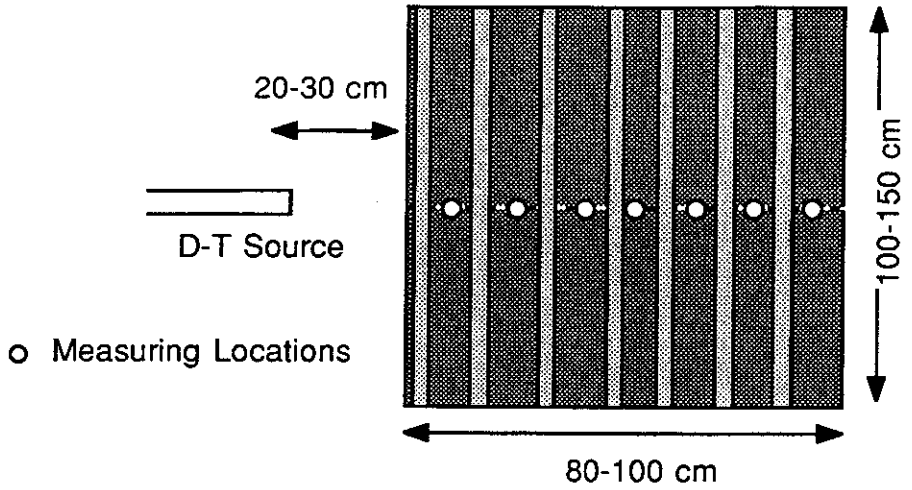

Figure 5.5-3. Example Bulk Shield Test Assembly – Heterogeneous Assembly

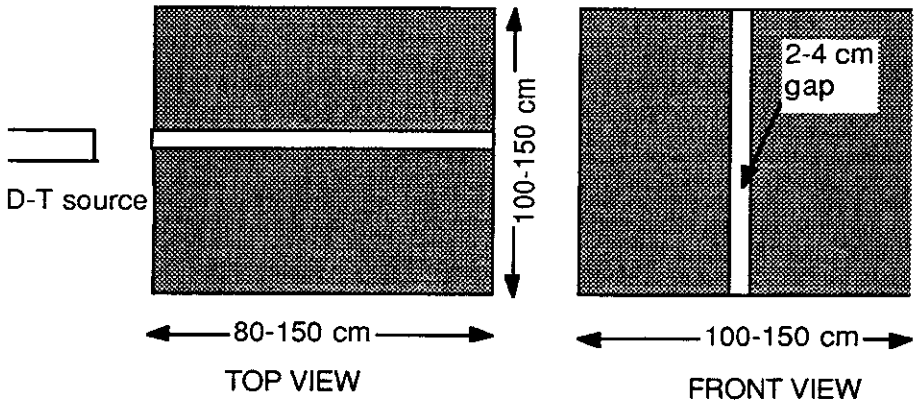

Figure 5.5-4. Example Bulk Shield Test Assembly With Discontinuities and Penetrations – Straight Plane Gap Assembly

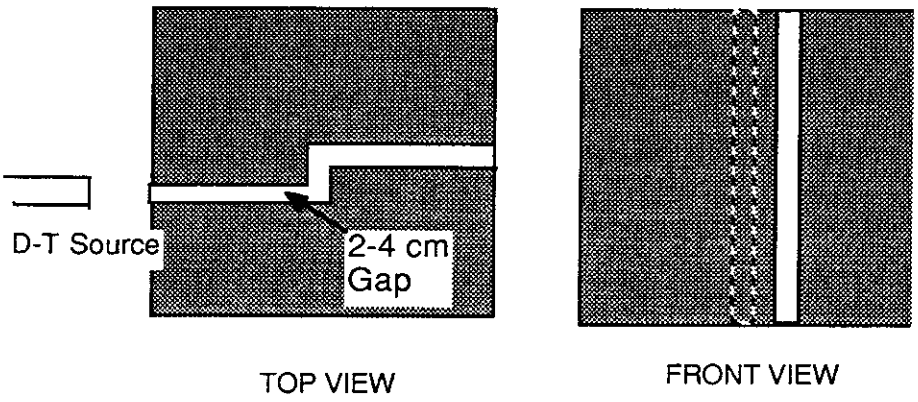

Figure 5.5-5. Example Bulk Shield Test Assembly With Discontinuities and Penetrations – Stepped Plane Gap Assembly

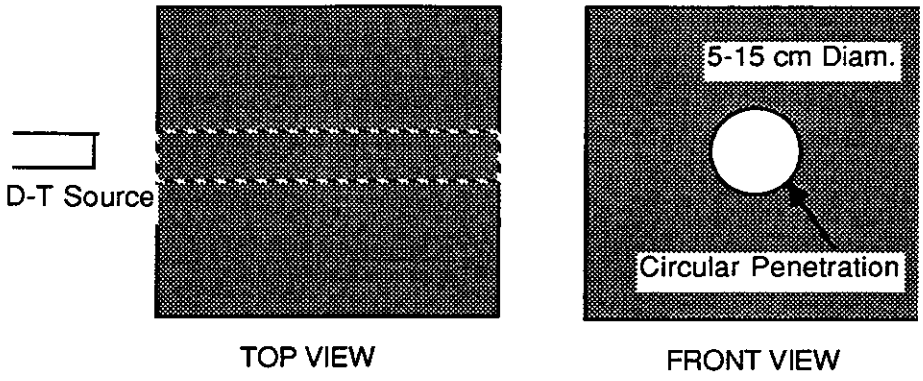

Figure 5.5-6. Example Bulk Shield Test Assembly With Discontinuities and Penetrations – Assembly With Circular (or Rectangular) Duct

Facility: An Intense 14-MeV neutron source is required to perform the above integral experiments. One of the U.S. facilities should be upgraded or reactivated. It is estimated that $1.5M is required to bring the ORNL 14-MeV shield facility to full operation while meeting the most current operational safety standards. However, this facility has 14-MeV neutron source intensity of only 10^9 n/s. For an intensity of 10^{13} n/s or higher, it is estimated that an additional $2M is needed. A new facility similar to the Japanese FNS facility with a similar intensity capability will cost ~$15-20M.

Cost and Time: It is estimated that ~$800k/year operating cost is required to perform a series of experiments for the validation of the bulk shield effectiveness (including penetrations experiments.) Operating cost include machine operation, test assembly materials and construction, and manpower. It is estimated that for each experiment, the manpower is ~8 man-months including operators, maintenance personnel, experimentalists and analysts. A 4-5 year period is required to accomplish this R&D task.

Shielding of Sensitive Components

Issues: # E.c.4 Shielding of final and turning mirrors (L)
E.c.5 Shielding of quadrupole magnets (HI)

Description: Damage to the final mirrors in a laser reactors is mainly caused by prolonged bombardment by high-energy neutrons causing displacements of the atoms of materials constituting these mirrors in addition to excessive heating that leads to thermal deformation and reduced performance. In a HI reactor, the superconducting quadrupole magnets are damaged by the radiation dose deposited in the insulator, displacements to the Cu stabilizer atoms leading to increase resistivity, etc. The R&D required to resolve these issues are two fold: (a) Experimental/theoretical validation of the microstructural changes that materials undergo under irradiation which lead to performance degradation, and (b) accuracies involved in quantifying (estimating) the

irradiation source term responsible for these microstructural changes. The former is a material life-time issue and is covered under the R&D requirements for materials (ISSUE E.) while the latter is related to the validation of the computational tools and data base required to quantify the nuclear environment at these sensitive components and behind the shield installed to protect these components.

An intense 14-MeV neutron source with intensities $>10^{14}$ n/s and continuous operation capability should be used in integral experiments devoted to resolve the shielding issues of (b) above. Experiments should be conducted first to characterize the boundary conditions and background levels prior to the shielding performance experiments. The configurations of these experiments are characterized by the implementation of a long penetration of a typical length of 10-20 m. The penetration could have a bend to resemble the laser (or some of the beamlets) paths in IFE reactors. A zone that has a highly neutron absorbing material could be located behind the bending to simulate the neutron trap situated at the back of the final mirrors in laser reactors. Due to the necessity of using long penetration in this class of integral experiments, the neutron source strength should be higher than 10^{14} n/s in order to achieve good statistics on the measurements performed at the far end of the penetration.

The surrounding shield material around this penetration could be made of conventional shielding materials (316SS+water; concrete) or innovative materials that have superior attenuation capabilities (SiC+Pb+B_4C+water). Measured parameters are: (a) Neutron spectrum ($E_n > 2$ MeV, 1 keV < E_n < 1 MeV), (b) Integrated fast neutron fluence (En> 0.1 MeV), (c) Gamma spectrum, and (d) Gamma heating. Figure 5.5-7 shows possible configurations relevant to these integral experiments. The validation of the prediction accuracies for these parameters at locations near and outside the outer surface of the test assembly is necessary in quantifying the level of confidence in calculating the damage parameters to the quadrupole magnets in HI reactors. Comparing calculated parameters to measurements near and behind the bend will indicate the prediction accuracies in assessing the damage to the final grazing incident mirrors in laser reactors. Performing measurements near the end of penetration will also assess the prediction accuracies of the nuclear environment at the turning mirrors in these reactors.

Facility: A very high intensity 14-MeV neutron source is required to perform the above integral experiments. For an intensity of 10^{14} n/s or higher, it is estimated that a new facility similar to the Japanese FNS facility with the capability of 10^{12} n/s intensity will cost ~$20-25 M.

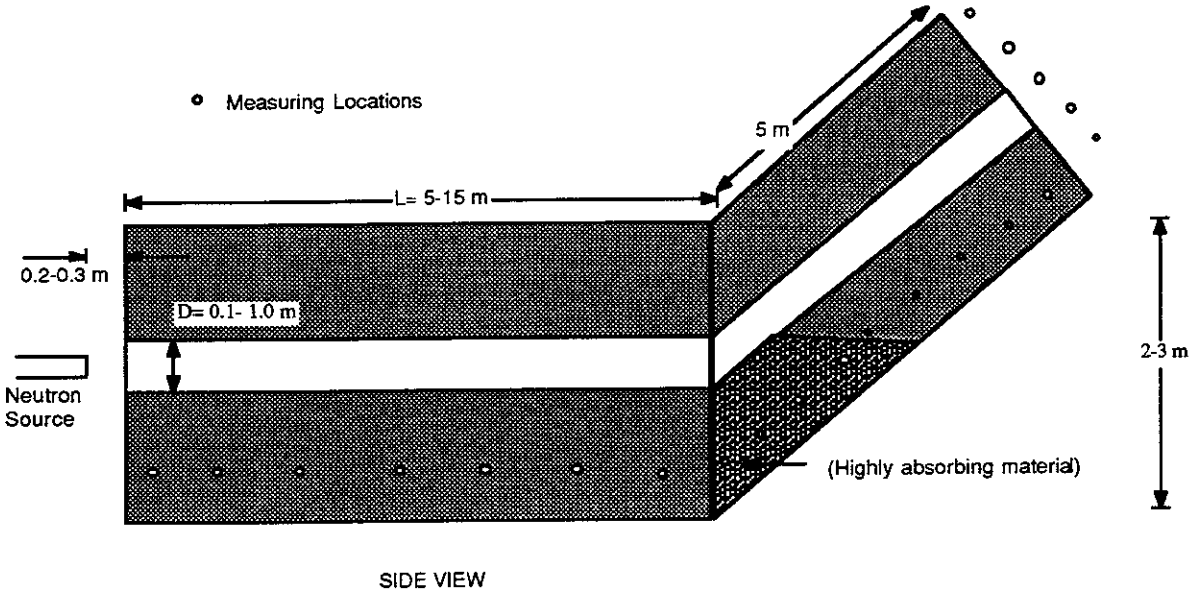

Figure 5.5-7. Proposed Configuration for Test Module for Verification of Mirror Protection and Quadrupole Magnet Protection Scheme

Cost And Time: It is estimated that ~$1-1.5M/year operating cost is required to perform a series of experiments that utilizes a relatively long test assembly composed of different shielding materials surrounding the penetration. Operating cost include machine operation, test assembly materials and construction, and manpower. It is estimated that for each experiment, the manpower is ~10 man-months including operators, maintenance personnel, experimentalists and analysts. two-three year period is required to accomplish this R&D task.

5.5.5 R&D for Tritium System - There are six major topics which should be included in the fuel cycle R&D program to achieve the objective of a practicable operating fusion plant.

(1) Demonstrate an advance fuel impurity treatment process - high temperature isotope exchange.
(2) Demonstrate a ceramic breeder tritium recovery process that allows extraction from a helium purge without oxidation - pressure swing adsorption.
(3) Demonstrate low inventory hydrogen isotope separation by cryogenic distillation.
(4) Demonstrate extended operation of integrated test loops with tritium.
(5) Develop and demonstrate the purification of the first wall protectant liquid lead with acceptable tritium inventories and losses.
(6) Demonstrate processing of solid, liquid and gaseous waste streams.

Facilities - The R&D plan assumes the use of current facilities (with modifications) where possible. All development and testing R&D could be accomplished in existing and under-construction tritium facilities in the U.S., Canada and Europe.

Prototype processing loops are planned to be tested in separate facilities. An integrated test stand of prototype processes would be assembled and demonstrated in a single, large facility.

Schedule - To demonstrate removal of tritium from impurity waste streams by high temperature isotope exchange (1995).

To demonstrate a process to remove tritium from helium purge gas from solid breeders (1997).

Demonstration scale test of new CD column concept to reduce tritium inventory (1997).

Demonstration scale test of waste processing (1997).

Integrated test loop demonstration (2000).

R&D Costs - The estimated R&D costs for the tritium system are $15M capital expenditure for facilities and $1.5M per year operating costs with a program duration of about ten years.

5.5.6 Safety and Environment - Many of the issues and R&D discussed for various reactor components relate to safety and environmental considerations. Some additional R&D specific to safety and environment is discussed in this subsection.

5.5.6.1 Overall Plant Tritium Inventory (Issue J.1) - See description of R&D requirements for Key Issue D.1.

5.5.6.2 Permeation of Tritium (Issue J.2)

Description - In order to resolve this issue, both the transport of tritium into the liquified lead and the retention of tritium by the lead must be understood. A program of experiments and modeling that would allow for these processes to be understood includes:

- Laboratory experiments to characterize the adsorption of tritium into liquid lead as a function of pressure and temperature.
- Laboratory experiments to characterize the desorption of tritium from the lead through the wall of the heat exchanger material as a function of pressure and temperature.
- The adsorption of tritium by sodium must also be studied via laboratory experiments, as a function of pressure and temperature.

Facility - A heat transfer laboratory which can handle tritium is needed to perform these experiments. Existing tritium experimental facilities may be suitable for this purpose.

Cost & Time -	With existing facility:	$250,000
	Without existing facility:	TBD
	Time period:	Within five years

5.5.6.3 Normal Operation Tritium Release (Issue J.3) - See description of R&D requirements for Key Issue 5.5.6.2.

5.5.6.4 Neutronic Cross Sections/Data Library for Activation Analysis (Issue J.4)

Description - Computational tools and data libraries used for activation analysis in the fusion community can be verified through decay rate measurements in a simulated fusion neutron spectra. Such validation has been initiated at UCLA for W and Zr. For example, the Prometheus study identified a large uncertainty in the O^{17} (n,α) cross section which results in about two orders of magnitude difference in the C^{14} production and radioactivity. Such uncertainty is critical as it has large impact on classification of waste disposal from the Li_2O breeder. However, extensive experimental and theoretical investigations are still needed. The R&D requirements with regards to the activation issue are common to both MFE and IFE.

Decay rate measurements can be done by examination of specimens following irradiation and removal from the irradiation facility. The tests would measure the decay gamma spectrum and count rate. Verification procedures include: (1) identification of decay photon spectra of the irradiated sample; (2) experimental decay rate calculations; (3) computer code simulation; and (4) comparisons of calculated and measured values and search for sources of discrepancies.

Facility Requirements - A facility with a fusion-like neutron spectrum is needed for the experiments. Such an environment can be generated by using 14 MeV neutrons (produced from a deuterium beam impinging on a tritiated target) surrounded by an assembly of materials in a configuration that simulates the fusion environment. In general, this type of facility is used for tritium generation and neutron cross section measurement. Existing facilities includes FNS facility in JAERI and others.

Cost and Time - A new facility similar to the FNS with neutron source intensity of 10^{12} n/s will cost ~$15M. It is estimated that for each experiment, the average manpower is about 3 man-months including irradiation, data analysis and validation of computational tools. The total program would last 5 years with annual operating cost of $600K.

5.5.6.5 Removing Decay Heat from Lead Coolant Under Accident Conditions (Issue J.5)

Description - Failure to cool the radioactive lead following a coolant spill might result in a local structure damage and releases to the environment. These tests seek to measure and locate the radioactive lead coolant under cooling break conditions. Research for this area includes the development of remote lead activity monitoring and remote lead cleanup system. In addition, verification tests of after-heat level would help assuring that adequate cooling is available.

Test Facility - A fluid loop with pressurizer, piping, pump, valve, break joints and any other components is desirable to simulate the lead coolant spreading behavior under a loss of coolant accident condition. The coolant and environmental pressures should be preserved and the size of test space should be large. The simulations should cover different break sizes and break locations. Decay heat measurement can be addressed in the same facility for decay rate measurements.

Cost and Time - It is estimated that the cost of the fluid loop is of the order of $500K. The task might take 1 year for planning, design and construction, with an additional year for performing experiments and data acquisition. The annular operating cost could be of the order of $300K.

5.5.6.6 Hydrogen Burn Due to Rupture of Diffusion Vessel

Description - Rather than experimental research, an engineering analysis is required to resolve this issue. This analysis would use existing methodology to calculate the effects of a hydrogen burn, and develop a design which would be able to sustain such an accident. Parameters which would be studies include: (a) the initial amount of hydrogen/tritium present, (b) the initial pressure and temperature within the diffusion vessel, (c) the rate of release of hydrogen/tritium from the diffusion vessel, (d) the amount of oxygen available. Existing computer programs which could be utilized include HECTOR and CONTAIN.

Facility - None

Cost & Time -	Cost:	$50,000
	Time period:	within six months

5.5.6.7 Detection of Local Dry Spots Prior to Failure (Issue J.7)

Description - These tests consist of the investigation of dry spot creation mechanism of FW, development of in-situ detection and repair techniques and development of radiation heat transport modeling capability in a partially-ionized gas environment.

Tests which address the formation of local dry spots on the first wall include the neutron irradiation effect on the porous SiC structure, structure degradation due to interactions with unburned pellet and deposition of corrosion product.

Experimental and modeling efforts of radiation heat transport in partially-ionized gas are covered under the R&D requirements for cavity vapor behavior. Estimation of time to failure for a local dry spot is about 19 minutes for a wall thickness of 0.5 cm. The above calculation assumed a local thermodynamic equilibrium condition for the cavity gas. Further analysis should consider the effects of non-thermodynamic equilibrium, gas excitation and self-shielding on the gas conditions.

Test Facility - Transport and deposition of corrosion product on SiC porous FW can be studied using a fluid loop with or without neutron sources. (Neutron yields neutron bulk heating which provides better simulation of coolant bulk temperature). The fluid loop consists of a vertical portion of SiC porous tube for creation of the film flow, with the rest of the loop made from stainless steel to simulate the heat transport loop. Measurements include coolant temperature, impurity content, and standard post-test examination of surfaces for corrosion. Experiments of irradiation effects on SiC structure require a fusion-like neutron spectra environment and are covered under the R&D requirements for materials.

A full size module might be needed to simulate the accessibility for tests related to in-situ repair technique development.

Cost and Time - It is estimated that the cost of the fluid loop facility without neutron source is of the order of $500K. The amount of time required for this task includes one year for design and construction, with an additional year for performing experiments, data acquisition and post test examination. The operating cost is of the order of $300K per year.

5.5.6.8 Detailed Accident Analysis (Issue J.8)

Description - In order to resolve this issue, detailed accident scenarios must be developed for each of the identified initiating events for each system in the plant. A more completely developed design is necessary for the development of the accident scenarios. Once the scenarios have been developed, the detailed accident engineering analysis would be initiated. During the accident analysis it is expected that various data/information will be identified as being required to complete the analysis, but is unavailable. Specific R&D needs to provide these data/information would evolve as the engineering accident analysis evolves.

Facility - None is required for the detailed accident engineering analysis to be performed.

The facilities required to resolve this issue depend on what data/information is identified during the detailed accident engineering analysis.

Cost & Time - Detailed accident engineering analysis:

Cost:	$1M (5 man-years)
Time period:	2 years

5.5.6.9 Removal of Contaminants from the Liquid Lead (Issue J.9)

Description - The tritium aspects of this issue are addressed in Key Issue 5.5.6.2. The first step to resolve this issue is to identify which are the potential contaminants and their expected amounts. Once this has been done, both the transport of contaminants into the liquid lead and the retention of contaminants by the lead must be understood. A program of experiments and modeling that would allow for these processes to be understood includes:

- Laboratory experiments to characterize the adsorption of contaminants into liquid lead as a function of pressure and temperature.
- Laboratory experiments to characterize the desorption of contaminants from the lead through the wall of the heat exchanger material as a function of pressure and temperature.
- The adsorption of contaminants by sodium must also be studied via laboratory experiments, as a function of pressure and temperature.

Facility - A heat transfer laboratory is need to perform these experiments. Such a laboratory may already exist (e.g., university, national laboratory).

Cost & Time -	With existing facility:	$1M
	Without existing facility:	TBD
	Time period:	Within five years

5.5.6.10 Impact of Large Quantities of Lead on Waste Disposal (Issue J.10)

Description - This is a regulatory issue to be resolved by the NRC.

This page intentionally left blank.

TABLE OF CONTENTS – CHAPTER 6 through 6.4

CHAPTER 6
CONCEPTUAL DESIGN SELECTION AND DESCRIPTION

This chapter describes the selection of the specific design choices for the two IFE reactor plant designs. The engineering details for the systems and subsystems are presented to describe the expected performance and operation of the complete reactor plants.

6.1 Introduction

Chapter 4 described the rationale for the major subsystems which influence the overall plant design. Early identification of key plant design options was critical in the design process. Subsequently, effort was directed toward the development of the conceptual design of systems and subsystems to integrate plant requirements .

Even though many of the key system options has been chosen with the expert judgement of the team and the aid of the systems code, each design team did not have sufficient knowledge to independently begin to design the optimal system. Moreover, a collection of individual optimal system designs may not prove to represent the overall optimal plant design. As the system designs began to evolve, systems performance and cost modeling was incorporated into the systems code to improve the modeling fidelity. Then the systems model was exercised to examine the available parameter space and determine micro or macro changes in the design configuration and operating parameter space. This process was iterated many times throughout the course of the study. However, not all the decisions could be quantified by the systems model, rather some decisions were based on qualitative judgements regarding the merits of safety, environmental attractiveness, reliability, and design conservatism.

One of the popular misconceptions held by the fusion community prior to this study was that the physical separation of the IFE driver from the reactor cavity implied nearly complete design independence for all the major systems. This study found that there is a profound amount of interaction among all the systems. The type of target influences driver illumination scheme, beam quality, fuel cycle, and cavity design. The wall protection choice affects energy conversion efficiency, waste handling capability, beam propagation across the cavity, and so on. Physical separation affords many benefits and design freedoms, however there are still significant and strong interactions among the systems which must be accommodated.

The system designs documented in this chapter constitute a conceptual design for a KrF laser reactor power plant and a heavy ion laser reactor power plant. Section 6.2, Design Point Selection discusses the development and evolution of the two respective design points. That section also contains high level parameter lists for the two reactors. More detailed parameters lists are presented in Appendices A and B. The overall reactor and plant configurations are presented in Section 6.3 along with a discussion of the design integration of the major systems. The maintenance approach and RAM analyses are also discussed . Following are the sections explaining the designs and analyses for the individual plant systems. This chapter concludes with a discussion of the rationale for the selection of the major materials used in the designs, principally the reactor cavity with the high radiation environment. There is a significant discussion of the safety and environmental analyses conducted during this study. The final section is an assessment of the economic analyses conducted for the two designs. A detailed cost basis is provided in Appendix C.

6.2 Design Point Selection

The selection of an optimum operating point in parameter space for inertial fusion power plants involves a trade-off between target gain G as a function of driver output energy E_D, the driver efficiency η, and the change in driver cost with output energy. The basis for this is illustrated by the simple power flow diagram shown in Figure 6.2-1. In this figure the driver power is related to the output energy through the pulse repetition rate RR, namely $P_D = RR\ E_D / \eta$. The thermal power depends on the effective energy multiplication in the blanket $M' = 1 + f_n(M-1)$ where f_n is the neutron fraction of the fusion power. To simply power the driver, the product of the driver efficiency and target gain ηG must satisfy the following relation $\eta G > 1 / \varepsilon M'$. Net power generation requires ηG in excess of $1 / \varepsilon M'$, typically by a factor of two or more. An advanced thermal conversion efficiency of 40% and effective blanket multiplication of 1.1 thus imply a minimal ηG of ~5 for economic power generation. If the driver efficiency is 5%, a target gain greater than 100 is required. If the driver efficiency improves to 20%, a gain greater than 25 will suffice.

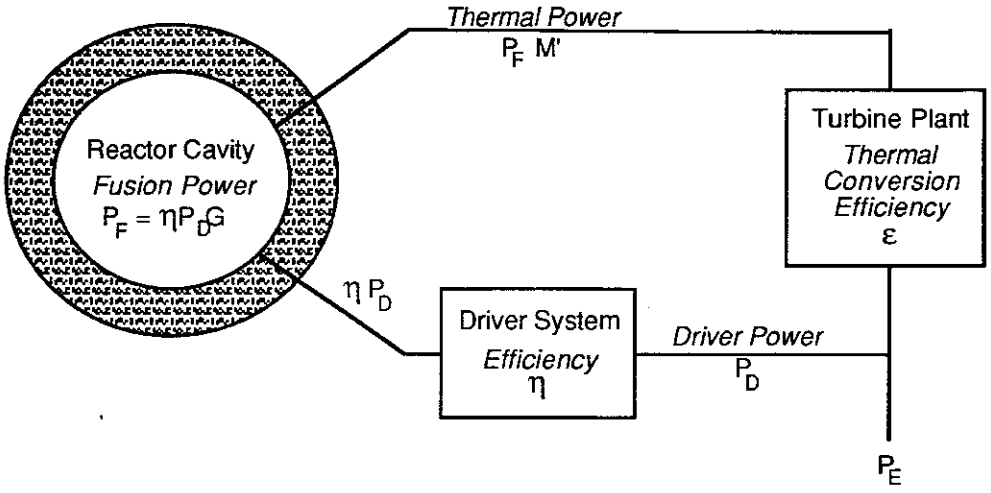

Figure 6.2-1. Simple Power Flow Diagram for an Inertial Fusion Power Plant

Systems modeling provides a basis for deciding how large an ηG is economically warranted. Typical target gain curves increase with driver output energy. Improved ηG is thus provided by increasing driver energy, but this implies a more costly driver. For a fixed-size plant, however, there can be a net cost savings because the driver is pulsed less frequently and therefore requires less input power. The size, hence cost, of the supporting plant equipment (reactor, steam generators, turbines, etc.) is thus reduced. The systems code quantifies this trade-off by parametrically modeling the size and cost of all major power plant systems. Incremental driver cost can then be weighed against the cost savings provided by higher target gain to determine the optimum size driver for the anticipated target gain curves.

This brings up an important point, namely that this process is intimately tied to the scaling of target gain with driver output energy. Gain curves for the present study were provided by a DOE-appointed Target Working Group (TWG). The TWG endeavored to level the technical optimism between the various laser illumination concepts (direct drive constant spot - CS, direct drive zoomed spot - ZS, and indirect drive - ID) and the indirect drive heavy-ion targets. For the laser driver, they provided their recommendations in the form of upper and lower bounds on the expected gain as a function of incident driver energy for each option. The TWG recommended an arithmetic mean of the upper and lower bound as a baseline gain curve for system studies that is represented by the constant spot curves. Figure 6.2-2 shows the resulting baseline gain curves for the KrF laser-driven target options.

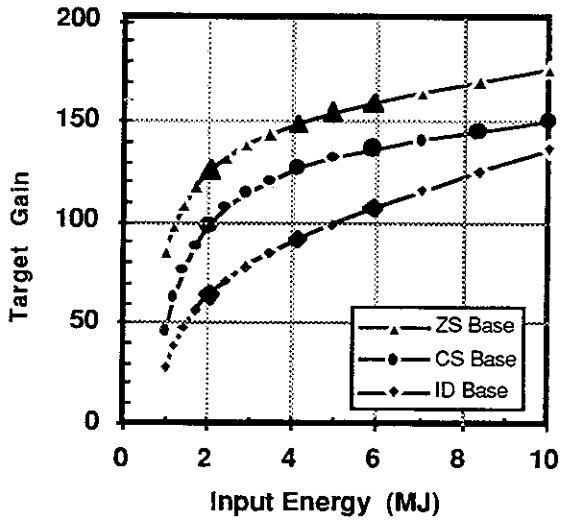

Figure 6.2-2. Baseline Gain Curves for KrF Laser Driver

The shape and magnitude of these curves directly influence the design point selection as discussed in the next section. The position of the ignition cliff ~2 MJ determines the minimum driver size whereas the slope of the curves determines the attractiveness of going to higher driver energy to improve ηG. Alternate target designs with different gain characteristics could push the design point to a different driver energy. This possibility is discussed in more detail in Section 5, Critical Issue 1, where economic considerations are used to determine the gain space region of interest for a smaller-size (100 MWe) power demonstration unit. It should also be noted that the significant disparity between the driver energy needed to achieve gain of ~100 for direct and indirect drive was the key reason that a direct-drive approach was selected for the present study. This is discussed in more detail in Section 4.6.

A final aspect of the systems modeling involves the fact that the code evaluated projected performance and cost between subsystems that in many cases employ technologies at vastly different stages of development. Efforts were made to normalize the cost projections across subsystems, but this is difficult where comparable hardware does not exist today. Costs were normalized to assumptions made for

recent MFE reactor studies[1-2] to provide a common basis for comparison. Elsewhere, costs were based on the best judgment of system experts. The economic scaling in the present systems model ICCOMO has evolved over many years. The models were originally developed as part of the STARFIRE reactor design study[3] and were adapted to IFE as part of the HIFSA project.[4] All cost models were updated to conform with the economic guidelines discussed in Section 3. A detailed description of the final cost models is presented in Appendix C.

The study guidelines indicated that costs are to be evaluated for a tenth-of-a-kind power plant. The study has conformed to this guideline and the rationale for doing so is presented in Appendix C. However, technology development will not be dictated by projected tenth-of-a-kind costs but rather by those for the first-of-a-kind system. The trade studies presented in this section include no learning curve adjustments—only first-of-a-kind costs. The results are therefore presented in the form of relative comparisons in order to avoid confusion in relating them to the tenth-of-a-kind costs discussed elsewhere.

6.2.1 Laser System Trade Studies - The Prometheus-L design point is the result of a number of different trade studies. These studies are summarized in Table 6.2.1-1. Many of these studies were evaluated within individual subsystems,

Table 6.2.1-1. Summary of Design Options Considered for KrF Laser System

Parameter	Baseline Value	Options/Range Considered
Target:		
Type	Direct Drive	Indirect Drive
Gain Curves	Average of Optim & Conserv	Optimistic, Conservative
Gain Curves	Average of Optim & Conserv	Zoomed Spot
Number Beams	60	30-90
Illumination	Tangential Focus	Nested Focus
Incident Energy (MJ)	4	2-8
Reactor Cavity:		
Wall Protection	Wetted Wall (Lead)	Dry Wall with Fill Gas
Breeder	Li_2O	FLiBe; LiPb Eutectic
Thermal Cycle (He Coolant)	Advanced Rankine	Direct Brayton
Coolant Pressure (MPa)	1.5	1-5
Driver System:		
Laser Amplifier	Electric Discharge with Raman Accumulator	Large Area E-Beam Pumped
Pulse Compression	Stimulated Brillouin Cell	Angular Multiplex, Hybrid
Amplifier Energy (kJ)	5.6	3-10
Amplifier Run Time (ns)	250	200-500
Optical Fluence (J/cm^2)	10	3-10
Final Mirror:		
Type	Grazing Incidence Metal on Ceramic Structure	Grazing Incidence Metal on Metallic Structure
Protection	Distance; Residual Gas; Deflection Magnets	Shutters; Cover Gas; Gas Prism

however, some trades could not be quantified within a subsystem. The systems code was used to resolve these trade-offs. The trade studies directed at choosing between technology options (e.g., indirect versus direct drive targets, single versus multiple beam LINAC, etc.) are discussed in Section 4. The discussion presented in this section concerns itself only with the rationale for selecting a certain operating range in parameter space for the baseline technology options.

In addition to design point selection, studies were also performed to assess the sensitivity of the overall performance to various subsystem technology assumptions, e.g., discharge laser intrinsic efficiency and output energy, optical damage limit, number of beamlines, etc. These studies indicate which research and development areas have the most leverage and thus might be considered the most critical.

Laser Design Point Selection and Sensitivity Studies - A 4 MJ driver energy was selected for the Prometheus-L design point based on the trade study summarized in Figure 6.2.1-1. This figure shows the relative driver capital cost, COE, and pulse repetition rate as a function of driver energy for the reference NLO driver architecture. The projected COE reaches a minimum at 4 MJ and rises slowly thereafter. As Figure 6.2-2 illustrates, the flatness of the direct-drive gain curves above the ignition cliff makes it unattractive to pay for the extra driver needed to achieve higher gains. In fact, a 3 MJ driver is projected to have performance nearly identical to the baseline system. The 4 MJ system was selected because the higher 8.2 pps repetition rate at 3 MJ was thought to provide inadequate time for reducing the lead vapor pressure in the cavity back to the 1-3 mtorr level required to prevent laser-induced gas breakdown. Cavity clearing was a key concern in the design of the Prometheus-L system as discussed in Section 6.8.

Figure 6.2.1-2 shows the sensitivity of the Prometheus-L design to key assumptions about the driver performance. The data displayed in the figure is summarized in Table 6.2.1-2 together with the parameters which were varied and their range of variation. In determining the change in COE, only the indicated parameter was allowed to vary, all other parameters were held constant. In many instances the change in COE could be offset to some extent by reoptimizing the overall design for the new conditions. For example, the lower gain predicted for the conservative curve would likely lead to the selection of a higher driver energy but this was not factored into the sensitivity study.

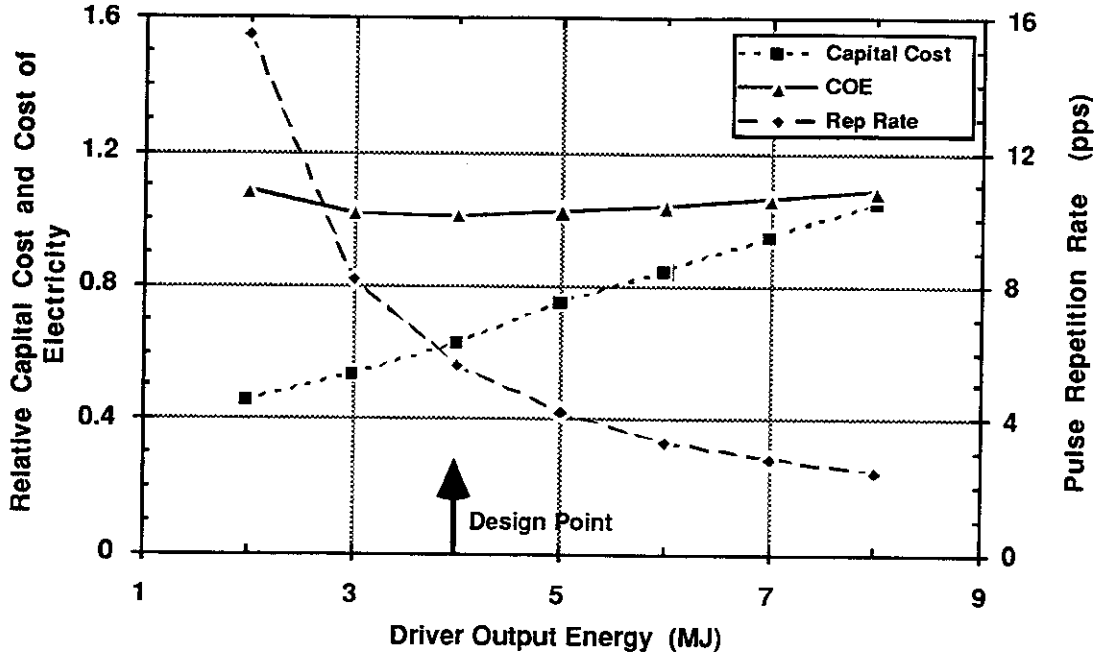

Figure 6.2.1-1. Scaling of Prometheus-L Driver Capital Cost, COE, and Pulse Repetition Rate with Driver Output Energy

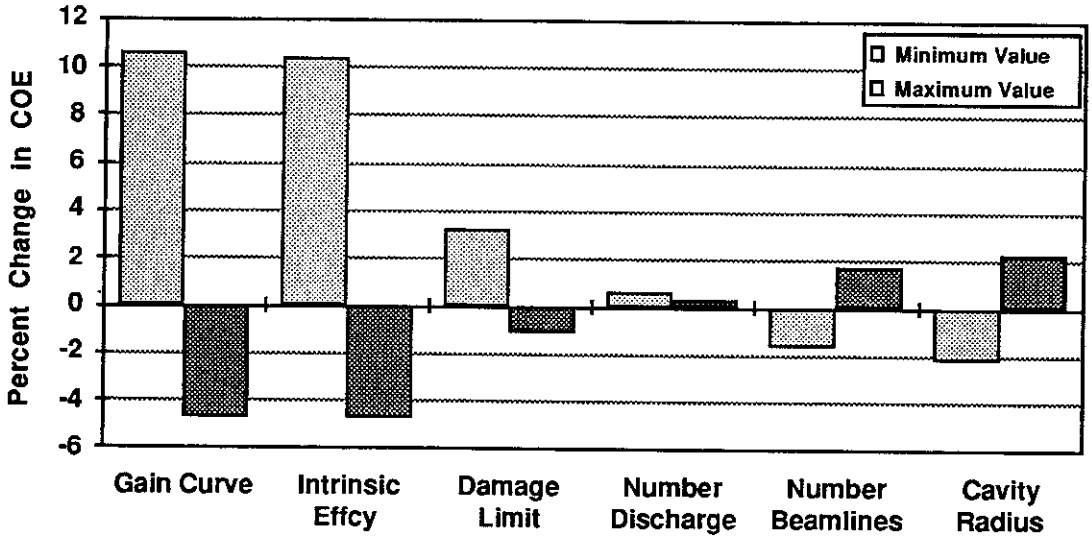

Figure 6.2.1-2. COE Sensitivity to Prometheus-L Design and Performance Assumptions

Table 6.2.1-2. COE Sensitivity to Variations in Key Prometheus-L Design Parameters

Parameter	Baseline Value	Minimum Value	Change in COE (%)	Maximum Value	Change in COE (%)
Gain Curve (Consvrt, Optm)	126	86	+10.6	165	-4.8
Laser Intrinsic Efficiency (%)	15	10	+10.3	20	-4.7
Optical Damage Limit (J/cm^2)	10	5	+3.2	15	-1.1
Num Dischg Lasers, Energy (kJ)	960, 6	240, 20	+0.6	2160, 2	+0.3
Number Final Beamlines	60	30	-1.7	90	+1.7
Cavity Radius (m)	5	4.5	-2.2	5.5	+2.3

Figure 6.2.1-2 also shows that COE depends most strongly on the gain curve assumption and the discharge laser intrinsic efficiency. The projected COE is 10% higher at the minimum value considered for these two parameters and drops 5% below the baseline value at their upper limit. These are sensitive parameters because there is very little ηG margin for the KrF laser driver since the overall efficiency is only 6.5%. Lowering the optical damage limit to 5 J/cm^2 causes a 3% increase in COE, while raising it to 15 J/cm^2 only decreases COE by 1%. There is thus little incentive to improve optical coatings beyond the 10 J/cm^2 point. COE is virtually independent of the discharge laser output energy even though the number of discharge lasers varies from 2160 down to 240. This is because the lasers are producing the same amount of total energy (4 MJ) in either case. Hence, the pulsed power energy requirement is the same and it is the major cost driver. Finally, a decrease in the number of beamlines from 60 to 30 or a reduction in cavity radius from 5 to 4.5 m would each lower COE by 2%. Conversely, COE would increase by 2% for 90 beamlines or if a 5.5 m cavity radius was needed to lower cavity vapor pressure.

6.2.2 Heavy Ion System Trade Studies - The Prometheus-H design point is based on a number of trade studies. These studies are summarized in Table 6.2.2-1. The heavy-ion driver has more scaling flexibility because it produces the requisite total energy by combining several ion beamlets at a discrete kinetic energy. The choice of ion charge state and kinetic energy lead to significant differences both in the accelerator configuration and in the target performance which must both be considered in determining the optimum design point. This section discusses these issues along with the results of sensitivity studies which were run to document the leverage of key design parameters on the overall system performance. Table 6.2.2-1 also highlights several trade studies which are discussed elsewhere in this report. The rationale for choosing a single versus multiple beam LINAC is presented in Section 4.1. The rationale for selecting a self-formed channel for cavity transport and the resulting target focal spot size and channel energy coupling is presented in Section 4.3. Finally, the rationale leading to the choice of a wall protection scheme identical to that for the laser system is presented in Section 4.4 and a discussion of target issues for the heavy ion system is presented in Section 4.6.

Table 6.2.2-1. Design Options Considered for Heavy Ion System

Parameter	Baseline Value	Options/Range Considered
Target:		
Type	Indirect Drive	
Ion Range (g/cm^2)	0.045 (4 GeV Lead)	0.025-0.2
Spot Size, Radius (mm)	3	2-5
Illumination	Two Sided	One Sided
Incident Energy (MJ)	7	4-9
Final Beam Trnsp Effncy (%)	90	70-100
Reactor Cavity:	Wetted Wall (Lead)	Same as Laser System
Driver System:		
LINAC Type	Single Beam with Storage Rings	Multiple Beam
LINAC Scaling	$\alpha = 0.2$; $\kappa = -0.15$	$\alpha = (0.2 - 0.5)$; $\kappa = (-0.2 - 0.0)$
Ion Type	+2 Lead	+1 to +3 Lead
Ion Energy (GeV)	4	4-8
Focusing Quads	Superconducting	Normal
Cavity Transport	Self-formed Channel	Ballistic; Pre-formed Channel

Figure 6.2.2-1 shows the gain curves provided by the TWG for the heavy ion system. These gain curves illustrate the strong influence which both beam spot size and ion energy have on the overall system performance. For a 7 MJ system with a 3 mm radius focal spot, the gain drops from ~100 at an ion kinetic energy of 2.4 GeV to 50 at 12.5 GeV. With a 4 mm radius spot, the change is even more dramatic going from a gain of 90 at 2.4 GeV to no gain at all. These large changes in gain, hence ηG, have a significant impact on the overall system performance which is a key aspect of the heavy ion trade studies.

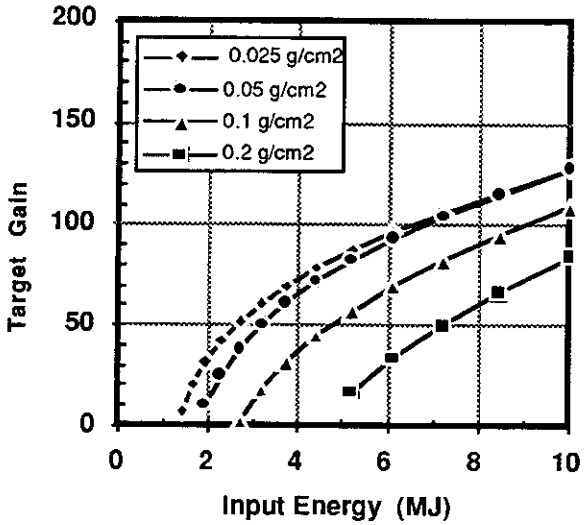

Figure 6.2.2-1. Baseline Gain Curves for Indirect-Drive, Heavy Ion Targets With a 3 mm Radius Focal Spot.

The systems code permits this gain variation to be traded off against the driver cost which tends to increase with ion energy. Figure 6.2.2-2 shows how LINAC size, cost and complexity scale with ion energy for a 7.8 MJ, single beam system operating at 5 pps. It shows that cost increases with ion energy because the LINAC length grows from 2200 m (1210 quads) at 4 GeV to 4200 m (1682 quads) at 8 GeV. The number of focusing quads is a significant cost factor. As a result, the lower energy system is favored from a cost standpoint in spite of the fact that more pulses per beam hence storage rings are required at 4 GeV (34 as compared to 18 at 8 GeV). This cost advantage must be weighed against the added technical risk of storing the beams for a longer time and the added complexity of the storage ring, final transport and final focus systems. System efficiency is also lower at 4 GeV (14.7% as compared to 16.6% at 8 GeV) because the induction cores are recycled more times per pulse. The Prometheus-H design point was chosen based on all these considerations.

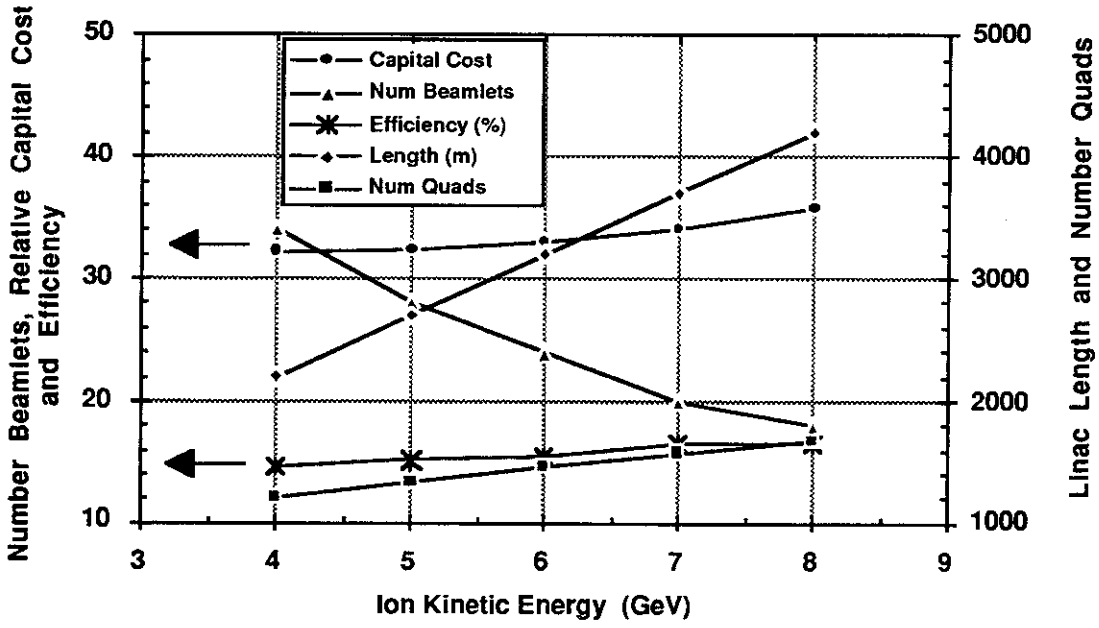

Figure 6.2.2-2. SB LINAC Size and Cost Scaling Vs. Ion Energy for a +2 Lead, 7.8 MJ and 5 pps System With Lee Lattice Scaling.[5]

One of the main induction LINAC design challenges involves the space charge limit on transportable current in a periodic focusing lattice. This limit necessitates multiple transport channels (typically > 10 beamlets) for heavy ion fusion drivers. Past systems studies[4] have envisioned a multiple beamlet lattice consisting of a closely packed quadrupole bundle surrounded by massive induction cores. The Prometheus-H design considers an alternative approach consisting of a single beam transport lattice coupled with intermediate storage rings to accumulate the required number of beamlets. In either case there is significant motivation to reduce the number of beamlets as much as possible in order to simplify the system design. Figure 6.2.2-2 shows that one way to reduce the number of beamlets is by increasing the ion energy. Unfortunately, this has an adverse effect on gain. In fact, Figure 6.2.2-1 shows that the

gain curves motivate the LINAC designer to work towards an ion energy of 4 GeV or less for lead ions. Design trade studies thus focused on alternative transport lattice configurations that would minimize the number of beams for a 4 GeV system.

The transport lattice scaling used for these trade studies is based on the following relations suggested by Maschke.[6] In these relationships, V is the local accelerator column voltage and I is the local individual beamlet current. These relations are used to define the number of beamlets N_B; the mean beam radius a; the space charge depressed phase advance per lattice period (depressed tune) σ; the beamlet bunch length $\delta = \tau\beta c$; and the number, length, and location of the focusing quads which are specified in terms of the lattice period 2L and the magnet occupancy (packing) fraction per lattice period η. In addition, several constraints based on physical limitations must be satisfied along with the relationship between beam energy and total charge.

Maschke[6] characterized the transport lattice scaling with LINAC voltage in terms of two parameters α and κ as summarized in Table 6.2.2-2. Lattice scaling suggested by Ed Lee[5] is a special case of this general parameterization as indicated where $\alpha = 0$, $\kappa = -1/4$ in the ramped gradient and $\alpha = 1/2$, $\kappa = 1/8$ in the fixed gradient sections.

Table 6.2.2-2. Prometheus-H Transport Lattice Scaling Model

Parameter	Maschke Scaling	Ed Lee Scaling[5] Ramped	Ed Lee Scaling[5] Fixed	Final Transport Scaling
Lattice Half Period, L	$V^{\alpha-\kappa}$	$V^{1/4}$	$V^{3/8}$	$I^{\zeta-1}$
Depressed Tune, σ	V^{κ}	$V^{-1/4}$	$V^{1/8}$	$I^{-\zeta}$
Beam Radius, a	$V^{\alpha/2-\kappa-1/4}$	Const	$V^{-1/8}$	$I^{\zeta-1/2}$
Bunch Length, δ	$V^{\alpha-1/2}$	$V^{-1/2}$	Const	$I^{\zeta-1}$
Packing Fraction, η	$V^{-3\alpha/2+\kappa+1/4}$	Const	$V^{-3/8}$	$I^{3/2-\zeta}$

The additional constraints involve the space charge limit on transportable current:

$$I_{max} = \frac{Q}{\tau N_B} = 1.56 \times 10^7 \sigma_o^2 \left(\frac{a}{2L}\right)^2 \left(\frac{A}{Z}\right)(\beta\gamma)^3, \qquad 6.2.2\text{-}1$$

where I_{max} is in amps, $Q = 10^6 Z E_B/E_{ion}$ is the required charge in coulombs (E_B in MJ and E_{ion} in GeV), A and Z are the ion atomic mass and charge state, and τ is the pulse length. The relation between normalized emittance $\varepsilon_n = \beta\gamma\varepsilon$ and phase advance:

$$\varepsilon_n = \sigma\left(\frac{a^2}{2L}\right)(\beta\gamma). \qquad 6.2.2\text{-}2$$

The relation between undepressed phase advance σ_o and the focal lattice properties:

$$\sigma_o = B_P\left(\frac{\eta a}{[B\rho]L^2}\right), \qquad 6.2.2\text{-}3$$

where B_P is the poletip field and $[B\rho] = 3.13\,\beta\gamma\left(\frac{A}{Z}\right)$ is the beam rigidity in T-m. (The poletip field is actually the magnetic field at the edge of the beam, so the maximum

field in the magnet is typically 1.5 to 2 times higher.) The relation governing the maximum rate that the voltage gradient can be increased in the ramped gradient section:

$$\frac{dV}{dx} \le 0.25\left(\frac{V}{\delta}\right)\left[\frac{1}{2} - \frac{V}{\delta}\left(\frac{d\delta}{dV}\right)\right]^{-1}. \qquad 6.2.2\text{-}4$$

And finally the practical limits on quadrupole packing fraction in the lattice $\eta < 0.80$ and quadrupole aspect (bore to length) ratio $a/\eta L < 0.25$.

These scaling relations are implemented by choosing values for the lattice scaling parameters with voltage along the LINAC α and κ, and with beamlet current I in the final transport (typically $\zeta = -0.8$). The undepressed phase advance $\sigma_o = 80°$ maximum poletip field $B_{PT} = 3$ T, desired final transport section length (typically 180 m), pulse length at the target (typically 7-8 ns), beam and ion energies are also specified. The code then searches for a number of beamlets and bunch length at the high energy end of the LINAC that do not violate the packing fraction and aspect ratio limits at either the injector end or in the final transport section where beamlet current increases rapidly due to bunching. If the constraints cannot be satisfied, the poletip field is reduced. The poletip field is typically reduced to ~2T before a solution is found for the combinations of α and κ considered here.

An examination of Table 6.2.2-2 shows that some combinations of α and κ are more attractive than others and the trade studies discussed here focus on them. Initial studies considered the Lee[5] choice for lattice scaling and these results were used in Figure 6.2.2-2. However, this scaling results in 34 beamlets at 4 GeV for a 7 MJ driver which presents a significant technical and design challenge both in the storage rings and the final focus. One logical alternative scaling involves setting $\alpha = 0.5$ and $\kappa = 0$. This is attractive because it leads to a common quadrupole size (a and ηL are both constant) down the entire length of the LINAC. Another alternative involves simply holding magnet bore size constant down the length of the LINAC, i.e., choosing $\kappa = \alpha/2 - 1/4$. The quadrupole length will vary for this family of scaling possibilities, but discrete steps can be provided by adjusting the magnet field strength slightly. It furthermore is desirable to have $\alpha < 0.5$ so that the magnet aspect ratio ($a/\eta L$) decreases along the LINAC to avoid problems with aberrations. This leads to values of $\kappa < 0$ which corresponds to letting the phase advance float downward along the LINAC length. This leads to a worst case final phase advance of 2.2° assuming $\sigma = 8°$ at the injector end, which should not be a problem.

Table 6.2.2-3 summarizes the results of these trade studies. The number of magnets is significantly reduced for $\alpha = 0.5$, from ~1200 for the Lee cscaling[5] to 356. Unfortunately, the number of beamlets nearly doubles, going from 34 to 66. This in

Table 6.2.2-3. Summary of LINAC Lattice Scaling Trade Studies for a 4 GeV, 7.8 MJ, +2 Lead System

Lattice Scaling		Number	Number	Final Pulse	Final Phase	Overall Driver System	
Alpha	Kappa	Beamlets	Quads	Length (ns)	Advance (deg)	Effcy (%)	Cost (M$)
0.50	0.00	66	356	150.0	8.0	7.50	765.0
0.40	-0.05	36	484	150.0	5.8	11.55	619.9
0.30	-0.10	18	760	150.0	4.2	18.05	645.1
0.20	-0.15	16	956	89.8	3.0	21.54	595.0
0.10	-0.20	38	982	18.3	2.2	17.05	447.6

turn lowers the overall efficiency to 7.5% due to increased induction core losses. The α=0.5 scaling was thus rejected for the final design point. However, the table shows that more attractive results occur as α is reduced from 0.5 to 0.2. The number of beamlets decreases from 66 to 16, the efficiency improves from 7.5 to 21.5% and the cost drops from $765 to $595 M. The cost trend continues for α = 0.1, but the other trends reverse. The turnaround is a result of the rapid drop in final pulse length that is required to prevent violating the quadrupole packing fraction constraint in the final transport section for values of α < 0.2. Based on this result, transport lattice scaling using α = 0.2 and κ = -0.15 was selected for the baseline design point.

To this point, the discussion has focused on the selection of LINAC parameters that minimize the number of beamlets for a given total output energy. An energy of 7.8 MJ was used for illustration purposes because it was selected for the Prometheus-H driver. This accounts for a 10% loss in the process of forming the cavity transport channel and coupling the driver output energy through the channel into the target as discussed in Section 6.5. Hence only 7 MJ of energy is actually assumed to be available for producing target gain. Figure 6.2.2-3 depicts the basis for selecting this driver energy. It shows that the projected COE has yet to reach a minimum at 9 MJ for the selected LINAC design configuration. The projected incremental driver cost for the single beam LINAC and the slope of the heavy-ion gain curves favor higher energies. The number of beamlets was originally a concern at this energy, more than 50 were anticipated for a 4 GeV system, however this concern is mitigated somewhat by the alternative lattice transport scaling which is projected to need only 22 beamlets at 9 MJ. Nevertheless, higher energy drivers certainly represent a greater development challenge both for the driver and the cavity with must withstand a higher yield. This realization coupled with the marginal improvement in COE above 7 MJ still justify it as a design point.

It is worthwhile here to note that the alternative lattice transport scaling really opens a more attractive heavy ion LINAC design window that previously was not accessible due to the large number of required beamlets. This can be understood by referring to the gain curves as shown in Figure 6.2.2-1. The gain falls off rapidly for ion energies above 5 GeV and is almost a factor of 2 lower for the 10 GeV ions typically proposed

in the past. In addition, lower energy ions are much less sensitive to variations in focal spot size. This is quantified in Table 6.2.2-4 which summarizes the sensitivity of COE to variations in key driver performance parameters.

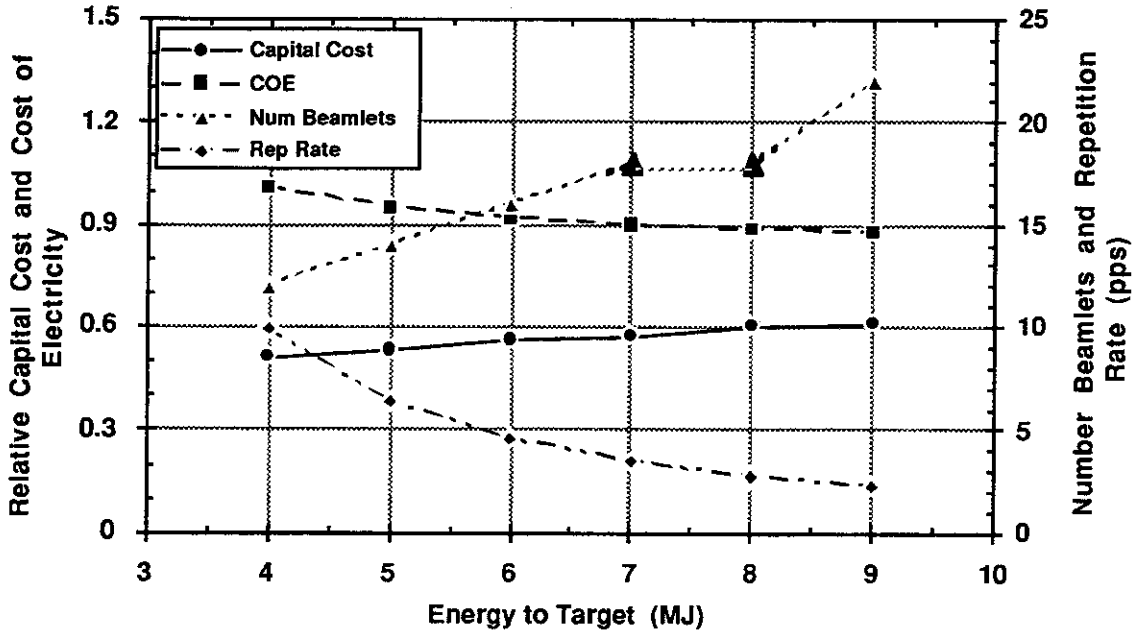

Figure 6.2.2-3. Scaling of Prometheus-H Driver Cost, COE, Repetition Rate, and Number of Beamlets with Output Energy

Table 6.2.2-4. COE Sensitivity to Variations in Key Prometheus-H Design Parameters

Parameter	Baseline Value	Minimum Value	Change in COE, Effcy*	Maximum Value	Change in COE, Effcy*
Focal Spot Radius (mm)	3	2	-2.1	4	+3.6
Spot Radius Change at 7 GeV**	3	2	-4.3	4	+8.6
Final Beam Transport Effcny (%)	90	80	+0.8	100	-0.6
Ion Kinetic Energy (GeV)	4	3	-2.7, -13.0	7	+18.2, +21.4
Core Flux Swing (T)	1.5	1.0	+1.7, +8.4	2.0	+0.1, -9.3
Ion Charge State	+2	+1	+24.5, +2.8	+3	-4.2, -4.4

* Change in driver efficiency is indicated only for parameters that influence it significantly

** Changes are normalized to 7 GeV system with 3 mm radius spot which is 18% higher than 4 GeV COE

These results highlight several key aspects of the Prometheus-H driver design. The primary one involves the improved cost and performance characteristics provided by the reduced ion kinetic energy. As is indicated, COE is 18% higher for a 7 GeV design due to the increased length of accelerator required at this energy. The number of beamlets is reduced from 18 to 6 at 7 GeV , but the single beam approach, coupled with the alternate transport scaling, eliminates most of the complication (hence cost) of

added beamlets at 4 GeV. The results also indicate that there is little motivation to further reduce beam energy. COE is 3% lower at 3 GeV but 32 beamlets are required at this energy which complicates the final transport and lowers driver efficiency by 13%.

An added benefit of the lower ion energy is reduced sensitivity to target gain curve characteristics. The results show that a 7 GeV system is twice as sensitive to spot size variations as the 4 GeV design point. This is important because it minimizes the effect which the poorly understood transport channel re-imaging properties may have on system performance. Insensitivity to transport channel properties is reinforced by the weak COE dependence on target coupling efficiency (beam energy loss in the transport channel). A doubling of energy loss (from 10 to 20%) would only increase COE by 1%. The results also indicate very weak COE dependence on Metglas flux swing. A low flux swing of 1.5 T was selected for the baseline design to reduce induction core energy losses since this was thought to be a key factor in the design of a single beam LINAC where the cores are recycled several times per pulse. Indeed, the driver efficiency changes by ±9 % as flux swing is varied from 1 to 2 T, however this causes only a 1 % change of COE. Finally, the results highlight that there is still a significant advantage to higher charge states for the single beam system, but that the payoff is limited beyond +2. The cost of electricity is 24 % higher for singly charged ions while it drops by 4 % for charge state 3. Unfortunately, the number of beamlets increases to 36 for +3 ions which may offset the indicated cost advantage once the engineering details of final transport and focusing are evaluated.

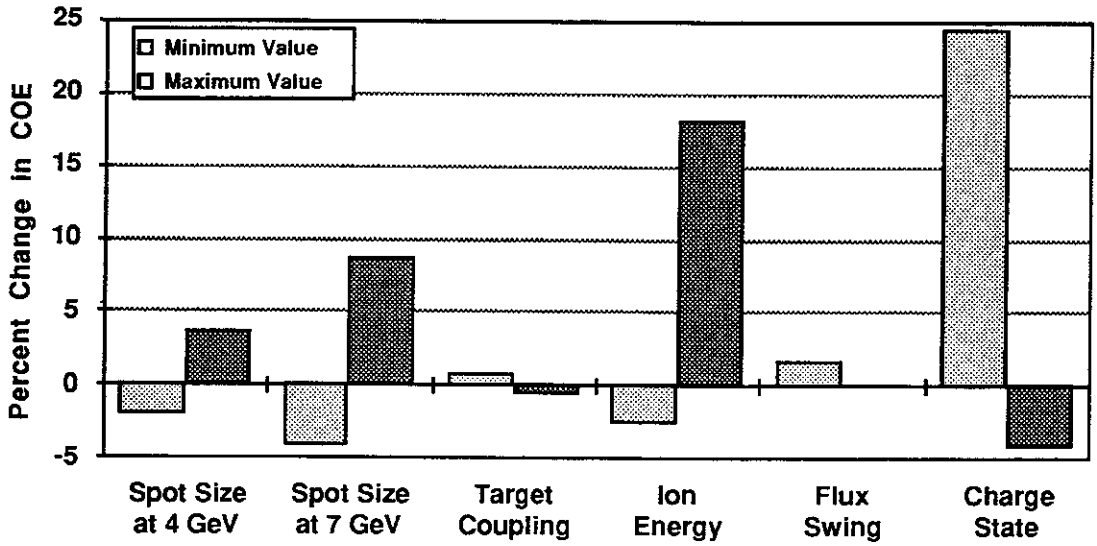

Figure 6.2.2-4. COE Sensitivity to Prometheus-H Design and Performance Assumptions

References for 6.2

1. F. Najmabadi, R. W. Conn, et al., "The ARIES-I Tokamak Reactor Study, Final Report,", UCLA-PPG-1323, 1991

2. M. A. Abdou, "FINESSE, A Study of the Issues, Experiments and Facilities for Fusion Nuclear Technology Research & Development," PPG-821, UCLA-ENG-84-30, 1984.

3. C. C. Baker, M. A. Abdou, et al., "STARFIRE - A Commercial Tokamak Fusion Power Plant Study," ANL/FPP-80-1, September 1980.

4. D. S. Zuckerman, et al., "Induction LINAC Driven Heavy Ion Fusion System Model," Fusion Technology, Vol. 13, #2, 1986.

5. Dr. Edward Lee, Lawrence Berkeley Laboratory, Personnel Communication, 1991.

6. Mr. Alfred Maschke, TRW, Personal Communication, 1991.

6.3 Configuration and Maintenance Approach

The configuration and maintenance approaches for both the Prometheus-L and Prometheus-H reactor concepts are described in this section. Prometheus-L is a 1000 MWe IFE power plant using a KrF excimer laser driver to deliver 4 MJ of energy through 60 beamlines 5.6 times per second to direct drive targets in the center of a cylindrical reactor cavity. Prometheus-H is a similar sized plant utilizing a heavy ion driver to deliver 7.8 MJ of energy through 14 beamlines 3.5 times a second to indirect drive targets in a similar reactor cavity.

A top down approach describes these two IFE plant configurations. A general site plan explains the overall arrangement of each power plant. Most of the plant buildings (administration, auxiliary, turbine, steam generator, target factory, and tritium processing) and sizes used in both concepts are similar; only the reactor and driver buildings differ in size and design approach. Descriptions of the driver systems, reactor systems, and heat transport system are provided Plan and elevation drawings define interfaces between these major subsystems with drawings illustrating major components arrangements.

The maintenance approach used to service reactor and driver systems vary depending on the location within the plant. The maintenance of all reactor systems within the bulk shielding walls will be totally remote. In both concepts, the reactor cavity is essentially the same. Therefore, common maintenance methods are employed. A vertical maintenance approach for all operations within the reactor vacuum vessel is envisioned. All interfacing systems which penetrate the bulk shielding walls are provided with enclosed, local shielding. Therefore, reactor systems and interfacing driver systems within the reactor building walls but outside the bulk shielding walls are maintained with a combination of remote maintenance and limited hands-on maintenance equipment. The maintenance method would depend on the type of maintenance to be performed.

6.3.1 Reactor Design Integration - This section presents design integration of the major subsystems in the two inertial fusion energy (IFE) reactor concepts. Detailed descriptions of the subsystems are presented in Sections 6.4 through 6.11.

6.3.1.1 Prometheus-L - Site plans for the Prometheus-L reactor design power plant are shown in Figures 6.3.1-1 through 6.3.1-3. These figures present a trimetric view of the plant site, a plan view of the plant site, and a building definition plan view, respectively. Prometheus-L site plans show the typical IFE power plant buildings (administration, auxiliary, turbine, steam generator, target factory, and tritium processing) arranged around the circular KrF laser driver building. This annular-shaped building is 153 m in outer diameter and contains all the laser driver

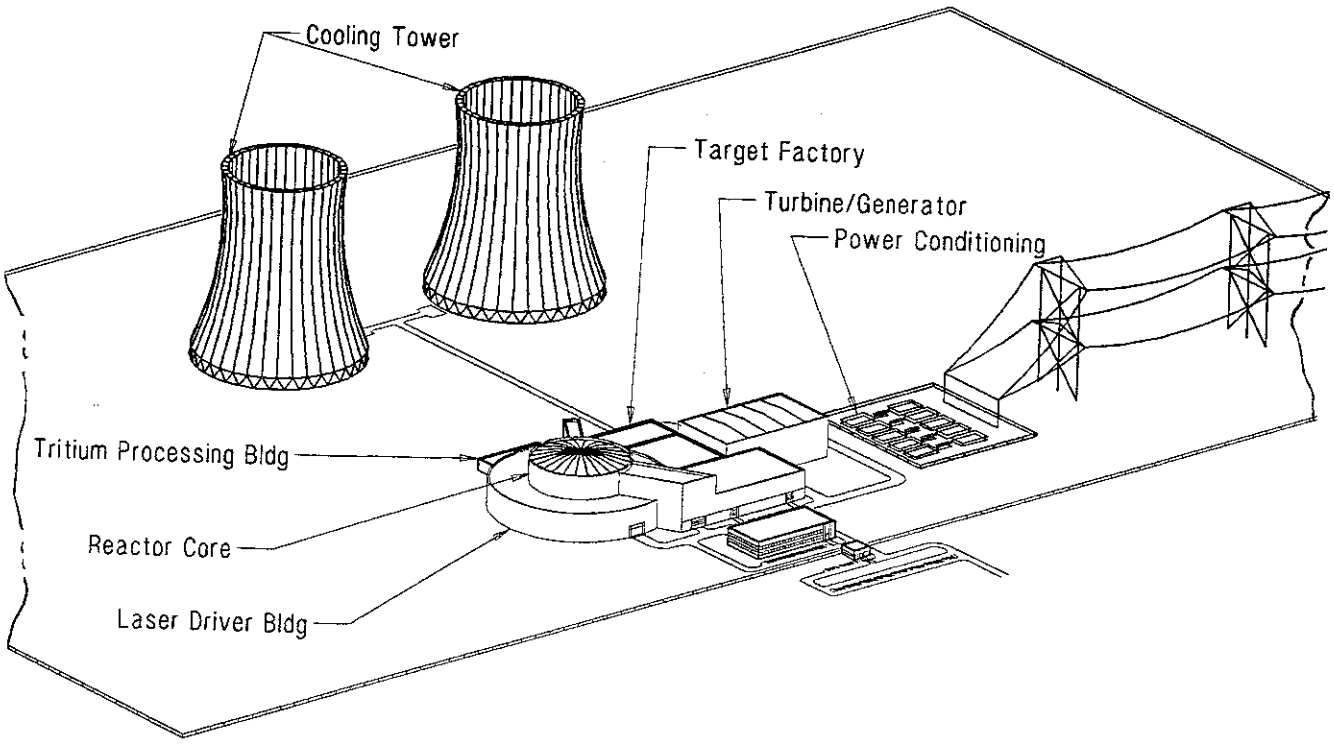

Figure 6.3.1-1. Prometheus-L Plant Site Trimetric View

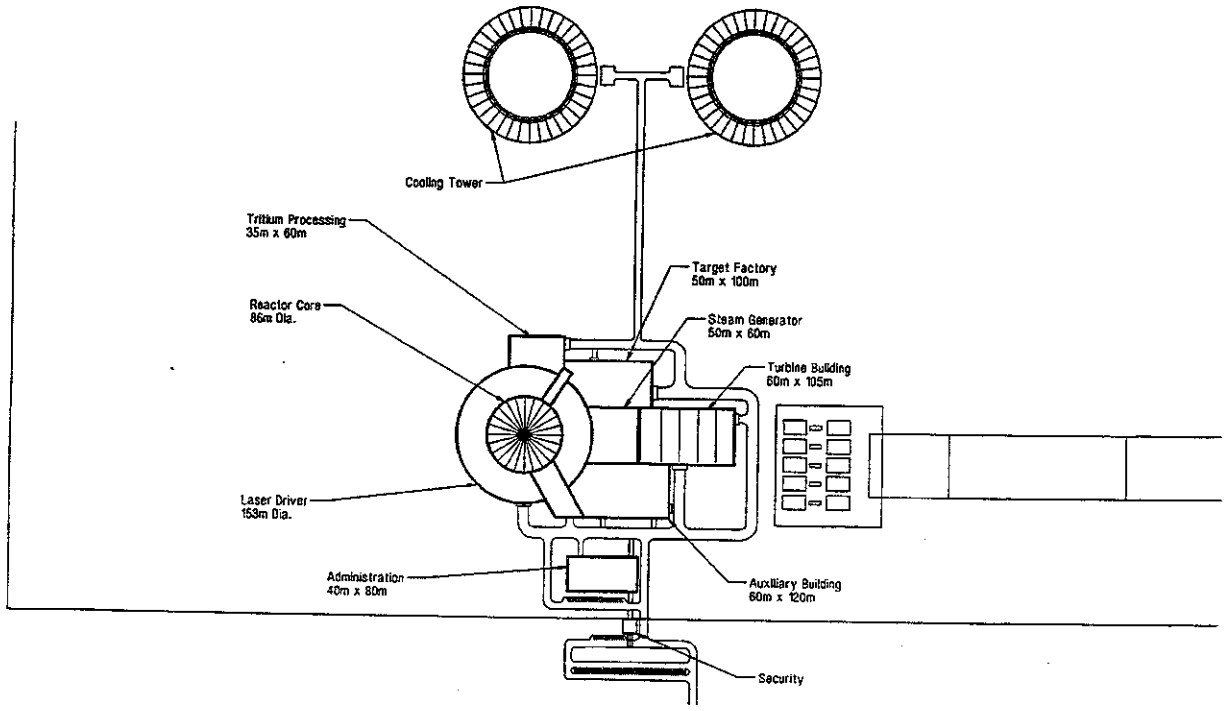

Figure 6.3.1-2. Prometheus-L Plant Site Plan View

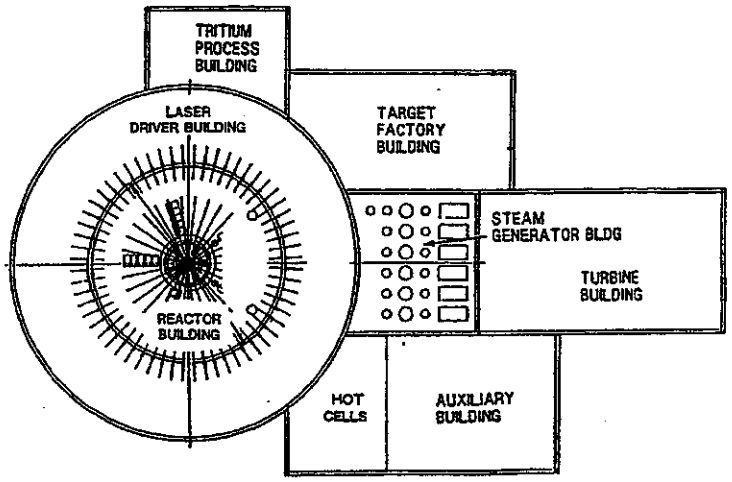

Figure 6.3.1-3 Prometheus-L Building Plan View

components to generate 60 individual laser beams. These 60 beamlines are arranged in an equally-spaced radial array and penetrate the inner wall of the driver building which is also the outer wall of the reactor building. The Prometheus-L reactor building is 86 m in diameter.

KrF Laser Driver-General Overview - The Prometheus-L reactor design concept employs a KrF excimer laser driver and a nonlinear-optical (NLO) system. This NLO system features an electric discharge laser subsystem, crossed forward Raman accumulator cells, and stimulated Brillouin scattering (SBS) cells. Upstream are typical front end elements which complete the 60-beam network including the master oscillator for all the beams, the beam splitter system, and the preamplifier/amplifier stages for each beamline. Theoretical and operational aspects of the overall system are described in detail in Section 6.5.1.

The laser driver delivers 4 MJ of energy to a target through 60 optical laser beamlines each with a gross energy of 67 kJ. Sixty (60) identical sets of driver output components (laser module, Raman accumulator, and SBS cell) are arranged in an equally-spaced radial array (6°) in the annular driver building and about the reactor building vertical centerline. Inside the reactor building, the 60 beams converge to enter the reactor cavity with two beams equally spaced every 12° as seen in the plan view. A plan view of the KrF laser and reactor buildings is shown in Figure 6.3.1-4.

Inside the driver building, the electric discharge lasers output beams are routed to the Raman accumulators and then to the SBS cells. Output beams from each of the 60 SBS cells are then directed to the cylindrical section of the reactor cavity. The

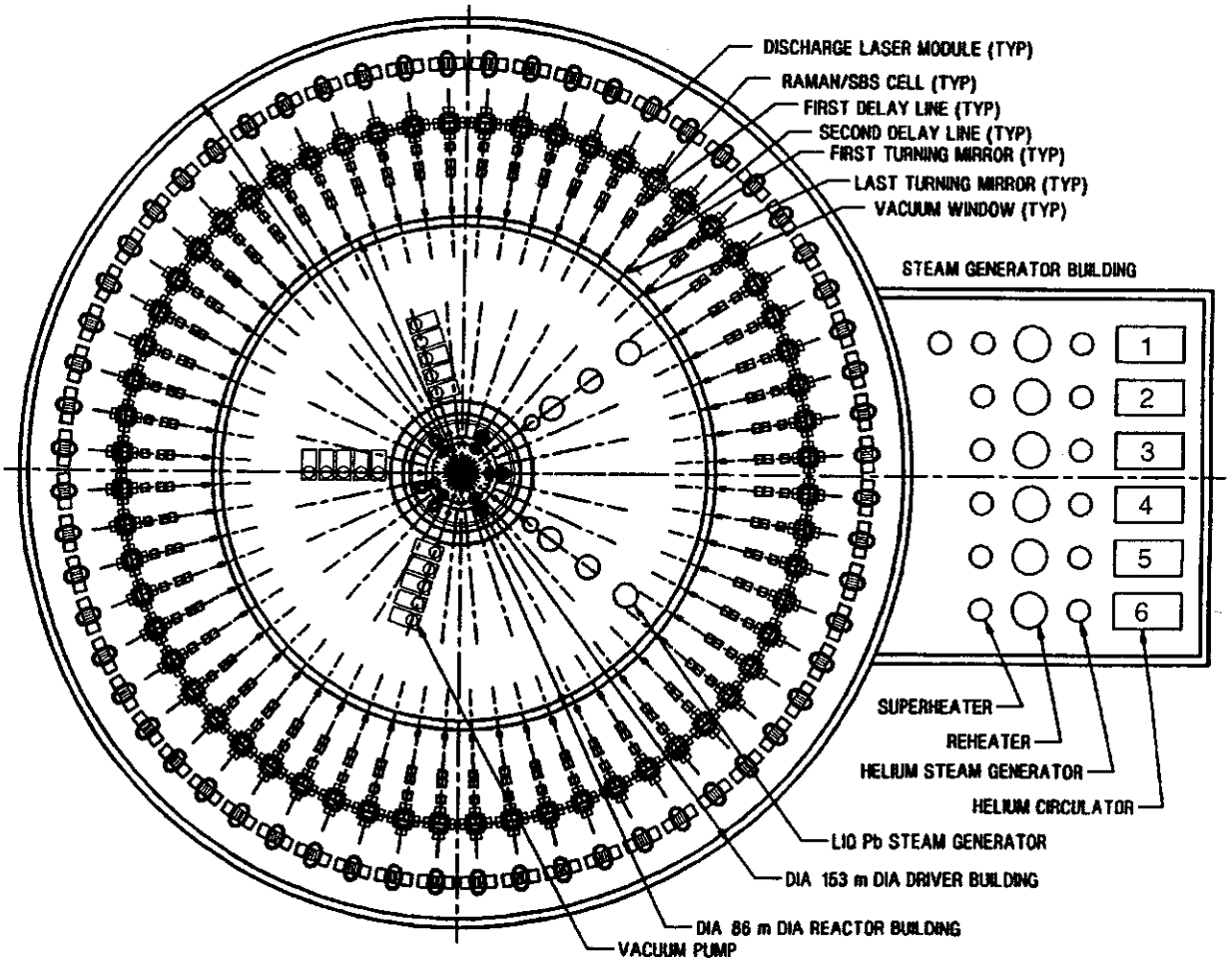

Figure 6.3.1-4. KrF Laser and Reactor Buildings – Plan View

location and orientation of the 60 beamline penetrations in the reactor cavity (to be discussed below in the Final Optics Subsystem Description) results in eight unique beamline routes from the SBS cell to the center of the reactor cavity. The eight unique beamline routes occur repetitively around the reactor cavity. These routes are shown in Figure 6.3.1-5 (typical five places) and Figure 6.3.1-6 (typical ten places), which are two cross-sectional elevation views. Some license has been taken with correct technical drawing of the these two views since the four routes in each figure upstream of the final focusing mirrors actually lie slightly out of the plane of the cross-sectional cut (along different radial arrays). The 90° doglegs in the beamlines are rotated either slightly into or out of the plane of the drawing. The route from final focus mirror to the center of the cavity on both figures lies in plane and is shown correctly.

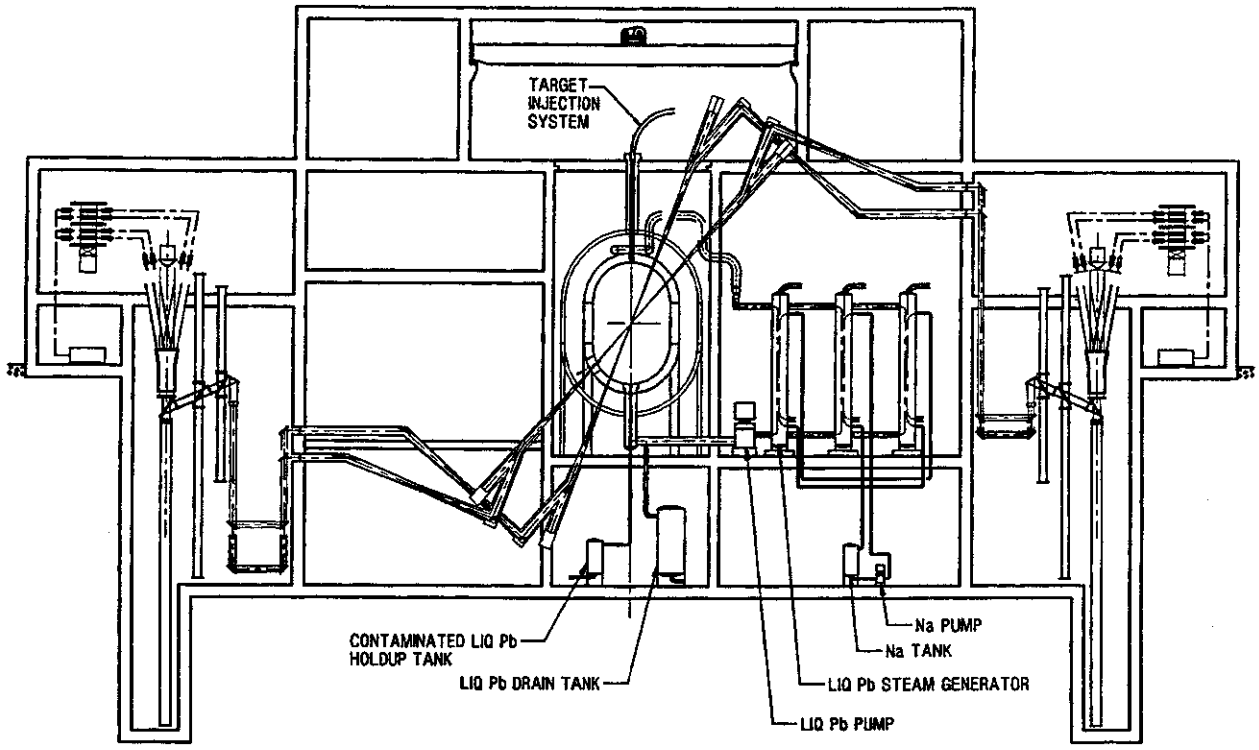

Figure 6.3.1-5. Elevation View - Typical Laser Beam Routing–5 Places

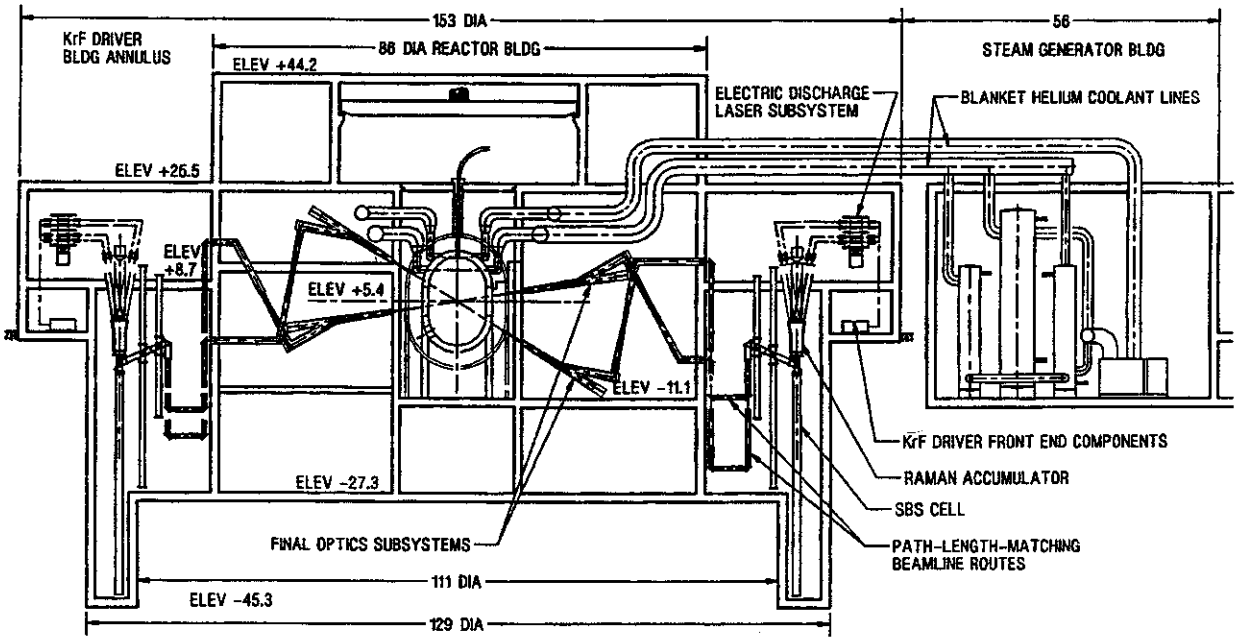

Figure 6.3.1-6. Elevation View - Typical Laser Beam Routing–10 Places

The output beam from each SBS cell is routed through four turning mirrors along a path within the driver building that will match the path lengths for all eight beams from the SBS cell to the center of the reactor cavity. From this path-matching route, the beams enter the reactor building through penetrations running radially inward toward the center of the reactor cavity. The wall penetration contains the vacuum window for each beamline. The driver building is pressurized with argon at ambient pressure. The operating pressure downstream of the vacuum window is $3x10^{-3}$ torr.

KrF Laser Driver-Electric Discharge Laser Subsystem - There are 60 electric discharge laser subsystems in the KrF driver system—one for each beamline. This subsystem consists of two electric discharge laser modules, three sets of stabilization coils, and the KrF gas flow system and is shown in Figure 6.3.1-7. The KrF gas flow system consists of inlet and outlet ducts, a helium-cooled heat exchanger, and a circulating fan. It circulates a mixture of KrF gas through four parallel paths in the two electric discharge laser modules. Each of the two discharge laser modules contains eight electric discharge lasers for a total of 16 lasers for each beamline. Thus, there is a total of 960 electric discharge lasers in the KrF driver. Each of the electric discharge lasers has a gross energy output of 4.2 kJ.

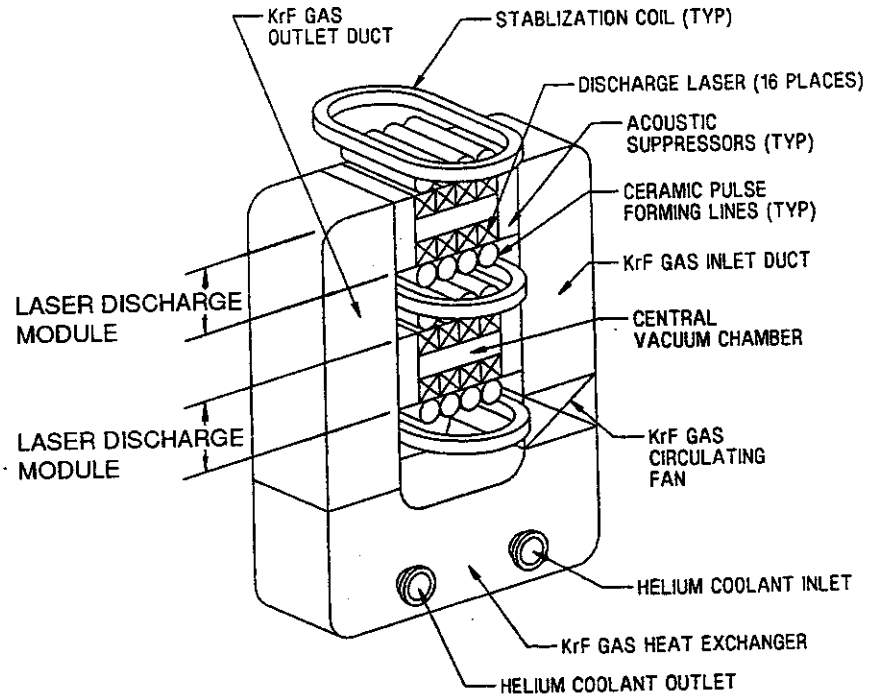

Figure 6.3.1-7. Electric Discharge Laser Subsystem

The KrF gas flow paths are shown schematically in Figure 6.3.1-8. To assure proper thermal control of the laser gas, a slug of KrF gas circulates through and clear each of the four parallel paths once for each of the 5.6 pulses per second. This yields a gas flow velocity of 15 m/s. The KrF gas is circulated by the fan through the lasers and then through the heat exchangers. The laser inlet gas temperature is 400°C and the outlet is 650°C. A cooler mixture of gas is assumed to be injected along the inner surface of the inlet and outlet windows of each laser to protect the windows from the higher temperature gases. Helium coolant is circulated through the heat exchanger to recover the resulting waste heat from the lasers. The helium is routed to a feedwater heat exchanger in the thermal transport system in the steam generator building where a total of 193 MW is recovered as feedwater preheat.

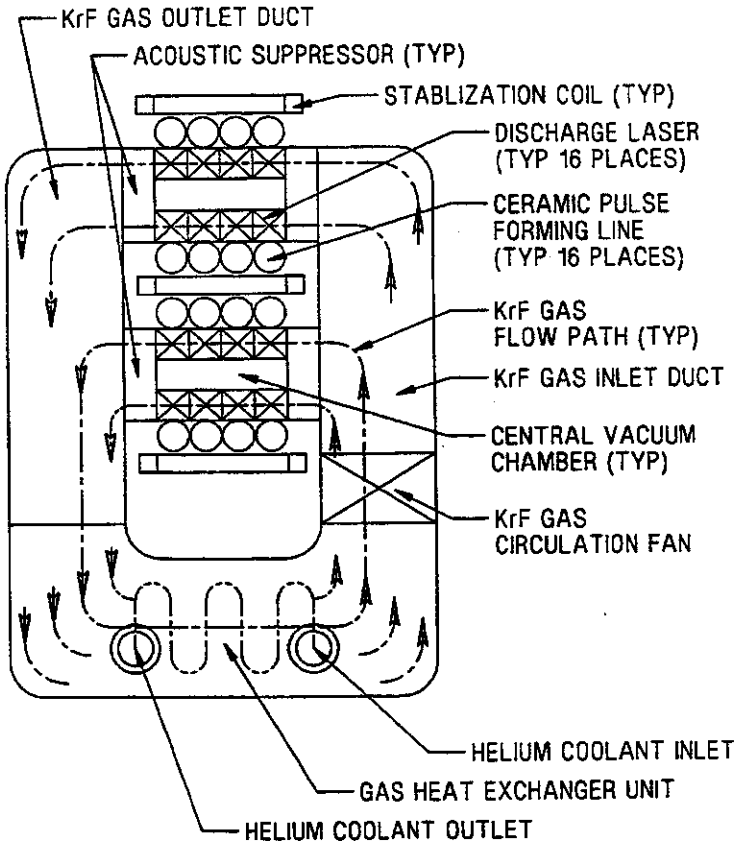

Figure 6.3.1-8. KrF Gas Flow Schematic for Waste Heat Recovery

Each electric discharge laser module contains eight discharge lasers arranged in four groups of two as shown in Figure 6.3.1-9. The discharge lasers are first clustered in groups of two lasers around a central vacuum chamber containing a pair of cathodes, one for each laser. Ceramic pulse forming lines and anodes (shown as the cylinders in Figure 6.3.1-9) are located on the outside of each laser. Stabilization coils are

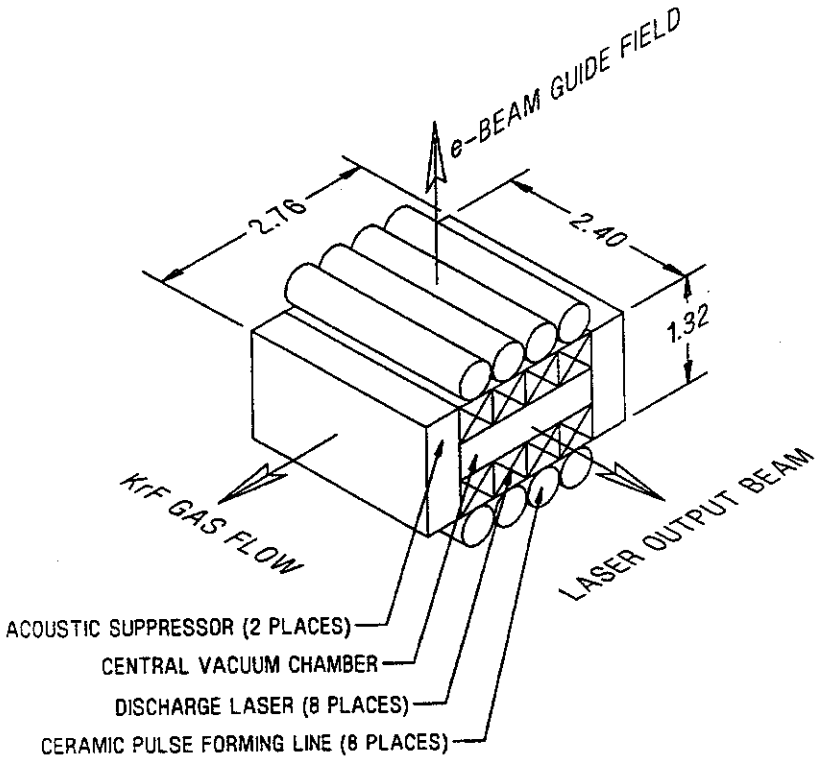

Figure 6.3.1-9. Electric Discharge Laser Module

located on the outside of the ceramic pulse forming lines as shown in Figure 6.3.1-7 forming a stabilizing magnetic field perpendicular to both the KrF gas flow direction and the laser beam direction (shown in Figure 6.3.1-9). Acoustic flow suppressors are located at the entrance and exit of the gas flow paths to maintain flow stability. A similar arrangement for discharge lasers has been suggested in previous KrF laser system studies.[1]

KrF Driver—Raman Accumulator/SBS Cell/Delay Line- Downstream of the electric discharge laser subsystem, the 16 discharge laser output beams are routed into the Raman accumulator (four beams on each of four sides) at an angle of 10° off the axial centerline. The Raman accumulator, SBS cell, and related components are shown in Figure 6.3.1-10. A larger Stokes seed beam (derived from the excimer pump beams upstream of the electric discharge laser subsystem) enters the Raman accumulator on the centerline of the Raman accumulator. Interaction of the 16 laser beams with the Stokes seed beam in the hydrogen gas environment of the Raman accumulator results in a highly amplified, long pulse Stokes beam exiting the downstream end of the Raman accumulator.

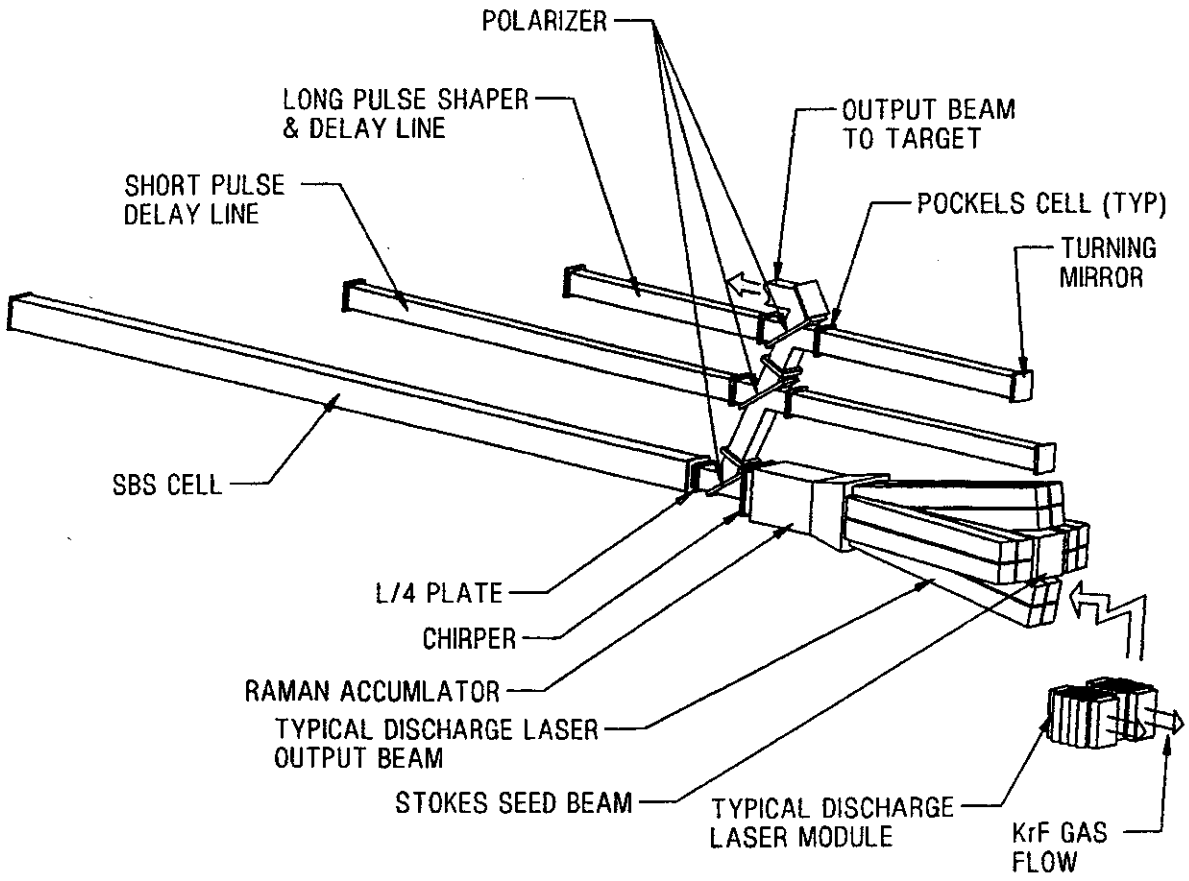

Figure 6.3.1-10. Raman Accumulator/SBS Cell/Delay Line

From the Raman accumulator, the long pulse Stokes beam passes through a chirper, a polarizer, and a quarter wave plate and enters the SBS cell. This 37.5-m long cell is filled with SF_6 gas and has a mirrored surface on the other end to reflect the entering beam back out the entrance window. The combination of these components produces a short pulse (6 ns) beam followed by a longer pulse length, depleted Stokes beam. (See Section 6.5.1 for a more complete description of this process.) The short pulse beam is the desired 6-ns pulse main beam with an energy of 70 kJ, while the longer pulse beam will be utilized to form a prepulse beam. When these beams come back out of the SBS cell and pass through the quarter wave plate, a frequency shift has occurred and the polarizer plate then reflects the beams off-axis in the direction of the short pulse delay line. (Since the 6-ns pulse main beam is in front of the longer, prepulse beam, the short pulse delay line inverts the time order of these beams.) Leaving the polarizer plate, the short pulse beam passes through a Pockels cell and strikes and is reflected off the next polarizer plate, this time into the short pulse delay line. Before the long prepulse beam enters this Pockels cell, the cell voltage is changed, which changes the polarity of the long prepulse beam such that it passes

through the polarizer plate in the short pulse delay line, proceeding on line toward the long pulse shaper and delay line.

The long prepulse beam now preceeds the short pulse main beam. Downstream, a combination of three Pockels cells are utilized to shape the prepulse beam to meet the prepulse requirements by alternately switching portions of the prepulse beam into and out of the long pulse shaper and delay line. The resulting prepulse beam (80 ns) continues downstream toward the target followed by the main beam (6 ns).

Turning mirrors route the prepulse and main beams from each of the 60 SBS cell/Raman accumulator arrangements in the KrF laser driver building into the reactor building beamlines. Delay lines allow path-length matching of all 60 beam paths. The 60 beamlines enter the reactor building through penetrations containing vacuum windows. The eight unique beam path routes discussed earlier are shown in Figures 6.3.1-5 and 6.3.1-6.

KrF Laser Driver - Final Optics Subsystem- The 60 beamlines enter the reactor cavity at angles defined by radial lines passing from the vertices to the center of a truncated icosahedron platonic solid with a pentagon/hexagon edge length ratio of 1.2. This orientation provides nearly uniform target illumination (<1% nonuniformity). This orientation of beamlines was envisioned for the Omega Upgrade facility at the University of Rochester. The resulting angular interface locations of the 60 beamlines with the reactor cavity are shown in the elevation view of the reactor cavity in Figure 6.3.1-11. Typical beams at each angular location off the vertical axis are rotated into view on both sides of the vertical axis to provide a visual indication of the beam orientations around the reactor cavity. If viewed from the top (plan view), two beams would be located on each radial plane approximately 12° apart as shown in the 3-D cavity/beamline drawing in Figure 6.3.1-12. A similar trimetric view is shown in Figure 6.3.1-13.

Typical final optics configuration contained within each beamline in the reactor building is shown in Figure 6.3.1-14. The optical characteristics of the mirrors within this region are presented in Section 6.5.1.6. From the outer diameter reactor building wall, each beamline enters on a horizontal radial array from the reactor vertical centerline. This penetration contains the vacuum window. Downstream of this window, the beams pass through a collimating mirror which focuses the beam to a point as it goes through a pinhole opening with an area of a few cm^2. This small opening allows the beam to enter the shielded region of the beamlines without releasing a significant amount of radiation. Each beamline contains an outer layer of shielding which is 25-cm thick. The shielded region runs from the pinhole opening to the beamline penetration in the bulk shielding wall. The shielding analyses for this region is presented in Section 6.8.4.1.

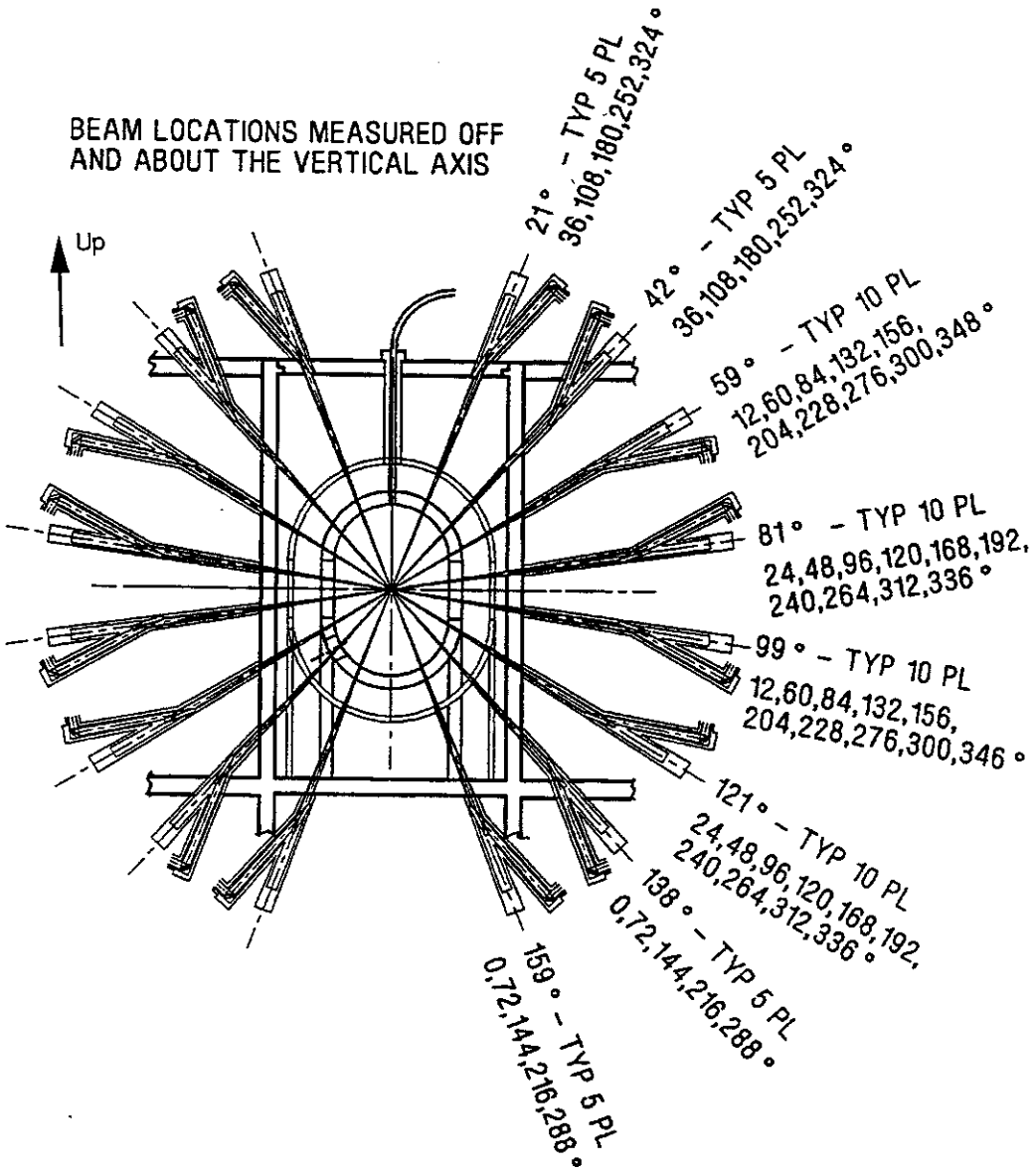

Figure 6.3.1-11. Angular Beamline/Reactor Cavity Interface Locations

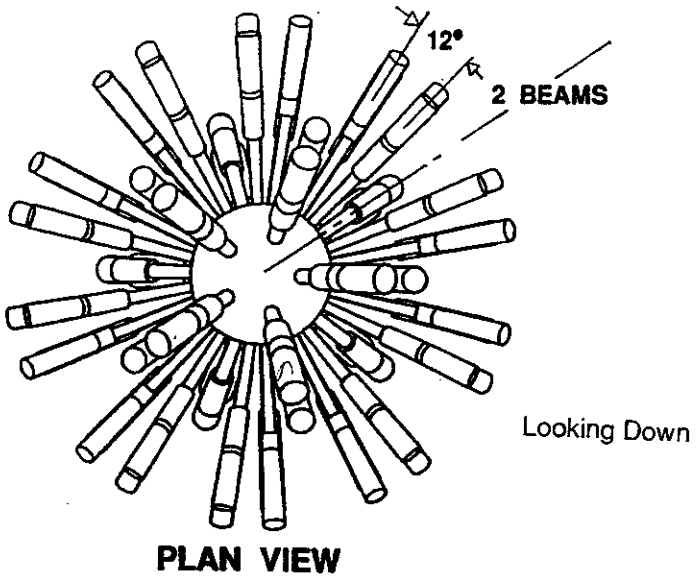

Figure 6.3.1-12. 3-D Beamline/Reactor Cavity Interface–Plan View

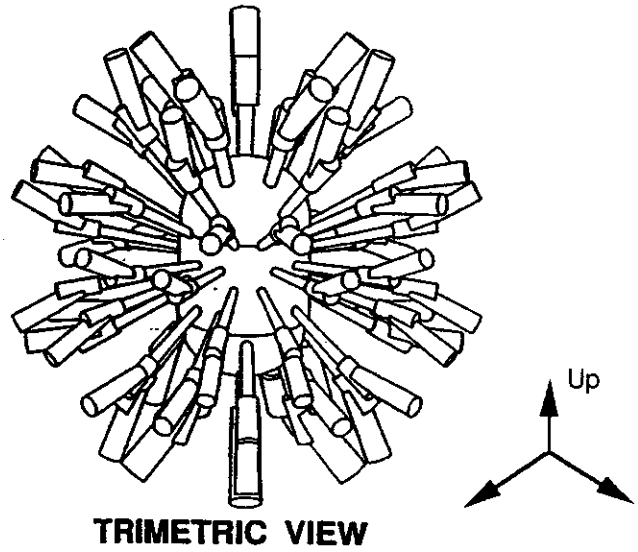

Figure 6.3.1-13. 3-D Beamline/Reactor Cavity Interface–Trimetric

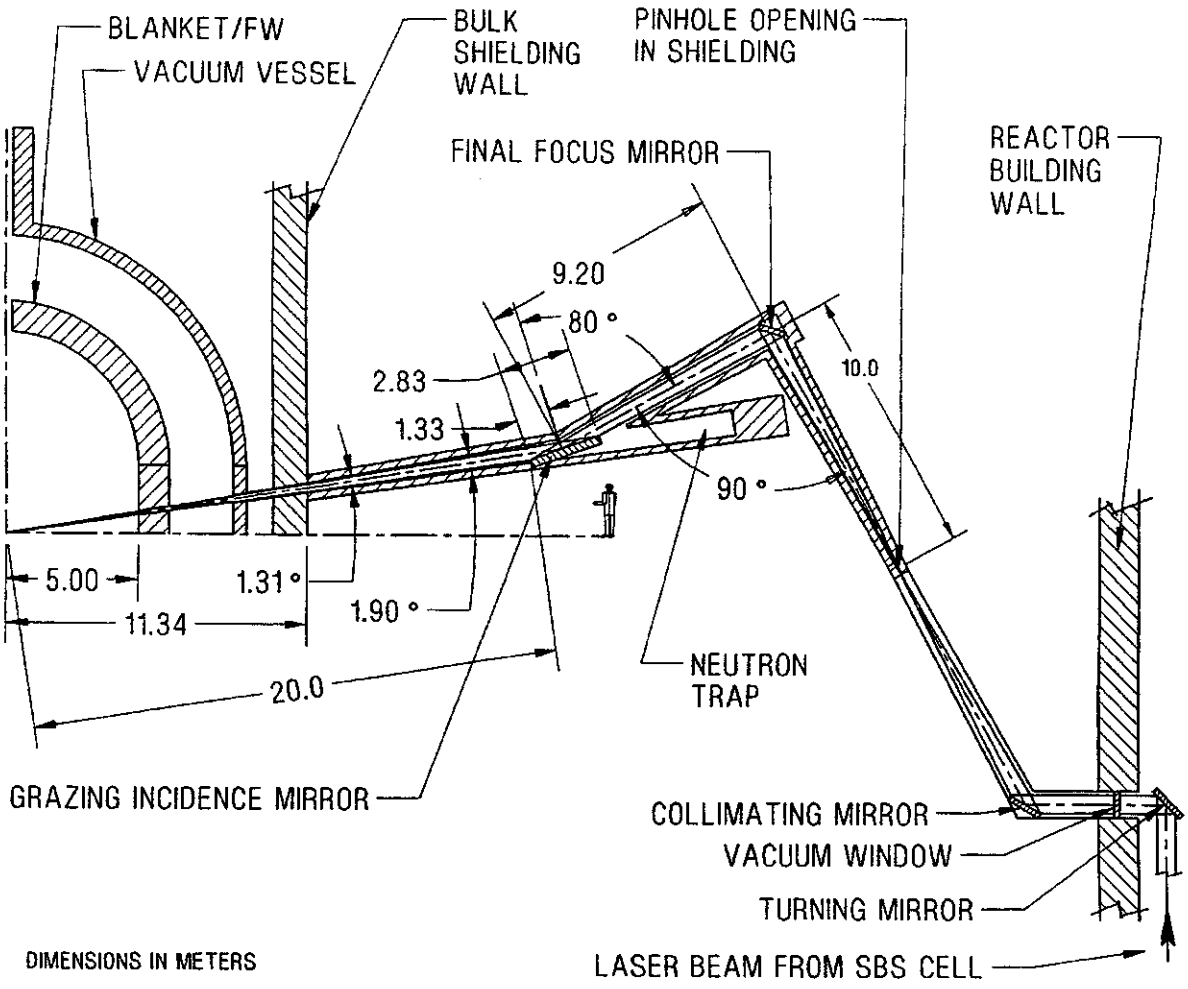

Figure 6.3.1-14. Final Optics Configuration–Reactor Building

After the pinhole, the beams tare directed downstream to the final focus mirror. This aspherical-shaped mirror, located 30 m from the center of the reactor cavity, serves to focus the beam to achieve a tangential illumination on the target at the cavity center.

The final mirror configuration is a grazing incidence metal mirror (GIMM) which is located 20 m from the cavity center. The GIMM uses a high reflective aluminum surface (1-2 mm thick) bonded to a silicone carbide ribbed structure with coolant channels. The angle of incidence of the GIMM in the beam path is 80°. This mirror is positioned in the direct line of sight with the first wall (FW) beamline openings (0.18-0.26 m in diameter). It protects the upstream final focus mirror from the radiation damaging environment. A neutron trap is located between the GIMM and the center of the reactor cavity. Shielding at the end of the neutron trap is 2 m thick. Analyses of the

GIMM and final focus mirrors suggest they are life-of-plant components; however remote maintenance methods are provided for mirror replacement and maintenance.

Protection for the GIMM and the final focus mirrors (as well as beam port walls) have been identified as a key development issue for the laser driver (see Section 5.4). The mirrors and ports must be protected from heating, blast, and radiation damage effects while not interfering with the laser beam propagation. Evaluation of this issue explored a number of protection methods as shown schematically in Figure 6.3.1-15. Protection methods include:

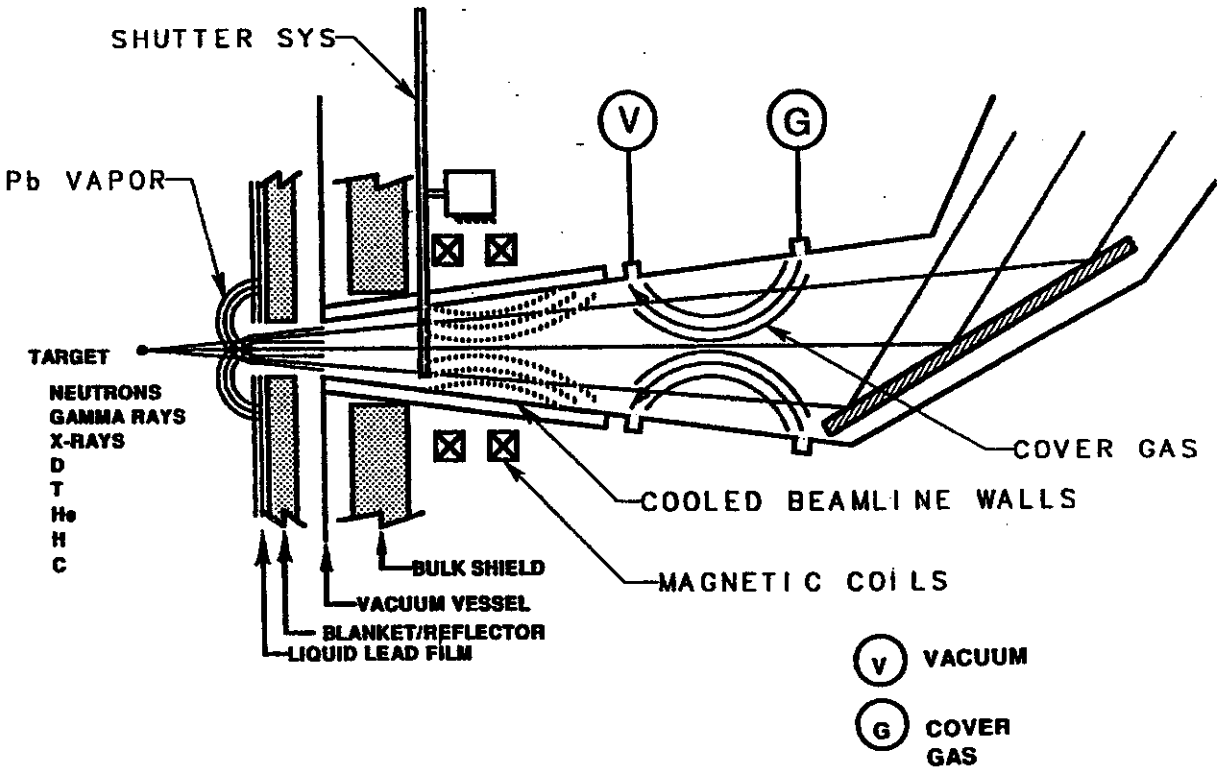

Figure 6.3.1-15. Schematic of Final Mirror Protection Methods

(1) Silicon carbide beam ports in a configuration similar to the FW panels with flowing liquid lead. The temperature of the lead would be maintained high enough to produce a lead vapor that protects the wall and mirror surfaces. Any condensed vapor on the GIMM surface would be vaporized by the prepulse beams.
(2) Residual lead vapor from the cavity could help attenuate the debris and x-rays before they reach the port area.
(3) A magnetic field could be provided by small magnet coils around the beamlines to deflect ions and electrostatically-charged particles.

(4) A cover gas, such as neon, injected in front of the GIMM could stop remaining x-rays and then be removed with vacuum pumps.
(5) Cooling the beamline walls below the GIMM surface temperature would help assure the condensable gases adhere to the walls instead of the optics.
(6) A shutter system could intercept lead droplets before they reach the optics, especially in the lower beamlines.

The baseline design employs a multilayer defense using all the above methods except the cover gas and cooled wall approaches. A neon cover gas resulted in extremely difficult vacuum pumping requirements. Instead, the baseline design provided a lead vapor cover gas by flowing hot lead through porous beamport walls and depending on the laser prepulse to remove any recondensing lead from the optic surfaces.

Prometheus-L Reactor Subsystems Overview - The subsystems that make up the reactor subsystem include the reactor vacuum vessel, vacuum pumping system, target injection, first wall, blanket, and the primary coolant systems. A wetted-wall reactor cavity concept is common to both the Prometheus-L and Prometheus-H reactor designs. The common cavity concept will be described in some detail for the Prometheus-L concept, and only the differences will be noted in the Prometheus-H description. All aspects of the cavity design are presented in detail in Section 6.8.

An elevation view of the central reactor cavity configuration is shown in Figure 6.3.1-16. The radial and elevation builds of the cavity are defined in this figure as is the dimensional configuration of the vacuum pumping system discussed below. Dimensions of the bulk shielding walls (1.3 m thick) are also defined.

Prometheus-L FW/Blanket Subsystem - The cavity first wall (FW) system employs liquid lead (Pb) which both cools and protects the silicon carbide (SiC) FW structure. Liquid lead bleeds through the porous first wall reactor facesheet, forming a protective liquid film on the surface. The microexplosion of the DT targets release three forms of fusion energy: neutrons, x-rays, and target debris ions. The energies from x-rays and target debris ions induce in surface heating of the Pb film, evaporating a portion of the film. As the film surface cools, the evaporated Pb condenses on the surface where the energy is conducted through the porous FW and is removed by convection into the flowing liquid Pb coolant. Also, a portion of the neutron energy is collected in the flowing Pb coolant as volumetric heating.

The SiC composite FW is 6 cm thick, with 5 cm diameter coolant channels. The film thickness of liquid Pb on the FW surface is 0.5 mm. Liquid Pb is pumped through the steam generator located in the reactor building to the top of the reactor cavity where it is distributed to the FW panels and flows downward to the collection header at the bottom of the reactor cavity. The general arrangement of the pumps, steam generator,

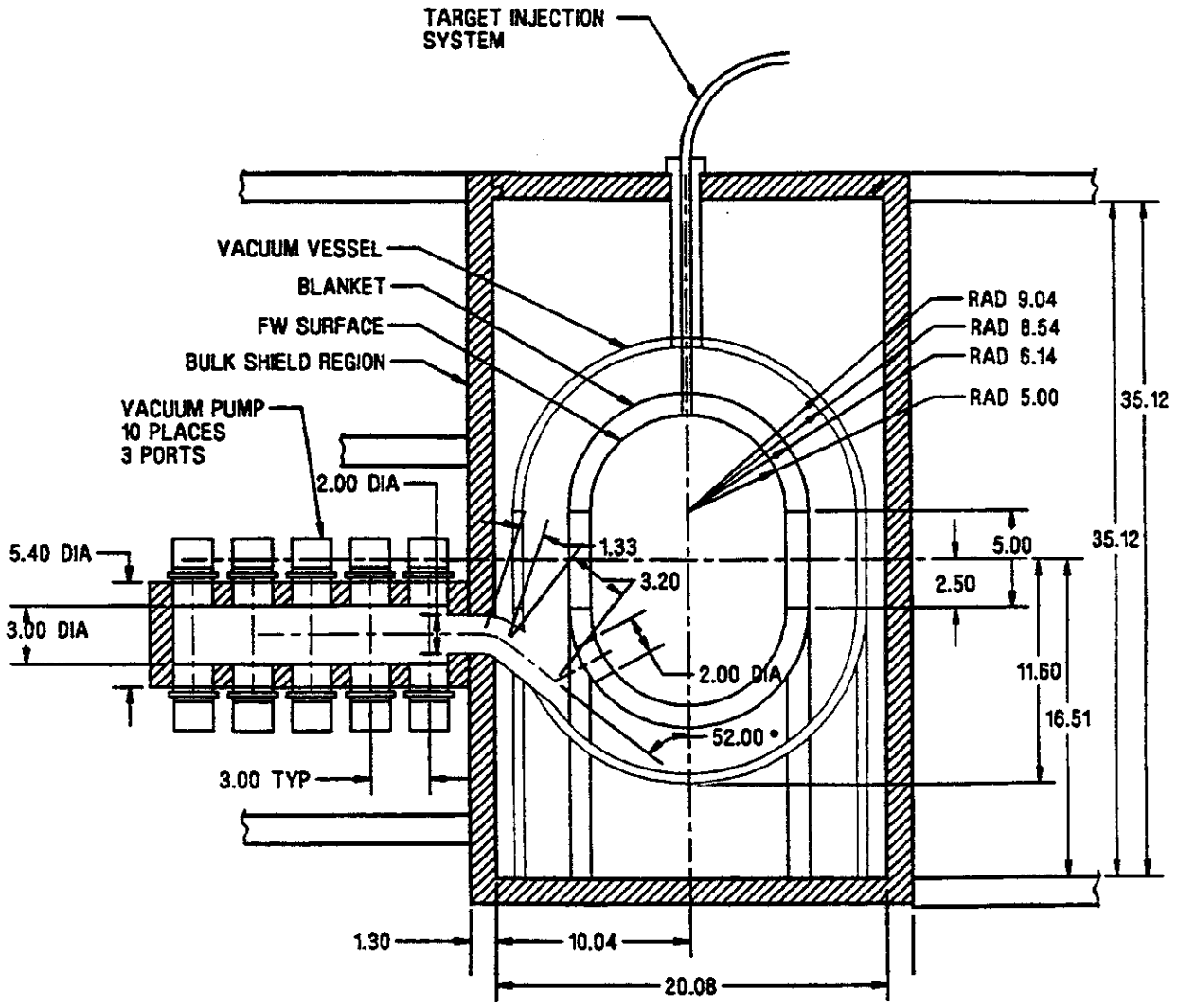

Figure 6.3.1-16. Elevation of Central Reactor Cavity Region

and inlet and outlet manifolds is shown in Figures 6.3.1-5 and 6.3.1-6. The liquid lead inlet/outlet temperatures are 375/525°C with pressures of 2.0/1.5 MPa, respectively.

The remaining useful neutron energy is captured in the blanket system. This helium cooled, solid breeder blanket system features SiC composite structure for a Li_2O peeble bed breeder with helium purge. The blanket section of the cavity is composed of stacked ring modules , each connected to helium manifolds in back of the blanket modules. Vertical supply and return headers supply helium coolant to/from the top of the reactor where inlet and outlet helium lines are located. (This configuration is shown in detail in the maintenance section of the report in Figures 6.3.2-4 and 6.3.2-5). Helium outlet lines connect the vacuum vessel to the helium steam generation components in the steam generator building. The general arrangement of

these components is shown in Figures 6.3.1-4 and 6.3.1-6. The hot helium flows through the steam generator releasing its energy to feedwater which is converted to steam for the power conversion system. A helium circulator driven by a steam turbine returns the helium back to the reactor blanket system via the helium inlet lines to the top of the reactor cavity. Tritium is bred in the breeder zones of the blanket and is collected by a separate helium purge system. The blanket tritium breeding ratio is 1.20.

The blanket inlet/outlet helium temperatures are 400/650°C with a inlet pressure of 1.5 MPa. The total pressure drop within the helium coolant system is 85 kPa with 33 kPa in the blanket. The total blanket thickness is 104 cm which is made up of 60 cm breeder zone, 20 cm reflector zone, 6.5 cm for inner/outer SiC structure, and 17.5 cm for internal plenum manifolding.

Prometheus-L Vacuum Pumping Subsystem - The propagation of the laser light beams within the reactor cavity required that the vacuum system pump the cavity to a base pressure of 1-3 mtorr prior to each pulse. Noncondensible gases of hydrogen, helium, deuterium, and tritium from each target implosion are pumped by a system of 30 vacuum cryopumps. These pumps are arranged in clusters of ten pumps, each at three radial locations around the reactor cavity. The detail configuration is shown in Figure 6.3.1-16. A reactor building cross-section in Figure 6.3.1-17 shows the vacuum

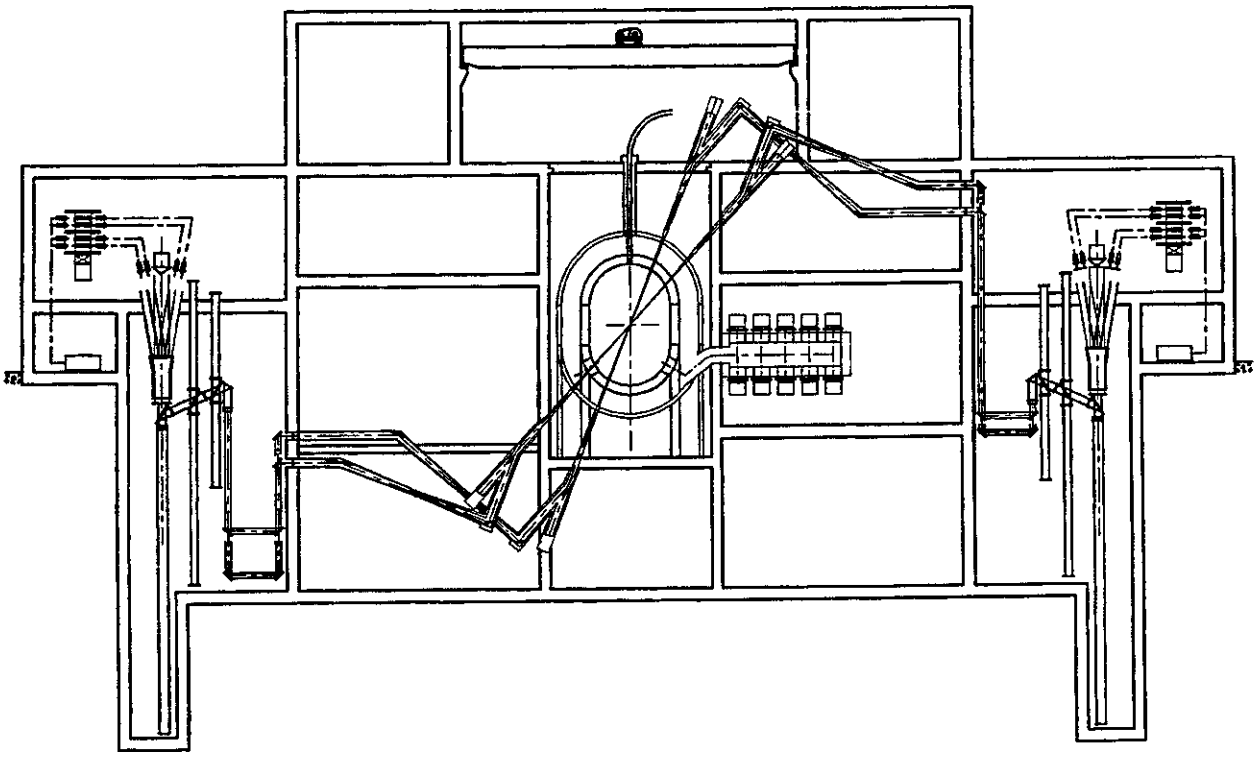

Figure 6.3.1-17. Vacuum Pumping/Reactor/Final Optics Systems Interface

pumping system relative to the cavity and laser beam lines. Pumps are attached to a 3-m diameter plenum which is connected to the vacuum vessel by a 2-m diameter duct attached to the vacuum vessel at each location. Radiation shielding 1-m thick surrounds this enclosure. Vaporized lead and carbon are assumed to recondense within the cavity or at the vacuum pump duct inlets. The design aspects of the vacuum pumping system are discussed in detail in Section 6.6.

Prometheus-L Target Injection System Reactor Interface - The Prometheus-L concept uses the direct-drive targets. An electromagnetic injection system injects targets into the reactor cavity at a rate of 5.65 per second (484 x 10^3 per day). The single shell targets are 6 mm in diameter. The target injection interface with the reactor cavity is shown in Figure 6.3.1-16. This injection system is discussed in detail in Section 6.4.4.

Prometheus-L Reactor Vacuum Vessel - The reactor vacuum vessel shown in Figure 6.3.1-16 provides the required pressure boundary for the reactor. A vessel radial build of 0.5 m is allocated for the overall structural arrangement although the overall actual vessel pressure boundary thickness will be only a few cm. The material for the vessel is a low activation ferritic steel material. There is some power loss through the FW/blanket system, thus the vessel will require heat removal capability. This could be an active, liquid cooled system or perhaps a passive, convective system over the outside of the vessel.

6.3.1.2 Prometheus-H - The Prometheus-H reactor power plant employs a single-beam linear induction accelerator (LINAC) driver design to deliver the necessary energy to the indirect drive targets. Site plans for the Prometheus-H reactor design power plant are shown in Figures 6.3.1-18 through 6.3.1-20. Presented are a trimetric view of the plant site, a plan view of the plant site, and a building definition plan view, respectively. These figures show the configurational arrangement of the heavy ion beam driver components and the interface with the 59-m diameter IFE reactor building. The heavy ion beam driver components are located in a network of tunnel complexes with a total length of 2700 m. Two main beam bundles enter the reactor building from two sides, 180° apart. Typical IFE power plant buildings (administration, auxiliary, turbine, steam generator, target factory, and tritium processing) complete the site complex. Notice that Figure 6.3.1-20 shows the routing of the LINAC with broken lines. Figures 6.3.1-18 and 6.3.1-19 show the site plan with the full 2700-m length of the heavy ion driver shown to scale.

Prometheus-H Driver - General Overview - This driver is a single-beam induction linear accelerator (LINAC) design which generates and accelerates a sequential series of 18 heavy ion beamlets with a total energy output of 7.8 MJ. The technical, theoretical, and operational aspects of this driver system are discussed in Section 6.5.2.

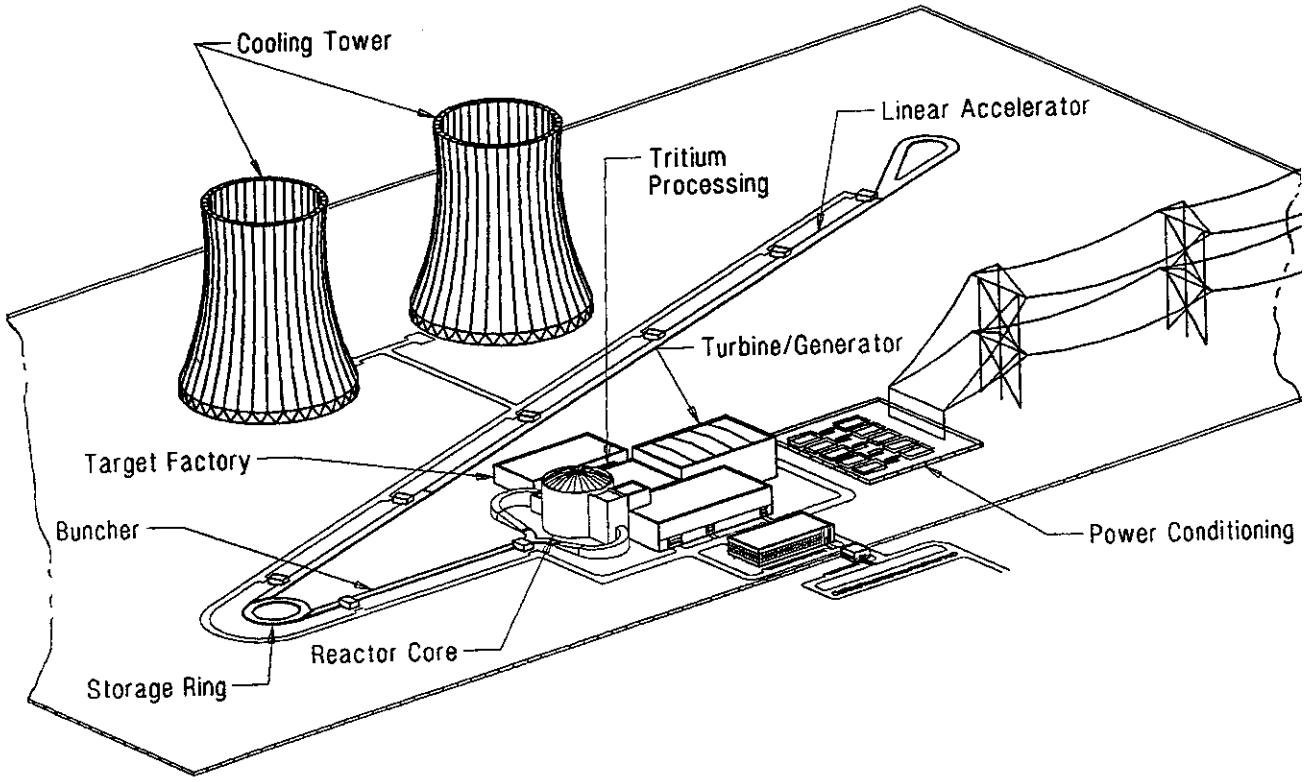

Figure 6.3.1-18. Prometheus-H Plant Site Trimetric View

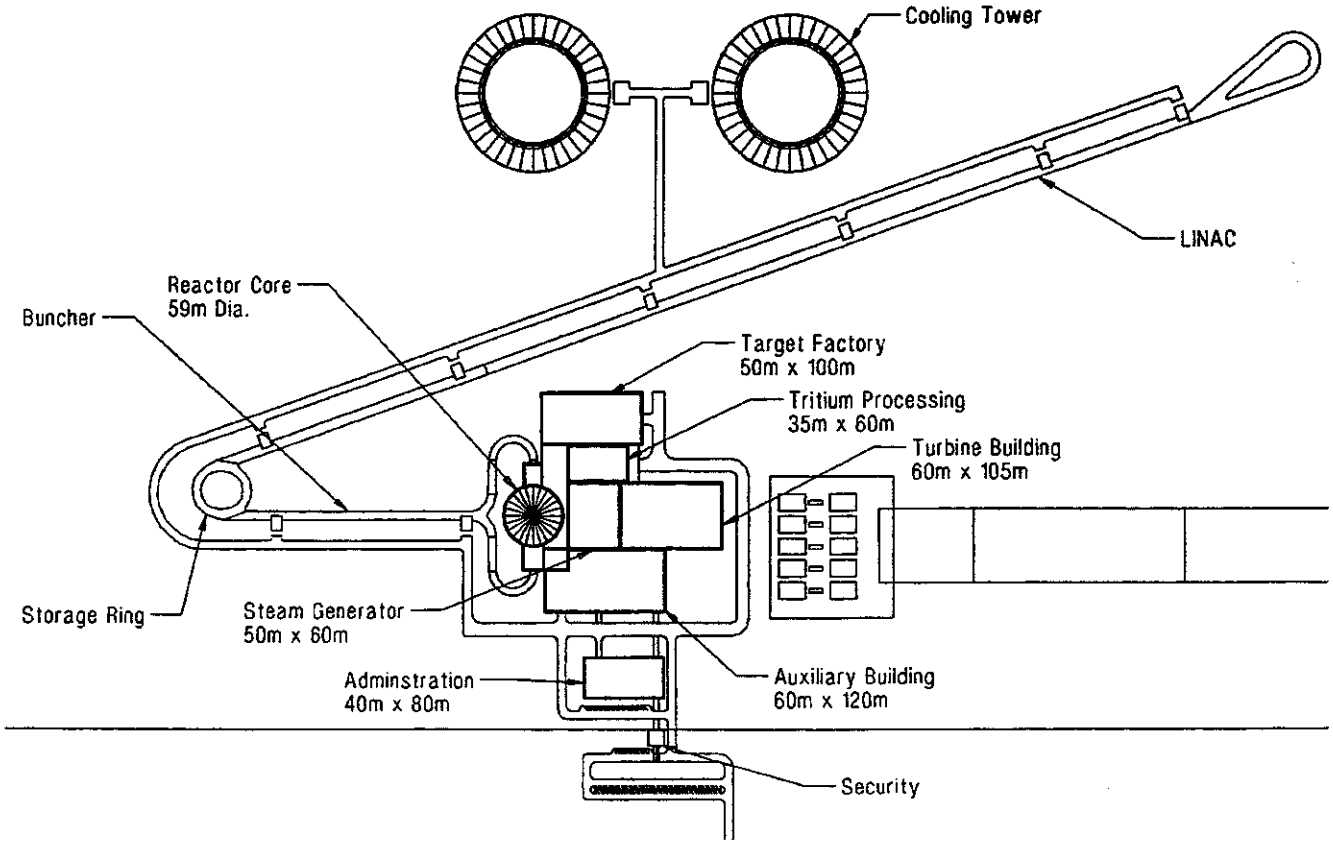

Figure 6.3.1-19. Prometheus-H Plant Site Plan View

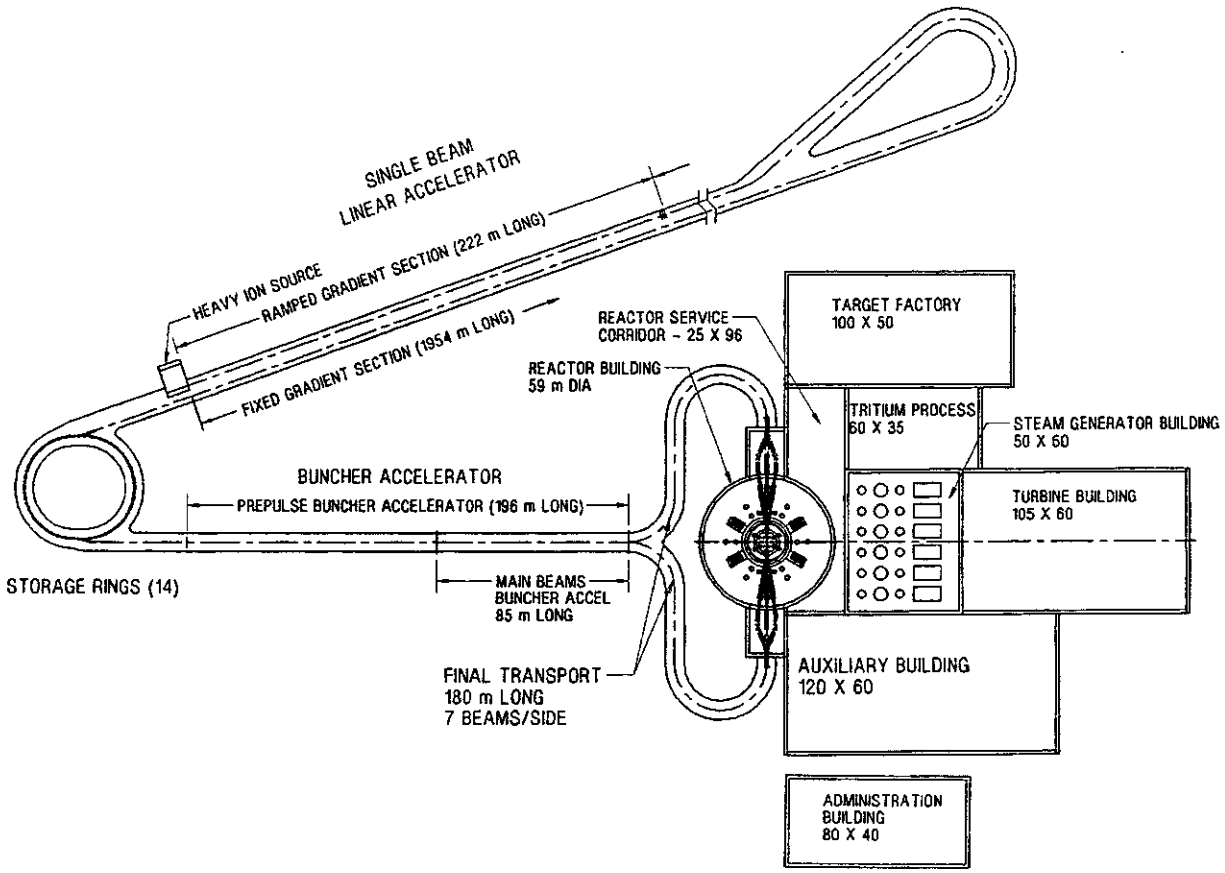

Figure 6.3.1-20. Prometheus-H Building Plan View

The major subsystems are the heavy ion LINAC, storage rings, buncher accelerator, final transport, final focus, and channel formation sections. The major components and general arrangement of these subsystems are shown in a sketch in Figure 6.3.1-21 with the final focus and channel formation subsystems located inside the reactor building not shown in detail. These subsystems will be discussed in the sections below. A heavy ion source on the front end of the LINAC generates and injects the 18 heavy ion (Pb) beamlets into the single-beamline LINAC section where they are accelerated to the desired energy state. From the LINAC section, the 18 beamlets are stored in a set of 14 vertically-stacked storage rings which store the beamlets (12 main and 6 prepulse beamlets) until the proper time for release. The six prepulse beamlets are stored in two storage rings with three sequential beamlets in each storage ring (one storage ring for each set of prepulse beamlets going to each side of the reactor). At the proper time, the beamlets from first the prepulse and then the main beamlet storage rings are simultaneously released into 14 parallel beamlines leading to the buncher accelerators. There are two separate buncher accelerators—one for the prepulse beamlets (196-m long) and one for the main beamlets (85-m long). The buncher accelerators compress the beamlet lengths to achieve the required pulse lengths for both the prepulse (30 ns) and main (7.3 ns)

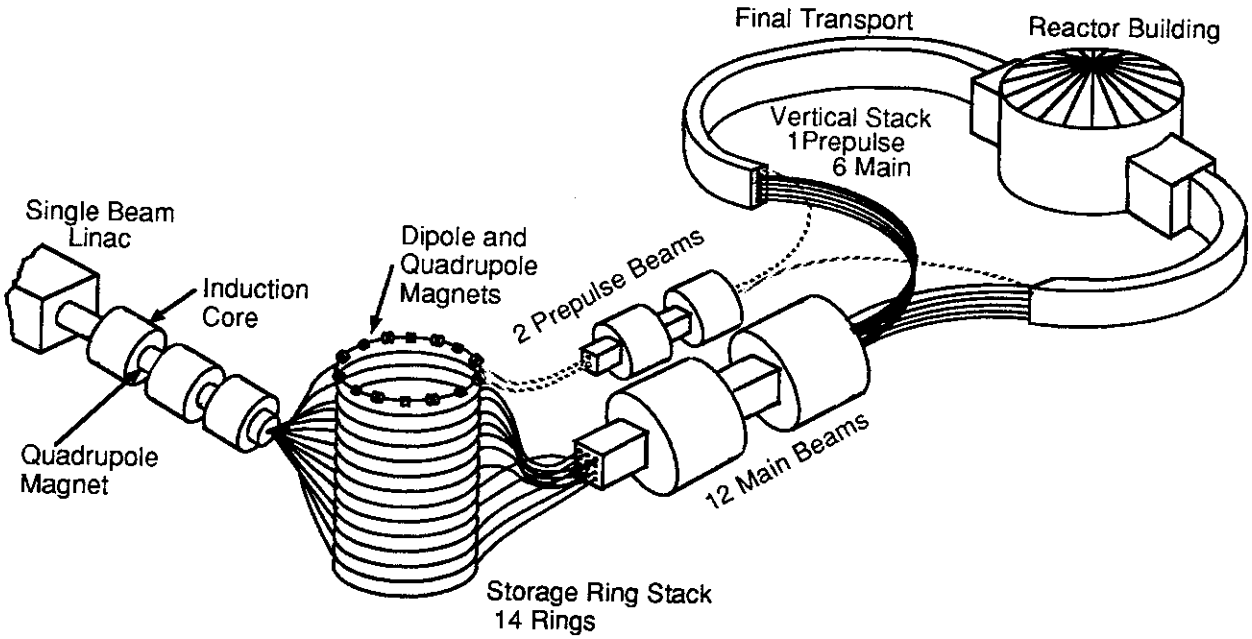

Figure 6.3.1-21. Schematic of Heavy Ion Driver Subsystems

beamlets. The buncher accelerator consists of 14 parallel beamlines—two for the prepulse beamlets and 12 for the main beamlets.

From the buncher accelerators, the prepulse and main beam routes separate into two identical 180 m long routes to the center of the reactor cavity. The typical routes enter the reactor building 180° apart with each route containing a vertical stack of seven parallel beamlines—six for the main beamlets and one for the prepulse beam (made up of three sequential beamlets). At the entrance to the reactor building system, the six main beams on each side are routed from the vertical stack to a conical array with a half angle of 8.54°, allowing all beams to be focused to a midplane point on the outer diameter face of the blanket cylindrical section. The prepulse beam line on the top of the vertical stack is routed to the horizontal, axial centerline of the conical array focusing on the same point. At this point, a lead-vapor gas jet forms an aero window over the 2-cm diameter cylindrical opening through the blanket module to the reactor cavity. This aero window serves as an electron stripping cell, allowing the beams to become one beam which is a highly charged, high current, self-pinched beam for transport through the final 5.64 m of cavity environment to the target at the center of the cavity. The prepulse beam arriving first forms a plasma channel for the following six main beams. All seven beams from each side (prepulse beams first, then main beams) strike the ends of an injected, indirect drive target in the center of the reactor cavity. The target implodes, releasing 719 MJ of energy to the reactor cavity at the rate of 3.5 pulses per second.

LINAC Subsystem - The LINAC subsystem consists of the heavy ion source/injector, ramped gradient sections, and fixed gradient sections. These components are located in a tunnel system with a nominal width of 10 m. In order to minimize the length of the tunnel network, a "hair-pin" arrangement of the tunnel system is used to house the 2200-m LINAC subsystem. The front end of this system is the heavy ion source and injector which contains all the components necessary to deliver heavy ion beams with the required properties to the ramped gradient portion of the LINAC. Representations of the source/injector portions of the LINAC subsystem were not developed in this study other than to represent the general location of the heavy ion source location on the site plan in Figure 6.3.1-20. The source/injector operates in "burst" mode, injecting a sequential set of 18 beamlets into the ramped gradient section at a repetition rate of 3.5 cycles per second. Specific parameters for the injector are discussed in Section 6.5.2.

The ramped and fixed gradient sections of the LINAC both accelerate and compress the injected beams traveling down the 2200-m length of the LINAC. The main components of the single beam LINAC are induction core modules and superconducting quadrupole magnets. These components are arranged in alternating fashion along the single beamline as shown in the schematic in Figure 6.3.1-21. The LINAC baseline configuration of the induction cores and the quadrupole magnets is shown in Figure 6.3.1-22. Note that the outer diameter and the length of the induction cores and the effective width of the superconducting quadrupole magnets change along the length of the LINAC system. Figure 6.3.1-22 shows those dimensions at three points—at the injector, at the transition between the ramped and fixed gradient sections, and at the end of the LINAC.

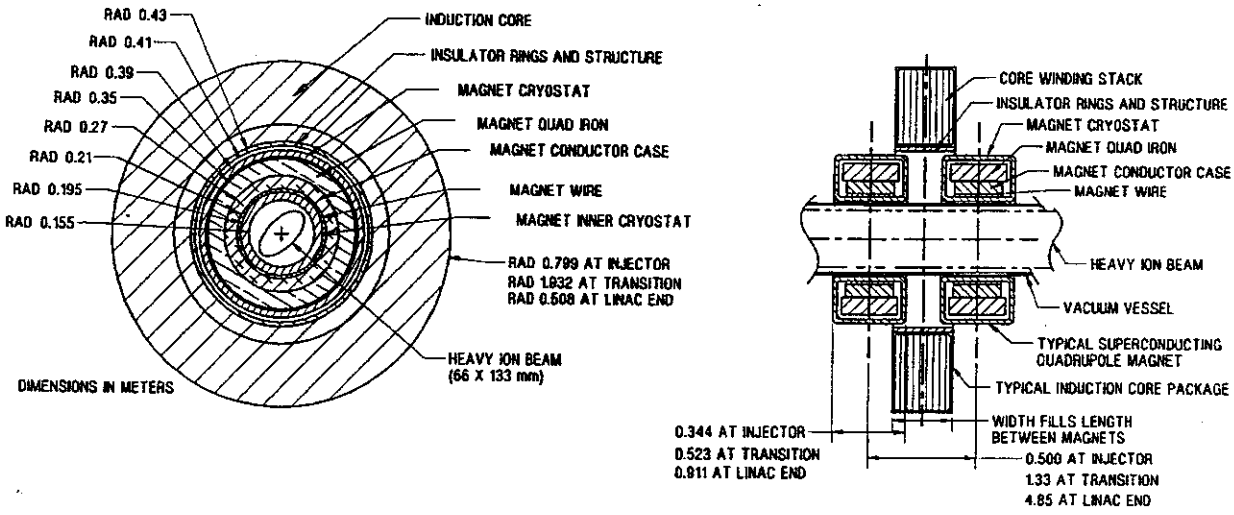

Figure 6.3.1-22. Configuration of Induction Cores and Quadrupole Magnets

The induction core modules function to accelerate the injected beamlets while the quadrupole magnets form the transport channel in between the induction cores. The ramped and fixed gradient sections function identically but differ in the allowed voltage gradient as a function of position along the accelerator length. The end of the ramped gradient section is defined as the point where the maximum gradient is reached. Section 6.5.2 describes the technical characteristics of these sections in more depth.

A typical cross-section of the LINAC subsystem tunnel complex at one of the maintenance buildings along the LINAC is shown in Figure 6.3.1-23. The maintenance buildings are located 200 m apart as shown in the site plans in Figures 6.3.1-18 and 6.3.1-19. These figures shows the single beamline, folded LINAC going in both directions—first down the tunnel system away from the heavy ion source and then back toward the storage ring tunnel complex.

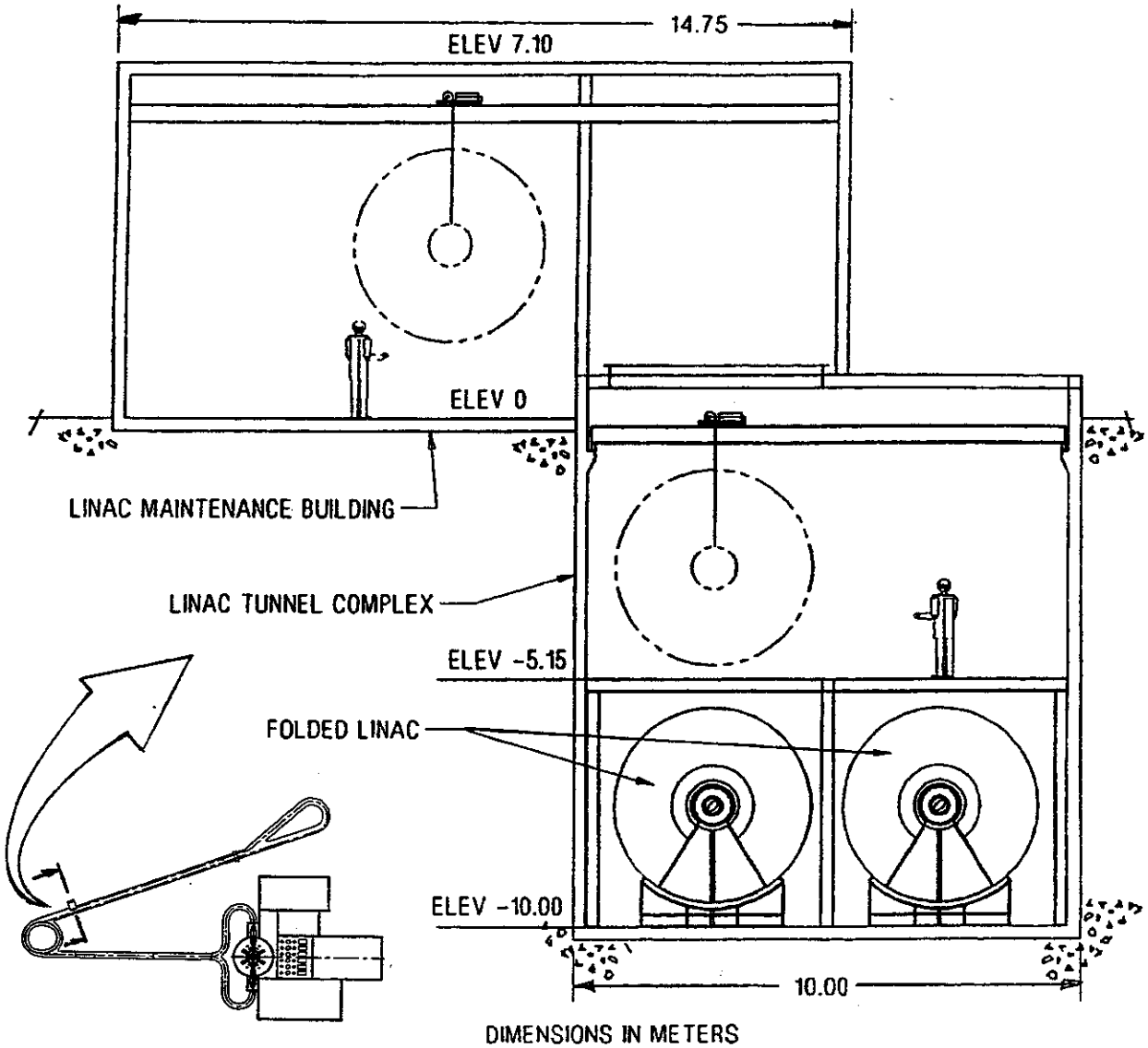

Figure 6.3.1-23. Typical Cross-Section LINAC Tunnel Complex

Storage Ring Subsystem - The single beam LINAC outputs the sequential array of 18 beamlets to a vertical stack of 14 storage rings as discussed above in the overview description. The storage rings store the beamlets until the proper timing for release toward the target in the reactor cavity. A network of beamlines with switching magnets routes the single beam output of the LINAC to the proper storage ring. A plan view of the storage ring is shown in Figure 6.3.1-24 which shows the arrangement of quadrupole and dipole magnets in two semi-circular arrangements with a short

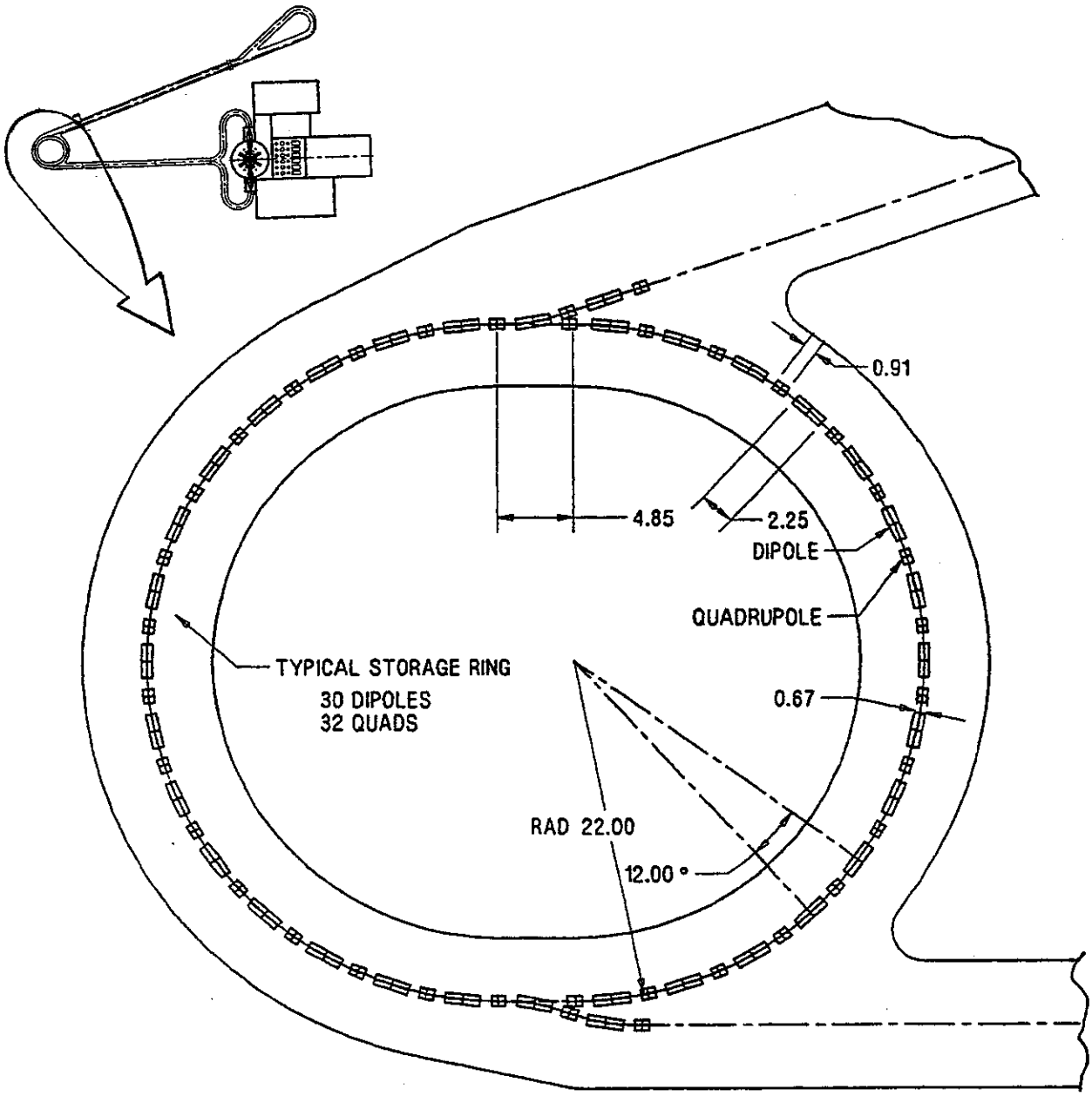

Figure 6.3.1-24. Storage Ring Plan View

straight section in between for switching the beamlines into and out of the storage rings. The vertical stack of 14 parallel beamlines in the storage ring is shown in the cross-sectional view of the storage ring tunnel complex in Figure 6.3.1-25. A detail in this figure shows the general arrangement of beamline components around the beamline.

Buncher Accelerator Subsystem - This subsystem functions to compress the overall length (head-to-tail length) of beamlets released from the storage ring complex to achieve the proper beam length at the time of impact with the target. Two sets of buncher accelerators are included in this subsection—one for the 2 prepulse beams (196 m long) and one for the 12 main beams (85-m long). The buncher accelerator components are identical in functional arrangement as the components in the main LINAC; i.e., the components again consists of a repeating arrangement of an induction core in between quadrupole superconducting magnets. However in the buncher accelerators, there are multiple, parallel beamlines. To reduce the number of induction cores, the parallel beamlines are grouped together and are run through a common induction core around all the parallel beams. Within the prepulse beam buncher accelerator, there are two parallel beam running through a common induction core. Similarly, within the main beam buncher accelerator, there are 12 parallel beamlines running through a common induction core. This is shown in the cross-section of the buncher accelerator tunnel complex in Figure 6.3.1-26.

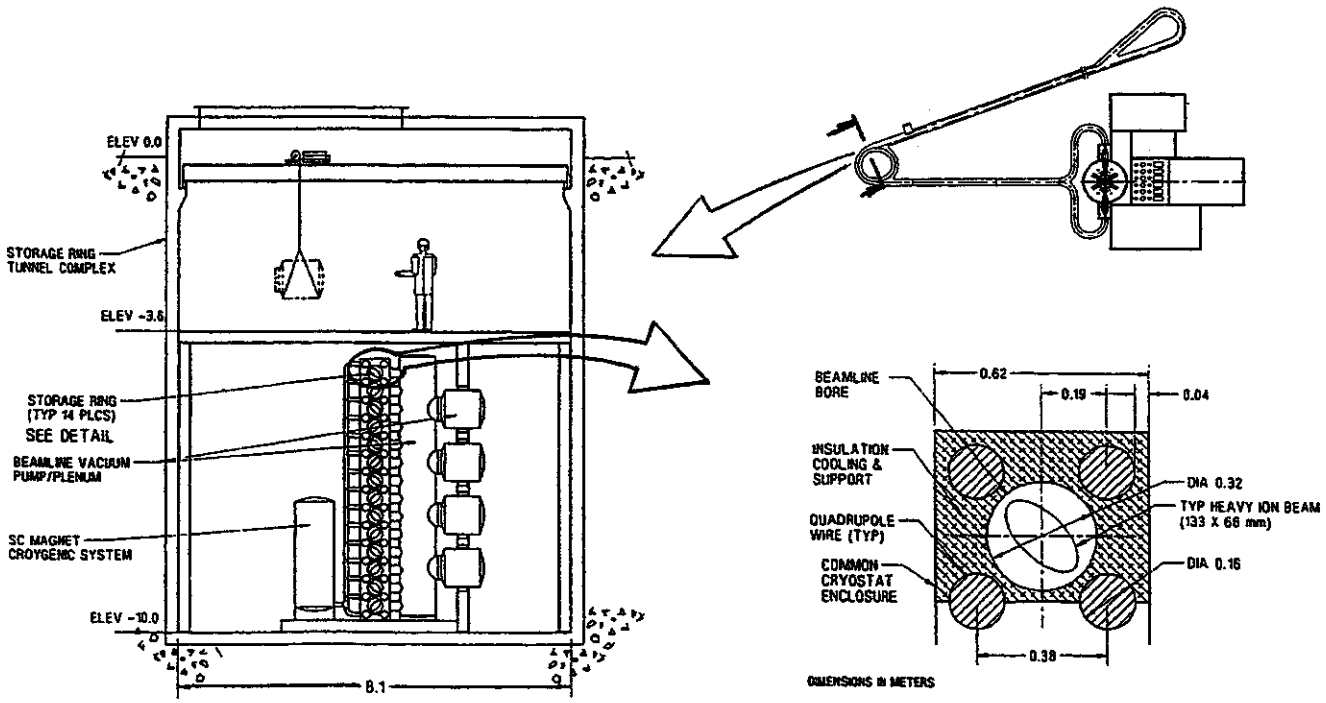

Figure 6.3.1-25. Storage Ring Tunnel Cross-Section and Typical Beam Detail

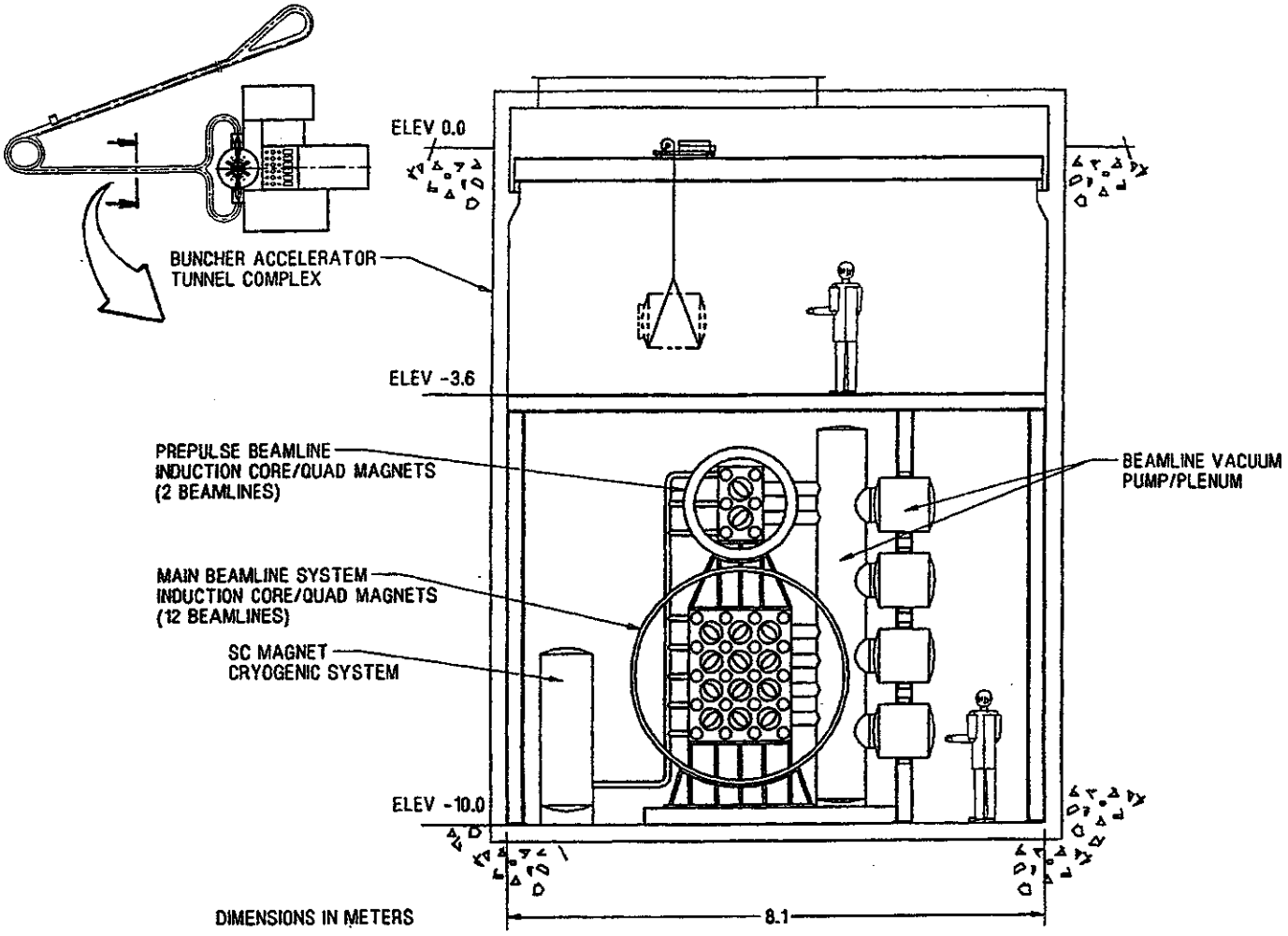

Figure 6.3.1-26. Buncher Accelerator Cross-Section

The beamlines exit the buncher accelerators at a common point and then divide up with one prepulse beam and six main beams routed to each side of the reactor building. The configuration and routing from LINAC to reactor is shown schematically in Figure 6.3.1-27 by the arrangement of the typical cross-sectional configurations of the beamlines in each major area. The configuration of components along the routes from each major area to the next consists of the parallel beamlines with alternating arrangement of quadrupole and dipole magnets. The quadrupole magnets maintain the channel transport and focus, and the dipole magnets are used to bend the beamlines along the curved paths. In pure straight sections with no bends, only quadrupole magnets are needed.

Final Focus Subsystem - The final focus subsystem consists of a triplet set of superconducting, quadrupole magnets in each beamline, and a final focus vacuum

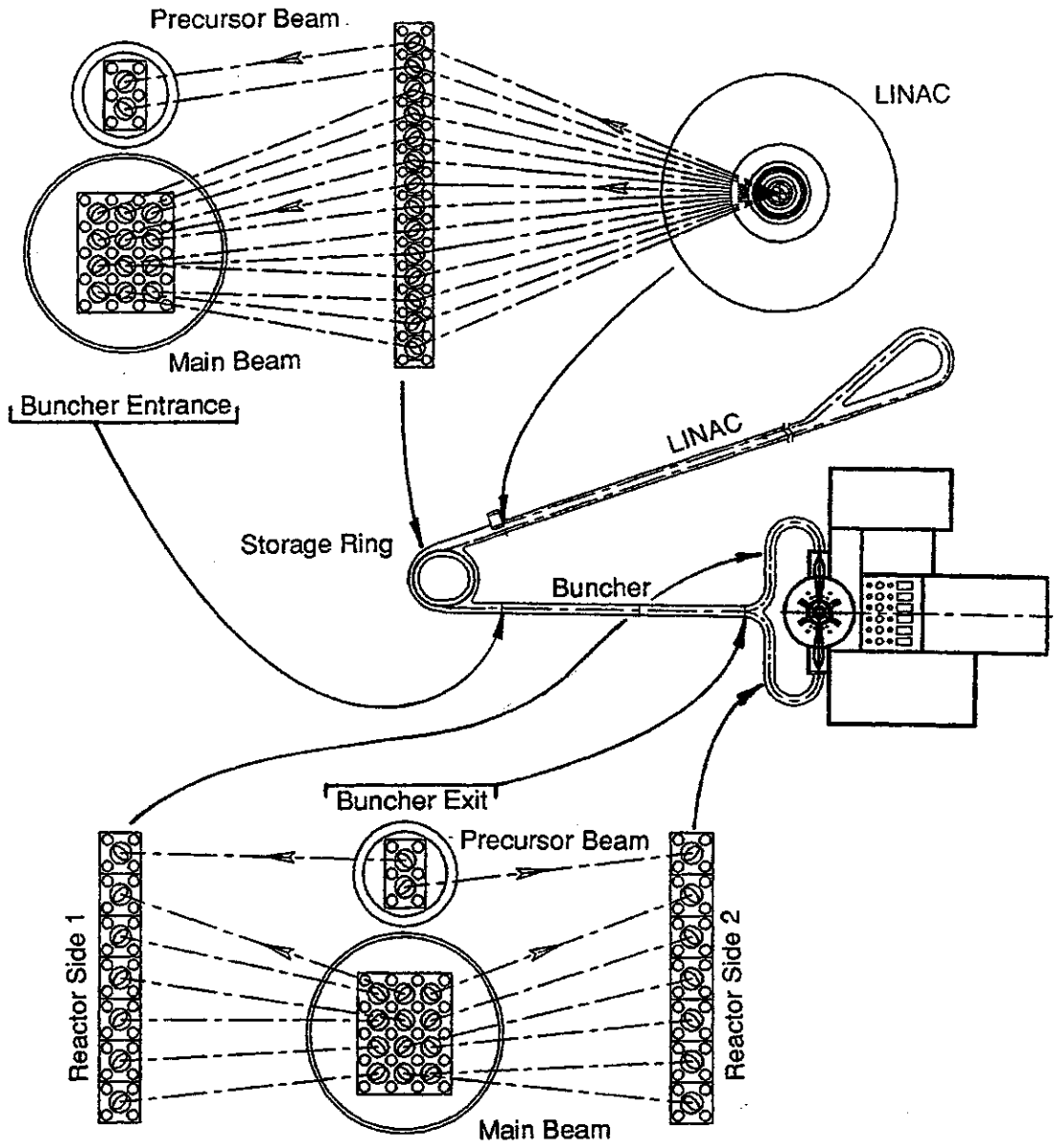

Figure 6.3.1-27. Beamline Configuration – Routing from LINAC to Reactor

enclosure. Components within this subsection are shown in Figure 6.3.1-28. The function of this subsystem is to accept the set of seven beams (six main and one prepulse) arriving from the last quadrupoles in the final transport section and to focus the beams on a common focal point which is on the outer diameter of the blanket cylindrical section. After passing through the triplet final focusing magnet sets, the beams proceed by ballistic transport to the focus point. To final focus the seven beams to a common point, the prepulse beam is routed from the vertically-stacked beamlines to a horizontal, on-axis position and the six main beams are routed from the vertical stack to an equally-spaced conical array around the center prepulse beamline. The

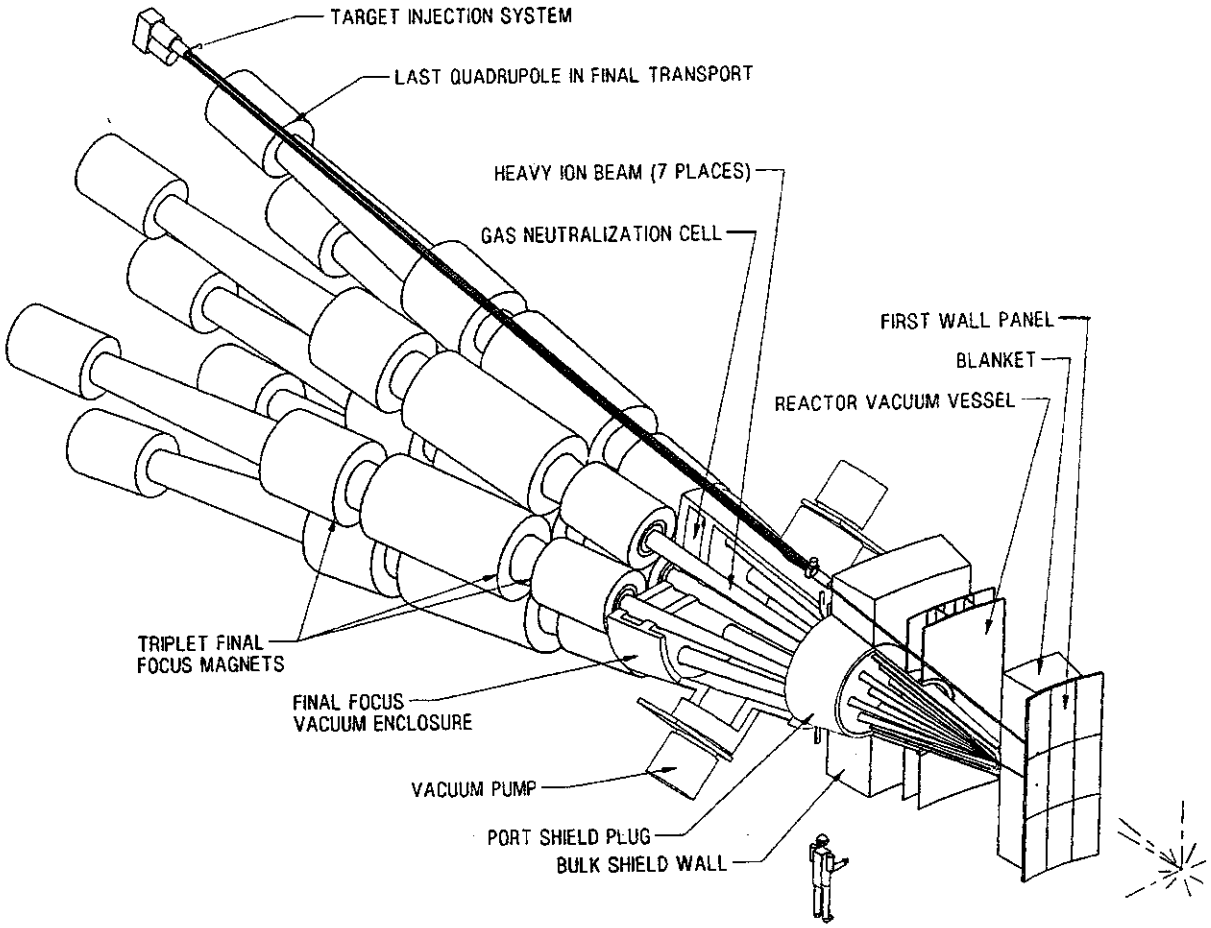

Figure 6.3.1-28. Heavy Ion Beam Final Focus Subsystem Configuration

conical array of six main beams has a half angle of 8.54°. The resulting interface with the reactor cavity is also shown in an elevation view in Figure 6.3.1-29 and in a plan view in Figure 6.3.1-30. The main beams in the conical array and the final focus vacuum pumps in Figure 6.3.1-29 and the vacuum pumps in Figure 6.3.1-30 have been rotated about the conical centerline into view for clarity.

The final focus vacuum enclosure provides an interface between the triplet magnet sets in each beamline and the outboard face of the cylindrical blanket modules at the midplane of the reactor cavity. This shielded, conical shaped enclosure forms an intermediate pressure boundary where a base vacuum pressure of 10^{-5} torr is maintained by a set of two cryopumps. The pressure boundary of the enclosure interfaces with the reactor vessel port extension at a flanged interface outside the bulk shielding wall as shown in Figure 6.3.1-31. The reactor vacuum vessel operates at a base vacuum pressure of 10^{-1} torr provided by a vacuum pumping system to be discussed below. The base vacuum pressure maintained within the beamlines

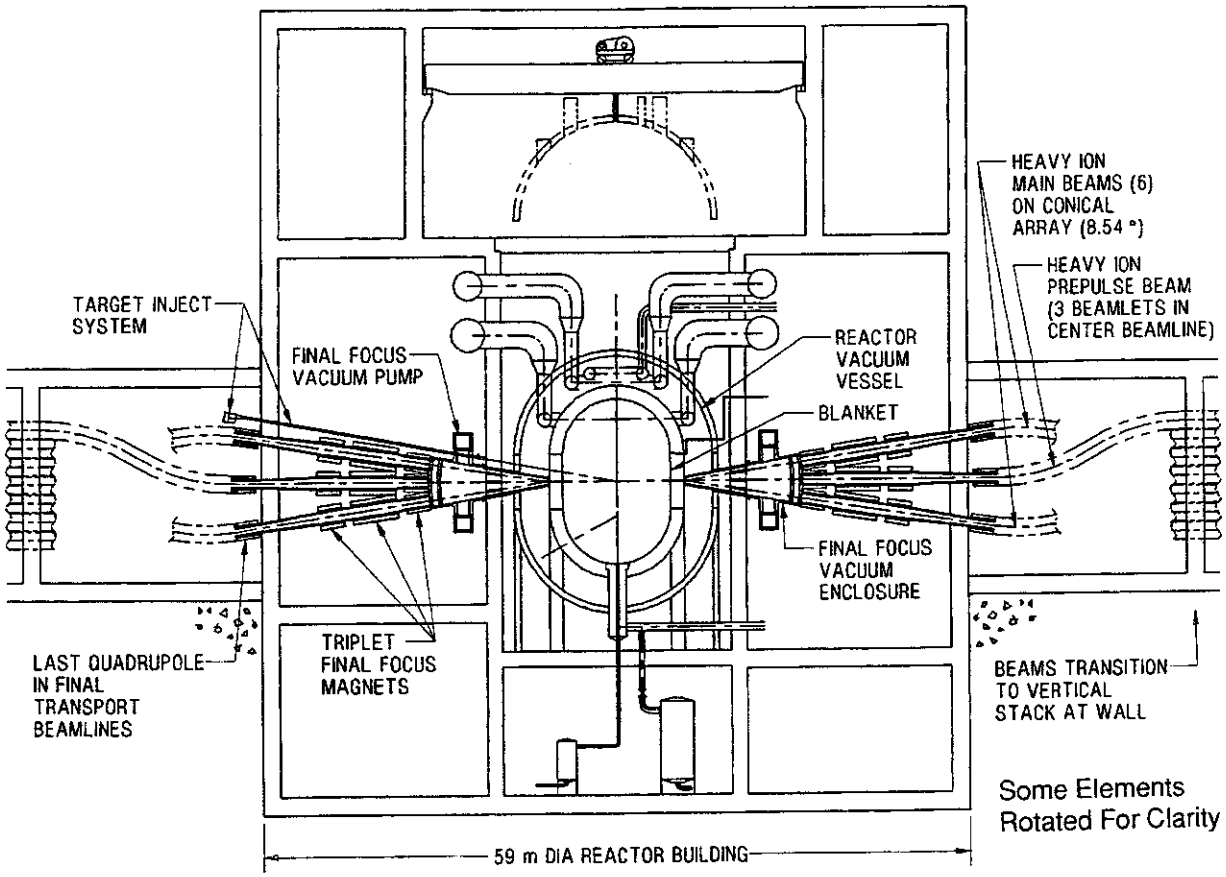

Figure 6.3.1-29. Elevation View – HI Beams/Reactor Systems Interface

passing through bore of all the magnets in the driver (from LINAC through final focus) is 10^{-9} torr. Thus, the final focus vacuum enclosure provides the intermediate vacuum pressure boundary between reactor cavity pressure of 10^{-1} torr and the beamline vacuum pressure of 10^{-9} torr.

As the seven beams enter the base of the final focus vacuum enclosure, they will pass through a gas neutralization cell formed by a double-bottom in the vacuum enclosure. Lead vapor gas will be puffed into this cell prior to the arrival of each set of beams in the 3.5 Hertz repetition rate. The gas neutralization cell functions to neutralize the charged, heavy ion beams allowing the beams to be focused to a small diameter (6 mm) focal spot just outside the blanket.

Channel Transport Subsystem - The final subsystem in the Prometheus-H driver system is the channel transport subsystem which is shown in Figure 6.3.1-31. It consists of a lead vapor gas jet system employed to form an aero window at the final focus point of the seven beams on each side of the reactor cavity. The aero window

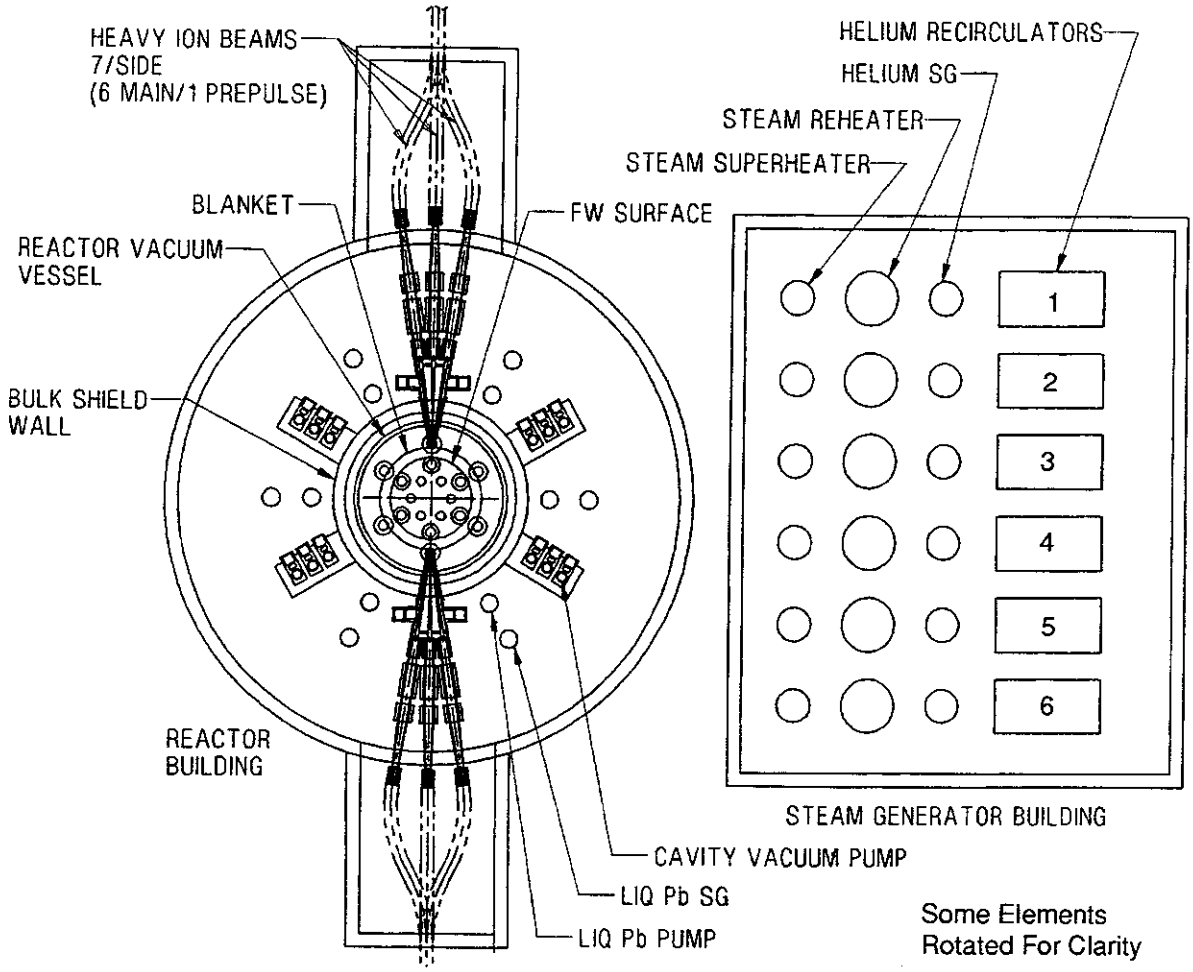

Figure 6.3.1-30. Plan View – HI Beams/Reactor Systems Interface

provides two functions. First, it provides a stream of lead gas vapor which serves as an electron stripping cell. This allows first the prepulse beam and then the six main beams to become a highly charged, high current, self-pinched beam for transport through the final 5.64 m of cavity environment to the target at the center of the cavity. Secondly, it separates the pressure boundary inside the reactor cavity from the pressure boundary inside the final focus vacuum enclosure.

The lead vapor gas jet line enters the final focus vacuum enclosure on the outside of the bulk shielding wall and is routed parallel to the main beam path. At the focus point, the 4x10-cm rectangular line bends on a 25-cm bend radius and intercepts the beam path at the focus point. The gas jet line is positioned to fit snugly against the outer face of the blanket module. At the focus point, the gas jet line has a 2-cm diameter hole through and at 90° to the gas jet flow path. The gas jet line contains a center 2x2-cm line containing the lead vapor gas. The center line is surrounded by an outer cell containing helium gas at 400°C to prevent the lead vapor from solidifying on the inner walls of the center gas jet line.

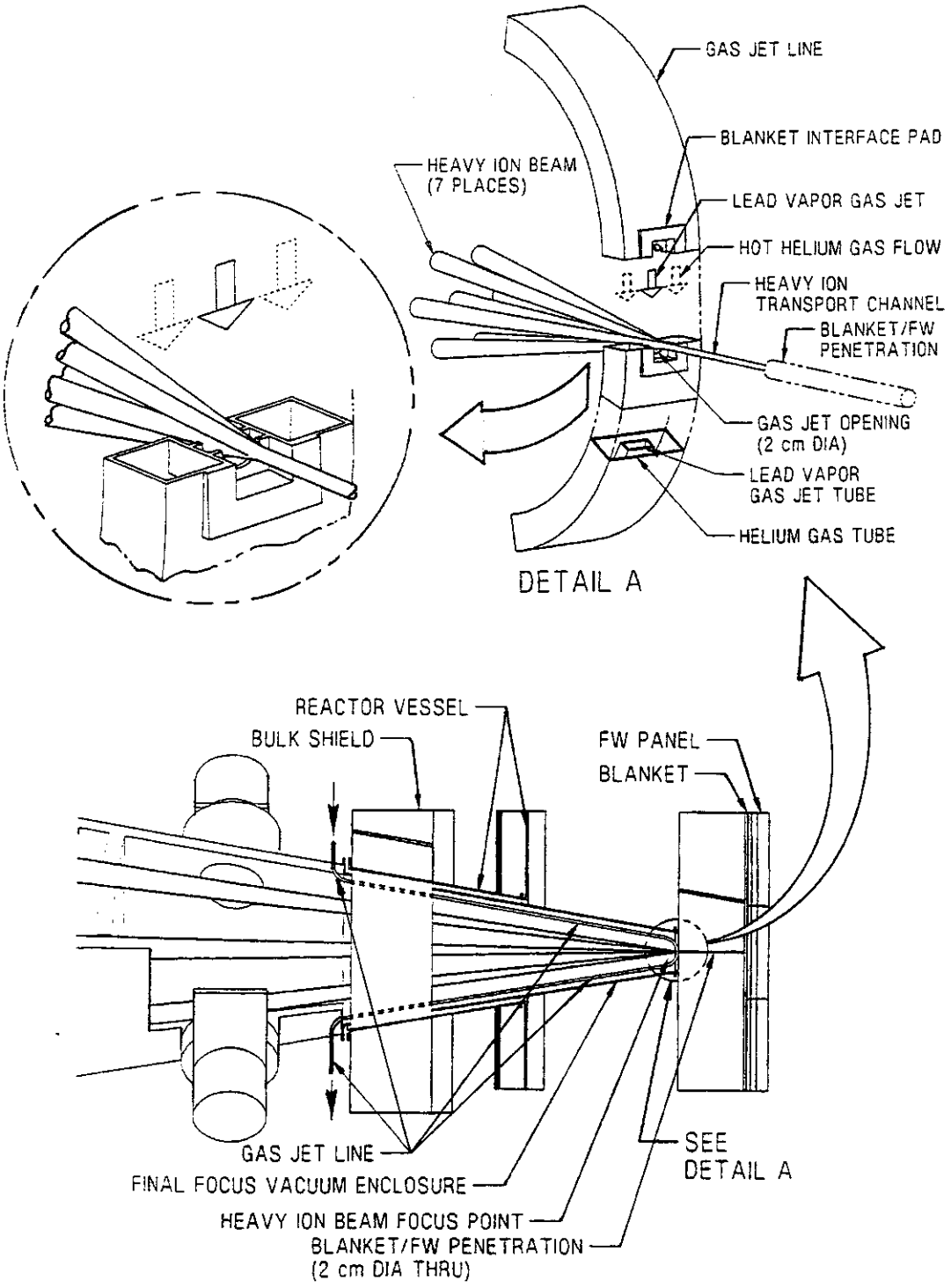

Figure 6.3.1-31. HI Beam Channel Transport Configuration

Prometheus-H Reactor Subsystems Overview - Since the type of cavity and heat transport designs for Prometheus-H are identical to the designs for Prometheus-L except for the overall, detail dimensions, the reactor subsystems for Prometheus-H will not be discussed in the same detail as for Prometheus-L. The discussions here and below will simply discuss the differences between the two designs. All aspects of the cavity and heat transport designs are presented in detail in Section 6.8 and 6.9, respectively.

An elevation view of the reactor systems is shown in Figure 6.3.1-32. This figure shows all the interfaces between the reactor cavity, vacuum pumping, and heat transport systems within the reactor and the steam generator buildings. The reactor building for Prometheus-H is smaller (59-m diameter and 66-m height) than the Prometheus-L building due to differences in number of beams and final focus subsystem differences between the two systems.

Prometheus-H FW/Blanket Subsystem - These systems are identical in design to the systems for the Prometheus-L design except for the dimensional differences. (See the subsystem description for Prometheus-L above for further definition.) The radial and veritical builds for Prometheus-H are shown in the elevation view of the central reactor cavity region in Figure 6.3.1-33. This figure is comparable to Figure 6.3.1-13 for Prometheus-L.

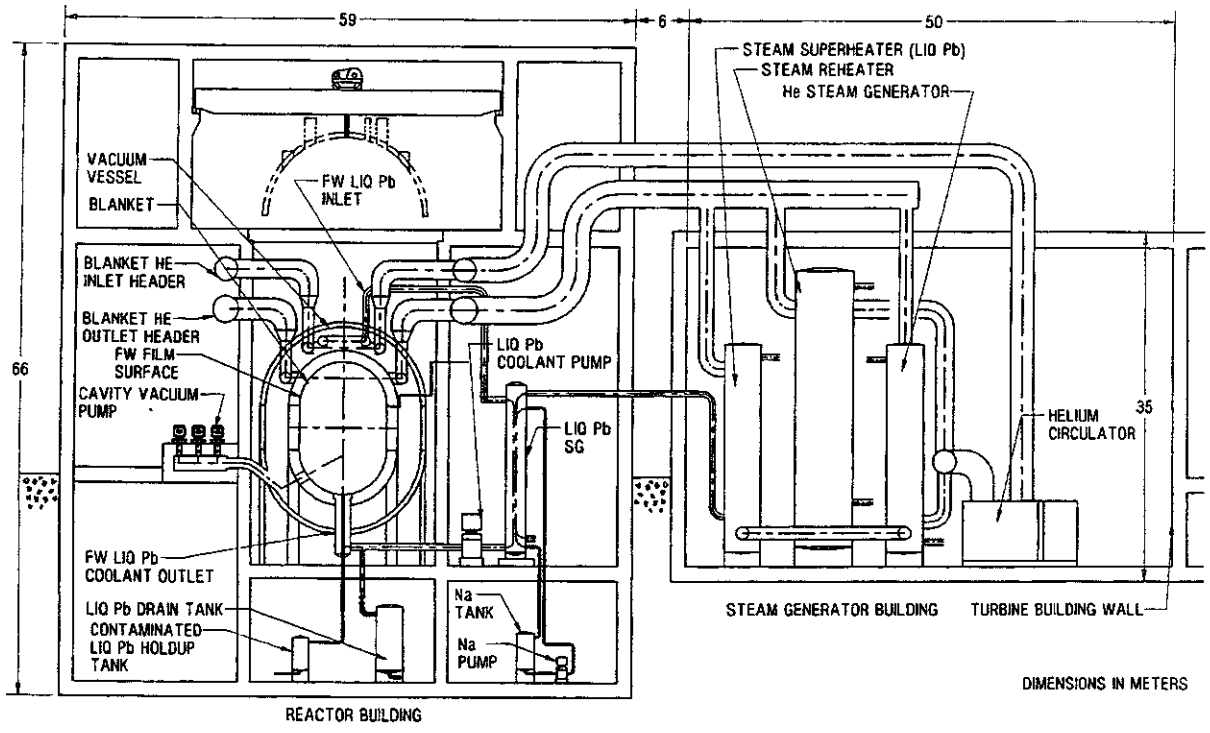

Figure 6.3.1-32. Elevation View – Reactor Systems/Heat Transport Interface

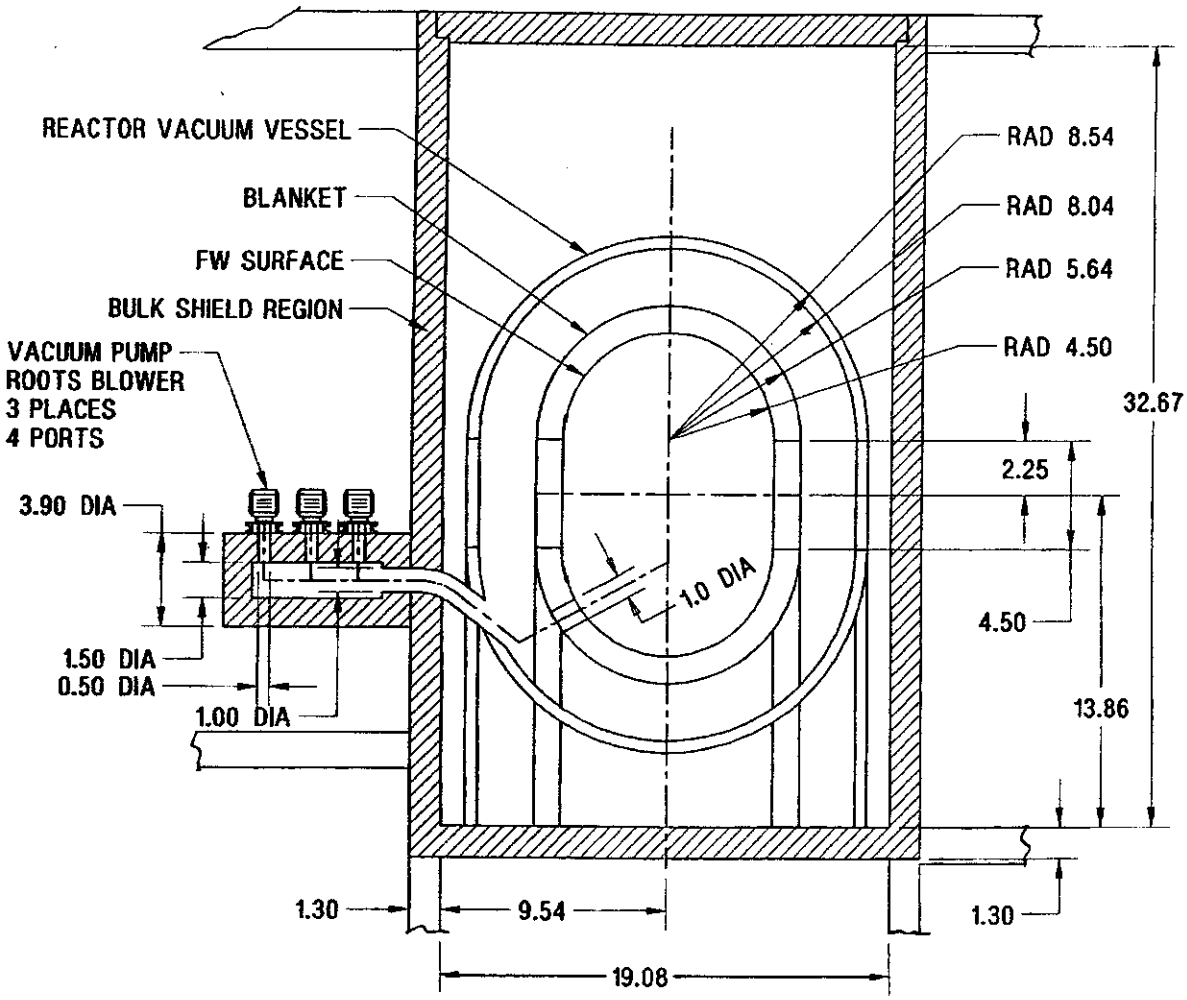

Figure 6.3.1-33. Prometheus-H Elevation of Central Reactor Cavity Region

Prometheus-H Vacuum Pumping Subsystem - The configuration of the vacuum pumping system for the reactor cavity is also defined by Figure 6.3.1-33. A system of three vacuum pumps on each of four ports pump the reactor cavity down to a base pressure of 10^{-1} torr, removing noncondensible gases of hydrogen, helium, deuterium, and tritium. The vacuum pumps are Roots blower pumping systems. The pumps are attached to a 1.5-m diameter plenum which is reduced to a 1.0-m diameter duct attached to the vacuum vessel at each port location. The inlet diameter for each pump is 0.5-m diameter. Four 1.0-m diameter holes through the blanket/FW subsystem complete the vacuum duct system to the inner cavity. For a technical description of the vacuum system operation, refer to Section 6.6

Prometheus-H Target Injection System Reactor Interface - The targets selected for the Prometheus-H concept are indirect drive targets. A pneumatic target injection system injects targets at the rate of 3.5 per second (302,400 per day). The injection system is described in more detail in Section 6.4. The target injection system is depicted by

Figure 6.3.1-34. The system feeds, loads, and pneumatically injects targets with an acceleration of 100 g's through rifled barrels 20-m long. Multiple barrels permit complete evacuation of each barrel prior to the next shot. A fast-acting gate valve on the muzzle end prevents the accelerating gas from entering the vacuum environment of the reactor cavity. A diagnostic chamber permits determination of the target position after launch down the ballistic guide tube. The guide tube provides a protected guide path through the bulk shield, vacuum vessel, blanket, and FW systems to the open cavity. This interface is shown in Figures 6.3.1-28 and 6.3.1-29.

Prometheus-H Vacuum Vessel - The reactor vessel design is the same as the design for Prometheus-L except for the dimensional differences due to the cavity radial and vertical build differences.

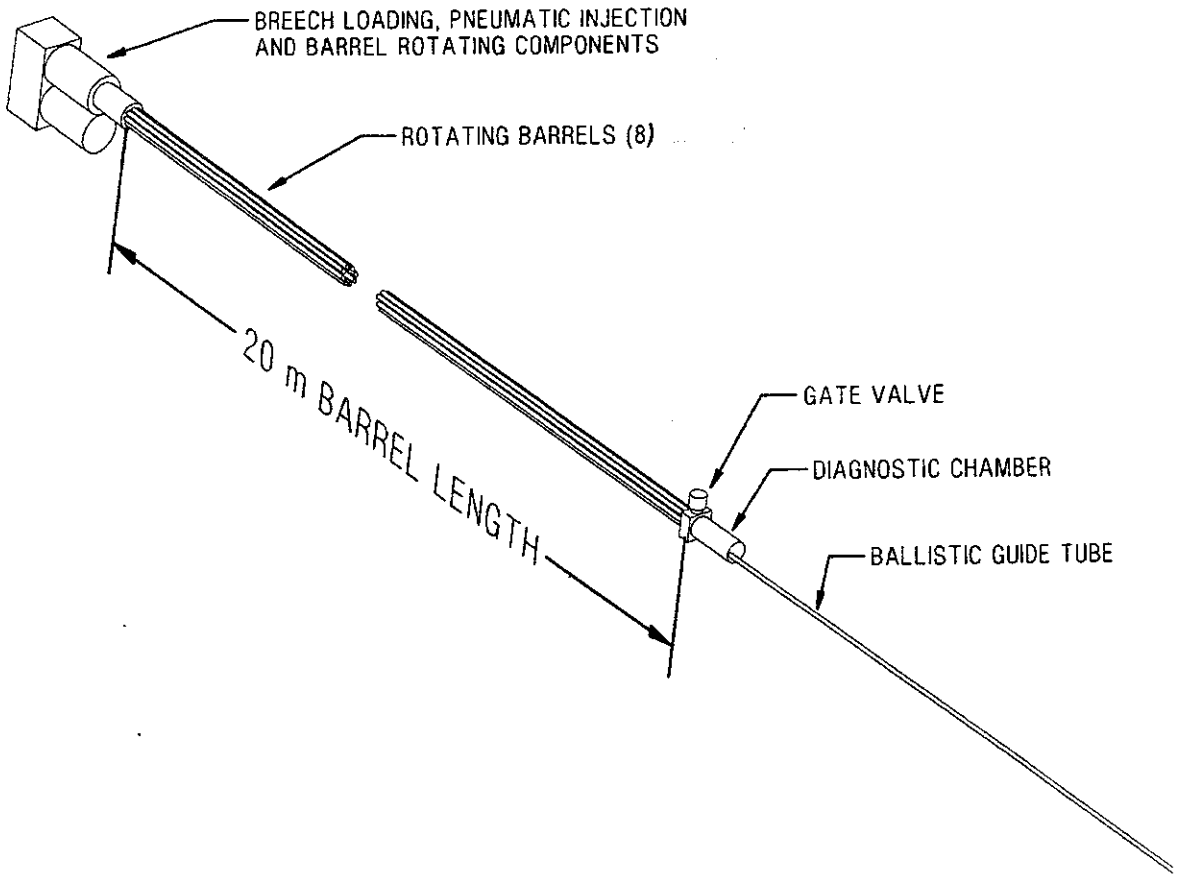

Figure 6.3.1-34. Prometheus-H Target Injection System

References for 6.3.1

1. D. B. Harris, N. A. Kurnit, D. D. Lowenthal, R. G. Berger, J. M. Eggleston, J. J. Ewing, M. J. Kushner, L. M. Waganer, D. A. Bowers, D. S. Zuckerman, "Future Developments and Applications of KrF Laser-Fusion Systems," Fusion Technology, 11, 705 (May, 1987).

6.3.2 Plant Maintenance Approach - The approach used to define plant maintenance takes into account two key factors. These factors are (a) maintenance prediction and planning systems which use artificial intelligence (AI) methods and (b) the continuing improvement of automation technology. Both scheduled and unscheduled maintenance were considered plant maintenance requirements. Maintenance needs were analyzed and the hazards in the plant were considered. The maintenance analyses were included in the reactor and plant design process. This resulted in a number of operational and availability advantages for the plant design considered in this study. Total remote maintenance was chosen for critical areas which results in no human exposure to radionuclides.

6.3.2.1 Maintenance Requirements - The major reactor and plant systems and components requiring maintenance were first determined during the study. These were selected based upon previous maintenance experience and consultation with the Prometheus team members regarding their respective system designs. The maintenance analysis effort then concentrated on critical areas which would have the most impact on the overall plant availability and maintenance costs. Table 6.3.2-1 lists the major maintenance items for the Prometheus power plants. The remaining plant items are addressed with a general allowance factor.

Maintenance Environment - There are many new and unique requirements which are associated with the IFE reactor plant designs. The reactor vessel operates with an internal pressure of a few mtorr for Prometheus-L and 100 mtorr for Prometheus-H. The low pressure regions extend into the laser beamlines out to the vacuum window at the Reactor Building wall for Prometheus-L. For Prometheus-H, the complete length of the heavy ion beam lines is at an even lower pressure (10^{-5} to 10^{-9} torr). During reactor operation, radiation levels of 1.8×10^7 rads per hour are expected inside the reactor hall, principally from neutrons out the back of the shield. X-ray and gamma-ray emissions will be present at a lower level. The shields are designed to limit the neutron flux level at the back of the shield to 2×10^6 n/cm^2·sec during operation which equates to a biological dose of 2.5 mrem/hr 24 hours after shutdown (2.5 mrads/hr for equipment). The reactor hall (the region outside the bulk shielding walls and inside the reactor building walls) environment will be inerted with CO_2 in order to minimize activation of the hall atmosphere. Only remote maintenance would be performed during reactor operation. After shutdown, hands-on maintenance could be accomplished for specific needs with remote maintenance being the preferred option.

If the beamlines are removed for maintenance, there would be the potential hazard of lead vapor from the first wall coolant. The potential for tritium leakage also exists but specific detritiation systems are provided in the reactor building for this purpose.

The laser building will be inerted with CO_2 as a design requirement. The building will have low level gamma radiation during operation. The operating KrF laser gas would

also present a maintenance hazard. The LINAC tunnel complex by comparison will have low level gamma radiation which will build up as a background dose during the life of plant.

Various other hazard sources such as lasers, high voltage power lines, and alpha emitters (e.g., uranium in the tritium storage getters) will exist. These are to be expected not only in the reactor building, target factory, driver buildings, and hot cell facility, but also associated with the transfer routes between these buildings. The hot cells and lead cleanup facilities will have comparatively high levels of radioactive contaminants.

Table 6.3.2-1 Major Maintenance Items

Major Items Common To Both Reactor Types

- First Wall Panels
- Blanket Modules
- Reactor Vacuum Pumps
- Blanket Tritium Extraction Pumps
- Reactor Computer Control System
- First Wall Lead Cooling Pump
- First Wall Coolant Heat Exchanger (lead to steam)
- Lead Drain Pump
- Lead Decontamination System
- Helium Extraction Pump
- Helium Decontamination System
- Tritium Extraction Loop
- Blanket Helium Coolant Pumps
- Blanket Coolant Heat Exchanger (helium to steam)
- Heat Exchangers
- Helium Low and High Pressure Reheaters
- Steam Turbines
- Alternators/Generators
- Transformers
- Target Factory

Laser Option Specific Items

- Target Injector (electromagnetic injection)
- Laser Amplifiers
- Gas Circulation Blowers
- Laser Gas Heat Exchanger
- Laser Optics Vacuum Backing Pumps
- Final Optical Elements

Heavy Ion Option Specific Items

- Target Injector (pneumatic injection)
- Heavy Ion Accelerator Modules
- Ion Beam Vacuum Backing Pumps
- Magnets

6.3.2.2 Fault Diagnosis and Maintenance Scheduling - Fault diagnosis and maintenance scheduling technology are evolving quickly. These capabilities are expected to be extensively used during the deployment of the fusion reactor power plants. Artificial intelligence-based tools will continue to be improved for both fault diagnosis and maintenance scheduling.
Built-in-test (BIT) systems for fault diagnosis are becoming more powerful with the capability to minimize the repair site diagnostic skills. The repair time is minimized by rapid selection of correct replacement parts and notification of the appropriate repair specialis. Built-in-test systems use both top-down and bottoms-up system models with a combination of driver software and firmware incorporated. Faults are analyzed by the driver software traversing a system failure modes model and selecting test results from the diagnostic firmware to define the failed part. Fault dependencies can be determined to predict future malfunctions or failures. The U.S. Navy has positive experience with BIT systems such as those used in the ANSAR8 surveillance system.

Scheduling systems have been used for many years in manufacturing. With the advent of low overhead computerized systems, applications in maintenance scheduling and coordination are being developed and used. Such systems allow optimization of maintenance personnel and equipment, thus minimizing plant downtime and the required spares inventory.

6.3.2.3 Maintenance Options - There are three general options for the maintenance of the fusion reactor plants.

- Hands-On Maintenance - This includes regular contact maintenance or contact maintenance in a controlled area with a partial or full change of clothing which may include a ventilated or "bubble suit".
- Semi-Remote Maintenance - Maintenance is accomplished using long handled-tools or from behind temporary shielding.
- Fully-Remote Maintenance - Maintenance is carried out with totally remote devices such as manipulators or robotic devices. The operator is removed from the work place.

The type of maintenance procedure adopted is determined by the degree of protection required, the hazards, and the type and intensity of radiation present. There is usually a time penalty associated with the semi-remote or fully-remote options. However, if the operation is highly repetitive, task automation may be employed to improve maintenance times.

6.3.2.4 Maintenance Approach Choices - The maintenance approach for a major power plant is optimized to maximize the plant availability. This is best achieved by use of planned maintenance actions on key systems in order to prevent expensive, unplanned plant outages.

Scheduled Maintenance - Scheduled maintenance consists of preventative maintenance actions both on a regular basis and during planned plant outages. Maintenance prediction and planning systems using AI techniques are used to schedule maintenance tasks for minimal downtime. These prediction and planning systems are used in conjugation with sensor input to identify parts with early wearout or potential failure tendencies. Identification of these parts allows replacement during the planned maintenance periods. Due to the lack of statistical data on this approach, the reliability, availability, and maintainability (RAM) analysis reported in Section 6.3.3 did not consider these potential benefits in availability.

Unscheduled Maintenance - Unscheduled maintenance consists of downtime due to unforeseen failures or premature wearout. Unscheduled maintenance is very costly and time consuming. Frequently only repair of one element is accomplished and no other parallel maintenance activities can be accomplished. Failure of components can happen at any time and under any load conditions, frequently at full load conditions. Other systems can be damaged as a result of the initiating failure. Replacement parts may not be available for immediate installation thus causing further delays. Unscheduled maintenance should be minimized to the greatest extent possible with scheduled maintenance.

6.3.2.5 Reactor Maintenance - The Reactor Equipment is the most important system relative to the availability parameter. The Reactor Equipment was chosen for the most extensive analysis in the study. Of the two Prometheus concepts, the laser-option reactor vessel was examined in more detail due to the more difficult access. Site layouts of the two reactor designs are shown in Figure 6.3.2-1. This figure illustrates the Reactor Building and the Hot Cells where maintenance will be performed on the removed radioactive components such as the wall and blanket modules. At the center of the laser Reactor Building, the 60 laser beamlines are shown. These beamlines, which are equally spaced around the complete sphere, proved to have the more difficult maintenance. Figure 6.3.2-2 is a cross-section through the laser-option Reactor and Driver Building which illustrates two of the laser drivers and four of the beamlines which penetrate the reactor chamber. Also shown are the plumbing and steam generators for the helium and lead primary coolant systems. Figure 6.3.2-3 illustrates the comparable heavy ion-driven Reactor Building with the diametrically opposed beam bundles.

The reactor designs for both reactor concepts are well suited for repair and replacement with the adopted vertical maintenance scheme. The top of the reactor vessel is removable with all internal parts lifted upwards. The only required bottom access is to the lead coolant outlet pipe and contaminated lead outlet pipe.

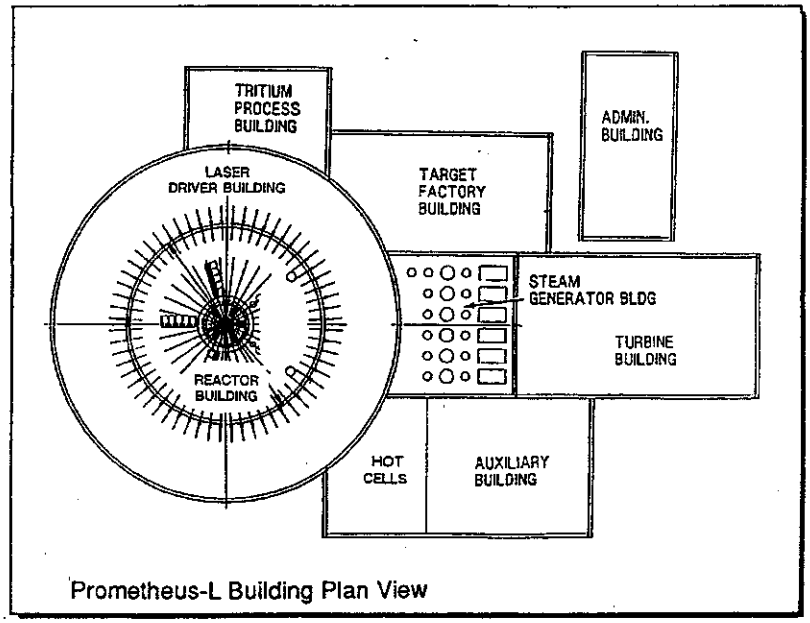

Prometheus-L Building Plan View

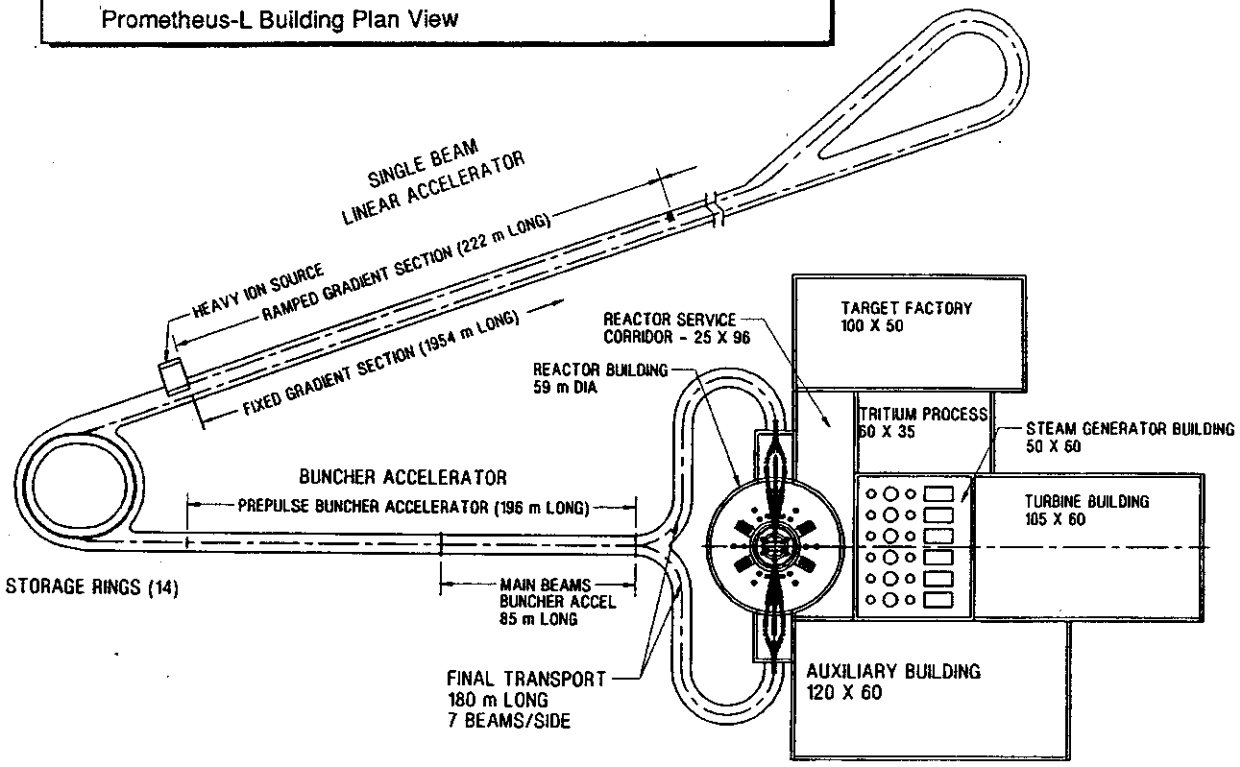

Prometheus-H Building Plan View

Figure 6.3.2-1 Plant Site Plans for Two Reactor Design Options

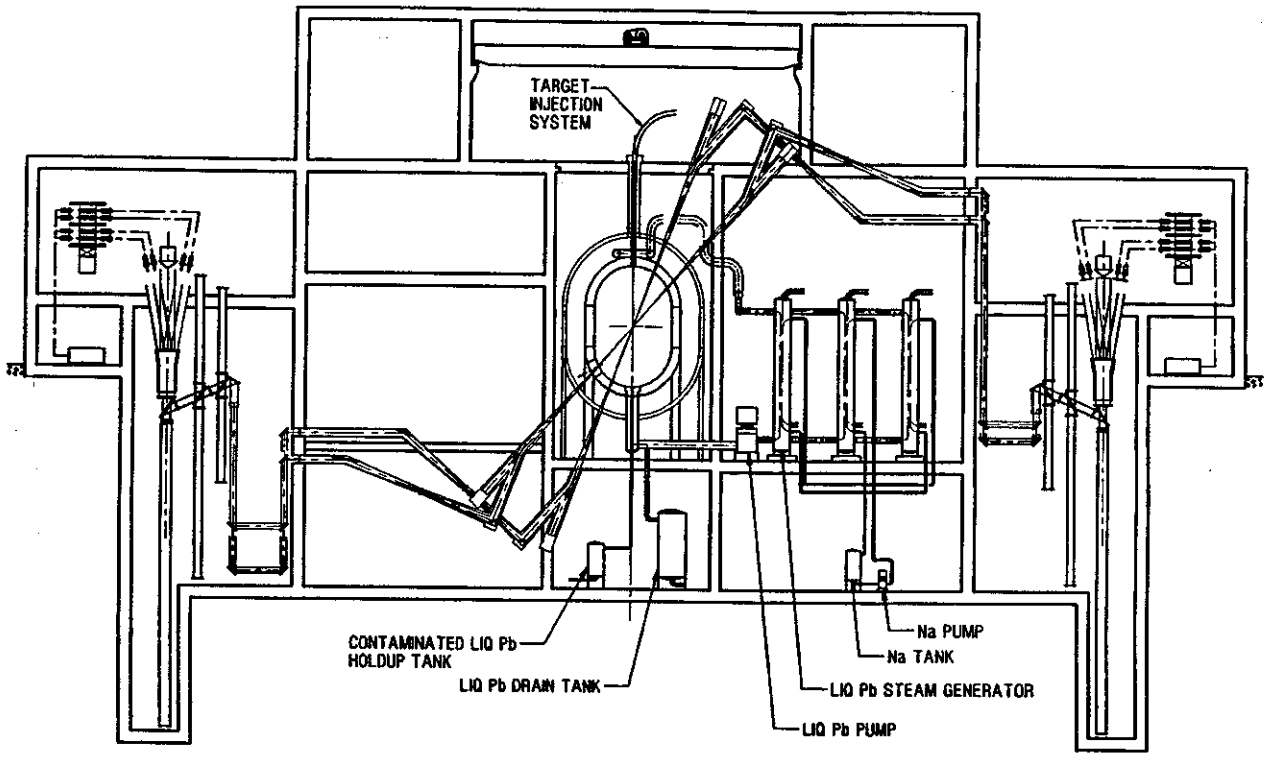

Figure 6.3.2-2 Reactor and Laser Building Layout Shown with the Primary Coolant Systems and a Portion of the Laser Beam Lines

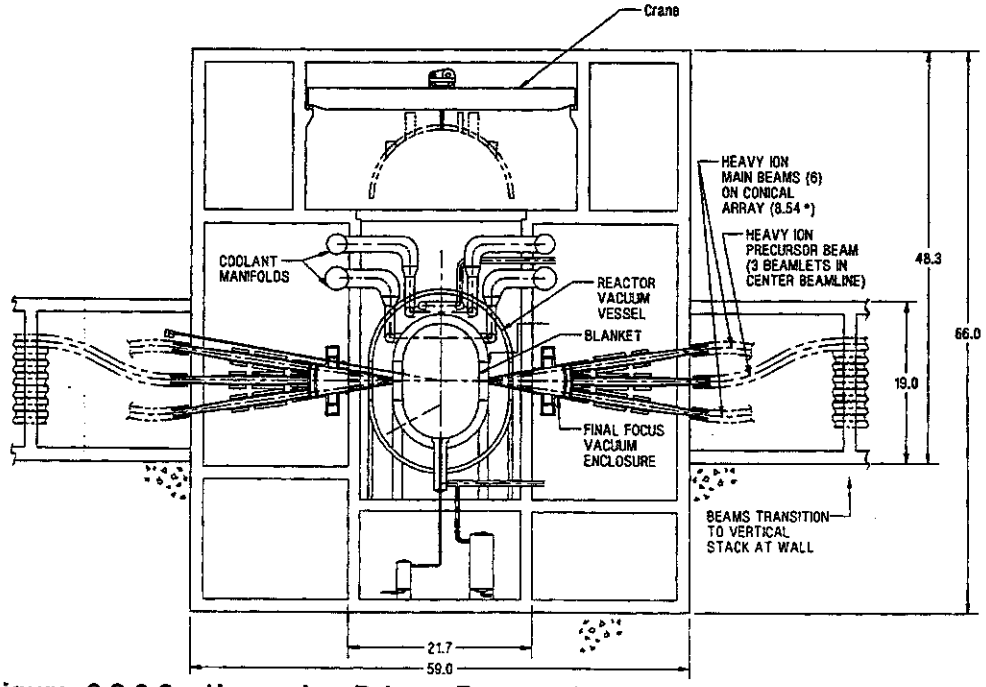

Figure 6.3.2-3 Heavy Ion-Driven Reactor has Two Beam Bundles Located on Opposite Sides of the Reactor Vessel

Figure 6.3.2-4 is a cross-section of the reactor which illustrates the major equipment components. The primary helium coolant inlet and outlet ducts enter from the top of the vessel. These ducts connect to coolant manifolds which in turn connect with the blanket modules. Lead coolant has separate inlet and outlet plumbing. Large vacuum ducting must also be disconnected to remove the blanket modules. To facilitate maintenance, the reactor vessel is subdivided into five equally-spaced sectors as shown in Figure 6.3.2-5. Each maintenance sector has independent supports and plumbing systems. Moreover, the blanket modules are divided into six separate vertical levels, each supplied by separate manifolds. More detail on the laser-driven reactor vessel with the beamlines in place is shown in Figure 6.3.2-6. The vacuum pumps are located outside the right-circular cylindrical bulk shield. Only the first wall, blanket, vacuum vessel, coolant piping, beamlines, and target injector are inside the shield boundary. The laser beams are projected to the center of the cavity for clarity.

A trimetric view of the heavy ion beam-driven reactor is shown in Figure 6.3.2-7. This vessel is slightly smaller with the radius of the first wall being 4.5 meters. The most discernible difference is the relative lack of penetrations in the heavy ion case. Only one of the ion beamline sets is shown in this view. The ion beams converge at the back face of the blanket. Only a two-centimeter diameter hole is required through the blanket and wall. The only sizable openings in the first wall are the vacuum pump ports. All other maintenance features of the two reactor chamber options are identical.

Reactor Assembly and Disassembly - Because the laser and the heavy ion-driven reactor have similar maintenance requirements and design concepts, the reactor vessel assembly and disassembly procedures have many common features. The procedures for the laser option will be discussed as the nominal case because it is the more demanding.

Many of the assembly and disassembly operations are conducted from the interior of the vessel with access from above. Typical of these activities is the removal of first wall panels every 5-10 years. External access to the reactor vessel is also required. Figure 6.3.2-2 illustrates the cylindrical bulk shield wall surrounding the reactor vessel. A circular shield cover will be removed vertically to provide overhead access. This will allow access to the coolant ducts and laser beamlines. The target injection system will also be accessible. Maintenance will be accomplished with long-reach manipulators from above and mobile devices from below or along the shield wall. Local contamination control boundaries will be erected to prevent the spread of contamination from worksites.

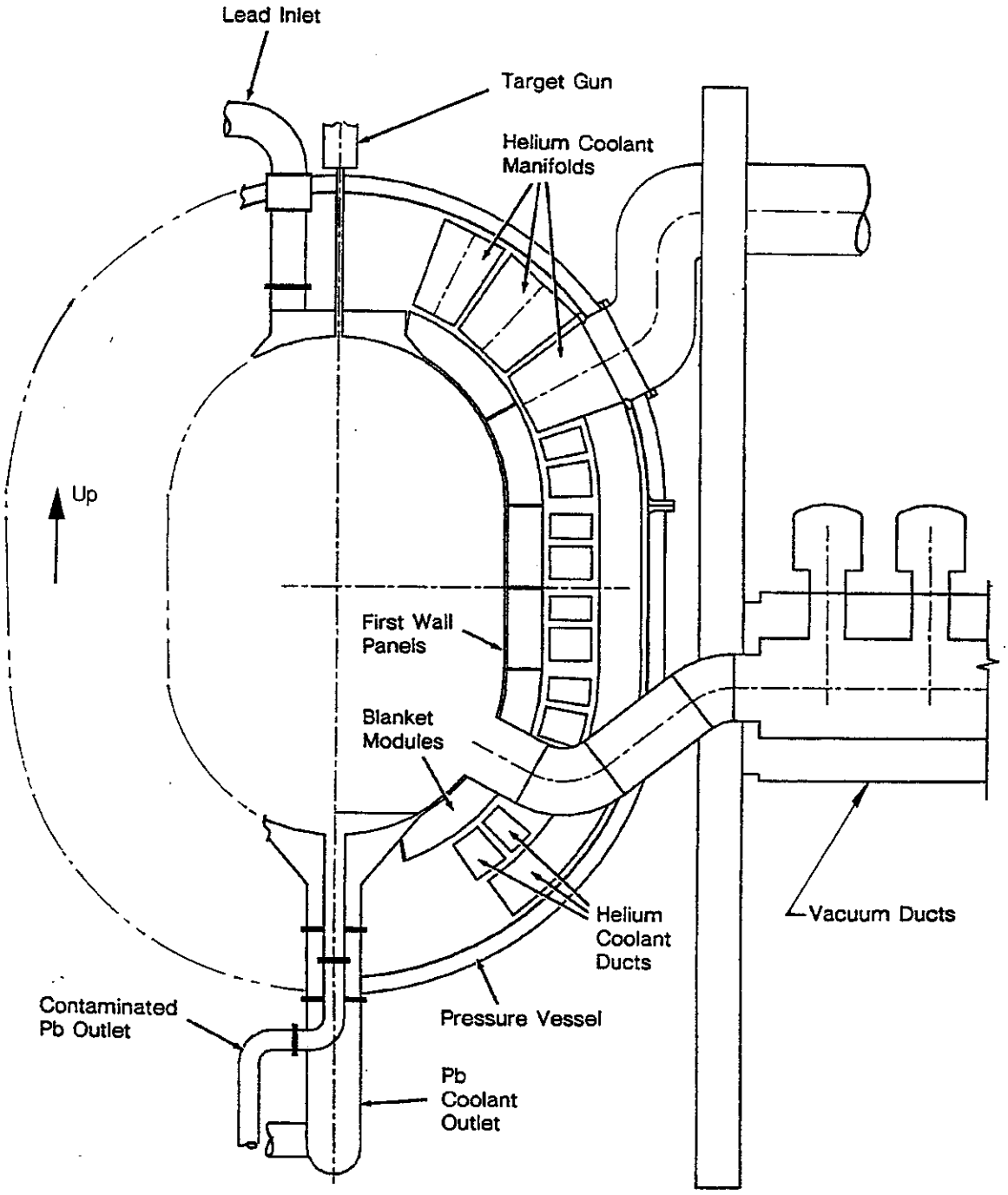

Figure 6.3.2-4 Reactor Vessel Cross Section with Major System Components Shown

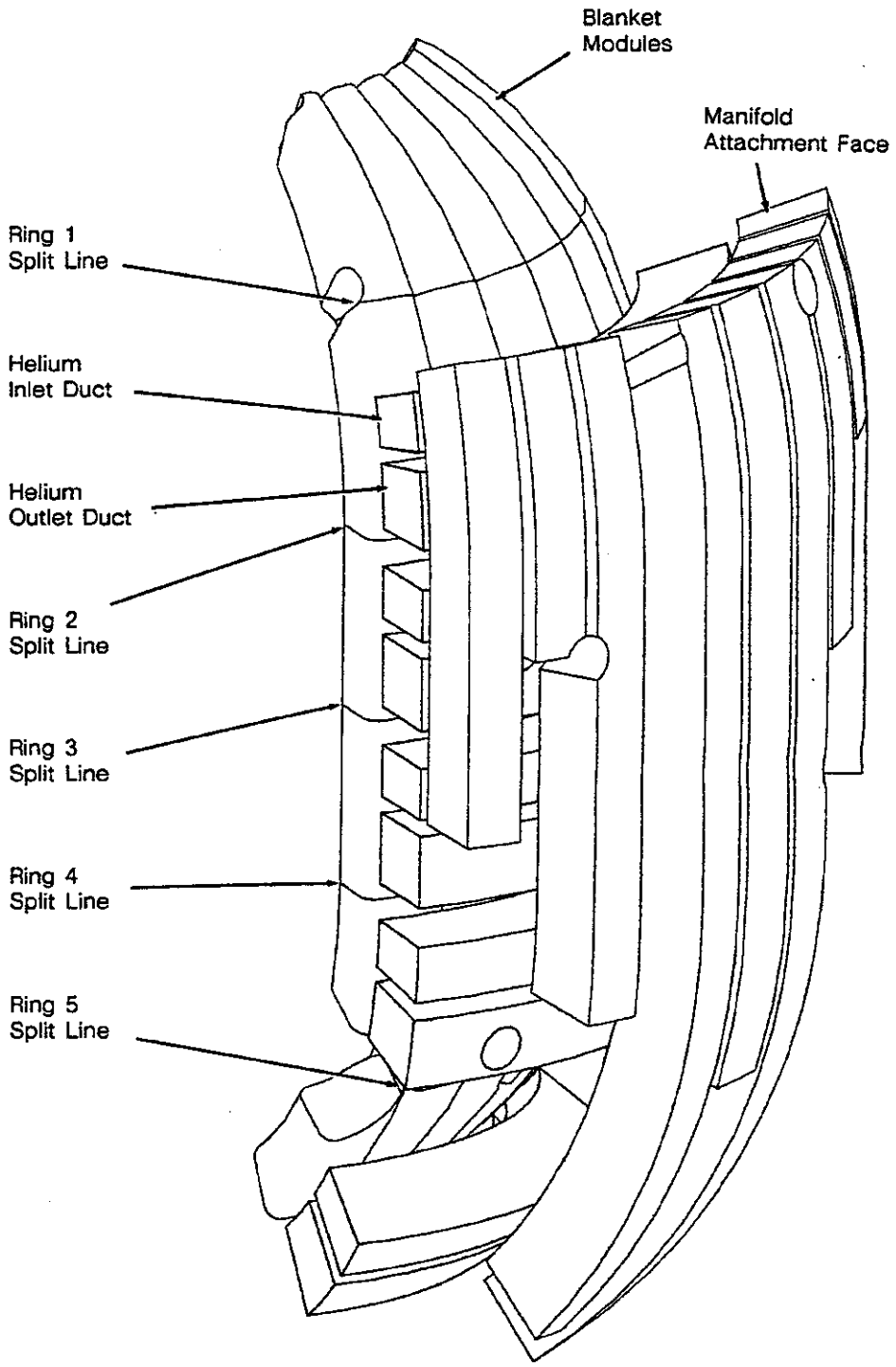

Figure 6.3.2-5 A Blanket Module Sector with Associated Coolant Ducts

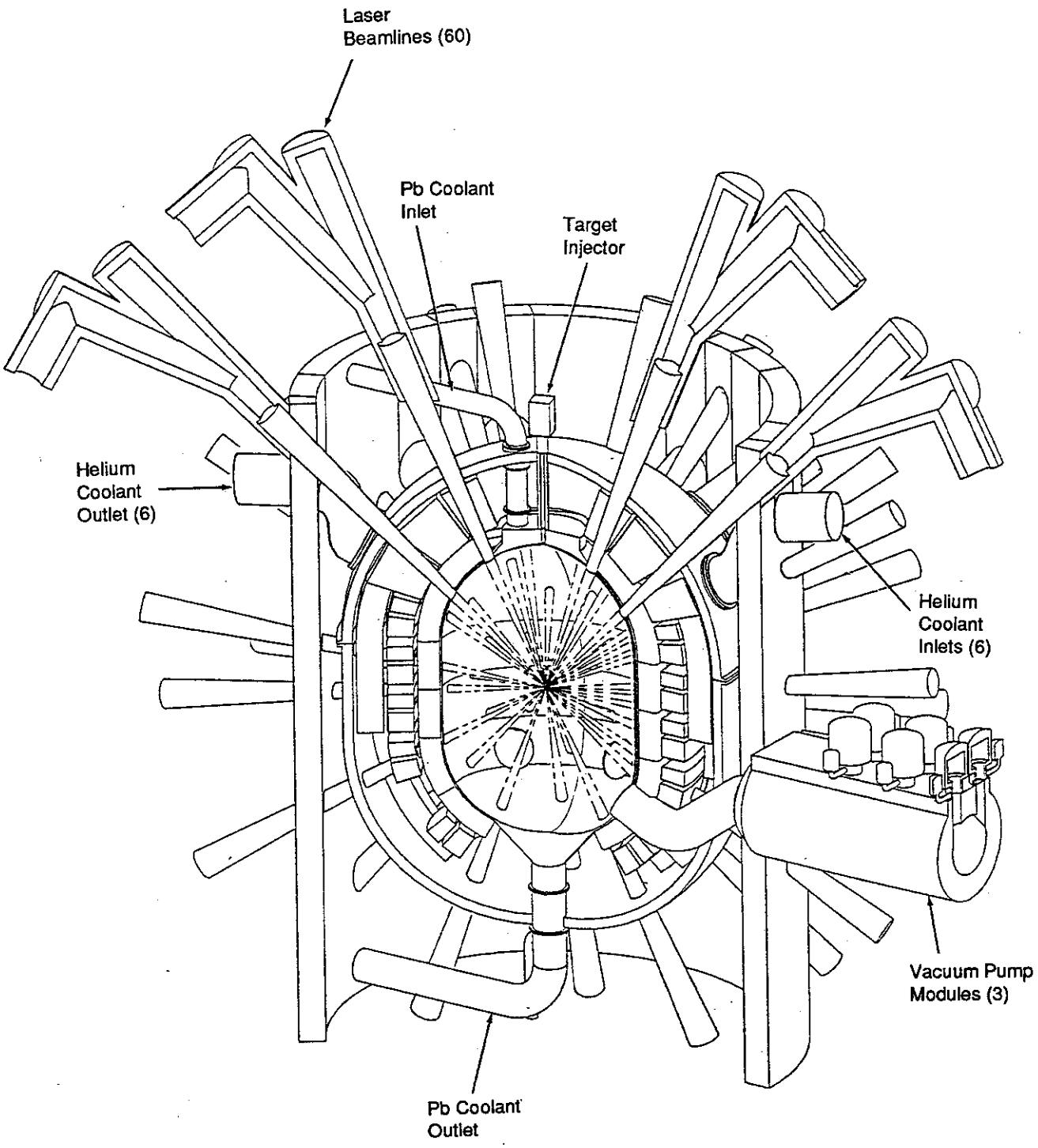

Figure 6.3.2-6 General Arrangement of the Major Laser-Driven Reactor Equipment

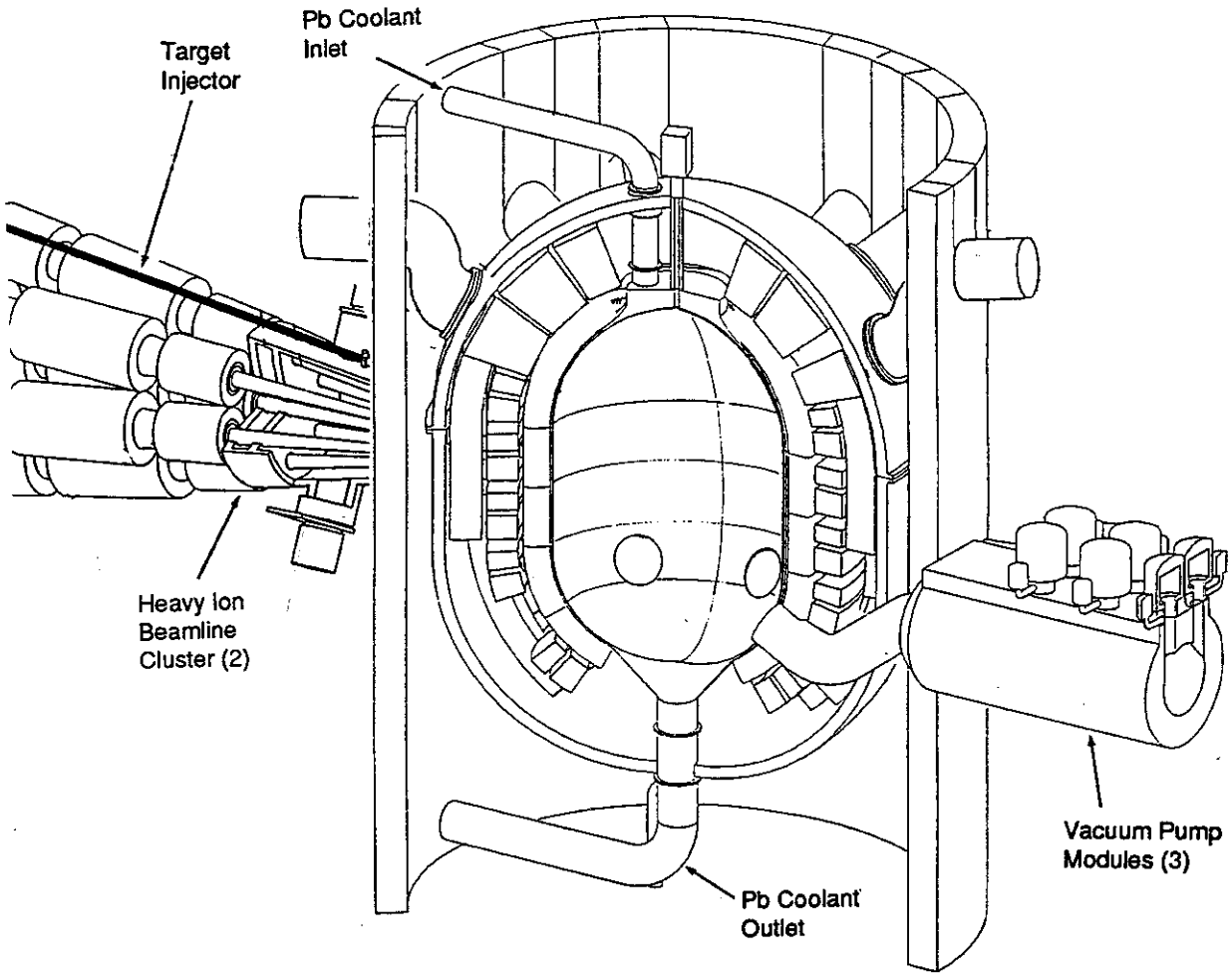

Figure 6.3.2-7 General Arrangement of the Major Heavy Ion-Driven Reactor Equipment

The general procedure for disassembly will be as follows:

(a) The lead coolant system is drained and the first wall is flushed of the lead coolant.
(b) The shield slabs in the floor of the upper access chamber, as shown in Figure 6.3.2-2, are removed to gain access to the reactor vessel. Figure 6.3.2-8 is a view looking downwards at the reactor vessel. The building floors are not shown for clarity. The remote maintenance equipment will then be installed and moved into position.
(c) Sections of the coolant plumbing (see Figures 6.3.2-9 and 6.3.2-10) will be removed to provide clear access to the top of the vessel.
(d) Sections of the laser beamline ducting are disconnected and removed.

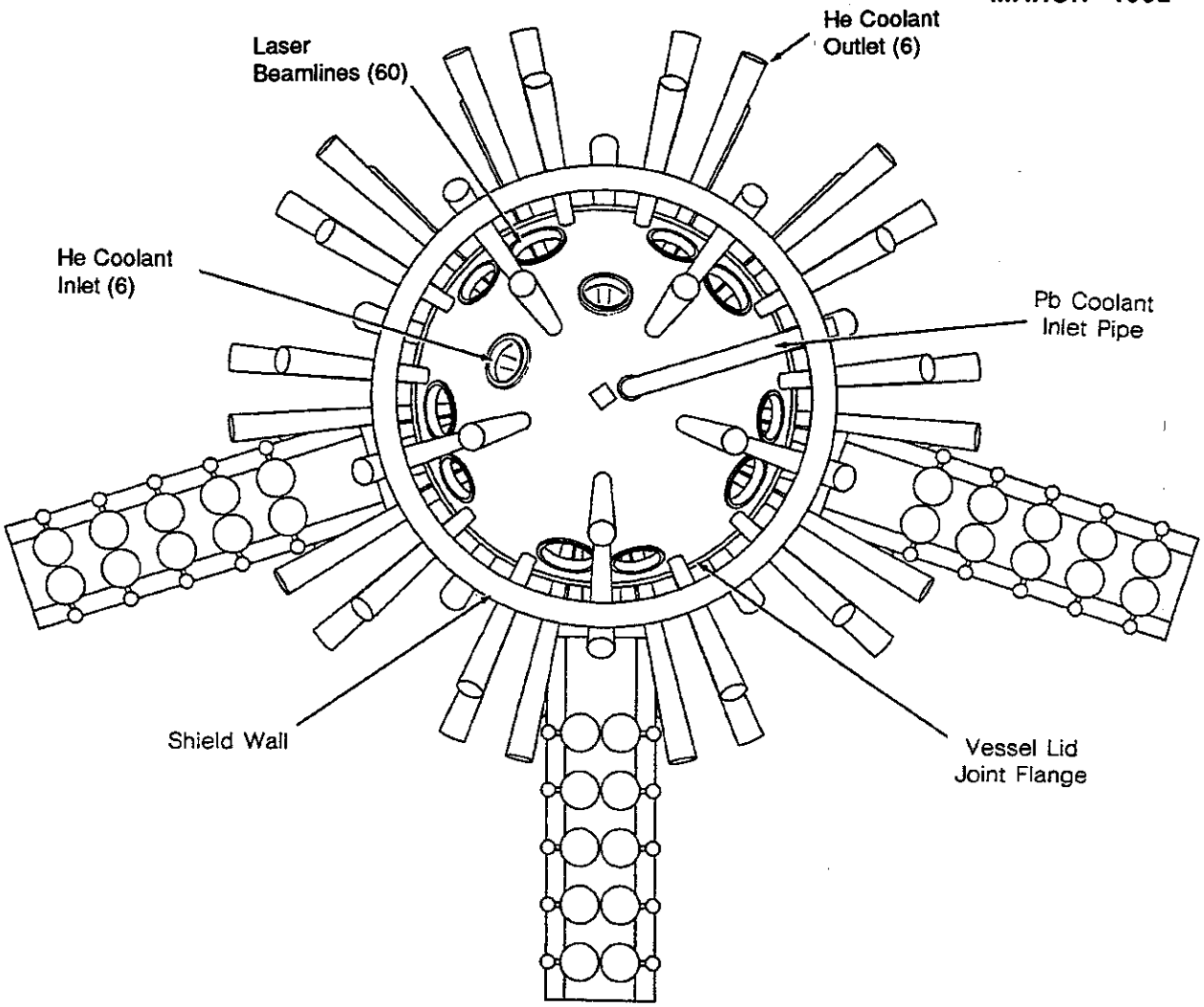

Figure 6.3.2-8 Access to Reactor Vessel with Upper Bulk Shielding and Helium Coolant Ducting Removed

(e) The target injection system is removed from the top of the reactor vessel. This procedure is further described in a following paragraph.

(f) The top of the reactor vessel is unbolted at the flange joint and any seal welds cut. Figure 6.3.2-11 illustrates a remote manipulator working on the attachment flange.

(g) Reactor vessel top is removed and placed in the upper access tunnel as shown in Figure 6.3.2-3 (heavy ion option).

(h) Helium manifolds are disconnected from the large helium inlet and outlet piping. Figure 6.3.2-12 shows the reactor vessel with the upper helium manifold removed and the manifold-to-duct attachment joint visible. Figure 6.3.2-13 shows the vessel with the helium manifold lifted clear.

(i) The first (top) blanket ring is removed after its support attach points are released, revealing the first wall dome as shown in Figure 6.3.2-14.

(j) The second blanket ring is removed after its support attach points are released. This enables removal of the first wall dome as shown in Figure 6.3.2-15.

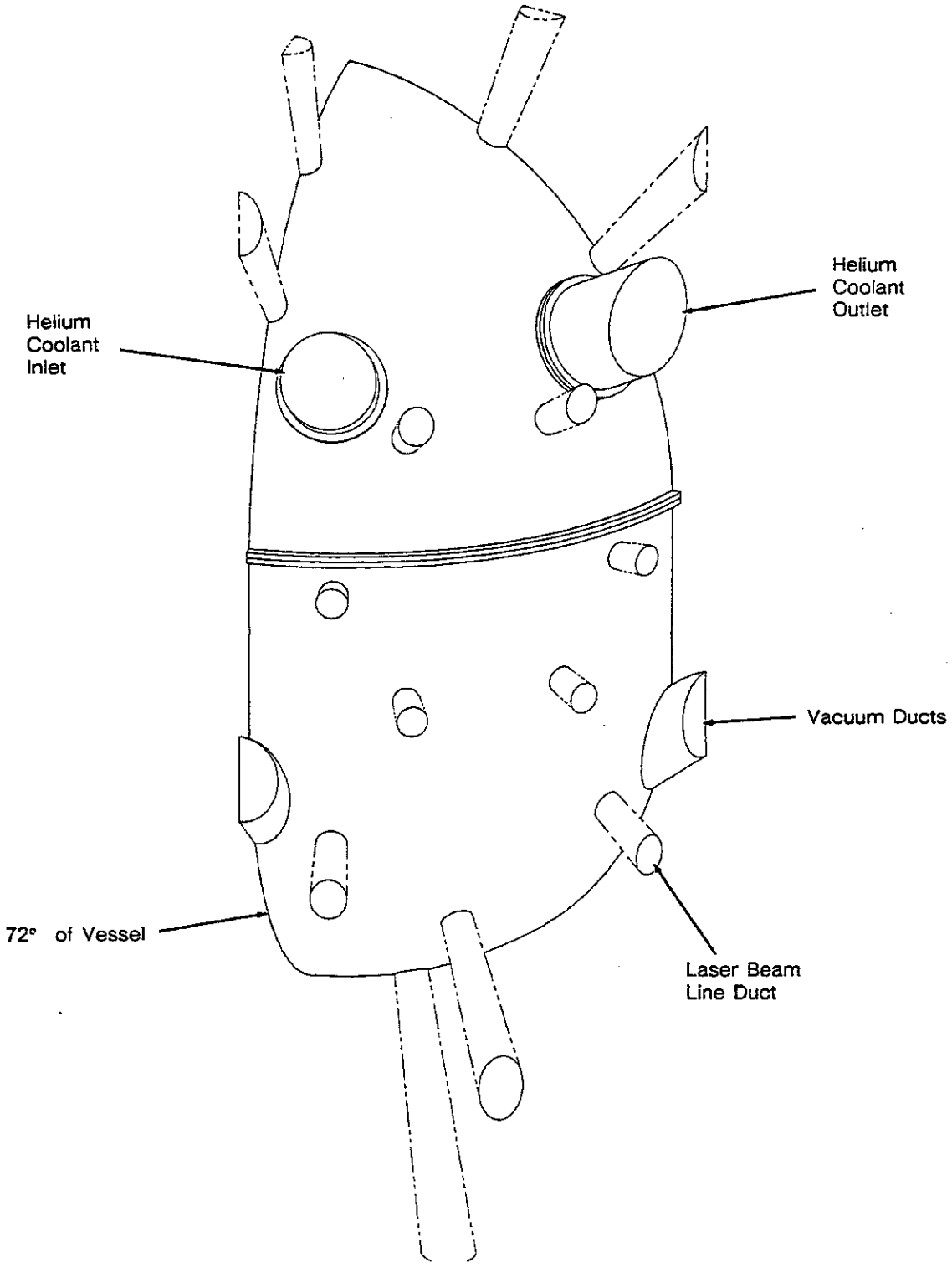

Figure 6.3.2-9 Segment of Reactor Vessel with Coolant Ducting

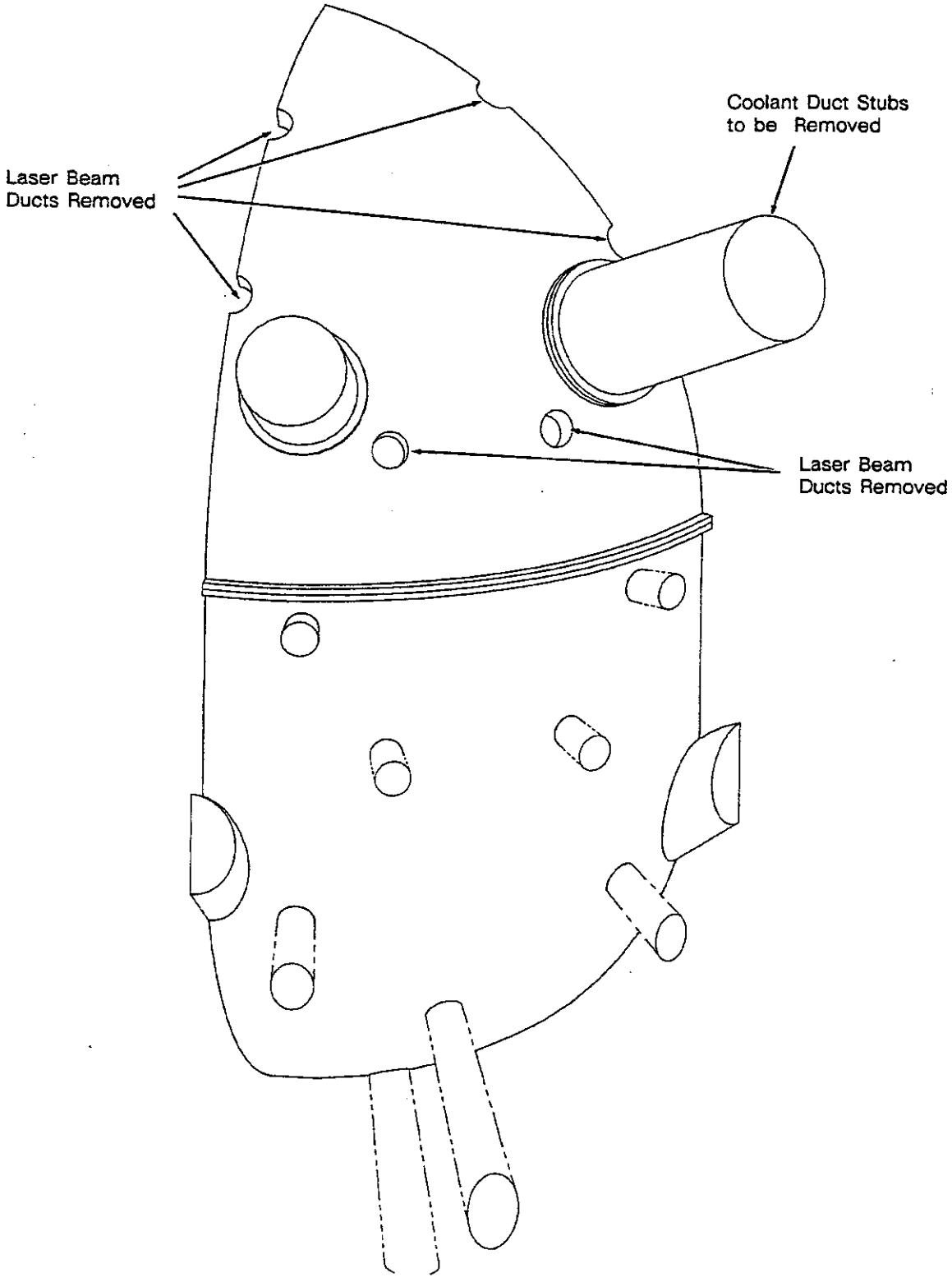

Figure 6.3.2-10 Segment of Reactor Vessel Showing Some Laser Ducts Removed

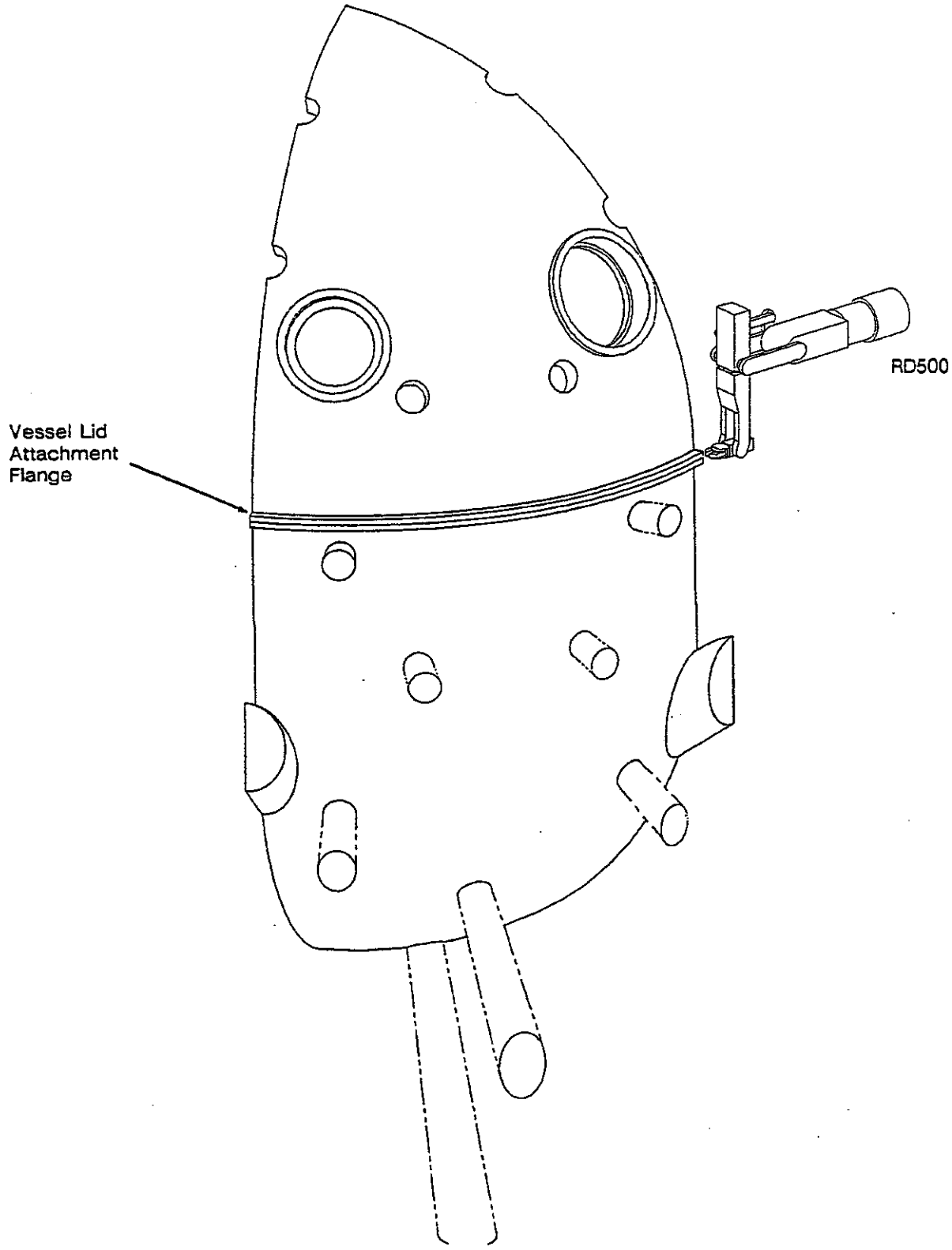

Figure 6.3.2-11 Remote Manipulator Working on Vessel Lid Attachment Flange

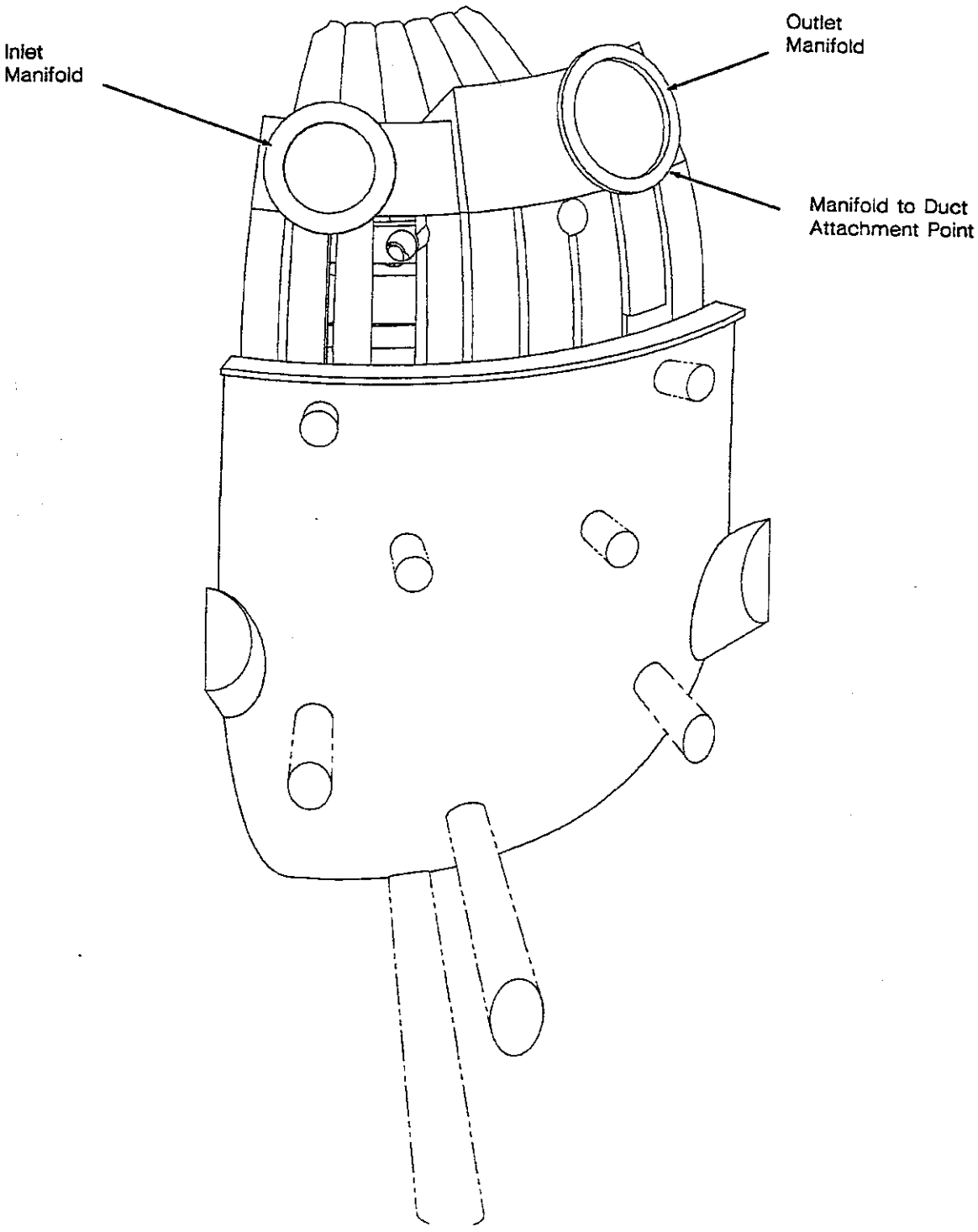

Figure 6.3.2-12 Reactor Vessel with Lid and Top Ring Manifold Removed

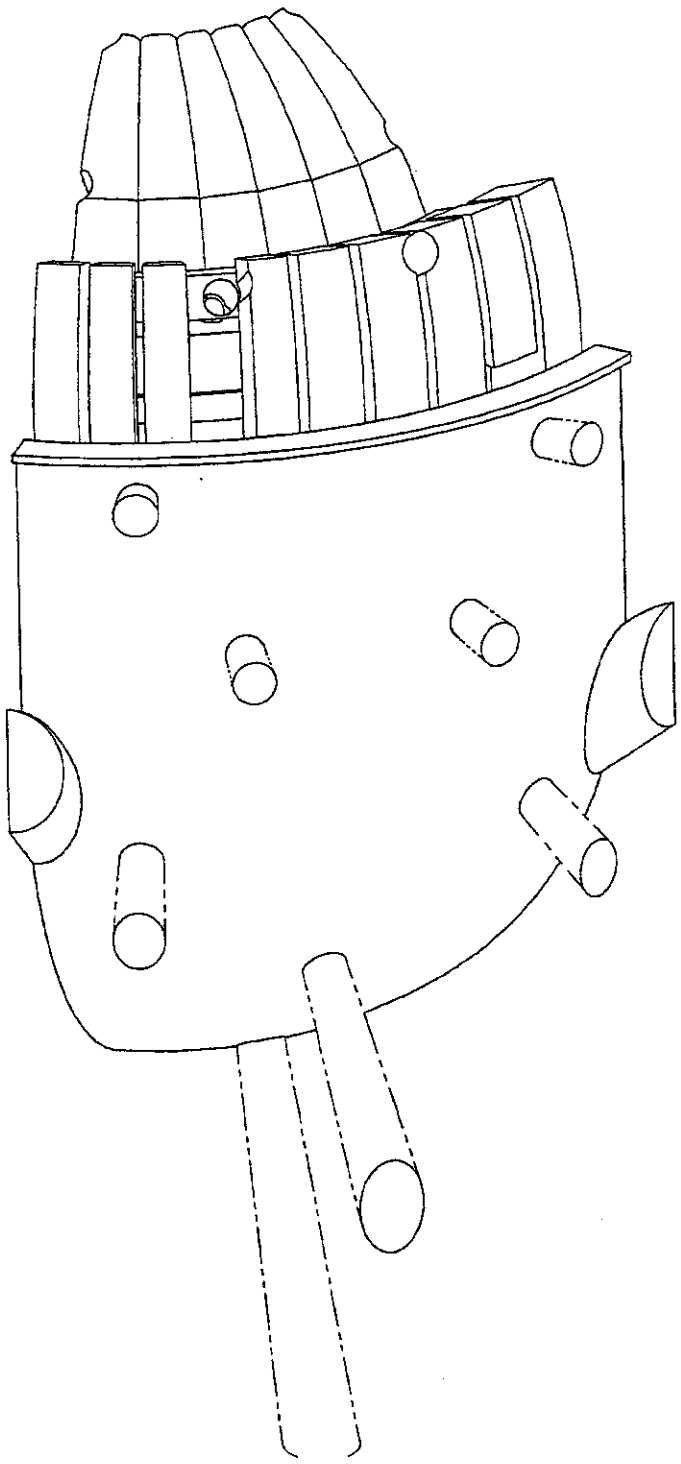

Figure 6.3.2-13 Reactor Vessel with Manifolds Removed

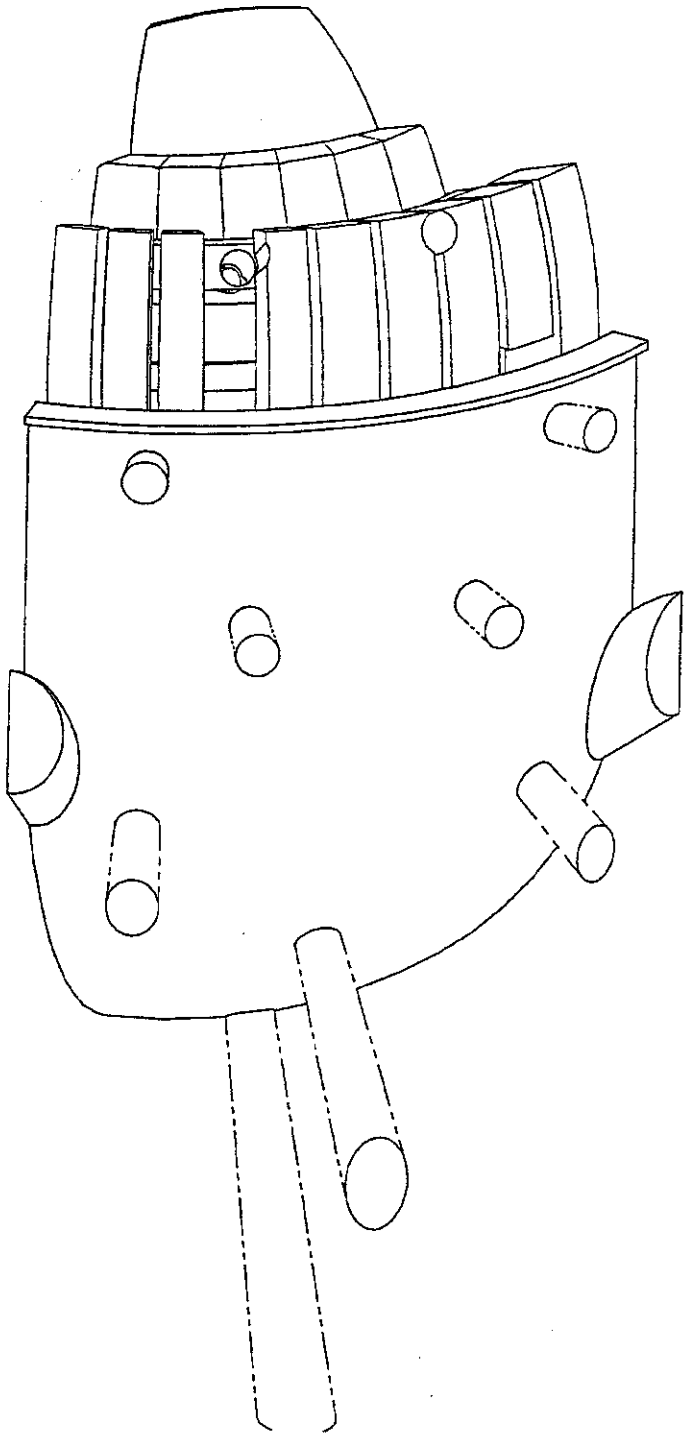

Figure 6.3.2-14 Reactor Vessel with Upper Blanket Ring Removed

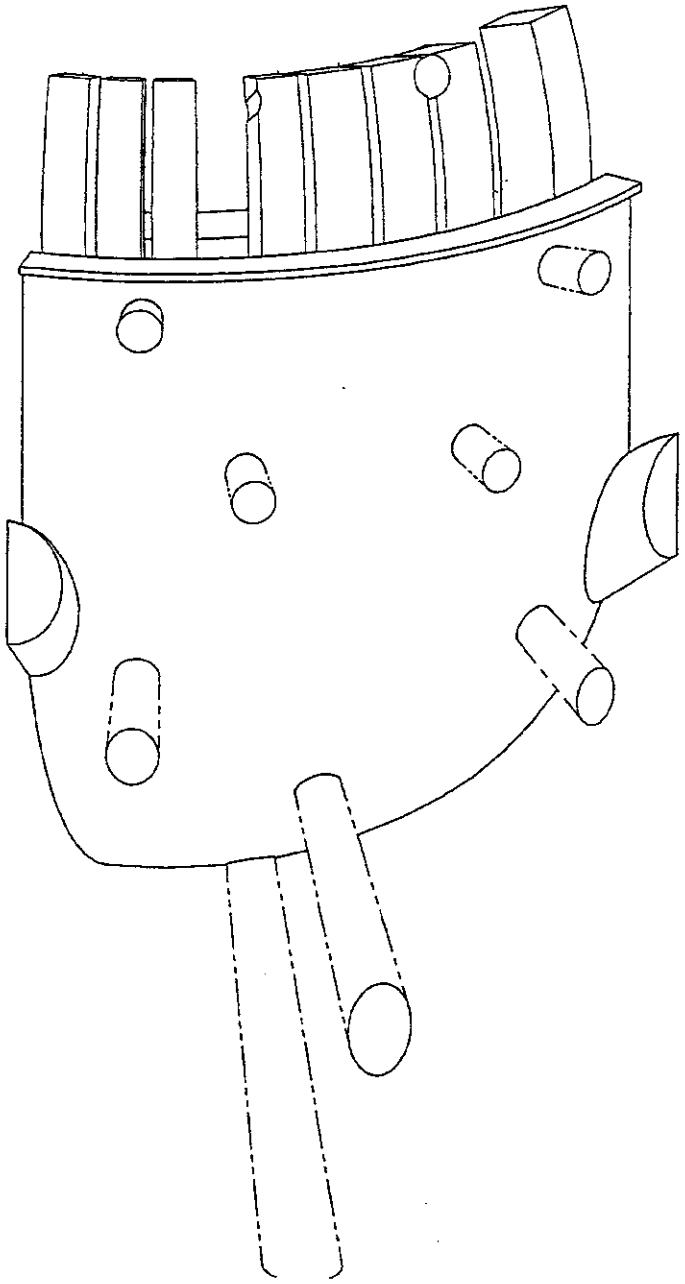

Figure 6.3.2-15 Reactor Vessel with First Wall Top Dome Removed

(k) The remainder of the blanket rings and first wall panels can then be removed in a similar sequence.

First Wall Attachment - The method of mounting and transferring loads from the first wall panels to the underlying structure was investigated to determine concept feasibility. A number of options were evaluated for the central cylindrical portion of the wall. This section of the wall is comprised of vertical wall panels as seen in Figure 6.3.2-16. These panels are assembled in a ring with the radial reaction taken by the blanket module edges. Figure 6.3.2-17 shows two options, composite leaf springs or adjustable wedges, for applying this preload. Detailed analyses of these approaches will be required as the design evolves.

6.3.2.6 Reactor Building Maintenance - Due to the number and the variation of components requiring maintenance in the Reactor Building along with the high level of the conceptual design study, only the maintenance of a few key systems were investigated to demonstrate applicable principles. Figure 6.3.2-18 illustrates the Reactor Building maintenance equipment and provisions. The bubbles indicate the location of various overhead cranes, mobile devices, and remote manipulators which are explained in the following figures and paragraphs.

Maintenance of the Target Injector System - The target injection system for the laser option is located at the top of the reactor and is mounted along the vertical axis of the machine. [The target injection system for the heavy ion beam option is located near the midline of the vessel in the vicinity of one of the beamline clusters.] The electromagnetic target injection system for the laser option is approximately 2 meters long. See Section 6.4.4 for additional information on this system.

This injection system is serviced from above as shown in Figure 6.3.2-19. Transportable power manipulators will be used in these service operations. Other maintenance equipment includes the overhead crane, target injector lifting rig, adjustable balancing beam, and assorted special purpose tools.

The target injection systems is removed from the operating position and transferred directly to the hot cell. This is achieved by attaching a lifting rig to the pellet feed line and disconnecting the feed line from the injector using the transportable power manipulator with an appropriate tool. When the line is free, it is lifted from the injector by the main crane. The main target injection system attachment locking device is disconnected and the injection system is removed by the main overhead crane for maintenance actions in the hot cell.

Final Mirror Maintenance - There are 60 laser beamlines symmetrically located around the reactor cavity. This arrangement provides the necessary direct drive target illumination uniformity. The beamlines are maintained with an interior pressure of a few mtorr. Bulk shielding is provided individually around each beamline out to and

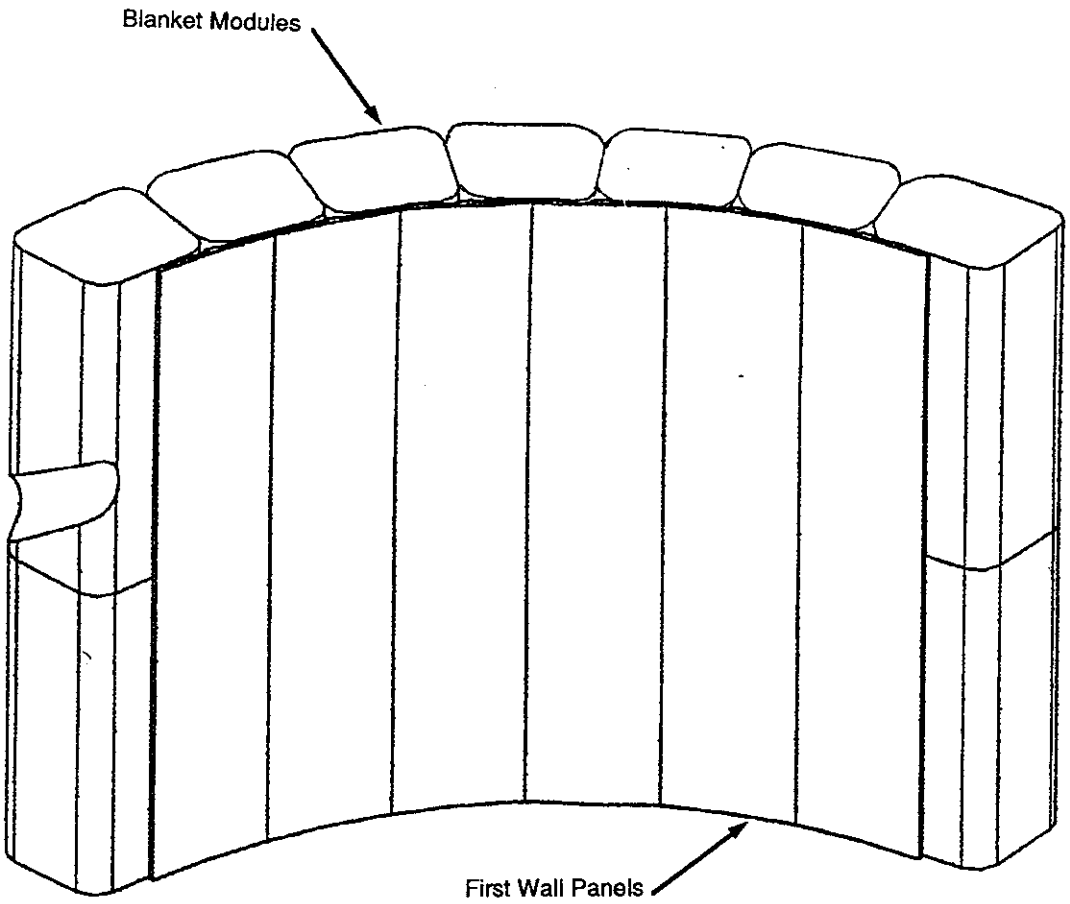

Figure 6.3.2-16 Vertical First Wall Panels are Attached to Blanket Modules

beyond the grazing incidence mirrors, the final mirrors, the neutron trap, and the neutron, which all lie inside the reactor building wall. Figure 6.3.2-20 illustrates a typical beamline arrangement and its principal elements. Both the grazing incidence metal mirror (GIMM) and the final focusing mirror must be replaced on a periodic basis, perhaps every 5 to 15 years depending upon material and coating developments. Beamline support structures allow attainment of the requisite beamline and mirror alignment requirements. The mirrors will also be cooled to maintain stable temperature and dimensional requirements. The mirrors will be removed and replaced with prealigned slide mounts to affect near final alignment. Final alignment will be accomplished with feedback from a surrogate target. Vernier adjustments will be made with the mirror mounts. Remote manipulators will be used to gain access to the mirror systems and remove/reattach the cooling fittings, if required.

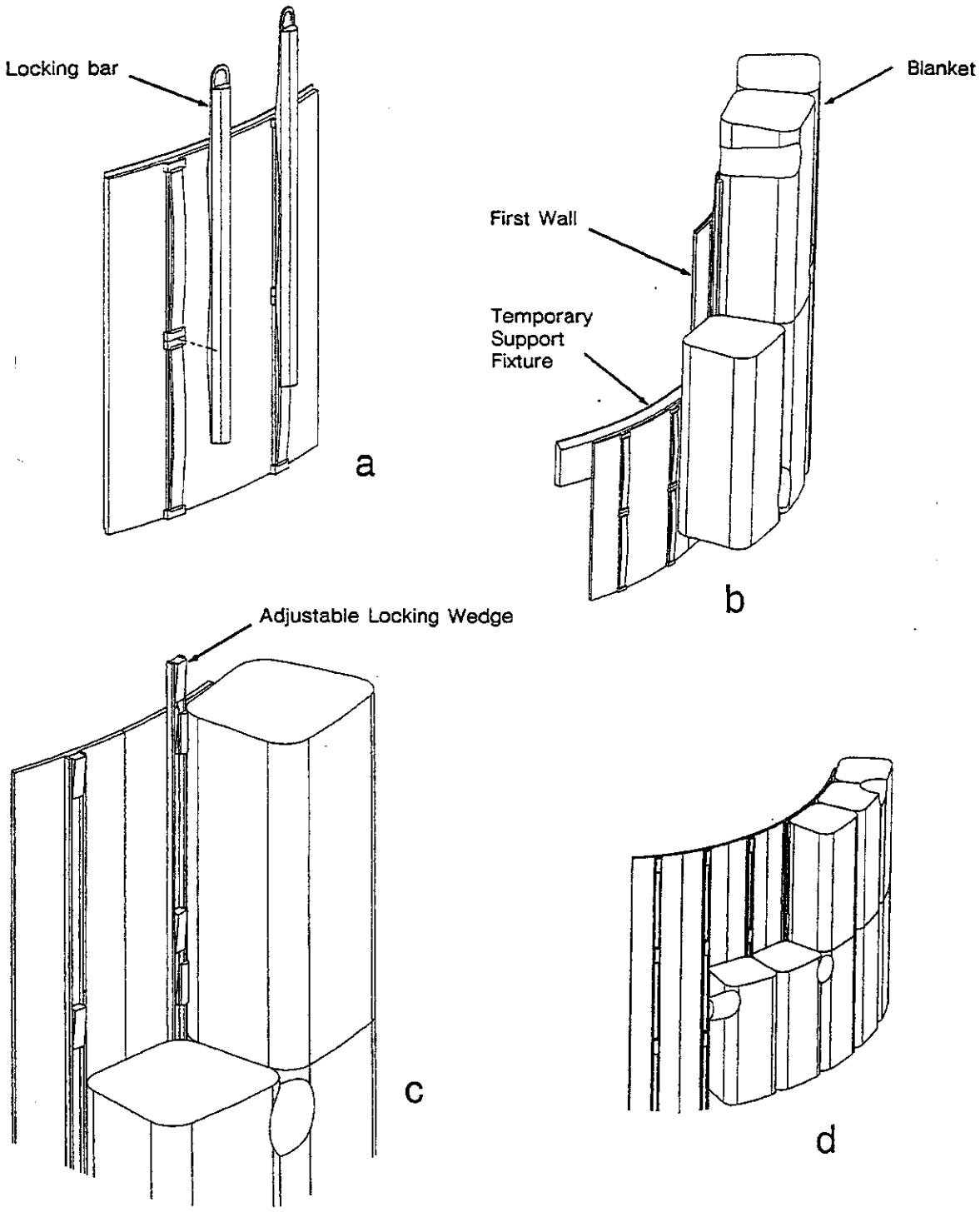

Figure 6.3.2-17 First Wall Attachment Options

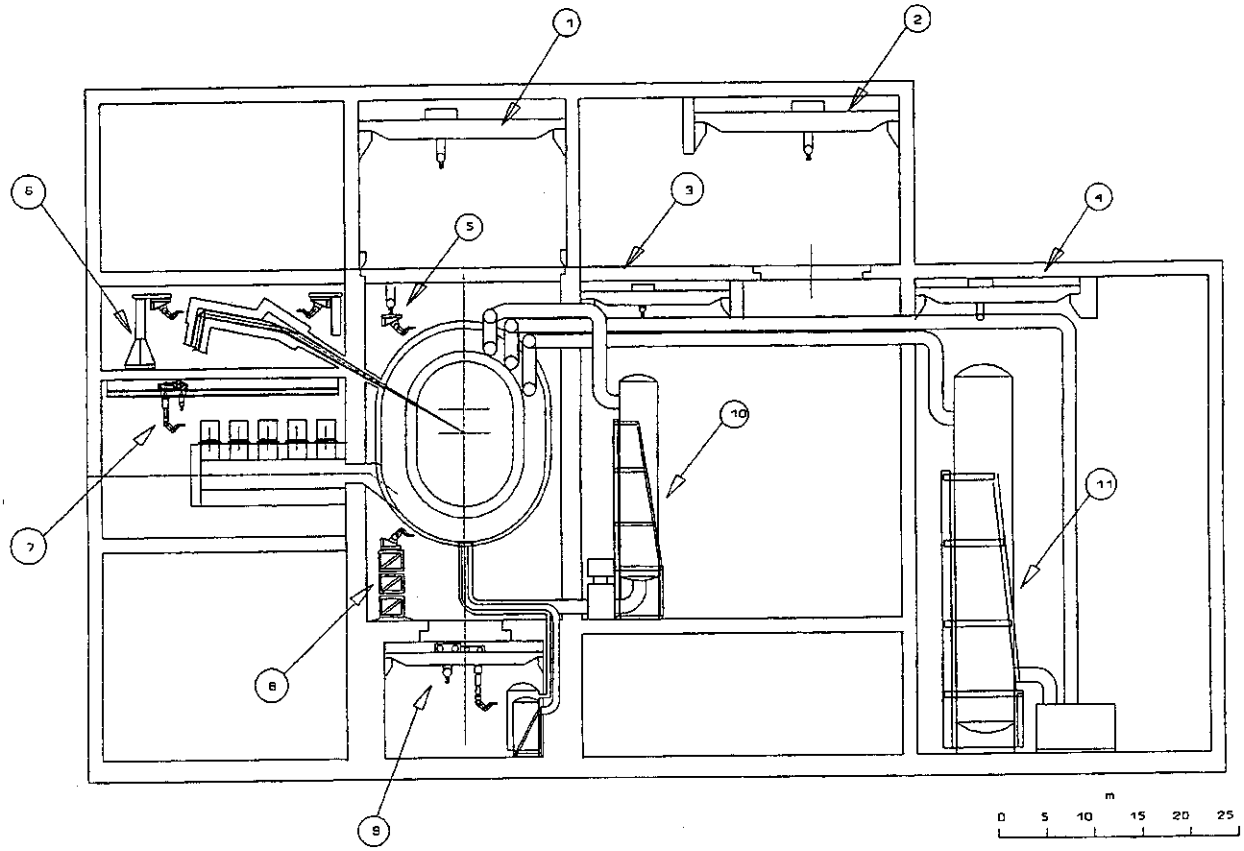

Figure 6.3.2-18 Reactor Building Maintenance Equipment and Provisions

Vacuum Pump Maintenance - The reactor chamber vacuum pumps are located on three main vacuum pump modules. Each pump module has ten cryogenic vacuum pumps on the upper surface of the module. The general arrangement is shown is several views on Figure 6.3.2-21. The vacuum pump provides pumping of the reactor chamber noncondensable gases to obtain a base pressure of a few mtorr. The lead condensation removes most of the condensable gases and traps some of the noncondensable gases. Figure 6.3.2-21 illustrates the relation of one of the vacuum modules compared to the beamlines and the wall/blanket sector.

The cryogenic vacuum pumps are very reliable. The only moving parts are the slide valves. During routine maintenance, these slide valves and pumps would be serviced or replaced. An overhead gantry crane would be used with a telescopic manipulator mast as shown in Figure 6.3.2-22. The mast has an interface with a dextrous and power manipulator. Pumps are mounted on manifolds such that the removal of the fixing clamp will allow vertical movement of the pump. Detailed maintenance will be accomplished in the hot cell.

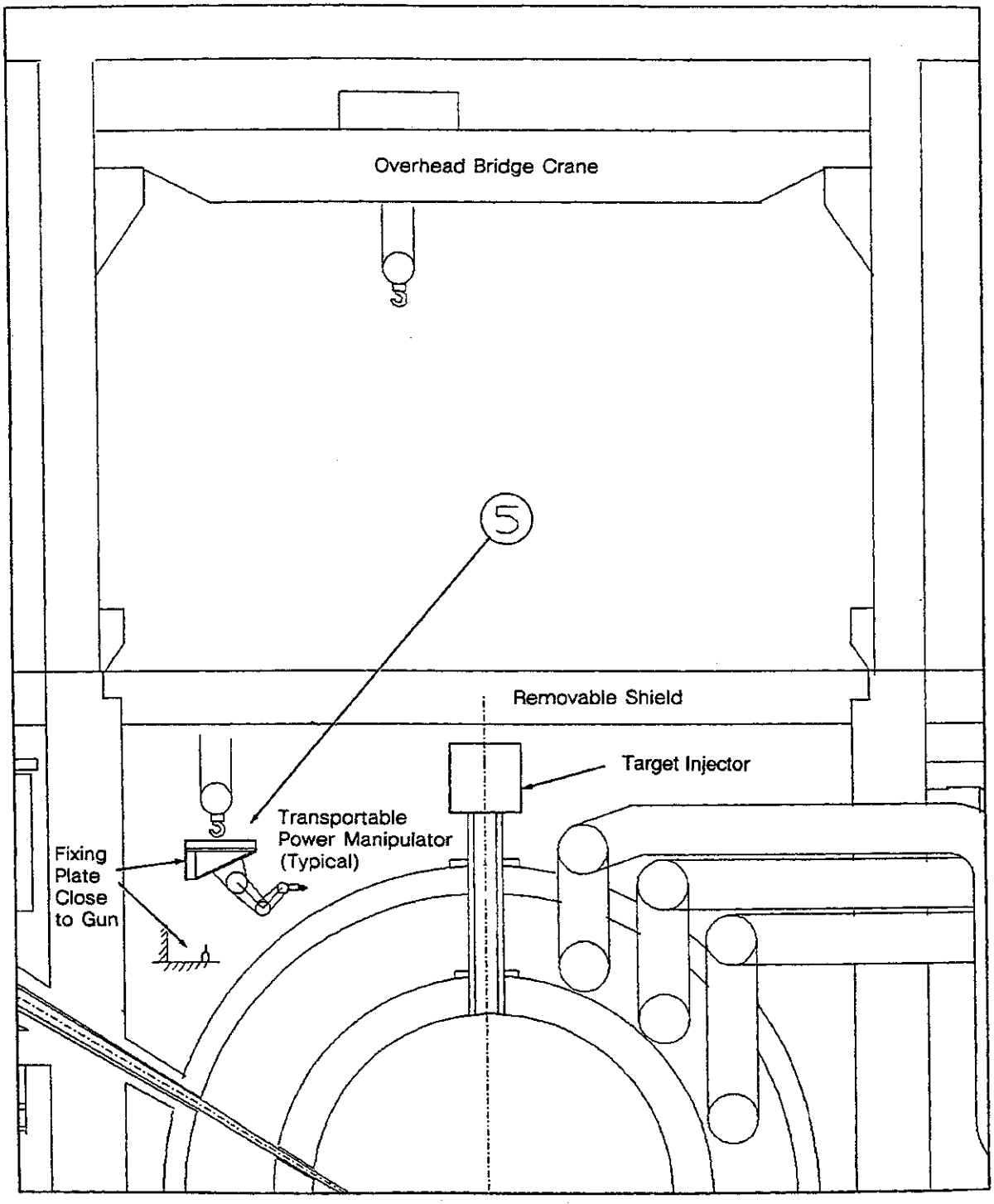

Note: For Exo-Vessel maintenance or preparation work prior to removing Cavity Cap, the Transportable Power Manipulator is attached to an installed base.

Figure 6.3.2-19 Main Bridge Crane and Exo-Vessel Maintenance of Target Injection System

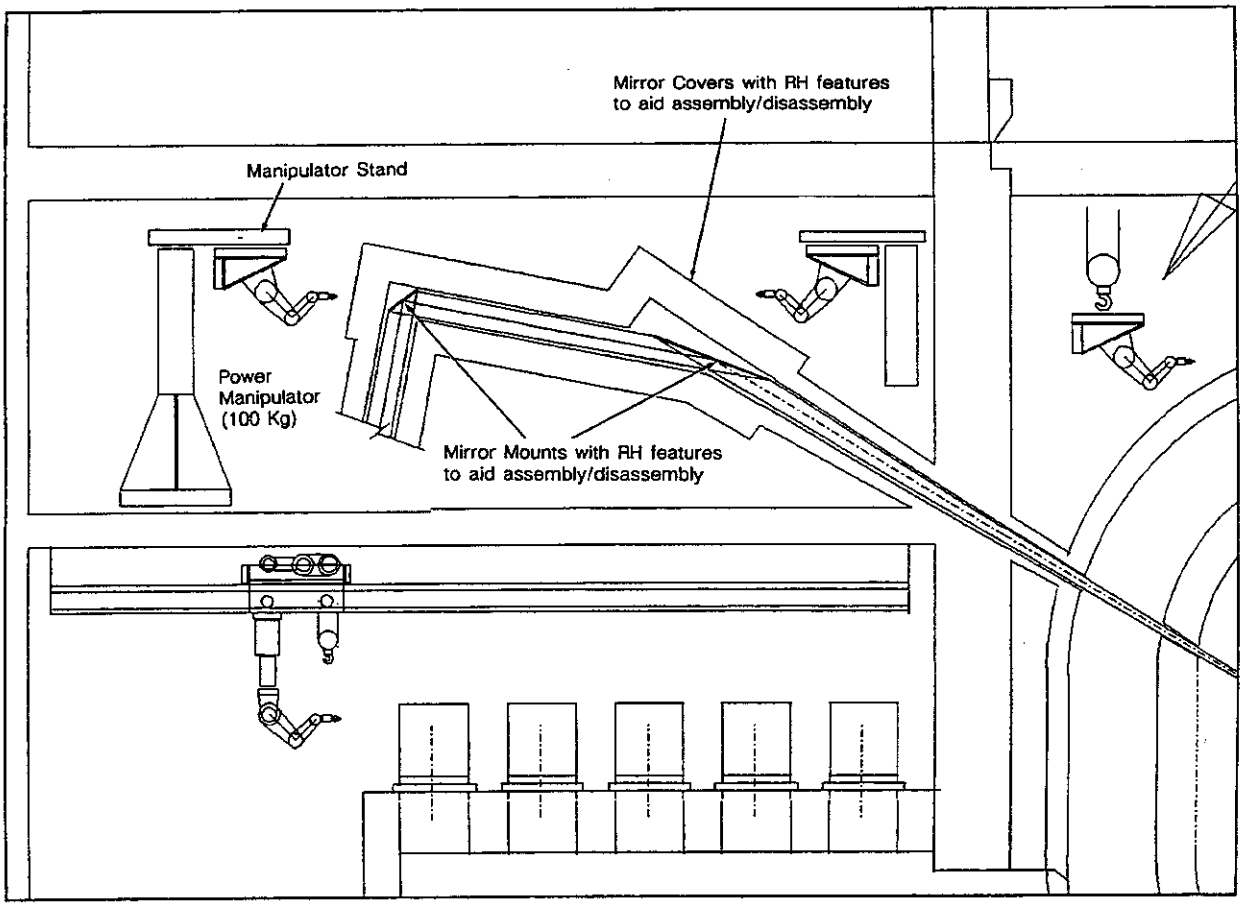

Figure 6.3.2-20 Remote Handling Equipment for Final Optical Elements

Liquid Lead Steam Generator Maintenance - Three liquid lead steam generators are mounted in the area outside the bulk biological shield at the -19 meter level. The liquid lead leaving the first wall cooling circuit, at the bottom of the reactor vessel, is pumped into the top of the steam generator. The lead flows downward through the generator, exiting to be returned to the top of the first wall system.

Liquid lead steam generators will require periodic maintenance and replacement. Before performing maintenance, the liquid lead must be drained from the entire circuit. A first wall liquid drain tank is located in the basement. Inspection and minor maintenance of tube headers can be made by accessing an entrance port at the bottom of the generator with a floor-mounted manipulator. Similarly, the bottom of the water circuit can be desludged by gaining access via a port at the bottom of the generator. For major repair, the steam generator would be replaced and repairs accomplished in the hot cell.

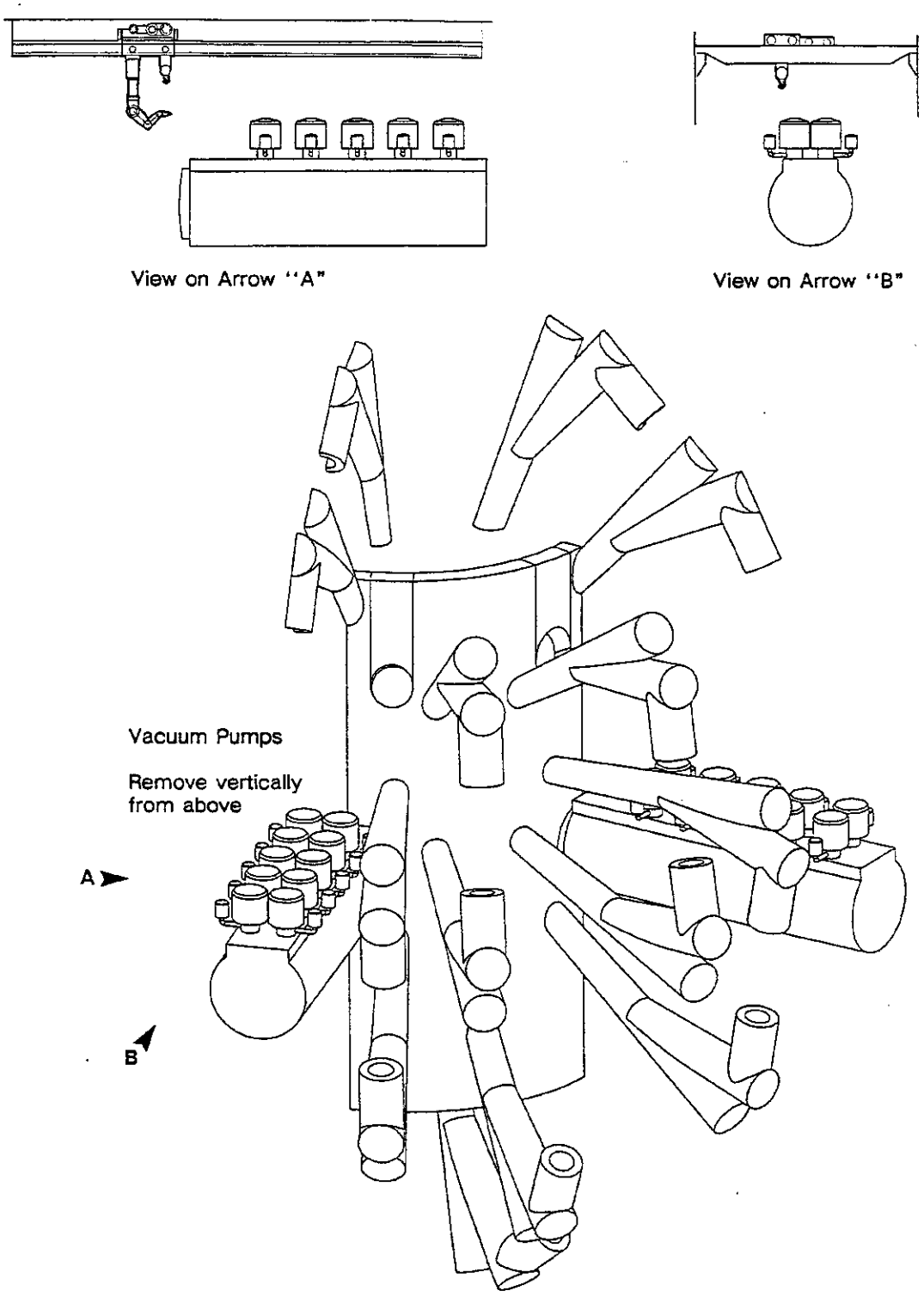

Figure 6.3.2-21 Sector of Bulk Shield Wall Showing Positions of Vacuum Pumps Relative to Laser Beamlines

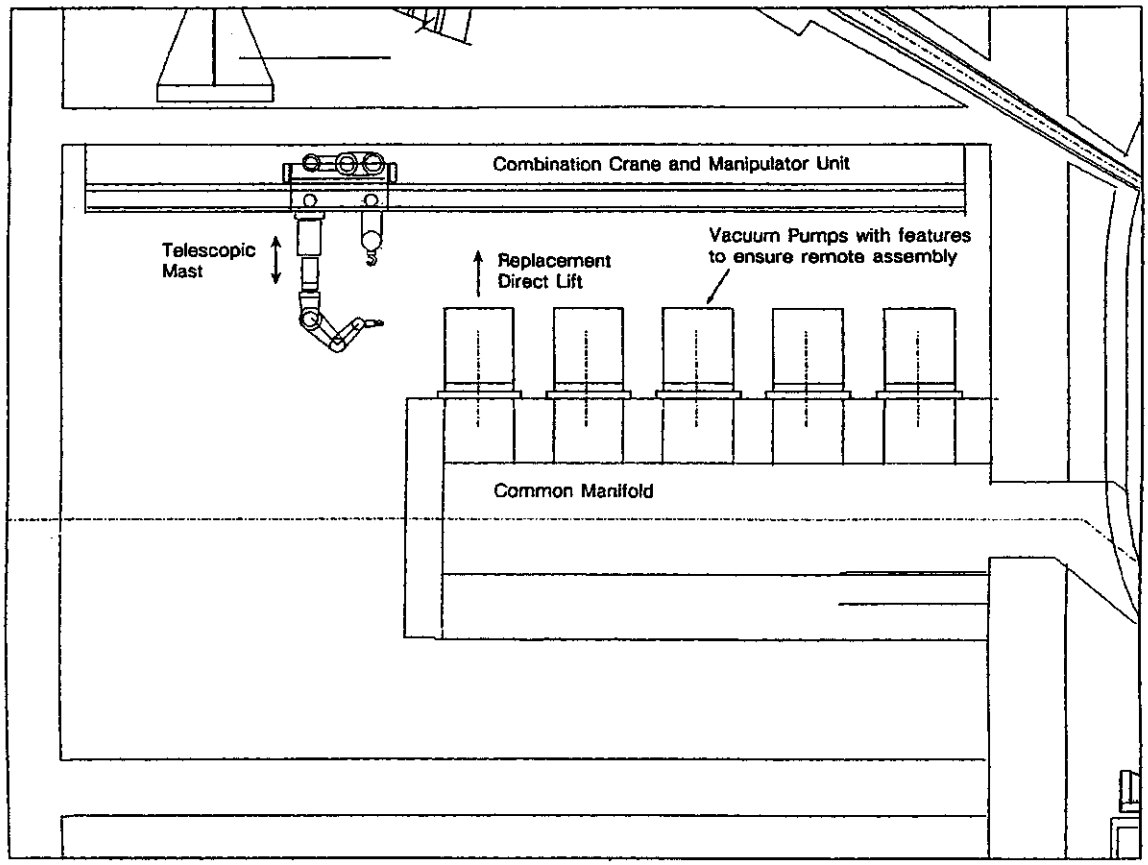

Figure 6.3.2-22 Schematic Arrangement of Remote Handling Equipment for Vacuum Pump Room

To facilitate handling and removal, steam generators are mounted in racks similar to those devised for chemical vessels in reprocessing plants. This arrangement is shown in Figure 6.3.2-23. Disconnection and lifting functions are carried out with a bridge crane and manipulator system (both dexterous and power). The rack is both a lifting rig and a strong back for the vessel. Vessels are normally connected to the feed lines by jumper pipes. When jumper pipes are disconnected and fasteners for the support rack are removed, an overhead crane can transfer the whole assembly from an operating position to the hot cell or decontamination facility. When replacing the unit, the rack has passive features which automatically locate the vessel and align the jumper pipe for remote connection.

Helium Steam Generator Maintenance - The helium steam generators are more remote from the reactor vessel. Levels of radiation are lower due to the environment and limited tritium migration within the helium coolant. However, there will be tritium in the coolant. Thus, the helium circuits must be detritiated to allow hands-on access with bubble suits. Figure 6.3.2-24 illustrates the size of the generators and maintenance with an overhead crane.

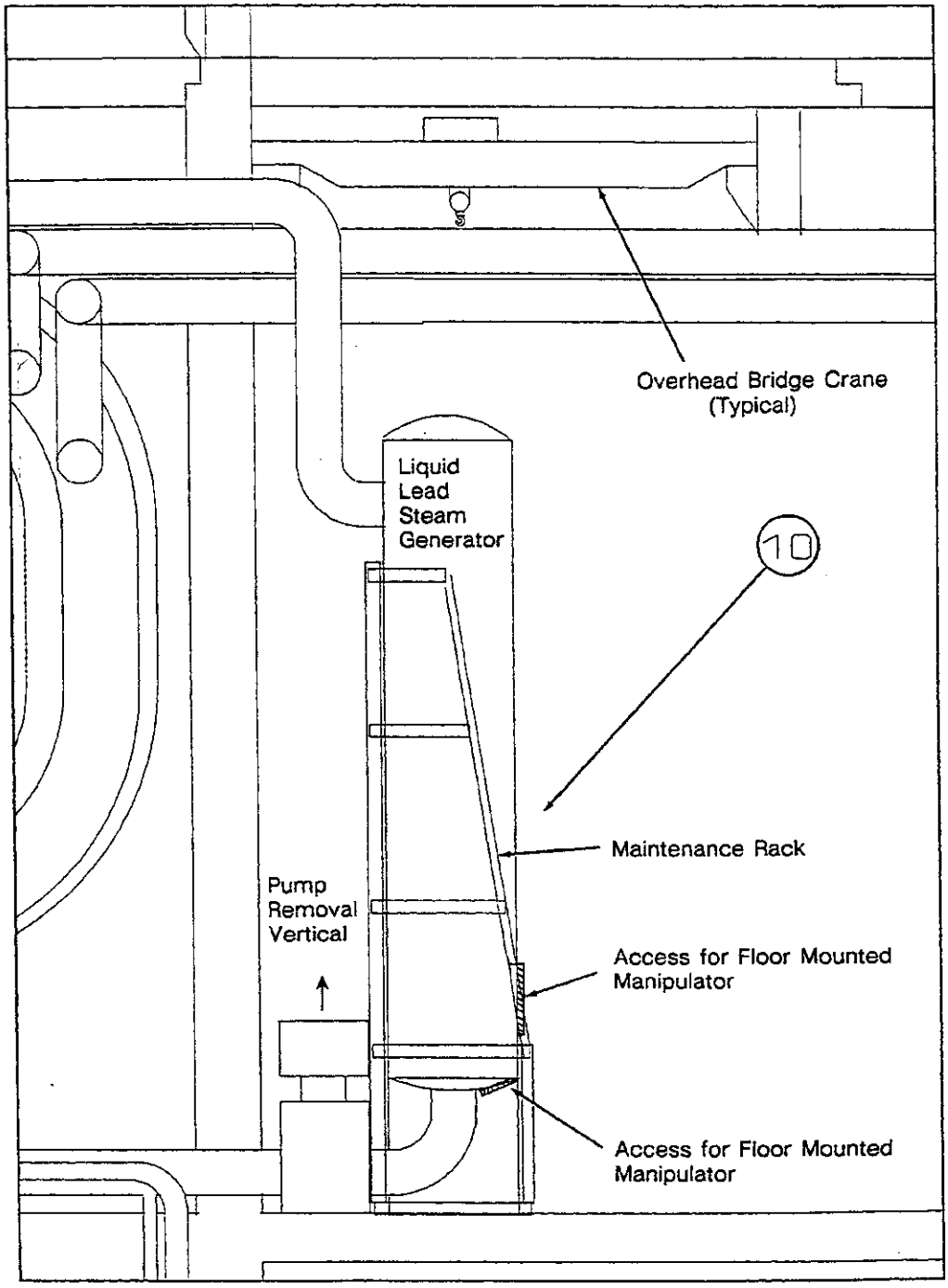

Figure 6.3.2-23 Lead-Steam Generator Maintenance

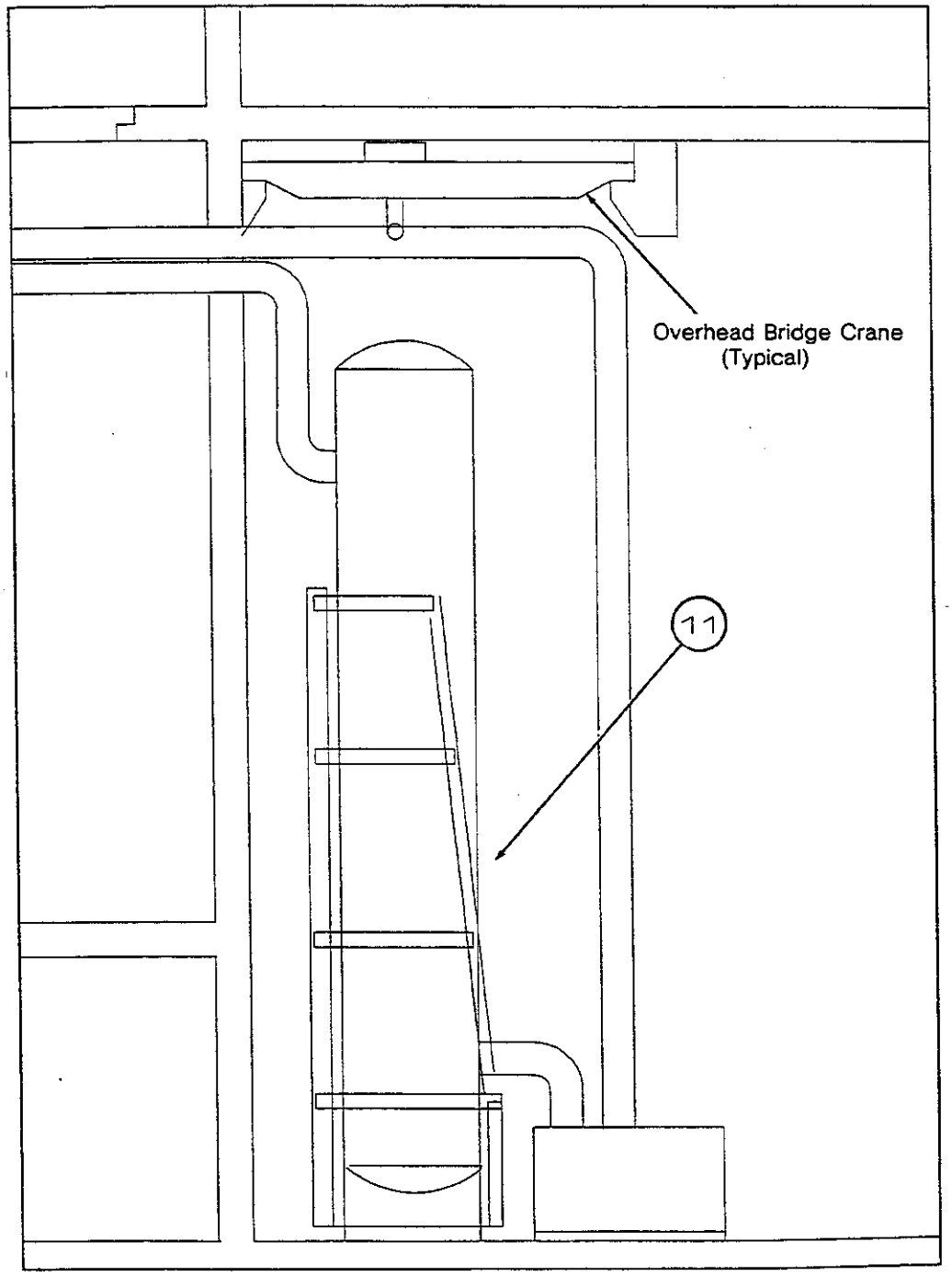

Note: For heat exchanger maintenance, access ports must be provided for the Floor-Mounted Manipulator

Figure 6.3.2-24 Helium-Steam Generator Maintenance

First Wall Liquid Lead Drain Tank Maintenance - The first wall coolant liquid lead drain tanks are located below the reactor vessel in the basement. To aid in replacement, the tanks are supported in equipment racks which are designed for remote replacement. Figure 6.3.2-25 shows the general arrangement and extent of the maintenance equipment. Minor maintenance actions on valves can be accomplished in place with replacement of parts. Larger items will require removal and replacement of the entire unit. The rack has location and alignment features which allow remote operations.

Contaminated Liquid Lead Hold Up Tank Maintenance - The contaminated liquid lead holdup tank is located in the basement alongside the drain tank. This tank collects the liquid lead which has a high level of contamination and is awaiting processing. The maintenance actions are identical to the liquid lead drain tanks.

6.3.2.7 Driver Building Maintenance - The two driver concepts chosen for Prometheus require different maintenance approaches and equipment. Figure 6.3.2-1 previously presented the site plan for the two reactors. The laser option uses an annular driver building, as shown in Figure 6.3.2-2, surrounding the reactor building. The laser driver is designed for an on-line maintenance of critical components in order to maximize the system availability. Moreover, the system is designed with enough redundancy in the main laser amplifier systems to accommodate a number of failures without adversely degrading the system performance in terms of target illumination uniformity. One of the critical driver system maintenance tasks is the replacement of the discharge laser power amplifier modules. Figure 6.3.2-26 illustrates the maintenance equipment used to replace the laser power amplifier modules which are approximately 0.44 m x 0.44 m x 2.0 m.

The heavy ion driver option uses a long but small cross-section tunnel to house the ion beam driver elements. A cross-section of the driver tunnel with overhead cranes was shown previously in Figure 6.3.1-23. The heavy ion driver maintenance will principally consist of change-out of the magnets and power supplies. The maintenance strategy chosen is simply an updating of the procedures used on existing accelerators such as CERN. A combination of heavy lift transporters and dexterous robots are deployed down the accelerator tunnel to perform the change-out operation remotely with human supervision. Figure 6.3.2-27 shows a typical existing setup for this type of operation. Due to the serial nature of the linear accelerator system where any major system failure causes the entire driver to be off line, the system will be optimized for high reliability and minimum maintenance times.

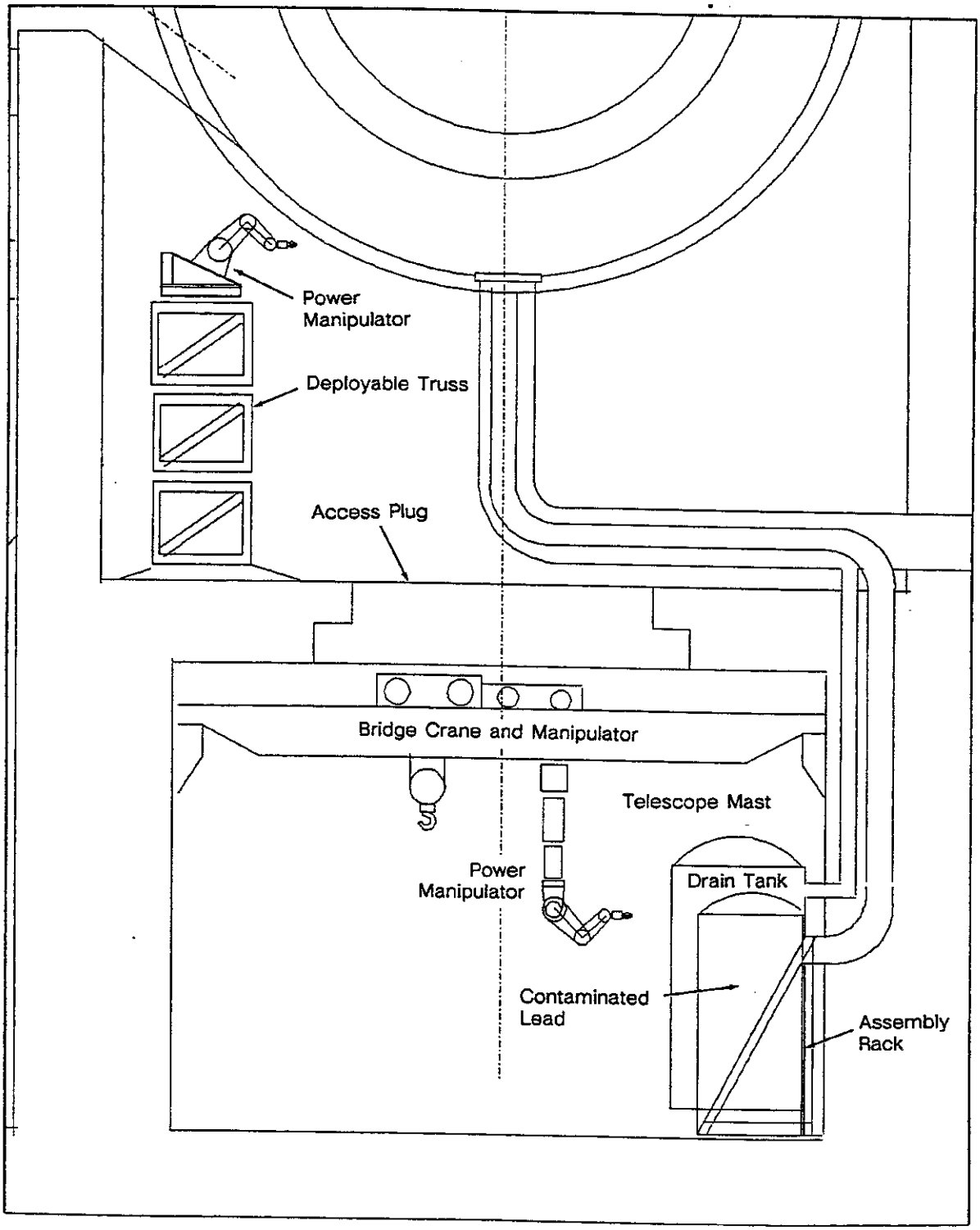

Figure 6.3.2-25 Lead Tank Maintenance

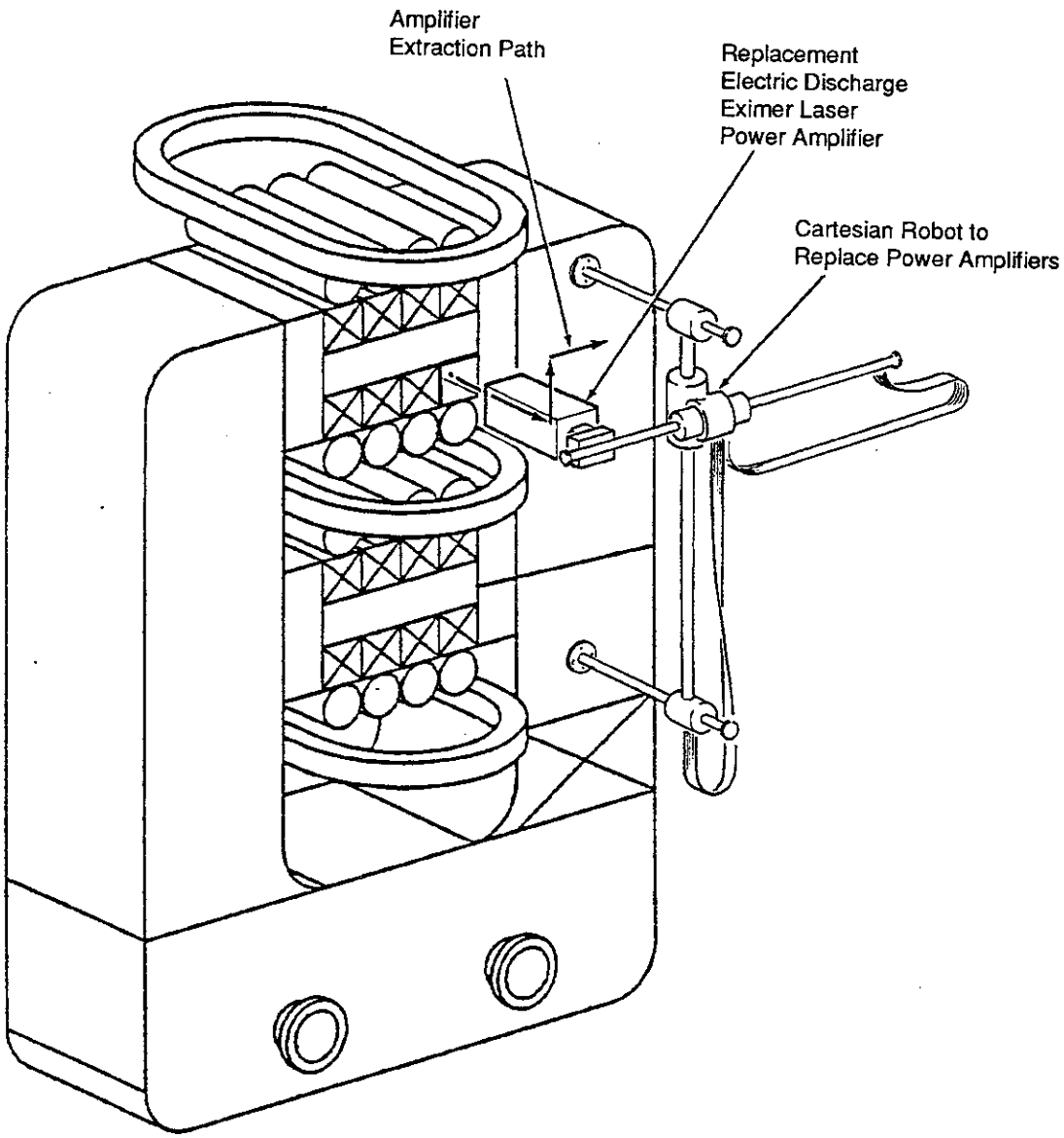

Figure 6.3.2-26 Maintenance of the Electric Discharge Power Amplifier Module

Tritium Building and Target Factory Maintenance - The Tritium Building and Target Factory both use a significant amount of process machinery. These types of applications are very suitable for a high degree of dedicated module replacement automation. In both of these applications, a failure of a critical element would cause the entire plant to be off-line. Thus the design approach is to have highly reliable components and systems, maximize the redundance of critical systems, and design the maintenance systems to minimize the maintenance times. The maintenance equipment associated with these functions were not considered in detail although general information can be found in Sections 6.4 (Target Factory), 6.7 (Fuel Processing), and 6.11 (Remote Maintenance Systems).

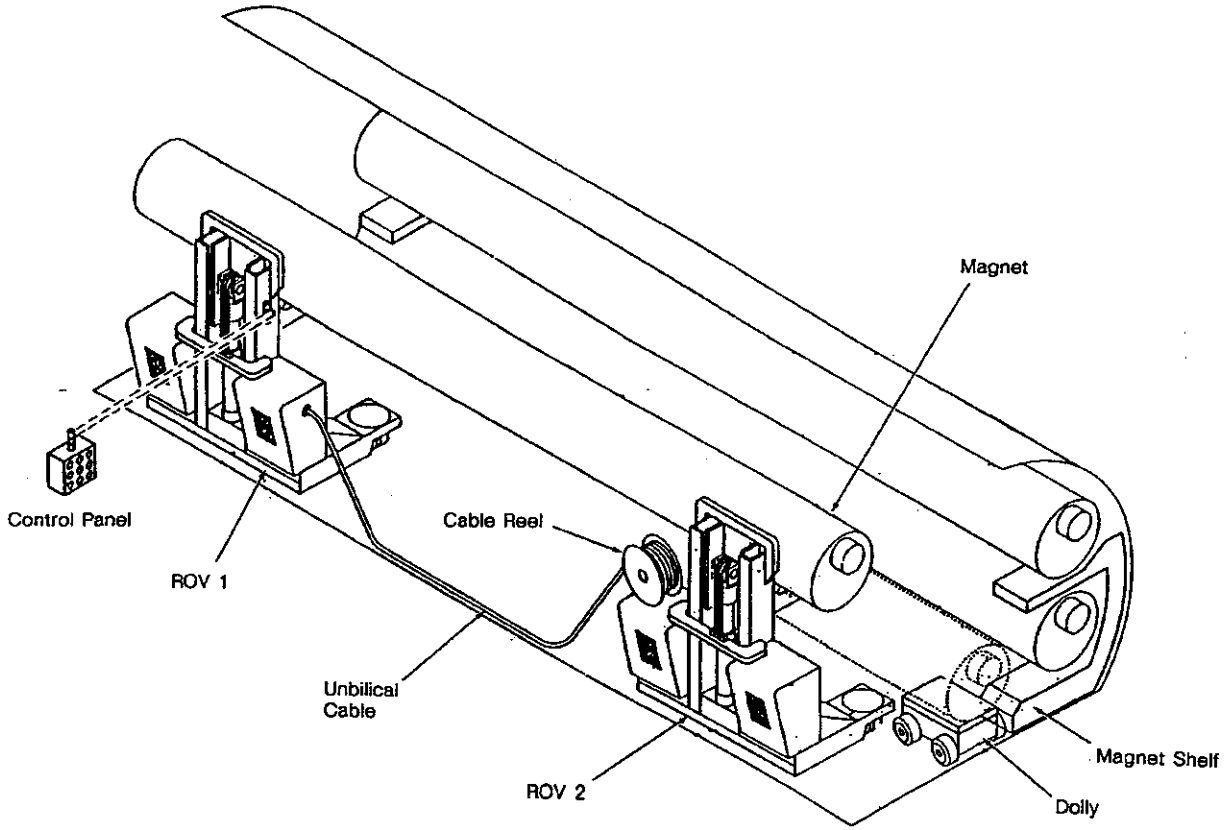

Figure 6.3.2-27 Typical Maintenance System for a Linear Accelerator

Turbine Building Maintenance - Experience in power plant turbine maintenance has been evolving over decades. The technology proposed in this design study is an extrapolation of current technologies. This involves significant hands-on maintenance using cranes and general purpose manipulators. However, we are forecasting for the 2030 timeframe, which would suggest increased automation would help speed and improve the maintenance of these systems. Autonomous cranes and smart tooling will reduce the manual labor role to that of supervision and technical expertise. Section 6.11 provides additional information on this subject.

Maintenance and Hot Cell Facilities - The normal mode of operation for maintenance in the majority of the plant is to remove and replace failed or worn equipment. This approach will provide the highest level of plant availability. This approach also reduces the sophistication of the local maintenance equipment to that required only for replacement and not for repair. For plant equipment with a high level of activation, the equipment will be transferred to a specialized hot cell for repair or disassembly and waste disposal. Figure 6.3.2-28 portrays the hot cell with a large number of reactor elements assembled in their operational configuration, perhaps in preparation for installation. Shown in the figure is a large overhead crane with a telescoping mast and a dexterous robot. The hot cell would have a large number of both general

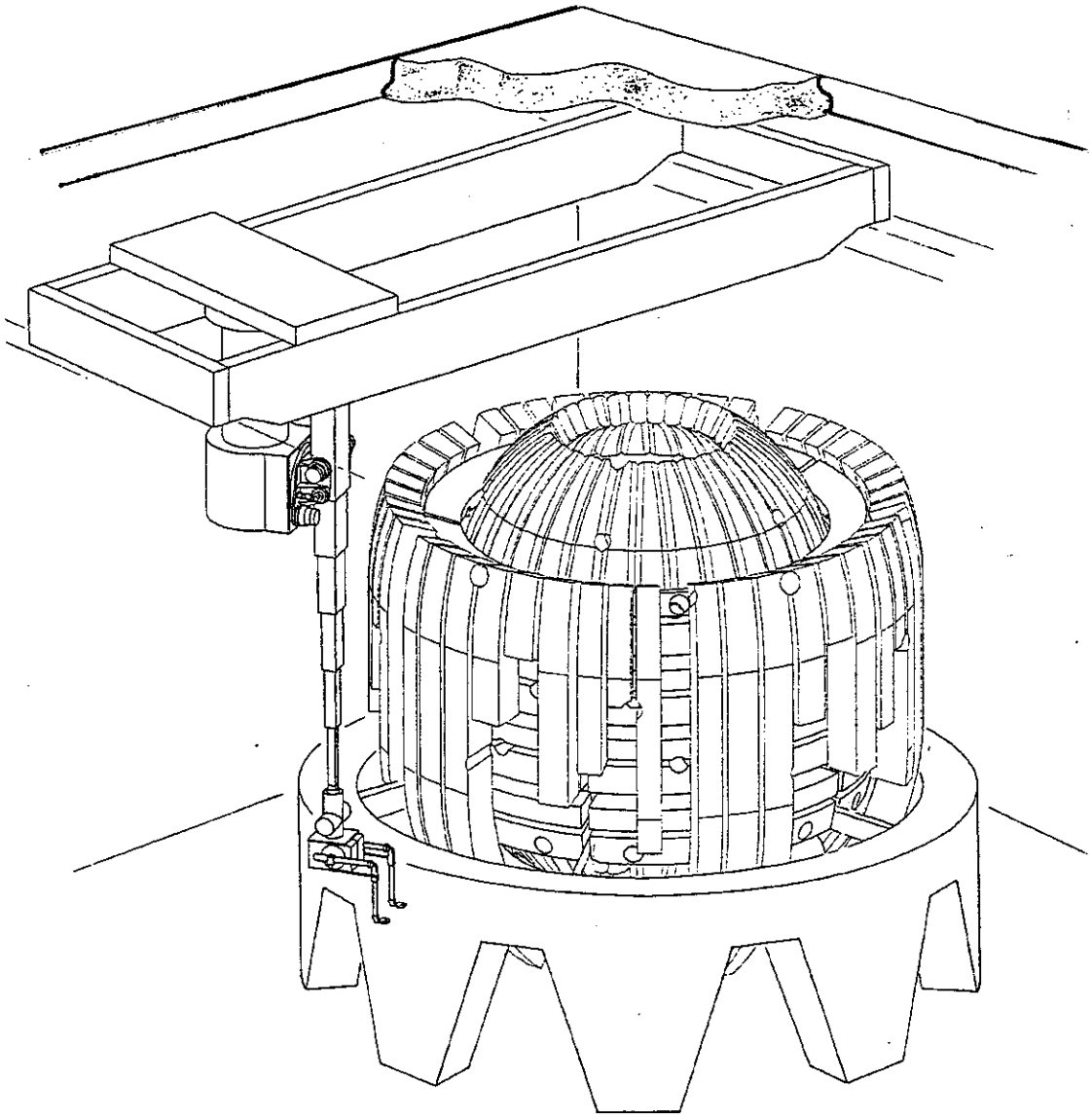

Figure 6.3.2-28 A Complete Set of Blanket Modules in the Hot Cell

purpose and specialized robots and manipulators for a variety of operations. The operations done in the hot cell include decontamination, failure analysis, disassembly, repair, system testing, and dimensional mockup (inspection). Due to the nature of the work accomplished in the hot cell, these are envisioned to be a complete range of operations from hands-on maintenance, human-assisted maintenance, and completely autonomous operations. Components which exhibit known and predictable wearout behavior are candidates for the more automated repair techniques.

6.3.3 Reliability, Availability, and Maintainability (RAM) Analyses - This section discusses the RAM analyses results along with the contributing factors. Production of economically competitive electric power is the ultimate goal of power plants. Several factors contribute to the production cost of electricity: net power, capital cost, operating cost, and plant availability. The plant must meet certain availability goals or attainment of all other performance and cost goals are meaningless. To achieve the plant availability goals, both plant reliability and maintainability requirements must be met.

6.3.3.1 Availability Summary - For both of the Prometheus reactor plant designs, analyses were conducted to determine the expected reliability and maintainability values of the key plant systems. These data were combined into the inherent availability for the respective subsystem or system. For this conceptual design, a complete analysis could not be accomplished because of the lack of complete technical definition of all systems. Rather, the major plant elements were analyzed which were estimated to account for 90% of the expected plant downtime. These data were then extrapolated to arrive at an estimated plant inherent availability value.

	Laser	Heavy Ion
Inherent Availability of Major Plant Elements	89.28%	90.68%
Projected Plant Inherent Availability	88.09%	89.64%

The conversion of the plant inherent availability into the average achieved availability takes into account the planned or unscheduled maintenance and the service shutdown for unplanned maintenance or repair. Typical of central station power plants, a 30-day annual shutdown is assumed. The longest scheduled task would take 15 days at three shifts per day. To account for a refit shutdown of 60 days every 5 years, an extra yearly shutdown allowance of 6 days is added.

	Laser	Heavy Ion
Total time per year, days	365	365
- Less scheduled annual shutdown, days	-30	-30
- Less refit allowance, days	- 6	- 6
Attempted run time, days	329	329
- Less unscheduled maintenance time*, days	-39.2	-34.1
Productive reactor time, days	289.8	294.9
Average achieved availability**, percent	79.4	80.8

* Unscheduled maintenance is computed from the plant inherent availability and the attempted run time.

** The average achieved availability is the ratio of the productive reactor time to the total time per year.

The estimated plant availability of 80% for the Prometheus reactors is well within the availability demonstrated by current commercial nuclear power plants. Table 6.3.3-1

Table 6.3.3-1 Reported Availability for Existing Power Plants (Reprinted from Nuclear Engineering International, August 1991)

Reactor name and country		Annual figures (for 12-months to end March 1991) Rank	Load factor, %	Avail., %
Kanwa 5	J	1	99.8	100.0
Kori 2	SK	2	99.4	100.0
Pt Lepreau	C	3	98.5	97.9
Fukushima II 4	J	4	96.4	97.3
Prairie Isl 1	US	5	96.1	99.7
Tokai 2	J	6	95.9	
TVO 1	SF	7	94.9	95.7
Embalse	A	8	94.0	94.3
Philippsburg 2	D	9	93.9	93.2
Sendai 1	J	10	93.6	100.0
Almaraz 2	E	11	92.9	
TVO 2	SF	12	92.6	94.3
Three Mile Isl 1	US	13	92.4	
Bruce 7	C	14	91.4	94.4
Paks 2	HU	15	91.0	
Fukushima I 6	J	16	90.9	91.8
Neckar 2	D	17	90.4	90.8
Emsland	D	18	90.4	90.8
Huntlerston B1	GB	19	90.2	98.1
Gundremmingen B	D	20	90.0	99.9
Paks 1	HU	21	89.9	
Waterford 3	US	22	89.6	92.3
Pilgrim	US	23	89.5	
Hatch 2	US	24	89.4	
Farley 1	US	25	89.4	
Ohi 2	J	26	89.4	
Tihange 2	B	27	89.2	
Shimane 2	J	28	89.1	90.2
Gosgen	CH	29	88.9	91.1
Hinkley Pt A1	GB	30	88.5	97.1
Tihange 3	B	31	88.4	
Byron 1	US	32	88.3	
Grohnde	D	33	88.1	89.9
Muehleberg	CH	34	88.1	90.3
Paks 3	HU	35	87.9	
Leibstadt	CH	36	87.9	
Takahama 3	J	37	87.7	
Tsuruga 1	J	38	87.6	
Doel 3	B	39	87.5	
Monticello	US	40	87.4	93.8
Pickering 5	C	41	87.4	89.3
Tihange 1	B	42	87.1	92.0
Bruce 6	C	43	87.0	88.8
Takahama 4	J	44	86.2	
Beznau 2	CH	45	86.0	86.4
Doel 4	B	46	86.0	
Wolsong 1	SK	47	85.9	85.5
Palo Verde 3	US	48	85.8	
Asco 2	E	49	85.8	88.2
Millstone 1	US	50	85.7	88.5
Prairie Isl 2	US	51	85.7	90.2
Hamaoka 3	J	52	85.4	
Asco 1	E	53	85.4	87.7
Lovisa 2	SF	54	85.3	88.0
Doel 1	B	55	84.8	
Kewaunee	US	56	84.8	
Vandellos 2	E	57	84.5	
Barsebaeck 1	S	58	84.4	
Paks 4	HU	59	84.4	
Lovisa 1	SF	60	84.3	87.3
Maanshan 2	TW	61	84.0	88.9
Diablo Canyon 2	US	62	83.9	90.8
Cofrentes	E	63	83.8	86.1
Point Beach 2	US	64	83.7	88.1
Beznau 1	CH	65	83.6	85.7
La Salle 1	US	66	83.6	86.5
Pickering 7	C	67	83.2	92.8
Hinkley Pt B2	GB	68	83.1	94.3
Shimane 1	J	69	83.1	83.2
Neckar 1	D	70	83.0	85.9
Ikata 2	J	71	83.0	
Dukovany 2	CS	72	82.9	88.6
Yonglwang 1	SK	73	82.4	85.7
Wolf Creek	US	74	82.3	87.2
Sendai 2	J	75	82.2	83.4
Point Beach 1	US	76	82.0	84.3
Bugey 2	F	77	81.9	95.2
Almaraz 1	E	78	81.9	
Barsebaeck 2	S	79	81.8	
San Onofre 2	US	80	81.7	89.0
Oconee 3	US	81	81.6	
Forsmark 3	S	82	81.5	93.7
Bruce 3	C	83	81.2	89.2
Dukovany 1	CS	84	81.1	84.8
Ringhals 4	S	85	81.1	92.2
Bruce 8	C	86	81.1	85.9
Arkansas 2	US	87	80.9	
Genkai 2	J	88	80.6	81.5
Isar 2	D	89	80.5	89.3
Vermont Yankee	US	90	80.5	
Bradwell 2	GB	91	80.4	99.9
Kruemmel	D	92	80.4	85.5
Mihama 3	J	93	80.0	

Reactor name and country		Annual figures (for 12-months to end March 1991) Rank	Load factor, %	Avail., %
Beaver Valley 1	US	94	79.9	88.8
Oconee 1	US	95	79.9	
St Lucie 1	US	96	79.8	
Trnastin 3	F	97	79.6	86.9
Catawba 1	US	98	79.5	
Bruce 5	C	99	79.5	81.7
Maanshan 1	TW	100	79.5	83.1
Susquehanna 2	US	101	79.4	
Brunswick 2	US	102	79.3	
Wylfa 1	GB	103	79.3	99.5
Ginna	US	104	79.0	
Flamanville 2	F	105	79.0	85.7
Unterweser	D	106	78.9	79.0
Surry 2	US	107	78.9	
Callaway 1	US	108	78.9	81.8
Dresden 3	US	109	78.9	90.6
Borssele	NL	110	78.9	81.4
Vogtle 1	US	111	78.9	
Ulchin 2	SK	112	78.7	80.0
Forsmark 2	S	113	78.6	92.7
K-Kariwa 2	J	114	78.6	82.6
Cooper	US	115	78.5	
Peach Bottom 3	US	116	78.4	
Oskarshamn 2	S	117	78.3	90.2
Dukovany 3	CS	118	78.2	86.6
Pickering 6	C	119	78.2	80.2
Dukovany 4	CS	120	77.9	84.1
Oskarshamn 3	S	121	77.8	88.8
Trillo 1	E	122	77.7	
Chinon B4	F	123	77.7	80.0
Shearon Harris	US	124	77.6	
Krsko	JU	125	77.5	86.0
Ikata 1	J	126	77.5	
Kori 4	SK	127	77.3	80.8
Ulchin 1	SK	128	77.2	80.1
Gentilly 2	C	129	77.1	
Gravelines B4	F	130	77.1	80.8
Quad Cities 2	US	131	77.1	85.4
Stade 1	D	132	76.8	80.4
Gravelines B3	F	133	76.7	79.2
Koeberg 2	SA	134	76.7	84.9
Diablo Canyon 1	US	135	76.5	80.6
Paluel 2	F	136	76.4	81.9
Forsmark 1	S	137	76.4	90.1
St Lucie 2	US	138	76.1	
Braidwood 2	US	139	76.1	
Gravelines B2	F	140	76.0	81.6
Gundremmingen C	D	141	75.8	85.8
Cruas 2	F	142	74.8	82.4
Zorita	E	143	74.8	
Limerick 2	US	144	74.8	
Gravelines C5	F	145	74.7	83.8
Dampierre 3	F	146	74.1	83.3
Fukushima II 2	J	147	73.9	74.3
Blayais 1	F	148	73.5	78.4
Grafenrheinfeld	D	149	73.4	77.0
Onagawa 1	J	150	73.4	67.4
Summer 1	US	151	73.0	
Tsuruga 2	J	152	72.9	
Ringhals 3	S	153	72.8	93.4
North Anna 2	US	154	72.7	79.7
Brokdorf	D	155	72.2	73.7
Cruas 1	F	156	72.2	84.9
Tomari 1	J	157	72.1	
Davis Besse 1	US	158	72.1	
Blayais 2	F	159	72.0	86.4
Paluel 1	F	160	71.9	78.0
Dungeness A1	GB	161	71.9	99.1
Garona	E	162	71.8	78.1
Hope Creek	US	163	71.7	
Belleville 2	F	164	71.5	76.3
Oyster Creek	US	165	71.4	
Sequoyah 1	US	166	71.2	
Paluel 3	F	167	71.0	77.0
Kori 3	SK	168	70.9	76.1
Sequoyah 2	US	169	70.8	
La Salle 2	US	170	70.6	75.1
Trnastin 2	F	171	70.6	79.7
Doel 2	B	172	70.6	
Ringhals 2	S	173	70.5	72.5
Farley 2	US	174	70.5	
North Anna 1	US	175	70.5	81.6
Oconee 2	US	176	70.4	
Kori 1	SK	177	70.2	74.4
Kuosheng 2	TW	178	70.0	75.3
Sizewell A1	GB	179	69.6	91.8
River Bend	US	180	69.5	
Pickering 8	C	181	69.4	78.4
Isar 1	D	182	69.3	86.5
Susquehanna 1	US	183	69.3	
San Onofre 3	US	184	69.2	73.1
Gravelines C6	F	185	69.2	79.0

Reactor name and country		Annual figures (for 12-months to end March 1991) Rank	Load factor, %	Avail., %
Philippsburg 1	D	186	69.1	70.1
Cruas 3	F	187	68.9	75.9
Oldbury 1	GB	188	68.8	99.6
Chinon B1	F	189	68.6	70.5
Chinon B2	F	190	68.3	84.7
Laguna Verde 1	MX	191	68.1	
Cruas 4	F	192	67.9	73.9
Nogent 1	F	193	67.8	73.4
Grand Gulf	US	194	67.8	
Crystal River 3	US	195	67.8	
Hatch 1	US	196	67.3	
St Laurent B1	F	197	67.3	70.3
St Alban 1	F	198	67.1	71.6
Surry 1	US	199	67.0	
Belleville 1	F	200	67.0	71.1
Millstone 2	US	201	66.9	70.0
Bugey 5	F	202	66.9	77.8
McGuire 1	US	203	66.9	
Ringhals 1	S	204	66.8	84.6
Takahama 1	J	205	66.6	
Blayais 4	F	206	66.5	72.8
Flamanville 1	F	207	66.5	80.5
Chinon B3	F	208	66.2	70.2
Trnastin 4	F	209	66.1	83.6
Fukushima I 2	J	210	66.1	67.3
Cattenom 2	F	211	66.0	71.5
Brunsbuttel	D	212	65.9	98.5
Fukushima II 1	J	213	65.8	66.5
Kuosheng 1	TW	214	65.4	80.0
Tokai 1	J	215	65.3	
Fessenheim 1	F	216	65.1	74.2
Catawba 2	US	217	65.1	
Chinshan 1	TW	218	64.7	69.7
Nogent 2	F	219	64.5	69.5
Fermi 2	US	220	64.4	
Yonglwang 2	SK	221	64.4	69.0
Chinshan 2	TW	222	64.3	77.4
Fukushima I 1	J	223	64.3	65.1
Beaver Valley 2	US	224	64.1	76.3
Wylfa 2	GB	225	64.1	81.1
Trnastin 1	F	226	64.0	72.5
Millstone 3	US	227	64.0	72.6
Perry 1	US	228	63.8	
Palo Verde 2	US	229	63.5	
Abucha	A	230	63.4	
Oskarsnamn 1	S	231	63.4	66.1
Byron 2	US	232	63.3	76.2
Indian Pt 3	US	233	63.2	66.3
St Laurent B2	F	234	63.1	69.3
K-Kariwa 1	J	235	62.9	63.6
McGuire 2	US	236	62.8	
Fukushima I 4	J	237	62.5	63.8
Biblis B	D	238	62.4	77.0
Paluel 4	F	239	62.4	69.4
Fort Calhoun 1	US	240	62.1	71.6
Pickering 2	C	241	62.1	77.3
Arnold	US	242	61.8	71.2
Hunterston B2	GB	243	61.4	67.4
Blayais 3	F	244	61.3	65.0
Trawsfynydd 2	GB	245	61.3	84.3
Mihama 1	J	246	61.2	
Bruce 4	C	247	61.2	68.0
Rajasthan 2	IN	248	61.0	
St Alban 2	F	249	60.9	65.2
Bugey 3	F	250	60.8	62.9
Mapp 1	IN	251	60.7	62.8
Mihama 2	J	252	60.6	
Braidwood 1	US	253	60.4	
Fugen	J	254	60.1	
Fukushima I 5	J	255	60.1	61.1
WNP 2	US	256	60.0	65.6
Vogtle 2	US	257	59.8	
Pickering 1	C	258	59.6	77.9
Limerick 1	US	259	59.0	
Hamaoka 2	J	260	59.0	
Peach Bottom 2	US	261	58.7	
Fitzpatrick	US	262	58.6	64.6
Hartlepool 2	GB	263	58.4	71.2
Gravelines B1	F	264	57.5	63.0
Dampierre 4	F	265	57.3	68.4
Heysham A2	GB	266	57.2	71.2
Salem 2	US	267	57.2	
South Texas 2	US	268	57.1	
Trojan	US	269	57.0	59.3
Bruce 2	C	270	56.8	64.0
Cattenom 1	F	271	56.6	63.2
Hinkley Pt B1	GB	272	56.3	63.3
Arkansas 1	US	273	56.2	
Dampierre 2	F	274	56.0	71.6
Cook 1	US	275	56.0	
Indian Pt 2	US	276	54.8	59.3
Palo Verde 1	US	277	54.7	
Quad Cities 1	US	278	54.5	60.0

Reactor name and country		Annual figures (for 12-months to end March 1991) Rank	Load factor, %	Avail., %
Bradwell 1	GB	279	54.5	64.1
Yankee Rowe	US	280	53.8	58.8
Maine Yankee	US	281	53.6	
Hartlepool 1	GB	282	53.2	63.2
Tarapur 2	IN	283	52.3	87.8
Oldbury 2	GB	284	51.9	72.3
Cook 2	US	285	51.7	
Chooz	F	286	51.6	73.0
Fessenheim 2	F	287	51.4	62.6
Tarapur 1	IN	288	51.3	76.6
Fukushima I 3	J	289	50.7	51.5
Turkey Pt 4	US	290	50.6	
Hinkley Pt A2	GB	291	50.4	63.6
Biblis A	D	292	50.3	53.3
Ohi 1	J	293	49.8	
Dungeness A2	GB	294	49.4	74.0
Salem 1	US	295	49.4	
Turkey Pt 3	US	296	46.7	
Genkai 1	J	297	46.6	48.6
Dampierre 1	F	298	46.2	49.3
Mapp 2	IN	299	45.7	
Bugey 1	F	300	44.7	66.1
Conn Yankee	US	301	43.8	50.8
Dresden 2	US	302	43.6	53.3
Wurgassen	D	303	43.5	45.0
Nine Mile Pt 2	US	304	43.1	55.4
Brunswick 1	US	305	43.1	
Heysham A1	GB	306	43.0	52.6
Torness 1	GB	307	41.9	48.0
Sizewell A2	GB	308	41.5	55.7
Angra 1	BR	309	41.4	81.0
Zion 1	US	310	41.2	45.1
Bugey 4	F	311	39.7	48.6
Darrington 2	C	312	38.3	
Robinson 2	US	313	38.3	
Trawsfynydd 1	GB	314	37.2	52.0
Koeberg 1	SA	315	36.8	45.4
Calvert Cliffs 1	US	316	36.1	41.0
Torness 2	GB	317	36.1	44.0
Clinton	US	318	35.3	
Zion 2	US	319	34.5	37.9
Seabrook 1	US	320	34.0	
Fukushima II 3	J	321	33.8	35.7
Nine Mile Pt 1	US	322	33.8	46.3
South Texas 1	US	323	32.5	
Dounreay	GB	324	31.5	36.4
Dungeness B1	GB	325	28.1	72.9
Palisades 1	US	326	27.4	
Phenix	F	327	25.8	28.9
Heysham B1	GB	328	25.5	33.5
Rajasthan 1	IN	329	24.1	
Heysham B2	GB	330	22.7	28.1
Pickering 4	C	331	21.6	25.5
Hamaoka 1	J	332	20.9	21.0
Narora 1	IN	333	20.7	
San Onofre 1	US	334	20.4	24.2
St Laurent 2	F	335	19.7	28.9
Takahama 2	J	336	17.8	
Bruce 1	C	337	16.2	28.3
Obrigheim	D	338	15.0	15.0
Dungeness B2	GB	339	7.6	26.0
Pickering 3	C	340	0.0	0.0
Calvert Cliffs 2	US	341	0.0	0.0
Browns Ferry 1	US	342	0.0	0.0
Browns Ferry 2	US	343	0.0	0.0
Browns Ferry 3	US	344	0.0	0.0
Mulheim Kariich	D	345	0.0	0.0
Creys Malville	F	346	0.0	0.0

is a summary of nuclear plant availabilities around the world which shows close to half the plants exceed 80% inherent availability. Additionally, these fission plants require periodic fuel replacement procedures which contribute to downtime. Fusion plants will be fueled continuously which would offer an availability advantage.

The 80% availability estimate is higher than that usually quoted for the comparable MFE conceptual design. There are several reasons for this difference. The Prometheus study devoted effort to analyze the reliability and maintainability of key systems and then calculate the availability of the plant rather than assume a likely range. The STARFIRE conceptual design adopted a value of 75% as an availability goal and then developed planned and unplanned maintenance activities to achieve the adopted goals. Most of the following MFE conceptual designs are built upon that premise.

The Prometheus power plants can achieve higher availability due to the more simple and reliable nature of the major plant elements. The reactor chamber is very simple with little interaction with the other plant elements. The two drivers have high levels of availability. The heavy ion driver has many magnet elements which must function in series, but the components are not highly stressed and are expected to have high reliability. The laser driver has a slightly lower reliability, but the ability to continue plant operation with several power amplifiers or beam elements not functioning, or functioning in diminished capacity, is highly beneficial. The laser driver has a higher degree of redundancy. The continued operation of the target plant is essential, thus the design is structured with a high degree of redundancy in all essential systems. The thermal conversion systems, electrical plant equipment, and balance of plant are improvements from the current proven systems. These systems will continue to make availability enhancements for the plant.

The availability of the Prometheus IFE power plants are expected to be approximately 80%. The difference between the two designs is not significant. Rather, the significant finding is that there is an availability advantage for IFE power plants. Moreover, the fusion power plants will be competitive with the availability demonstrated by current nuclear fission power plants.

6.3.3.2 RAM Introduction - Reliability, Availability and Maintainability (RAM) analysis was performed on a conceptual design for a tenth-of-a-kind commercial electric power plant. The concept features an inertial confinement nuclear fusion reactor representing the design maturity expected for a plant starting operation in 2045. Two design options were considered for the driver systems: the laser driver and the heavy ion driver.

The methodology of the RAM analysis process is defined in Subsection 6.3.3.3. The source data used in the analysis for the common and distinct elements of the two

design options are described in Subsections 6.3.3.4 and 6.3.3.5. The analysis results are presented and discussed in Subsection 6.3.3.6. The design impact of the RAM study is discussed in Subsection 6.3.3.7.

6.3.3.3 Reliability, Availability and Maintainability Methodology - The RAM analysis is a numerical process. Results are determined by source data which are combined numerically in a manner representing the complexity and interdependence of plant components.

The plant is divided into subsystems and major components, for each of which reliability and maintainability data is determined. Subsystems that do not impact on plant availability, such as personnel services, are not considered.

The mathematical treatment of the data assumes that all component failures result in a plant outage of duration equal to the mean repair time. The exception to this is where parallel redundancy exists, since this allows operation to continue during repairs unless a second equipment fails while repairs are taking place. With redundancy, the outage is reduced. It is also assumed that spare components and support equipment are available on demand, repair procedures start immediately following failure, and restarting the plant requires negligible time.

Availability is calculated as follows:

(a) Identify plant components that impact availability
(b) Determine failure rates and repair times of components
(c) Define maintenance strategy and redundancy
(d) Calculate inherent availability of both drivers
(e) Calculate inherent availability of other key (reactor) parts
(f) Calculate overall inherent availability for key parts
(g) Estimate effect of balance of plant parts on overall availability
(h) Calculate overall inherent availability
(i) Determine annual maintenance shutdown times
(j) Determine refit shutdown time and interval
(j) Calculate achieved plant availability

Inherent Availability - Inherent availability A_I is the probability that a system or equipment used under stated conditions in a properly supported environment will operate satisfactorily at any given time. It accounts for outage due to corrective maintenance. Although A_I excludes preventative maintenance, logistics, and administration outages, the reliability data used assume that preventative maintenance is performed as specified. Failures are assumed to occur randomly with constant probability, ignoring infancy failures, design bugs, and wear out failures after prolonged operation.

A_I is computed from the Mean Time Between Failure (MTBF) and the Mean Time To Repair (MTTR) as follows:

$$A_I = \frac{1}{1+O_I} \text{ where outage is represented by } O_I = \frac{MTTR}{MTBF}$$

For a subsystem consisting of N identical equipment, the value of O_I is increased by the factor N. However, when one equipment is on hot standby (redundant), outage only occurs if a second equipment fails while the first is under repair:

$$A_I = \frac{1+(2N-1)O_I}{(1+NO_I)(1+NO_I-O_I)}$$

For a system consisting of several subsystems and major components, the outage is determined by:

$$\frac{MTTR}{MTBF} = \frac{MTTR1}{MTBF1} + \frac{MTTR2}{MTBF2} + \frac{MTTR3}{MTBF3} + \cdots$$

MTTR and MTBF can be obtained by analyzing records of the use of field-deployed equipment where these exist for identical or closely similar equipment. Alternatively, they can be calculated as follows:

MTTR =	Fault isolation time	+ item retrieval time
	+ preparation time	+ disassembly time
	+ interchange or repair time	+ alignment time
	+ re-assembly time	+ verification or inspection time

$MTBF = \frac{1}{\lambda}$ where λ is the statistical failure rate of an individual part.

All the above MTTR and MTBF values are in hours; λ is millions of hours.

Achieved Availability - The computation of A_A factors the calculated value of A_I to incorporate the impact of regular servicing, preventative maintenance, logistics and administration, and periodic shutdowns for major refits including end of life equipment replacement. For the IFE reactor generating station, these are factored using overall values typical of fission plant practice and computed values for design specific data. The factoring calculations are provided in Section 6.3.3.1.

6.3.3.4. Failure Rates and Maintenance Source Data - Failure rates and maintenance times for subsystems and major components are used as source data for the RAM analysis process. The validity of this source data is determined by the relevance of the available data sources.

For a mature technology, data is readily available based on field experience. This is the case for the non-nuclear portions of the plant such as electrical generation.

For the new technology to be used in the reactor and related subsystems, field experience is unavailable. Where applicable, field data on similar equipment is adjusted using expert opinion to allow for changes of duty cycle, conditions of operation, etc.

In a few cases no similarity with existing, field deployed equipment can be found. For these cases the source data is entirely based on expert opinion, allowing for technological maturity to be expected in a tenth-of-a-kind plant.

Redundancy is specified in the given descriptions of several subsystems and major equipment. Generally the need for redundancy is determined by the need to maintain a safety-related system or to improve inherent availability. In addition, if a related subsystem is already redundant, it may be feasible to integrate the component parts of the two subsystems, making both redundant.

The estimated failure rate and repair time for each subsystem and major component is listed in Table 6.3.3-2; MTBF values are for single equipment, not the quantity needed for the subsystem. Table 6.3.3-2 also contains notes on such issues as redundancy and on-line maintenance. The sources for the data listed in Table 6.3.3-2 are discussed in the following paragraphs.

Sixty-six percent of the reliability and maintainability data is based on established data or similarity to field deployed equipment, 12% is derived from detailed analyses, and 22% represents totally new technology for which opinions were obtained from experts in these fields. This mix of data sources provides an acceptable level of confidence in the validity of the data. Whenever possible, to further improve confidence, subsystems with new technology are decomposed into components with available field data, as shown in Table 6.3.3-3 for the Heavy Ion Driver.

The established data which was derived from field service records and published data is available from the following sources:

Reliability Statistics Manual (Summarized in Table 6.3.3-4), Production and Transmission Branch, Nuclear Generation Division, Ontario Hydro

Non-electrical Parts Reliability Data (NPRD), Reliability Analysis Center, Rome, NY.

Table 6.3.3-2. IFE Failure Rates and Repair Times for Subsystems

Item	Data Sources	Description	Notes	MTBF (HRS)	MTTR (HRS)
Target Factory	Dr. Douglas Drake, KMS Fusion Inc.; Dr. Steven Wineberg, NPRD	Large facility for producing 300,000 to 500,000 cryogenic fuel pellets per day. Deuterium and tritium are injected into plastic capsule which is then frozen and sealed. High pressure and cryogenics are used.	Cryogenics is a mature field, but expect problems with pressure system. Subjective evaluation, no data from field or similar equipment. Deuterium and tritium supply failure rate considered elsewhere. Assumed that isolated pellet non-conformance is rejected by automatic inspection system. Special design features required to achieve MTTR.	2924	24
Target Injector	Dr. Alice Ying, UCLA; Dr. Douglas Drake, KMS Fusion, Inc.	System injects fuel targets into reactor cavity. Precisely aligned before assembly. Coolant flows round cavity penetration which is screened from fusion reaction.	Subjective evaluation, no data from field or similar equipment. MTTR and MTBF (three years) are estimated. Target gun to be inspected at same time as first wall.	26280	24
Laser Power Amplifier	Dr. Gary Linford, TRW	960 amplifiers used with a pulse rate of 5 Hz. Associated power units, blowers, gas units. Each amplifier weighs approx. 100 Kg. A single failure will not shut reactor down.	Pulses per year = 1.6 x 10^8. Required amplifier failure rate is 1 in 10^{10}, current rates are 10^8. One hundred times reliability improvement is realistic in this recent field. Replacement requires disconnection from gas flow circulation system. Sixty sets of 16 units, assumed one unit in a set can fail without reactor outage. Redundant.	556000	8
Laser Gas Circulation Blowers	NPRD Table 6.3.3-3	Provides laser amplifier cooling; 10 sets of 16 blowers. One blower supplies 6 amplifiers. Gas is circulated at 100 KPa.	Loss of one blower reduces laser power by 7% which is assumed not enough to shut down reactor. Field data on similar devices used. Redundant system.	411000	194

Table 6.3.3-2. IFE Failure Rates and Repair Times for Subsystems (Cont.)

Item	Data Sources	Description	Notes	MTBF (HRS)	MTTR (HRS)
Laser Heat Exchanger	NPRD Table 6.3.3-3	One heat exchanger per six amplifiers, as blowers.	Redundant, as gas circulation blowers.	367174	98
Final Optics	NPRD SPAR, Solar Array Program Records	The final optics consists of a pointing and alignment system using three magnetic actuators each (and associated power units) for 60 grazing incidence mirrors.	The optics themselves are unlikely to fail unless the vacuum chambers become contaminated (assumed once every ten years). Field data on similar devices used.	450000	4
Laser Optics Backing Pumps	NPRD Table 6.3.3-3	Laser Optics Backing Pumps evacuate laser optics. Pumps operate at 135 Pa. Pumps are duplicated for each of 60 beamlines.	Field data on similar devices used. Redundant. A hard vacuum is not required so MTBF data for normal pumps used. MTBF for vacuum pump is normally 64,666.	114929	194
Heavy Ion Driver	Table 6.3.3-2	Two systems, each comprising a source and a linear particle accelerator, storage rings and a final transport section. Superconducting magnets used.	Assumed warm iron magnets, which are not cycled during normal operation, and heavy duty cryogenic system to reduce warm-up and cool-down times to achieve needed MTTR.	2190	24
Reactor First Wall Panels	Dr. Nasr Ghoniem, UCLA Table 6.3.3-4	Thirty full length porous silicon carbide panels line the inside the reactor cavity, cooled with liquid lead which also coats and protects the inner surface.	Totally new technology, no material or application experience base. Lifetime estimated at three years. MTBF = 175,200 hours (6.7 x lifetime for passive unit) with considerable surface stress.	175200	120
First Wall Lead Cooling Pump	NPRD Table 6.3.3-4	Two centrifugal pumps, one on standby.	Field data on similar devices used.	114929	84

Table 6.3.3-2. IFE Failure Rates and Repair Times for Subsystems (Cont.)

Item	Data Sources	Description	Notes	MTBF (HRS)	MTTR (HRS)
First Wall Heat Exchanger (lead to steam)	NPRD Table 6.3.3-4	A heat exchanger consist of a fan or compressor, cooling pipes and the operating fluid. There is one heat exchanger in the plant.	Field data on similar devices used	367175	98
Blanket Assembly	Table 6.3.3-4; Dr. Nasr Ghoniem, UCLA	The blankets are hollow silicon carbide panels filled with Li_2O granules which are cooled with helium. Exposure to neutrons breeds tritium.	Totally new technology, no material or application experience base. Lifetime estimated at five years. MTBF = 876,000 hours (20 x lifetime for passive unit) with no moving parts. 180 units per reactor.	876000	240
Blanket Helium Coolant Pumps	NPRD Table 6.3.3-3, Table 6.3.3-4	Centrifugal blower pumps operating at 1.5 MPa. Two pumps for each of the five helium/steam heat exchangers, one of each pair acting as standby (redundant).	Field data on similar devices used. Redundant.	114929	72
Blanket Heat Exchanger (Helium to steam)	NPRD Table 6.3.3-4	Five helium-to-steam heat exchangers used.	Similar to lead-to-steam heat exchanger. Values factored for increased quantity.	367175	98
Blanket Tritium Extraction Pumps	NPRD Table 6.3.3-3	Blanket Tritium Extraction Pumps feed blanket tritium to the tritium extraction loop. Two pumps for redundancy.	Field data on similar devices used. Redundant.	114929	194
Tritium Extraction Loop	NPRD Ronald Matsugu and Otto Kveton, CFFTP; Paul Gierszewski	The tritium extraction loop consists of a circulating pump pair, a molecular sieve bed with heaters, liquid nitrogen cooling, valves and tanks.	Cryogenic absorber use proven technology. The system is mostly static except for the pumps. Field data on similar devices used where appropriate. 24 hour warmup/cooldown time assumed for cryogenic system.	43647	72

Table 6.3.3-2. IFE Failure Rates and Repair Times for Subsystems (Cont.)

Item	Data Sources	Description	Notes	MTBF (HRS)	MTTR (HRS)
Reactor Vacuum Pumps	NPRD Table 6.3.3-3	Ten reactor vacuum pumps used at each of three ports.	Field data on similar devices used. Redundant.	64666	194
Lead Decontam-ination System	NPRD	No description provided.	Assume MTBF and MTTR are similar to the Tritium Extraction Loop, but cooldown/warmup times reduced.	43647	48
Lead Drain Pump	NPRD Table 6.3.3-3	No specification, assumed similar to Tritium Extraction Pump	Field data on similar devices used. Redundant.	114929	194
Reactor Computer Control System	J. Richardson, OH Table 6.3.3-3	The computer control system is a safety system; therefore, a hot standby system is always available.	Computer system has a prescribed unavailability of $1x10^{-3}$ MTBF computed to achieve this. Redundant.	223776	224
Helium Extraction Pump	NPRD Table 6.3.3-3	Assumed similar to blanket tritium extraction pumps. Two pumps for redundancy.	Field data on similar devices used. Redundant.	114929	194
Helium Extraction Loop	NPRD	Similar to the tritium extraction loop.	No specific data available so data assumed similar to the tritium extraction loop.	43647	72
Heat Exchangers, Helium Low and High Pressure Reheaters	NPRD Table 6.3.3-3, Table 6.3.3-4	Similar to lead-to-steam heat exchanger. Two reheaters in the circuit.	Field data on similar devices used.	367175	98

Table 6.3.3-3. Heavy Ion Driver: Failure Rate and Repair Time Analysis

DATA SOURCES:

SSC Laboratory, TRIUMF and Fermilab, and NPRD Data

DESCRIPTION:

Comprises ion source, LINAC, storage rings, and final transport. Only components that are significant contributors to failure rates and repair times shown.

DESIGN NOTES:

Data assumes welded warm iron magnets, infrequent thermal cycling, minimum Lorentz force stresses. Heavy duty cryogenics reduce warm-up and cool-down time. Focusing and steering magnets have similar characteristics. Neutron bombardment is insufficient to cause brittle welds. Estimates final transport magnet count.

FAILURE RATE:

Where lifetime is quoted, MTBF values are 10 x Lifetime. Redundant function data shown in the format (functions used) + (% redundancy).

Device	Magnets	Cells	HV Supplies	Injectors	Pumps
Lifetime/Basis	Fermilab	Est.	$2x10^{11}$ shots		
Unit MTBF hours	4,000,000	556,000	800,000	114,929	114,929
Unit MTTR hours	24	2	2	2	194
Units per:					
Ion Source	0	0	1	1	1
LINAC	878	439	439	0	12
Storage Rings	64	0	0	0	4
Final Transport	96	0	0	2	2
Unit Totals	1,038	439	440	3	19

NOTE:

Vacuum pumps fully redundant with hot standby.

Table 6.3.3-4. In-Service Reliability Records

Equipment	Units	MTTR
Pumps/Gas Blowers	16	194
(number of records)		10
(at hours)		1935
Heat Exchangers	16	404
(number of records)		5
(at hours)		2019
Active Computer Safety Systems	2	224
(number of records)		1
(at hours)		224

6.3.3.5 Maintainability Task Analyses - For complex, highly design-specific subsystems, maintenance field data is not available. These tasks were identified, and maintainability task analyses were performed. Table 6.3.3-5 summarizes the maintainability task analyses.

Table 6.3.3-5. Maintainability Task Analysis Summary

Item	Activity	Estimate (Hours)
1	Remove Hemispherical Pressure Vessel Top	46
2	Remove (One) First Wall Panel	4
3	Replace First Wall Panel	4
4	Remove (One) Blanket Module	4
5	Repair Blanket Module	4
6	Replace Blanket Module	4
7	Remove and Replace First Wall Panel in Third Layer	120
8	Remove and Replace Blanket Module in Third Layer	240
9	Remove First Wall Lead Coolant Pump	19
10	Replace First Wall Lead Coolant Pump	23
11	Remove First Wall Lead Coolant Heat Exchanger	25
12	Replace First Wall Lead Coolant Heat Exchanger	31
13	Remove Blanket Helium Coolant Pump	15
14	Replace Blanket Helium Coolant Pump	21
15	Remove Blanket Helium Coolant Heat Exchanger	21
16	Replace Blanket Helium Coolant Heat Exchanger	28
17	First Wall Panel Inspection	49.8
18	Blanket Inspection	41

6.3.3.6 Reliability, Availability and Maintainability Analysis Results - The results of the A_I analysis of key reactor plant parts are shown in Table 6.3.3-6. The impact on availability of large quantities of identical equipment and redundancy in some subsystems has been accounted for in the calculations. The A_I of key plant items is then factored down by considering remaining equipment and the effect of human mistakes. The A_I values for key plant parts are defined as contributing to 90% of unplanned maintenance down time. Human factors derating K are not included (normally between 1.1 and 1.6) due to anticipated benefits of maintenance planning (see Section 6.3.2).

The overall plant A_A accounts for all outages throughout the life of the plant. It is computed from A_I by factoring in allowances for random failures in the rest of the plant (about 40% of total), 30-day shutdowns at yearly intervals, and major refits at longer intervals. Yearly 30-day outages for scheduled inspection, and adjustment and service are typical practice for existing commercial nuclear fission generating plants. The outage times for major reactor refits and the interval between them take into account the expected life of the Blanket and First Wall and the total replacement times for them as calculated in Table 6.3.3-5 and summarized in Table 6.3.3-7. Note that these times include a concurrent portion since the First Wall must be removed to access the blanket.

Table 6.3.3-6. IFE Inherent Availability Computations

Subsystem	MTBF Factor	Redundancy	Sets	MTTR	A_j	
Target Subsystem						
Target Factory	2924		1	24	99.18	
Target Gun	26280		1	24	99.90	
Laser Driver Option Only						
Laser Amplifier	556000	16	60	8	99.98	
Laser Amplifier Blower	411000	16	10	194	99.46	
Laser HX	367174	16	10	98	99.82	
Final Optics	450000		60	4	99.94	
Optics Backing Pumps	114929	2	60	194	97.98	
Complete Laser Driver						97.24
Heavy Ion Driver Option Only						
Magnets	4000000		1038	24	99.38	
Induction Cells	556000		439	2	99.84	
HV Supplies	800000		440	2	99.89	
Injectors	114929		3	2	99.99	
Vacuum Pumps	114929	2	19	194	99.79	
Complete Heavy Ion Driver						98.91
First Wall						
Reactor First Wall	175200		30	120	97.98	
Coolant Pumps (Pb)	114929	2	1	84	99.99	
Coolant HX (Pb/Water)	367175		1	98	99.97	
Blanket						
Blanket Assembly	876000		180	240	95.30	
Blanket Coolant Pumps (He)	114929	2	5	72	99.99	
Blanket HX (He/Water)	267175		5	98	99.81	
Tritium Extraction Pump	114929	2	1	194	99.99	
Tritium Extraction Loop	43647		1	72	99.83	
Reactor Miscellaneous						
Reactor Vacuum Pumps	64666	10	3	194	99.27	
Lead Decontamination S/S	43647		1	48	99.89	
Reactor Lead Drain Pump	114929	2	1	194	99.99	
Reactor Control S/S	223776	2	1	224	99.99	
He Extraction Pump	114929	2	1	194	99.99	
He Extraction Loop	43647		1	24	99.94	
Summary						
Laser Option						89.28
Heavy Ion Option						90.68

Note: HV = High Voltage S/S = Subsystem HX = Heat Exchanger

Table 6.3.3-7. Summary of Blanket and First Wall Reliability and Maintainability Data

Item	Life (hours)	Replacement Time (hours)	Equivalent Outage (hours/year)
Blanket	43800 (5 yrs)*	260	52
First Wall	26280 (3 yrs)*	212	71

* The final design for the Blanket and First Wall predicted lifetimes of 10 and 5 years, respectively.

For comparison, the reactor outage for 16 Ontario Hydro CANDU (Nuclear Fission) reactors for the period 1987 through 1991 was 184,196 hours, including 160,384 hours for refitting several older reactors. The balance of 23,812 hours' outage were for non-refit reasons and occurred during an estimated 540,416 hours attempted reactor run time. These values are distorted by an unusually high number of major refits during the period, equating to 73.7% achieved availability which is low due to the refits and 95.6% for inherent availability which is high since many reactors were recently commissioned or refitted. The two values bracket the value used for the fusion reactor. Table 6.3.3-1 previously showed a recently reported selection of nuclear plant availabilities from around the world. Nearly 50% of the reporting power plants had availability exceeding 80%.

6.3.3.7 Design Notes - In order to achieve the availability computed for the fusion reactor generating station, the assumptions embedded in the computations must be realized in the final design. The most significant assumptions are outlined below.

Target Factory - Because of its complexity and high pressure technology, the target factory has a relatively poor MTBF. Thus, it is important to implement a redundant design. In order to reduce its impact on the reactor A_I to a manageable level, the design must achieve a MTTR of 24 hours. MTTR was originally calculated at 105 hours.

Laser Amplifiers - Large numbers of these are used. The value for MTBF is a significant improvement over what is achieved currently, representing expected design improvements in this immature field. In order to further reduce the impact of laser amplifier failure rates on the reactor A_I to a manageable level, each group of 16 amplifiers serving a beamline should continue to function with one unit under repair. If the resulting 6% power loss has an unacceptable effect on reactor performance, then a 17th (redundant) unit is required. The design should facilitate repair of the amplifiers while the reactor is on-line. (This is a general requirement for all redundant units.)

Laser Heat Exchanger - The calculated figure for MTTR (98 hours), based on Table 6.3.3-4 calculations applicable to the first wall heat exchanger, is significantly less than field records (404 hours). It is believed to be a reasonable value but the design should accommodate the requirement if it is a design challenge. It is assumed that the heat exchangers are arranged in groups similar to the laser amplifier blowers to provide a measure of redundancy. An integrated blower/heat exchanger design would be advantageous if feasible.

Optics Backing Pumps - The MTBF of 114,929 hours is taken from pump data and is better than the typical vacuum pump MTTR which is 65,666 hours. This is justified on the grounds that the vacuum required is not an especially good one. However, it may represent a design challenge.

Heavy Ion Driver - The MTTR of 24 hours is a target for the complete exchange of a superconducting magnet including warm-up and cool-down. It may represent a significant design challenge and probably involves the use of a warm iron design, which cools down and warms up more rapidly than a cold iron design since the iron core is outside the cryostat. The cryogenic equipment requires extra capacity. The use of techniques to accelerate magnet removal, replacement and alignment, including automated beam vacuum pipe cutting and rejoining, has been explored for the proposed KAON Factory at TRIUMF, Vancouver, and the MTTR is believed to be feasible.

6.3.4 Design for Decommissioning - Fusion reactors using a deuterium/tritium cycle have the advantage over fission reactors in that there is no radioactive spent fuel to be disposed of; the reactor structure is the only radioactive waste at the end of plant life. Use of low activation materials was chosen to keep activation to a minimum. The choice of total remote maintenance for key parts is expected, by itself, to greatly simplify and reduce the cost of final disassembly. The design process, therefore, took into account not only maintenance but also final disassembly.

6.4 Target and Target Fabrication

Target physics issues are not addressed in this section or in this report as all pertinent data have been supplied by the DOE Target Working Group (TWG).[1,2] Data on target gain and physics used in this report is also found in the TWG's recommended guidelines[1,2] and are summarized in Chapter 3. The question of illumination symmetry for direct drive targets may be considered a target physics issue and is discussed in Reference 1. However, the information supplied by the TWG pertains to beams with a $\sin^2 x/x^2$ profile. It will be much easier to supply beams with a somewhat different profile using the laser system proposed in this report (see Section 6.5). The question of illumination symmetry is, therefore, discussed in Section 6.4.1 to show that the proposed system will not lead to a deterioration in target performance over that prescribed in the TWG guidelines. Illumination symmetry is also used to examine the effect on target performance of various laser system malfunction scenarios.

The issue of target fabrication is addressed in Section 6.4.2. Alternative target fabrication techniques are reviewed and specific methods are chosen for this reactor design. Additionally, the question of target survivability is addressed in view of the various thermal, structural, and other stresses encountered by the target in the reactor system.

Section 6.4.3 is devoted to the target factory. It includes a discussion of the overall layout of the facility including the fabrication and inspection techniques employed therein. The section concludes with a discussion of target production costs and target factory staffing requirements.

The target injection system is covered in Section 6.4.4. Acceleration systems are proposed for both direct and indirect drive targets. Target tracking and beam steering systems are defined for both target types.

6.4.1 Target Performance - Data on illumination symmetry for direct drive targets was provided by the TWG for a 60-beam arrangement similar to the one described in Sections 6.3 and 6.8. As mentioned above, this information was obtained assuming a $\sin^2 x/x^2$ beam profile. However, it may be much easier and economical to generate beams with a flat, "top hat" profile with the laser system described in Section 6.5. The question of illumination symmetry for such beams has, therefore, been examined to insure that there is no unacceptable decline in performance from the data provided by the TWG.

6.4.1.1 Illumination Symmetry - Illumination symmetry and uniformity requirements on a direct-drive spherical target irradiated with multiple laser or other beams has been studied by a number of authors.[3-5] A formalism that has often been used to study uniformity of illumination is described in Reference 5. In this method, the

irradiation pattern on the sphere is broken down into spherical harmonics. Additional detail is added by using a single beam factor evaluated by tracing rays through the target plasma. A geometrical factor is also used to account for the number and orientation of the beams.

A view factor computer code was developed to study illumination symmetry for this reactor design study. The code uses algorithms common to similar codes developed to study radiation transport problems. However, the code has a number of unique capabilities not common to other view factor codes, such as the ability to model highly collimated beams arranged in arbitrary geometries and pointing in arbitrary directions. Although quite different from the formalism described in Reference 5, the code gave similar results on benchmark problems. The code breaks the target surface into some large number of elements of approximately equal area. It then uses information on the geometry and apodization of the illuminating beams to solve the geometric problem of where within the sheaf of each beam each of the target surface elements is intersected. This makes it possible to determine how much energy is received from each beam by each surface element. These quantities are summed for all the beams and the results are compared, allowing conclusions to be drawn regarding variations in illumination over the target surface. It is possible to introduce beam mispointing errors either manually or randomly, and to introduce energy imbalances between the beams. It is also possible to keep track of illumination symmetry as the target travels through space. At present, only surface illumination effects are modeled. The algorithm is flexible enough to allow for simulation of volumetric absorption effects should this become necessary. However, illumination symmetry results supplied by the TWG were closely duplicated without resorting to volumetric modeling. Unless otherwise noted, the results described in the following paragraphs apply to beams that have a top hat profile. The results were obtained for target surfaces subdivided into 500 surface elements. Greater surface resolution than this did not significantly change the results for the 60-beam system modeled. The beams were arranged as shown in Sections 6.3 and 6.8.

Figure 6.4.1-1 shows the effect on illumination symmetry of variations in the ratio of beam radius to target radius. This ratio is, of course, 1.0 for tangential focus. In an IFE reactor, the target would implode during illumination by a beam of uniform radius, causing the ratio to vary from 1.0 at the start to around 2.0 at the end of the laser pulse. For zoomed illumination systems, the ratio would stay at about 1.0 throughout the pulse. The curves in Figure 6.4.1-1 were generated assuming perfect beam energy balance with no mispointing. Under these ideal conditions, the top hat beam apodization results in a deterioration of illumination symmetry compared to the $\sin^2 x/x^2$ profile. The rapid drop off in performance seen for ratios less than 1.0 is especially pronounced for the flat profile. Clearly, illumination must be at least tangential for a flat apodization and, preferably, somewhat greater to allow for mispointing and beam jitter. The symmetry above a ratio of 1.0 is very flat, as

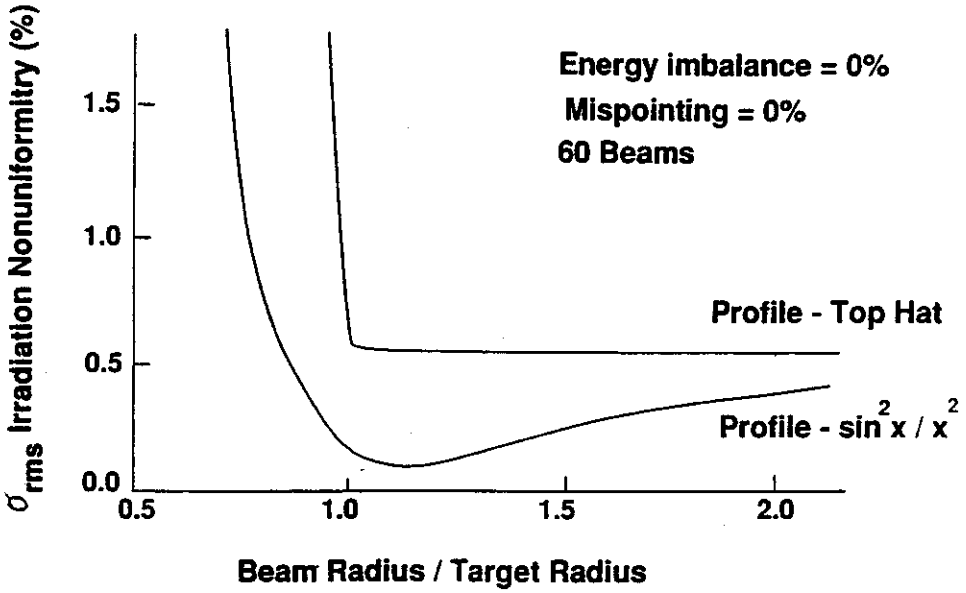

Figure 6.4.1-1. Beams with Top Hat Profiles Deliver Acceptable Illumination Symmetry

expected, since the intensity of the beam does not vary at any point in a cross section. For very large ratios, the $\sin^2 x/x^2$ profile begins to look flat to the target and begins to approach the top hat curve.

Evidently, under otherwise perfect conditions, some sacrifice in performance is made by going to flat beams. However, above a ratio of 1.0, the irradiation nonuniformity is still significantly below the target figure of 1.0 set by the TWG. It is, therefore, apparent that top hat beams can potentially meet reactor illumination symmetry requirements.

It is unlikely that the perfect beam pointing and energy balance conditions assumed above can actually be achieved in a working reactor. Figure 6.4.1-2 shows the effect on irradiation uniformity of random beam pointing errors. Beams were configured so that tangential illumination would have occurred in the absence of pointing errors. The curves in the figure were generated by choosing a maximum pointing error, and then mispointing each beam by a random fraction of this amount between 0.0 and 1.0. As these errors increase, the superiority of beams with the $\sin^2 x/x^2$ apodization becomes less marked and, eventually, disappears entirely. Interestingly, beam mispointing causes 60-beam systems with both apodizations to exceed the critical 1% root mean square irradiation nonuniformity level when the maximum mispointing exceeds about 0.07 of the target radius. This shows that beams with the top hat profile will not cause reactor performance to deteriorate faster than the $\sin^2 x/x^2$ apodization in the presence

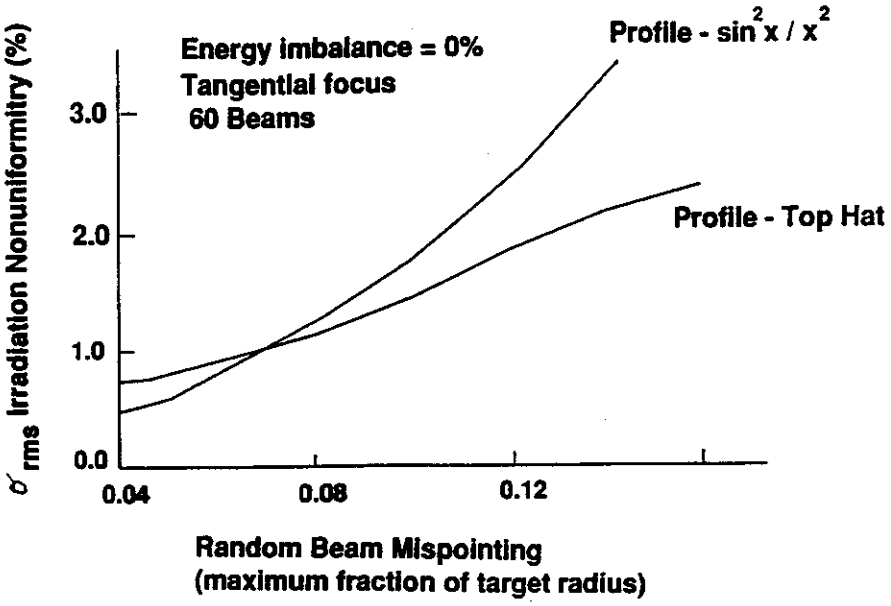

Figure 6.4.1-2. Top Hat Beam Performance Is Not Significantly Worse than that of Beams With $\sin^2 x/x^2$ Profiles in the Presence of Random Mispointing Errors

of small mispointing errors. In particular, the critical 1.0% illumination nonuniformity level will not be exceeded faster with top hat beams. This is significant because some mispointing error is probably unavoidable. It is noted that qualitatively similar curves to those shown in Figure 6.4.1-2 were obtained using different sets of random numbers. It was not, however, possible to conduct sufficient runs to determine statistically accurate error bars at all points.

The most likely laser system malfunction for the direct drive reactor proposed here would entail the loss of 1/16 of one beam, or 1/960 of overall laser energy. Results of such a malfunction are shown in Figure 6.4.1-3. The resulting illumination nonuniformity would not be significantly greater than that predicted under ideal conditions. Target performance would not suffer any significant decline. Also shown in Figure 6.4.1-3 is the result of the much more unlikely loss of one fourth of a single beam. Even under these conditions, the irradiation nonuniformity under otherwise ideal conditions does not exceed 1% for beam radius to target radius ratio greater than 1.0. Again, comparison with Figure 6.4.1-4 shows that performance of beams with the top hat profile is not significantly poorer than those with the $\sin^2 x/x^2$ apodization for loss of 1/4 beam. Calculations show that the loss of one entire beam out of the 60 would result in failure to properly implode the target for both apodizations.

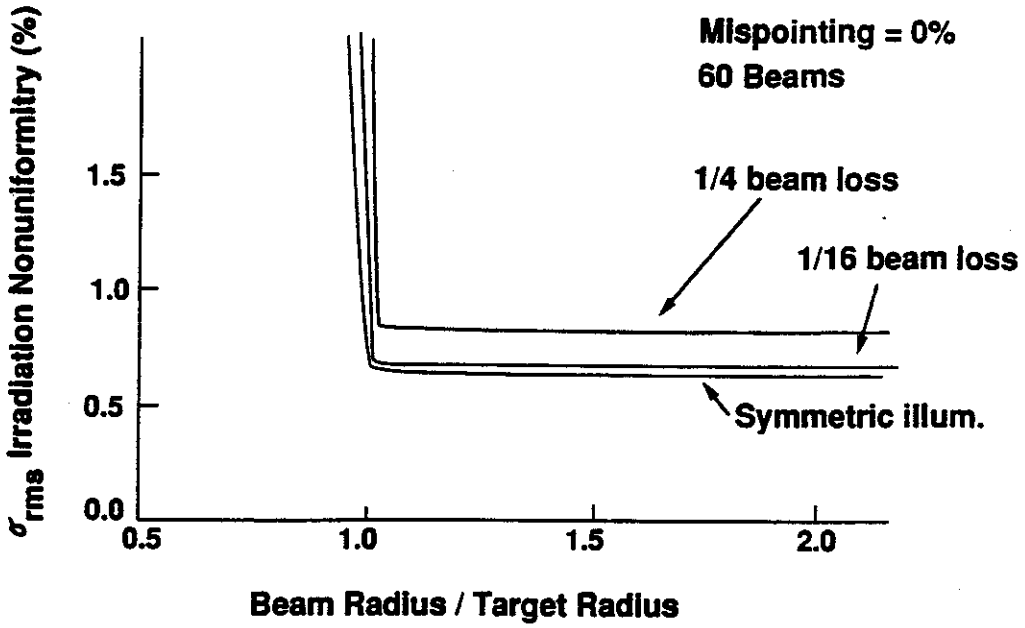

Figure 6.4.1-3. Reasonable Loss Scenarios Do Not Lead to Target Failure with Top Hat Beams

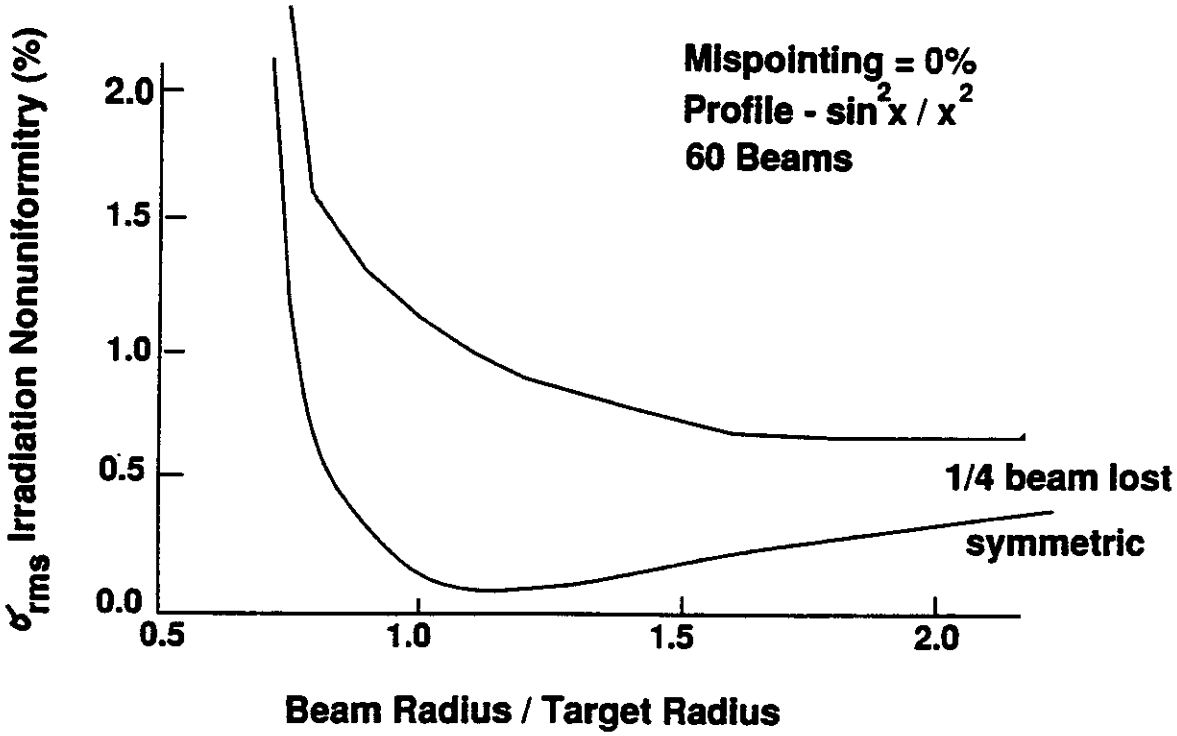

Figure 6.4.1-4. Beams With $\sin^2 x/x^2$ Profiles Do Not Show Significantly Better Performance in Beam Power Imbalance Scenarios

6.4.1.2 Target Heating in the Reactor Cavity - In the proposed direct drive reactor design, sabots will be used to protect the targets during acceleration in the injection system. However, the sabots will be separated from the targets before they enter the reactor cavity. The unprotected targets must reach the firing point before the cryogenic fuel layer is heated above the triple point by radiation and interaction with the gases in the cavity. Excessive target heating could force a reduction in the pulse repetition rate or redesign of targets with shine shields, ablative layers, or other protective schemes. Previous studies have raised serious concerns about the ability of unprotected targets to survive their journey through the cavity.[6] However, higher ambient cavity temperatures and/or pressures were assumed in many of the studies. For example, a cavity temperature of 2000°C was assumed in the Solase report.[6] We assume that cavity temperature will not exceed 600°C during target transit. Note that the target will not enter the cavity region until the cavity temperature and pressure are nearly at equilibrium conditions. Radiation tends to dominate the heat transfer to the target. Since radiation is proportional to the fourth power of the absolute temperature, serious problems at 2000°C do not imply that similar difficulties will exist at 600°C.

The target heating problem was examined with the aid of a 3D spectral method computer code. It was used to solve the non-linear heat equation,

$$\rho c_p \frac{\partial T}{\partial t} = \text{div} \left(k(T) \nabla T \right) + q$$

where:

- ρ = density in g/cm^3
- c_p = constant pressure heat capacity in joules/deg-g
- k = conductivity in watts/deg-cm
- q = volumetric heat source (non-zero only in DT ice)
- T = temperature in °K

and the boundary conditions were,

$$k_{shell} \frac{\partial T}{\partial n} = Q \text{ watts/cm}^2 \text{ (heat flux on shell surface).}$$

The code used Chebyshev polynomials and grid points in radius and spherical harmonic functions and grid points in latitude and longitude (spherical coordinates). A domain decomposition method was used making it possible for all parameters, such as k, c_p, q and r to vary discontinuously across material boundaries. Shell heat capacity was assumed constant at 1.754 joules/deg-g. The code can allow for temperature-dependent conductivities. However, since this dependence is not well understood at very low temperatures, shell conductivity was also assumed constant for each run. A range of plausible conductivities were then checked in separate runs.

Target temperature distributions were checked after 0.1 seconds, a maximum assumed transit time of targets through the cavity. (Note that the final design for the direct drive injection scheme reduces the target transit time to 0.0375 seconds for a velocity of 200 m/s over a distance of 7.5 m. This conservative estimate will compensate for time to accelerate capsule and transit through the shielded blanket region.) The target examined was that prescribed by the target working group scaled to a driver energy of 4 MJ. An ambient pressure of 3 mtorr was assumed for the direct drive (DD) targets. A sample of the results obtained with the code is shown in Table 6.4.1-1.

Table 6.4.1-1 Effects of Cavity Environment on Direct Drive Targets After 0.099 sec. (3.0 mtorr H)

Ambient Temp, K	Shell Thermal Conductivity, W/K/cm	Ice/Vapor Temp, K	Ice/Shell Temp, K	Outer Shell Temp, K
2000	1.0×10^{-3}	11.17	11.87	776.30*
700	2.0×10^{-3}	10.23	10.30	18.20
800	2.0×10^{-3}	10.39	10.50	24.00
1000	2.0×10^{-3}	10.91	11.21	4.18
2000	2.0×10^{-3}	19.68	29.62*	556.90*
700	4.0×10^{-3}	10.80	10.95	15.89
1000	4.0×10^{-3}	13.03	13.96	34.53
700	8.0×10^{-3}	11.45	11.68	14.36
1000	8.0×10^{-3}	15.40	16.99	28.17

* Shell outer surface temperature above CH damage threshold and/or DT ice temperature exceeds the triple point.

Table 6.4.1-1 shows that, at 3.0 mtorr, much higher temperatures than those expected in the reactor design presented here for DD targets would be necessary to cause significant target damage or deterioration, even in the unlikely case that the target absorbed all the radiative energy impinging on its outer surface. No shine shield or other special precautions would be necessary to avoid target thermal damage in the reactor cavity. Should the expected DD reactor cavity temperature and pressure during target injection prove unrealistically low, it would still be possible to overcome target heating problems by increasing injection velocity, thereby decreasing the amount of time the target is exposed to the cavity environment. According to the data presented in Reference 7, the DD targets should survive accelerations much higher than those required by the design presented here.

Ambient pressures in the indirect drive reactor cavity during target injection are expected to be similar to those for direct drive. Since ID heavy ion targets are completely enclosed in a radiation case, they are inherently more resistant to problems with overheating than their direct drive counterparts. A simple analysis of heat conduction in such targets shows that, even at pressures of 100 mtorr, no DT ice

melting will occur after 0.1 seconds. In other words, at design temperatures, indirect drive targets should be able to survive ambient pressures more than an order of magnitude higher than expected within the target cavity. Furthermore, at the 500 K to 600 K cavity ambient temperatures expected in the indirect drive reactor system proposed here, no significant damage to the radiation case material should occur.

6.4.2 Target Fabrication - In this section fabrication methods for the major components of direct and indirect drive targets are discussed. Many of the techniques described have actually been used to produce targets for IFE experiments. Unfortunately, none of them has succeeded in demonstrating a capability to mass produce reactor size targets. In large part, this probably results from the lack of an immediate need for a large quantity of reactor size targets and the consequent lack of R&D funds devoted to their development. It should be straightforward, for example, to fabricate radiation cases for indirect drive targets and sabots for direct drive using existing technology. In spite of the many promising fabrication techniques described below, however, the same cannot be said of target shells. Reactor size shells can certainly be made using very expensive microfabrication and micromachining techniques. However, fabrication of such shells has not yet been demonstrated using droplet generators, microencapsulation, and other promising techniques for economical mass production. In the following section the case is made that this should not necessarily disqualify these techniques from consideration as candidates for reactor target mass production.

6.4.2.1 Target Shell Fabrication - Numerous techniques have been tried for producing target shells for experimental IFE facilities. A number of these show promise as methods for mass producing targets for IFE reactors. Some of the techniques are reviewed below. The methods described do not represent an exhaustive list. For that matter, it is quite possible that none of them will be chosen to produce targets for future reactors. A glance at "The Journal of Vacuum Science and Technology," or a similar publication in the field of applied chemistry is enough to impress one with the huge number of techniques that may someday have an impact in controlled fusion. Significant research and development resources have not yet been committed to developing ways of mass producing reactor size plastic target shells. When they are, it is not unlikely that new techniques will be developed which will supersede all the processes described here. The goal of this section is not to prescribe what the eventual shell fabrication technology will be. Rather, it is to make the case that, if necessary, reactor-size targets could be economically mass produced, if not with off-the-shelf technologies, at least with modest extensions thereof.

Historically, the vast majority of experimental laser fusion target shells have been composed of glasses of various types. Such shells can be produced by injecting drops of aqueous solutions of the glasses into the top of a drop tower or vertical tube furnace. Glass shells are formed as the drops fall through the furnace and are

collected at the bottom. This technique offers excellent control over shell mass and size. However, it is limited to a relatively narrow range of compositions and production of relatively small shells.[8] In a somewhat similar but more versatile technique, the components of the glass are placed in solution and converted into a gel. This material is crushed into a fine powder. A sieving step separates the powder into particles of the desired size. The material is then introduced at the top of the drop tower. It is possible to produce plastic shells using variations of the above techniques. However, it will probably be impossible to produce simple blown shells at the size and thickness levels necessary for IFE reactors.[9] Fortunately, promising alternatives to the procedures outlined above have been demonstrated. Some of these are described below.

Droplet Generators/Microencapsulation - In the various versions of microencapsulation, polymer layers are formed around droplets of volatile liquid in a suspending medium. The liquid is then removed by evaporation or some other exchange procedure leaving behind a plastic shell. In one version of the process,[10] an aqueous phase is emulsified in an organic solution of the desired polymer; subsequently, the oil/water emulsion is poured into a second water phase yielding a water/oil/water emulsion. The solvent is driven off thermally, leaving polymer shells containing water. The water is removed by gently heating the shells in vacuum. This procedure has been used to make CH shells. In an adaptation of the same process, CH shells with PVA permeation barriers have been produced. In the method described above, droplets are formed by rapid stirring of the mixture. This allows for little control over droplet size and thickness. To alleviate this problem, droplet generators with double and even triple nozzles have been introduced. These make it possible to exert much greater control over shell geometries. Shells can be produced from the droplets by allowing them to fall through heating towers or introducing them into a microencapsulation medium.

It presently appears unlikely that blown shells with diameters greater than about 1 mm can be produced within the tolerances demanded for inertial fusion targets. Droplet generators combined with microencapsulation are a promising alternative. Targets of the size and thickness needed for future IFE reactors have not yet been created using these techniques. However, there has, yet been no great demand for them. There is much room for progress in this field if significant research and development funds are made available. This seems justified considering the adaptability of these processes to the demands of mass production and their ability to produce uniform, seamless shells with excellent surface characteristics.

Micromachining - Several micromachining techniques have been used with good success to produce targets larger than those generally available from such processes as microencapsulation and drop tower blowing.[11,12,13] The term micromachining will be used to refer to a number of techniques that have been applied for fusion target

fabrication, including, among others, single point diamond turning, diamond sawing, laser drilling, and mechanical polishing. A significant application is in the creation of hemispheres that can be mated to form target shells.

The application of single point diamond turning to production of IFE targets was pioneered at Los Alamos and Livermore National Laboratories.[14,15] The technology existed before the need for fusion targets arose. However, the delicate nature of the work involved made it necessary to refine control of temperature, vibration, etc., on existing devices. Reported applications have included machining of support stalks from mandrels used to facilitate plastic coating of glass spheres. Extremely smooth surface finishes can be achieved in this way. It may be possible to apply a similar technique in future target factories as a final finishing technique for shell surfaces. Single point diamond turning has also been used to create hemispherical shells. In one technique, a convex mandrel was first machined. A layer of coating material was then deposited over the mandrel, and excess material was machined away. The mandrel was then dissolved to leave a hemispherical shell. Variations of this process have been used to produce shells with a step across the edge to facilitate mating. Stringent tolerances and surface finishes are necessary to successfully mate hemispheres for fusion target applications. This is a serious objection to the use of hemisphere mating for target mass production. Single point machining is one way of meeting the required tolerances. However, control of large numbers of such lathes in a future factory would be a daunting task.

Laser cutting has also been used to produce hemispherical sections by rotating the surface of a hollow shell through the focal point of the laser beam. However, the finite cut width of the laser beam makes it very difficult to produce hemispheres that can be accurately remated in this way.

Laser drills have been used to create tiny holes in target shells, which can then be used to introduce high-Z gases for use as diagnostics. A similar technique could be used in a target factory as part of a drill and fill operation should the tritium inventories and fill times required by the diffusion filling process prove excessive.

The so-called void formation method, which has been used to create large glass and plastic shells,[16] employs several micromachining techniques. The process consists of forming a spherical bubble in molten material, then grinding away the excess material to form a shell. The material can be rotated during the process to minimize the effect of bubble movement. In an application of this technique reported in the literature, the molten material solidified into a cylindrical mass after void formation. A diamond cutting wheel was used to cut a rough cube containing the bubble from this mass. Diamond saws were then used to form a rough sphere. The capsule is then placed in a lapping system consisting of three lapping mandrels, as shown in Figure 6.4.2-1, which is capable of grinding and polishing the surface to any desired thickness.

Large, seamless, uniform shells can be created in this way. Unfortunately, the process is extremely labor intensive, and is an unlikely candidate for mass production of targets.

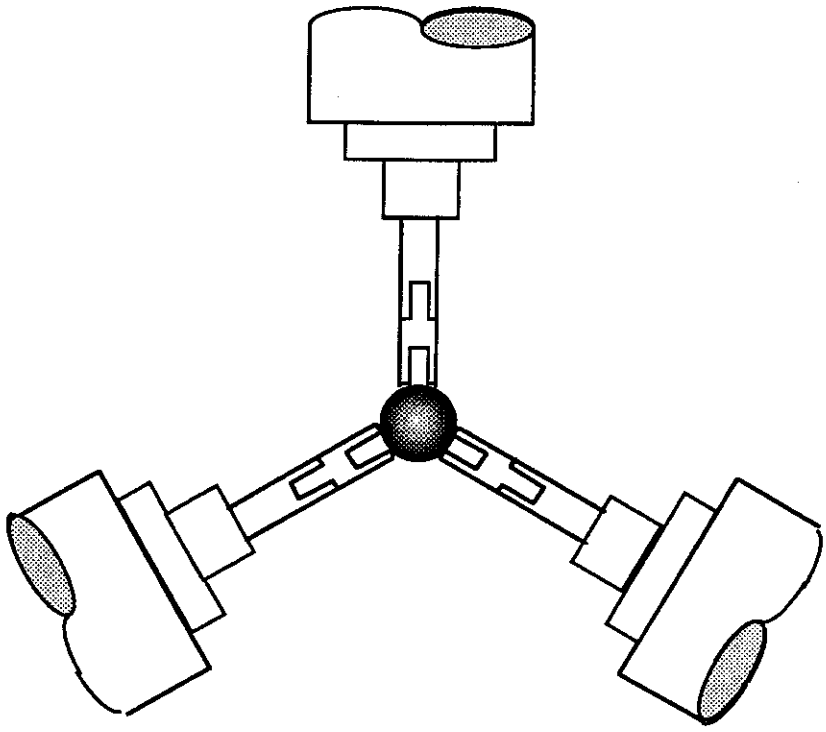

Figure 6.4.2-1. Shell Held in Place by Three Laps, Driven by Independently Controlled Motors

Hemisphere Fabrication and Joining - Hemispheres can easily be filled with fuel and then joined together to form target shells. Lengthy diffusion filling steps requiring large tritium inventories can be avoided in this way. Unfortunately, it may be difficult to produce the hemispheres with sufficient precision for fusion target applications and keep their costs within reasonable bounds at the same time. Micromachining techniques for producing hemispheres have already been described above. Other methods which are more promising for eventual mass production include chemical etching and solid-state processes.[17,18]

One such technique takes advantage of the relatively advanced state of development of glass shells for fusion applications. Such shells are sputter coated with a copper release layer and then embedded in epoxy. The epoxy is then reactive ion etched in oxygen down to the equator of the glass shell. When the shell is removed from the epoxy, a negative hemispherical mold is left behind in the epoxy surface. This surface is replicated using a silicone rubber compound. The positive rubber replica is used as a master mold for making any number of final molds. This is done by curing a drop of photoresist on the rubber master mold. Once a metal substrate is epoxied over the top of the photoresist and allowed to cure, the silicone master can be peeled away for

eventual reuse, leaving the photoresist final mold mounted on the metal substrate. These molds can then be coated with any chosen shell material. Hemispherical shells with excellent surface quality have been produced using this method. Unfortunately, the size of the high quality blown glass shells used in the process is presently limited to about 1 mm. Production of thick shells with fine edge tolerances is also difficult using the method.

A method that shows more promise for producing large, thick, hemispherical shells borrows techniques developed in the semiconductor industry. The mass production of silicon computer chips provides ample evidence of the utility of such techniques in producing large numbers of identical objects.

In the basic process, hemispherical cavities are first formed in silicon wafers using batch photolithography and isotropic etching. Techniques exist for creating self-aligned flanges on the edges of these cavities. Once a hemispherical cavity is formed, its surface can be doped with a material that renders it insoluble to silicon etchant. The remainder of the wafer can then be etched away leaving a hemispherical shell. Alternatively, the hemispherical cavities can be used as molds for other material. To create thick shells, the entire cavity can be back filled with a selected material, which is then polished down to the level of the original masking layer on the surface of the silicon wafer. A hemispherical cavity is then formed in this material using the same photolithographic pattern definition and isotropic etching techniques used to create the original hemispheres. The finished hemispherical shell can then be freed from the surrounding wafer. Large, thick shells with excellent surface finish can be made in this way.

Target Shell Fabrication for the Prometheus Reactors - Droplet generators combined with microencapsulation have been chosen as the target shell fabrication technique for the Prometheus reactors. As already pointed out above, shells of the size and thickness necessary for future reactors have not yet been demonstrated using these processes. However, this reflects the lack of research and development devoted to production of reactor-size targets more than the unsuitability of droplet generators and microencapsulation for producing them. The very fact that there is so much potential for progress in this area is a good reason for not overdesigning shell fabrication facilities at this point. Even in the unlikely event that no further progress is made in these technologies, ancillary technologies in combination with some of the other techniques described above could be used, taking shells produced by droplet generators/microencapsulation as a starting point, to produce shells suitable for fusion reactors. Glow discharge polymerization (GDP), for example, has been used to fabricate CH coatings on fuel shells. It could be used to increase the thickness of polymer shells. It produces hard, strong, tough surfaces and good adhesion to existing surfaces has been demonstrated.[19] Significant technological progress has been made recently in achieving smooth surface finishes using GDP. Other promising

coating technologies exist which, alone or in combination with micromachining steps for grinding away excess material, could be used to increase the thickness of shells as necessary.

For purposes of designing the overall target fabrication facility a shell production procedure similar to that shown in Figure 6.4.2-2 is assumed. Provision for extra coating steps and generation of droplets with multiple layers is not shown in the figure. This does not reflect the belief that no such procedures will be necessary, but that it is impossible to predict their exact nature at this point.

6.4.2.2 Fuel Filling Procedure - Diffusion filling has been chosen as the fueling method for this design. It relies on the extremely high permeability of CH shells to hydrogen to allow filling within reasonable times. The fueling process will begin with a preheat step to drive residual gases out of the target shells. The preheat step will have dual benefit of degassing shells and making them stronger at the same time. The goal will be to constantly maintain optimum filling rates during the entire process while avoiding damage to the shells due to excess pressure.

The diffusion filling process would take place in a pressure vessel such as that shown in Figure 6.4.2-3. Empty shells received from the shell fabrication area would be introduced into the low pressure end of such vessels through a pressure lock. A number of the pressure vessels, perhaps as many as ten to fifteen, could be arranged in parallel. This would allow for periodic maintenance or replacement of individual vessels and an excess filling capacity should this be necessary, for example, to provide targets to other facilities, or to store targets on site for immediate restart after

short reactor shutdowns. Once loaded into the diffusion filling vessels, targets would be automatically conveyed through a number of zones of gradually increasing pressure separated by pressure locks. Maximum fill pressures would be about 800 to 1200 atmospheres. A heating system would maintain temperatures in the vessels at constant levels. A temperature of approximately 200°C would be optimum for rapid target fill, but it may be necessary to limit actual temperatures in the vessels to around 100°C to avoid softening damage to the polystyrene shells as well as excess leakage of tritium through the vessel walls and deterioration due to hydrogen corrosion and embrittlement. A limited amount of breakage of faulty target shells could be expected under the extreme conditions in the pressure vessels. However, experience with diffusion filling of the much more fragile experimental targets now in use has shown that neighboring shells seldom suffer significant surface or other damage when this happens. Fill times will depend on the exact thickness and state of polymerization of the plastic shells. However, assuming permeabilities near those of the experimental CH shells produced to date, fill times will likely be about 24 to 36 hours. The larger of these numbers is used in estimating required tritium inventories.

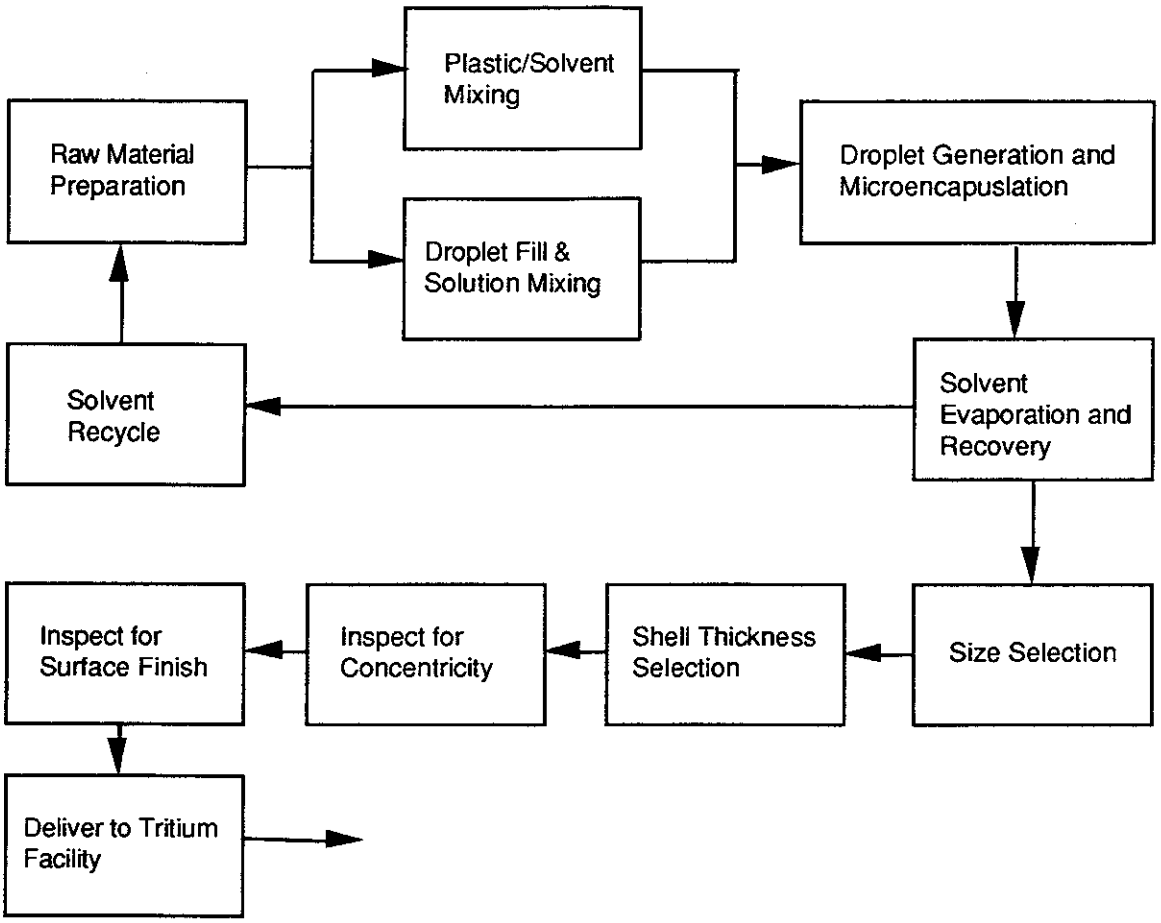

Figure 6.4.2-2. Target Costs Can Be Kept Low if Present Shell Production Technologies Can Be Enhanced to Produce Reactor-Sized Targets

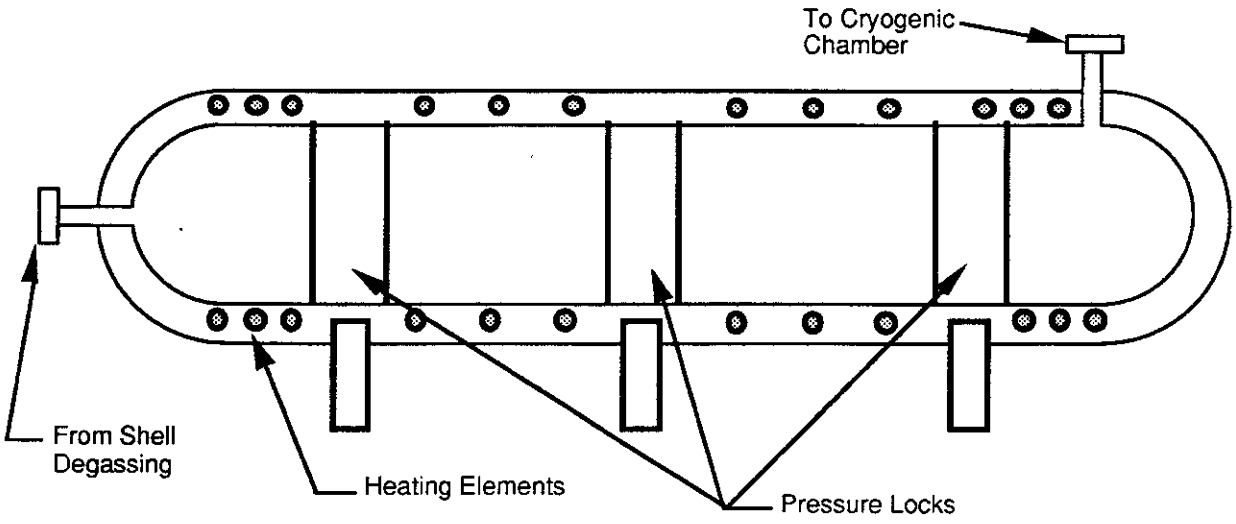

Figure 6.4.2-3. Pressure Vessel for Diffusion Filling

Hydrogen attack and hydrogen embrittlement of the pressure vessels could pose severe problems if conventional steel vessels are used in the diffusion filling process. In hydrogen attack, methane forms internally, causing the steel to swell and lose strength, eventually resulting in material failure. This mode of failure is uncommon at temperatures less than 200°C, but may become a problem at the extremely high pressures necessary for diffusion filling.[20] Hydrogen embrittlement refers to a complex of physical processes that are still not thoroughly understood. However, its effects can be devastating at much lower pressures and temperatures, leading to reduced fatigue life, surface blistering, internal fissuring, and reduced stress rupture.[21] Certain varieties of austenitic stainless steels have shown good resistance to hydrogen damage. However, even they are not immune.[22] The best solution to this problem would seem to be the use of aluminum pressure vessels. Aluminum and related alloys seem to be practically unaffected by hydrogen damage, even at high pressures. This characteristic is not dependent on the formation of an oxide layer, and is true of weldments as well as the base metal.[23] Some deterioration in the ability of aluminum to resist hydrogen damage is seen when hydrogen at high temperatures and pressures is combined with a high relative humidity. However, such problems should not arise as long as care is taken to control humidity.

Tritium inventories required in a factory depending on the diffusion filling process may be higher than those in facilities relying on some competing processes. However, they need not be excessive. The density of solid DT is 0.213 g/cm^3. The target would have a layer of this material about 600 microns thick if scaled to a driver energy of 5 MJ. The total DT mass would be about 7.5 mg. To provide such a mass, the entire interior of the target must be filled with DT gas at a pressure of approximately 600 atmospheres. This means that, in the final stage of the filling process, it would be necessary to surround the target with DT gas at a considerably greater pressure to assure a rapid fill. In the early stages of filling, outside gas pressure would be considerably less if the stepwise filling process outlined above is used. One can assume an average fill pressure for the entire process of around 500 atm, corresponding to a gas density of around 0.1 g/cm^3 at a fill temperature of 100°C. The CH shells must be surrounded by this pressurized DT during the entire diffusion filling step, which will take approximately 36 hours. Close packed spheres have a packing fraction of 0.74. The figure for randomly packed spheres is usually given as somewhere at the high end of the 0.5 to 0.6 range. Allowing a reasonable amount of space for automatic conveyor mechanisms, pressure locks, etc., one can conservatively choose a packing fraction of 0.5.

For a repetition rate of 4 Hertz, around 350,000 targets will be consumed per day. This implies that 525,000 targets will be in the diffusion filling stage if the fill time is 36 hours. Assuming the targets have a radius of 3 mm, each will occupy a volume of around 0.11 cm^3, and enclose a space of around 0.08 cm^3. For the 0.5 packing fraction cited above, 525,000 targets must then be surrounded by approximately

60,000 cm^3 of DT at 500 atmospheres. This gas will have a total mass about 6.5 kg, corresponding to about 4.0 kg of tritium. The average fill pressure in the targets during the process will be about 250 atmospheres. The 525,000 targets will, therefore, contain about 0.003 grams of additional DT each on average during the fill, accounting for another 0.95 kg of tritium.

If the beta heating process described below takes another four hours, another 87,500 targets will be in this stage of production at any time, corresponding to another 0.40 kg of tritium.

The total tritium required in the beta heating and diffusion filling stages alone, then, is around 5.35 kg. Inventory in piping, stored targets, compressors, etc., will likely bring the total inventory in the factory to around 7.0 kg. This corresponds to an activity of 6.8×10^7 curies. Thus, the diffusion filling process requires a rather high tritium inventory. However, it will require none of the potentially expensive and technically difficult mechanical processes described above, such as drilling, plugging, gluing, molding, etc. It will not be necessary to provide for the individual fueling of each of several hundred thousand targets per day. Human intervention in the filling process could be kept to a minimum, making it possible to keep personnel requirements in the tritium fill section of the factory low, thus enhancing the overall safety of the plant. Furthermore, diffusion filling makes it possible to avoid surface seams, cracks, holes and other imperfections occurring at mechanically joined or drilled surfaces that could potentially cause degradation in target performance, perturbation of the beta heating process and target disintegration under high acceleration.

A possible drawback to diffusion filling is potential tritium irradiation damage to the CH shells during the relatively long fill times. Significant damage to inner layers could occur in less than 100 hours.[24, 25] This can be a problem in small, experimental targets, where such damage can lead to shell failure. It is most unlikely that tritium irradiation will lead to such problems in reactor-size targets with their much thicker shells.

6.4.2.3 Creation of Uniform Fuel Layers - Excellent results have been achieving with the fast-refreeze method in creating uniform fuel layers for targets with diameters up to a millimeter and fuel layers of a few microns.[26] However, for the shells with radii of several millimeters and proportionally thick fuel layers, this method is not successful.[27] Use of low-Z foams as wicks for liquid DT has also been proposed as a way of creating uniform layers. Unfortunately, foam targets would have significantly lower gain than ones of similar size with free-standing ice layers. (TWG communication)

The beta heating method is proposed for creating uniform DT ice layers. This method relies on several simple physical phenomena to create uniform DT ice layers in spherical targets.[28] The relatively low energy beta released in the decay of the

radioactive tritium component of the DT ice is absorbed close to its emission point within the ice layer. This leads immediately to the generation of thermal gradients in nonuniform layers. The DT layer within a plastic shell can be modeled as a closed, solid-vapor system. In such a system, temperature gradients must be released by sublimation. In thick regions of ice, relatively more energy will be released because of the greater number of decaying tritium atoms. This will cause the thick regions to become warmer and the ice in such regions to sublime faster. In the thin regions the opposite is the case. Sublimation is slower and ice redeposition is faster. This process will continue in a spherically symmetric system until the ice layer is uniform as shown in Figure 6.4.2-4. The beta heating process could be used in conjunction with other, simpler techniques to increase the speed of the overall redistribution process. Air tumbling, for example, might be used during initial freezing of the ice to produce approximately even layers. This would shorten the time necessary for the beta heating process to create targets with ice layers sufficiently uniform to achieve high gain. Feasibility of this preliminary tumbling step would depend on such factors as potential damage to surface finish. Application of external thermal gradients could also be used as a preliminary step to generate nearly uniform ice layers.[29] Whether such preliminary steps will be needed depends, of course, on the ice redistribution rates in the beta heating process itself. Recent computer and experimental results seem to indicate that they can be eliminated.[30,31]

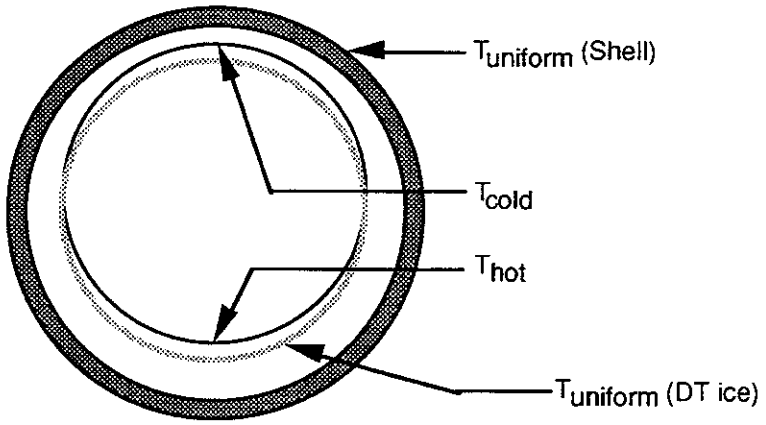

Figure 6.4.2-4. Energy From Beta Decay Can Form a Uniform Solid Layer of DT Fuel

The question remains of whether the process would be fast enough for mass production in an IFE reactor target factory. Fast ice redistribution to form uniform layers would be necessary to avoid deterioration of targets due to radiation damage and to eliminate the need for excessive tritium inventories. Recent theoretical and experimental work indicates that ice layers with sufficient uniformity for reactor targets can be achieved in a matter of a few hours, depending on such factors as target size and the thermal conductivity of the shell material. Redistribution rates found using the 2D code mentioned above are shown as a function of shell wall conductance in Figure 6.4.2-5. The relatively low thermal conductance of the CH shell means that

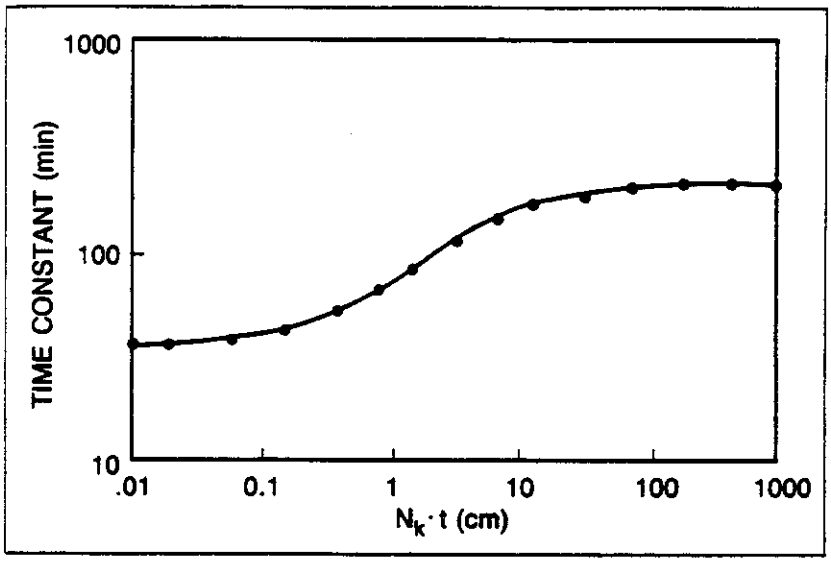

Figure 6.4.2-5. The Thermal Conductivity of the Shell Material Is an Important Factor in Determining the Rate of Heat Transfer. N_k is a Factor Used to Normalize the Thermal Conductivity of the Shell Material to that of Glass.

predicted e-folding time constants will fall on the left side of the curve in the figure. Experimental results obtained using a thick-walled copper cylindrical with sapphire windows bear out these optimistic theoretical predictions.[30] DT ice redistribution due to beta heating within a 5.74 mm enclosure led to nearly uniform layers within three hours. Faster rates can be expected with actual targets due to the low thermal conductivity of CH compared to copper.

The target factory design proposed here in allows four hours for the beta layering step, a time that seems reasonable in view of the available evidence and the possibility of creating reasonably uniform layers by such preliminary steps as air tumbling.

6.4.2.4 Indirect Drive Target Case Fabrication and Mating - The capsule for indirect drive targets will be similar to the direct drive targets, and will be fabricated and filled in the same way. The radiation case must then be mated to the capsule under cryogenic conditions. Incorporated in the case is a support structure to provide target position and ability to survive acceleration while providing good illumination symmetry. This configuration also happens to be the best for target performance and would be easiest to manufacture. The exact configuration chosen will depend on target performance requirements, which are beyond the scope of this report. However, it should be possible to cheaply mass produce targets in either configuration.

Indirect Target Engineering Model - After the project decision to use the indirect drive (ID) target as the baseline target for the heavy ion driver, a study was conducted to determine the feasibility of mass producing the targets, techniques of handling and injecting the target, and the survivability of the target. Indirect laser targets have been successfully used in experiments, but only on a single shot basis, perhaps suspended or positioned on a pedestal within the test chamber. Care was taken in the fabrication of these limited-production targets to obtain the performance or experimental results desired. Likewise, the thermal and handling environments were tailored to minimize design and physics constraints.

To date, there has been no need to propose or design a mass-produced, commercial, indirectly-driven fusion target as it is not needed for the present or planned experiments. Therefore, to determine within this unclassified study the engineering feasibility of an indirectly-driven target, not the physics feasibility, an engineering model was proposed for evaluation and study.

General Target Model Guidelines - The indirect target is designed for the heavy ion driver system although the design could easily be adapted to the laser driver system. The DT capsule contained within the outer case is similar to direct drive capsules. The outer radiation case enclosing the DT capsule is assumed to be cylindrical with energy converter regions located on the two ends of the heavy ion target case. A laser indirect target would have apertures on the two ends instead of the energy converter regions. The target would be injected into the reactor cavity along its longitudinal axis with an induced spin to provide stabilization.

The Target Working Group (TWG) considered both single- and double-sided illumination schemes for the heavy ion, indirectly-driven target.[1,2] However, the TWG felt the two-sided target should be employed as the baseline because of the speculative nature of the single-sided illumination.[2] Thus two energy converter regions will be used, one in each end of the cylinder on the axis of symmetry. The TWG-supplied heavy ion ID gain curves,[1] shown in Figures 3.3-8 and 3.3-9, indicate focal spot sizes from 4 to 10 mm in diameter, depending on the ion range (R) and driver energy chosen. For the driver design point chosen, the converter region geometry was determined. This converter geometry allows for some beam misalignment with respect to the target. An engineering model of the converter region was defined. The converters will be affixed to the inner surface of the radiation case. One of the engineering analyses addressed the question of the minimum thickness of the radiation case to withstand the acceleration forces of the injection systems, which was tentatively chosen to be 100 g's for the indirect target. The case geometry is configured to ease fabrication and reduce stress concentrations. If target physics constraints would require other configurations, these features could easily be changed.

The initial effort was to determine if the acceleration loads of 100 g's would cause buckling or distortion of the case walls or ends. The dimensions of the case were held to the minimum to reduce the hydrogen and carbon gas load to be introduced into the cavity. As the ion beams interact with the energy converter region, soft x-rays are created and bathe the inside of the case and the DT sphere. To efficiently contain the X-ray radiation, lead was chosen for use in the case to be compatible with the wall protectant.

The central capsule should be supported so as not to significantly disturb the illumination of the capsule. For the calculations as to the elastic strength of the case walls, the weight of the central capsule was transferred to the walls, but the mass of the support was neglected. The mass of the case walls, converter regions, and the support mechanism was estimated.

For the target to have the proper thermal conditions when it reaches the center of the cavity, the entire target must be at cryogenic temperatures up to and including the injection operation. During a preliminary investigation, no CH compounds were found to exhibit adequate structural properties at these cryogenic temperatures. Other materials that can easily withstand the operating environment with adequate structural properties may not be suitable from a physics standpoint and desirable additions would not be attractive from a materials handling standpoint. However, specific structural properties were used as representative of an improved CH plastic to be engineered for this application.

Radiation Case Wall Structural Analysis - A Nastran finite element model was constructed with 1155 nodes, 1155 QUAD elements, and 36 TRIA elements to model the case. For the wall thickness trade study, the internal DT capsule was represented as a point mass in the center of the case with a structure carrying the load to the case walls. The analysis was conducted using a Nastran inertial relief analysis method. A pressure of 3.3 kPa (0.47 psi) behind the target will impart approximately 100 g's acceleration. The maximum case wall stress is 0.079 MPa that is well within the allowable limits of the material. Thus the case can easily withstand the acceleration load of 100 g's.

The internal support structure was more difficult to postulate and analyze. Room temperature stress properties were used to estimate allowable designs based upon capsule survivability during acceleration and resultant deflection and vibration modes. An increase in the thicknesses assumed may be dependent upon the cryogenic allowable stress levels in the to-be-determined material. In the search for suitable materials for this engineering study, the choice was limited to available commercial materials. It was found this material will easily withstand the imposed acceleration stresses and the resultant vibrational displacements would probably be acceptable even at cryogenic temperatures. The deflection was predicted under full acceleration

loading. The calculated natural frequency of the capsule is approximately 1500 Hz. Assuming a conservative damping coefficient of 0.1% (low damping), the capsule would oscillate within the case approximately 75 times during the transit of 10 meters from the end of the injection system to the center of the reactor chamber (50 ms). With this damping coefficient, the amplitude at T = 0 would be negligible.

Summary of Indirect Target Structural Analyses - An engineering model of the indirect drive (ID) target was defined using commercially available materials. Structural analysis of this model indicated the outer radiation case wall would easily withstand the desired acceleration loads of 100 g's. An acceptable structural support technique is proposed provided adequate structural properties can be obtained in suitable materials. For the materials and properties assumed, the stresses and deflections were within acceptable engineering limits.

Summary of Indirect Target Material Requirements - The above engineering target model provides baseline data for the material's usage and waste product generation within the reactor cavity.

Fabrication of the Indirect Target - The manufacturing process for the indirect target is designed to support a pulse rate of the heavy ion driver reactor of 3.5 pulses per second. The operations are divided into ambient and cryogenic processes as is indicated in Figure 6.4.2-6. Duplicate facilities with excess capacity are planned to reliably produce the required quantities. Buffer queues are also planned to assure 100% target availability for the reactor. The reactor will require 12,600 targets per hour or 300,000 per day. The rates of production and cryogenic atmosphere necessitate inclusion of the inspections into the automation scheme. In the interest of minimizing the tritium inventory, a Just In Time (JIT) inventory philosophy is anticipated using a partnership with the supplier to provide the safety stock required.

The design of the target lends itself to the fabrication techniques employed in the pharmaceutical industry, although somewhat larger in diameter. The case will be fabricated in two half cylinders to allow the tritium capsule to be attached with its support structure centered in the cylinder. Several alternatives are available to close the case. One alternative is to store the right half of the case at room ambient and slide it over the section with the capsule that will be at cryogenic temperature. The subsequent shrinking of the material as it approaches the cold temperature will create a bond. Two other alternatives address bonding the two sections together. The application of ultra sonic welding is a viable candidate. The energy is applied to the point where bonding is required and a localized rise in temperature results that creates a bonded butt joint. The other alternative is to rotate the mating bodies in opposite directions and create an inertial weld of the butted surfaces. Both alternatives would require the buffer stores in the cryogenic environment to have temperature stability.

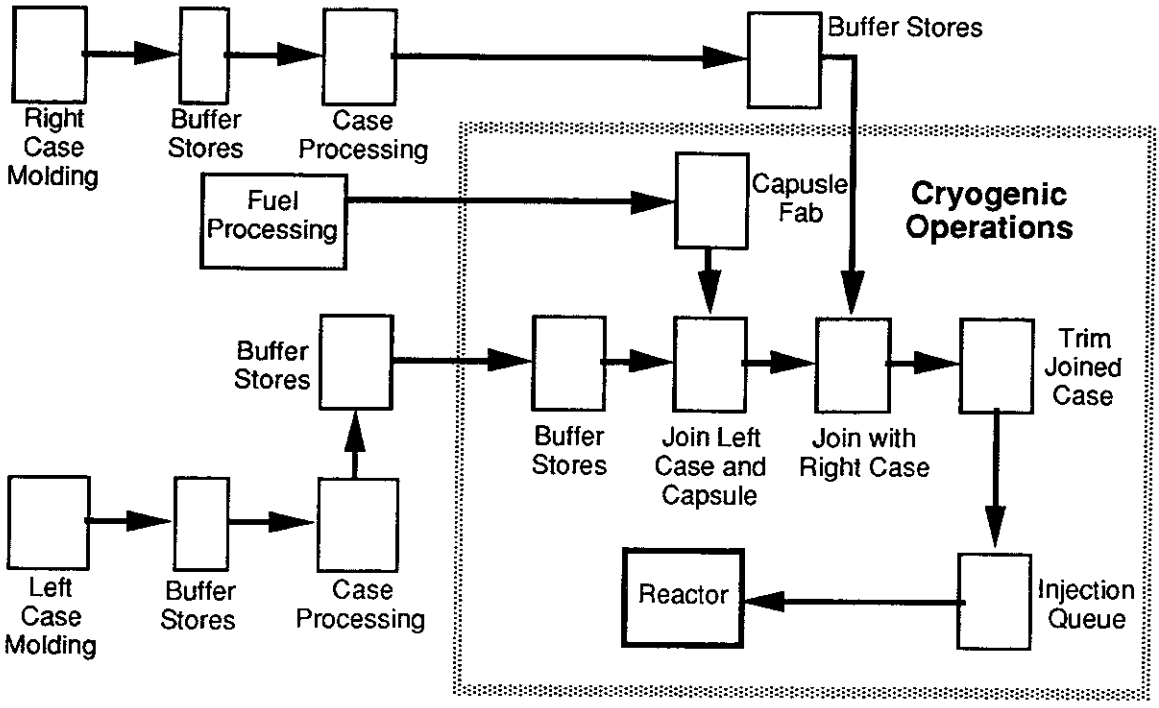

Figure 6.4.2-6. Indirect Target Production Process

The fabrication of the case sections would be done in multi-cavity molds. The half cylinders would be formed with an extrusion or blow molding process that would hold the tolerances on the diameter to a few thousandths of an inch and wall thickness to a fraction of a thousandth of an inch. The cylinder ends can be trimmed to the desired length. The extrusion die would be designed to form the converter section and the constant thickness walls. With molds of 100 cavities and the short cycle time, the utilization would be less than 12 hours per day that would allow ample time for machine and mold maintenance. Space cavity inserts and the possibility of operating with missing cavities would assure adequate supply. A 24 to 36-hour buffer stock would be adequate. The availability of two machines, one dedicated to each half, would provide further insurance against a stoppage.

The vapor deposition facilities will require special fixturing for multi-unit processing. The number of units has not been determined but, based on other applications, a minimum of three work cells would be required. These ambient temperature operations need to be adjacent to the cryogenic operations since the lead will be recovered from the reactor exhaust stream and reused in this process. The facility design will be required to prevent lead escaping into the atmosphere inside the ambient room as well as to the exterior.

The fuel capsule will be manufactured in a process similar to the laser direct drive target, of similar materials. A diffusion process will be used to fill the capsule with DT. The capsules will be fabricated and inspected in a JIT process for injection to minimize

the tritium inventory. Multiple parallel production lines will be utilized to assure the necessary reliability values.

The DT capsules will be mated initially with one half of the radiation case and the capsule support structure in the cryogenic environment. The assembly of the remainder of the case will occur in the next work cell using one of the proposed methods of attachment. The next work cell will deflash (trim) the cases, if necessary, and load them into a transportation fixture for the injection queue.

The equipment design specifications will provide for in-process inspection internal to the equipment with attribute data acquired for process control purposes. Appropriate "no touch" measurement techniques such as laser micrometers or air gaging will be used for data acquisition. Built in processors would provide continuous statistical analysis of the output. The initial designs will be built around a requirement that 35% of the work stations in any piece of equipment be available for future growth to provide flexibility for future changes to the process and unanticipated problems.

6.4.3 Target Factory Definition - Targets for inertial fusion experiments conducted to date have been hand crafted at great expense in time and money. Occasionally, single targets are made with precise individual features such as surface bumps, thin coatings of exotic materials and doping with trace elements. Production methods in target factories for future IFE reactors will be radically different. These factories will need to economically mass produce hundreds of thousands of standardized targets per day. At the moment there is not even general agreement on what fabrication methods will be most appropriate or even, in the case of indirect drive, what the targets will look like. Nevertheless, there is good reason to believe that this technological challenge can be met. Reactor targets will be small and complex. It will be necessary to built them to exact specifications. Experience in other industries shows us that novel products with all of these characteristics can be produced economically. Semiconductor chips, for example, have even smaller features that must be cheaply fabricated to similarly demanding specifications in hundreds of thousands of copies. Similar examples can be cited in industries producing everything from electronic equipment, pharmaceuticals, and small mechanical devices, to optical equipment and even toys. Obviously, in our present state of technological uncertainty, the advances of tomorrow can quickly make the designs of today obsolete. Nevertheless, it is still useful to consider the general layout, potential fabrication and inspection steps, special safety and containment precautions and approximate staffing requirements of future target factories, if only to make the case that mass production of reactor targets is possible and can be done cheaply enough to make fusion power economically attractive.

6.4.3.1 General Factory Layout - The target factory concept for direct drive targets will be discussed first. Many of the production steps for direct drive targets will be found in the indirect drive target factory as well. Operations peculiar to the indirect drive factory will be discussed in a separate subsection.

The proposed target factory will be separated into two distinct sections. Operations requiring the handling of tritium will be carried out in one section, referred to hereafter as Zone II, and all other production steps in the other section, referred to as Zone I Gross dimensions of both sections will be approximately 50 m x 50 m. Figure 6.4.3-1 shows the functional relationships between the major operations requiring space in the factory. It is, of course, premature to consider detailed architectural planning at this point. However, the general layout of Zone I is expected to reflect the diagram in Figure 6.4.3-1 to the extent that actual production steps, which are shown in the large rectangle, will be carried out in a large, central bay area. All other operations, such as administration, maintenance, etc., will be carried out in peripheral areas. This arrangement will allow the greatest flexibility in accommodating changes in production steps due to technological improvements in materials, fabrication techniques, etc.

The majority of the resources in terms of space and manpower in Zone I will be devoted to production and delivery of finished target shells to Zone II. In addition, significant resources will be devoted to inspection and recycling of used sabots and fabrication of new ones to make up for normal attrition. Finally, Zone I will contain facilities for production of radiation case elements for indirect drive targets. All production steps will be carried out in a number of parallel lines that will provide redundant capacity to allow periodic maintenance of individual line elements and, if necessary, production of targets for other facilities.

The basic technologies chosen for target shell fabrication are dual-nozzle droplet generators combined with microencapsulation. As already pointed out above, production of significant numbers of reactor size targets has not yet been demonstrated with this combination of technologies. In spite of this, their choice does not necessarily entail any technological leap of faith. They are certainly capable of producing the large numbers of target shells required for reactor operations. If significant resources are devoted to research and development in this area, it is not unlikely that variations will be found which are capable of turning out target shells with the required thickness and size. Even in the event that no such process is found, these methods can be used in combination with shell coating and micromachining steps to produce reactor-size targets. The question is whether they can do it economically. The evidence from many other industries where demand has led to the inexpensive manufacturing of small and complex items suggests that they can.

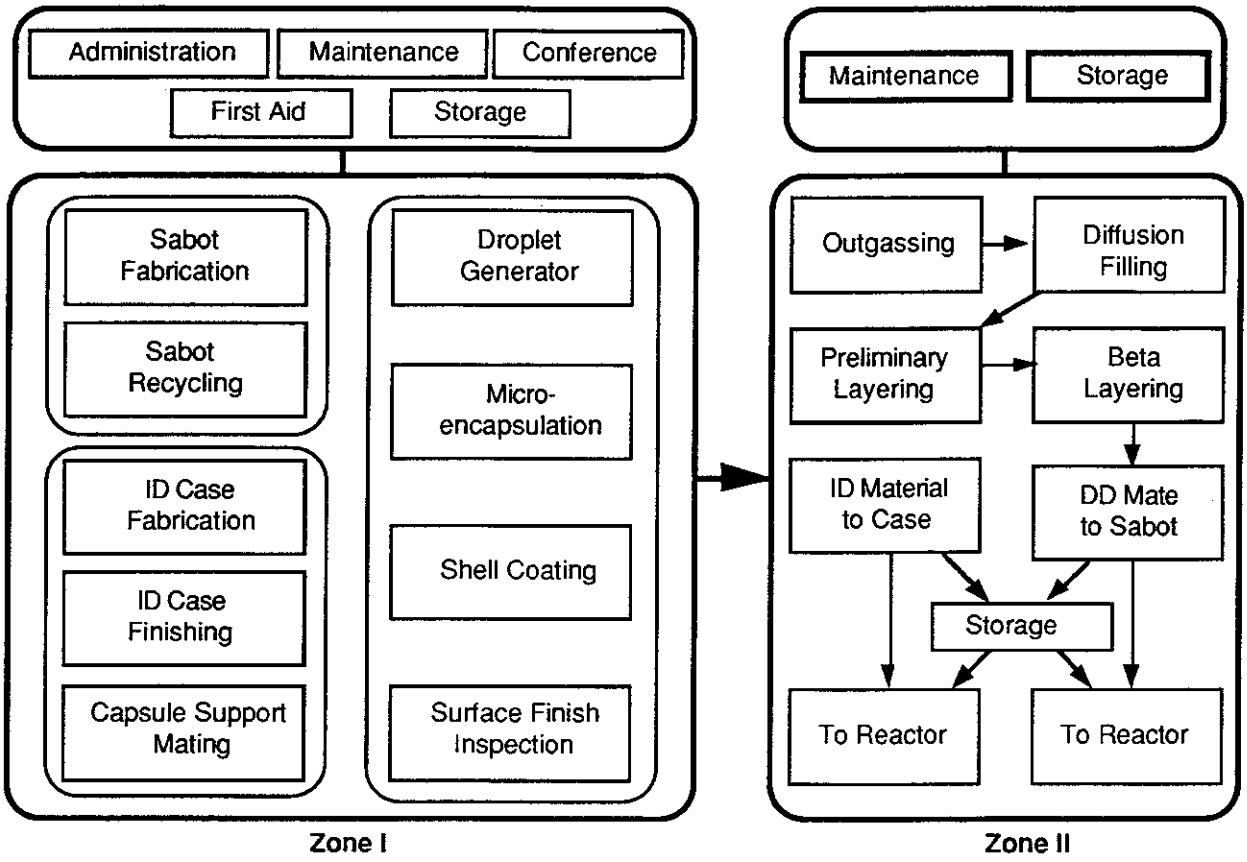

Figure 6.4.3-1. Functional Relationships for Buildings in Target Factory

At the moment, no need is foreseen for coating steps other than those required for fabrication of the main shell. The target prescribed by the TWG has no additional elements required by any peculiarities of the reactor design proposed here. The open bay design of Zone I could accommodate such steps if necessary; however, finished target shells will be subjected to a final heating and outgassing step before delivery to Zone II or vacuum storage.

In addition to fabrication of the main target shell, provision is made in Zone I for reception and inspection of used sabots from the target injection system and production of new sabots to replace those damaged or worn. Sabots will be used only for direct drive targets. Indirect drive targets are completely enclosed in a radiation case that will provide sufficient protection to the target capsule during the acceleration process. Sabots are considered precision parts in this design. An example is shown in Figure 6.4.3-2. The target will be seated loosely in the nose of the sabot. The sabot must be designed so as not to damage the capsule or impart a transverse velocity component to the target on release of the capsule. Sabots will be injection molded of thermoplastic and then finished by machining with high tolerance tools. The

ferromagnetic material shown in Figure 6.4.3-2 will be mechanically attached to the sabot. It is expected that sabots will be reused an average of 20 times.

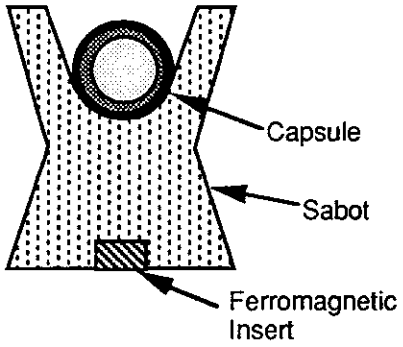

Figure 6.4.3-2. Direct-Drive Sabots Must Be Precisely Machined to Insure a Straight Trajectory for the Loosely Seated Capsule

Finally, indirect drive cases and auxiliary parts will be produced in Zone I. Indirect drive cases are not considered precision parts. However, they must be made to reasonable tolerances as they will be in direct contact with the injection system barrel during target injection. The left and right radiation case components will be molded. Finally, capsule support structures will be attached to the open ends of both case components to provide support for the target capsules. As shown in Figure 6.4.3-1, all components produced in Zone I will then be transferred to Zone II for DT fueling operations.

Zone II will be designed to provide for tritium containment and all systems therein will be designed to operate with as little human intervention as possible. Application of artificial intelligence and robotics will be used in all production and inspection steps. The need for a human presence in Zone II will be limited, as much as possible, to provision for periodic maintenance. High pressure and cryogenic barriers in Zone II are as shown in Figure 6.4.3-3.

Target capsules arriving in Zone II will be introduced into diffusion filling vessels such as the one shown in Figures 6.4.2-3 and 6.4.3-3. Four to six of these aluminum vessels will operate in parallel to provide redundant capability to provide for standard maintenance and continuous plant operation in case of failure of any of the vessels. The target capsules will be mechanically conveyed through internal locks in the vessels to allow for gradually increasing external DT pressure and maintaining optimum filling rates. Optimum fill temperatures of around 100°C will be maintained in the vessels with the aid of external heating and cooling elements. Depending on the exact size and polymerization of the target capsules, diffusion filling will take from 24 to 36 hours.

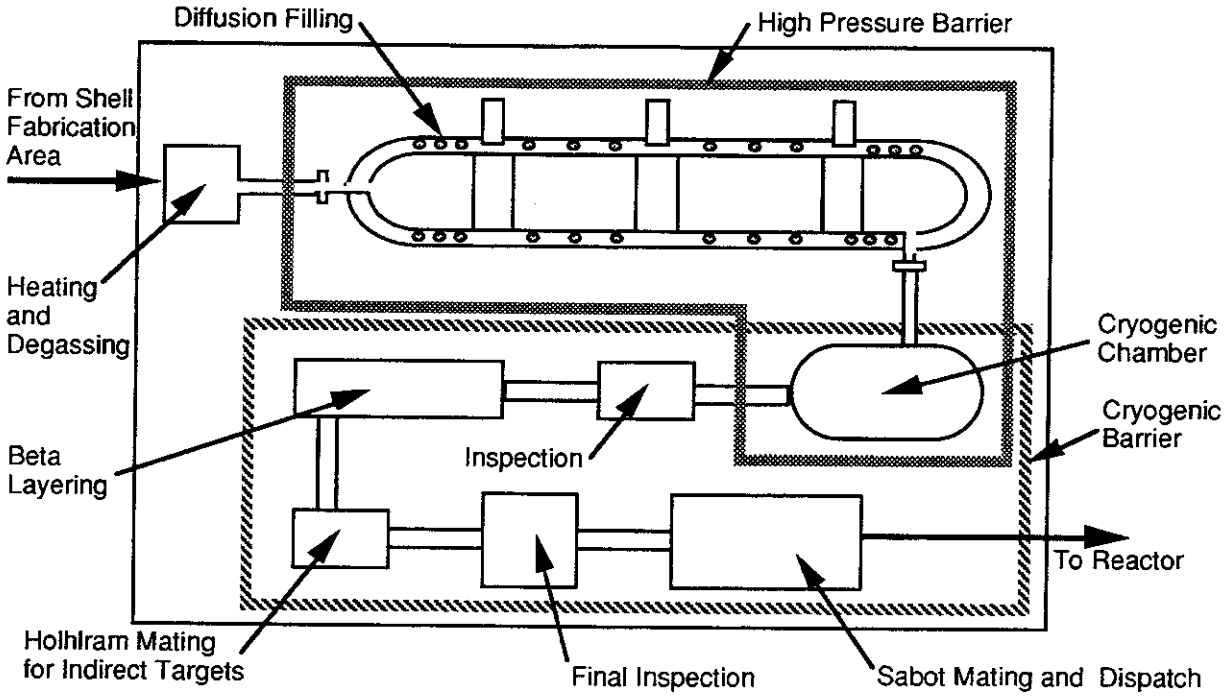

Figure 6.4.3-3. Zone II Layout for Direct and Indirect Drive Targets Shows High Pressure and Cryogenic Barriers

After diffusion filling, capsules will be removed to separate containment vessels and cooled to cryogenic temperatures. This could be done in a high pressure DT environment if necessary to prevent excessive fuel loss due to outgassing during the cooling process. The ambient gas would be cooled to near cryogenic temperatures with the target capsules and pumped off at the appropriate time.

At this point, indirect drive target capsules would be mated to their radiation cases. This process will take place at cryogenic temperatures using precooled parts. Ideally, case components will be fabricated with sufficient accuracy to lock firmly together, holding the capsule in place.

Direct drive targets will be suspended between layers of thin (<1.0 mm) plastic film and also be cooled with gaseous helium during the beta layering step. Next, they will be mated to their sabots. At this point, both types of target will normally be delivered to the reactor for immediate injection. Some provision will be made for short term storage, but the shelf life of the targets is expected to be quite short (<100 hours) due to radiation damage to the inner surface of the CH shell and it will be necessary to thermally isolate them during storage.

Inspection of Target Components - Inspection of components will take place after all major target fabrication steps. In principle, inspection of parts such as sabots and indirect drive case elements could be done visually by a staff of inspection personnel. However, this would be expensive and, in the case of opaque components such as

target shells, impractical. Fully automated inspection with the aid of artificial intelligence and pattern matching and recognition techniques is preferred. Limited application of such techniques has already been demonstrated in the field of optical interferometry for glass shells, as shown in Figure 6.4.3-4. For opaque parts, x-ray microscopy is proposed.[32,33] This technique lends itself to batch target characterization, and is capable of detecting target flaws at the submicron level.

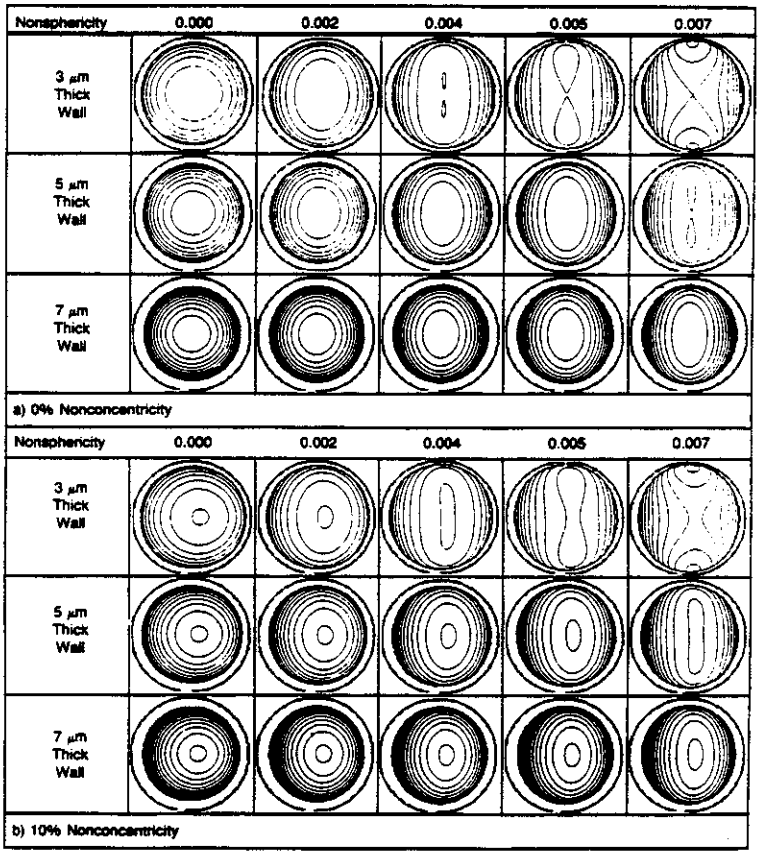

Figure 6.4.3-4. Computer Generated Interferometric Reference Patterns Suggest the Possibility of Mass Inspection with the Aid of Pattern Matching and Artificial Intelligence

Target Costs - Target costs are estimated according to a model proposed by Pendergrass, et. al.[34] In this model, costs are divided into three components: target factory capital charges, nontritium materials costs, and nonfuel, nonmaterials O&M costs. Simple algorithms are supplied for computing these costs that depend on a number of fixed parameters as well as variables intrinsic to individual reactor designs. Default values supplied for the parameters have been used here unless otherwise noted. Appendix C, Section C.3.7, has more detail on the nominal capital costs, repetition rates, and reject fractions used to arrive at the final cost values.

The form of the capital cost model is

$$C_F = \sum_{i=1}^{N_s} C_{FRi} \left(\frac{P_{Ai}}{P_{AR}} \right)^{a_i}$$

Eq. 6.4.3-1

where C_F is the total target capital cost (M$), C_{FRi} is the reference capital cost increment for the target factory section to manufacture target substructure i (M$), N_S is the number of substructures, P_{Ai} is the required annual production capacity for the section of target factory that produces target substructure i (1/yr), P_{AR} is the reference annual production capacity of the target factory (10^8/yr), and a_i is a production capacity scaling exponent of the section of the target factory to manufacture target substructure i. The Pendergrass model distinguishes between two inspection models, depending on whether inspection takes place of each major target component as it is completed or only of finished targets. For the designs proposed here, the first model is appropriate. The target rejection model for this type of inspection is

$$P_{Ai} = \frac{P_A}{\prod_{k=i}^{N_s} (1-F_k)}$$

Eq. 6.4.3-2

where P_A is the design target factory annual production capacity and F_k is the fraction of targets rejected for failure to meet specifications for target substructure k. For the direct drive reactor, there are two significant target substructures: the single-shell target fuel capsule and the sabot. A reference capital cost of $122M (escalated to 1991$) was given for the target shell manufacturing facilities. No value was given for the sabot manufacturing. Capital costs for the sabot should be much lower in view of the simplicity of the design and the potential for reuse of sabots. C_{FRi} for sabots was asssumed to be $5M for a total nominal capital cost of $127M. The default rejection fraction for the fuel capsule of 0.02 was used, and a sabot rejection fraction of 0.01 was assumed. Substituting the Prometheus laser option values of repetition rate into Eq. 6.4.3-1 yields:

C_F(direct drive) = $134.92M

Sabots are not required with the indirect drive targets. Instead, a radiation case with energy convertor regions is used. The nominal capital cost for this element is assumed to be $37M. A nominal captial cost of $145M is assumed for the fuel capsule

that may be somewhat more complex. The nominal capital for the indirect drive target totals $182M. The default rejection fraction of 0.02 is assumed for the radiation case. The added energy convertors contributes an additional 0.01 rejection fraction. The fuel capsule default rejection rate is retained at 0.02. Again, substituting these values into Eq. 6.4.3-1 yields:

C_F(indirect drive) = $143.62 M

Materials costs for both designs are insignificant in view of the inexpensive choice of target materials and the possibility of recycling the lead in indirect drive radiation cases. Pendergrass et. al. give reference materials costs of 0.015 and 0.025 $/target for direct and indirect drive laser targets expressed in 1986$. For the designs proposed here, these numbers are much too high. It was assumed the laser direct drive materials costs are $0.010 per target and the HI indirect drive materials costs are $0.014 per target. Refer to Appendix C for the relevant cost estimating relationships. Heavy ion target materials were higher due to the addition of the energy converter structures.

Nonfuel, nonmaterials O&M costs include personnel costs, the annual target factory interim replacement cost, annual maintenance materials cost and O&M cost for other supplies and materials. The algorithm used to determine personnel costs is

$$C_p = (0.001\ \text{k\$/M\$}) \sum_{j=1}^{N_{JC}} N_{Rj} C_{PRj} \left(\frac{P_A}{P_{AR}} \right)^{d_j} \qquad \text{Eq. 6.4.3-3}$$

where N_{JC} is the total number of job categories, N_{Rj} is the reference number of persons required for a job category, C_{PRj} is the reference annual cost per employee in job category j, and d_j is the exponent for scaling of number of staff required for job category j (1.0 if category scales, 0.0 if not) with design target factory annual production capacity. Some of the data used in the above equation are shown in Table 6.4.3-1. The format and defaults in Reference 36 have been used in the table where appropriate. However, some modifications are introduced which reflect the idiosyncrasies of the design presented here.

Table 6.4.3-1
Target Factory Staffing Requirements (10^8 Targets/Yr)

Position	Salary 91$	Plant Staff Capsule		Rad Case	Indirect Drive O&M		Direct Drive O&M	
		Fixed	Scalable	Scalable	Fixed	Scalable	Fixed	Scalable
Plant Manager	82.8	0.5			41.4	0.0	41.4	0.0
Secretary	29.8	1.0			29.8	0.0	29.8	0.0
Clerk Storekeeper	30.3	1.0			30.3	0.0	30.3	0.0
Auditor Bookkeeper	38.6	1.0			38.6	0.0	38.6	0.0
Janitor	22.4	1.0			22.4	0.0	22.4	0.0
Target Mfg Specialist	55.1	2.0			110.1	0.0	110.1	0.0
Quality Control Engineer	55.1	1.0			55.1	0.0	55.1	0.0
Electrical Engineer	55.1	0.5			27.5	0.0	27.5	0.0
Mechanical Engineer	55.1	0.5			27.5	0.0	27.5	0.0
Chemist	55.1	2.0			110.1	0.0	110.1	0.0
Health Physicist	55.1	1.0			55.1	0.0	55.1	0.0
Laboratory Technician	32.3	6.0		1.0	193.8	82.8	193.8	0.0
Shift Supervisor	60.1	2.5			150.3	0.0	150.3	0.0
Senior Operator	51.2	5.0			255.9	0.0	255.9	0.0
Operator	46.8		5.0	5.0	0.0	468.3	0.0	234.1
Assistant Operator	41.4		5.0		0.0	206.9	0.0	206.9
Maintenance Supervisor	46.8	2.5			117.1	0.0	117.1	0.0
Mechanical Maint Tech	41.4		5.0	2.5	0.0	310.4	0.0	206.9
Electrical Maint Tech	41.4		5.0		0.0	206.9	0.0	206.9
Inst. & control Maint Tech	41.4		5.0		0.0	206.9	0.0	206.9
Quality Assurance Tech	41.4		5.0	2.5	0.0	310.4	0.0	206.9
Security Specialist	34.0	5.0			170.0	0.0	170.0	0.0
Peak Maint FT Equiv	48.0		5.0	2.5	0.0	360.3	0.0	240.2
TOTALS					1434.9	2102.3	1434.9	1508.9
						3537.3		2943.8

Use of the above numbers for personnel cost estimation gives

C_P(direct drive) = \$4.15M/yr
C_P(indirect drive) = \$3.91M/yr

The algorithm for annual target factory interim replacement cost is,

$$C_{IR} = F_{IR}C_F \sim \$1.35M \text{ (DD)}, \sim \$1.44M \text{ (ID–HI)} \qquad \text{Eq. 6.4.3-4}$$

where F_{IR} = interim replacement annual cost factor, with a default of 0.01. In addition to the above, the annual maintenance materials cost,

$$C_{MM} = F_{MM}C_{MP} = \$6.22M \text{ (DD)} = \$5.85M \text{ (ID–HI)} \qquad \text{Eq. 6.4.3-5}$$

where F_{MM} is a maintenance materials cost factor with a default of 1.5 and C_{MP} is total annual maintenance personnel cost computed using a formula analogous to Eq. 6.4.4-3, and the reference fixed annual cost for supplies and expenses O&M costs is

$$C_{SE} \sim \$0.6M/\text{year} \qquad \text{Eq. 6.4.3-6}$$

6.4.4 Target Injection and Tracking - Injection systems capable of firing multiple targets at rates greater than those needed for IFE reactors have already been in existence for several years. They were designed to refuel tokamaks in the magnetic fusion program.[35,36,37] Magnetic fusion injection systems have shown that cryogenic pellets can be injected at the velocities and repetition rates required in IFE reactors. Many target injection techniques developed for magnetic fusion may eventually find application in inertial fusion. However, significant differences exist between the two approaches to fusion in the requirements they place on target injection systems. The pellets used in magnetic confinement systems are merely chunks of solid H_2 or D_2. The goal is to accelerate them to extremely high velocities, enabling them to penetrate to the center of the tokamak plasma. They are significantly more tolerant of high acceleration and surface abrasion than inertial fusion targets, and there is no need to delicately synchronize their velocities with a system of laser or particle beams. Target injection systems are presented here for the direct and indirect versions of Prometheus which address the technological challenges unique to each system.

6.4.4.1 Direct Drive Target Injection System - Choice of a direct drive target injection system is conditioned by the fact that it will probably be necessary to deliver direct drive targets in a sabot. Unprotected targets would be subjected to unacceptable levels of surface abrasion and thermal gradients during acceleration. Assuming a sabot is necessary, such questions must be answered as how to separate the target from the sabot prior to injection into the reactor cavity and how to recover the sabot for reuse. In addition, the synchronization and tracking problem inherent in IFE must be solved. An electromagnetic acceleration system is proposed as the best option for meeting these technological challenges.[38]

An example of the proposed direct drive target and sabot and a schematic of the injection system is shown in Figure 6.4.4-1. Targets will arrive from the target factory already mounted in their sabots. The sabot end cap is designed only to protect and hold the target in place during transit from the factory to the reactor, and will be removed shortly before the target is fired. Targets in both the DD and ID designs will be accelerated to 200 m/sec. The direct drive target will be injected through the first wall at a point about 7.5 meters from the beam aiming point. The target will traverse the cavity in approximately 37 msec. The target will enter the cavity about 140 msec after the previous shot, a sufficient time for cavity temperature and pressure to fall to levels which will not adversely affect the target (see Section 6.4.1.2). The injection system will have a 2-meter long injection module as shown in Figure 6.4.4-1. The module will be synchronized to provide the design repetition rate of 5.65 Hertz. Accelerations of about 1000 g will be imparted to the direct drive targets. Solid D_2 pellets have withstood accelerations of 5×10^6 g without breaking,[39] suggesting that thick DT shells such as those shown in Figure 4.6.1-1 will easily withstand accelerations more than three orders of magnitude smaller.[40] However, the situation is complicated by the strong dependence of the yield stress of solid hydrogen on

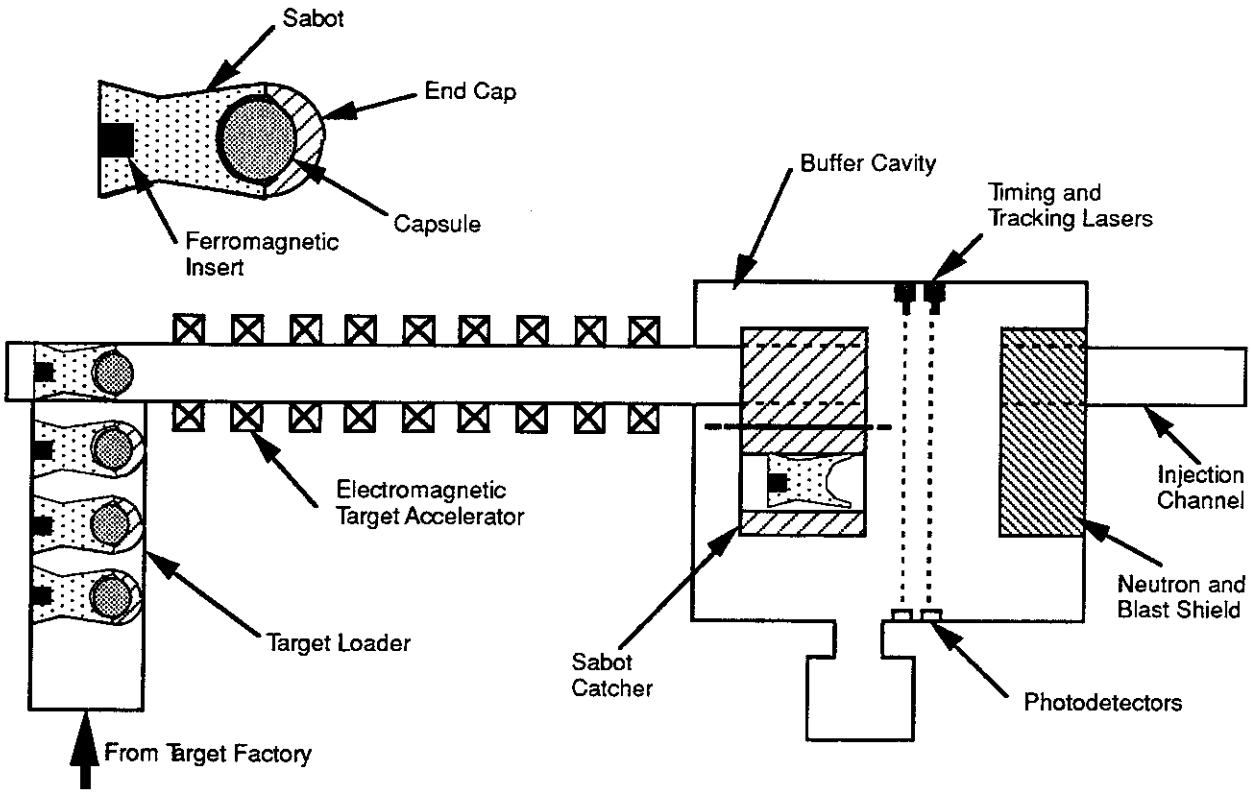

Figure 6.4.4-1. Schematic of One of the Eight Direct Drive Pellet Injection Modules

temperature. The solid targets mentioned above were at temperatures of about 12K. Yield stresses for solid hydrogen near the triple point are much less.[41] It is assumed here that fuel temperatures of less than 15K are acceptable.

Acceleration will take place on the principle of a linear synchronous motor, and a number of ferromagnetic materials exist which are capable of accelerating the target and sabot to 200 m/sec over a distance of two meters assuming achievable mean effective gradients $\delta_x B$ of the magnetic induction B of the accelerator coils of around 100 T/m.[38] The system has the advantage of requiring no medium in the barrel unlike railguns and, of course, pneumatic systems.

The injection system for the direct drive target will be mounted at the top of the reactor cavity, injecting downward into the cavity, as shown in Figure 6.4.4-2. After leaving the injection system barrels, targets will pass through a sabot catcher into a diagnostic chamber. There, a system of optical interrupters will be used to transmit position and timing information to the driver beams. Such systems are already in use in magnetic fusion pellet injection systems.[42,43] Timing information will be provided by a pair of light barriers or beams through which the target must pass on its way to the reactor cavity. Directional information, i.e., data on how far the target will deviate from a

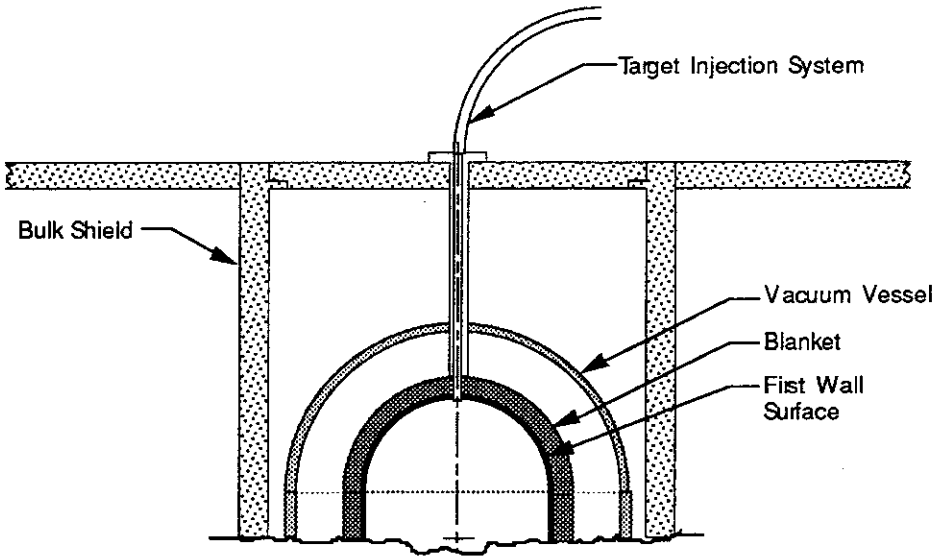

Figure 6.4.4-2. Electromagnetic Direct Target Injection System Employed in the Laser-Driven Reactor

straight line path, will be provided by interrupters oriented orthogonal to each other and to the target's direction of travel. In one such system devised for cylindrical targets which might be adapted for spherical targets, white light is broken down into a spectrum across the target path.[44] The parts of the spectrum interrupted by the target provide data on its exact location. It will be possible to steer the beams to hit targets within a radius of a few millimeters from the nominal aiming point on a shot to shot basis. Since targets must hit within this volume after leaving injector barrels located over ten meters away, it will be necessary to keep the transverse and longitudinal velocity scatter to a few millimeters per second. This requirement will be challenging with targets which are accelerated while seated in a sabot. It will be necessary to manufacture the sabots to precise specifications and inspect them after each shot. They will be decelerated before reaching the sabot catcher to prevent excessive impact damage.

The injector barrel will be enclosed in a thermal jacket and cooled by a continuous flow of helium. A number of similar systems for cooling barrels of magnetic fusion pellet injectors are described in the literature.[45]

6.4.4.2 Indirect Drive Target Injection System - Injection of indirect drive targets is complicated by their inherent fragility. Ideally, the target capsule would be suspended within the radiation case without any support structures whatsoever. Unfortunately, this is impractical in the real world. As disussed in Section 6.4.2.4, these capsules must be supported with a light weight structures, compatible with the required target physics and be capable of withstanding an acceleration of 100 g's. In

order accelerate targets to the optimum velocity of 200 m/sec, injection system barrels approximately 20 meters long will be necessary.

Indirect drive targets enjoy some inherent protection from friction and overheating because they are completely enclosed in radiation cases. Sabots will, therefore, not be used with the HI design. Pneumatic acceleration has been chosen in order to eliminate the need for ferromagnetic or other special materials in the target's radiation case. Numerous pneumatic pellet injection systems capable of repetitive injection have been built for fueling tokamaks, and their technology is, consequently, significantly more mature than that of competing electromagnetic systems. Their major drawback is the need for a propellant gas.

Ideally, the longitudinal axis of the heavy ion indirect drive target should be aligned with the two diameter, two HI beam sets. Unfortunately, the final focus coils prevent coaxial injection. Instead the injection system will be aligned 10° off the horizontal beam axis. A diagram of the indirect drive injection system is shown in Figure 6.4.4-3. An eight barrel system will be used. This will provide sufficient time for each barrel to be reloaded, fired and evacuated while maintaining a repetition rate of 3.54 Hertz. The barrels will be fired by electronically opening a magnetic valve[46,47] to the D_2 propellant gas reservoir, as shown in Figure 6.4.4-4. A piston in the reservoir will maintain constant accelerating pressure behind the target during its approximately 0.2 second trip down the barrel. Its movements will be controlled by automatic interpretation of data from a quartz pressure transducer mounted in the propellant gas cavity. An advantage of the requirement for low acceleration is that it allows the use of cold propellant gas. Thus, a potential source of target overheating is avoided.

A problem inherent in pneumatic injection systems is how to avoid contaminating the reactor cavity with propellant gas. Fortunately, the magnetic fusion community has already provided many of the answers on how to deal with this problem.[48,49] Piezoelectric pressure transducers will be mounted along the length of the barrel to sense the passage of the target. This information will be relayed to gate valves on the muzzle of each barrel.[50] The gate valve will be closed immediately after passage of the target, and the propellant gas in the sealed barrel will then be pumped out.

After leaving the injector barrel and passing through the diagnostic chamber, targets will travel ballistically down guide tubes through the bulk shielding, blanket and first wall. These will be slightly curved to account for the drop in the trajectory due to gravitational forces on the way to the aiming point.

Indirect drive targets must be properly oriented during beam illumination of the energy convertor regions. It is therefore necessary to impart a spin to them to prevent them from tumbling. This will be accomplished by rifling the injector barrels. Small tabs will be molded on the radiation cases to accept the rifling.

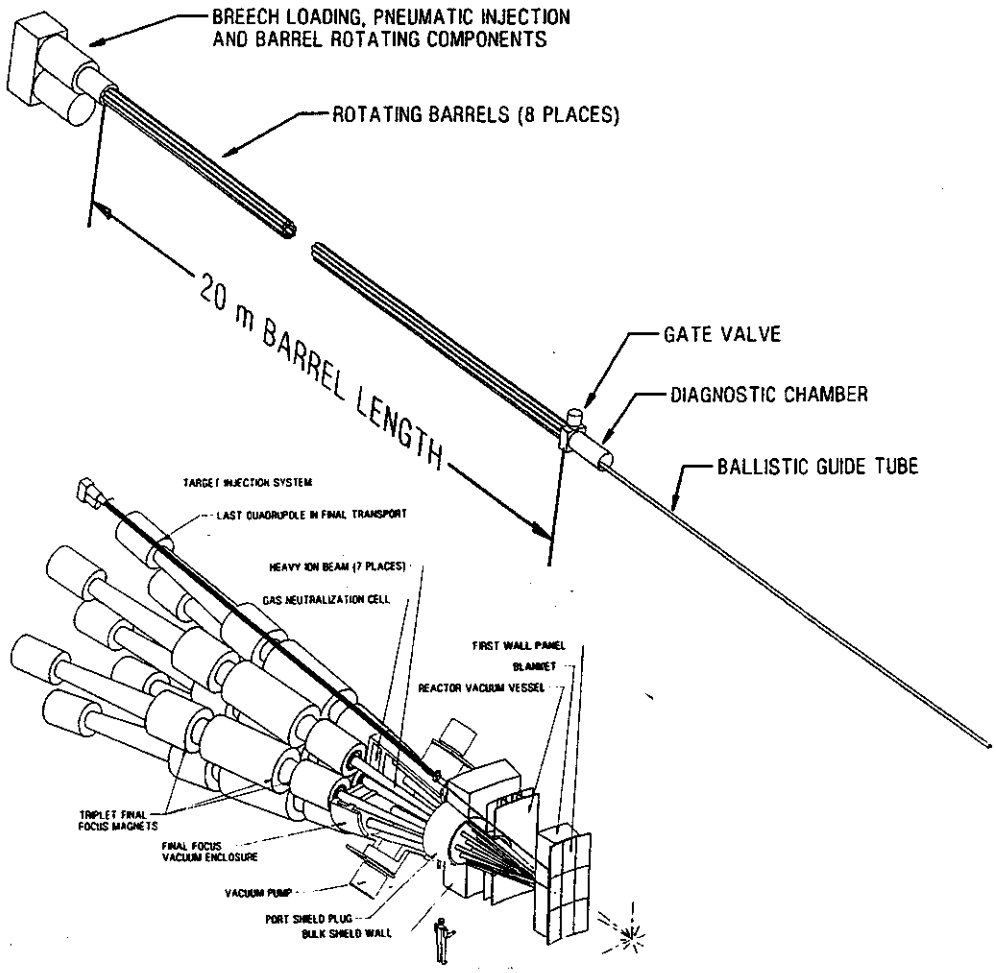

Figure 6.4.4-3. Pneumatic Indirect Target Injection System for Heavy Ion-Driven Reactor

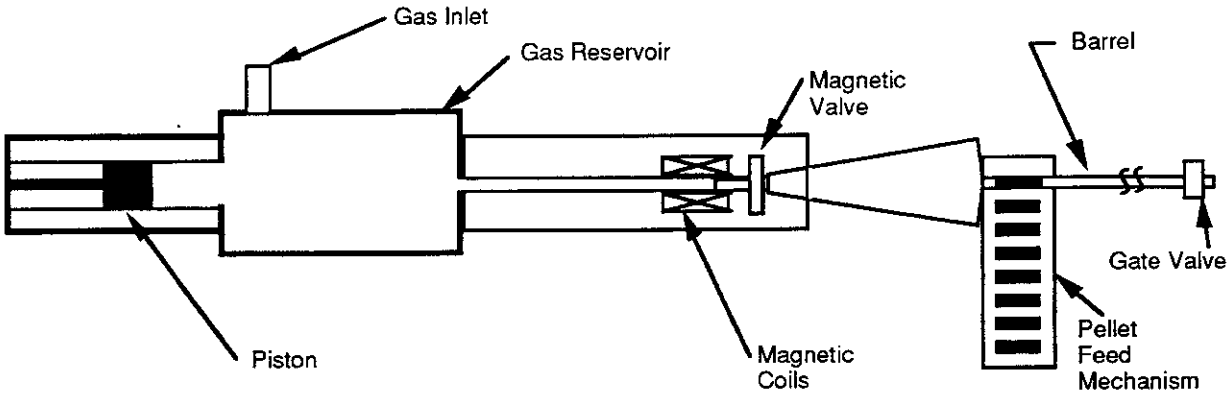

Figure 6.4.4-4. Constant Gas Pressure Is Maintained During Acceleration by a Piston in the Gas Reservoir.

References for 6.4

1. R. C. Davidson, et al., Inertial Confinement Fusion Reactor Design Studies Recommended Guidelines, Prepared for the Department of Energy, Office of Fusion Energy, September, 1990.

2. Roger O. Bangerter, "Revised Target Information for ICF Reactor Studies", 28 February 1991.

3. J. E. Howard, Appl. Opt., 16, p. 2764.

4. J. B. Trenholme and E. J. Goodwin, "Nova Target Illumination Studies," Laser Program Annual Report - 1980, LLNL Report UCRL-50021-80, Livermore, CA.

5. S. Skupsky and K. Lee, J. Appl. Phys., 54, p. 3662.

6. SOLASE - A Conceptual Laser Fusion Reactor Design, UWFDM-220, Section IX-B-1, December, 1977.

7. P. C. Souers, Hydrogen Properties for Fusion Energy, University of California Press, Los Angeles, 1986, pp. 85-87.

8. T.P. O'Holleran, R.L. Downs, D.A. Steinman and R.L. Crawley, *Journal of Vacuum Science and Technology*, 18 (3), pp. 1242-1243.

9. L. A. Scott, et. al., Journal of Vacuum Science and Technology A, 8 (3), pp. 1736-1740.

10. U. Kubo and H. Tsubakihara, Journal of Vacuum Science and Technology A, 5 (4), pp. 2778-80.

11. R. L. Downs, 1987 KMS Annual Report, p. 74.

12. L. A. Scott, et. al., op. cit.

13. H. W. Deckman, Journal of Vacuum Science and Technology, 18 (3), pp. 1171-1174.

14. J. K. Feuerherd and E. H. Farnum, Journal of Vacuum Science and Technology, 18 (3), pp. 1284-1287.

15. D. E. Day and C. P. Wang, Final Report to Los Alamos National Laboratory, Contract No. 9-X66-5788D-1, 1987

16. L. A. Scott, et. al., op. cit.

17. I. S. Goldstein, F. Falk and J. Trovato, Journal of Vacuum Science and Technology, 18 (3), pp. 1175-1178.

18. K. D. Wise, M. G. Robinson and W. J. Hillegas, Journal of Vacuum Science and Technology, 18 (3), pp. 1179-1182.

19. R. L. Downs, KMS Fusion, Inc. Annual Report, 1986, p. 90.

20. H. H. Johnson, Hydrogen in Metals, Proceedings of an international conference on the effects of hydrogen on materials properties and selection and structural design, pp. 35-49, 23-27 September, 1973.

21. A. R. Troiano, Hydrogen in Metals, Proceedings of an international conference on the effects of hydrogen on materials properties and selection and structural design, pp. 3-15, 23-27 September, 1973.

22. M. R. Louthan, Jr., Hydrogen in Metals, Proceedings of an international conference on the effects of hydrogen on materials properties and selection and structural design, pp. 53-77, 23-27 September, 1973.

23. M. O. Speidel, Hydrogen in Metals, Proceedings of an international conference on the effects of hydrogen on materials properties and selection and structural design, pp. 249-285, 23-27 September, 1973.

24. SOLASE, op. cit., p. IX-A-16.

25. R. L. Downs, op. cit., p. 89

26. A. J. Martin, KMS Fusion, Inc. Annual Report, 1986, p. 92.

27. KMS Fusion, Inc. Annual Report, 1985, pp. 99-102.

28. A. J. Martin, R. J. Simms, and R. B. Jacobs, Journal of Vacuum Science and Technology A, 6, p. 1885.

29. V. Varadarajan, K. Kim and T. P. Bernat, Journal of Vacuum Science and Technology A, 5 (4), pp. 2750-2754.

30. J. K. Hoffer and L. R. Foreman, Journal of Vacuum Science and Technology A, 7 (3), pp. 1161-1164.

31. A. J. Martin, KMS Fusion, Inc. Annual Report, 1988, pp. 13-17.

32. R. M. Singleton and J. T. Weir, Journal of Vacuum Science and Technology, 18 (3), p. 1264.

33. Hyo-gun Kim and M. D. Wittman, Journal of Vacuum Science and Technology A, 5 (4), pp. 2781-2784.

34. J. H. Pendergrass, D. B. Harris, and R. J. Dudziak, Fusion Technology, 13, pp. 375-395.

35. H. Sorenson, et. al., Proceedings of the 15th Symposium on Fusion Technology, Utrecht, The Netherlands, pp. 704-708, 19-23 September, 1988.

36. K. Sonnenberg, et. al., Proceedings of the 15th Symposium on Fusion Technology, Utrecht, The Netherlands, pp. 715-719, 19-23 September, 1988.

37. S. K. Combs, et. al., Journal of Vacuum Science and Technology A, 6 (3), pp. 1901-1904.

38. R. Kreutz, Fusion Technology, 8, pp. 2708-2720.

39. P. Michelson et. al., Proceedings of the 15th Symposium on Fusion Technology, Utrecht, The Netherlands, pp. 700-703, 19-23 September, 1988.

40. Y. C. Fung, Foundations of Solid Mechanics, Prentice-Hall, Inc., Englewood Cliffs, N. J., 1965, p. 191.

41. P. C. Souers, Hydrogen Properties for Fusion Energy, University of California Press, Los Angeles, p. 85, 1986.

42. K. Kawasaki, et. al., Proceedings of the 15th Symposium on Fusion Technology, Utrecht, The Netherlands, pp. 724-728, 19-23 September, 1988.

43. S. K. Combs, et. al., Proceedings of the 15th Symposium on Fusion Technology, Utrecht, The Netherlands, pp. 709-714, 19-23 September, 1988.

44. W. Bailey, et. al., Proceedings of the 15th Symposium on Fusion Technology, Utrecht, The Netherlands, pp. 720-723, 19-23 September, 1988.

45. H. Sorenson, et. al., op. cit.

46. K. Kawasaki, et. al., op. cit.

47. H. Hiratsuka et. al., Proceedings of the 15th Symposium on Fusion Technology, Utrecht, The Netherlands, pp. 729-732, 19-23 September, 1988.

48. K. Kawasaki, et. al., op. cit.

49. H. Sorenson, et. al., op. cit.

50. Ibid.

This page intentionally left blank.

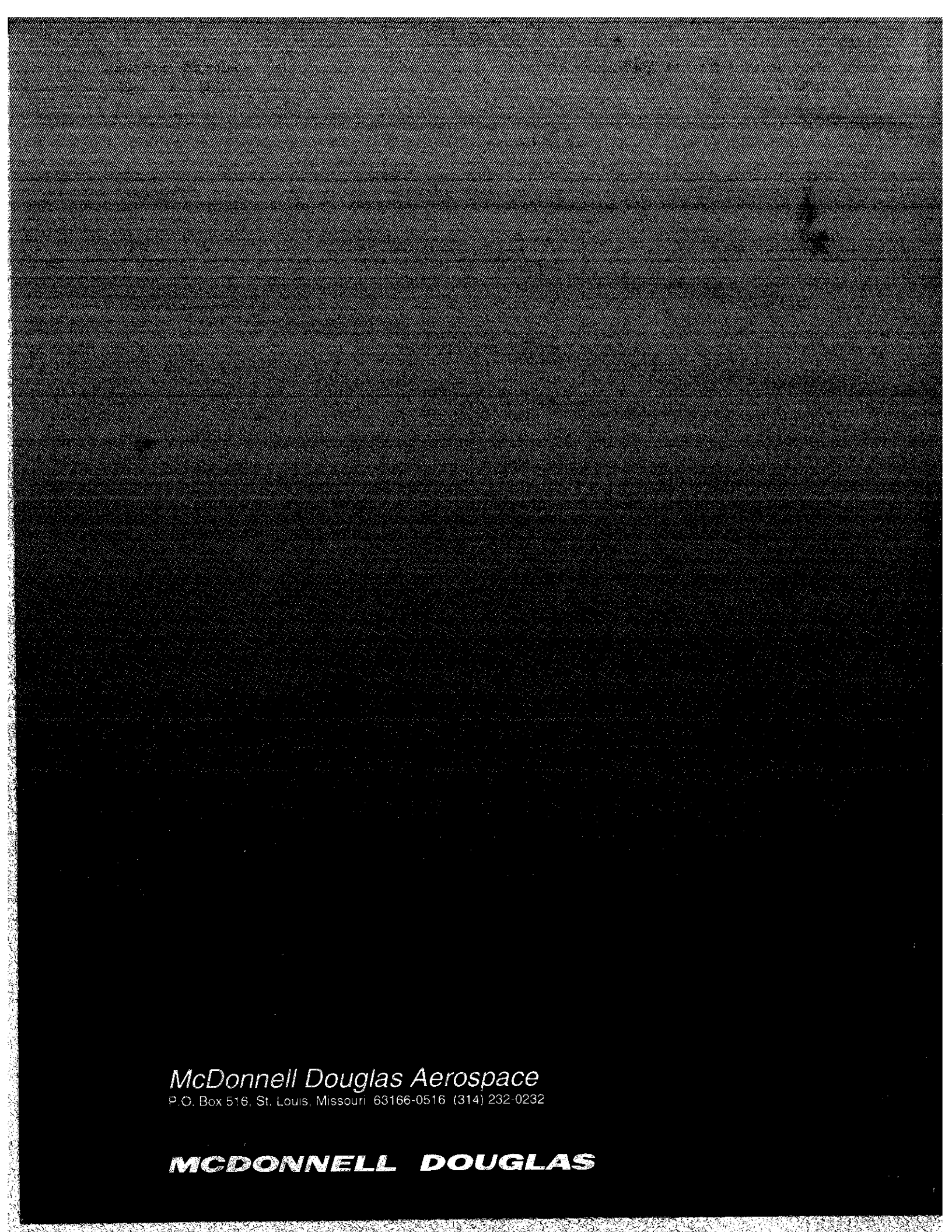

McDonnell Douglas Aerospace
P.O. Box 516, St. Louis, Missouri 63166-0516 (314) 232-0232

MCDONNELL DOUGLAS